Gesellschaft für Anlagen-
und Reaktorsicherheit
(GRS) gGmbH

ATHLET

Validation

GRS-P-1 / Vol. 3
Rev. 8

Gesellschaft für Anlagen-
und Reaktorsicherheit
(GRS) gGmbH

ATHLET 3.4.0

Validation

T. Hollands
S. Buchholz
V. Di Nora
N. Dünne
D. Eckert
M. Junk
A. Krüssenberg
A. Rezchikova
P. Schöffel
A. Wielenberg

November 2023

GRS-P-1 / Vol. 3
Rev. 8

Abstract

This report describes the validation status of ATHLET, which is the best-estimate system thermal-hydraulics code for the simulation of operational, transient, design basis and design extension conditions without core degradation in nuclear reactors. ATHLET is part of the GRS system code package AC². This report is part of the overall documentation for the release AC² 2023.

This report starts with a brief overview of ATHLET. Then, the general validation strategy for ATHLET is described, the validation matrices for ATHLET are presented and the validation calculations on specific tests in these matrices are referenced. In addition, participations in International Standard Problems with ATHLET and DRUFAN, the ATHLET predecessor code, are briefly summarized. In a separate chapter, the quality assurance procedures for performing validation for ATHLET are explained in some detail. Thereafter, validation calculations on in total twelve facilities for the current release ATHLET 3.4 are presented and compared to experimental data and ATHLET 3.3.1 results. Finally, guidance is given on performing uncertainty analyses with the GRS method with representative model input parameter uncertainties.

Overall, ATHLET 3.4 has been demonstrated to be validated for safety analyses of LWR reactors (PWR including VVER and BWR). ATHLET 3.4 is also validated for analyses in the spent fuel pool of LWR reactors and most scenarios in pool-type research reactors. No claims on the validation status of ATHLET 3.4 for reactor designs with working fluids other than water are made.

Acknowledgements

The development and validation of ATHLET and the associated documentation are funded by the German Federal Ministry for the Environment, Nature Conservation, Nuclear Safety and Consumer Protection (BMUV) based on decisions of the German Bundestag.

Over the more than 40 years of continuous validation of ATHLET and its predecessors, a very large number of people, both former GRS employees as well as external experts have contributed to the current version of ATHLET. Here, we want to acknowledge the work of those experts who have made major contributions to the validation of ATHLET: Christine Bals, Henrique Austregesilo, Maria Burwell, Peer Dräger, Horst Glaeser, Johannes Geppert, Udo Graf, Gerhard Höppner, Adela Hora, Wolfgang Horche, Michael Hrubisko, Rudolf Kirmse, Georg Lerchl, Klaus Liesch, Wolfgang Luther, Pavlos Papadimitriou, André Petry, Winfried Pointner, Franz Ringer, Heinz-Günther Sonnenburg, Jürgen Steinborn, Fritz Steinhoff, Klaus Trambauer, Ivan Vojtek, Jonas Wack, Adly Wahba.

Thanks are also due to H. Gasteiger, Ulrike Gocht, C. Györi, András Keresztúri, Alexandr V. Kotsarev, Eckard Krepper, Wolfgang Lischke, Mikhail Lizorkin, Radim Meca, O. I. Melikhov, V. I. Melikhov, A. Moskalev, Sergei P. Nikonov, Frank Schäfer, Manfred Schall, Aleksei I. Suslov, T. Thiele, Istvan Trosztel, Bernd Vandreier, Johannes Weisbrod and Hans-Dieter Wierum.

List of Contents

List of Figures

List of Tables

1 Overview of ATHLET

The thermal-hydraulic computer code **ATHLET** (**A**nalysis of **TH**ermal-hydraulics of **LE**aks and **T**ransients) is being developed by the Gesellschaft für Anlagen- und Reaktorsicherheit (**GRS**) for the analysis of operational conditions, abnormal transients and all kinds of leaks and breaks in nuclear power plants. The aim of the code development is to cover the whole spectrum of design basis and beyond design basis accidents (without core degradation) for **PWRs, BWRs, SMRs and future Gen IV reactors** with one single code.

The main code features are:

- advanced thermal-hydraulic modelling (compressible fluids, mechanical and thermal non-equilibrium of vapor and liquid phase)
- availability of diverse working fluids: light or heavy water, helium, sodium, potassium, lead, lead-bismuth eutectic, supercritical carbon dioxide, molten salts as well as user-provided single-phase (non-boiling) working fluids
- heat generation, heat conduction and heat transfer to single- or two-phase fluid considering structures of different geometry, e.g. rod or pebble bed
- interfaces to specialized numerical models such as 3D neutron kinetic codes or 3D CFD codes for coupled multiphysical and multiscale simulations
- control of ATHLET calculation by call backs to programming language independent user code enabling the coupling of external models
- plug-in technique for user provided code extensions
- modular code architecture
- separation between physical models and numerical methods
- numerous pre- and post-processing tools
- portability
- continuous and comprehensive code validation

ATHLET is applied by numerous institutions in Germany and abroad.

The development and validation of ATHLET is sponsored by the German Federal Ministry for Economic Affairs and Energy (BMWi) based on decisions by the German Bundestag.

1.1 Range of Applicability

ATHLET has been developed and validated to be applied for all types of design basis and beyond design basis incidents and accidents without core damage in light water reactors, like PWR, BWR, VVER, and RBMK. For accidents with core damage, **ATHLET-CD** (**C**ore **D**egradation) has been developed providing extensions for the simulation of the mechanical fuel behaviour, core melting and relocation, debris bed formation as well as fission product release and transport within the reactor system. ATHLET-CD uses the same input deck as ATHLET supplemented by data required by the core degradation models.

The range of working fluids covers **light and heavy water** enabling the transition between subcritical and **supercritical fluid states**. In addition, further coolants can be simulated as working fluids: **helium, sodium, potassium** as well as **non-boiling fluids liquid lead, lead-bismuth eutectic, molten salts** and **user-provided fluids**. These extensions, aiming at the simulation of future Generation IV reactor designs, are still subject to further development and validation.

ATHLET is a 1D system code, ATHLET is not a 3D CFD code. ATHLET thermal hydraulic models generally assume fully developed flow on dimensions (0.01 m to 10 m) and pressures (0.01 MPa to 30 MPa) typical of nuclear facilities. Details of turbulence, of boundary layer, and viscous energy dissipation between flow layers are neglected, interfacial area and momentum terms are treated in a simplified manner, and 3D flow effects cannot be investigated in detail. Similarly, heat conduction in structures generally is 1-dimensional using averaged, engineering level heat transfer correlations. While ATHLET can be applied outside of these constraints with some success, it has not been validated for them.

1.2 Code Structure

ATHLET is written in Fortran. The code features a modular code structure that allows an easy maintainability and expandability of the modelling basis to satisfy the demands of

new applications and future reactor designs. The code is composed of four basic modules that focus on the calculation of phenomena relevant for safety analyses of a nuclear power reactor:

- Thermo-Fluid dynamics (TFD)
- Heat Conduction and Heat Transfer (HECU)
- Neutron Kinetics (NEUKIN)
- Control and Balance-of-Plant (GCSM)

The TFD system of ordinary differential equations is solved fully implicitly with the numerical integration method FEBE. Other independent modules (e.g. large models with own time advancement procedure) can be coupled without structural changes in ATHLET by means of dedicated interfaces.

1.3 Fluid Dynamics

The TFD module of ATHLET employs a modular network approach for the representation of a thermal-hydraulic system. A given system configuration can be simulated just by connecting basic fluid dynamic elements, called **thermo-fluid dynamic objects (TFOs)**. There are several TFO types, each of them is applied with a selected fluid dynamic model. All object types are classified into three basic categories:

The TFD module of ATHLET employs a modular network approach for the representation of a thermal-hydraulic system. A given system configuration can be simulated just by connecting basic fluid dynamic elements, called **thermo-fluid dynamic objects (TFOs)**. There are several TFO types, each of them is applied with a selected fluid dynamic model. All object types are classified into three basic categories:

- **Pipe objects** employ a one-dimensional TFD model describing the transport of fluid. After nodalisation according to input data, a pipe object can be understood as a number of consecutive nodes (**control volumes**) connected by flow paths (**junctions**). A special application of a pipe object, called single junction pipe, consists of only one junction, without any control volumes.
- **Branch objects** consist of only one control volume. They employ a zero-dimensional TFD-model of non-linear ordinary differential equations or algebraic equations.

- **Special objects** are used for network components that exhibit a complex geometry, e.g. the cross connection of pipe objects aligned in parallel for the generation of a multidimensional network.

This object structure has been developed in order to allow the coupling of models of different physical formulation and spatial discretization, which are to be employed in certain network domains.

ATHLET offers two different sets of model equations for the simulation of the fluid-dynamic behaviour:

- The **5-equation model** with separate conservation equations for liquid and vapor mass and energy, supplemented by a mixture momentum equation. It accounts for thermal and mechanical non-equilibrium and includes a mixture level tracking capability.
- The **Two-fluid model** with fully phase-separated conservation equations for liquid and vapor mass, energy, and momentum (without mixture level tracking capability).

The spatial discretization is performed on the basis of a **finite-volume staggered-grid approach**. The mass and energy equations are solved within control volumes, and the momentum equations are solved over junctions connecting the centres of the control volumes. The solution variables are the pressure, vapor temperature, liquid temperature and vapor mass quality within a control volume, as well as the mass flow rate (5-eq. model) or the phase mass velocities (6-eq. model) in a junction, respectively.

Two types of control volumes are available. Within the so-called “ordinary” control volume, a homogeneous mass and energy distribution is assumed. Within the “non-homogeneous” control volume, a **mixture level** is modelled. Above the mixture level, steam with water droplets, below the mixture level, liquid with vapor bubbles may exist. The combination of ordinary and non-homogeneous control volumes provides the option to simulate the motion of a mixture level through vertical components.

A full-range **drift-flux model** is available for the calculation of the relative velocity between the fluid phases. The model comprises all flow patterns from homogeneous to separated flow occurring in vertical and horizontal two-phase flow. It also takes into account counter current flow limitations in different geometries.

Moreover, both fluid-dynamic options allow for the simulation of **non-condensable gases**. This applies for water as well as for the liquid metal and molten salt working fluids. Fluid properties are provided for hydrogen, nitrogen, oxygen, air, helium, argon, krypton, xenon, carbon monoxide, and carbon dioxide. Additional mass conservation equations can be included for the description of **boric acid** or **zinc borate** transport within a coolant system as well as for the transport and release of **nitrogen dissolved** in the liquid phase of the coolant.

Both the 5-equation model and the two-fluid model employ the one-dimensional conservation equations for mass, momentum and energy. By means of a spatially two- or three-dimensional TFO arrangement, these models allow for a simplified multidimensional simulation. In order to enhance the capability of ATHLET with regard to the simulation of complex, multidimensional flow phenomena, a **thermal-hydraulic 2D/3D model** has been developed. It extends the balance equations of the two-fluid model. Both 2D and 3D momentum equations for liquid and vapor are available.

For pipe objects applying the 5-equation model, there is also the possibility to use the method of integrated mass and momentum balances (**EIMMB**), an option for fast-running calculations, mainly in the frame of a nuclear plant analyser. With the application of the EIMMB-Method, the solution variables are now the average object pressure, the mass flows at pipe inlet and outlet, and the local qualities and temperatures. The local pressures and mass flow rates are obtained from algebraic equations as a function of the solution variables.

Another fluid-dynamic option, applied exclusively for the steady state calculation, consists of a 4-equation model with balance equations for liquid mass, vapor mass, mixture energy and mixture momentum. The solution variables are the pressure, vapor mass quality and enthalpy of the dominant phase within a control volume, and the mass flow rate in a junction. The entire range of fluid conditions, from subcooled liquid to superheated vapor including thermal non-equilibrium is taken into account, assuming the non-dominant phase to be at saturation.

1.4 Numerical Methods

The **time integration** of the thermo-fluid dynamic model is performed with the general-purpose ODE-solver **FEBE** (Forward-Euler, Backward-Euler). It provides the solution of a

linear system of ordinary differential equations (ODE) of first order, splitting it into two subsystems, the first being integrated explicitly, the second implicitly. Generally, the **fully implicit** option is used in ATHLET. Each thermo-fluid dynamic object provides a subset of the entire ODE system, which is integrated simultaneously by FEBE.

The linearization of the underlying model equation system is done numerically by calculation of the Jacobian matrix. A **block sparse matrix package** (FTRIX) is available to handle the repeated evaluation of the Jacobian matrix as well as the solution of the resulting system of linear equations in an efficient way. Alternatively, scalable solvers from the PETSc and MUMPS libraries can be used for the numerical calculations via the Numerical Toolkit (NuT) plug-in.

A **rigorous error control** is performed based on an extrapolation technique. According to the error bound specified by the user, the time step size and the order of the method (> 2) are adequately determined by FEBE for every integration step.

1.5 Heat Conduction and Heat Transfer

The simulation of the heat conduction in **structures, heat exchangers, fuel rods, electrical heaters and spheres** (pebble bed) is performed by the basic module **HECU**. It permits the user to assign heat conduction objects (HCOs) to all thermal-fluid dynamic objects of a given network.

The one-dimensional heat conductor module HECU provides the simulation of the temperature profile and the energy transport in solid materials. The model has the following characteristics:

- The shape of a HCO is constant in time.
- The model can simulate the one-dimensional temperature profile and heat conduction in plates normal to the surface, as well as in hollow or full cylinders and spheres in the radial direction.
- Optionally, two-dimensional heat conduction can be simulated considering the axial direction of plates and cylinders.
- In each HCO, up to three material zones can be modelled. A material zone is simulated by a user-defined number of temperature layers. The material zones can be

separated by a geometrical gap and a corresponding heat transfer coefficient. Furthermore, the model enables the calculation of the temperature in TRISO coated particles.

- The HCOs can be coupled on left and/or right side to TFOs by consideration of the energy transport between heat conductor surface and the surrounding fluid. It is also possible to simulate a fluid temperature as boundary condition for the HCO by means of control (GCSM) signals.
- The HCOs are automatically split into heat conduction volumes (HCVs) according to the nodalisation of the adjacent TFOs and to user input.
- Heat generation can be considered in material zones. The specific heat generation rate per volume unit is assumed to be distributed uniformly either within a material zone or a temperature layer.
- Radiation heat transfer between different HCOs can be taken into account.

The **heat transfer package** covers a wide range of single phase and two-phase flow conditions of water. Correlations for critical heat flux and minimum film boiling temperature are included. Evaporation and condensation directly at heating or cooling surfaces are calculated. A quench front model for bottom and top reflooding is also available. Special heat transfer correlations are available for supercritical water, liquid metal working fluids and helium considering specific geometries (e.g. rod bundle or pebble bed).

1.6 Nuclear Heat Generation

The nuclear heat generation is generally modelled by means of the neutron kinetics module **NEUKIN**. For the simulation of electrically heated rods or for a simplified, straight-forward representation of a reactor core, the total generated power as a function of time or any other quantity can optionally be given.

The generated **nuclear reactor power** consists of two parts: the prompt power from fission and decay of short-lived fission products, and the decay heat power from the long-lived fission products. The steady state part of the decay heat and its time-dependent reduction after a reactor scram are provided in form of a GCSM signal. The time-dependent behaviour of the prompt power generation is calculated either by a point-kinetics model

or by coupling to a 3D neutron kinetics code. An input-specified fraction of the total power is assumed to be produced not in the fuel but directly in the coolant.

The **point-kinetics model** is based on the application of the well-known kinetics equations for one group of prompts and for six groups of delayed neutrons. The reactivity changes due to control rod movement or reactor scram are given by a GCSM signal. The reactivity feedback effects for fuel temperature, moderator density and moderator temperature are calculated either by means of dependencies given by input tables or with reference reactivity coefficients. If the boron tracking model is applied, the reactivity feedback due to changes in the boron concentration will be also taken into account.

The module NEUKIN also offers a general interface for coupling of **3D neutronic models**. Several 3D codes for rectangular and hexagonal geometries have been successfully coupled to ATHLET with this interface, e.g., FENNECS, QUABOX/CUBBOX, TORT-TD, PARCS or DYN3D.

1.7 Simulation of Components

Specific models are provided for the simulation of **valves, pumps, accumulators, steam separators, steam and gas turbines, compressors, steam condensers, single and double ended breaks, fills, leaks, and boundary conditions** for pressure and enthalpy. The steam separator model is an empirical approach for the calculation of carry-over and carry-under flows by means of input functions of the inlet mass flow rates, of the void fraction in the separator region, and of the mixture level outside the separator. Abnormal separator conditions like flow reversal or flooding can be simulated.

In general, major plant components (e.g., pressurizer, steam generators) can be modelled by connecting thermo-fluid dynamic objects (TFOs) and heat conduction objects (HCOs) via input data. For compact heat exchanger designs like plate heat exchanger or helical coil heat exchanger dedicated models are available.

Critical flow, e.g. **discharge flow**, is calculated by a one-dimensional thermal non-equilibrium model with consideration of the given flow geometry. The module CDR1D generates automatically tables of critical mass fluxes applied in ATHLET for the interpolation

of the critical mass flow rates. Optionally, a homogeneous equilibrium model and the Moody discharge model are available.

1.8 Simulation of Control and Balance-of-Plant

The simulation of balance-of-plant (BOP) systems within ATHLET is performed by the basic module **GCSM** (General Control Simulation Module). GCSM is a block-oriented simulation language for the description of control, protection and auxiliary systems.

The user can model control circuits or even simplified fluid systems just by connecting basic functional blocks (e.g., switch, adder, integrator). Most of the system variables calculated within the fluid dynamics, neutron kinetics or within other ATHLET modules can be selected as input to these functional blocks (process variables). The output of such control blocks can be fed back to the thermo-fluid dynamics in form of hardware actions (e.g., valve cross sectional area, control rod position) or boundary conditions (e.g., temperature, heat and mass sources).

The GCSM module allows for the representation of fluid dynamic systems (e.g., steam line, condensate system) in a very simplified way (quasi stationary approach) with the advantage of requiring very little computing time in comparison with the fluid dynamics module.

GCSM also provides an interface to a library that contains detailed models with fixed structure and own input data for plant components (e.g. heat exchanger or even containment model) or for control systems (e.g. power control or system pressure control for typical power plants). The **GRS containment codes CONDRU and COCOSYS** have been coupled to ATHLET by means of this interface. In addition, GCSM comprises a flexible interface that enables the coupling of ATHLET with user provided code, that implements external models, new controller types, specific signals, or complete BOP models.

1.9 Code Handling

ATHLET provides a free-format, hierarchically structured input. Both the generation and the maintenance of the ATHLET input decks are facilitated by several copy functions and by the use of a flexible parameter technique during input data processing, which helps to avoid the repeated typing of identical or similar input data and adaptation of existing

inputs to different configurations. An extended checking of both the input data and the program processing helps the user to discover input errors or modelling weaknesses affecting both code performance and physical results.

ATHLET provides a **restart capability**. The program execution can be **parallelized** on computers with shared memory architecture using the Fortran OpenMP standard. ATHLET runs under different computer operational systems (MS Windows ®, Unix).

The ATHLET Program Package comprises a series of **auxiliary programs** to support both the ATHLET users and developers in the application and development of ATHLET:

- AGM: **A**THLET **G**CSM **M**odeler for graphical setup and testing of control systems and generation of GCSM input data.
- AIG: **A**THLET **I**nput **G**raphics for graphical representation of the TFO and HCO network specified in the input model.
- GIG: **G**CSM **I**nput **G**raphics for graphical representation of the structure of GCSM controllers.
- Several programs for the post-processing of plot data (concatenation, merging, algebraic operations)
- APTPlot: Generates time and locus diagrams exploiting the structure of the input model.
- ATLAS: Dynamic visualization of the simulation results on the basis of AIG and GIG pictures.
- Several programs for the analysis of the Jacobian matrix (interdependencies, Eigenvalues, …), mainly for code development and debug purposes.
- Furthermore, ATHLET can be applied as process model of the **ATLAS/ATALSneo plant simulator** providing full interaction and extended data visualization. ATLAS and ATLASneo are also components of the AC² software package.

ATHLET is also closely linked with the GRS computer programs **SUSA** and **MCDET**. Both enable uncertainty and sensitivity analyses of ATHLET simulation results.

1.10 Code Coupling

ATHLET is part of the **AC² software package**, which comprises the GRS codes ATHLET, ATHLET-CD and COCOSYS, includes the 3D nodal neutronics code FENNECS and is complemented by the interactive simulator software ATLAS/ATLASneo and some productivity tools.

To allow **multiphysical or multiscale simulations**, ATHLET has been coupled successfully to various computer codes by means of dedicated coupling interfaces. The following figure depicts the essential interfaces that are realized for ATHLET. Depending on the characteristic time constants of the coupled processes, the coupling techniques used range from weak form (e.g., data transfer after completed time step) to strong or semi-implicit form (i.e., mutual iteration of the codes' results for each sub step of the FEBE extrapolation algorithm, used for coupling with CFD codes).

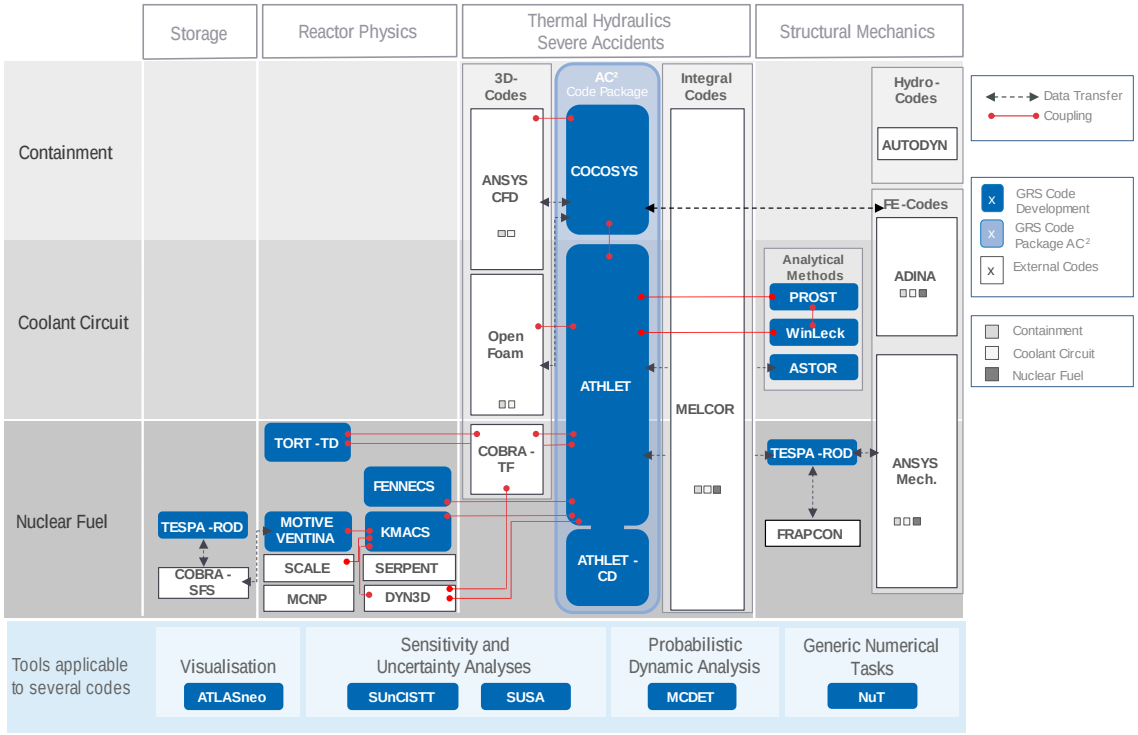

Fig. 1.1 GRS nuclear simulation chain and code coupling

Moreover, ATHLET can be extended by user provided feature implementations. The **plug-in concept** enables the users to apply ATHLET more individually by either requesting a specific extension from GRS or even by developing the needed feature on their own. Such plug-ins have to be created as separate shared libraries on Linux systems or DLLs under Windows. In case a plug-in binary is placed within the *plugin* directory of an

ATHLET installation, ATHLET will register it at start up and invoke it if the applied input file demands its use. The parts or phases of the simulation that can be extended by plug-ins are specified by ATHLET.

Another option for controlling the simulation by user code is offered by using the shared library version (MS Windows: dll / Linux: so) of ATHLET. This library provides the main entry of ATHLET via the exported routine symbol athlet_. This variant allows to implement a user program that calls ATHLET as a subroutine. In this case the simulation process can be controlled in an *"event oriented"* manner by associating the so-called **call-back routines** before calling ATHLET. An *event* can be considered as a certain and named point in the simulation flow, like *input done*, *begin of timestep*, *end of timestep*. These points have been made available as the so-called **hooks**, at which a user might associate routines that instruct ATHLET what to do at this point before continuing the simulation. Hash maps, which include pointers to exported ATHLET variables, are accessible by both the user code and ATHLET. They enable inter-code data transfer of e.g., physical fields or GCSM control block states.

1.11 Validation

The development of ATHLET was and is accompanied by a systematic and comprehensive validation program. The validation is mainly based on pre- and post-test calculations of separate effects tests, integral system tests including the major **International Standard Problems**, as well as on actual plant transients. A well-balanced set of tests has been derived from the **CSNI Code Validation Matrix** emphasizing the German combined ECC injection system. The tests cover phenomena which are expected to be relevant for all types of events of the envisaged ATHLET range of application for all common LWRs including advanced reactor designs with up-to-date passive safety systems. The validation of ATHLET for SMR designs and future Gen IV reactors is underway.

2 General Validation Strategy

2.1 Objectives and Definitions

Computer codes like ATHLET aim to simulate the system behaviour of nuclear power plants as realistic as possible ('best estimate'). These computer codes are used to investigate

- incidents and accidents of different scenarios and their consequences,
- the effectiveness of emergency procedures.

The process carried out by comparing code predictions with experimental measurements or measurements in a reactor plant (if available) is called validation /IAEA 16/, /GRS 21/. A code or code model is considered validated when sufficient testing has been performed to ensure an acceptable level of predictive accuracy over the range of conditions for which the code is foreseen to be applied. Accuracy is a measure of the difference between measured and calculated quantities taking into account uncertainties and biases in both. Bias is a measure, usually expressed statistically, of the systematic difference between a true mean value and a predicted or measured mean. Uncertainty is a measure of the scatter in experimental or predicted data /CSNI 89/. The acceptable level of accuracy is judgmental and will vary depending on the specific problem or question to be addressed by the code. The procedure for specifying, qualitatively or quantitatively, the accuracy of code predictions is also called code assessment.

The international literature distinguishes between the term’s 'validation' and 'verification'. As explained in /JAC 23/, verification is an important element of the overall quality assurance process during code development, where the conformance of the source code to the specifications and underlying intentions is tested and where the code is checked on coding errors and other bugs. Within this context, a mathematical model, or the corresponding computer code, is verified if it is demonstrated that the code behaves as specified, i.e., that it is a proper mathematical representation of the conceptual model, and that the equations are correctly encoded and solved. Verification may include the demonstration of convergence of the calculated results during a process of reduction of time steps and the size of the nodes of simulation. Also, the comparison of results for a specific model with exact mathematical solutions and with the results obtained by similar codes may fall under the term verification. In this context, the comparison with measured

values is not part of the verification process, it is rather a validation task. The term verification, however, has often been used synonymously with validation and qualification /CSNI 89/. In the past, the term verification was used in the frame of the ATHLET code validation work, including comparisons between calculations and measurements.

2.2 Validation Matrices for Light Water Reactors

The validation of codes is mainly based on pre-test and post-test calculations of separate effects tests, integral system tests, and transients in commercial plants. An enormous amount of test data, usable for code validation, has been accumulated in the last decades. In the year 1987 the Committee on the Safety of Nuclear Installations (CSNI) of the Nuclear Energy Agency (NEA) in the Organization for Economic Co-Operation and Development (OECD) issued a report compiled by the Task Group on the Status and Assessment of Codes for Transients and ECC /NEA 87/. It contains proposed validation matrices for LOCA and transients, consisting of the dominating phenomena and the available test facilities, and the selected experiments. The Task Group on Thermal Hydraulic System Behaviour updated the integral test matrices /NEA 96/ and extended their work to separate effects tests /NEA 93/.

The systematic validation of ATHLET is based on a well-balanced set of integral and separate effects tests derived from the CSNI proposal, emphasizing however the German combined ECC injection system which has been investigated in the UPTF, PKL and LOBI facilities.

The validation methodology distinguishes between the validation of individual code models and the assessment of the overall system simulation. The individual code models are validated against separate effects tests in full or at least large-scale test facilities. The overall assessment is based on pre- and post-test calculations of integral tests, and comparisons with available plant transients.

To systemize the selection of tests for code validation, the so-called 'Cross Reference Matrices' have been first established. Based on these matrices, phenomenologically well-founded sets of experiments have been defined, for which comparison of measured and calculated parameters forms the basis for establishing uncertainty ranges of test calculation results. The matrices also permit identification of areas where further research may be justified.

In the Cross Reference Matrices (Fig. 2.1 to Fig. 2.11), the relevant physical phenomena, which are known or assumed to occur during transients or loss-of-coolant accidents in different types of NPPs are listed, together with the experimental facilities suitable for reproducing these effects and the test types of interest. The relationship of phenomenon versus test type indicates which phenomena are expected to occur in which types of tests. The relationship of test facility versus phenomenon indicates the suitability of the test facilities for code validation of the different phenomena, and the relationship of test type versus test facility indicates which types of tests are performed in which test facilities.

The matrices for Western PWRs and BWRs are focused mainly on integral system tests and operational data from power plants. For PWR facilities, six individual matrices were prepared (Fig. 2.1 to Fig. 2.6), differentiating between:

- large breaks
- small and intermediate leaks for PWRs with U-tube steam generators
- small and intermediate leaks for PWRs with once-through steam generators
- transients
- transients under shut-down conditions
- accident management for a non-degraded core.

The matrix for small and intermediate breaks in PWRs with once-through steam generators (Fig. 2.3) has been developed to address particular phenomena, which are unique to this reactor type. For BWR facilities, two individual matrices have been established (Fig. 2.7 to Fig. 2.8) differentiating between loss-of-coolant accidents and transients.

For Russian VVER facilities, three matrices have been compiled by the OECD /NEA 01/ differentiating between large breaks, small and intermediate breaks, and transients (Fig. 2.9 to Fig. 2.11). Different to the matrices for Western NPPs, they include test facilities for separate effects tests. Furthermore, they distinguish between the plant types VVER-440/213 and VVER-1000. However, these matrices have not been updated. The more current state of the VVER related tests performed is given in Tab. 2.2, Tab. 2.4, and Tab. 2.7.

The LWR design types of PWR, BWR or VVER are included under 'Test Facility' since the analyses of transients and accidents in actual power plants are valuable for validation as they are not subject to scaling distortions and can expose simulation problems.

The relationship of phenomenon versus test type is rated at one of three levels:

- occurring: which means that the particular phenomenon does occur in that kind of test (plus sign in the matrix),
- partially occurring: only some aspects of the phenomenon occur (open circle in the matrix),
- not occurring (dash in the matrix).

The relationship of phenomenon versus test facility is rated at one of four levels:

- suitable for code assessment: a facility is designed in such a way as to simulate the phenomenon assumed to occur in the plant, and it is sufficiently instrumented to reveal the phenomenon (plus sign in the matrix),
- limited suitability: the same as above, but with restrictions due to imperfect scaling or insufficient instrumentation (open circle in the matrix),
- not suitable (dash in the matrix),

The relationship of test type versus facility is also rated at one of three levels:

- performed: the test type is useful for code assessment purposes (plus sign in the matrix),
- performed but of limited use: this kind of test has been performed in the facility, but it has limited usefulness for assessment purposes due to poor scaling or lack of instrumentation (open circle in the matrix),
- not performed (dash in the matrix).

For VVER plants two further relationships are included to account for the different reactor designs:

- plant type versus phenomenon and
- plant type versus test facility.

The matrices for VVER reactor types date from 2001 /NEA 01/. At this time, the suitability in particular of the PSB-WWER facility for several phenomena could be only estimated. Therefore, a new rating 'expected to be suitable' had been introduced. Meanwhile, numerous experiments have been performed proving the suitability of these facilities for code assessment (see tables in chap. 2.2.1).

MATRIX I: CROSS REFERENCE MATRIX FOR LARGE BREAKS IN PWRs		Test Type			Test Facility						
Test type vs. phenomenon + occurring o partially occurring - not occurring **Test facility vs. phenomenon** + suitable for code assessment o limited suitability - not suitable **Test type vs. test facility** + performed o performed but of limited use - not performed or planned		Blowdown	Refill	Reflood	CCTF 1:25	LOFT 1:50	BETHSY 1:100	PKL 1 : 145	LOBI 1:712	SEMISCALE 1:1600	UPTF 1:1 (1)
Phenomena	Break flow	+	+	+	o	o	o	o	o	o	o
	Phase separation (condition or transition)	o	+	+	+	+	+	+	+	+	+
	Mixing and condensation during injection	o	+	+	o	o	o	o	o	o	+
	Core wide void + flow distribution	o	+	+	o	o	o	o	o	-	o
	ECC bypass and penetration	o	+	o	+	+	-	o	o	-	+
	CCFL (UCSP)	o	+	+	o	o	o	o	o	-	+
	Steam binding (liquid carry over, ect.)	-	o	+	o	o	-	o	o	o	o
	Pool formation in UP	-	+	+	o	o	o	o	o	o	+
	Core heat transfer incl. DNB, dryout, RNB	+	+	+	o	+	+	+	o	o	-
	Quench front propagation	o	o	+	+	+	+	+	-	+	-
	Entrainment (Core, UP)	o	o	+	o	o	+	o	o	o	+
	Deentrainment (Core, UP)	o	o	+	o	o	o	o	o	o	+
	1- and 2-phase pump behavior	+	o	o	-	o	-	o	+	+	-
	Noncondensable gas effects	-	o	o	-	-	o	-	-	-	o
Test Facility	CCTF	-	o	+							
	LOFT	+	+	+	Important test parameters: - Break location/break size - Pumps off/pumps on - Cold leg injection/combined injection						
	BETHSY	-	-	+							
	PKL	o	+	+							
	LOBI	+	+	-							
	SEMISCALE	+	+	+	(1) UPTF integral tests						
	UPTF	o	+	+							

Fig. 2.1 Cross Reference Matrix for Large Breaks in PWRs

MATRIX II: CROSS REFERENCE MATRIX FOR SMALL AND INTERMEDIATE BREAKS IN PWRs		**Test Type**							**Test Facility**								
Test type vs. phenomenon + occurring o partially occurring - not occurring **Test facility vs. phenomenon** + suitable for code assessment o limited suitability - not suitable **Test type vs. test facility** + performed o performed but of limited use - not performed or planned		Stationary test addressing energy transport on primary side	Stationary test addressing energy transport on secondary side	Small leak overfeed by HPIS, secondary side necessary	Small leak without HPIS overfeeding, secondary side necessary	Intermediate leak, secondary side not necessary	Pressurizer leak	U-tube rupture	PWR 1:1	LOFT 1:50	LSTF 1:50	BETHSY 1:100	PKL-III 1:145	SPES 1:430	LOBI-II 1:712	SEMISCALE 1:1600	UPTF TRAM 1:1 (2)
Phenomena (3)	Natural circulation in 1-phase flow, primary side	±	+	+	o	-	+	+	+	±	+	+	+	±	+	±	-
	Natural circulation in 2-phase flow, primary side	±	-	o	±	±	o	-	-	±	+	+	+	±	+	±	o
	Reflux condenser mode and CCFL	±	-	-	±	±	-	-	-	o	+	+	o	o	o	o	+
	Asymmetric loop behavior	-	-	+	±	-	o	+	-	-	o	+	+	±	o	o	+
	Break flow	-	-	+	±	±	+	+	-	+	+	+	+	±	+	±	o
	Phase separation without mixture level formation	±	-	o	±	±	+	o	-	o	+	+	+	±	+	o	+
	Mixture level and entrainment in SG second side	-	+	+	±	±	+	+	-	-	+	+	+	o	o	-	-
	Mixture level and entrainment in the core	±	-	-	±	±	+	-	-	o	+	+	+	o	o	o	o
	Stratification in horizontal pipes	±	-	-	±	±	-	-	-	±	+	o	o	±	o	o	+
	Phase separation in T-junct. and effect on break flow	-	-	-	±	±	-	-	-	o	o	o	o	o	o	-	+
	ECC-mixing and condensation	-	-	o	±	±	+	+	-	o	o	o	o	o	o	o	+
	Loop seal clearing	-	-	-	±	±	o	-	-	±	±	±	±	±	±	±	+
	Pool formation in UP/CCFL (UCSP)	±	-	-	o	±	+	-	-	o	o	o	o	o	-	o	+
	Core wide void and flow distribution	±	-	-	o	±	+	-	-	o	o	o	o	-	-	-	o
	Heat transfer in covered core	±	+	+	±	±	+	+	o	±	±	±	±	±	+	±	-
	Heat transfer in partly uncovered core	±	-	-	o	±	-	-	-	±	±	±	±	o	o	o	-
	Heat transfer in SG primary side	±	o	o	±	±	o	o	-	o	±	±	±	±	+	o	-
	Heat transfer in SG secondary side	o	+	+	±	±	+	+	-	o	±	±	±	o	+	o	-
	Pressurizer thermohydraulics	o	-	o	o	±	+	+	o	o	o	o	o	o	o	-	+
	Surge line hydraulics	o	-	-	o	±	+	o	-	o	o	o	o	o	o	o	+
	1- and 2-phase pump behavior	-	-	-	o	±	-	-	o	o	o	o	o	o	+	±	-
	Structural heat and heat losses (1)	±	-	o	±	±	o	o	-	o	o	o	o	o	o	o	o
	Noncondensable gas effects	±	-	-	-	-	-	-	-	-	o	o	o	-	-	o	+
	Boron mixing and transport	±	-	+	±	±	+	+	-	-	-	-	-	-	-	-	o
Test Facility	PWR	-	-	o	-	-	+	+									
	LOFT	-	-	+	±	±	+	-									
	LSTF	±	+	±	+	+	+	±									
	BETHSY	±	±	±	+	+	+	±									
	PKL-III	±	+	±	±	±	+	+									
	SPES	±	+	+	±	-	-	-									
	LOBI-II	±	+	+	±	±	+	+									
	SEMISCALE	o	o	+	±	±	+	+									
	UPTF, TRAM	-	-	-	-	±	+	-									

(1) Problem for scaled test facilities
(2) UPTF integral tests
(3) For intermediate breaks phenomena included in large break reference matrix may be also important

Fig. 2.2 Cross Reference Matrix for Small and Intermediate Breaks in PWRs

MATRIX III: CROSS REFERENCE MATRIX FOR SMALL AND INTERMEDIATE BREAKS IN PWRs WITH OTSG (IN ADDITION TO THE MATRIX FOR PWRs WITH UTSG)

Phenomenon
+ suitable for code assessment o limited suitability - not suitable

Test type vs. test facility
+ performed
o performed but of limited use
- not performed or planned

		Test Type							Test Facility				
		Stationary test addressing energy transport on primary side	Stationary test addressing energy transport on secondary side	Small leak overfeed by HPIS, secondary side necessary	Small leak without HPIS overfeeding, secondary side necessary	Intermediate leak, secondary side not necessary	Pressurizer leak	OTSG-tube rupture	PWR	Univ. Maryland (lowered loop) 1:500	MIST (lowered loop) 1 : 817	OTIS (raised loop) 1 : 1686	GERDA (raised loop) 1 : 1686
Phenomena (2)	Natural circulation in 1-phase flow, primary side	+	+	+	o	-	+	+	+	+	+	+	+
	Natural circulation in 2-phase flow, primary side	+	-	o	+	+	o	o	-	+	+	-	+
	Boiler condenser mode	+	-	-	+	+	-	-	-	+	+	+	+
	Asymmetric loop behaviour	-	-	+	+	-	o	+	-	+	+	-	-
	Break flow	-	-	+	+	+	+	+	-	+	+	+	o
	Phase separation without mixture level formation	-	-	o	+	+	+	o	-	+	+	-	-
	Mixture level and entrainment in SG secondary side	-	+	+	+	+	+	+	-	o	+	o	o
	Mixture level and entrainment in the core	-	-	-	+	+	+	-	-	-	-	-	-
	Stratification in horizontal pipes	-	-	-	+	+	-	-	-	o	o	-	-
	Phase separation in T-junct. and effect on break flow	-	-	-	+	+	-	-	-	-	-	-	-
	ECC-mixing and condensation	-	-	o	+	+	+	+	-	o	o	-	o
	Loop seal clearing	-	-	-	+	+	o	-	-	+	o	-	-
	Pool formation in UP/CCFL (UCSP)	-	-	-	o	+	+	-	-	-	-	-	-
	Core wide void and flow distribution	-	-	-	o	+	+	-	-	o	o	-	-
	Heat transfer in covered core	+	+	+	+	+	+	+	o	o	o	+	+
	Heat transfer in partly uncovered core	-	-	-	o	+	-	-	-	-	-	-	-
	Heat transfer in SG primary side	+	o	o	+	+	o	o	-	+	+	o	o
	Heat transfer in SG secondary side	o	+	+	+	+	+	+	-	o	o	o	o
	Pressurizer thermohydraulics	-	-	o	o	+	+	+	o	o	o	-	-
	Surge line hydraulics	-	-	-	o	+	+	o	-	-	-	-	-
	1- and 2-phase pump behavior	-	-	-	o	+	-	-	o	o	o	-	-
	Structural heat and heat losses (1)	+	-	o	+	+	+	o	-	o	o	o	o
	Noncondensable gas effects	+	-	-	-	-	-	-	-	+	+	+	+
	Boron mixing and transport	+	-	+	+	+	+	+	-	-	-	-	-
	Intermittent two-phase natural circulation	-	-	-	+	+	o	o	-	+	+	+	+
	Natural circulation-core, vent valve, downcomer	+	o	+	+	+	+	+	o	+	+	+	+
	Refill of loops	-	-	+	+	o	+	-	-	+	+	o	+
	Superheating in secondary side	+	+	+	+	+	+	+	+	+	+	+	+
Test Facility	PWR	-	-	o	-	-	+	o					
	Univ. Maryland	+	+	+	+	-	+	+					
	MIST	+	+	+	+	-	+	+					
	OTIS	+	+	+	+	-	+	-					
	GERDA	+	+	+	+	-	+	-					

(1) Problem for scaled test facilities

(2) For intermediate breaks phenomena included in large break reference matrix may also be important

Fig. 2.3 Cross Reference Matrix for Small and Intermediate Breaks in PWRs with OTSG

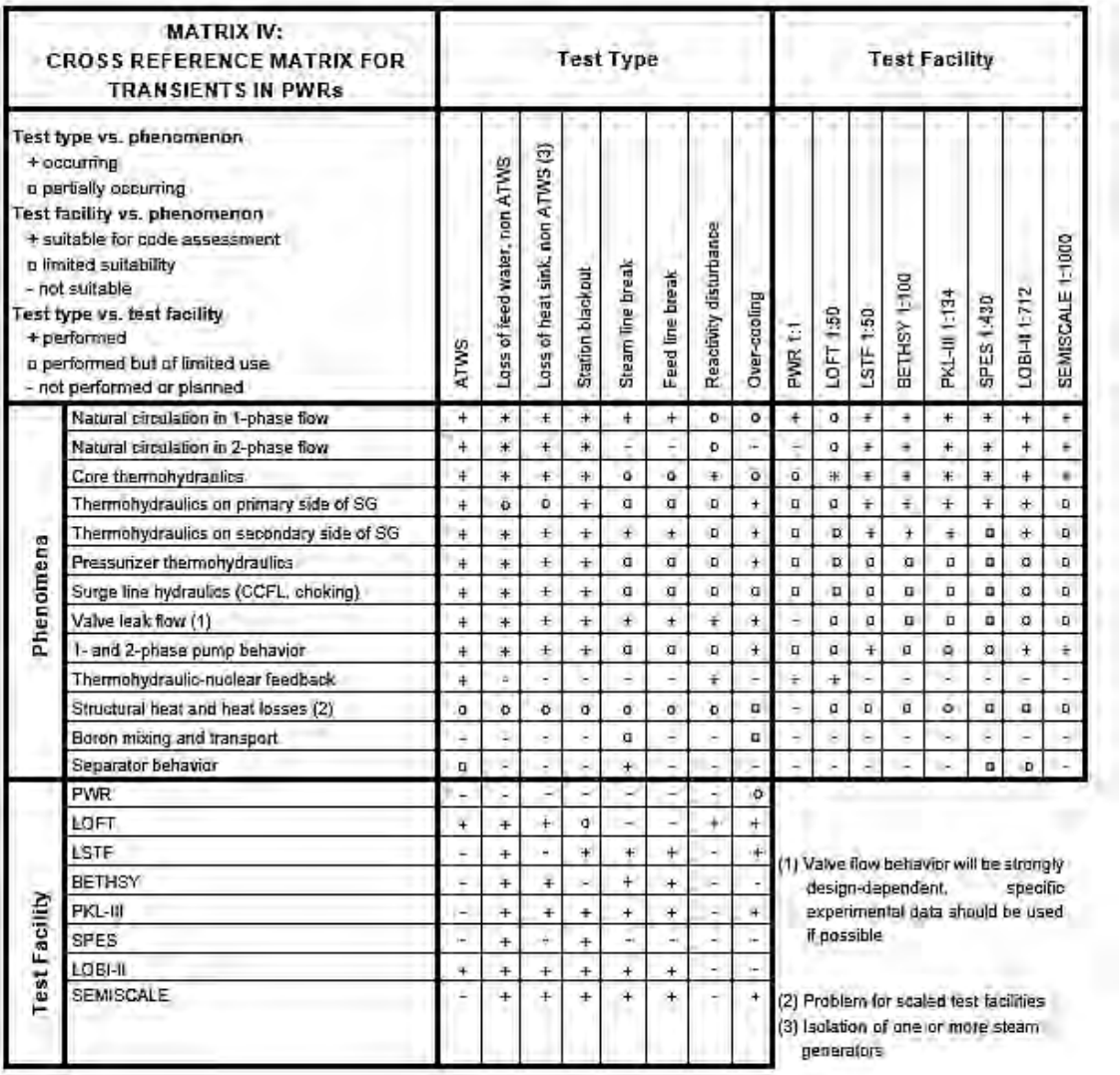

MATRIX IV: CROSS REFERENCE MATRIX FOR TRANSIENTS IN PWRs		Test Type								Test Facility							
Test type vs. phenomenon + occurring o partially occurring Test facility vs. phenomenon + suitable for code assessment o limited suitability - not suitable Test type vs. test facility + performed o performed but of limited use - not performed or planned		ATWS	Loss of feed water, non ATWS	Loss of heat sink, non ATWS (3)	Station blackout	Steam line break	Feed line break	Reactivity disturbance	Over-cooling	PWR 1:1	LOFT 1:50	LSTF 1:50	BETHSY 1:100	PKL-III 1:134	SPES 1:430	LOBI-II 1:712	SEMISCALE 1:1000
Phenomena	Natural circulation in 1-phase flow	+	+	+	+	+	+	o	o	+	o	+	+	+	+	+	+
	Natural circulation in 2-phase flow	+	+	+	+	-	-	o	-	-	o	+	+	+	+	+	+
	Core thermohydraulics	+	+	+	+	o	o	+	o	o	+	+	+	+	+	+	+
	Thermohydraulics on primary side of SG	+	o	o	+	o	o	o	+	o	o	+	+	+	+	+	o
	Thermohydraulics on secondary side of SG	+	+	+	+	+	+	o	+	o	o	+	+	+	o	+	o
	Pressurizer thermohydraulics	+	+	+	+	o	o	o	+	o	o	o	o	o	o	o	o
	Surge line hydraulics (CCFL, choking)	+	+	+	+	o	o	o	o	o	o	o	o	o	o	o	o
	Valve leak flow (1)	+	+	+	+	+	+	+	+	-	o	o	o	o	o	o	o
	I- and 2-phase pump behavior	+	+	+	+	o	o	o	+	o	o	+	o	o	o	+	+
	Thermohydraulic-nuclear feedback	+	-	-	-	-	-	+	-	+	+	-	-	-	-	-	-
	Structural heat and heat losses (2)	o	o	o	o	o	o	o	o	-	o	o	o	o	o	o	o
	Boron mixing and transport	-	-	-	-	o	-	-	o	-	-	-	-	-	-	-	-
	Separator behavior	o	-	-	-	+	-	-	-	-	-	-	-	-	o	o	-
Test Facility	PWR	-	-	-	-	-	-	-	o								
	LOFT	+	+	+	o	-	-	+	+								
	LSTF	-	+	-	+	+	+	-	+								
	BETHSY	-	+	+	-	+	+	-	-								
	PKL-III	-	+	+	+	+	+	-	+								
	SPES	-	+	-	+	-	-	-	-								
	LOBI-II	+	+	+	+	+	+	-	-								
	SEMISCALE	-	+	+	+	+	+	-	+								

(1) Valve flow behavior will be strongly design-dependent, specific experimental data should be used if possible

(2) Problem for scaled test facilities

(3) Isolation of one or more steam generators

Fig. 2.4 Cross Reference Matrix for Transients in PWRs

MATRIX V: CROSS REFERENCE MATRIX FOR TRANSIENTS AT SHUT-DOWN CONDITIONS IN PWRs		Test Type				Test Facility		
Test type vs. phenomenon + occurring o partially occurring - not occurring **Test facility vs. phenomenon** + suitable for code assessment o limited suitability - not suitable **Test type vs. test facility** + performed o performed but of limited use - not performed or planned		Loss of RHR with no opening	Loss of RHR with openings	Loss of RHR with dam in HL	Boron dilution at shut-down	LSTF	BETHSY	PKL III
Phenomena	Pressurization due to boiling	+	+	+	-	+	+	+
	Reflux condenser mode and CCFL	+	+	o	-	+	+	o
	Asymmetric loop behavior	-	o	+	-	+	+	+
	Flow through openings (manholes, vents)	-	+	+	-	+	+	-
	Mixture level formation in upper plenum and hot legs	+	+	+	-	+	+	+
	Mixture level and entrainment in the core	+	+	+	-	+	+	+
	SG siphon draining	-	-	+	-	+	-	-
	Asymmetry due to the presence of a dam	-	-	+	-	+	-	-
	Stratification in horizontal pipes	+	+	+	-	+	o	+
	Phase separation in T-junctions and effect on flow	-	+	+	-	o	o	o
	ECC mixing and condensation	+	+	+	-	o	o	o
	Loop seal clearing and filling	+	+	+	-	+	+	-
	Pool formation in UP/CCFL (UCSP)	-	-	-	-	-	-	-
	Core 3D thermalhydraulics	+	+	+	+	o	o	o
	Heat transfer in covered core	+	+	+	-	+	+	+
	Heat transfer in partially uncovered core	+	+	+	-	o	o	-
	Heat transfer in SG primary side	+	+	+	-	+	+	+
	Heat transfer in SG secondary side	+	+	+	-	+	+	+
	Pressurizer thermalhydraulics (1)	-	x	x	-	o	o	o
	Surge line thermalhydraulics (1)	-	x	x	-	o	o	o
	Structural heat and heat losses	-	-	-	-	-	-	o
	Noncondensable gas effects	+	+	+	-	+	+	+
	Boron mixing and transport	-	-	-	+	-	-	-
	Thermalhydraulics-nuclear feedback	-	-	-	+	-	-	-
Test	LSTF	+	+	+	-			
	BETHSY	-	+	-	-			
	PKL III	+	-	-	-			

(1) x is dependent on opening location:
+ pressurizer manhole open
- pressurizer manhole closed

Fig. 2.5 Cross Reference Matrix for Transients at Shutdown Conditions in PWRs

MATRIX VI: CROSS REFERENCE MATRIX FOR ACCIDENT MANAGEMENT FOR A NON-DEGRADED CORE IN PWRs		Test Type					Test Facility						
Test type vs. phenomenon + occurring o partially occurring - not occurring **Test facility vs. phenomenon** + suitable for code assessment o limited suitability - not suitable **Test type vs. test facility** + performed o performed but of limited use - not performed or planned		High pressure primary side feed and bleed	Low pressure primary side feed and bleed	Secondary side feed and bleed	RCP-Restart in a highly voided PCS	Primary to secondary break with multiple failures	LOFT 1:50	LSTF 1:50	BETHSY 1:100	PKL-III 1:145	SPES 1:430	LOBI-II 1:712	UPTF TRAM 1:1 (2)
Phenomena	Natural circulation in 1-phase flow, primary side	+	-	+	-	+	+	+	+	+	+	+	-
	Natural circulation in 2-phase flow, primary side	+	+	+	-	+	+	+	+	+	+	+	o
	Reflux condenser mode and CCFL	-	-	+	-	+	o	+	o	o	o	o	+
	Asymmetric loop behavior	+	+	+	+	+	-	o	+	+	+	o	+
	Break flow	+	+	o	+	+	+	+	+	+	o	+	o
	Phase separation without mixture level formation	+	+	+	+	+	o	+	+	+	+	+	+
	Mixture level and entrainment in SG secondary side	-	-	+	-	+	-	+	+	+	o	o	-
	Mixture level and entrainment in the core	+	+	+	o	+	o	+	+	+	o	o	o
	Stratification in horizontal pipes	+	+	+	o	+	+	+	o	o	o	o	+
	Phase separation in T-junct. and effect on break flow	+	+	o	-	+	o	o	o	o	o	o	+
	ECC-mixing and condensation	+	+	+	-	+	o	o	o	o	o	o	+
	Loop seal clearing	o	o	+	o	+	+	+	o	o	+	+	+
	Pool formation in UP/CCFL (UCSP)	+	+	+	-	+	o	o	o	o	o	-	+
	Core wide void and flow distribution	+	+	+	+	+	o	o	o	o	-	-	o
	Heat transfer in covered core	o	o	+	-	+	+	+	+	+	+	+	-
	Heat transfer in partly uncovered core	+	+	+	+	+	+	+	+	+	o	o	-
	Heat transfer in SG primary side	-	-	+	o	+	o	+	+	+	+	+	-
	Heat transfer in SG secondary side	-	-	+	o	+	o	+	+	+	o	+	-
	Pressurizer thermohydraulics	+	+	o	o	+	o	o	o	o	o	o	+
	Surge line hydraulics	+	+	o	o	+	o	o	o	o	o	o	+
	1- and 2-phase pump behavior	o	o	+	+	+	o	o	o	o	o	+	-
	Structural heat and heat losses (1)	+	+	+	+	+	o	o	o	o	o	o	o
	Noncondensable gas effects	o	+	+	+	+	-	o	o	+	-	-	+
	Accumulator behavior	-	+	+	-	o	o	+	+	+	+	+	+
	Boron mixing and transport	+	+	+	+	+	-	-	-	-	-	-	o
	Thermohydraulic-nuclear feed back	-	-	-	+	-	-	-	-	-	-	-	-
	Separator behavior	-	-	-	-	-	-	-	-	-	-	-	-
Test Facility	LOFT	-	-	+	-	-							
	LSTF	+	+	+	-	o							
	BETHSY	+	+	+	-	+							
	PKL-III	o	+	+	+	-							
	SPES	+	+	+	-	+	(1) problem for scaled test facilities						
	LOBI-II	+	+	+	-	+	(2) UPTF integral tests						
	UPTF, TRAM	o	+	-	-	-							

Fig. 2.6 Cross Reference Matrix for Accident Management for a Non-Degraded Core in PWRs

MATRIX VII: CROSS REFERENCE MATRIX FOR LOCAs IN BWRs		Test Type						Test Facility						
Test type vs. phenomena + occurring o partially occurring - not occurring Test facility vs. phenomenon + suitable for code assessment o limited suitability - not suitable Test type vs. test facility + performed o performed but of limited use - not performed or planned		Large steam line break with fast depressurization	Large break below water level with fast depress.	Small break without depress. before ADS actuation	Intermediate break with slow depress.	Spray line break	Refill - reflood	BWR 1:1 (1)	TBL 1:382, 2 chan., full pow., full height	ROSA III 1:424, 4 channels	TLTA 1:624, 1 chan., full power	FIST 1:624, 1 chan., full pow., full height	FIX 2 1:777, 1 chan., full pow., full height	PIPER1 1:2200, 1 chan., full height
Phenomena	Break flow	+	+	+	+	+	o	-	o	o	o	o	o	+
	Channel and bypass axial flow and void distribution	+	+	+	+	+	+	o	+	o	+	+	+	+
	Core wide radial void distribution	o	o	+	+	+	+	o	o	+	o	o	o	-
	Parallel channel effects-instabilities	-	-	+	+	+	+	-	o	+	-	-	-	o
	ECC bypass	-	-	o	o	o	+	-	o	o	o	o	-	+
	CCFL at UCSP and channel inlet orifice	o	+	-	+	+	+	-	o	o	-	o	o	o
	Core heat transf. incl. DNB, dryout, RNB, surf. to surf radiation	+	+	o	+	o	+	-	+	+	+	+	+	+
	Quench front propagation for both fuel rods and channel walls	-	-	-	-	-	+	-	+	+	+	+	-	+
	Entrainment and deentrainment in core and upper plenum	+	+	o	o	o	+	-	-	o	o	o	-	o
	Separator behavior incl. flooding, steam penetration and carryover	+	+	o	o	o	-	o	+	o	o	+	o	o
	Spray cooling	-	-	o	o	o	+	-	o	o	o	o	-	+
	Spray distribution	-	-	o	o	o	+	-	-	o	-	-	-	-
	Steam dryer - hydraulic behavior	+	-	o	o	-	-	o	o	o	o	o	-	o
	One and two phase pump recirc. behavior incl. jet pumps	o	o	+	+	+	o	o	o	o	o	o	o	-
	Phase separation and mixture level behavior	+	+	+	+	+	+	-	o	+	o	+	+	o
	Guide tube and lower plenum flashing	+	+	-	o	o	-	-	+	+	+	+	+	+
	Natural circulation - core and downcomer	-	-	+	o	o	+	+	+	o	o	+	+	+
	Natural circulation core bypass, hot and cold bundles	-	-	+	o	o	+	-	o	o	o	o	o	o
	Mixture level in core	-	-	+	o	o	+	-	+	+	+	+	+	o
	Mixture level in downcomer	+	+	+	+	+	+	-	+	o	o	+	+	o
	ECC mixing and condensation	-	-	+	o	+	+	-	o	o	o	o	-	o
	Pool formation in upper plenum	o	o	-	o	o	+	-	o	o	o	o	o	o
	Structural heat and heat losses	o	o	o	+	+	+	-	+	o	o	o	o	o
	Phase separ. in T-junction and effect on break flow	-	-	+	o	+	-	-	-	-	-	-	-	+
Test Facility	BWR	-	-	-	-	-	-							
	TBL	+	+	+	+	-	+							
	ROSA III	+	+	+	+	-	+							
	TLTA	+	+	-	+	-	+							
	FIST	+	+	+	+	-	+							
	FIX 2	-	+	-	+	-	-							
	PIPER 1	-	+	+	+	-	+							

(1) These are non-LOCA data but may be used for assessment

Fig. 2.7 Cross Reference Matrix for LOCAs in BWRs

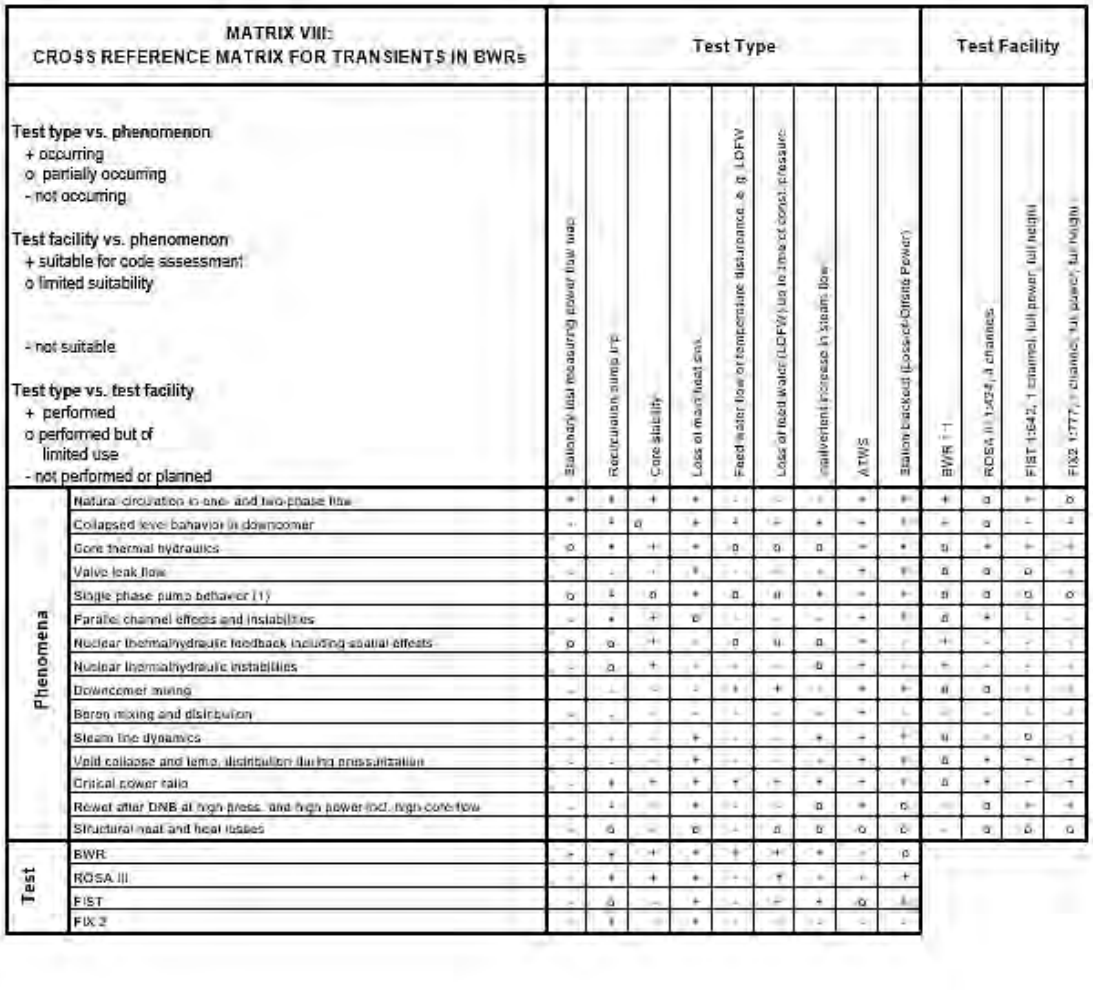

MATRIX VIII: CROSS REFERENCE MATRIX FOR TRANSIENTS IN BWRs		Test Type									Test Facility			
Test type vs. phenomenon + occurring o partially occurring - not occurring Test facility vs. phenomenon + suitable for code assessment o limited suitability - not suitable Test type vs. test facility + performed o performed but of limited use - not performed or planned		Stationary test measuring power flow map	Recirculation pump trip	Core stability	Loss of main heat sink	Feed water flow or temperature disturbance, e. g. LOFW	Loss of feed water (LOFW) run to intact const. pressure	Inadvertent increase in steam flow	ATWS	Station blackout (Loss-of-Offsite Power)	BWR 1:1	ROSA III 1:424, 1 channel	FIST 1:543, 1 channel, full power, full height	FIX2 1:777, 7 channels, full power, full height
Phenomena	Natural circulation in one- and two-phase flow	+	+	+	+	-	-	-	+	+	+	o	+	o
	Collapsed level behavior in downcomer	-	+	o	+	+	-	+	+	+	-	o	-	+
	Core thermal hydraulics	o	+	+	+	o	o	o	+	+	o	+	+	+
	Valve leak flow	-	-	-	+	-	-	+	+	+	o	o	o	-
	Single phase pump behavior (1)	o	+	o	+	o	o	+	+	+	o	o	o	o
	Parallel channel effects and instabilities	-	+	+	o	-	-	-	+	+	o	+	-	-
	Nuclear thermalhydraulic feedback including spatial effects	o	o	+	-	o	o	o	+	-	+	-	-	-
	Nuclear thermalhydraulic instabilities	-	o	+	-	+	-	o	+	-	+	-	-	-
	Downcomer mixing	-	-	-	-	+	+	-	+	+	o	o	-	-
	Boron mixing and distribution	-	-	-	-	-	-	-	+	-	-	-	-	-
	Steam line dynamics	-	-	-	+	-	-	+	+	+	o	-	o	-
	Void collapse and temp. distribution during pressurization	-	-	-	+	-	-	-	+	+	o	+	-	+
	Critical power ratio	-	+	+	+	+	+	+	+	+	o	+	-	+
	Rewet after DNB at high press. and high power/incr. high core flow	-	+	-	+	-	-	o	+	o	-	o	+	+
	Structural heat and heat losses	-	o	-	o	-	o	o	o	o	-	o	o	o
Test	BWR	-	+	+	+	+	+	+	-	o				
	ROSA III	-	+	+	+	-	+	-	-	+				
	FIST	-	o	-	+	-	-	+	o	+				
	FIX 2	-	+	-	+	-	-	-	-	-				

Fig. 2.8 Cross Reference Matrix for Transients in BWRs

MATRIX IX: CROSS REFERENCE MATRIX FOR LARGE BREAKS IN VVERs

CSNI
+ covered by
o partially covered
- not covered

Plant type vs. phenom.
+ fully specific to VVER
o partially specific
- not specific

Test type vs. phenom.
+ occuring
o partially occuring
- not in list

Test facility vs. phenom.
+ suitable for code assessment
o limited suitability
- not suitable
x expected to be suitable

Test type vs. test facility
+ already performed
o performed but of limited use
- not performed

Plant type vs. test facility
+ covered by
o partially covered
- not covered

		CSNI	Plant Type: VVER-440/213	Plant Type: VVER-1000	Test Type: Blowdown	Test Type: Reflood	Test Type: Refill	Test Facility: System Tests: PSB-VVER	PM-5	SB	ISB-VVER	Separate Effects Tests: Data bank (EREC)	LWL	REWET-II	IVO-CCFL	SKN	SVD-1	SVD-2	TVC-440	EVTUS	KS	TOPAZ	SG-NPP
Phenomena	Break flow	+	-	-	+	+	+	x		+	x	+											
	Phase separation	o	+	o	o	+	+	x			x				o								
	Mixing and condensation during injection	o	+	+	o	+	+	x			x												
	2-phase flow in SG primary and secondary side	-	o	o	o	o	o	x			x												
	Core wide void + flow distribution	o	+	+	o	+	+	x	o		-												
	ECC downcomer bypass and penetration	o	+	+	o	o	+	-			-												
	UP injection and penetration	-	+	+	o	+	+	x		+	x			+				+	+				
	CCFL (UCSP)	o	+	+	o	+	+	x	+		x				+								
	Steam binding (liquid carry over, ect.)	o	o	o	-	+	o	x		+	x												
	Pool formation in UP	o	+	+	-	+	+	x	+		x												
	Core heat transfer incl. DNB, dryout, RNB	o	+	+	+	+	+	x	o	+	x		+			+	+	+	o	o	+			
	Quench front propagation	o	+	+	o	+	o	x		+	x		+	+			+	x	+	o		+		
	Entrainment (Core, UP)	-	+	o	o	+	o	x	o	+	x			+				x	o					
	Deentrainment (Core, UP)	-	+	o	-	+	o	x	o	+	x			+				x	o					
	1 - and 2-phase pump behavior	-	+	+	+	o	o	x			-												
	Noncondensable gas effects	-	o	o	-	+	+	x			+													x
Facility System	ISB-VVER		o	+	-	-	-																	
	PSB-VVER			+	-	-	-																	
	SB		+	+	+	+	+																	
	PM-5			+		+																		

Fig. 2.9 Cross Reference Matrix for Large Breaks in VVERs

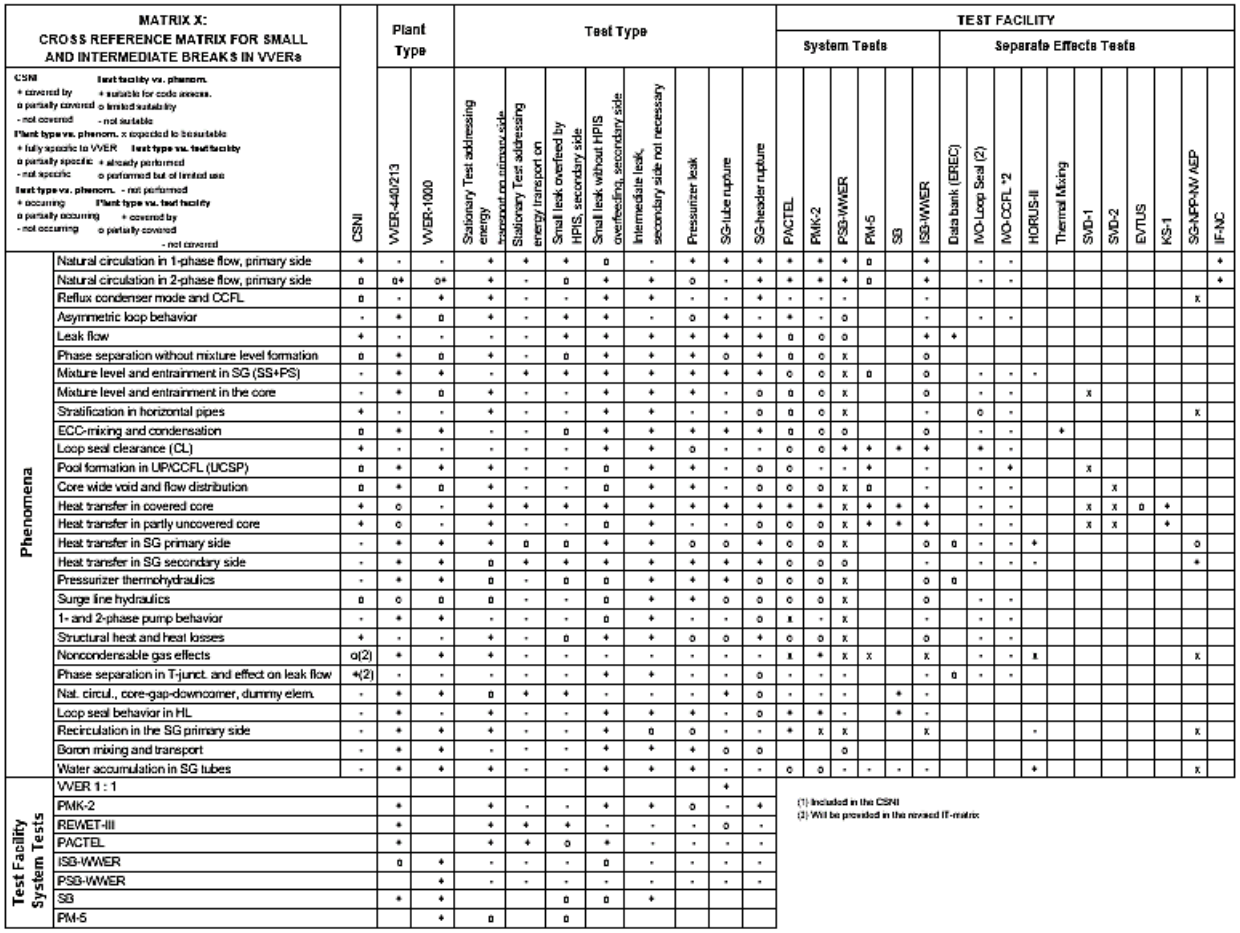

MATRIX X: CROSS REFERENCE MATRIX FOR SMALL AND INTERMEDIATE BREAKS IN VVERs		CSNI	Plant Type		Test Type								TEST FACILITY: System Tests						Separate Effects Tests														
			VVER-440/213	VVER-1000	Stationary Test addressing energy transport on primary side	Stationary Test addressing energy transport on	Small leak overfeed by HPIS, secondary side	Small leak without HPIS overfeeding, secondary side	Intermediate leak, secondary side not necessary	Pressurizer leak	SG-tube rupture	SG-header rupture	PACTEL	PMK-2	PSB-WWER	PM-5	SB	ISB-WWER	Data bank (EREC)	IVO-Loop Seal (2)	IVO-CCFL *2	HORUS-III	Thermal Mixing	SVD-1	SVD-2	EVTUS	KS-1	SG-NEPP-NV AEP	IF-NC
Phenomena	Natural circulation in 1-phase flow, primary side	+	-	-	+	+	+	o	-	+	+	+	+	+	+	o		+		-	-							+
	Natural circulation in 2-phase flow, primary side	o	o+	o+	+	-	o	+	+	o	-	+	+	+	+	o		+		-	-							+
	Reflux condenser mode and CCFL	o	-	+	+	-	-	+	+	-	-	+	-	-	-			-									x	
	Asymmetric loop behavior	-	+	o	+	-	+	+	-	o	+	-	+	-	o			-		-	-							
	Leak flow	+	-	-	-	-	+	+	+	+	+	+	o	o	o			+	+										
	Phase separation without mixture level formation	o	+	o	+	-	o	+	+	+	o	+	o	o	x			o											
	Mixture level and entrainment in SG (SS+PS)	-	+	+	-	+	+	+	+	+	+	+	o	o	x	o		o		-	-	-							
	Mixture level and entrainment in the core	-	+	o	+	-	-	+	+	+	-	o	o	o	x			o		-	-			x					
	Stratification in horizontal pipes	+	-	-	+	-	-	+	+	-	-	o	o	o	x			-		o	-						x	
	ECC-mixing and condensation	o	+	+	-	-	o	+	+	+	+	+	o	o	o			o		-	-	+							
	Loop seal clearance (CL)	+	-	-	-	-	-	+	+	o	-	-	o	o	+	+	+	+		+	-								
	Pool formation in UP/CCFL (UCSP)	o	+	+	+	-	-	o	+	+	-	o	o	-	-	+		-		-	+			x					
	Core wide void and flow distribution	o	+	o	+	-	-	o	+	+	-	o	o	o	x	o		-		-	-				x				
	Heat transfer in covered core	+	o	-	+	+	+	+	+	+	+	+	+	+	x	+	+	+		-	-			x	x	o	+		
	Heat transfer in partly uncovered core	+	o	-	+	-	-	o	+	-	-	o	o	o	x	+	+	+		-	-			x	x		+		
	Heat transfer in SG primary side	-	+	+	+	o	o	+	+	o	o	+	o	o	x			o	o	-	-	+						o	
	Heat transfer in SG secondary side	-	+	+	o	+	+	+	+	+	+	+	o	o	o			-		-	-	-						+	
	Pressurizer thermohydraulics	-	+	+	o	-	o	o	+	+	+	o	o	o	x			o	o										
	Surge line hydraulics	o	o	o	o	-	-	o	+	+	o	o	o	o	x			o		-	-								
	1- and 2-phase pump behavior	-	+	+	-	-	-	o	+	-	-	o	x	-	x			-		-	-								
	Structural heat and heat losses	+	-	-	+	-	o	+	+	o	o	+	o	o	x			o		-	-								
	Noncondensable gas effects	o(2)	+	+	+	-	-	-	-	-	-	-	x	+	x	x		x		-	-	x						x	
	Phase separation in T-junct. and effect on leak flow	+(2)	-	-	-	-	-	+	+	-	-	o	-	-	-			-	o	-	-								
	Nat. circul., core-gap-downcomer, dummy elem.	-	+	+	o	+	+	-	-	-	+	o	-	-	-		+	-											
	Loop seal behavior in HL	-	+	-	+	-	-	+	+	+	-	o	+	+	-		+	-											
	Recirculation in the SG primary side	-	+	+	+	-	-	+	o	o	-	-	+	x	x			x				-						x	
	Boron mixing and transport	-	+	+	-	-	-	+	+	+	o	o			o														
	Water accumulation in SG tubes	-	+	+	+	-	-	+	+	+	-	-	o	o	-	-	-	-				+						x	
Test Facility System Tests	VVER 1 : 1										+																		
	PMK-2		+		+	-	-	+	+	o	-	+																	
	REWET-III		+		+	+	+	-	-	-	o	-																	
	PACTEL		+		+	+	o	+	-	-	-	-																	
	ISB-WWER		o	+	-	-	-	o	-	-	-	-																	
	PSB-WWER			+	-	-	-	-	-	-	-	-																	
	SB		+	+			o	o	+																				
	PM-5			+	o		o																						

(1) Included in the CSNI
(2) Will be provided in the revised IT-matrix

Fig. 2.10 Cross Reference Matrix for Small and Intermediate Breaks in VVERs

MATRIX XI: CROSS REFERENCE MATRIX FOR TRANSIENTS IN VVERs

CSNI
+ covered by
o partially covered
- not covered

Plant type vs. phenom.
+ fully specific to VVER
o partially specific
- not specific

Test typ vs. phenom.
+ occurring
o partially occurring
- not occurring

Test facility vs. phenomenon
+ suitable for code assessment
o limited suitability
- not suitable
x expected to be suitable

Test type vs. testfacility
+ already performed
o performed but of limited use
- not performed

Plant type vs. test facility
+ covered by
o partially covered
- not covered

		CSNI	Plant Type		Test Type									TEST FACILITY												
														System Tests							Separate Effects Tests				
			VVER-440/213	VVER-1000	ATWS	Loss of feed water, non ATWS	Loss of heat sink, non ATWS	Station blackout	Steam line break	Feed line break	Cool down prim. feed and bleed	Reactivity disturbance	Over-cooling	VVER 1:1 (1)	PACTEL	PMK-2	PSB-WWER	PM-5	ISB-WWER	BD	Data bank (EREC)	VEERA	REWET II	SVD-2	Mixing Model
Phenomena	Natural circulation in 1-phase flow	+	-	-	+	+	+	+	+	+	+	o	o	+	+	+	+	o	+			-	-		
	Natural circulation in 2-phase flow	o	o+	o+	+	+	+	+	-	-	o	o	-		+	+	+	o	+			-	-		
	Core thermohydraulics	o	+	o	+	+	+	+	o	o	o	+	o	+	+	+	x	o	+			+	+		
	Thermohydraulics on primary side of SG	-	+	+	+	o	o	+	o	o	+	o	o	+	o	o	x		o			-	-	+	
	Thermohydraulics on secondary side of SG	-	+	+	+	+	+	+	+	+	+	o	o	+	o	o	x		-			-	-		
	Pressurizer thermohydraulics (2)	-	+	+	+	+	+	+	o	o	o	o	+	o	o	o	o		o		o	-	-		
	Surge line hydraulics (CCFL, chocking) (2)	o	o	o	+	+	+	+	o	o	o	o	o	o	o	o	x		o			-	-		
	1- and 2-phase pump behaviour	-	+	+	+	+	+	+	o	o	o	o	o		x	-	x		-			-	-		
	Thermohydraulic-nuclear feedback	o	+	+	+	-	-	-	+	-	-	+	- +	+	-	-	-		-			-	-		
	Structural heat and heat losses (3)	+	-	-	o	o	o	o	o	o	o	o	o		o	o	o		+			-	-		
	Boron mixing and transport	o(4)	+	+	-	-	-	-	o	-	-	-	o		x	-	x	-	-	+		+	+		+
Test Facility System Tests	VVER 1 : 1		+	+																					
	PMK-2		+		-	o	-	o	-	-	-	-	-												
	PACTEL		+		-	o	-	o	-	-	-	-	o												
	ISB-WWER		o	+	-	-	-	-	-	-	-	-	-												
	PSB-WWER			+	-	-	-	-	-	-	-	-	-												
	PM-5			+																					
	BD		+	+																					

(1) Volumetric scaling
(2) For phenomena requiring separate effects test, e.g. ressurizer behavior, see small leak cross reference matrix
(3) Problem for scaled testfacilities
(4) Included in the CSNI SET matrix

Fig. 2.11 Cross Reference Matrix for Transients in VVERs

2.2.1 Integral Tests Validation Matrices for ATHLET

Based on the Cross Reference Matrices (Fig. 2.1 to Fig. 2.11), well balanced sets of tests were selected for the ATHLET validation based on the criteria presented in the CSNI report /NEA 96/. The criteria for selection are:

- each phenomenon should be addressed in test facilities of different scale,
- all test types should be included.

If feasible, each thermal-hydraulic phenomenon and each test type should be addressed by at least two facilities of different scale. A total of approximately 50 test types results in about 100 integral tests for code validation. The validation work is shared between GRS and independent organizations.

During the selection process, a number of additional factors were considered, including:

- representativeness of facility and experiment to expected reactor conditions,
- quality and completeness of experimental data (measurement and documentation),
- relevance to safety issue,
- selected test must clearly exhibit the addressed phenomena,
- high priority to International Standard Problems (ISP), counterpart and similar tests (for more explanations see /NEA 96/),
- challenge to system codes.

Where counterpart tests or similar tests were identified between two or more facilities, they were included in order to address questions relating to scaling and facility design compromises. For the accident management matrix, priority was given on how realistically the test represents typical accident management procedures.

A periodic updating of the matrices may be necessary to include new relevant experimental facilities and tests, and to include improved understanding of existing data as a result of further validation.

The integral tests selected for ATHLET validation are presented in Tab. 2.1 to Tab. 2.13. An overview of the different integral test facilities indicating the number of selected tests for each category (e.g. large breaks, small breaks, etc.), and the current status of calculated experiments is shown in Tab. 2.14 and Tab. 2.15.

Importantly, the validation tests for ATHLET do include qualification tests for plant-specific analysis simulators maintained by GRS /POI 94/, /HOR 95/, /POI 96/, /HOR 98/, /POI 99/, /DRÄ 00/, /DRÄ 02/ against transient data for the specific plants. These analysis simulators have been maintained and used by GRS in diverse activities. Most are currently still in use and are qualified by GRS /POI 17/, /PAL 18/, /PAL 20/. In line with good practice, before the release of ATHLET 3.3 it was checked against a set of standard analysis simulator tests that results and performance of the new version are adequate.

Tab. 2.1 Large Breaks in PWRs (Matrix I)

Test Facility	Test No.	Brief Description	Calcula-tion done by	ATHLET Version	Reference
UPTF	-2	Double ended cold leg break, cold ECC injection, EM-case			
UPTF	-27B	Double ended cold leg break, cold ECC injection, BE-case	RUB	Mod1.2B	/WEI 01/
UPTF	-18	Double ended cold leg break, combined ECC injection, EM-case	TÜV Bayern	Mod1.0D	/GAS 91/
UPTF	-28	Double ended cold leg break, combined ECC injection, BE-case			
UPTF	-19	50% Break in the cold leg, combined ECC injection, EM-case			
UPTF	-24	Vent valve test, double ended cold leg break, EM-case, downcomer and cold leg ECC			
CCTF	C2-19/79	Double ended cold leg break, combined ECC, EM-case	FZR	Mod1.2C	/KRE 01/
CCTF	C2-20/80	Double ended cold leg break, combined ECC, BE-case	TÜV Bayern	Mod1.0D	/KRY 91/
CCTF	C2-04/62	Double ended cold leg break, cold ECC, EM-case, base case	FZR	Mod1.2C	/KRE 01/
CCTF	C2-12/71	Double ended cold leg break, cold ECC, BE-case	Battelle	Mod1.2B	/SCH 00/
LOFT	L2-5	Double ended cold leg break, loss of external power, decoupled pump flywheel	Battelle	Mod1.2B	/SCH 00/
LOFT	LP-LB-1	Double ended cold leg break, loss of external power	GRS	DRUFAN Current	/WAH 86/ Sect. 0
LOBI	A1-06	Double ended cold leg break, combined ECC injection	Battelle	Mod1.0 B	/SCH 89/
LOBI	A1-66	Double ended cold leg break, cold ECC injection	Battelle	Mod1.0 B	/SCH 89/

Test Facility	Test No.	Brief Description	Calcula-tion done by	ATHLET Version	Reference
PKL-II	B2	Double ended cold leg break, combined ECC injection	TÜV Nord	Mod1.2C	/WIE 00//
PKL-II	B5	Double ended cold leg break, cold leg ECC injection	TÜV Nord	Mod1.2C	/WIE 00/

Tab. 2.2 Large Breaks in VVERs (Matrix IX)

Test Facility	Test No.	Brief Description	Calcula-tion done by	ATHLET Version	Reference
PSB WWER	XT-2x25-02	2 x 25% break in hot leg	Kurchatov	Mod2.0A	/MOS05b/

Tab. 2.3 Small and intermediate breaks in PWRs (Matrix II)

Test Facility	Test No.	Brief Description	Calcula-tion done by	ATHLET Version	Reference
UPTF TRAM	A7	5% cold leg break, hot leg ECC injection	GRS	Mod1.1D	/DRÄ 98/
UPTF TRAM	A6	5% cold leg break, cold leg ECC, similar to LSTF-SB-CL-18	GRS	Mod1.1A	/BUR 94/ /PAP 96/
ATLAS	SB-DVI-09	50% Break of a DVI Line of the APR-1400 (ISP-50)	GRS	Mod2.2A	/AUS 13a/
ATLAS	A1.1	Station Blackout (SBO) with asymmetric cooling via one steam generator	GRS	Mod3.0B	/HOL 16/
ATLAS	A5.1	1% cold leg break, failure of HPI and secondary side depressurization (counterpart test to LSTF SB-CL-32)	GRS	Mod3.1A	/HOL 16/

Test Facility	Test No.	Brief Description	Calcula-tion done by	ATHLET Version	Reference
LOFT	LP-SB-1	2% hot leg break, main coolant pumps switched off	GRS	DRUFAN	/POI 84a/
LOFT	LP-SB-2	2% hot leg break, main coolant pumps running	GRS	DRUFAN	/POI 84b/
LOFT	LP-SB-3	1% cold leg break	GRS	Mod1.0D	/DRÄ 91/
LOFT	L3-2	15% cold leg break			
LSTF	SB-CL-18	5% cold leg break, ISP-26	GRS	Current	Sect. 5.1
LSTF	SB-CL-21	5% cold leg break, similar to BETHSY 6.2 TC and LOBI BL-34			
LSTF	SB-CL-32	1% cold leg break, failure of HPI and secondary side depressurization	GRS	Mod3.0A	/HOL 16/
LSTF	IB-HL-01	17% hot leg break (Test 1 of OECD ROSA-2 Project)	GRS	Mod2.2B	/AUS 13b/
LSTF	IB-CL-03	17% cold leg break (Test 2 of OECD ROSA-2 Project)	GRS	Mod2.2B	/AUS 13b/
LSTF	IB-CL-05	13% cold leg break (Test 7 of OECD ROSA-2 Project)	GRS	Mod2.2B	/AUS 13b/
PKL-III	A 4.1	1% cold leg break, LP, HP ECC, pressurizer level test	GRS	Mod0	/AUS 89/
PKL-III	AC-1	Reflux condenser mode (similar to LOBI A1-92)			
PKL-III	B 3.2B	Natural circulation with different mass inventories and flow resistances (similar to LSTF ST-NC-08)			
PKL-III	B 3.5.1	Cooldown of a PWR with 100K/h under reflux condenser mode with 4 SG at 2% power			
PKL-III	B 4.3	System behaviour during nitrogen injection under reflux condenser conditions	TÜV Nord	Mod1.1C	/WIE 98/
PKL-III	B 4.1	System behaviour during nitrogen injection under single phase natural circulation conditions in primary side	GRS	Mod1.1B	/RIN 95/

Test Facility	Test No.	Brief Description	Calculation done by	ATHLET Version	Reference
PKL-III	C 6.1	24 cm^2 cold leg break, cooldown of a PWR with 100K/h, isolation of 2 SG, nitrogen injection from 2 accumulators	TÜV Nord	Mod1.2A	/WIE 98/
PKL-III	C 3.2	Reflux condenser with 0.8MPa and increasing SG Power (1%-20%)			
PKL-III	D 2.1	Small CL leak, start of natural circulation with HP, LP, accumulator injection into two loops	GRS	Mod1.2D	/STE 02//
PKL-III	D 2.2	Small HL leak, start of natural circulation with LP injection into four loops	GRS	Mod1.2D	/RIN 03/
PKL-III	E 2.2	Small CL leak, start of natural circulation with HP and LP injection into two CLs	GRS	Mod2.0A	/STE 04/
PKL-III	E 2.3	Small HL leak, start of natural circulation with HP injection into two HLs and accumulator injection into 4 HLs	GRS	Mod2.0B	/STE 06a//
PKL-III	F 1.1	Small 21 cm^2 CL leak, ECC injection into 4 CLs, secondary side depressurization with 56K/h. Experimental boundary conditions correspond to Framatome and Westinghouse Design.			/BUR 05/
PKL-III	F 1.2	Systematic study of the accumulation of low borated water during reflux condenser mode depending on the water inventory, pressure and reactor power. Concentration of low borated water at heat exchanger exits during two-phase natural circulation and reflux condenser			/BUR 05/
PKL-III	F 1.3	Small HL leak in the primary circuit, ECC injection into 2 HLs, accumulator injection into 4 HLs, LP injection into 2 CLs and 2 HLs, secondary side depressurization with 100K/h. Disruption of the natural circulation in all coolant loops during reflux condenser operation.			/BUR 05/
PKL-III	F 1.4	Small 26 cm^2 CL leak, ECC injection into 2 CLs, accumulator injection into 4 HLs and 4 CLs, without LP injection, secondary side depressurization with 120K/h;			/BUR 05/
PKL-III	H 2.1	Station Blackout (SBO)	GRS	Mod3.0A	/HOL 16/
PKL-III	H 2.2, Run 2	Station Blackout (SBO)	GRS	Mod3.0A	/HOL 16/
PKL-III	H 4.1	Cool-down under natural circulation conditions with isolated, water-filled steam generators	GRS	Mod3.0A	/HOL 16/

Test Facility	Test No.	Brief Description	Calcula-tion done by	ATHLET Version	Reference
PKL-IV	I2.2 (runs 1,2,3)	Intermediate break LOCA with safety injection and borated water	KIT	Mod 3.1A	/XU 22/
PKL-IV	I2.2 (run 3)	Cold leg IBLOCA with BDBA (Beyond Design Basis Accident) conditions to resemble the IBLOCA experiments at the LSTF facility within the OECD/NEA ROSA-2 project. 17% break size, HPSI and LPSI: 1out of 4 loops, cold side 2 Accs, cold side.	GRS	Mod3.1A	/MAR 22/
BETHSY	4.1a	Two phase natural circulation with different mass inventories in the primary circuit	GRS	Mod1.0D	/STE 91/
BETHSY	5.1a	Variation of mass inventories in the secondary circuit	GRS	Mod1.1A	/RIN 93a/
BETHSY	3.4a	Natural circulation with 2 isolated SGs, similar to PKL III B3.1	Battelle	Mod1.1A	/SCH 94/
BETHSY	4.3b	Multiple steam generator U-tube rupture	GRS	Mod1.1A	/RIN 93b/
BETHSY	4.1a TC	Two phase natural circulation with constant core power 5%	Battelle	Mod1.1C	/SCH 98a/
BETHSY	6.2 TC	5% cold leg break, without HP ECC, similar to LSTF-SB-CL-18 and LOBI-BL-34	Battelle	Mod1.1C	/SCH 98a/
BETHSY	7.2 c	Reflux condenser mode with nitrogen in primary circuit	Battelle	Mod1.1C	/SCH 98a/
LOBI II	A2-77A	Primary side behaviour with different mass inventories	GRS	Mod1.0D	/KIR 89/
LOBI II	A1-82	LOCA with 1% cold leg break, hot leg HP ECC injection	GRS	Mod1.2D	/RIN 01a/
LOBI	A2-81	LOCA with 1% cold leg break, cold leg HP ECC injection, ISP-18	GRS	Mod1.0D	/BUR 89/
LOBI II	A1-91	1% cold leg break, with hot ECC injection	Battelle	Mod1.0B	/SCH 89/
LOBI II	BL-01	5% cold leg break	GRS	Mod1.0D	/KYN 89/
LOBI II	A1-83	10% cold leg break			
LOBI	B-R1M	25% cold leg break	Battelle	Mod1.0B	/SCH 89/

Test Facility	Test No.	Brief Description	Calcula-tion done by	ATHLET Version	Reference
LOBI II	BL-34	6% cold leg break, similar to LSTF-SB-CL-21 and BETHSY 6.2 TC			

Tab. 2.4 Small and intermediate breaks in VVERs (Matrix X)

Test Facility	Test No.	Brief Description	Calcula-tion done by	ATHLET Version	Reference
PMK		ATWS with stuck open pressurizer relief valve, loss of feedwater	GRS/KFKI	Mod1.2A	/HOR 99/
PMK		7,4% cold leg break with N_2 injection, secondary side bleed and feed	GRS/KFKI	Mod1.1B	/GYÖ 95/
PMK		7,4% cold leg break without N_2 injection, secondary side bleed and feed	GRS/KFKI	Mod1.1B	/GYÖ 95/
PMK		7,4% cold leg break, secondary side bleed and feed, IAEA SPE-4	GRS/Kurt.	Mod1.1A	/STE 95/
PMK		0,5% cold leg break, secondary side bleed and feed	NRI/GRS	Mod1.1D	/VOJ 00a/
PMK		Surge line break	NRA/GRS	Mod1.2A	/VOJ 01/
ISB		Small break in cold leg, Russian Standard Problem No. 1 (SSP-1)	FZR	Mod1.1A	/KRE 96/
ISB		Intermediate break in cold leg without HP injection, Russian Standard Problem No. 2 (SSP-2)	GRS	Mod1.1C	/STE 98a/
ISB		Intermediate break in cold leg with HP injection, Russian Standard Problem No. 3 (SSP-3)	INRNE/GRS	Mod1.2A	/VOJ 00b/
ISB		11,2% break of connection pipe to the upper plenum, 1 HP injection	NRI/GRS	Mod1.1D	/VOJ 00a/
ISB		11,2% break of connection pipe to the upper plenum, 2 HP injections	NRI/GRS	Mod1.1D	/VOJ 00a/
ISB		0,5% break in cold leg with HP injection	NRI/GRS	Mod1.1D	/VOJ 00a/

Test Facility	Test No.	Brief Description	Calculation done by	ATHLET Version	Reference
PSB	Analytical Exercise	Primary-to-secondary (PRISE) 100mm leakage at the head of the hot collector of steam generator 4 with a seizure (full opened position) of related BRU-A (Turbine bypass valve with steam dump to the atmosphere)	GRS	Mod2.0B	/STE 05/
PSB	PSh-1.4-04	1.4% leakage from primary to secondary side	GRS NR Rez	Mod2.0B Mod2.0B	/MEL 08/ /MEL 08/
PACTEL	ITE-06	Natural circulation, ISP-33	GRS THZ	Mod1.0E	/STE 94/ /LIS 93/
PACTEL	SBL-03	0,04% break, 3,3% power			
PACTEL	SBL-04	1% break, 3,3% power			
PACTEL	SBL-07	0,04% break 3,3% power, pressurizer isolation			
PACTEL	SBL-22	Small break in lower plenum, one- and two-phase natural circulation, reflux condenser mode	THZ HSZG	Mod1.1C Mod1.1D	/LIS 93/, /LIS 97/ /ALT 98/
PACTEL	LSR-10	Loop seal refilling test	THZ	Mod1.1 B	/LIS 96/
PACTEL	SIR-11	Stepwise reduction of coolant inventory			
PACTEL	SIR-20	Natural circulation with lower pressure at 4,0MPa (prim. side) and 1,2MPa (sec. side), reduction of water inventory	THZ HSGZ	Mod1.1 D Mod1.1D	/VAN 98/, /VAN 99a/ /ALT 98/
PACTEL	SIR-21	Natural circulation with lower pressure at 1,6MPa (prim. side) and 0,3MPa (sec. side), reduction of water inventory	THZ HSGZ	Mod1.1 D Mod1.1D	/VAN 99a/ /ALT 98/

Tab. 2.5 Small and intermediate breaks in PWRs with once-through steam generators (Matrix III)

Test Facility	Test No.	Brief Description	Calcula-tion done by	ATHLET Version	Reference
GERDA	160 702	20% break in pump seal	ABB/GRS	Mod1.0D	/STF 91/

Tab. 2.6 Transients in PWRs (Matrix IV)

Test Facility	Test No.	Brief Description	Calcula-tion done by	ATHLET Version	Reference
LOFT	L9-3	ATWS, loss of feedwater			
LSTF	ST-NC-41	Stepwise cooldown procedure with SG isolated and empty on the secondary side (Test 6 of OECD ROSA-2 Project, Counterpart test to PKL-III G2.1)	GRS	Mod2.2B	/AUS 13b/
PKL-III	A1.2	Asymmetric cooldown of a PWR with one pump and 3 isolated SG			
PKL-III	A2.1	Cooldown of a PWR with 4 SG and loss of offsite power, similar to LOBI A1-87			
PKL-III	A2.2	Cooldown of a PWR with station blackout, 3 SG			
PKL-III	A3.2	Restart of a main coolant pump, with upper head steam/gas cushion			
PKL-III	A5.2	Loss of feedwater of 1 SG			
PKL-III	B2.1	Secondary side depressurization with 50K/h in case of emergency power with 3 isolated steam generators and standing main coolant pumps	GRS	Mod 1.0E	/BRÄ 93/
PKL-III	B3.1	Cooldown with one of four steam generators	GRS	Mod 1.0E	/SEN 94/
PKL-III	F4.1	Inherent boron dilution under reflux-condenser conditions as function of primary coolant inventory	GRS	Mod 2.1B	/AUS 10/

Test Facility	Test No.	Brief Description	Calcula-tion done by	ATHLET Version	Reference
PKL-III	F4.2	Inherent boron dilution (GRS-LOBI Scenario)	GRS GRS	Mod 2.1B Mod 2.1B	/AUS 10/ /POI 08/
PKL-III	G2.1 Run 3	Stepwise cooldown procedure with SG isolated and empty on the secondary side	GRS	Mod 2.2B	/AUS 13b/
PKL-III	G3.1	10% steam line break; OECD/PKL 2 Benchmark	GRS	Mod 2.2A	/DEL 11/
PKL-III	G4.1 Run 2	Systematic study on heat transfer under reflux-condenser conditions	GRS	Mod 2.2B	/AUS 13b/
LOBI-II	A1-87	Cooldown of a PWR			
LOBI-II	A2-90	Loss of offsite power, ATWS	GRS	Mod3.0A	/LER 12/
LOBI-II	BT-01	10% steam line break	GRS	Mod1.0D	/GEP 90/
LOBI-II	BT-12	Steam line break	Battelle	Mod1.0B	/SCH 89/
GKN-2		Load rejection (2.4.92)	GRS	ATLAS	/HOR 98/
GKN-2		Reactor trip (18.10.91)	GRS	ATLAS	/HOR 98/
GKN-2		Trip of one main coolant pump (20.5.93)	GRS	ATLAS	/HOR 98/
KKU		Load rejection (17.2.99)	GRS	ATLAS	
KKU		Turbine trip, reactor trip (6.6.98 and 14.10.98)	GRS	ATLAS	/DRÄ 00/
KKU		Planned reactor cooldown (26. - 27.6.99)	GRS	ATLAS	/DRÄ 00/
KKP-2		Pump failure (1 of 4; 19.11.98)	GRS	ATLAS	/DRÄ 02/
KKP-2		Fault of load control (21.5.99)	GRS	ATLAS	/DRÄ 02/

Test Facility	Test No.	Brief Description	Calcula-tion done by	ATHLET Version	Reference
KKP-2		Turbine trip (28.2.01)	GRS	ATLAS	/DRÄ 02/
KKP-2		Reactor trip (8.10.00)	GRS	ATLAS	/DRÄ 02/
KKP-2		Planned reactor cooldown (23.7.00)	GRS	ATLAS	/DRÄ 02/
KBR		Simulation of a SG tube rupture (start-up test; 21.11.86)	GRS	ATLAS	/HOR 95/
KBR		Turbine trip (14.8.93)	GRS	ATLAS	/HOR 95/
KBR		Load rejection (11.3.91)	GRS	ATLAS	/HOR 95/
KBR		Inadvertent closing of a feedwater control valve, reactor trip (25.4.95)	GRS	ATLAS	/HOR 95/

Tab. 2.7 Transients in VVERs (Matrix XI)

Test Facility	Test No.	Brief Description	Calcula-tion done by	ATHLET Version	Reference
PACTEL	LOF-01	Loss of feedwater (1 loop, 75 KW power)	THZ	Mod1.1A	/LIS 94/
PACTEL	LOF-04	Loss of feedwater (3 loop, 166 KW power)	THZ	Mod1.1A	/LIS 94/
Greifswald (U4)		Quick electrical power reduction by 100 MW	GRS	Mod1.0D	/POI 91/
Greifswald (U4)		Commissioning test: loss of two main coolant pumps	GRS	Mod1.0D	/POI 91/
Dukovany		Failure of 1, 2, 3 and 6 main circulation pumps	NRI/GRS	Mod1.1A	/ARN 97/
Dukovany		Reactor scram and turbine trip caused by EP1 signal	NRI/GRS	Mod1.1D	/VOJ 00a/
Bohunice		Transient following the signal 'Pressure in primary system below 8.3 MPa'	NRA/GRS	Mod1.1D	/VOJ 01/
Kosloduj (U6)		Coast down of two neighboring out of four main circulation pumps	INRNE/GRS	Mod1.2A	/VOJ 00b/
PKL-III	B2.1	Secondary side depressurization with 50K/h in case of emergency power with 3 isolated steam generators and standing main coolant pumps	GRS	Mod 1.0E	/KRE 99/

Tab. 2.8 Transients at shutdown conditions in PWRs (Matrix V)

Test Facility	Test No.	Brief Description	Calcula-tion done by	ATHLET Version	Reference
PKL-III	B 4.5	Loss of residual heat removal system during mid-loop operation	GRS	Mod1.2B	/STE 01/
PKL-III	E 3.1	Loss of residual heat removal system during 3/4-loop operation; OECD/PKL Benchmark	GRS	Mod2.0B	/STE 06b/
PKL-III	F 2.1	Loss of residual heat removal system with different water inventories and varied upper head bypasses	GRS	Mod2.1B	/WIE 08/
PKL-III	G1.1	Parameter study on heat transfer mechanisms in the SG in the presence of nitrogen for a 3/4 -loop operation	GRS	Mod2.2A	/WIE 10/

Test Facility	Test No.	Brief Description	Calcula-tion done by	ATHLET Version	Reference
BETHSY	6.9a	Loss of residual heat removal system during mid-loop operation, pressurizer manways open			
BETHSY	6.9c	Loss of residual heat removal system during mid-loop operation, pressurizer and SG outlet plenum manways open, ISP 38	GRS/Kurt.	Mod1.1D	/MOS 97/
BETHSY	6.9d	Loss of residual heat removal system during mid-loop operation, primary system half open			

Tab. 2.9 Transients at shutdown conditions in VVERs

Test Facility	Test No.	Brief Description	Calcula-tion done by	ATHLET Version	Reference
PMK		Primary circuit opened, water level reduction	GRS/KFKI	Mod1.1B	/GYÖ 95/
PMK		Primary circuit opened, isolation of a cold leg	GRS/KFKI	Mod1.1B	/GYÖ 95/

Tab. 2.10 Accident management for non-degraded core in PWRs (Matrix VI)

Test Facility	Test No.	Brief Description	Calcula-tion done by	ATHLET Version	Reference
Primary bleed and feed procedures					
TRAM	B1	Steam release from the pressurizer at constant system pressure	GRS	Mod1.1C Mod1.1D	/KIR 96/ /SCH 98b/

Test Facility	Test No.	Brief Description	Calculation done by	ATHLET Version	Reference
TRAM	B2	Steam release from the pressurizer with depressurization			
TRAM	B3	Steam release from the pressurizer with depressurization, alternative ECC injection			
PKL-III	B1.6	Loss of off-site and on-site power			
PKL-III	C1.2	Small leak with station blackout, primary side accident management-procedures	GRS	Mod1.1C	/RIN 96/
PKL-III	C5.2	Loss of offsite power, primary side bleed and feed followed by secondary side bleed and feed	GRS	Mod1.1D	/STE 98b/
LOBI II	BT-02	Primary feed and bleed procedures after a complete loss off feedwater	Battelle	Mod1.0E	/SCH 93a/
BETHSY	5.2a	Two phase natural circulation with empty SG secondary side and primary accident management procedures			
BETHSY	5.2c	Primary feed and bleed procedures after a complete loss off feedwater	FZR	Mod1.1D	/KRE 98a/
Secondary bleed and feed procedures					
PKL III	B1.2	Complete loss of feedwater, injection of water due to flashing in feedwater line, mobile pump	GRS GRS	Mod1.1B Mod1.1D	/GEP 96/ /SCH 98b/
PKL III	C2.2	Primary depressurization after a SG tube rupture			
PKL III	C4.2	Complete loss of feedwater, injection of water due to flashing in feedwater line and feedwater tank,			
PKL III	D1.2	System behaviour during a station blackout with small leak and secondary accident management- procedures	GRS	Mod1.2B	/STE 99a/

Test Facility	Test No.	Brief Description	Calcula-tion done by	ATHLET Version	Reference
PKL III	G7.1	1.5% hot leg break with failure of high-pressure injection and secondary side depressuri-zation (Counterpart test to LSTF SB-HL-18)	GRS	Mod2.2B	/AUS 13b/
LOBI II	BT-17	Complete loss of feedwater, similar to PKL III B1.2	Battelle	Mod1.0E	/SCH 93a/
BETHSY	9.1b	0.5% break in the cold leg without high pressure injection (ISP-27)	GRS	Mod1.1A	/POI 92a/
BETHSY	5.2d	Station black-out in combination with auxiliary feedwater failure	GRS	Mod1.1B Mod1.1D	/RIN 94/ /SCH 98b/
BETHSY	9.3	SG tube rupture with loss of feedwater and failure of high-pressure injection	FZR	Mod1.1D	/KRE 98b/
LSTF	SB-PV-09	1.9% pressure vessel upper head break with total failure of high-pressure injection	GRS	Mod2.1A	/AUS 07/
LSTF	SB-PV-10	0.1% break in bottom of pressure vessel and failure of high-pressure injection asymmet-rical steam generator secondary side depressurization as AM action	GRS	Mod2.1A	/AUS 10/
LSTF	SB-HL-18	1.5% hot leg break with failure of high-pressure injection and asymmetrical steam gener-ator secondary side depressurization as AM action (OECD ROSA-2 Project Test 3)	GRS	Mod2.2B	/AUS 13b/

Tab. 2.11 Accident management for non-degraded core in PWRs (Matrix VI)

Test Facility	Test No.	Brief Description	Calcula-tion done by	ATHLET Version	Reference
PACTEL	SBL-31	0.22% cold leg break, 3 loops, secondary side bleed and feed	THZ	Mod1.2A	/VAN 99a/
PACTEL	SBL-33	0.44% cold leg break, 3 loops, secondary side bleed and feed	THZ	Mod1.2B	/VAN 99b/

Tab. 2.12 Small, intermediate and large breaks in BWRs (Matrix VII)

Test Facility	Test No.	Brief Description	Calcula-tion done by	ATHLET Version	Reference
ROSA III	Run 912	5% pipe rupture in the recirculation line, failure of the high-pressure core spray system, ISP-12	TÜV Bayern	Mod1.0E	/GAS 93/
ROSA III	Run 984	2,8% pipe rupture in the recirculation line in a BWR facility	GRS	Mod1.0C	/HRU 92/
ROSA III	Run 916	50% pipe rupture in the recirculation line, failure of the high-pressure core spray system	GRS	Current	Sect. 0
ROSA III	Run 983	200% pipe rupture in the recirculation line, failure of one emergency diesel for the low-pressure injection system	GRS	Mod1.0A/ FLUT	/POI 89/
ROSA III	Run 952	100% steam line rupture	GRS	Mod1.0E	/HRU 93/
FIST	6SB2C	2,8% pipe rupture in the recirculation line, similar to ROSA III Run 984	GRS	Mod1.0E	/HRU 95/
FIST	6MSB1	100% steam line rupture	GRS	Mod1.1A	/ARI 95/

Tab. 2.13 Transients in BWRs (Matrix VIII)

Test Facility	Test No.	Brief Description	Calcula-tion done by	ATHLET Version	Reference
ROSA III	Run 971	Loss of offsite power, failure of the high-pressure core spray system	TÜV Bayern	Mod1.0E	/BOR 93/
FIST	6PMC1	ATWS	GRS	Mod 2.1B	/AUS 10/
KRB		Turbine trip (2.10.87)	GRS	ATLAS	/POI 94/
KRB		Reactor trip (18.10.90)	GRS	ATLAS	/POI 94/
KRB		Temperature transient at pressure vessel bottom (8.5.93)	GRS	ATLAS	/POI 94/
KKK		Loss of main heat sink (17.1.91)	GRS	ATLAS	/HÖP 93/
KKK		Reactor trip (29.10.91)	GRS	ATLAS	/POI 96/
KKK		Steam line isolation (18.7.90)	GRS	ATLAS	/POI 96/
KKP-1		Loss of main heat sink (22.3.96)	GRS	ATLAS	/POI 99/
KKP-1		Reactor trip (6.3.96 and 3.12.96)	GRS	ATLAS	/POI 99/
KKP-1		Planned reactor cooldown (11.1.96)	GRS	ATLAS	/POI 99/

Tab. 2.14 Summary of ATHLET validation integral experiments and incidents for western design facilities (total / performed analyses)

Facility or Plant	Scale	Pressurized Water Reactors					Boiling Water Reactors	
		Large breaks	Small and medium breaks	Transi-ents	Transi-ents with loss of RHRS	AM	LOCAs	Transi-ents
UPTF/ TRAM	1:1	6 / 2	2 / 2			3 / 1		
CCTF	1:25	4 / 4						
LOFT	1:50	2 / 2	4 / 3	1 / 0				
LSTF	1:50		5 / 4			3 / 3		
BETHSY	1:100		7 / 7		3 / 1	5 / 4		
PKL	1:145	2 / 2	13 / 8	12 / 7	3 / 3	8 / 5		
ATLAS	1:288		1 / 1					
LOBI	1:712	2 / 2	8 / 6	4 / 3		2 / 2		
GERDA*	1:1686		1 / 1					
ROSA-III	1:424						5 / 5	1 / 1
FIST	1:642						2 / 2	1 / 1
German Konvoi				3 / 3				
KBR				4 / 4				
KKU				3 / 3				
KKP-2				5 / 5				
KKP-1								3 / 3
KRB								3 / 3
KKK								3 / 3
TOTAL		16 / 12	41 / 32	32 / 25	6 / 4	21/15	7 / 7	11 / 11

*) PWR with once-through steam generators

Tab. 2.15 Summary of ATHLET validation integral experiments for Russian design facilities (total / performed analyses)

Facility	Scale	Large breaks	Small and medium breaks	Transi-ents	Transi-ents with loss of RHRS	AM
PMK	1:2070		6 / 6		2 / 2	
ISB	1:3000		6 / 6			
PACTEL	1:305		9 / 5	2 / 2		2 / 2
PSB WWER	1:300	1 / 1	3 / 3			
Greifswald (U4)	1:1			2 / 2		
Dukovany	1:1			2 / 2		
Bohunice	1:1			1 / 1		
Kosloduj (U6)	1:1			1 / 1		
TOTAL		1 / 1	24 / 20	8 / 8	2 / 2	2 / 2

2.2.2 Separate Effects Test Validation Matrices for ATHLET

Whereas integral experiments are usually designed to follow the behaviour of a reactor system in various off-normal or design basis accident or design extension conditions, separate effects tests (SETs) focus on the behaviour of a single component, or on the characteristics of one thermal-hydraulic phenomenon. Main advantages of separate effects tests are:

- the existence of clear boundary conditions,
- measurement instrumentation can be chosen to study one particular phenomenon,
- reduced possibility of compensating modelling errors during code validation,
- systematic evaluation of accuracy of a code model across a wide range of conditions up to full reactor plant scale,
- steady state rather than transient observations possible.

The construction of a separate effects test matrix is an attempt to collect the best sets of available test data for code validation, assessment and improvement, from the wide range of experiments that have been carried out world-wide in the field of thermal hydraulics.

At the beginning of the code assessment work, it was considered that sufficient comparison with separate effects tests data would be undertaken and documented by code developers. Therefore, only limited further validation against separate effects test data would be necessary. This expectation has shown to be unrealistic. It has since been recognized that continued comparison of calculations with separate effects test data is necessary to investigate the applicability of codes, especially where a quantitative evaluation of prediction accuracy is required, for further code model improvement, and to ensure the overall quality of the recent code version. A key issue concerning the application of best estimate codes to plant calculations is quantitative code assessment. Quantitative code assessment is intended to allow predictions of nuclear power plant behaviour to be made with a well-defined uncertainty. Most methods for achieving this quantification of uncertainty rely on assigning uncertainties to the modelling by the code of individual phenomena, for instance by the determination of reasonable ranges which key model parameters can cover and still produce results consistent with data. This interest has placed a new emphasis on separate effects tests over and above that originally envisaged for model development. For more information on uncertainty analyses with ATHLET, see chap. 6.

A further incentive for simulating separate effects tests in addition to tests carried out in integral facilities is the difficulty encountered in scaling predictions for phenomena from integral test facilities (which are often at a small scale) to plant applications. Where a phenomenon is known to be highly scale-dependent and difficult to model mechanistically, there is a strong case for conducting separate effects tests at full scale. In general, it is desirable to have a considerable overlap of data from different facilities, since successfully predicting data from different facilities provides some confirmation that a phenomenon is well understood. While both integral test data and separate effects test data are appropriate for code validation, for model development and improvement there should be a preference for separate effects test data.

A total of 67 thermal-hydraulic phenomena of interest in LWR LOCA and transients are listed in Tab. 2.16. This table is taken from the OECD/CSNI report on the separate effects test matrix /NEA 93/. All representative phenomena occurring during a LOCA or transient are included. However, several phenomena are combined under a general heading in some cases, such as various instances of counter-current flow limitation, and of critical flow. It should also be emphasized that some phenomena are dependent on each other, for instance spray effects and condensation. There are different types of

phenomena, varying from those such as interphase friction which is a very basic attribute of a two-phase flow, to those such as loop seal clearing, which is essentially a system phenomenon, localized in its occurrence but very dependent on events and conditions elsewhere in the loop. In such cases, the influences from the loop have to be provided as boundary conditions. A detailed description of these phenomena can be found in /NEA 93/.

This list of phenomena forms one axis of the SET facility cross reference matrix. The second axis of the matrix consists of the 187 facilities identified as potential sources of separate effects test data. For each test facility, the phenomena addressed by the corresponding experimental research programme have been indicated in these matrix tables, yielding the SET cross reference matrix for test facilities and thermal-hydraulic phenomena.

A number of specific experiments were selected from those facilities which are included in the cross-reference matrices described above. These selected tests versus phenomena establish the individual code validation matrix (Tab. 2.17). An overview of the different separate effects test facilities indicating the number of selected tests as well as the current status of calculated experiments is shown in Tab. 2.18.

Tab. 2.16 List of relevant phenomena for LWR transients and LOCAs

0	Basic Phenomena	Evaporation due to depressurization Evaporation due to heat input Condensation due to pressurization Condensation due to heat removal Interfacial friction in vertical flow Interfacial friction in horizontal flow Wall-to-fluid friction Pressure drops at geometric discontinuities Pressure wave propagation
1	Critical flow	Breaks (1), Valves (2), Pipes (3)
2	Phase separation / vertical flow with or without mixture level	Pipes / plena (1), Core (2), Downcomer (3)
3	Stratification in horizontal flow	Pipes
4	Phase separation at branches	Branches
5	Entrainment / De-entrainment	Core Upper plenum Downcomer Steam generator tube Steam generator mixing chamber (PWR) Hot leg with ECC injection (PWR)

6	Liquid-vapor mixing with condensation	Core Upper plenum Downcomer Lower plenum Steam generator mixing chamber (PWR) ECC injection in hot and cold legs (PWR)
7	Condensation in stratified conditions	Pressurizer (PWR) Steam generator primary side (PWR) Steam generator secondary side (PWR) Horizontal pipes
8	Spray effects	Core (BWR) Pressurizer (PWR) OTSG secondary side
9	Countercurrent flow / CCFL	Upper tie plate Channel inlet orifices (BWR) Hot and cold leg Steam generator tube (PWR) Downcomer Surge line (PWR)
10	Global multidimensional fluid temperature, void and flow distributions	Upper plenum Core Downcomer Steam generator secondary side
11	Heat transfer:Natural or forced convection Subcooled / saturated nucleate boiling DNB / Dryout Post critical heat flux Radiation Condensation	Core, steam generator, structures Core, steam generator, structures Core, steam generator, structures Core, steam generator, structures Core Steam generator, structures
12	Quench front propagation / rewetting	Fuel rods Channel walls and water rods (BWR)
13	Lower plenum flashing	
14	Guide tube flashing (BWR)	
15	One- and two-phase impeller-pump behaviour	
16	One- and two-phase jet-pump behaviour (BWR)	
17	Separator behaviour	
18	Steam dryer behaviour	
19	Accumulator behaviour	
20	Loop seal filling and clearance (PWR)	
21	ECC bypass / downcomer penetration	
22	Parallel channel instabilities (BWR)	
23	Boron mixing and transport	
24	Non-condensable gas effects (PWR)	
25	Lower plenum entrainment	

Tab. 2.17 Summary of ATHLET validation separate effects tests

Test Facility	Test No.	Brief Description	Calcula-tion done by	ATHLET Version	Reference
ACHILLES		Reflooding in bundle with 69 electrically heated rods (6 tests)	GRS	Mod2.2B	/TIB 15/
Bartolomej	1 ... 21	Subcooled and saturated nucleate boiling at high pressure	GRS	Mod2.1B	/TRA 09/
BATTELLE	SWR 2R	Break of a steam line, ISP-6	GRS	DRUFAN	/STE 89/
BATTELLE	SL1	Break of a feedwater line	GRS	DRUFAN	/RIN 83/
KWU-Karlstein	RS 37 C	Blowdown heat-transfer			
CREARE	1/5	CCFL in downcomer	RUB	Mod1.1D	/WEI 98/
CREARE	1/15	CCFL in downcomer	RUB	Mod1.1D	/WEI 98/
CREARE	1/30	CCFL in downcomer	RUB	Mod1.1D	/WEI 98/
ECTHOR		Clearance of a water filled loop seal by a forced air flow through the loop	RUB	Mod1.0E	/SCH 93b/
Elektrogorsk 108 (E-108)		Steam line break. RBMK-1500 reactor type.	GRS-ISAG	Mod1.2A	/WEB 98/
FEBA	Series I	Reflooding in a 5x5 full length rod bundle	RUB	Mod2.2B	/TIB 15/

Test Facility	Test No.	Brief Description	Calcula-tion done by	ATHLET Version	Reference
FLECHT-SEASET	31701	US SP 9A: Bundle reflood at high flooding rate	GRS GRS	Mod1.2D Mod3.0A	/TES 01/ /TIB 15/
	31805	US SP 9B: Bundle reflood at low flooding rate	GRS GRS	Mod1.2D Mod3.0A	/TES 01/ /TIB 15/
GE VESSEL	5702-16	Blowdown test with top leak	GRS	Mod0.0B	/KIR 87/ /SKO 88a/
GE VESSEL	5803-2	Blowdown test with bottom leak	GRS	Mod0.0B	/KIR 87/ /SKO 88a/
HCGS		Heat transfer in helically coiled heat exchangers with parameters typical for Small Modular Reactors (SMR) like NuScale	RUB	Mod.3.2	/KRI 22/
HDR	V 45	Break of a steam line	GRS	DRUFAN	/STE 89/
HDR	V 21.1	Break of a feedwater line	GRS	Mod1.0D	/POI 92b/
HDR	V 21.3	Break of a feedwater line			
HDR-COCO	E 33.1131	Steam condensation at ECC water: 0.4 MPa, Steam surplus, Rt=0.8	GRS	Mod1.0E	/TES 93/
HDR-COCO	E 33.1142	Steam condensation at ECC water: 0.4 MPa, Steam deficiency, Rt=1.2	GRS	Mod1.0E	/TES 93/
HDR-COCO	E 33.1168	Steam condensation at ECC water: 0.4 MPa, Steam deficiency, Rt=3.0	GRS	Mod1.0E	/TES 93/
HDR-COCO	E 33.1241	Steam condensation at ECC water: 2.5 MPa, Steam surplus, Rt=0.8			

Test Facility	Test No.	Brief Description	Calcula-tion done by	ATHLET Version	Reference
HDR-COCO	E 33.1246	Steam condensation at ECC water: 2.5 MPa, Steam deficiency, Rt=1.6			
HDR-COCO	E 33.2331	Steam condensation at ECC water: 7.0 MPa, Steam surplus, Rt=0.8			
HDR-COCO	E 33.2338	Steam condensation at ECC water: 7.0 MPa, Steam deficiency, Rt=3.0			
Henry tests		Critical flow modelling	KIT	Mod3.1	/XU 21/
IVO		Clearance of a water filled loop seal, test sloping inlet D=80mm, VVER 440	GRS	Mod1.0A	/SKO 88b/
IVO		Clearance of a water filled loop seal, test straight inlet D=80mm, VVER 1000	GRS	Mod1.0A	/SKO 88b/
IVO		Clearance of a water filled loop seal, D=850mm, VVER 1000	GRS	Mod1.0A	/SKO 88b/ /SON 94/
IVO-CCFL		CCFL in fuel element head and fuel bundle (air-water)	RUB	Mod1.0B	/WEI 00/
HORUS	PCHS 5,9,10,11	Injection of steam in VVER SG tube; closed exit collector; condensation	THZ	Mod1.1B	/FJO 94/
HORUS	PCHS 23,25,30,36	Injection of steam in VVER SG tube; closed exit collector; condensation	THZ	Mod1.2B	/GOC 00/
HORUS	PCHS 25,30	Injection of steam in VVER SG tube; closed exit collector; condensation	HSZG	Mod1.1C	/FJO 98/
HORUS	POHS 1,3,5	Injection of steam in VVER SG tube; open exit collector; condensation	THZ	Mod1.1B	/FES 93/
HORUS	PCHG 7	Injection of steam in VVER SG tube with N_2 gas; closed exit collector; condensation	THZ	Mod1.1C	/FJO 96/
HORUS	POHG 9	Injection of steam in VVER SG tube with N_2 gas; open exit collector; condensation	THZ	Mod1.1C	/FJO 96/

Test Facility	Test No.	Brief Description	Calcula-tion done by	ATHLET Version	Reference
HORUS	PCHN 5,6,8,10	Injection of steam and N_2 gas in VVER SG tube; closed exit collector; condensation	THZ	Mod1.2B	/GOC 00/
HORUS	PCHN 6,10	Injection of steam and N_2 gas in VVER SG tube; closed exit collector; condensation	HSZG	Mod1.1C	/FJO 98/
KFA		Onset of flow instabilities in research reactors at low pressure	GRS	Mod2.1B	/TRA 09/
KFA		Analysis of the research reactor behavior during transients and leakage accidents	KFA	Mod1.0E	/HAI 93/
MARVIKEN	Test 22	Blowdown test with critical flow in subcooled fluid conditions	GRS	Mod0.0A	/RIN 87/
NEPTUNUS	Y 05	Pressuriser transient, d=800mm	GRS	Mod1.0 B	/HOB 89/ /FOR 90/
OMEGA Bundle	Test 9	PWR rod bundle behaviour during blowdown	GRS	Mod1.1C	/GLA 94a/
PATRICIA	GV 2	SG swell level (8 steady state tests, 3 transient tests)	RUB	Mod1.1D	/WEI 96/
PERICLES		3 Boil-off tests (steady state) in rectangular bundle, p=0.3-0.55 MPa	GRS	Mod1.0B	/FOR 90/
PERICLES		Reflooding in an array of 3 bundles of 7x17 rods each (6 tests)	GRS	Mod2.2B	/TIB 15/
ROCOM	T6655	Density driven mixed experiments (3 runs)	GRS	Mod2.1C	/HOR 09/
	T6655_Y1	Density difference 0.25%			/BUR 05/

Test Facility	Test No.	Brief Description	Calculation done by	ATHLET Version	Reference
ROCOM	01, 01a, 02	Small 50 cm^2 HL leak, start of natural circulation with HP injection into two HLs and accumulator injection into 4 HLs, secondary side depressurization with 100K/h. Boundary conditions of the PKL-III E2.3			/BUR 05/
ROCOM	Tests 1.1-1.3	Coolant mixing in downcomer during a MSLB scenario (Complementary tests to PKL-3 G3.1 in the frame of the OECD/NEA PKL-2 Project	GRS	Mod3.0A	/AUS 13b/
ROCOM	Tests 2.1, 2.2	Coolant mixing in downcomer during a MSLB scenario (Complementary tests to PKL-3 H in the frame of the OECD/NEA PKL-3 Project	GRS HZDR	Mod3.0B 3.2	/PAN 15/ /CEU 15/ /DIA 22/
RS 77		Thermodynamic nonequilibrium, evaporation	GRS	Mod1.1A	/RUA 96/
SCTF	S3-09/713	Double ended cold leg break, cold leg ECC, EM-case			
SCTF	S3-10/714	Double ended cold leg break, cold leg ECC, BE-case			
SCTF	S3-11/715	Double ended cold leg break, combined ECC, BE-case			
SCTF	S3-13/717	Double ended cold leg break, combined ECC, EM-case			
SCTF	S3-14/718	Double ended cold leg break, cold leg ECC, flat power profile			
SCTF	S3-16/720	Double ended cold leg break, cold leg ECC, steep power profile			
SUPER MOBY DICK		Phase separation with lateral outlet			
SUPER MOBY DICK		Critical flow; d=5.2 mm, d=15.5 mm	GRS	DRUFAN	/BUR 85/
THETIS		8 Boil-off Tests (steady state) in circular bundle, p=0.5-4.0 MPa	GRS	Mod1.0B	/FOR 90/

Test Facility	Test No.	Brief Description	Calcula-tion done by	ATHLET Version	Reference
THTL	FE712B, FE714B, FE714C, FE105B, FE212A, FE105D	Simulation of supercooled and saturated boiling. The THTL (Thermal-Hydraulic Test Loop) test facility consists of an electrically heated channel that replicates a core channel of the Advanced Neutron Source Reactor (ANSR) of reduced width	GRS		/LER 07/
KfK T-Junction Test Facility		T-junction tests	GRS	Mod1.1C	/SKO 95/
TOSHIBA - Vessel		Blowdown test with vessel boil-off	GRS	Mod1.0E	/STO 92/
TPTF	Nr.6	6 Boil-off tests in bundles, (p=3.0, 7.0, 11.9 MPa)	GRS	Mod1.0D	/RIN 91/
TPTF		Test in horizontal pipe, stratified flow	GRS	Mod1.1C	/SON 94/ /POM 96/
Techn. Univer-sität Hannover		CCFL in bundle			
UPTF	5A	CLI, CCFL Downcomer	GRS	3.3	/JUN 22/
UPTF	5B	CLI, CCFL Downcomer, break in cold leg			

Test Facility	Test No.	Brief Description	Calcula-tion done by	ATHLET Version	Reference
UPTF	6	CLI, CCFL Downcomer	RUB GRS	Mod1.2D Mod3.1A	/WEI 02/ /HOL 16/
UPTF	7	CLI, CCFL in downcomer	RUB GRS GRS	Mod1.2D Mod2.1A Mod3.0A	/WEI 02/ /WIE 06/ /AUS 13b/
UPTF	8A	Flow regime dependent condensation in cold/hot leg during HLI and CLI, resp.	GRS	Mod1.2B 3.3	/RIN 01b/, /JUN 22/
UPTF	9	Flow regime dependent condensation for combined ECC injection			
UPTF	10A	Upper tie-plate water breakthrough in countercurrent flow	GRS	Mod1.0D	/BUR 92a/
UPTF	10B	Liquid entrainment in steam flow from core to SG	RUB	Mod1.1D	/WEI 98/
UPTF	10C	CCFL core / UP	RUB GRS	Mod1.1D Mod 2.1B	/WEI 98/ /AUS 10/
UPTF	11	CCFL in hot leg, reflux condensation	GRS	Mod1.0D	/SON 90a/
UPTF	15 Run123	HLI, CCFL in fuel element head plate during ECC injection into intact HL, large break			
UPTF	20	UPI, CCFL in fuel element head plate during upper plenum injection	Pitscheider GRS	Mod1.0C Mod2.1B	/THI 90/ /SCH 08/
UPTF	22	DCI, Vent valve test			
UPTF	23	DCI, Vent valve test			
UPTF	25A	CLI, Entrainment in DC			
UPTF	25B	CLI, Entrainment in DC			
UPTF	26 Run 230	HLI, CCFL behaviour in hot leg, effect of scoop injection in hot leg	GRS	Mod1.0D	/SON 90b/
UPTF	29	Upper plenum de-entrainment	Pitscheider	Mod1.0C	/THI 91/

Test Facility	Test No.	Brief Description	Calcula-tion done by	ATHLET Version	Reference
UPTF	30	HLI, CCFL in fuel element head plate during HP injection into intact HL, small leak	GRS	Mod1.0D	/BUR 92b/
UPTF	Z1	Liquid entrainment in steam flow from downcomer to cold leg during reflood phase; steam condensation during cold water injection			
UPTF	Z3	CCFL in Downcomer during the postulated large break in cold leg	GRS RUB GRS	Mod1.0D Mod1.2D Mod3.1A	/BUR 92c/ /WEI 02/ /HOL 16/
UPTF TRAM	A1	Core cooling flow in hot leg ECC injection			
UPTF TRAM	A2	Stratified flow in hot leg ECC	Pitscheider	Mod1.0E	/FEI 93/
UPTF TRAM	A4	Reflux condenser with ECC injection			
UPTF TRAM	A5	Clearance of a water filled loop seal	RUB	Mod1.1A	/WEI 96/
UPTF TRAM	C1	ECC injection in the cold leg of a water filled PWR; thermal mixing in cold leg and down-comer	GRS GRS	Mod1.2E Mod2.2B	/LER 02/ /SCH 12/
UPTF TRAM	C2	ECC injection in steam-filled cold leg; influence of N_2 on condensation	GRS	Mod1.2B	/BUR 01/
UPTF TRAM	C3	Mixing of mass flows with different temperatures	GRS	Mod1.2E	/BUR 03/

Tab. 2.18 Summary of ATHLET validation separate effects tests (total / performed analyses)

Test Facility	Nr. of Tests	Test Facility	Nr. of Tests	Test Facility	Nr. of Tests
ACHILLES	1 / 1	Bartolomej	1 / 1	Battelle	2 / 2
CREARE	3 / 3	ECTHOR	1 / 1	FEBA	1 / 1
FLECHT	2 / 2	GE VESSEL	2 / 2	HDR	3 / 2
HDR-COCO	7 / 3	HORUS	6 / 6	IVO	3 / 3
IVO-CCFL	1 / 1	KFA	1 / 1	KfK T-Junction	1 / 1
KWU-Karlstein	1 / 0	MARVIKEN	1 / 1	NEPTUNUS	1 / 1
OMEGA	1 / 1	PATRICIA	1 / 1	PERICLES	2 / 2
ROCOM	4 / 4	RS77	1 / 1	SCTF	6 / 0
S MOBY DICK	2 / 1	THETIS	1 / 1	TOSHIBA-V.	1 / 1
TPTF	2 / 2	TU Hannover	1 / 0	UPTF	20 / 10
UPTF-TRAM	7 / 5				
TOTAL	87 / 61				

2.3 Validation for Passive Safety Systems

Particularly advanced Gen III+ and IV reactor designs rely more and more on passive safety systems for design basis accident and design extension conditions control and mitigation. Their range of applicability comprises ECC injection, residual heat removal, pressure reduction, flow limitation, etc. The functional capability of passive safety systems is based on key physical principles such as gravitation, buoyancy, condensation, and evaporation. Compared to active systems typically used in operating reactor designs, passive systems exhibit different operational conditions and by far smaller driving forces. In addition, their instantaneous working point is not defined but determined by the overall conditions in the facility. Thus, a separate code validation for passive safety systems or even further code elaboration becomes indispensable.

In the frame of the long-time general code validation procedure, ATHLET proved to be capable to capture basic phenomena that are characteristic for the operation of passive systems, e.g., single and two-phase natural convection processes or condensation/evaporation in heat exchangers of different shape. Unfortunately, only few experimental data of separate effect tests investigating in detail the practicality of passive

safety systems are publicly available until now. However, ATHLET could be validated against several dedicated test cases. Tab. 2.19 provides an overview of selected experiments. Some of the test cases are also included in the tables of the preceding chapters of the manual in hand.

Tab. 2.19 Validation cases for passive safety systems

Facility	Test	Brief Description	Calculation done by	Code Version	Reference
INKA	2_12_1 1_10_85_ 13_1	Stationary and transient emergency condenser tests simulating heat removal and primary side steam condensation in the KERENA BWR design	GRS	Mod3.0B	/BUC 15/ /BUC 18/
INKA	EASY-4	Integral test on functionality of the passive systems emergency condenser and building condenser in the KERENA BWR design	GRS	Mod3.0B Mod3.3	/BUC 18/
NOKO Jülich	Emergency condenser capacity	Analysis of an emergency condenser employing one slightly inclined heat exchanger pipe bundle	FZR GRS	Mod1.1C Mod3.0B	/SCH 98 c/ /SCH 15/
ATLAS	Test A1.2	Passive Auxiliary Feedwater System during a Station Blackout	GRS	Mod3.0B	/AUS 16/
UPTF TRAM	A6	Cold leg accumulator injection after 5% cold leg break	GRS	Mod1.1A	/BUR 94/
PERSEO	7, 9	Investigation of the stability of the system for two different liquid levels in the HX-Pool as well as long-run behaviour	GRS	3.2.1 3.3	/BUC 19/ /BUC 20/ Sect. 5.5
PASI	Pre-tests	Analysis of the thermosiphon behaviour (150kW, 100kW, 50kW)	GRS		/DAV 22/
	PAS-01	Characterization of the cooling system behavior with three different heating powers. Analysis of the loop flow resistance	GRS	3.3.1	/BUC 23 a/
GENEVA		Containment cooling condenser in the KERENA BWR design	TUD	Mod3.1C	/MAN 21/

The validation activities for passive safety systems are also relevant for pool configurations which are found in spent-fuel pools and pool-type research reactors. It has been demonstrated that ATHLET can be successfully applied to research reactors /KOP 20/, complemented by additional /WON 20/, /WON 21/. Together with extant validation on passive safety systems and 3D pool behaviour, this allows the conclusion that ATHLET

is validated for pool-type research reactor applications as long as specific characteristics of the fuel assembly (e.g., metallic fuel and its failure modes) or specific installations of a research reactor (helium-cooled cold neutron source) do not play a decisive role for scenario progression. Similarly, ATHLET has been successfully applied to spent-fuel pools (also in the context of severe accident analyses with ATHLET-CD) /WEB 19/, /KRÜ 19/. Consequently, the available validation for pool-type geometries allows the conclusion that ATHLET is validated for spent fuel pool applications, unless would require very specific dedicated models such as, e.g., a heavy load drop with mechanical damage to the fuel. Both for pool-type research reactors and for spent fuel pools, applying the mixture level to a parallel channel nodalisation when transition to pool boiling is expected is currently discouraged, as it is bound to produce substantial mass errors.

2.4 Validation for GEN IV Reactors

Originally, ATHLET has been developed to be applied for the analysis of the behaviour of Light Water Reactors (LWR) under transient or accident conditions. Meanwhile, the additional working fluids heavy water, helium, the liquid metals lead, lead-bismuth eutectic (LBE) and sodium have been implemented into the code, together with some models and correlations related to these coolants. These extensions are not only relevant for operating reactors like sodium fast reactors or CANDU reactors (to which ATHLET has been or can be applied), but also required for the modelling of so-called GEN IV reactors, which use different fluids in the coolant circuits and are currently under development or investigation internationally. Presently, the following reactor types are considered as the most promising ones:

- (Very) high temperature gas cooled reactor (V)HTGR (helium cooled)
- Sodium cooled fast reactor SFR (coolant is liquid sodium)
- Lead cooled fast reactor LFR (liquid lead or LBE)

The new core designs aim at different advantages compared to LWRs, among them

- increased overall efficiency of the NPP,
- improved fuel utilization and sustainability,
- improved passive or even inherent safety,
- improved reliability,

- reduced risk of proliferation.

Another innovative reactor design is the so-called Accelerator Driven Sub-Critical System (ADS) with LBE as coolant and target. This design enables the transmutation of long-lived fission products into short-lived ones.

In addition to the new coolants, the design of these reactors is quite different to those of common LWRs. In particular, the geometry of and the coolant flow inside the reactor vessel differ strongly from LWRs. Moreover, the nuclear core of (V)HTGRs may consist of graphite pebbles or may have a (prismatic) graphite block structure.

Different to LWRs, no systematic validation matrices have been set-up for GEN IV reactor's design and thermal-hydraulic phenomena up to now. Nevertheless, all major system codes have been extended for these types of reactors, and validation work is underway.

The validation of the ATHLET extensions for GEN IV reactors has started a few years ago. Besides many test calculations in the frame of the ATHLET development proving the capability of the code to model these coolants and to produce 'reasonable' results, some verification work has been performed up to now (Tab. 2.20). One subject of this work was the simulation of different transients and accident scenarios in the MYRRHA/XT-ADS concept which is planned to be built at the Belgian Nuclear Research Center SCK-CEN /PAL 13/. Up to now, no measured date is available, the ATHLET results have been compared with those obtained with the RELAP5 computer code.

Tab. 2.20 Validation cases for GEN IV reactors

Facility	Test	Brief Description	Calculation done by	Code Version	Reference
HERO-2	Open-extended case. Closed tests: 1, 2, 3, 7 ,8	Characterization of bayonets heat exchange. Application in heavy liquid metal GEN-IV	UJV	Mod3.2	/POL 22/
HERO-2	Open-extended case. Closed tests: 1 - 21	Characterization of bayonets heat exchange. Application in heavy liquid metal GEN-IV	USTUTT	Mod3.2	/POL 22/
KASOLA,code-to-code comparison	Drainage test	Emergency drainage of the KASOLA test facility, working fluid sodium	GRS	Mod3.0A	/HRI 15/
MHTGR-350, code-to-code comparison	OECD MHTGR benchmark	OECD code benchmark for prismatic MHTGR-350-MW core designs	GRS	Mod3.0B	/CRO 15/
MYRRHA code-to-code comparison		Simulation of nominal conditions and accidental scenarios in the spallation loop of MYRRHA facility (LBE)	GRS	Mod3.0A	/PAL 13/
TALL	T.01.09	European FP7 project THINS, ATHLET - ANSYS CFD coupled calculations of transition from forced to natural convection, working fluid LBE	GRS, TUM	Mod3.0A	/PAP 15a/

2.5 Validation for Coupled Code Systems

In the past, various interfaces were developed in order to couple ATHLET with other codes. This work enables multi-scale and multi-physical simulations and, by that, extends the code's scope of application. Fig. 2.12 depicts available code couplings. Regarding the interface concept, pure data transfer interfaces, e.g. for provision of appropriate boundary conditions for subsequent code application, and true coupling interfaces based on simultaneous code execution can be distinguished. Depending on the characteristic time constants of the coupled physical processes, the coupling is realized in weak or strong form, where the latter refers to mutual data transfer on ATHLET sub-timestep level, sometimes also including mutual iteration of both codes' results to comply with defined convergence criteria.

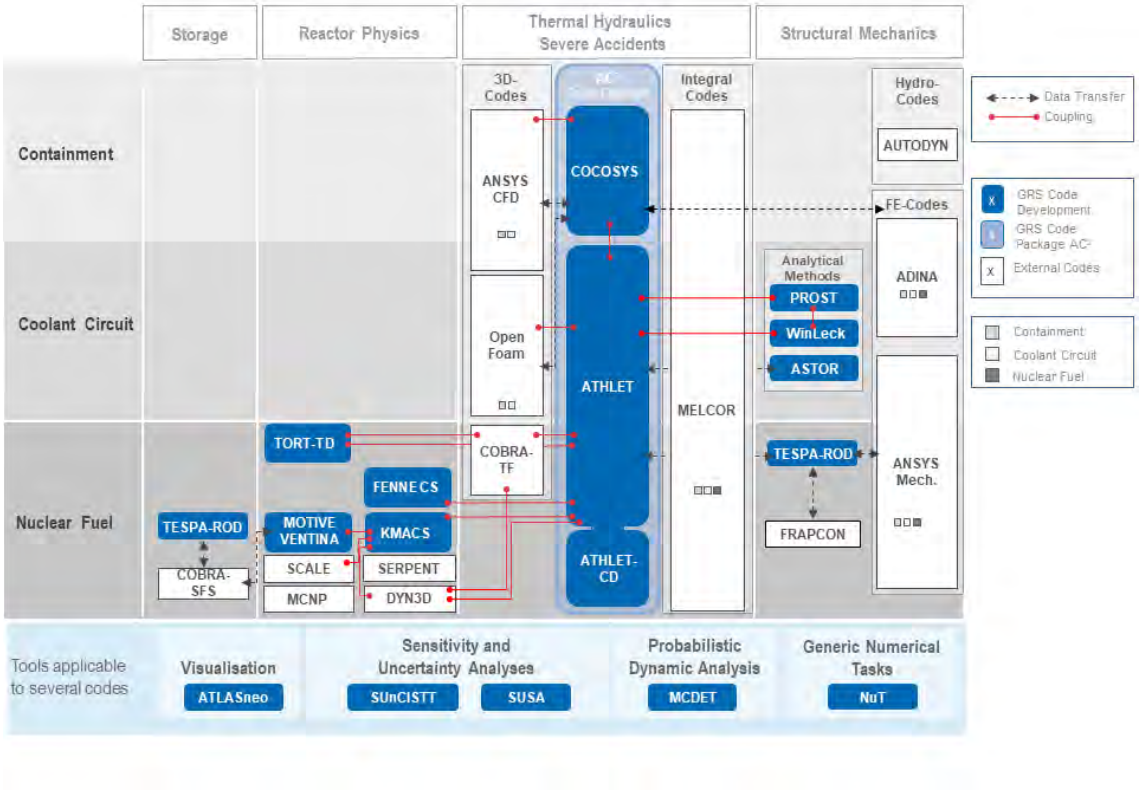

Fig. 2.12 Codes coupled with ATHLET

2.5.1 Coupling with CFD Codes

In several reactor transients and accidents, 3D flow phenomena relevant for nuclear safety issues occur in various parts of a NPP. Examples are boron dilution events or the main steam line rupture leading to a strongly asymmetric coolant distribution in the reactor pressure vessel which may propagate into the nuclear core. For these cases, the degree of coolant mixing of deborated and borated water or of hot and cold water, respectively, particularly in the downcomer and the lower plenum is of essential significance for the distribution of the boron concentration and the coolant temperature at the core entry, which in turn determines the local nuclear power production in the core.

TH system codes like ATHLET are based on balance equations solved in 1D direction. Although simulation networks with 3D topology can be generated and applied for safety analyses, their solution remains of 1D type, neglecting mixing and turbulence terms in the momentum equations. Computational fluid dynamics (CFD) codes, in turn, are able to model complex flow processes by means of true 3D approaches with high resolution in space and time. Unfortunately, CFD simulations require substantial CPU resource

and/or calculation time. Thus, the application of these tools for the complete NPP to be analysed is presently not feasible.

Since 3D processes, in general, are significant only in some locations of the NPP, coupled system and CFD code packages are developed and applied, where only that part of the facility is modelled in detail with a CFD code, where highly relevant 3D phenomena need to be resolved in detail, and the remaining (much larger) part is modelled with the system code.

For that purpose, ATHLET has been coupled with the CFD codes ANSYS CFD /LER 09/, /PAP 19/ and OpenFOAM /HER 16/, /SEU 19/. The validation of these coupled code system is presently underway. Besides many test calculations in the frame of the development of the coupling proving its feasibility, the implementation on a computer cluster, and the correctness of the achieved results (by comparison with stand-alone calculations), some validation work has been performed up to now. Tab. 2.21 provides an overview.

2.5.2 Coupling with 3D Neutronics Codes

For ATHLET, coupling interfaces to several 3D neutronics codes are provided (see Fig. 2.12). The development of multi-physics methodologies requires comprehensive validation procedures. For that purpose, NEA/OECD defined and conducted benchmarks that permit the verification of best-estimate neutronics / thermal-hydraulics coupled code systems for LWR. The benchmarks were addressed to complex transients with core plant interaction. Examples are the PWR coolant transient benchmark /KOL 11/ or the BWR turbine trip benchmark /LAN 04/.

A selection of cases employed for the validation of the ATHLET / neutronics code coupling against PWR and BWR of both western and Russian design is presented in Tab. 2.22. A lot of additional validation work has been performed for specific combinations, e.g. for ATHLET/DYN3D by Helmholtz-Zentrum Dresden-Rossendorf on Western type LWR as well as VVER designs /GRU 98/, /ROH 10/, /KOZ 15/, and for ATHLET/BIPR-VVER 1.0 by Kurchatov Institute on VVER designs /NIK 08/, /KOT 20/. Importantly, as preparation of the successful certification of ATHLET/BIPR-VVER 1.0 in the Russian Federation /FED 18/, the special version ATHLET 2.1A_A was certified for safety analyses of VVER reactors in the Russian Federation /FED 14/.

Tab. 2.21 Validation cases for coupling with CFD codes

Facility	Test	Brief Description	Calculation done by	Code Version	Reference
Double T-junction (PSI)	Double T-junction experiment	Fluid-fluid mixing in a double T-junction. ATHLET coupling with ANSYS.	GRS	Mod3.0A	/PAP 14/
LSTF	ROSA V, Test 1.1	PTS issue during the injection of cold emergency coolant into the cold leg of a PWR filled with hot water. ATHLET coupling with ANSYS.	GRS	Mod2.2B	/PAP 12/
LSTF	ROSA V, Test 1.1	PTS issue during the injection of cold emergency coolant into the cold leg of a PWR filled with hot water. ATHLET coupling with OpenFOAM.	GRS	Mod.3.3	/MIS 23/
TALL	T.01.09	Transition from forced to natural convection after pump trip. TALL facility comprises 3D test section and employs working fluid LBE. (European FP7 project THINS) . ATHLET coupling with ANSYS.	GRS, TUM	Mod3.0A	/PAP 15b/

Tab. 2.22 Validation cases for coupling with 3D neutronics codes

Facility	Test	Brief Description	Calculation done by	Code Version	Reference
ASTRID	Code-to-code	Core coolant inlet temperature ramp	GRS (PARCS / ATHLET, FENNECS/ ATHLET)	3.3	/SEU 22/
Elektro-gorsk 108 (E-108)	ATWS case	4000 MW Loss of Alternate Current Power ATWS case. RBMK-1500 reactor type.	GRS-ISAG (QUABOX/ CUBBOX-HYCA)	Mod1.1D	/WEB 98/
Kalinin-3 VVER-1000	MCP trip	Switching-off of one of the four operating main circulation pumps at nominal power (OECD/NEA Kalinin-3 coolant transient benchmark)	GRS/KI (QUABOX/ CUBBOX, BIPR)		/NIK 11/
Kursk-1 RBMK-1000	Vapor reactivity coefficient measurement (2010)	Modelling of vapor reactivity coefficient measurement in RBMK-1000	SEC NRS / GRS (QUABOX/ CUBBOX)	Mod2.2A	/KHR 15/
Peach Bottom-2 (GE BWR/4)	Turbine trip transient	BWR turbine trip (OECD/U.S. NRC BWR TT benchmark)	GRS (QUABOX/ CUBBOX)		/LAN 04/
PWR Boron Transient	Code-to-code	Postulated boron transient in PWR	GRS (QUABOX/ CUBBOX, TORT-TD)		/VEL 09/
Rostov-2		Operational transient of a VVER-1000 reactor. ATHLET coupling with DYN3D	GRS	Mod3.3	/TRA 22/
Three Mile Island-1 PWR	Code-to-code	Overcooling transient after main steam line break at 114% of nominal power (OECD PWR MSLB Benchmark)	GRS (QUABOX/ CUBBOX)		/LAN 03/
VVER-1000	Code-to-code	Main steam line break outside the containment (OECD/NEA VVER-1000 coolant transient benchmark V1000CT-2)	GRS/KI (BIPR)		/KOL 11/

3 International Standard Problems

Assessing the safety of nuclear installation requires the use of a number of highly specialized tools: computer codes, experimental facilities and their instrumentation, special measurement techniques, methods for testing components and materials, and so on. A highly effective way of increasing confidence in the validity and accuracy of such tools is provided by International Standard Problem (ISP) Exercises, in which they are evaluated against one another and/or agreed standards /NEA 89/, /NEA 00/. The OECD/CSNI Nuclear Energy Agency promoted International Standard Problems mainly for OECD countries, the IAEA mainly for Eastern European Countries.

For example, predictions of different computer codes or different users using the same computer code version for a given physical problem may be compared with each other and with the results of a carefully controlled experiment, which could also be a real plant transient. This kind of comparative exercise is clearly suitable for an international venture. Moreover, ISPs enable code users to gain experience and to demonstrate their competence. ISPs are performed as 'open' or 'blind' problems. In an open Standard Problem, the results of the experiment are available to the participants before performing the calculations, while in a blind Standard Problem the results are locked until the calculation results are made available for comparison.

The objectives of International Standard Problems according to /OEC 04/ are:

1. Contribute to a better understanding of postulated and actual events.
2. Compare and evaluate the capability of best estimate computer codes to predict controlled experiments and actual plant transients, and thus improve confidence in them as assessment tools for safety questions.
3. Suggest necessary improvements in the code.
4. Improve the ability of the code users.
5. Provide information for quantifying code uncertainties and hence safety margins in design or licensing criteria.
6. Suggest necessary experiments to reduce technical ambiguities which are discovered by the ISP.

The selection and analysis of ISPs should be based on the following:

1. Selections must be made with respect to relevance to the stated objectives and to safety priorities.
2. Both integral and separate effects experiments (as well as actual plant transients) may be considered.
3. Best estimate computer codes should preferably be used.
4. The analysis should be fully documented.

While code validation is primarily a task for institutions developing codes requiring considerable financial resources for performing a large number of calculations and comparing relevant experimental results with calculated data, ISP exercises can be considered as a supplementary activity validating appropriate code applications through the analyses of experts also different from the code developers. The application of the same code by different code users provides insight into the so-called user effect on calculated results /AKS 95/. The list of thermal-hydraulic International Standard Problems performed by OECD/CSNI is given in Tab. 3.1.

Tab. 3.1 OECD/CSNI International Standard Problems on thermal-hydraulic tests

ISP	Date	Title	CSNI Report No.
1	1975	Edwards' Pipe (discharge, pressure waves)	-
2	1975	Semi-scale: Test 11 (LB LOCA blowdown)	-
4	1978	Semi-scale MOD1: Test S-02-6 (6% SB LOCA)	16, 50
5	1979	LOFT: Test L1-4 (isothermal non-nuclear blow-down)	29 (+ addendum)
6	1979	Battelle: Test SWR-2R (steam line break)	30
7	1979	ERRSEC (reflooding experiment of LOCA, SET)	55
8	1979	Semi-scale MOD1: Test S-06-03 (LB LOCA, counterpart test to LOFT L2-3)	38
9	1981	LOFT: Test L3-1 (2.5% LOCA)	66
10	1981	PKL-I: Test K9 (LB LOCA refill and reflood)	64
11	1984	LOFT: Tests L3-6/L8-1 (2.5% LOCA)	73
12	1982	ROSA-III: Run 912 (5% LOCA in BWR)	100
13	1983	LOFT: Test L2-5 (LB LOCA)	101
15	1983	FIX-II: Experiment 3025 (31% LOCA in BWR)	102
18	1987	LOBI-MOD2: Experiment A2-81 (1% LOCA)	133
19	1987	PHEBUS: Test 218 (nuclear fuel behavior during LB LOCA)	131
20	1988	DOEL-2: Steam generator tube rupture event	154
21	1989	Piper-One: Test PO-SB-07 (1.6% and 2.8% LOCA in BWR)	162
22	1990	SPES: Test SP-FW-02 (loss of feedwater transient)	174 and NEA/CSNI/R(92)7
25	1991	ACHILLES: N_2 injection from accumulators and best estimate reflood rates (effect of accumulator gas during LOCA reflood)	NEA/CSNI/R(91)11
26	1992	LSTF: Test SB-CL-18 (5% cold leg LOCA)	NEA/CSNI/R(91)13
27	1992	BETHSY: Test 9.1b (0.5% LOCA with Loss of HP Injection)	NEA/CSNI/R(92)20
33	1992	PACTEL: Test ITE-06 (VVER-440 natural circulation behaviour)	NEA/CSNI/R(94)24
38	1995	BETHSY: Test 6.9c (loss of residual heat removal system during mid-loop operation	NEA/CSNI/R(97)38
42	2003	PANDA: Long term passive containment cooling system performance, 6 phases	NEA/CSNI/R(2003)6 NEA/CSNI/R(2003)7
43	2001	Univ. of Maryland College Park: Boron dilution, 2 tests	NEA/CSNI/R(2000)22

ISP	Date	Title	CSNI Report No.
50	2010	ATLAS: 50 % Break of DVI Line	NEA/CSNI/R(2012)6
51	2019	ACME: 2-inch SB LOCA	

Experiments selected to support ISP exercises are usually exceptionally well documented; they play a prominent role in the ATHLET validation matrices. GRS has participated in almost all thermal-hydraulic ISPs using ATHLET (or former DRUFAN, all essential models have been incorporated into ATHLET). The official comparison reports acknowledge the high quality of the obtained results and good agreement with experimental data compared with other computer codes. All ISP participations using ATHLET/DRUFAN are given in Tab. 3.2.

Tab. 3.2 Participations with ATHLET / DRUFAN in OECD/NEA/CSNI International Standard Problems

ISP	Facility	Country	Year	Subject	Program	Ref.
1	Edwards' Pipe	UK	1975	Discharge, pressure waves	DRUFAN-01	/GAR 73/
6	Battelle	Germany	1979	BWR steam line break	DRUFAN-01	/WIN 78/
8	Semi-scale	USA	1979	LB LOCA	DRUFAN-01	
11	LOFT	USA	1984	SB LOCA	DRUFAN-02	
13	LOFT	USA	1984	LB LOCA	DRUFAN-02	/BUR 79/
18	LOBI	EC	1987	SB LOCA	DRUFAN-02	/STÄ 84/
26	ROSA-IV-LSTF	Japan	1989	5% SB LOCA	ATHLET 1.0/FLUT N081)	/KUK 92/
27	BETHSY	France	1991	0.5% SB LOCA with AM	ATHLET 1.0/FLUT N081)	/CLE 92/
33	PACTEL	Finland	1994	VVER Natural Circulation	ATHLET 1.0	/PUR 94/
38	BETHSY	France	1996	Mid-Loop Operation	ATHLET 1.1	/LAV 95/
50	ATLAS	Korea	2010	50 % Break of DVI Line	ATHLET 2.2A	/CHO 12/
51	ACME		2019	2-inch SB LOCA	ATHLET 3.3	/GUO 22/

The OECD/CSNI International Standard Problems focussed on the investigation of the thermal-hydraulic phenomena appearing in western type of NPPs. For the analysis of phenomena and processes related to NPPs with Russian design, several experiments

of VVER integral test facilities have been declared as Standard Problems. In Tab. 3.3 a list of VVER-related Standard Problems calculated with ATHLET is given.

Tab. 3.3 Participations with ATHLET / DRUFAN in IAEA International Standard Problems for WWER

SP	Facility	Country	Year	Subject	Program	Ref.
SPE-4	PMK-2	Hungary	1993	SB LOCA, sec. side feed and bleed	ATHLET 1.1	/IAEA 95/
SSP-1	ISB	Russia		SB LOCA	ATHLET 1.1	/EREC 95/
SSP-2	ISB	Russia		Intermediate break LOCA, no HP inj.	ATHLET 1.1	/EREC 97/
SSP-3	ISB	Russia		Intermediate break LOCA, with HP inj.	ATHLET 1.1	/STE 99b/

4 Quality Assurance Procedures

The main objective of ATHLET development is providing a simulation code that can be used for deterministic safety analyses of nuclear facilities and to support safety cases submitted to a nuclear regulator. Such a code has to meet some high-level requirements, which are formulated in applicable regulation. Experts validating ATHLET should be aware of the overall requirement in IAEA GSR Part 4, Requirement 18: “Any calculational methods and computer codes used in the safety analysis shall undergo verification and validation.” /IAEA 16/, p. 26. Further guidance on quality assurance and the verification and validation of system codes can be found in IAEA SSG-2, Rev. 1, section 5 /IAEA 19/. It is recommended to read this section carefully. In addition, there are applicable norms, e.g. ISO/IEC 90003:2018 or ISO/IEC 25010:2011 and good practices for software development in the nuclear field like e.g. /ODA 00/. Validation of models and software used in the safety assessment of nuclear facilities is required by applicable national regulation in numerous countries, e.g. Germany /SIA 15/, France /ASN 17/, Russia /ROS 12/, Spain /CON 98/, U.K. /ONR 19/, and U.S.A. /NRC 05/. Therefore, the validation of ATHLET summarized in this report is an essential part of the overall quality assurance process for ATHLET development.

The software development process implemented at GRS has been defined against this background. Fig. 4.1 below gives an overview of the process. ATHLET is part of the overall AC² development performed at GRS. Therefore, the AC² quality management approach is fully applicable to ATHLET. In short, the process defines the following phases for the actual development process, explained here for a new feature:

- **Design**: Specification of the feature and definition of an implementation, verification, and validation plan
- **Implementation** of the feature in the source code
- **Verification** of the feature with appropriate unit-tests and simple test cases accompanying the development
- **Validation** of the feature against suitable experiments, where the new feature will have a relevant impact, and validation against the set of standard validation cases for ATHLET.

A more detailed description of the ATHLET development can be found in the ATHLET Programmer's Manual. In this section, the aspects of the overall quality assurance process relevant for validation are explained in more detail.

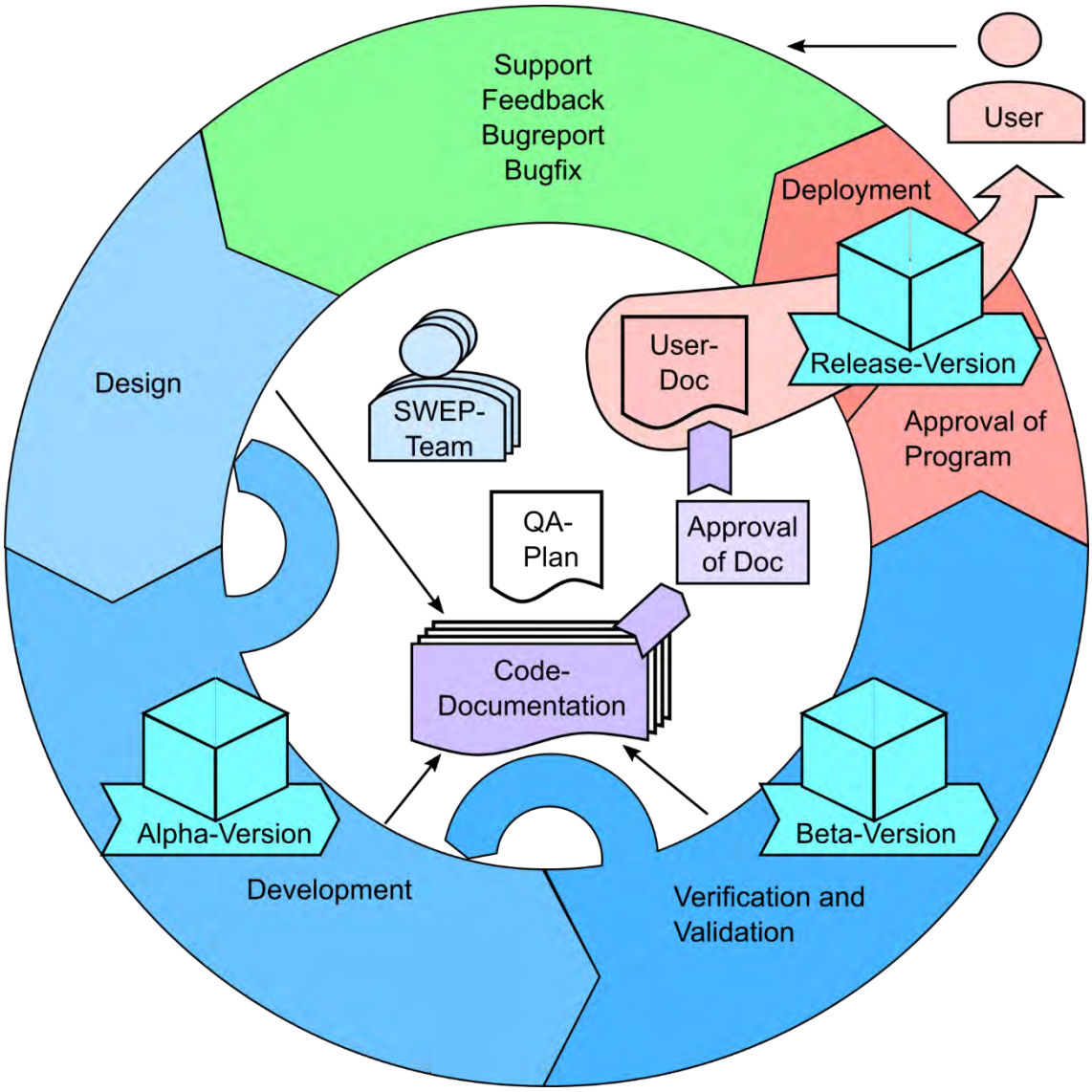

Fig. 4.1 Software development process at GRS /GRS 21/

The **validation** of ATHLET is based on the validation matrices described above. GRS is continuously performing validation of ATHLET both against new test data, standard validation cases and by performing non-regression testing via continuous integration (CI) via the GitLab server operated by GRS. Different to SSG-2, Rev. 1 /IAEA 19/, comparison on ATHLET results against simple basic tests, e.g. single CV simulation models, and checking that the simulation results conform to specified solution, is assigned to the verification phase as it properly happens during code development and implementation. Consequently, ATHLET validation entails SET, IET and plant transients.

There are two main approaches for validation used for ATHLET:

1. Simulating an experiment or a plant transient with ATHLET and comparing the code results against available **measurement data**. Using expert judgement, it is then concluded if the validation calculation was successful or not, if there are any issues with code performance and predictiveness, and if there are any residual matters.

2. Comparing ATHLET results **against other codes** (system codes or CFD codes) for a benchmark case with clearly specified geometry, initial and boundary conditions. Again, using expert judgement, it is then determined if ATHLET adequately simulates the scenario, if deviations between the codes are significant and if there are any indications for a code weakness that need to be addressed.

Obviously, validation against actual plant data and experiments should be preferred over code-to-code validation when feasible. Nonetheless, code-to-code comparisons and benchmarks are informative as to the overall performance of system codes and the models used therein.

Whenever feasible, validation should be performed by **independent experts**, i.e. experts not directly involved in the development and implementation of a new feature or model. The validation by GRS will provide some independent validation for new developments eventually, but this aspect should be addressed in the validation plan. Also, validation and plant transient simulations should be done by experts, who are sufficiently familiar with the code, the relevant phenomena, and the reactor technology the validation case applies to. Support from experienced supervisors should be available. This is important for two reasons, firstly for setting up an adequate input deck for the validation case, and secondly for making appropriate expert judgements on the validation results. Moreover, an in-depth understanding of ATHLET models (see the Models and Methods report) or access to the source code will be helpful, particularly if the ATHLET calculation does not arrive at the intended result. For code validation external to GRS, particularly in academia, acquiring the necessary **skills** and **experience** might not always be easy. As GRS supports external validation activities, there are firstly ATHLET trainings offered by GRS available to ATHLET users. Moreover, if external validation activities have been discussed with and endorsed by the ATHLET validation team in advance, GRS validation experts can give advice and support during such activities.

One further important element of **external validation** should be done by code users who apply ATHLET for deterministic safety analyses of nuclear facilities. The input deck for a

nuclear facility should be qualified against suitable commissioning, normal operation and observed transient data /IAEA 19/. Consequently, such **plant model qualification** tests should be run also whenever a new release version is applied for safety analyses. Assessing qualification tests results obtained with the new release against previous code versions and available measurement data allows to identify problems in the input deck or in the code. In the latter case, please inform GRS about the issue.

When deciding on **validation cases** to be investigated for ATHLET, the following aspects should be considered:

- The validation case targets one or more models or features recently added to the ATHLET master or release version.
- The validation case is new and has not yet been performed for ATHLET. Also, if the last validation is older than 10 years, a repetition with the recent version is generally sensible.
- The validation case is part of an international benchmark.
- The geometry and the conditions in the test facility are representative of an actual nuclear facility (minimisation of scaling distortions).
- The test facility description is comprehensive and sufficiently detailed for the development and qualification of a detailed ATHLET model.
- The measurement values are of adequate resolution and accuracy for the quantities of interest, the test instrumentation is sufficiently detailed.
- The validation case is suitable for derivation of uncertainty ranges.
- The validation case is suitable for integration into CI on GitLab.

Obviously, ATHLET should be capable of actually performing successfully in the intended validation. It would, e.g., be futile to try to validate ATHLET for the detailed prediction of flow and temperature fields on a sub-channel level, for two-phase flow in microchannels, or for water ingress into the hot core of a gas-cooled reactor with graphite-coated fuel pebbles – in all these cases ATHLET lacks important models and will not be able to achieve the validation results with sufficient precision.

The ATHLET validation matrices are based on a large set of tests, some of which are publicly available, and some are subject to confidentiality agreements. For obvious

reasons, validation should preferably be done against test results, which are publicly available. Still, GRS is always interested in further validation of its codes. Consequently, if you are interested in contributing to the external validation of ATHLET in the framework of research and education, please contact the ATHLET validation team as to the availability of GRS validation input decks. Conversely, if you want to validate ATHLET against new and or confidential experiments not yet in the ATHLET validation matrix, please contact the ATHLET validation team as well. As GRS is interested in keeping validation cases available, transferring the input deck and validation data to GRS should be explored.

When performing a validation calculation for ATHLET, it is important to clearly define the **scope** of the validation. The following points need to be taken into account.

- Identify the relevant phenomena for which ATHLET is to be validated specifically and derive the relevant model outputs and related measurement data on which ATHLET performance will be judged as a **figure of merit**.
- Derive the **nodalisation** required for ATHLET to adequately simulate the facility and the phenomena of interest. Determine if nodalisation studies need to be performed as part of the validation.
- Identify the ATHLET models to be varied as **sensitivity cases** for the validation calculation. This should include a comparison of existing ATHLET models vs. a new implementation, but should also consider, e.g., 5-equation model vs. 6-equation model thermal hydraulics or standard numerics vs. usage of NuT, etc. as applicable and sensible.
- Check, if during the course of the test and/or for the ATHLET simulation the occurring states likely are at or near bifurcation points or more complicated attractors for topologically distinct regions in the phase space of the test (i.e., so-called **cliff-edge effects** are relevant). At least in such cases, performing an **uncertainty analysis** with the GRS method /GLA 08a/ should be seriously considered, if feasible. For that, the sample size should be chosen so that several figures of interest can be controlled simultaneously and/or the rank order is comparatively high so that percentiles are better determined.
- Determine the necessary sensitivity cases on simulation model **stability** and **convergence**, e.g., by varying integration settings like `EPS`, `GRESCH`, `HMAX`, or the `FCLIMx` settings under `CW INTEGRAT`. Similarly, determine if both **serial** and

parallel program versions should be applied and if different settings for NuT should be used during the calculation.

- If applicable, define **restart** points at which the consistency of a restart with the reference calculation can be checked.
- Define acceptance criteria on **mass errors** (both overall as well as for short time periods) as computed by ATHLET under the `TFDGENERAL` output.
- Discuss with the ATHLET validation team if the validation case should be prepared for use in the **CI** under GitLab.

The validation calculation should be done based on this scope. The input deck should be refined until either a good agreement of test data to ATHLET predictions is reached, or a conclusion is reached that ATHLET is not adequately simulating the test in question. While grid-convergence is not applicable to a 1D system code as understood for CFD-codes because the 1D models are often not scale- and/or nodalisation-independent (including for multi-channel representations), it should be checked if the code prediction is at least qualitatively stable under refinements of the nodalisation by increasing the number of CVs in relevant TFOs. In all of this, however, changes to the validation input deck should be limited to those that firstly are necessary to capture the **relevant phenomena** of the scenario and that secondly are realistically **applicable to nuclear reactor and facility** input decks. Increasing the resolution of the nodalisation or fine-tuning several of the model parameters accessible via the input away from default values can serve a valid purpose in the context of validation. These would include derivation of nodalisation recommendations, analysing limits and predictiveness of ATHLET models, deriving improvements to existing models, and identifying the need for new models and features. However, for applications where experimental data are missing, such refinements would either not be possible, lead to unreasonable simulation times, or might even lead to the suppression of valid code predictions not in line with user expectations and should therefore be avoided. Consequently, validation calculations should be done with models that are comparable to models used in safety analyses.

Another important question is which ATHLET **version** should be used for validation calculations. The following rules are applicable generically, but for a specific case the ATHLET validation team might decide to select a different version for the validation.

- Validation should support the on-going development in a timely manner. Consequently, validation should be performed on adequately stable feature branch or

master versions as foreseen in the validation plan of a new development. As these are **alpha versions** of ATHLET, the selection of specific versions as a basis for validation requires coordination between the development and validation team. Similarly, regular non-regression testing via CI should be performed on the master branch and possibly long-running development branches.

- Validation in support of a release obviously needs to happen on the designated **beta versions** defined by the ATHLET development team.
- Participation in **code benchmarks** or similar activities should be done with release versions. If necessary and sensible, a beta version might be used, if agreed to by the ATHLET validation team.
- **External validation** activities should generally use release versions, unless in support of own or shared developments.

Finally, **non-validation applications** should generally only be done with release versions. This does apply to safety research as well as input model qualification and improvement unless such activities are included into the validation activities for the current development by the ATHLET validation team. Application of ATHLET for **safety analyses in support of safety cases** should only be done with release versions. Please note relevant good practice as described in IAEA SSG-2, Rev. 1, for the use of computer codes in safety assessments /IAEA 19/. Importantly, in addition to qualifying the input deck you should consider validating the release version of ATHLET for your purposes against suitable qualification tests for your model.

4.1 Validation supported by GitLab

It is good practice that input decks used for validation are subject to version control, they should therefore be managed via git and/or GitLab. In the Programmer's Manual /JAC 23/, a more detailed explanation for using GitLab when developing for ATHLET is given. The process described can be transferred to validation work. This is why this section only gives additional guidance relevant specifically to validation calculations.

For each facility, a separate project should be created under GitLab. As facilities might change significantly over the years, it might be necessary to define several projects corresponding to the major configurations or evolutions in a facility. In the project for a facility, a base input deck should be stored. The base input deck should describe the whole

geometry of the facility. Configuration variants should also be included in the input deck as practicable. Usage of parameters will facilitate configuration control for the base input deck. Changes to the base input deck should be checked using CI under GitLab. The actual tests should be variants of the base input deck. They can be generated using the `INCLUDE` directive in the input deck. For this to work smoothly, the base input deck might have to be split in several files as well. Input decks for specific tests can be stored either in the repository (and thus project) of the base input or they are placed in their own repository.

The base input deck should be qualified against suitable steady state commissioning tests and simple test data for the facility, if available. These tests should be included in the CI for the validation project and should be regularly checked to ensure consistency of the base input deck. The test-specific input decks should – to the extent possible and sensible – utilize ATHLET parameters (under CW `PARAMETERS`) and tables (under CW `TABLES`) to set the initial and boundary conditions for a test. Using separate files for the `TOPOLOGY` section and the list of HCOs under CW `HEATCOND` allows for effective configuration control. This might have to be complemented by separate files at least for sections of the GCSM input (e.g., if process signals are no longer available for certain configurations). If changes to the test-specific input decks are pushed to GitLab, it should at least be checked if the input deck still starts the transient phase via CI. While it is possible and for some sensitivity cases perhaps even comfortable to use interactive simulation via ATLAS, this is not recommended for baseline validation cases, because interactively defined simulations might not be fully reproducible using the available input data.

The workflow for validation should be defined under GitLab using **issues** and – if available and sensible – epics. Relevant changes to an input deck should be covered by issues so as to be traceable. Again, **merge requests** should be derived from issues under GitLab whenever sensible. Similar to code development, it is sensible to use feature branches to improve or change an input deck. A review of input deck changes might be required by the ATHLET validation team before merging it into the master. In any case, the input deck changes should only be merged if a (full) validation simulation has been successfully performed as documented in GitLab. A review of changes to the base input deck by a second expert might be sensible. Moreover, changes to the base input deck should be merged only after testing them against several of the specific validation cases, as applicable and agreed with the ATHLET validation team. To the

extent feasible, CI under GitLab should be used to perform these confirmatory calculations.

4.2 Documentation of Validation

As validation calculations produce a considerable amount of output data, it is not feasible to store artefacts of non-essential calculations on GitLab in the long-term. Similarly, it will not be practicable to document simulation results comprehensively in a GitLab issue. For this reason, dedicated validation should be documented in a separate report. Depending on the level of detail required for the documentation, GRS uses technical notes, technical reports, and GRS-reports for documentation. Publication of results in a scientific journal or as a conference contribution is also a valid means of documentation and generally encouraged. For any documentation of validation results, respect good scientific practices as, e.g., formulated by the Deutsche Forschungsgemeinschaft /DFG 21/.

As to the documentation of validation, the following needs to be considered.

- The base input deck and its main configurations for specific validation tests should be described in a separate **input deck description** report. This report will often not be published in full. It should be quite detailed so that other experts can understand the rationale in setting up the input deck, the information it is based on, its nodalisation, any simplifications and important modelling choices, the configuration of the GCSM model as well as the usage of the input deck to perform specific validation calculation. The input deck description should include the results of qualification calculations. The report should be maintained and updated to the current status of the base input deck as soon as a result obtained with the input deck is published (in a journal, conference or as part of code documentation for a release or patch).
- The original **sources** used to develop the input deck, setting up the initial and boundary conditions and the sources for the experimental data have to be cited. See also /DFG 21/. Copies of the referenced publications should be put on file (depending on the rights to these publications either as hard copies or as electronic copies) as part of the supplementary documentation for ATHLET validation. For experimental data, designated storage location should be used, as determined by the ATHLET validation team. If data subject to **non-disclosure agreements** are used, this should be clearly stated, and the report should be marked accordingly.

- The validation report should include a brief description of the **facility**, the specific **test** under investigation, its realisation in the facility, and the main **test results**. It should also include a brief description of the ATHLET **simulation model** used for the validation, the settings used for **initial and boundary conditions** as well as relevant **sensitivity cases**. The **version** of ATHLET used for validation should be specifically stated. Similarly, additional **plugins**, particularly user-supplied ones, or **other changes** compared to a release version have to be explained.

- The report should compare the results of the ATHLET simulation to measured values or other code results. Comparisons should be done on a carefully selected set of quantities (**figures of merit**) that allow judgements as to the quality of ATHLET's prediction. Such results should be presented in tables and/or figures (for time series). The report should discuss the results and provide conclusions on the **quality of prediction** as well as the need for improvements in the code or the input deck. In case there are issues with ATHLET's predictiveness, possible root causes in ATHLET models or the ATHLET source code should be identified.

- Analogously, results of **sensitivity cases** should be presented with the informative comparisons between reference calculation and experimental values.

- When evaluating results, the report should consider the implications of **scaling**. As most test facilities are scaled down (geometrically, but also regarding pressure, temperature, etc.) compared to actual nuclear reactors and as ATHLET models are optimised for reactor conditions, scaling distortions need to be analysed when judging the quality of ATHLET predictions.

- The **numerical performance** of the validation calculation should be investigated and discussed in the report. This should – at a minimum – include an evaluation of integral CPU use and the investigation of time step size. Notable and prolonged intervals of low time step size should be discussed.

- If reasonable and applicable, the consistency of **restarts** to the reference calculation should be demonstrated for a small set of restart points.

- In connection to numerical performance, the **mass errors** for working fluids and non-condensable gases in the different fluid systems of the facility should be analysed and discussed. Notable changes in mass error (e.g., steep jumps) should be discussed in relation to time step size behaviour and physical processes during periods of interest.

- If applicable, the report should draw conclusions as to the range of **uncertainty** of ATHLET predictions as well as model input uncertainties. This is particularly relevant, if results of an uncertainty analysis are discussed as part of the validation.
- The report should formulate **conclusions** and **recommendations** both for the further **development** of ATHLET as well as for the **application** of ATHLET (e.g., nodalisation guidance) for test facilities and particularly reactor applications.
- Remaining **residual matters** should be clearly identified and documented.

A formal validation report should be reviewed by a second experienced expert before it is finalised and filed or published. Some of the above can be relaxed or omitted as determined by the ATHLET validation team on a case-by-case basis. For external validation activities, please contact the ATHLET validation team for further guidance on validation documentation.

4.3 Release Procedures

The overall release procedure for ATHLET (and also AC²) is described in the ATHLET Programmers Manual. The following is therefore restricted to the specifics for the validation of ATHLET prior to a release.

Before the release of a new ATHLET version, either as a general release or as an internal release (some patch versions are available only within GRS), a set of experiments from the validation matrices is calculated to check the overall capability of the new code version as the final step of the overall quality assurance process. These tests consist of:

- samples (standardized calculation examples) provided with ATHLET,
- relevant separate effects tests, and
- the 'basis' validation cases.

The use of samples and separate effects tests depends on type and scope of changes in the code between two releases (particularly for patch releases). The selected test cases ensure that changes applied to solve one modelling problem do not affect other individual models or the overall simulation capability in an unacceptable manner. A further intention is to compare the results of the new version with those of earlier versions.

For beta versions designated from time-to-time by the ATHLET development team for the used in specific research projects, an analogous but even more simplified process is applied. Relying on the CI performed on the master und GitLab and considering dedicated verification and validation results performed on alpha versions, it can be concluded in specific cases that a certain tagged commit in the master can be used as a beta version.

The set of basis validation cases consists of 4 integral tests, which cover a wide range of thermal-hydraulic phenomena applicable to safety analyses for nuclear reactors. These tests run automatically on the CI server if commit of the source code is done by the code developer:

PWR tests:

- LOFT LP-LB-1 (200% break in cold leg, cold leg ECC water injection)
- LSTF-SB-CL-18 (5% break in cold leg, cold leg ECC water injection)

BWR tests:

- ROSA III-916 (50% break in recirculation line)

VVER tests:

- ISB-WWER SSP 2 (rupture of one UP ECC injection line)

In addition to the comparison with the experimental data, three kinds of tests are performed on several validation calculations:

- restart tests,
- optimization tests, and
- check of portability.

The restart capability is checked to ensure that all necessary data are stored in the restart file. Usually, a validation calculation is performed in one run, with one or more restart time points defined during the transient. Afterwards, a restart time point is selected, and a restart run is per- formed. The code must continue the calculation after a restart with identical results in comparison to the original run, if the input is not changed. (Note that

adding or removing a restart point can sometimes unavoidably lead to changes in results, as restart points influence time step size shortly before they are reached.)

ATHLET can be executed in parallel mode utilizing several CPUs sharing a common memory (SMP computer architecture). This parallelization is based on the OpenMP standard. Parallel ATHLET simulations must provide results which are identical to those achieved with serial applications. Moreover, data conflicts like race conditions must be reliably avoided. These requirements are periodically proven through the comparison of appropriate test cases.

Most of the FORTRAN compilers available on different platforms offer several levels of compiler optimization. Optimization is a valuable tool to improve runtime performance, i.e., to reduce the computational time for a given code application. Some options, like loop optimizations or inlining, can affect processing sequences and can cause significant deviations of calculated results. The adopted procedure for ATHLET is to run one or more validation calculations on a given platform with the debug option (no optimization) of the corresponding compiler, and then to repeat the calculations with the optimization level recommended for the applied compiler (default). Both calculations must produce quasi-identical results (unless the case is at or near an attractor for a cliff-edge effect, see above). Eventual noticeable deviations are investigated thoroughly. They can indicate incorrect programming, or even compiler malfunctions. Some examples have been reported in /TRA 97/.

One main feature of ATHLET – including its tools – is the that it can be run under Windows as well as Linux. Prior to a code release, a subset of test cases is run on reference Windows and Linux distributions at GRS. Code results between Linux and Windows versions have to be quasi-identical as well. Similarly, the whole AC² distribution including the tools provided therein is tested on these platforms.

5 Selected Validation Calculations for the Current Code Version

This chapter presents the analyses of the integral experiments included in the base validation matrix. These examples cover a wide range of thermal-hydraulic phenomena and give an insight into the actual performance of the current code version when applied to new challenging experimental findings.

At present, the following calculations are included in this chapter:

- LSTF Run SB-CL-18
- ROSA III - Run 916
- LOFT LP-LB-1
- ISB Test SSP-2
- PERSEO Tests 7 and 9
- EASY-4
- Selected reflooding experiments (FEBA, FLECHT, PERICLES)
- Mantilla 2-inch and 4-inch tests
- TPTF 8-inch and 4-inch tests

The test facilities cover a (volumetric) scaling range from 1:3000 up to 1:50. The post-test calculations include the simulation of an ATWS transient, three small break calculations for three different reactor types (PWR, BWR and VVER), and a large break LOCA simulation. Both the 5-eq. and the 6-eq. model as well as the local and integrated mass and momentum balance method are applied. In some cases, models are applied even if the related physical process does not appear in the experiment or has no measurable effect on the results - provided the calculated results are not affected. With this, the applicability of these models and the plausibility of the results shall be proven.

Besides that, several code features are applied for these calculations, amongst others:

- one-dimensional modelling of the break region for the calculation of the critical discharge rates,
- mixture level tracking model,
- quench front propagation model,
- simulation of non-condensable gases,
- entrainment.

A detailed list of the model options applied for the individual calculations is given in the corresponding sections below.

5.1 LSTF Run SB-CL-18

5.1.1 Test Facility

The LSTF (Large Scale Test Facility) is a 1:48 volumetrically scaled model of a Westinghouse-type 3423 MW_t four loop PWR. The LSTF facility has the same major component elevations as the reference PWR to simulate the natural circulation phenomena, and large loop pipes (hot and cold legs of 207 mm in diameter) to simulate the two-phase flow regimes and phenomena of significance in an actual plant. The LSTF equipment can be controlled in the same way as that of the reference PWR to simulate long term operational transients. Furthermore, LSTF is designed to be operated at the same high pressures and temperatures as the reference PWR.

Fig. 5.1 and Tab. 5.1 show the structure and major dimensions of the LSTF, respectively. The four primary loops of the reference PWR are represented by two equal-volume loops. A detailed LSTF system description is presented in /JAE 85/.

The hot and cold legs are sized to conserve the volume scaling and the ratio of the length to the square root of pipe diameter L/D 0.5 for the reference PWR in expectation that the flow regime transitions in the primary loops can be simulated appropriately by taking this scaling approach.

Over 2500 instrumentation locations are available for making various types of measurements in LSTF. Most numerous (about 70 %) are the thermocouples that measure the fluid (TE) and wall (TW) temperatures and temperature differences (DT). There are also about 400 conduction probes (CP) distributed throughout the primary and secondary systems, which indicate the presence or absence of liquid or vapor. Other conventional instruments include, amongst others, pressure (PE) and differential pressure (DP) transducers, liquid level meters (LE) based on differential pressure measurements, and flow meters (FE) using an orifice, venturi nozzle or simple nozzle. Advanced two-phase flow instruments include drag discs (MF) and three-beam gamma densitometers (DE) for measurement of momentum flux and fluid density, respectively.

Tab. 5.1 Major design characteristics of LSTF and PWR

	LSTF	**PWR**	**PWR/LSTF**
Pressure(MPa)	16	16	1
Temperature(K)	598	598	1
No. of fuel rods	1064	50952	48
Core height(m)	3.66	3.66	1
Fluid volume V(m^3)	7.23	347	48
Core power P(MW)	10	3423(t)	342
P/V(MW/m^3)	1.4	9.9	7.1
Core inlet flow(t/s)	0.0488	16.7	342
Downcomer gap(m)	0.053	0.260	4.91
Hot legD(m)	0.207	0.737	3.56
L(m)	3.69	6.99	1.89
$L \cdot D^{-0.5}(m^{-0.5})$	8.15	8.15	1.0
$A \cdot L(m^3)$	0.124	2.98	24.0
No. of loops	2	4	2
No. of tubes in steam generator	141	3382	24
Length of steam generator tube (average) (m)	20.2	20.2	1.0

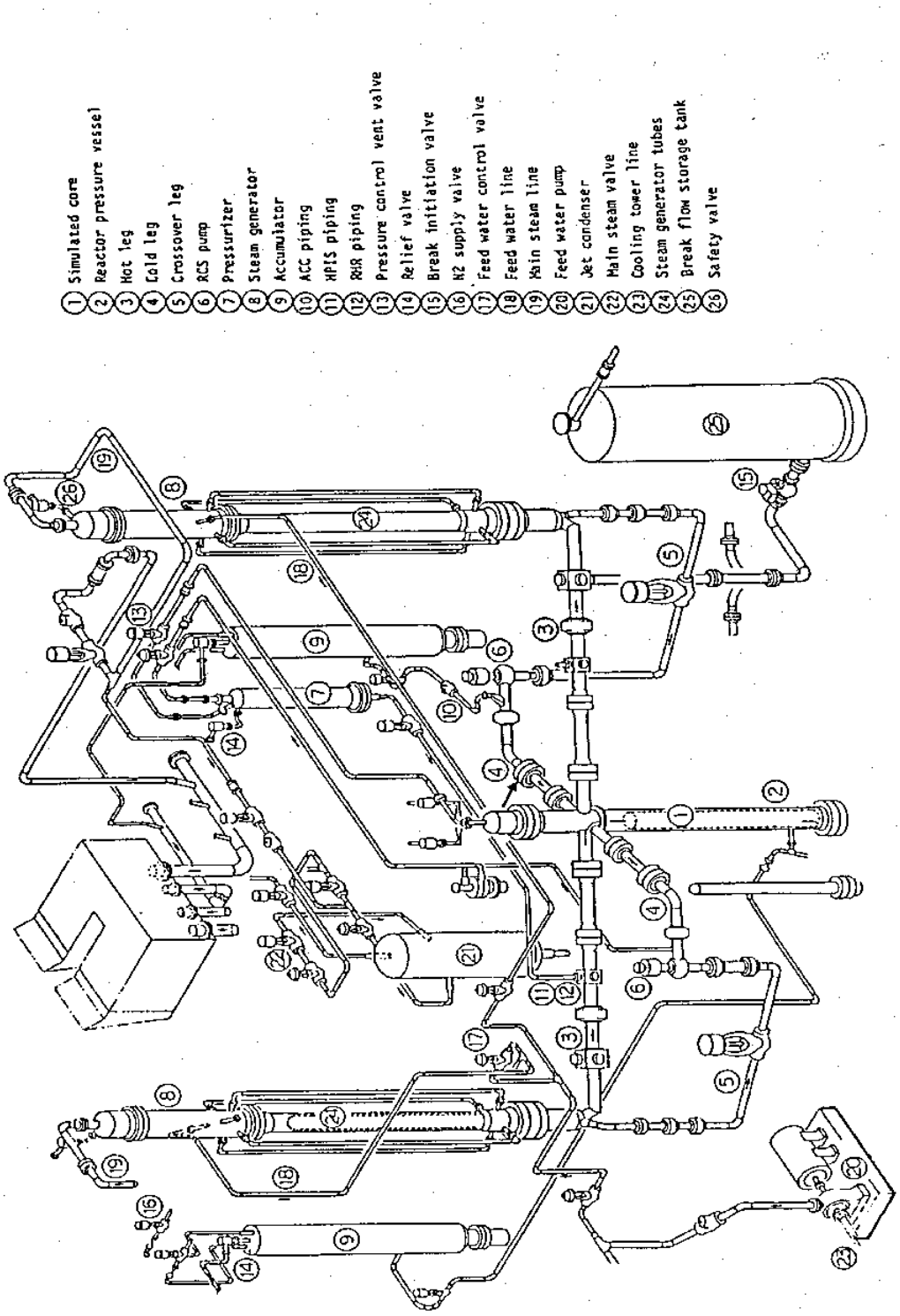

Fig. 5.1 General overview of LSTF /JAE 89a/

5.1.2 Test Conditions and Conduct

The major initial conditions of the LSTF 5 % cold leg break test, Run SB-CL-18, and a detailed description can be found in /JAE 89a/.Both the initial steady state conditions and the test procedures were designed to minimize the effects of LSTF scaling compromises on the transients during the test.

The most important design scaling compromise is the 10 MW maximum core power limitation, 14 % of the scaled reference PWR rated power. The steady-state condition is restricted to a core mass flow rate that is 14 % of the scaled value, to simulate the reference PWR temperature distribution in the primary loop. The desired primary coolant flow rate was established by reducing the pump speed with the flow control valves in the cross-over legs fully open. The primary loop flow rate was then increased at the time of break to improve the similarity of the LSTF to the reference PWR by increasing the pump speed.

The primary-to-secondary heat transfer must also be maintained at 10 MW, i.e., 14 % of the scaled value. Since the LSTF steam generators are geometrically scaled to the reference PWR, the 14 % primary-to-secondary heat transfer rate is established by raising the secondary temperature such that the primary pressure and temperature are representative of the reference PWR.

Major operational set points and conditions including emergency core cooling system (ECCS) actuation logic for this test are shown in /RIN 90/.

After the break occurred at time zero, the primary system depressurizes quickly. At a pressurizer pressure of 12.97 MPa, the reactor scrams. Loss of offsite power concurrent with the reactor scram is assumed and the primary coolant pumps are tripped to begin coast down and the core power begins to decrease along the pre-programmed decay curve. The power decay curve used in the test takes into account the actinides and delayed neutron effects and gives a slower decrease than the ANS standard. The SG auxiliary feedwater is assumed to fail to simplify the transient.

At a pressurizer pressure of 12.27 MPa, the safety injection signal is sent that trips ECCS to be actuated at respective pressure set points. However, the high-pressure charging system and the high-pressure injection system are assumed to fail in the test. The accumulator system and the low-pressure injection system (LPIS) are specified to initiate

coolant injection into the primary system at pressures of 4.51 and 1.29 MPa, respectively. The accumulator-cold system injects into the cold leg A and the accumulator-hot system into the cold leg B. The water temperatures of ACC-cold and ACC-hot tanks are the same and the ratio of accumulator injection flow rate into cold leg A and into cold leg B is 3:1. This injection method is adopted for good simulation of ECC injection flow rate to each cold leg in the LSTF.

The break point is located in the loop B cold leg (loop without the pressurizer) between the reactor coolant pump and the reactor pressure vessel. The break orientation is horizontal.

5.1.3 Input Dataset

5.1.3.1 Nodalisation

Fig. 5.3 and Fig. 5.4 show the nodalisation used for the ATHLET analysis of the LSTF SB-CL-18 test /RIN 90/. Except for the fuel rods, the heat conduction volumes for the simulation of the facility structures are not included in these figures. The nodalisation includes the following numbers of network elements:

CVs for primary system:	543
CVs for secondary system	26 (each loop)
CVs for emergency cooling system	14
Junctions in total	741
ODEs for thermo-fluid dynamic	3154
Heat conduction volumes	512
ODEs for heat conduction	2076

Thermo-fluid objects

The following aspects were considered for the choice of nodalisation of the fluid system /RIN 90/:

Core

The simulation of the partial dry-out required a fine axial division of the core. The level of division is matched to the axial core power distribution (19 CV with 203 mm length). The

core consists of rod bundles of three different performance classes: Mean (M) with 100% nominal power, Low (L) with 66% nominal power, and High (H) with 151% nominal power (see positions in Fig. 5.2 a). A one channel modelling of the core turned out to be not sufficient. The used five channel representation enables the simulation of the inhomogeneous fluid conditions in the core in a more realistic way. Fig. 5.2 b) shows the modelling of the core. One channel represents the middle-powered channels (PV-COR-Av). To simulate the influence of the two loops on the core, there are two channels representing each remaining performance class: The high-powered channels (PV-COR-HA and -HB) and the low-power channels (PV-COR-LA and -LB). An exchange between these channels is considered via cross connection objects (PV-CORE-CC1 to -CC6). The form loss coefficient for cross flow through tube bundles was calculated with correlations from the VDI Heat Atlas /VDI 10/.

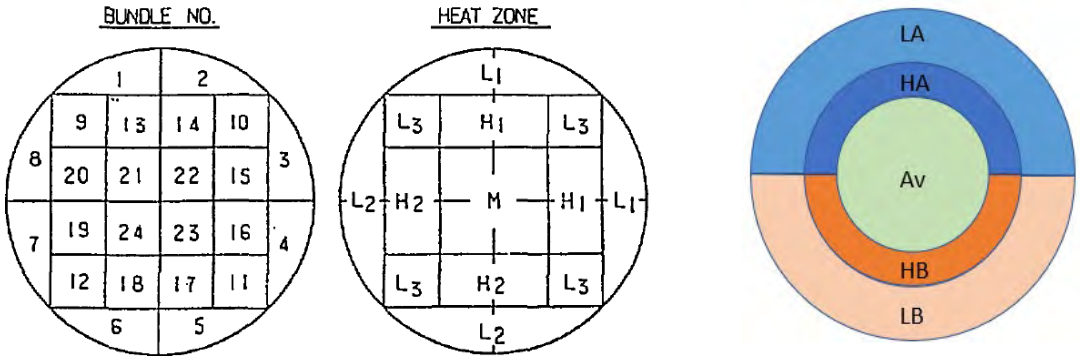

a) b)

Fig. 5.2 Fuel bundle performance distribution in a) the facility /JAE 89a/ and b) the ATHLET input deck

Core bypasses

In the LSTF facility, three core bypasses exist which promote the pressure balancing between the upper plenum and the downcomer:

a) Upper head bypass
This bypass carries nominally 0.3 % of the core mass flow via 8 spray nozzles and the control rod tubes (TFOs PV-DC-A-4, -B-4 and PV-BYP-UHI, -UHO).

b) Upper downcomer - upper plenum bypass
This bypass has no matching part in the Westinghouse reactor. It is an undesired leakage of the LSTF facility. The flow area is unknown. It depends on the thermal and mechanical load of the vessel. From JAERI specification, a bypass mass flow of

0.085 % of the nominal core mass flow is used here for the calculations (TFOs PV-BYP-DCA and -DCB).

c) Downcomer - hot leg bypass
This bypass carries nominally 0.1 % of the core mass flow and simulates the reactor bypass at the breakthrough of the hot leg through the downcomer (TFOs PV-BYP-HLA and -HLB).

Downcomer

To consider the asymmetric cold leg ECC injection and the influence of the break location, the downcomer is split into two parallel channels (PV-DC-A-x and -B-x) interconnected via the TFOs PV-DC-CC-x.

Control rod guide tube

The control rod guide tubes connect the upper core with the upper head. There is only a small flow during normal conditions. However, during the transient, the pressure in the upper head is released. The correlated TFOs PV-BY-Av-2, PV-BY-HA-2, PV-BY-HB-2, PV-BY-LA-2, PV-BY-LB-2.

Circuits

The bends in the circuit are flow limiting cross-sections. Correct modelling of the counter current flow limitation requires a detailed nodalisation of the elbow in the hot leg and in the pump seal. The flow channel in the main coolant pump is modelled in a sophisticated manner in order to simulate the overflow baffle of the pump case. This baffle enables the swell of emergency cooling water at the cold side of the leg.

U-tube steam generator

A difference in the behaviour of the long and the short U-tubes is observed in the experiment. The U-tubes are modelled by two channels accounting the results from the experiment. The SG inlet and outlet plena are nodalised considering the strong differences in the cross sections. The cross sections in the main coolant pipes, the SG plena, and the U-tube bundles are related like 1.0 : 6.1 : 4.6. The SG plena represent a strong cross

section increase and a distinctive phase separation can be expected. A splitting of the SG plena into 4 parts is used to get a realistic mass distribution.

Pressurizer

The pressurizer is heated with a PI-controlled heat source. The heating stops after the break occurs.

Upper head

The upper head is heated with a PI-controlled heat source. The heating stops after the break occurs.

Upper downcomer - upper plenum

A fine nodalisation is applied for the realistic modelling of the bypass in this part.

ECC piping

The fluid temperatures in the ECC injection nozzles indicate that, before the ECC injection started, the ECC water in the injection lines was considerably warmer than the accumulator water. Therefore, the injection lines are sub-divided into 5 CVs and a linear initial temperature profile is specified to approach the measured temperature time history.

Upper plenum interior (Heat conduction objects)

There are HECU components representing the control rod guide tubes, the support columns, and the upper core support plate. The interior of the control rod guide tubes consisting of control tubes and spacer are not modelled.

Heater rods

The radial power distribution of the heater rods is represented by three different groups of heater rods:

360 rods	14118 W	radial peaking factor 1.51
180 rods	9350 W	radial peaking factor 1.00
524 rods	6171 W	radial peaking factor 0.66

These heater rods are distributed to the two core channels according to the radial power distribution in the core (HCOs `HPV-CORI-x` and `HPV-CORO-x`). Every heater rod HCO is sub-divided into 9 HCVs.

Steam generator U-tubes

The 151 U-tubes of one SG are sub-divided into two groups representing 57 long and 84 short U-tubes, each with 14 HCVs and 12 HCVs, resp.

Structures

The major wall and internal structures of the reactor vessel, coolant pipes, pressurizer, and the steam generators are represented by HCOs, considering the heat losses to the environment

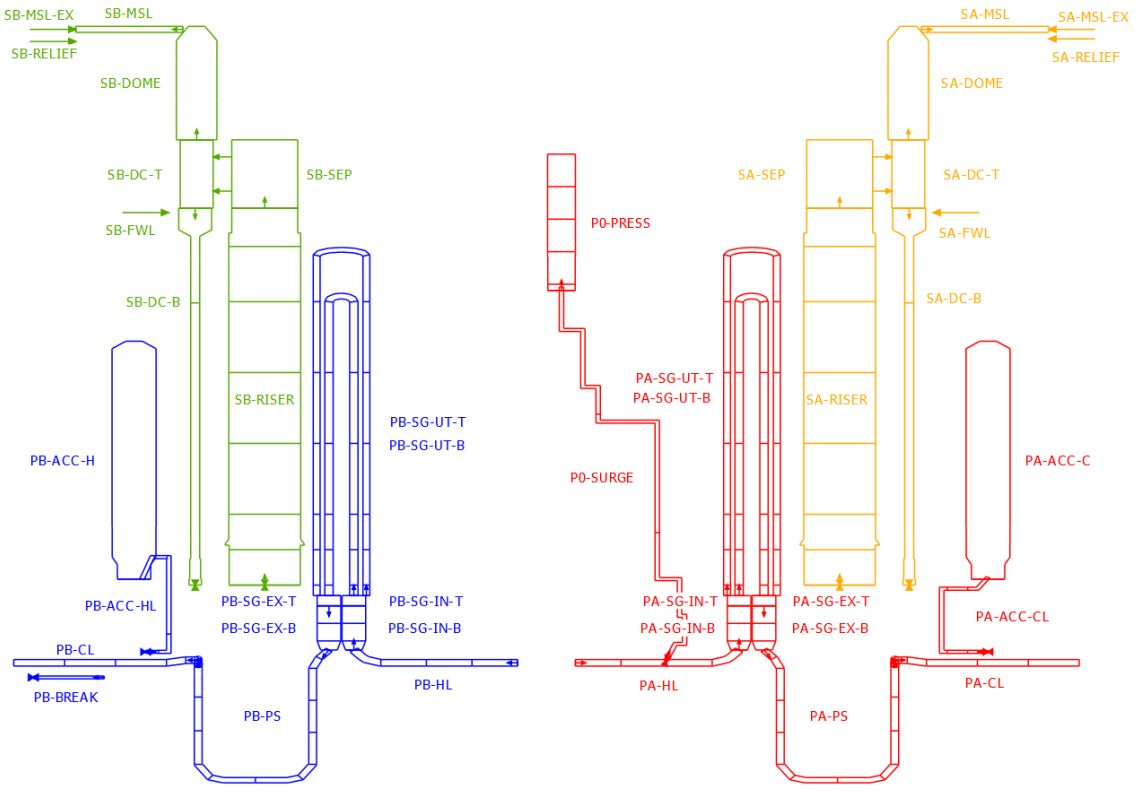

Fig. 5.3 LSTF: Nodalisation of the loops

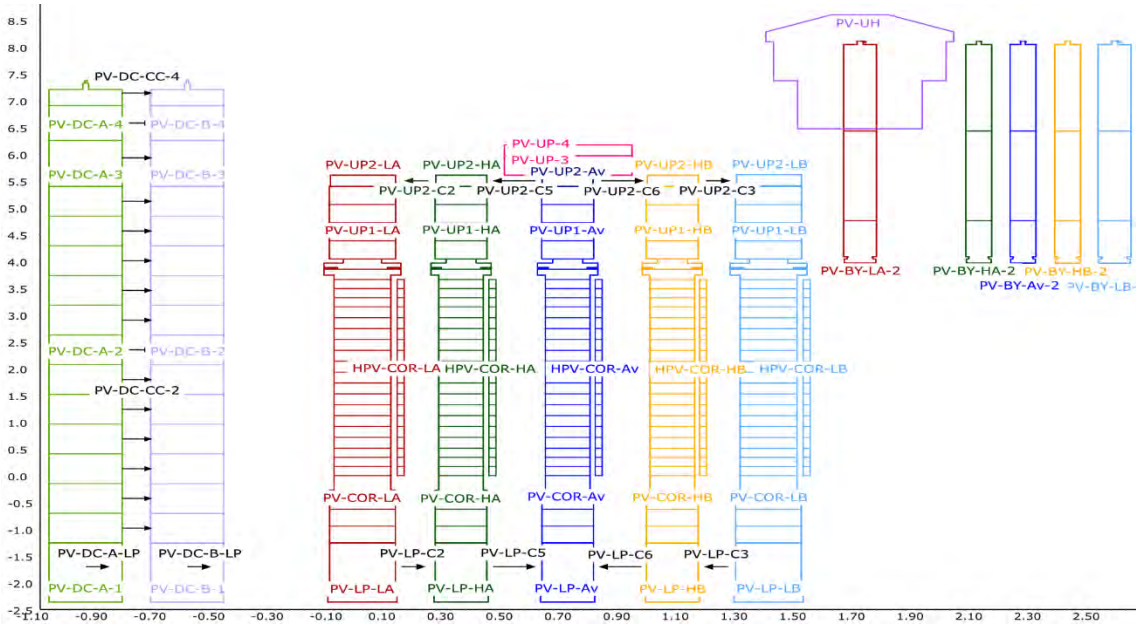

Fig. 5.4 LSTF: Nodalisation of the pressure vessel

5.1.3.2 Model Options

Following model options are applied:

- For the primary side of the test facility, the 6-eq. model is applied with the exception of the pressurizer and the break, where the 5-eq. model is chosen. The secondary side is completely simulated with the 5-eq. model.
- The T-junction model is applied to the entrance section of the break pipe. The critical discharge mass flow is calculated with the CDR1D model.
- The T-junction model is also applied at both ends of the pressurizer surge line to simulate the vapor pull-through when the mixture level reaches the surge line nozzle, as well as the vapor flow and liquid entrainment in case of a pressurizer in-surge.
- The multi-component model is used for the simulation of the nitrogen cushion in the accumulator.
- The condensation rates are calculated with the ATHLET direct condensation model.
- Evaporation and condensation at heating and cooling surfaces are considered.
- The Martinelli-Nelson friction model is used with all roughness $4 \cdot 10^{-5}$ m.

5.1.4 Main Results

Fig. 5.5 to Fig. 5.43 compare ATHLET results with the corresponding experimentally measured parameters for a variety of physical quantities, proving the quality of the ATHLET simulation. Additionally, results achieved with ATHLET 3.4 and ATHLET 3.3.1 are shown to also evaluate the progress of model development. The experimental result includes the designation of the measurement which is a combination of a two-letter prefix indicating the type of measurement and a number unique to each instrument location. Detailed information on the measurements and instrumentation system can be found in /JAE 89b/.

The calculated pressure on the primary side (Fig. 5.5) agrees very well with the experiment with two exceptions. In the early phase of the depressurization (20 s to 60 s), the pressure drops too far. The reason could be the over-prediction of the heat flow to the secondary side in that time period, which can be derived from the too fast increase of the pressure on the secondary sides of the steam generators (Fig. 5.6 and Fig. 5.7) after the closure of the main steam valves. During the late phase of the accumulator injection, the pressure drops too far caused by the overestimation of the steam condensation on the cold ECC water. The pressures on the steam generators secondary side are governed by the three times opening of the steam generator relief valves, and after that by the heat flow to the primary side.

The loop mass flows were measured in the two loop seals (Fig. 5.8 and Fig. 5.9). As already mentioned, the pump speed was temporarily increased immediately after break initiation to establish the scaled nominal loop mass flow. Due to the assumption of loss of offsite power the pumps were tripped and coasted down. The increase of the loop mass flows at about 150 s is caused by the clearance of the pump seals. After that, two phase flow occurs at the measurement position which could not been exactly measured by the venturi meters.

The begin of the accumulator injection is predicted little late (Fig. 5.10). The flow rate is underestimated during the following 200 s and subsequently overpredicted for 150 s (Fig. 5.11). There are no significant differences between the ATHLET version 3.4 and the version 3.3.1. Due to the overprediction of the steam condensation at the cold ECC water, the accumulator injection is terminated later than in the experiment and too much liquid is injected after 640 s.

The integrated break mass flows are compared in Fig. 5.12. The experimental data was derived from the leakage catch tank level. There is a significant discrepancy after 140 s with underestimation of both simulation runs. Regarding the break mass flow, there are two data sources from the experiment: A venturi flow measurement and additionally the mass flow derived from the catch tank level rise. Fig. 5.13 compares the datasets with the simulated break mass flow. The venturi flow measurement shows significant higher mass flow after 140 s compared to the values derived from the catch tank level rise. However, it could be expected higher accuracy for measuring the catch tank level. The underestimation of the break mass flow in the simulations during the period from 140 s to 200 s seems to be responsible for the significant differences of the integrated break mass flow since earlier deviations seem to compensate themselves. The density measurement upstream of the break orifice (Fig. 5.14) indicates entrained liquid between 550 s and 650 s. This phenomenon does not lead to a significant increase of catch tank level, which also indicates very low flow rate and wrong venturi measurement. The break is located behind a bend at its outside (see arrow in Fig. 5.1). It can be expected that the centrifugal force of the stratified liquid flow from the accumulator injection point towards the reactor vessel leads to an increased liquid fraction upstream the break. Parameter studies performed varying the leak mass flow (e.g. with a lowered elevation of the break nozzle), showed that the two periods of core uncover sensitively depend on the leak flow. Regarding the break flow, there are no significant differences notable for the two ATHLET versions.

The calculations of the densities in the hot legs of the two loops (Fig. 5.15 and Fig. 5.16), match very well the measurement during the first 550 s after break. Due to the ECC, the density in the hot legs increase around 600 s. Both ATHLET versions expect the density increase around 70 s later.

The calculated densities in the cold legs (Fig. 5.17 and Fig. 5.18) fit the experimental results well. After 480 s, there are deviations, and the density is underestimated.

After the main coolant pump coast down, the differential pressures are determined by the liquid distribution in the test facility since there are only low fluid velocities in the primary system. In general, the agreement of the calculation with the experiment is good, in some locations even excellent. For example, the first period of core uncovery (around 140 s, Fig. 5.19) is described well by ATHLET. Also, the time point of pump seal clearance is calculated well. The two ATHLET versions produce nearly the same results.

The pressure difference between downcomer and upper head fit the experimental results well (see Fig. 5.20). The pressure difference between downcomer and upper plenum is underestimated during the Zero-transient and the first 120 s after the break (see Fig. 5.21). The later results by 500 s fit the experimental data very well. After, there are differences between the experimental data and the simulations. The two ATHLET versions produce nearly the same results.

In Fig. 5.22 the measured fluid temperature in the upper head is compared with the ATHLET result calculated above the mixture level (which is initiated at ca. 20 s). After ca. 400 s, the steam becomes superheated due to the heat flow from the hot structures, which is not reflected by the calculation. A similar behavior can be observed in the upper downcomer (Fig. 5.23), where the mixture level model is not applied. Therefore, too much liquid is entrained by ATHLET, and the superheating is under-predicted. The temperature in the upper plenum is predicted well but little too high around 500 s as shown in Fig. 5.24. The calculated fluid temperature at the core entry (Fig. 5.25) is predicted very well by ATHLET within the first 550 s after break. Later, it is slightly overpredicted until it is underpredicted after 650 s. The measured temperatures in the ECC nozzles (Fig. 5.26 and Fig. 5.27) indicate that the water in the ECC injection lines is initially clearly warmer than that in the accumulators. This is considered in the calculation by a relatively fine nodalisation of the injection lines (5 CVs) and by the specification of an adequate initial temperature profile. The temperature increase at 650 s and 850 s is prevented by the one-way valves at the ECC nozzles in the ATHELT model. The nevertheless, the fluid temperatures in the cold legs downstream the ECC injection points are calculated significantly too low after 450 s (Fig. 5.28 and Fig. 5.29). There are no significant differences between the two ATHLET versions regarding the fluid temperatures described in in this paragraph.

The calculated vapor temperatures in the hot leg fit the experimental results well (see Fig. 5.30 and Fig. 5.31). During the Zero-Transient, there is no vapor. Hence, ATHLET sets the vapor temperature equal to the boiling temperate.

The fuel rod temperatures show the core heat-up during two periods of core uncover. The first core uncover is caused by manometric forces due to the asymmetric liquid holdup in the steam generator U-tubes and in the pump seals, and it is terminated after pump seal clearing at about 140 s. The second core uncover around 500 s which is observed only in the upper part of the core is caused by boil-off of the vessel inventory and terminated by the accumulator injection. In Fig. 5.32 to Fig. 5.40, the cladding

temperatures calculated for the hot rod of the high-performance core channels are compared with the minimum and maximum values measured at 9 levels. The calculated temperature excursions are within the measurement spread and the maximum temperatures at level 1-3 are predicted very precise. The maximum values are underpredicted at level 4-6. To the higher core levels, the maximum temperatures during the first core cover are more and more underestimated. At level 7 and 8, a temperature peak is only indicated and at the highest rod level, the rod temperature seems to be conserved. In few cases, quenching is predicted to late at different levels in the lower rod half. The two ATHLET versions have this quenching issue each at different levels. This is due to the different predictions of the heat transfer mode. When quenching occurs delayed, the switch from transition boiling to subcooled nucleate boiling is simulated too late. The second dry out period is predicted well but quenched about 40 s too late. Besides the general uncertainties concerning the liquid distribution during the transient, the further reasons are possibly deviations of the break mass flow as well as the deviations of the accumulator injections. There are no significant differences between the ATHLET version 3.4 and version 3.3.1. regarding the cladding temperatures.

Finally, the Fig. 5.41 to Fig. 5.43 document the performance of the ATHLET simulation concerning numerical effort and conservation of the coolant mass balance. No numerical problems appeared, and the maximum mass error of ca. 1.75 kg is negligible compared to the initial primary side mass inventory of about 5500 kg (without accumulators). Both compared ATHLET versions performed even well.

Summarizing the comparison of the ATHLET calculation with the experimental results, it can be stated that, in general, the calculated parameters show a good, some of them even excellent agreement with the measurements. ATHLET is able to simulate all main phenomena appearing during that type of transient investigated by this LSTF experiment. Overall, there are no significant differences between ATHLET version 3.4 and ATHLET version 3.3.1.

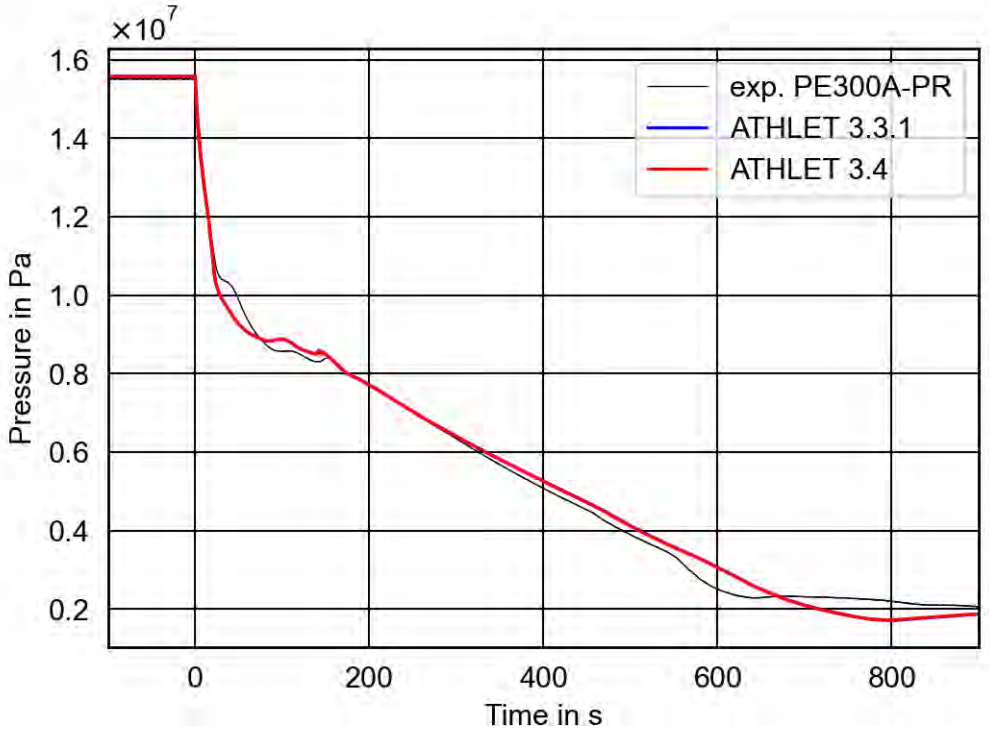

Fig. 5.5 Pressure in pressurizer

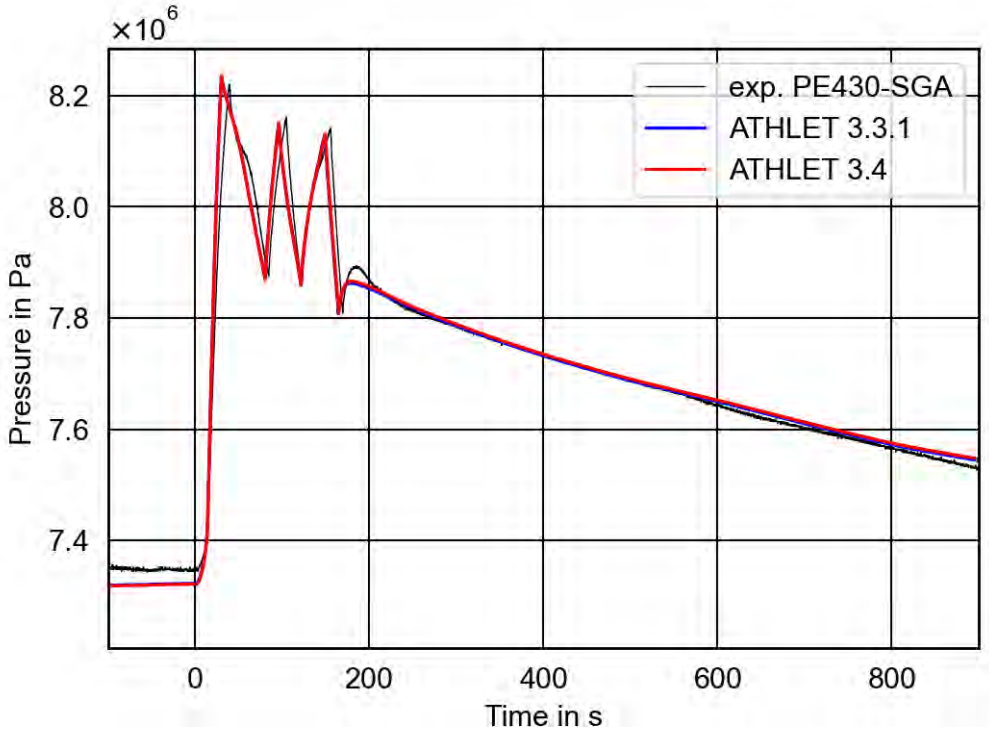

Fig. 5.6 Pressure in intact loop (A) SG dome

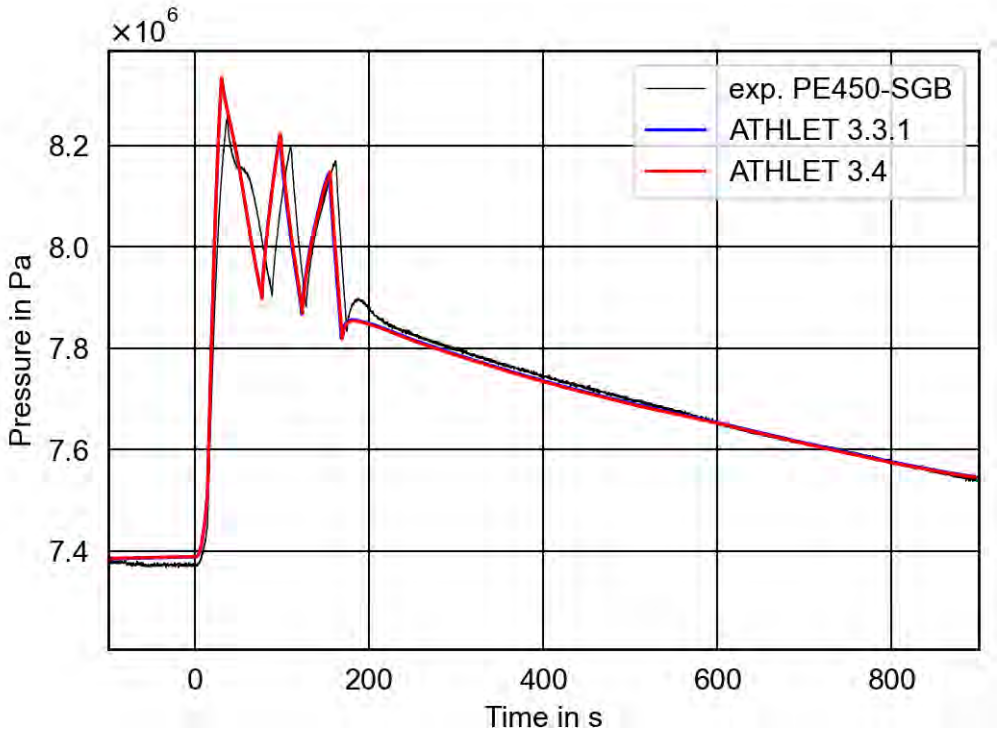

Fig. 5.7 Pressure in broken loop (B) SG dome

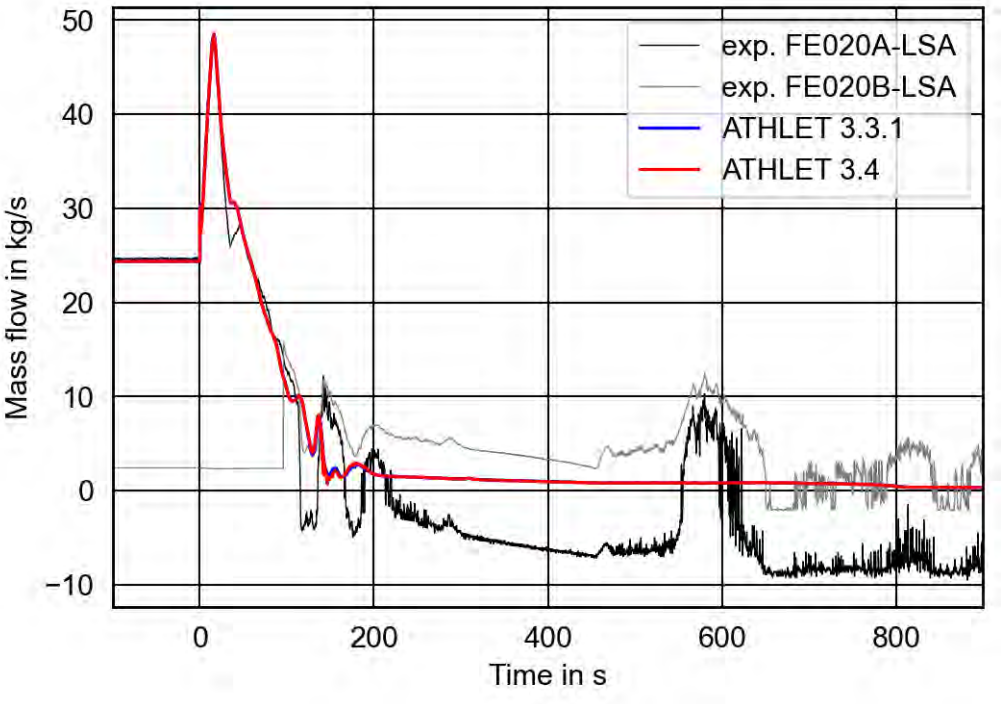

Fig. 5.8 Mass flow in loop seal of intact loop (A)

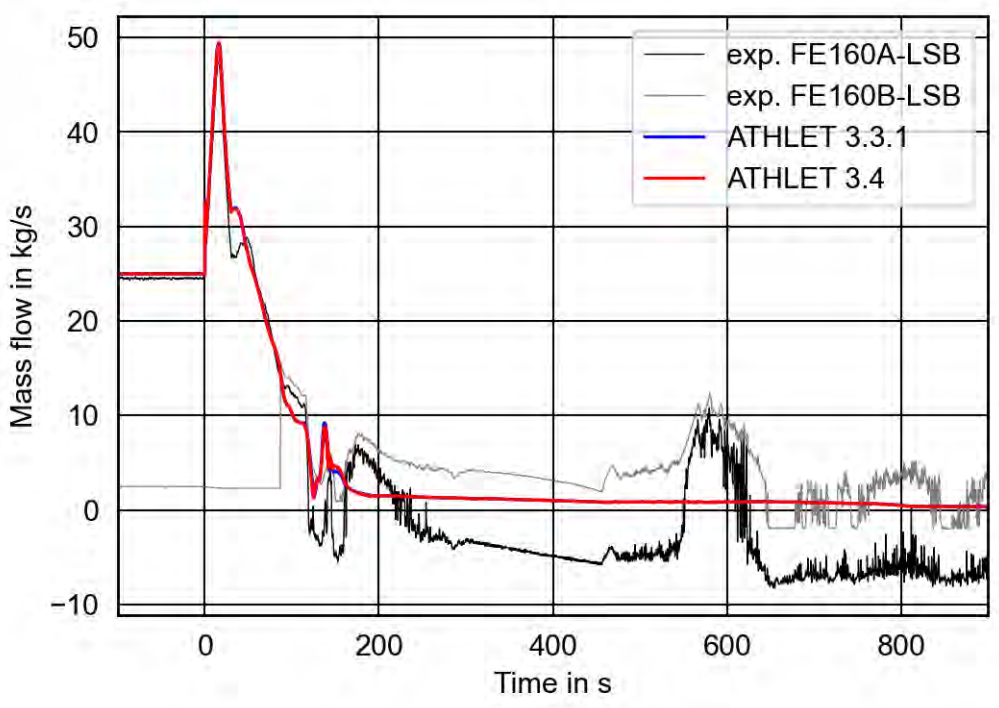

Fig. 5.9 Mass flow in loop seal of broken loop (B)

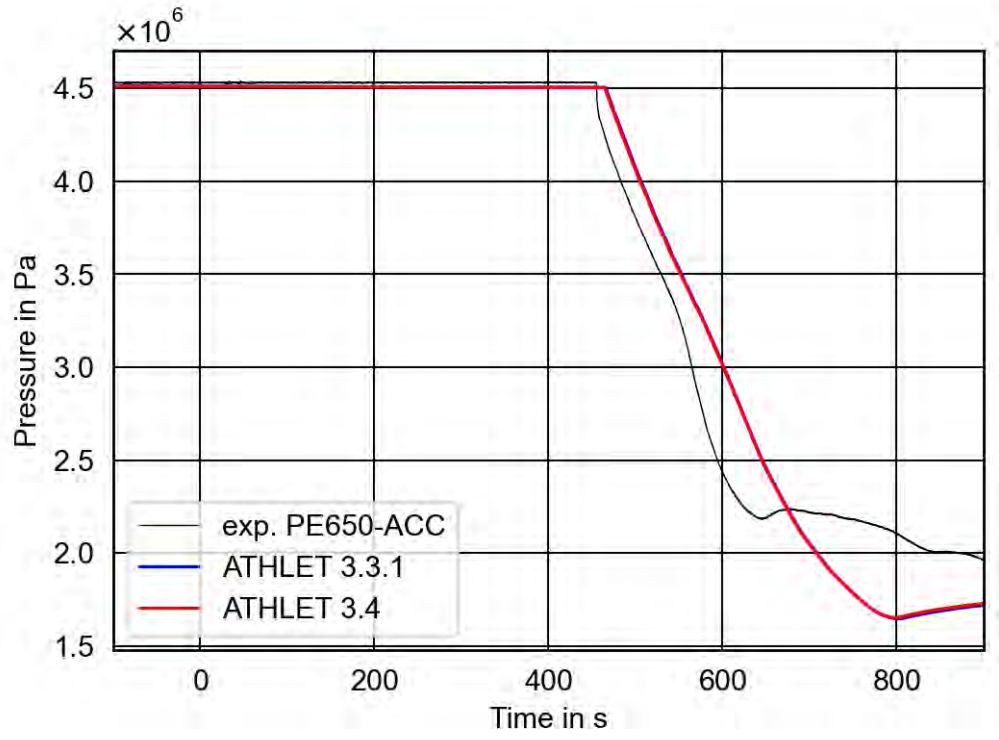

Fig. 5.10 Pressure in the accumulator of intact loop (A)

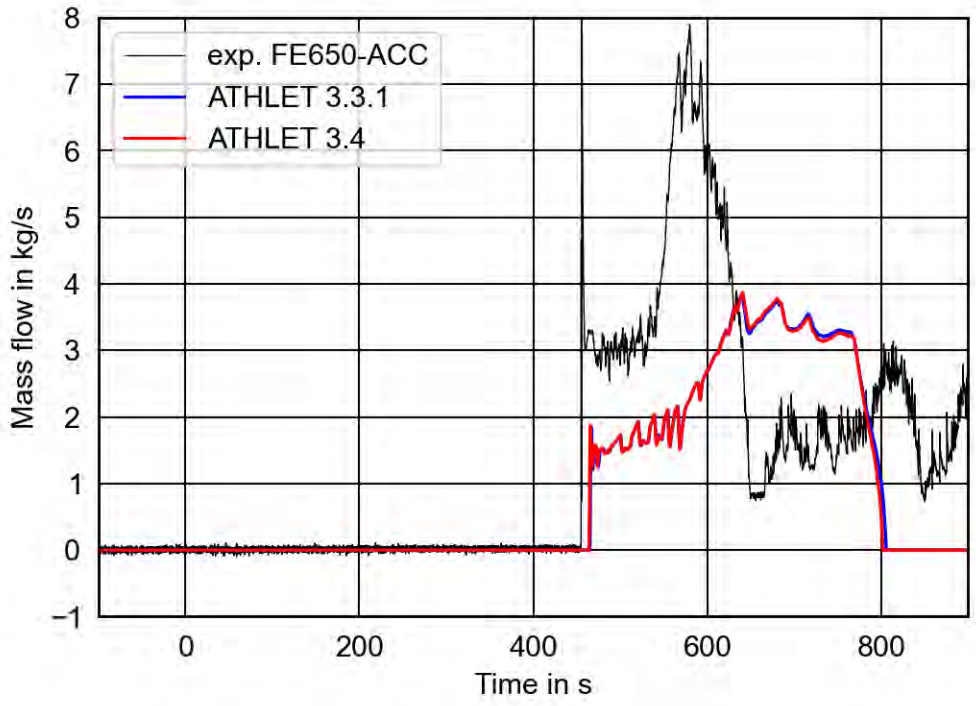

Fig. 5.11 Injection mass flow of the accumulator in intact loop (A)

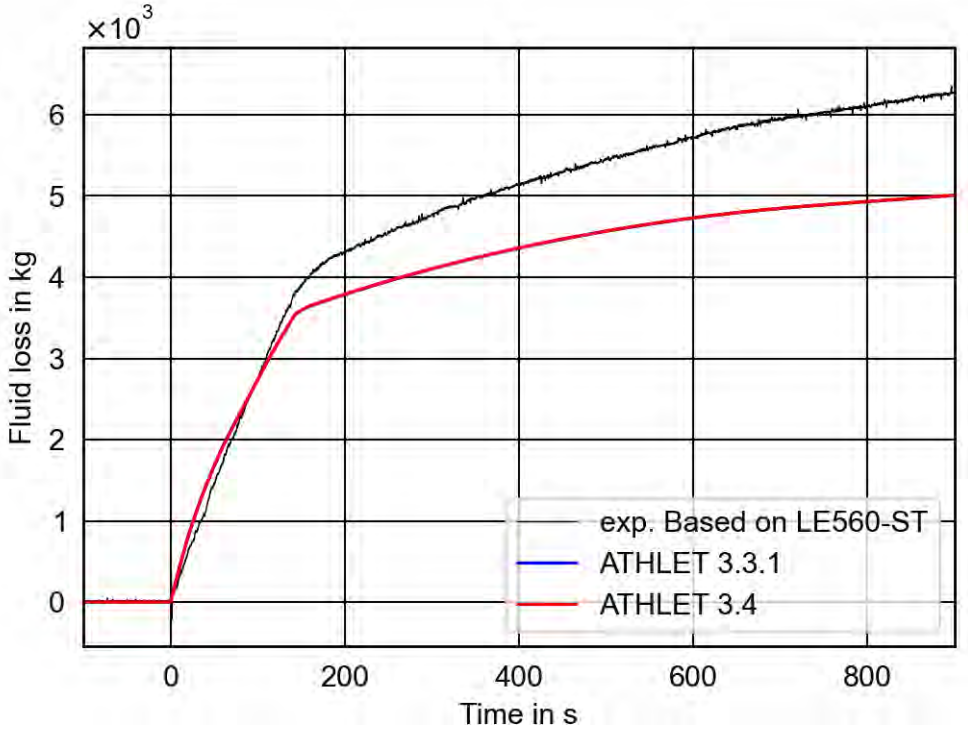

Fig. 5.12 Integrated break mass flow

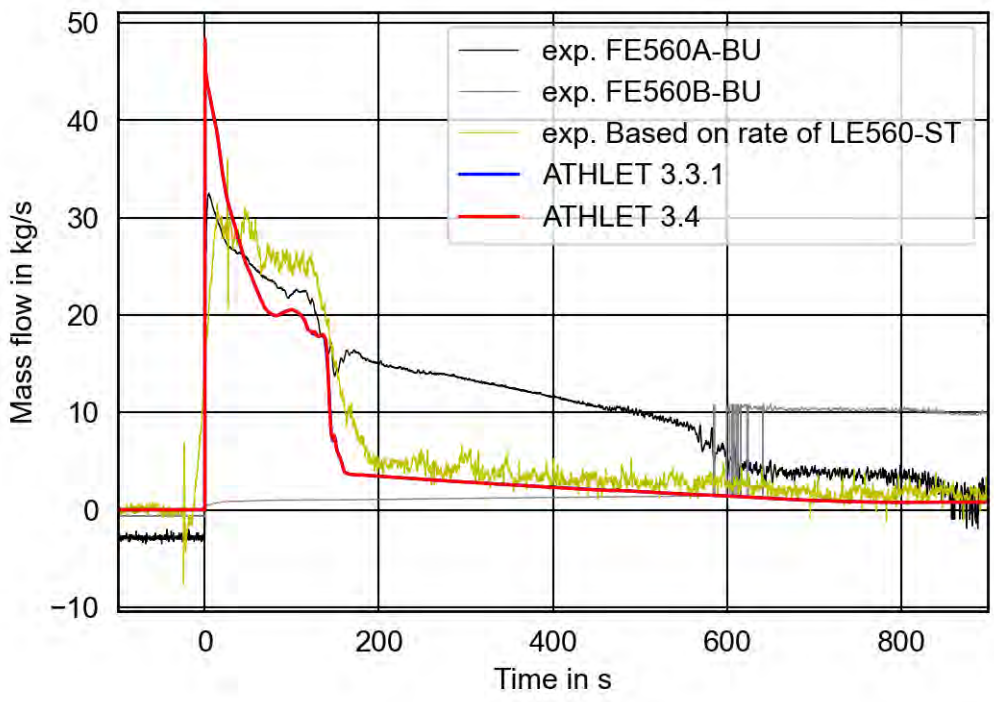

Fig. 5.13 Break mass flow

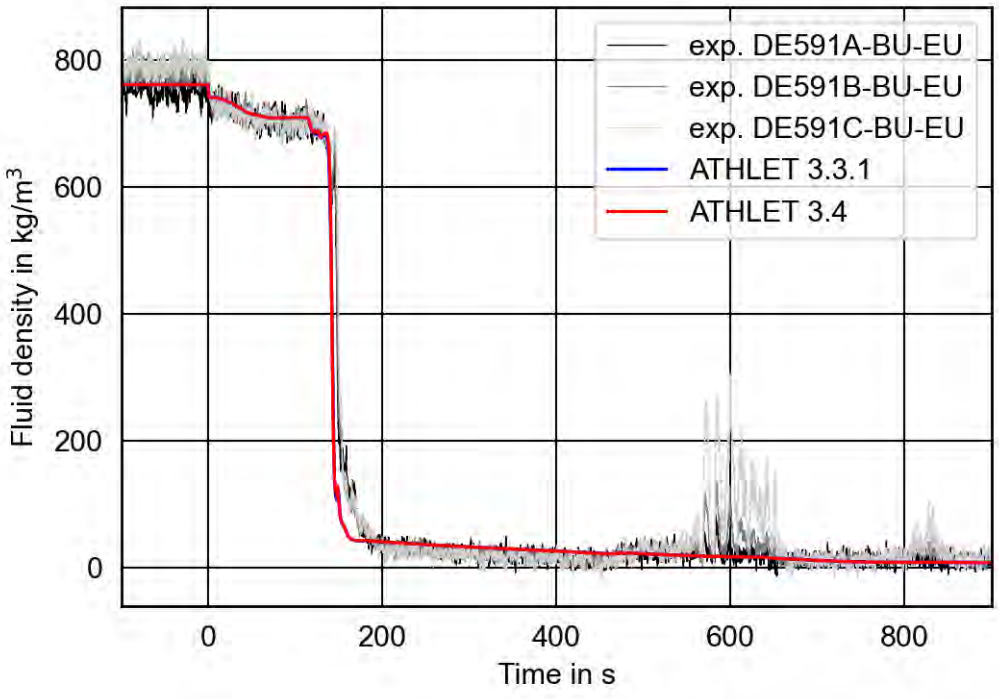

Fig. 5.14 Fluid density upstream break orifice

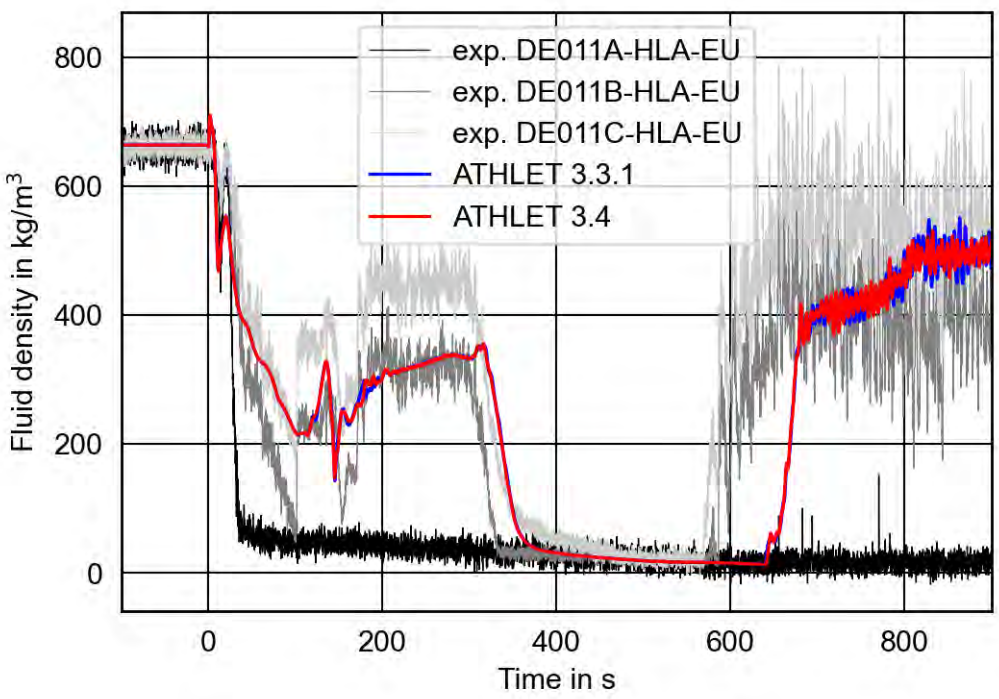

Fig. 5.15 Fluid density in hot leg A

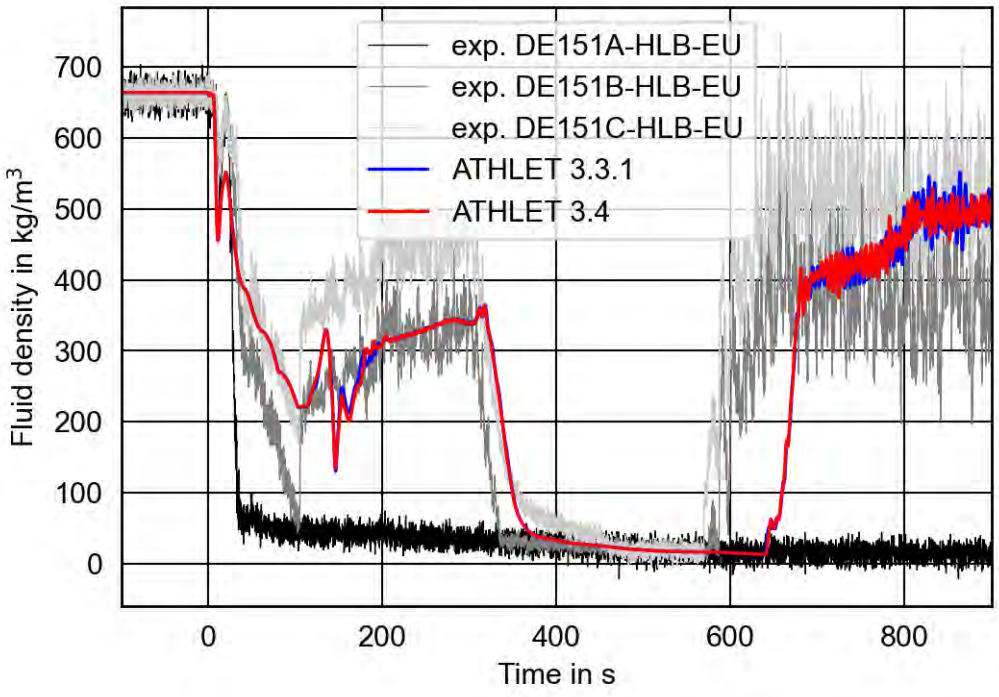

Fig. 5.16 Fluid density in hot leg B

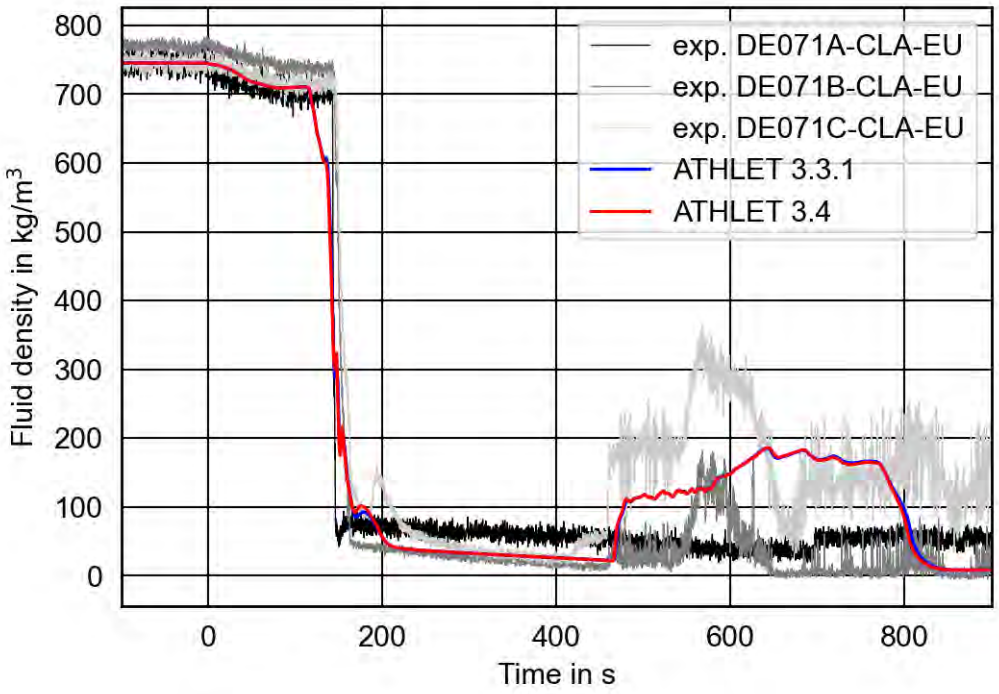

Fig. 5.17 Fluid density in cold leg A

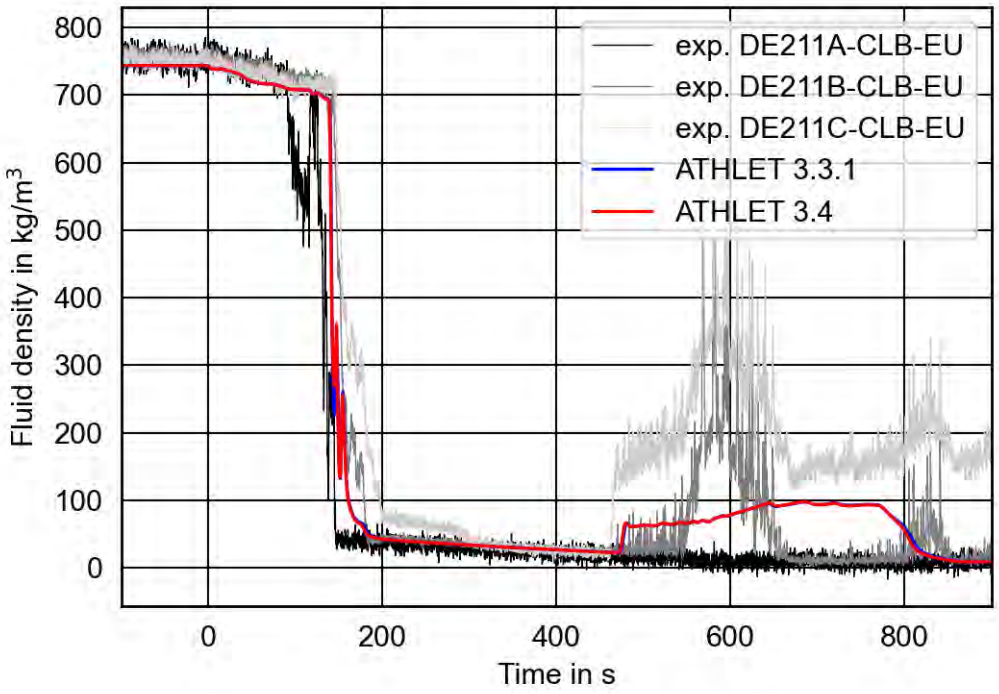

Fig. 5.18 Fluid density in clod leg B

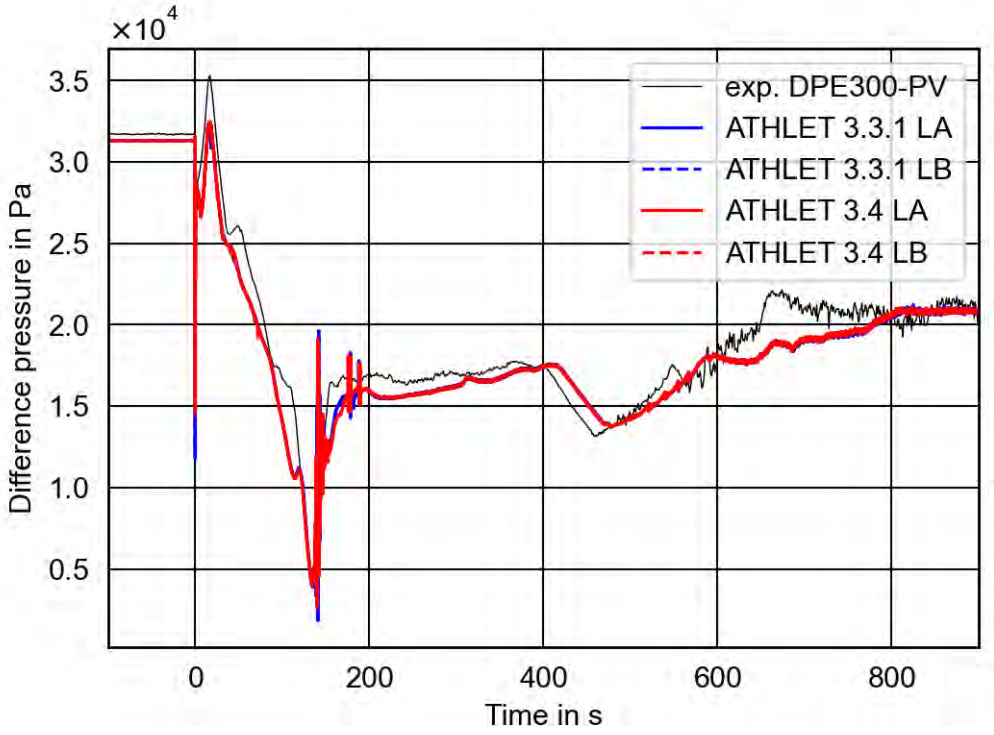

Fig. 5.19 Differential pressure across core

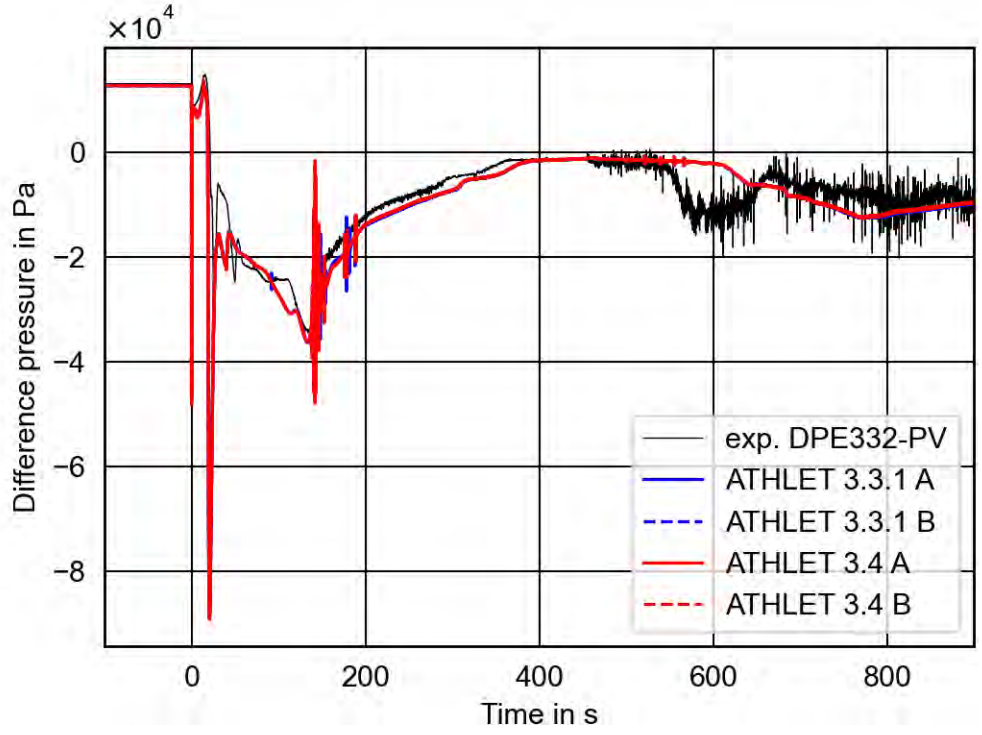

Fig. 5.20 Differential pressure between downcomer and upper head

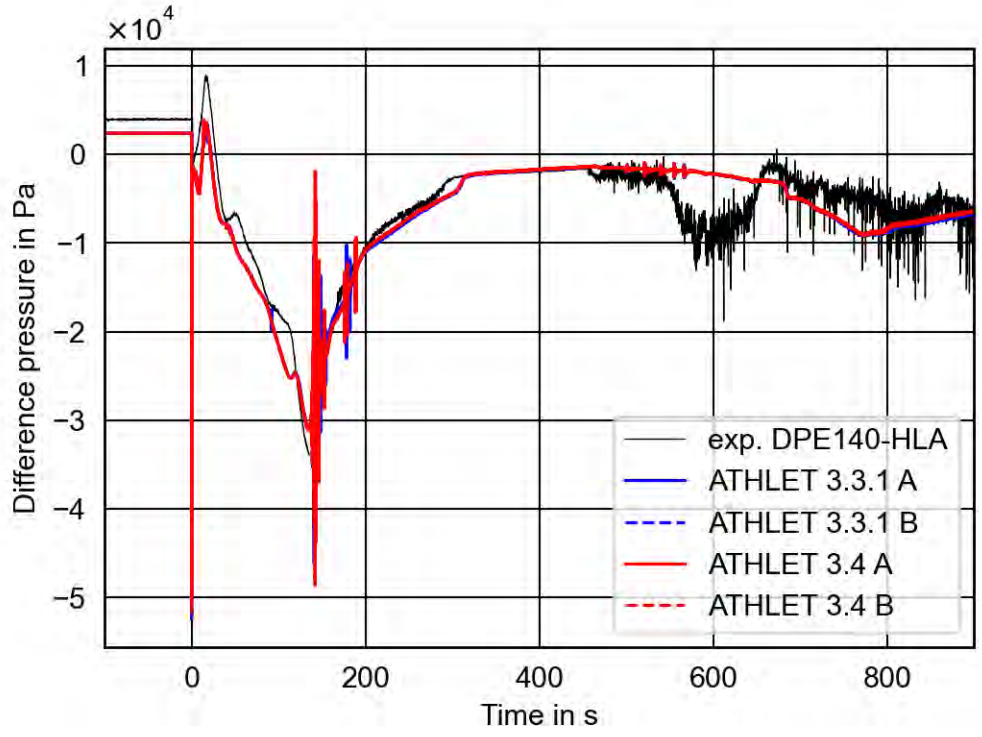

Fig. 5.21 Differential pressure between downcomer and upper plenum

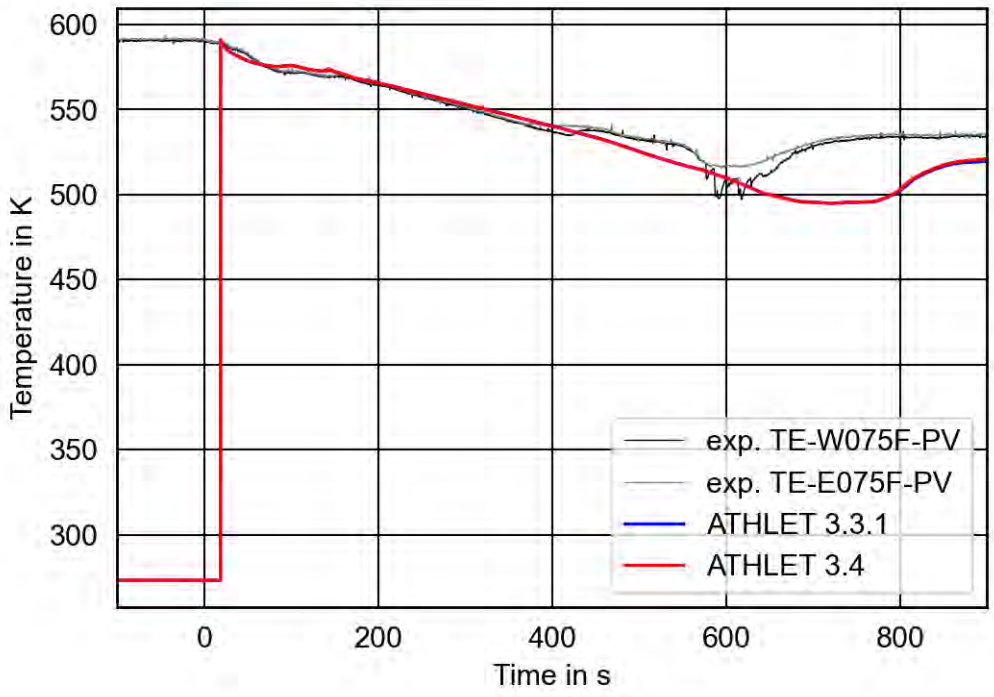

Fig. 5.22 Fluid temperature in the upper head (above mixture level)

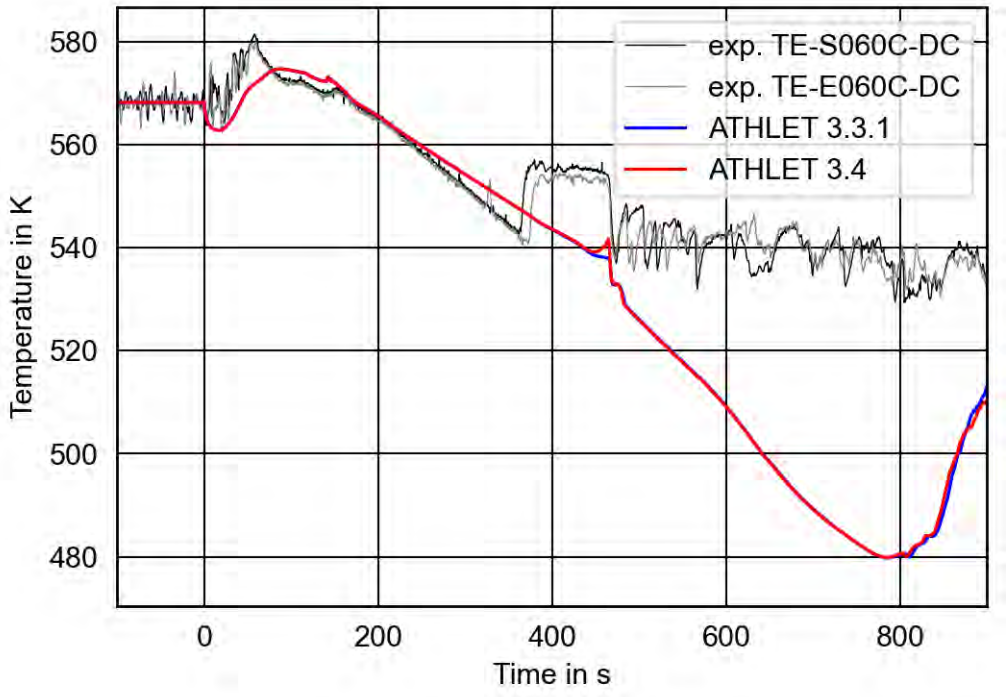

Fig. 5.23 Fluid temperature in upper downcomer

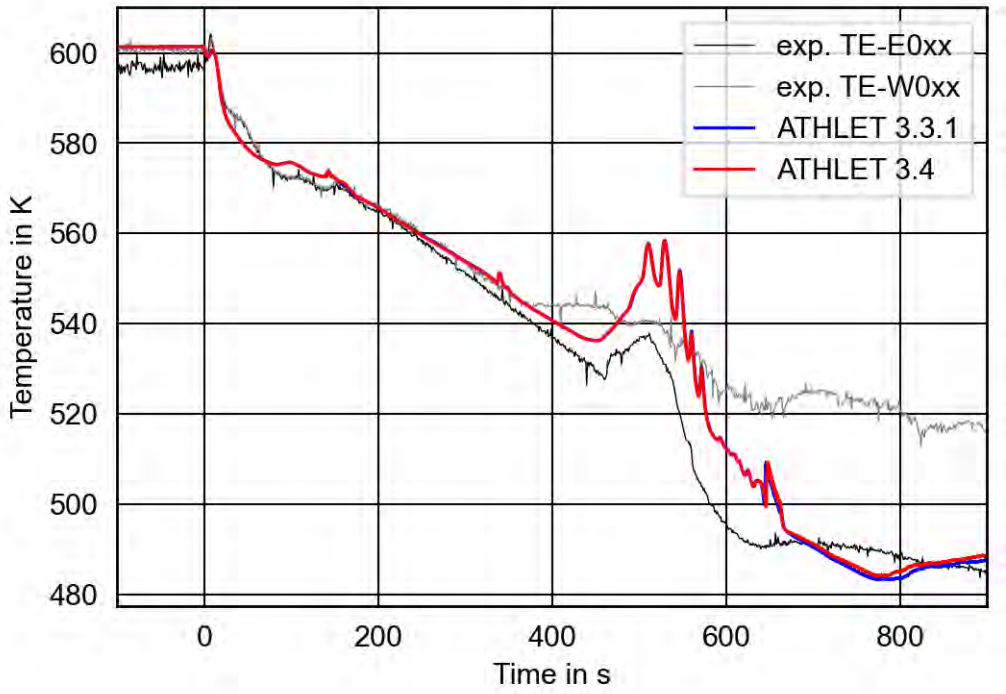

Fig. 5.24 Fluid temperature in the upper plenum

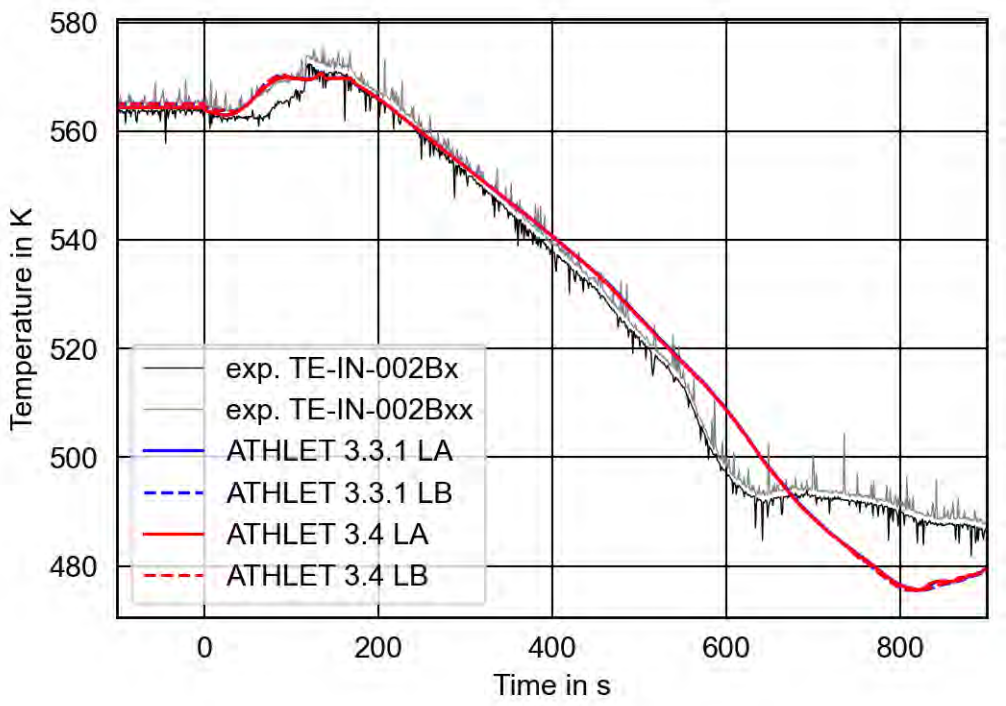

Fig. 5.25 Fluid temperature at the core entry

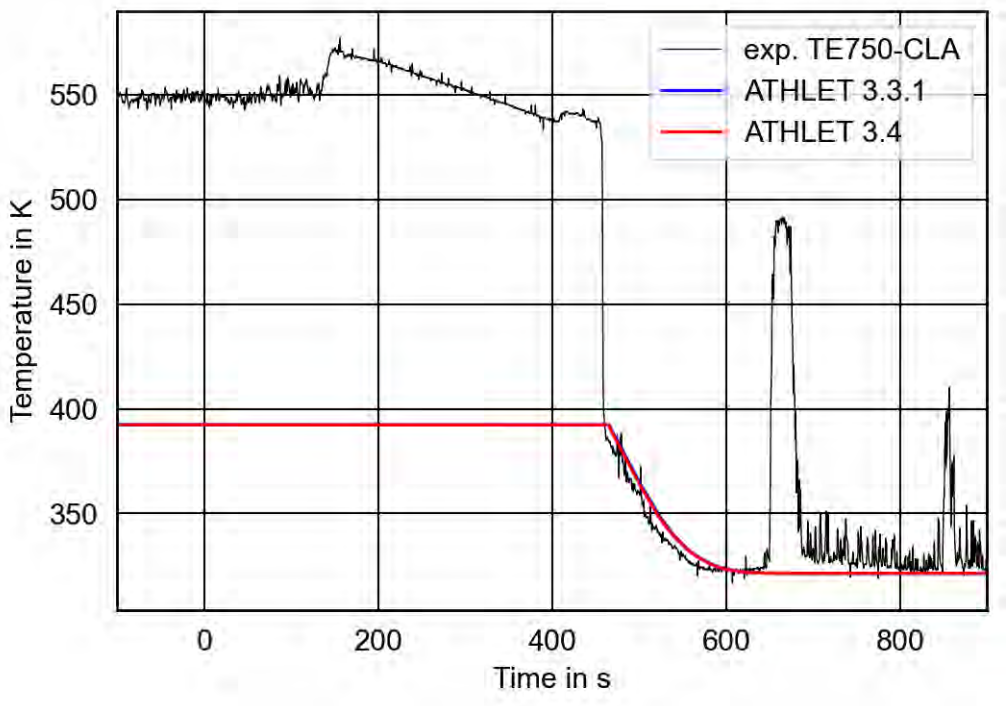

Fig. 5.26 Fluid temperature in the ECC nozzle of the intact loop (A)

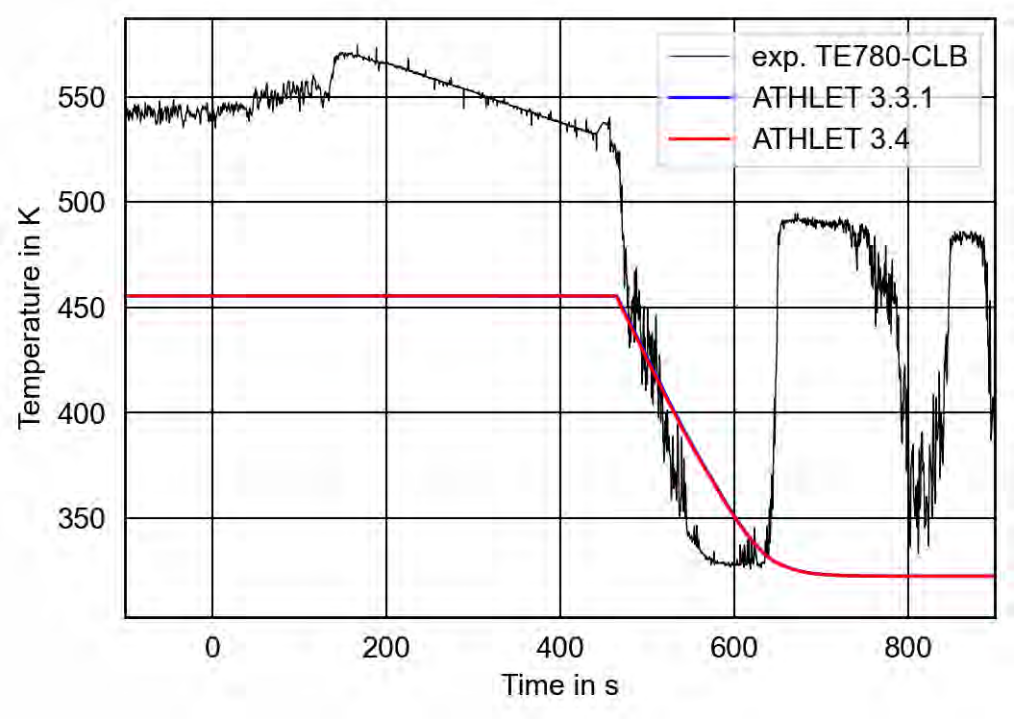

Fig. 5.27 Fluid temperature in the ECC nozzle of the broken loop (B)

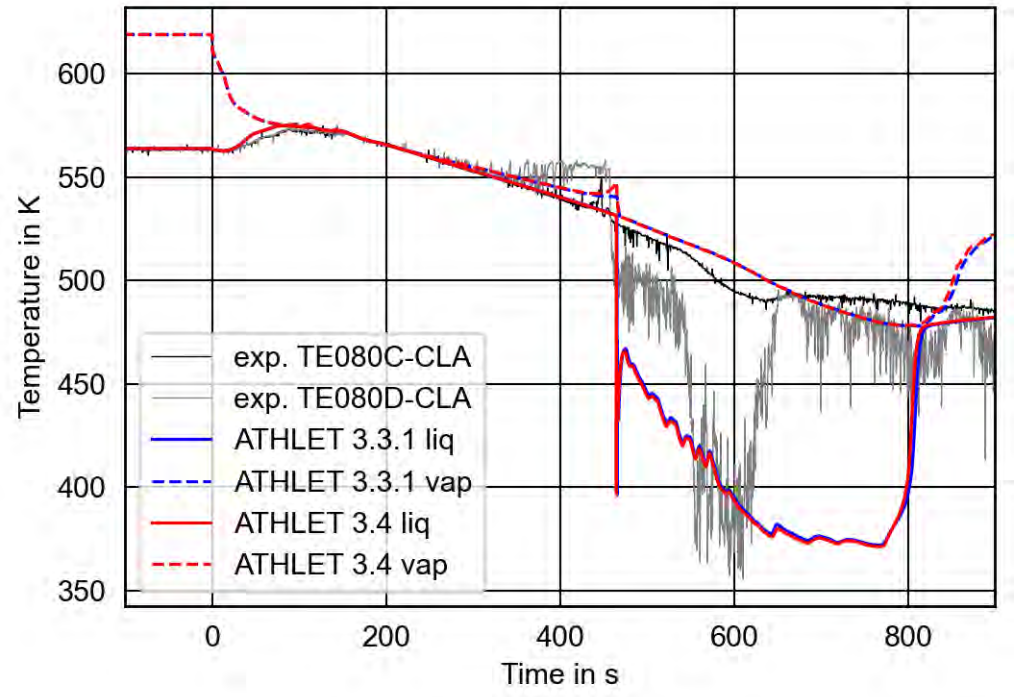

Fig. 5.28 Fluid temperature in the cold leg A (vessel side)

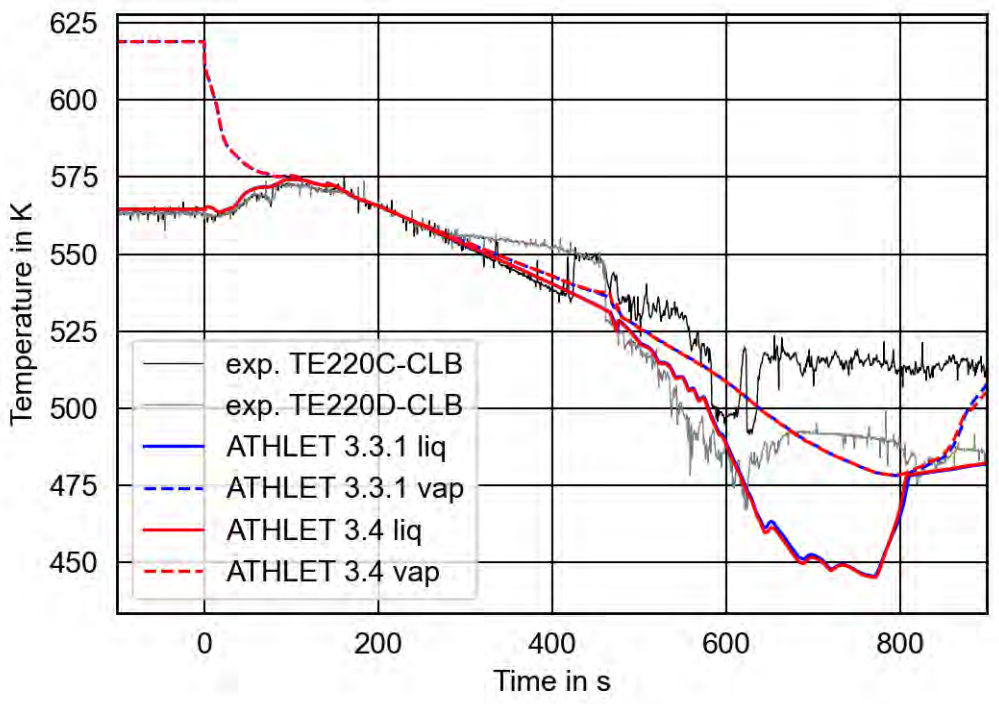

Fig. 5.29 Fluid temperature in the cold leg B (vessel side)

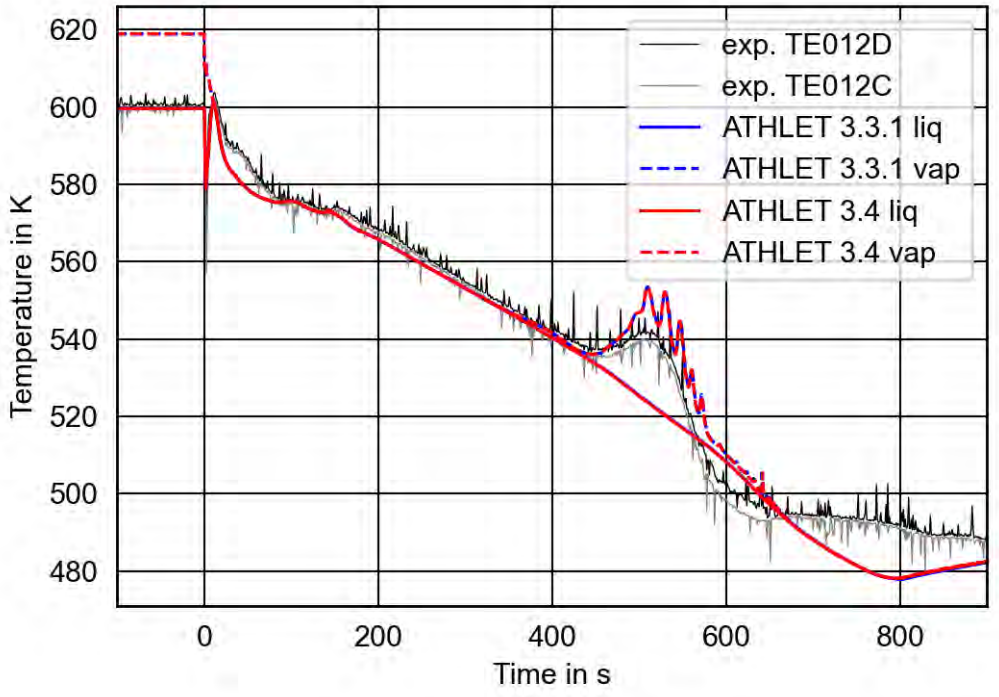

Fig. 5.30 Fluid temperature in the hot leg A (vessel side)

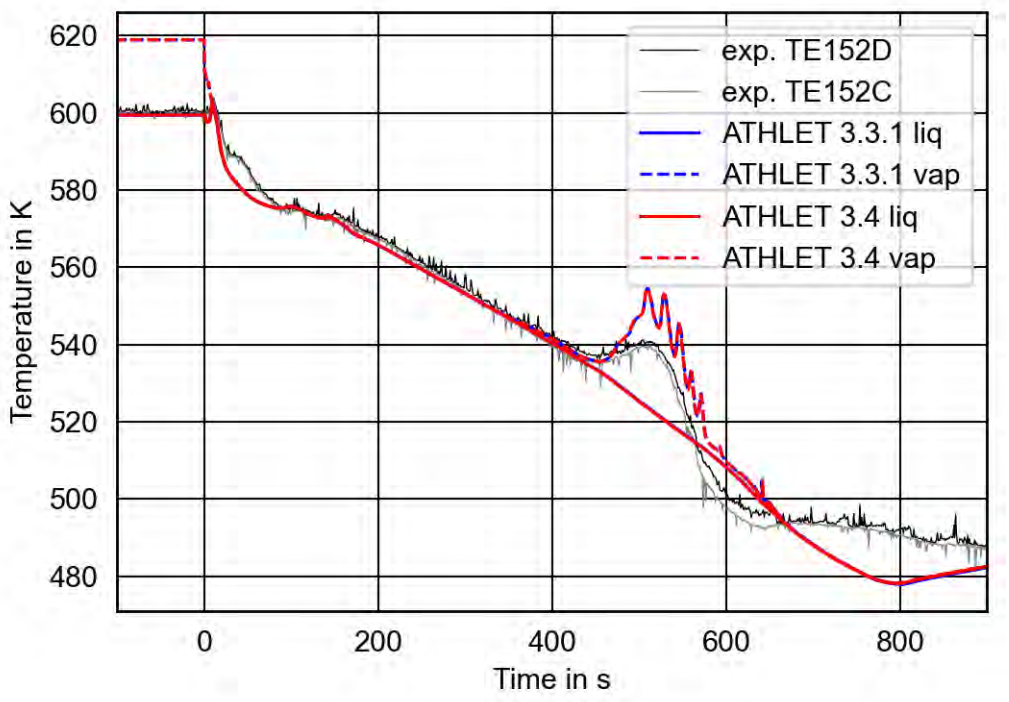

Fig. 5.31 Fluid temperature in the hot leg B (vessel side)

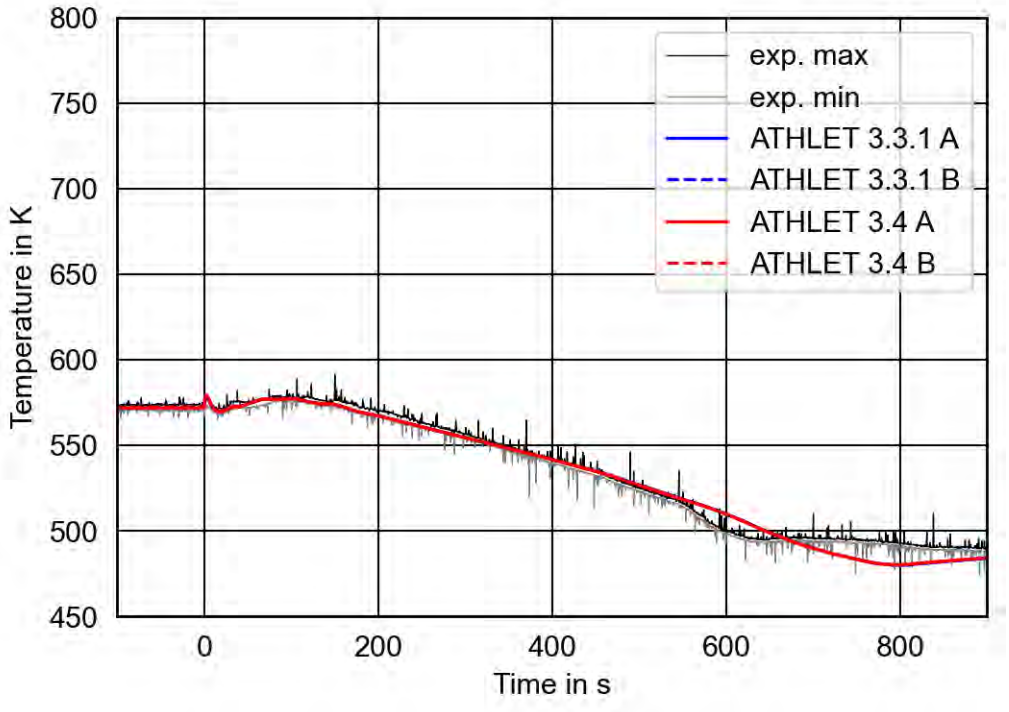

Fig. 5.32 Hot rod cladding temperature (HPV-COR-HX #1)

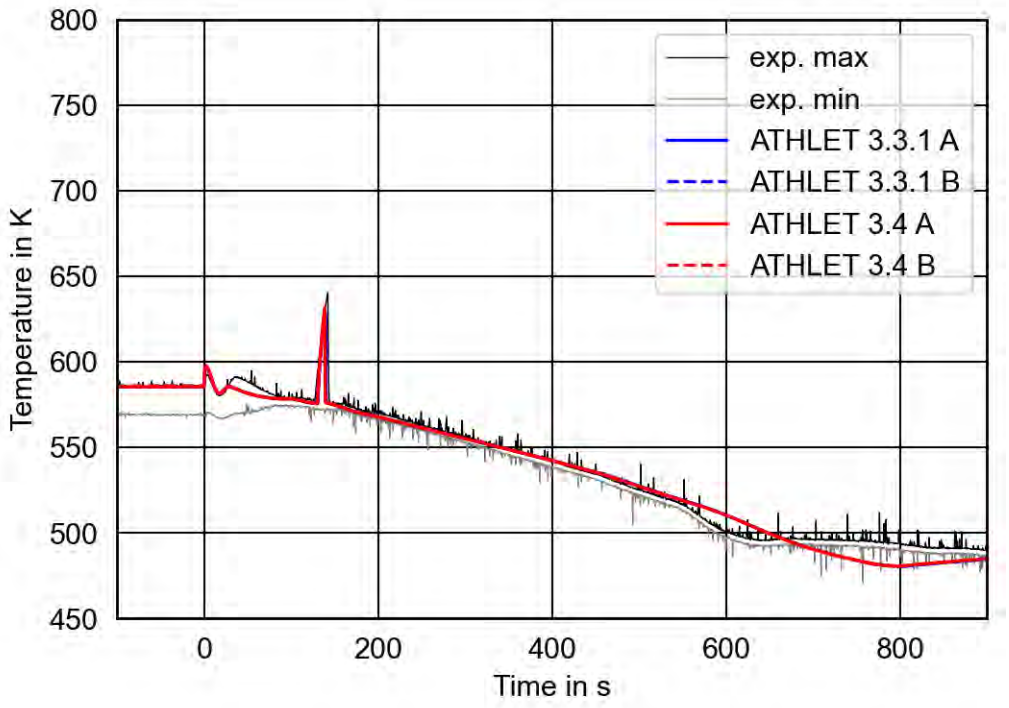

Fig. 5.33 Hot rod cladding temperature (HPV-COR-HX #2)

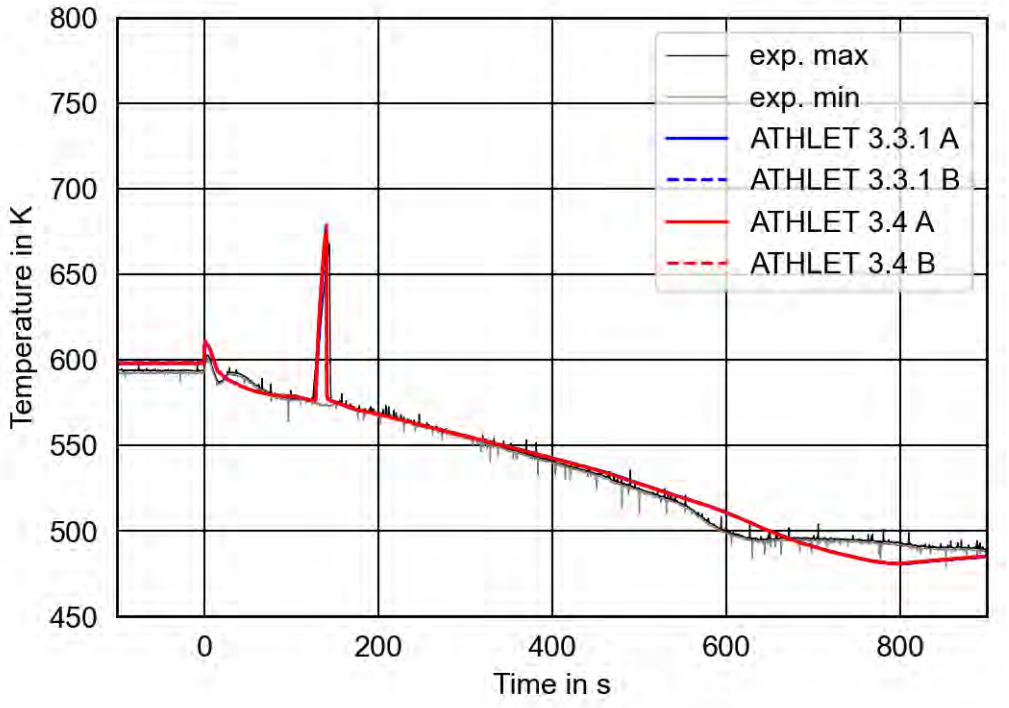

Fig. 5.34 Hot rod cladding temperature (HPV-COR-HX #3)

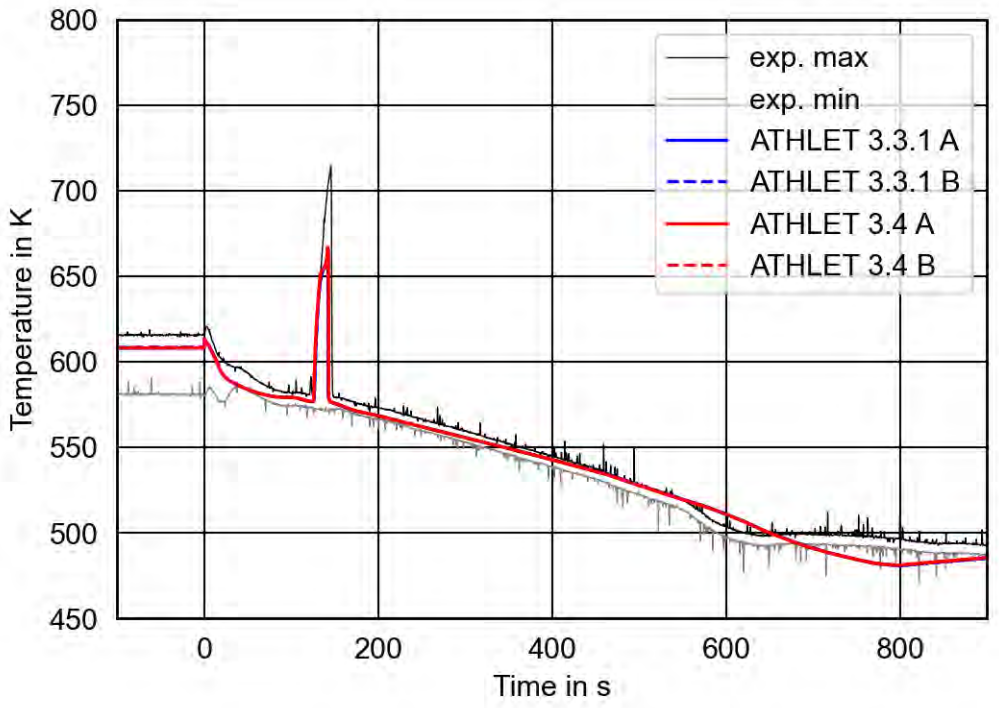

Fig. 5.35 Hot rod cladding temperature (HPV-COR-HX #4)

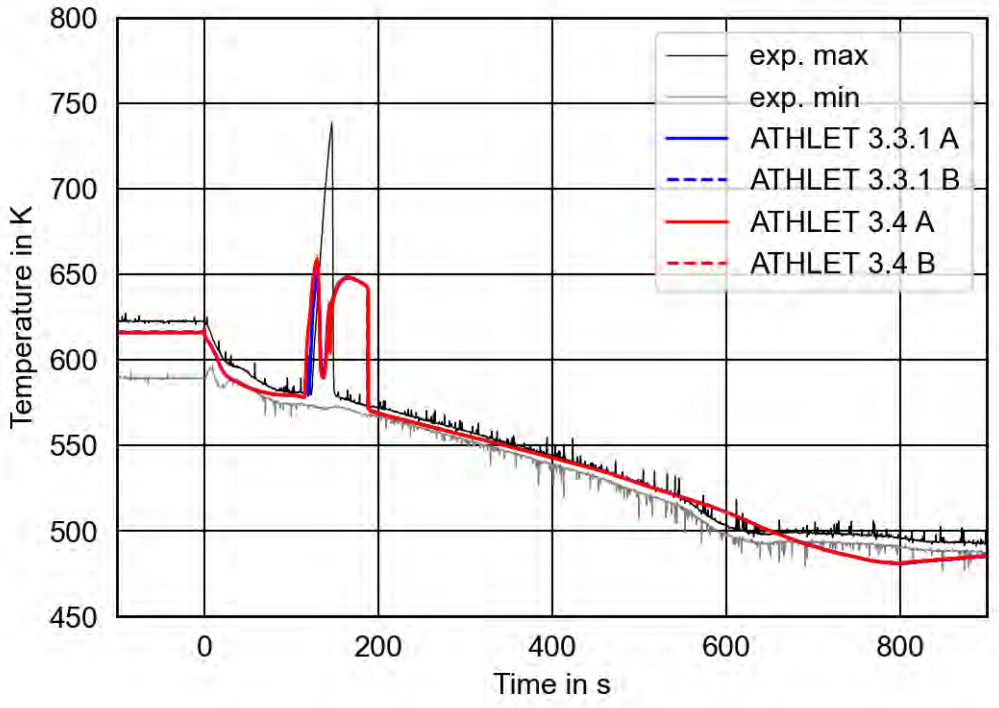

Fig. 5.36 Hot rod cladding temperature (HPV-COR-HX #5)

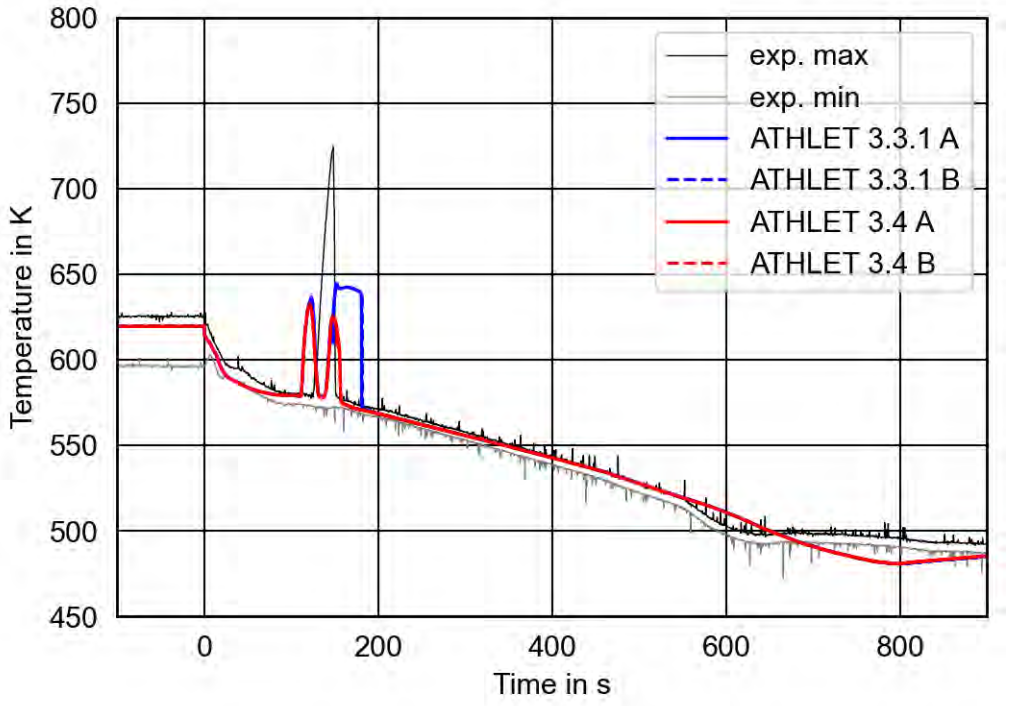

Fig. 5.37 Hot rod cladding temperature (HPV-COR-HX #6)

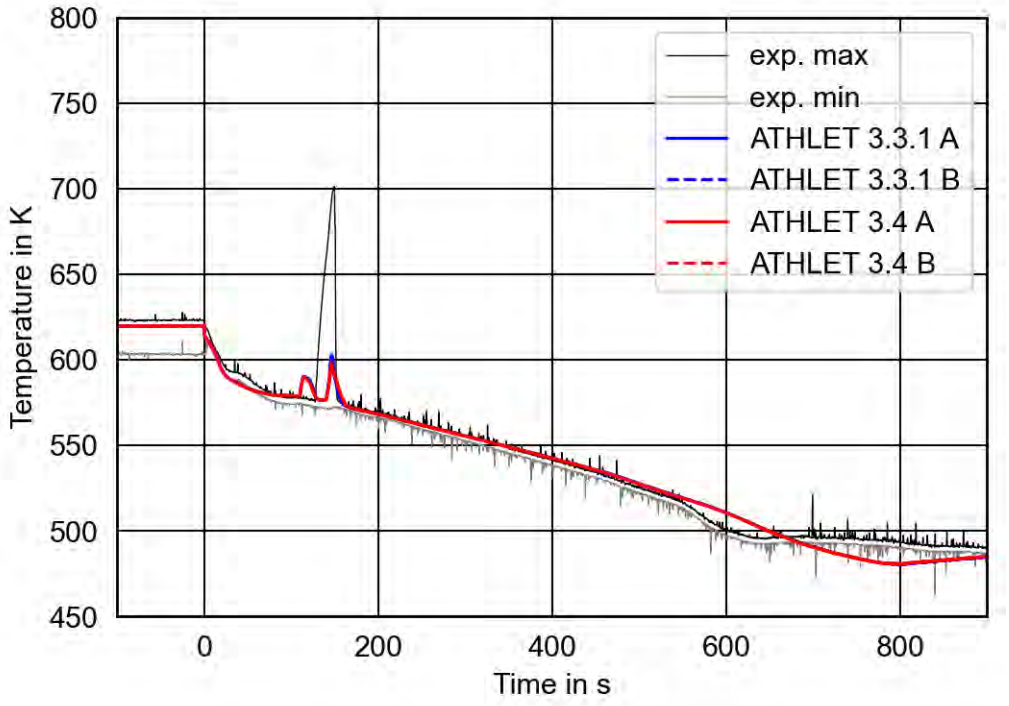

Fig. 5.38 Hot rod cladding temperature (HPV-COR-HX #7)

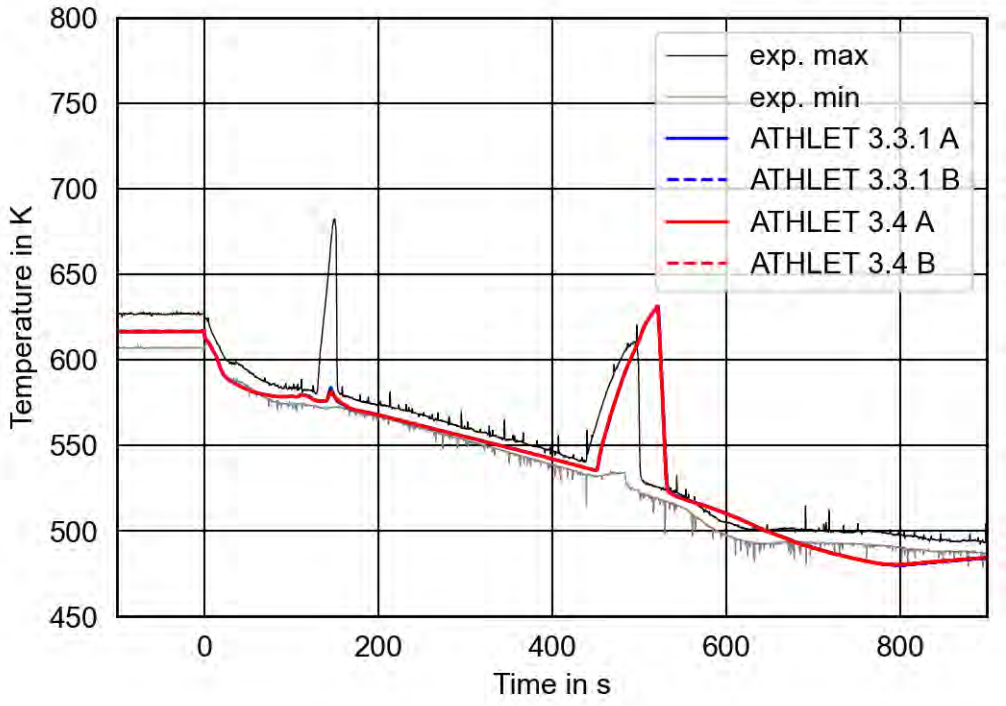

Fig. 5.39 Hot rod cladding temperature (HPV-COR-HX #8)

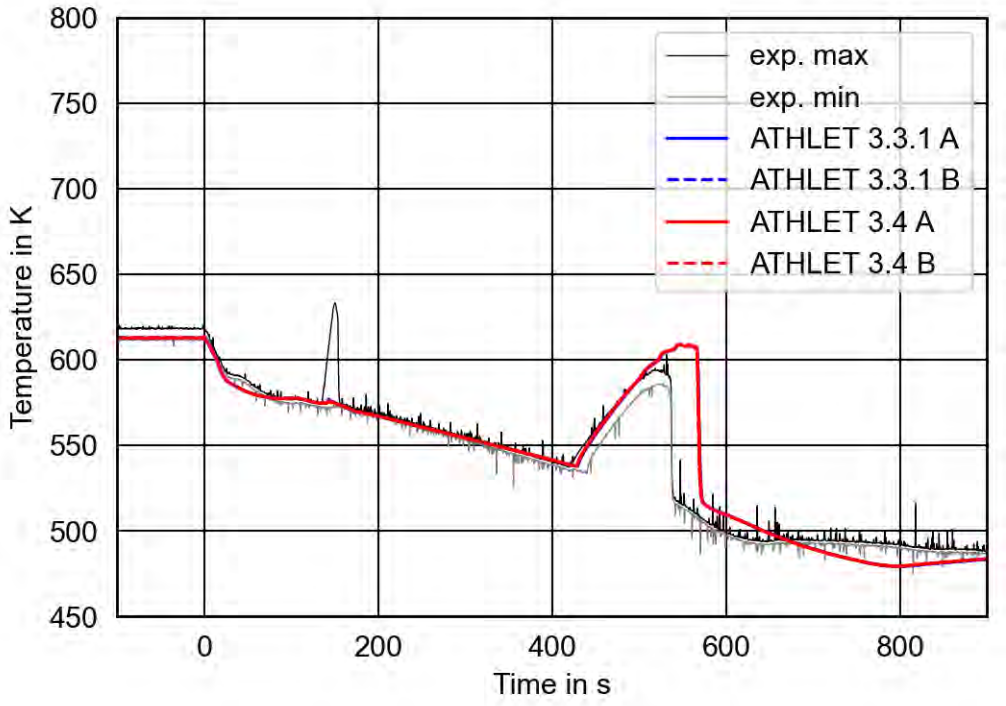

Fig. 5.40 Hot rod cladding temperature (HPV-COR-HX #9)

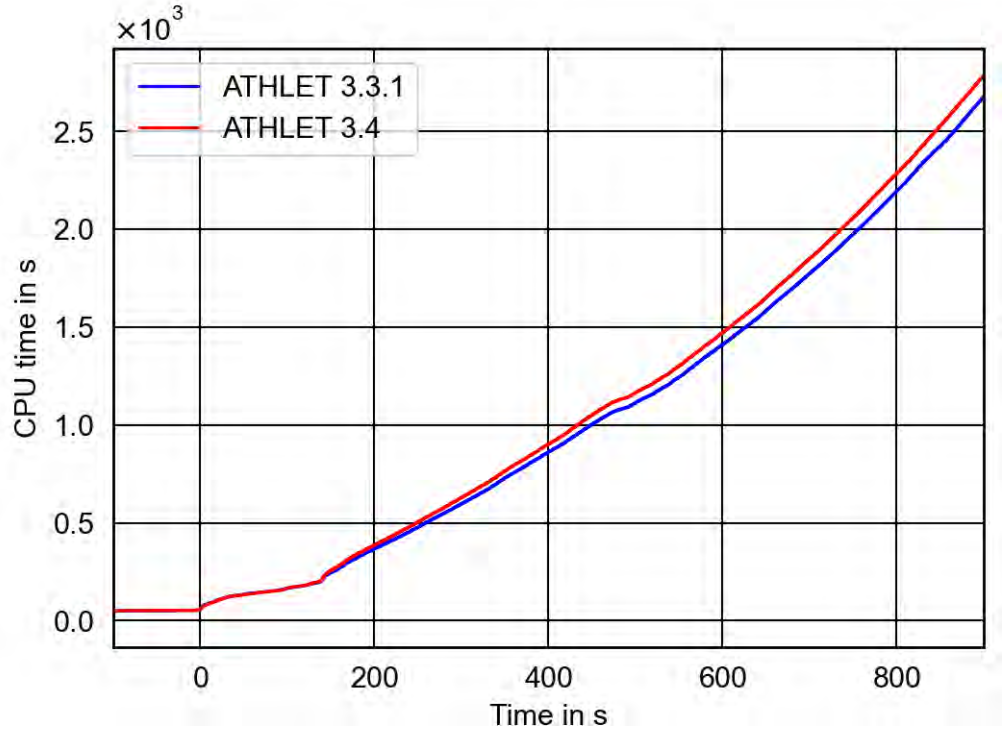

Fig. 5.41 CPU time consumption

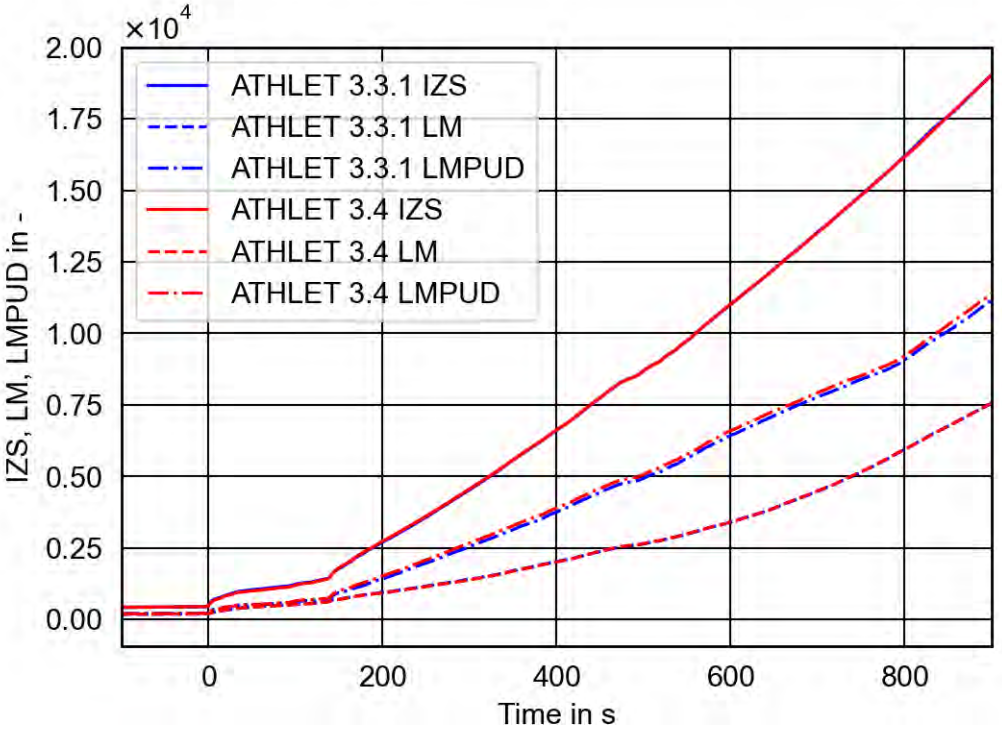

Fig. 5.42 Number of time steps (IZS) and Jacobian complete (LM) and partial updates (LMPUD)

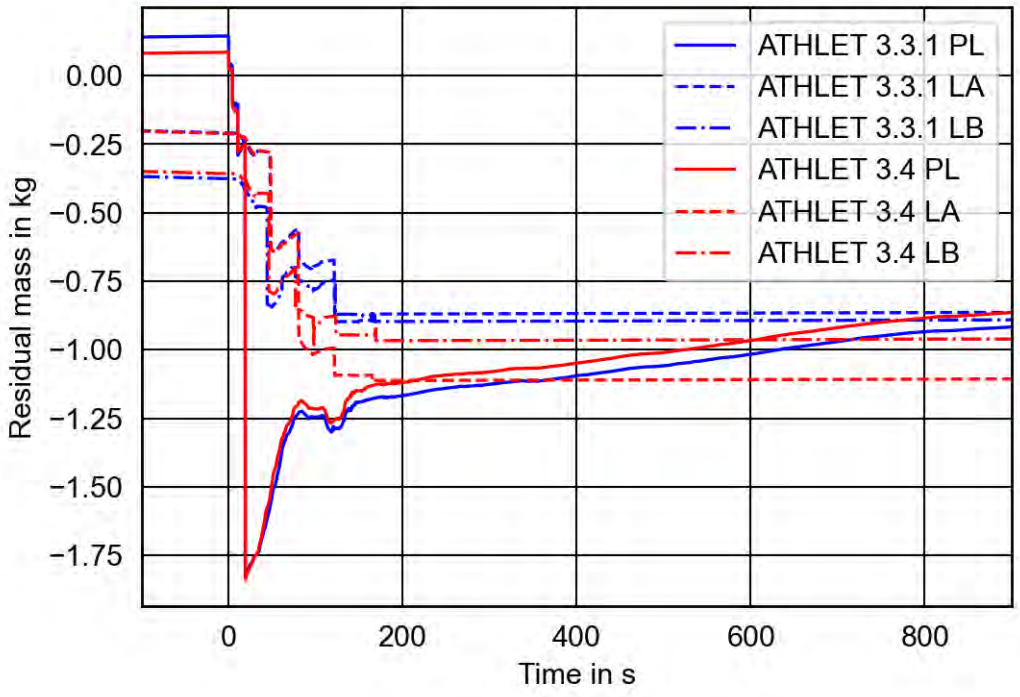

Fig. 5.43 Mass error in the TFD system: Primary loop (PL), secondary loop A (LA), secondary loop B (LB)

5.1.5 Main Findings

The results of the simulation of LSTF SB-CL-18 show that ATHLET 3.4 predicts the main phenomena during the sequence in good agreement to the experimental observations like primary pressure, break flow rates and cladding temperatures at low and middle rod altitude. The highest deviations are calculated for the ECC injection mass flow, the cladding temperatures at high rod levels, and the fluid temperatures in the upper downcomer.

Generally, the code version ATHLET 3.3.1 predicts a quite similar behavior of the sequence.

5.2 ROSA-III – Run 916

5.2.1 Test Facility

The ROSA-III facility is a volumetrically scaled (1:424) BWR system with an electrically heated core designed to study the response of the coolant system, the core, and the ECCS during a postulated LOCA. The facility is instrumented such that various thermal-

hydraulic parameters are measured and recorded during the test. The test facility consists of four subsystems. These subsystems are the pressure vessel, the steam line and the feedwater line, the recirculation loops, and the ECCS. Fig. 5.44 illustrates the configuration of the facility.

The ROSA-III pressure vessel includes various components simulating the internal structures of the reactor vessel in the BWR system. The interior of the vessel is divided into the core, the lower plenum, the upper plenum, the downcomer annulus, the steam separator, the steam dome, and the steam dryer. The core consists of four half-length model fuel assemblies and a control rod simulator. Each fuel assembly contains 62 heater rods and 2 supporting rods spaced in an 8 x 8 square lattice and supported by spacers and upper and lower tie plates. The heater rods are heated electrically with a chopped cosine power distribution along the axis. The effective heated length is 1880 mm, one half of the active length of a BWR fuel rod. The electric power supplied to the 'hot' model fuel assembly 'A' is 1.4 times larger than the power supplied to each of the other assemblies. The heater rods in each assembly are divided into three groups in terms of heat generation rate. The relative power generation rate of a heater rod in each group is 1.1, 1.0, and 0.875, respectively. Orifice plates are inserted at the core inlet to control the core inlet flow.

The steam line is connected to the steam dome of the pressure vessel. A control valve is installed in the steam line to control the steam dome pressure in steady state before the initiation of the tests. The steam line has a branch in which the automatic depressurization system is installed. The feedwater is supplied from the feedwater tank through the feedwater line and the feedwater sparger in the downcomer annulus. The recirculation lines consist of two loops. Each line is furnished with a recirculation pump and two jet pumps. The jet pumps are installed outside the pressure vessel to simulate the relative volume and the relative height to the core.

Two break simulators and a quick shut-off valve are installed in one of these loops to simulate the various break conditions. Each break simulator consists of a nozzle to determine the break size and a quick opening valve to initiate the test. The break mode (the double-ended or the split), the break size, and the break location can be changed. The diameter of the largest nozzle available is 26.2 mm. Several flow nozzles of different size are prepared to vary the break size.

The ROSA-III facility is furnished with all kinds of the ECCS available in the BWR system, i.e., the high-pressure core spray (HPCS), the low-pressure core spray (LPCS), the low-pressure coolant injection (LPCI), and the automatic depressurization (ADS) systems. The HPCS and the LPCS provide the cooling water from the top of the core. The LPCI injects the cooling water into the core shroud. Each ECCS consists of a pump, a tank, piping, and a control system. More detailed information of the facility design is available in references /ANO 80/, /ANO 81/.

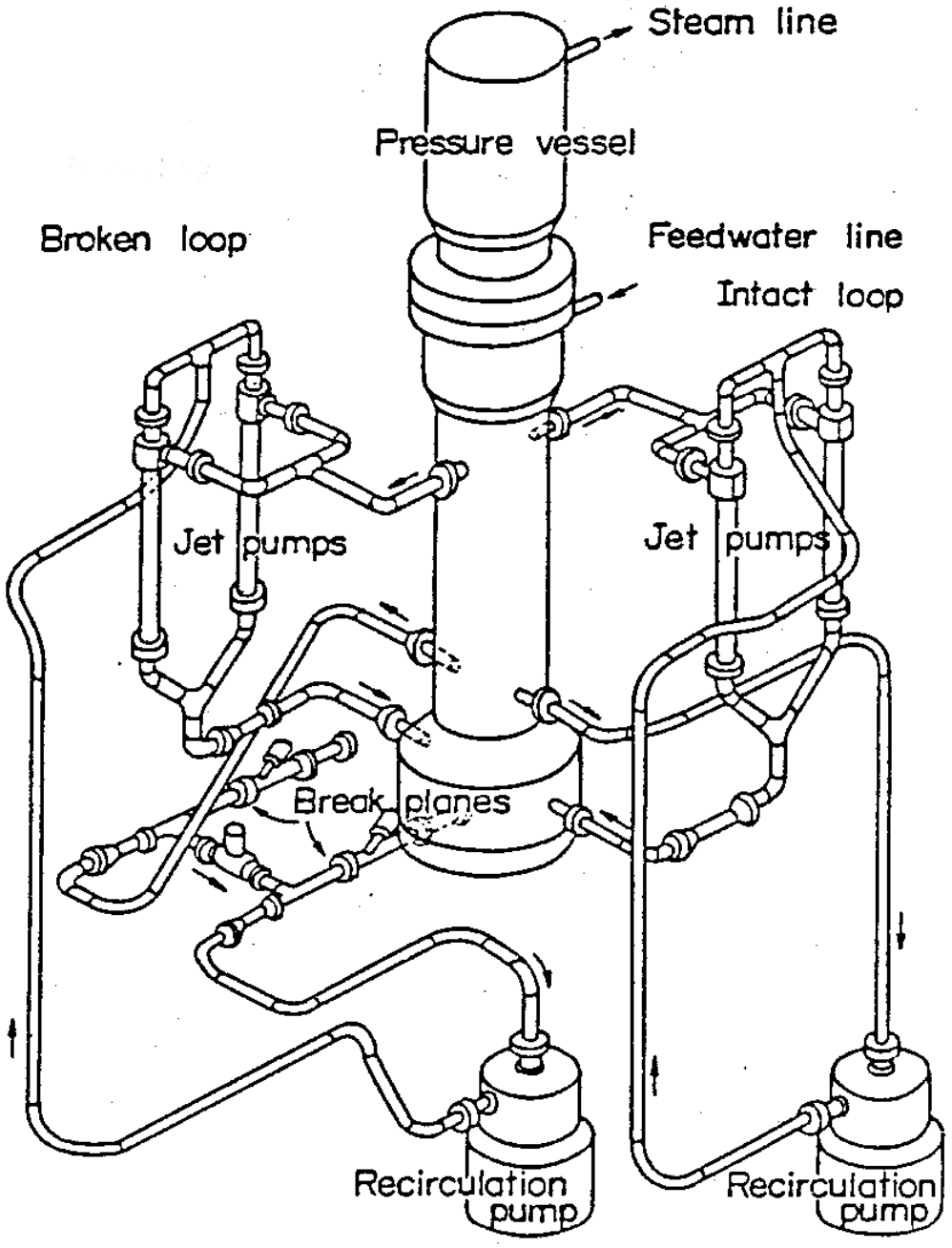

Fig. 5.44 Test Facility ROSA III Run 916

5.2.2 Test Conduct

Run 916 was a 50 % break test at the recirculation pump suction in one of the two recirculation lines /YON 85/. A sharp-edged orifice was used as a break plane. The break

area is determined by inserting an orifice or a nozzle upstream of the QOBV. Blowdown is initiated by opening the blowdown valve B.

The initial conditions of Run 916 are listed in Tab. 5.2. The subcooling at core inlet is 11.2 K, the estimated quality at the core outlet is 14.2 %. The core power is 3.963 MW before the break initiation which is 44 % of the 9 MW steady state power based on the conservation of the power to volume ratio in the reference BWR. The core power is changed during the transient after the break initiation. The power is kept constant for the first 9.0 s and reduced along a curve simulating the total heat transfer rate in the core of the reference BWR (the delayed neutron fission power, the decay power of fission products and actinides and the stored heat in the nuclear fuel) neglecting the stored heat of ROSA-III heater rod. The maximum linear heat generation rate of the peak power rod is 16.7 kW/m before break initiation.

The steam flow before MSIV closure is limited by an orifice of 18.0 mm ID (inner diameter) installed upstream of the MSIV CV-130. The feedwater supply is terminated at 2 s after the break by closing the valve AV-112 in the feedwater line. However, feedwater remained in the piping between the valve AV-112 and the feedwater sparger and flashed during the transient after the pressure dropped below the saturation pressure.

The coolant recirculation pumps are tripped at the break initiation. The liquid level signals in the downcomer are used to actuate the ECCS and to close the MSIV. The downcomer level in the steady state operation is set at the scram level L3 (5.00 m above the bottom of the pressure vessel) and L1 and L2 levels are 4.25 m and 4.76 m, respectively. The L2 level signal is used to close the MSIV with a time delay of 3 s and to actuate HPCS with time delay of 27 s. The L1 level signal is used to actuate LPCS, LPCI and ADS with time delay of 40 s, 40 s and 120 s, respectively. The above lag times of 3 s, 27 s, 40 s and 120 s are used in a safety analysis of the reference BWR. LPCS and LPCI could inject cooling water after the primary system pressure is reduced below 2.16 MPa and 1.57 MPa, respectively. Specified system pressures for actuating LPCS and LPCI were decided from the pump characteristics used in the safety analysis of the reference BWR. The test was terminated after the whole core was quenched at 255 s after break initiation.

Tab. 5.2 Initial conditions for ROSA-III test Run 916

Parameter	Measured value	ATHLET
Steam dome pressure (MPa)	7.32	7.32
Lower plenum (C)	277.7	280.9
Core inlet mass flow (kg/s)	16.5	16.6
Core power (kW)	3963	3960
Max. linear heat generation rate channel A (kW/m)	16.7	16.7
Max. linear heat generation rate channel B (kW/m)	11.9	11.9
Feedwater temperature (C)	216	216
Feedwater mass flow (kg/s)	2.1	2.1
Steam mass flow (kg/s)	2.03	2.1
Water level in PV (m)	5.0	4.8
ECCS water temperature (C)	40	40

5.2.3 Input Dataset

5.2.3.1 Nodalisation

Fig. 5.45 shows the nodalisation used in the ATHLET calculation /POI 89/. The heat conduction volumes for the simulation of the facility structures are not included in this figure. The nodalisation includes the following numbers of network elements:

Branches	11
Pipes	30
CVs	167
Junctions	180
ODEs for thermo-fluiddynamic	863
Heat conduction volumes	159
ODEs for heat conduction	833

The downcomer and the steam dome are divided in 7 TFOs. This fine nodalisation is required to simulate all connecting pipes, the separator, and the dead end of the lower downcomer. For all downcomer objects the mixture level model is applied.

The geometry of the loops is exactly represented. The hydraulic parameters of the recirculation pumps in the loops are determined by homologous curves. Only the single-

phase head curves are known for the ROSA-III pumps, therefore the two-phase curves have been derived from the Semi-scale pump data. Since no momentum curves are available, the pump speed history has been specified as a table according to the experimental measurement.

The TFOs NOZZLEI/B, JETPUMPI/B, and DISSUSORI/B simulate the jet pumps of the intact and the broken loop. The pressure recovery in the diffusor pipe is calculated via the standard momentum equation, the momentum mixing and the suction effect, however, are simulated with a GCSM controlled pump model taking into account the given jet pump characteristics.

The objects LPBOTTOM, LPCON, LPBOTR and LPTOP represent the lower plenum. This fine nodalisation is required to simulate the phase separation processes below the flow limiting cross areas in a realistic way. The 4 rod bundles are modelled by two channels. The object CORE1 represents the bundles B, C and D with a radial power factor of 0.91, CORE2 simulates bundle A with a radial power factor of 1.27. The objects COREOUT and COREIN simulate the head of the bundle and bundle inlet plenum.

The heater rods are modelled by one hot rod and the remaining number of averaged rods. A realistic modelling of the axial power shape is given by 24 axial CV's (arranged from bottom to top), each three of them assigned to one CV. The heater rods are divided in 3 radial materials (heat conductor, isolation and cladding).

The upper plenum and the separator are modelled by the objects RISER and SEPARATOR. The RISER TFO is divided in 4 CVs in order to simulate the phase separation below the separator.

The TFO BYPASS comprises the guide tubes, the reflector and the bundle bypass. COREINBY represents the holes connecting the bundle inlet plenum with the bypass.

The GCSM controlled fill components FEEDWATER and STEAML simulate the steady state feedwater injection and the steady state as well as transient steam removal, resp. The actual volume of the feedwater line is represented by the TFO FEEDWL to consider the flashing and injection process after the pressure has dropped below the feedwater saturation pressure. The ECC injection is performed via the fills HPCS, LPCS, and LPCI2, where the high-pressure injection is assumed to fail.

In all vertical objects including flow limiting flow areas, a fine nodalisation in the region below these areas is used. In this way, a correct simulation of possible counter-current flow limitations can be ensured.

In addition to the heater rods, all relevant structures are considered. To reduce the number of HCVs (to save CPU time) some of them are concentrated to a reduced number of HCOs conserving both the volume and the surface of the structures.

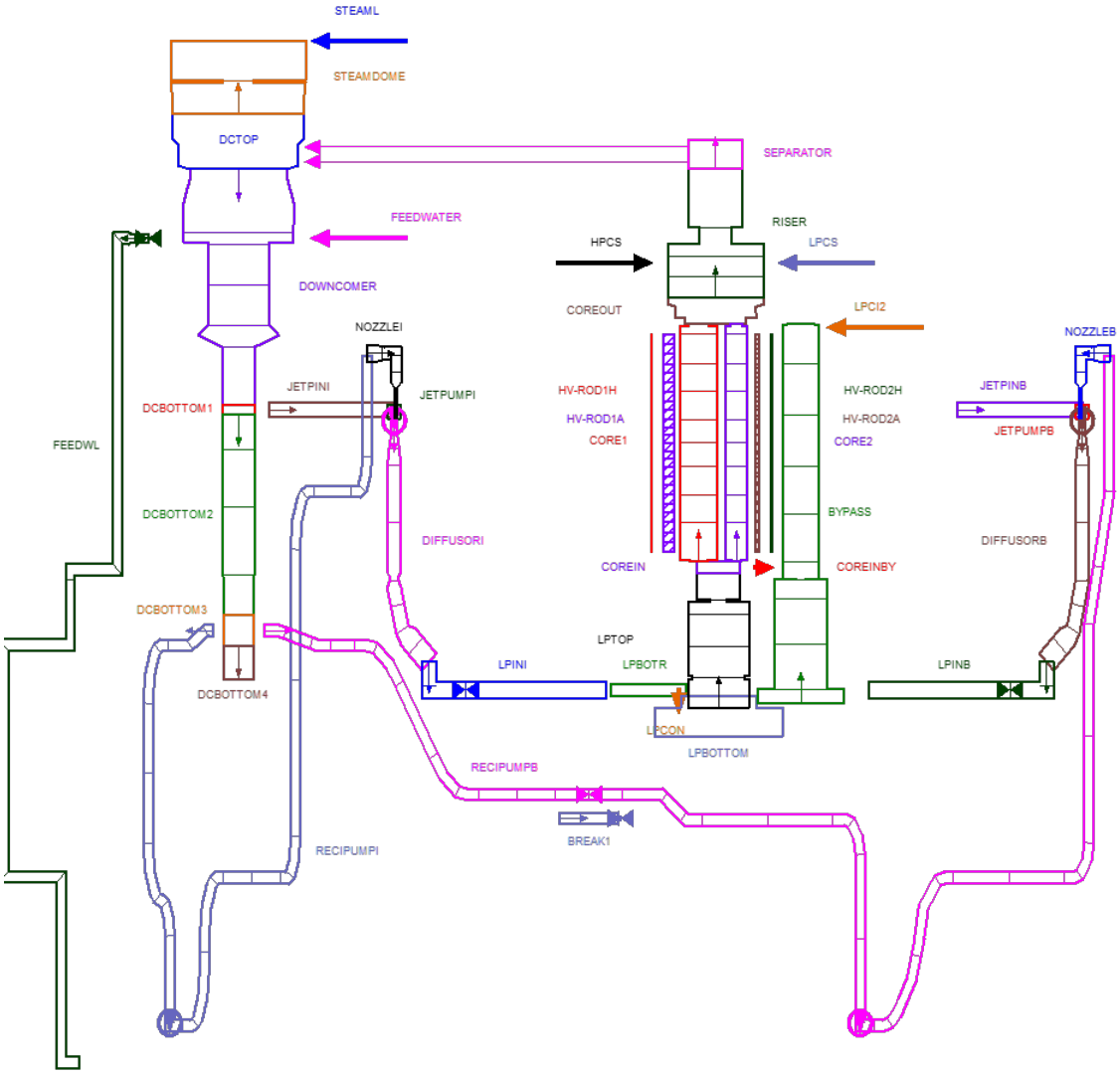

Fig. 5.45 Nodalisation of ROSA III for ATHLET

5.2.3.2 Model Options

Following model options are applied:

- The 5-eq. model with the flooding-based drift model is applied for all TFOs. Corresponding to the geometry, the pipe, bundle, or annulus drift flux option is selected.
- The relative velocity in the bundle inlet diaphragm is calculated with a special flooding-based drift model correlation for bundle inlet orifices of boiling water reactors.
- The critical discharge mass flow is calculated with the CDR1D model. A contraction factor of 0.8 is applied for vapor discharge flow.
- The T-junction model is applied for the entrance from the downcomer to the broken loop recirculation line.
- The friction losses are calculated with the Martinelli-Nelson model applying a constant Darcy-Weisbach friction factor of 0.012.
- The condensation rates are calculated with the ATHLET direct condensation model.
- Evaporation and condensation at heating and cooling surfaces are considered.
- The quench front model is applied to the heater rods.

5.2.4 Main Results

Fig. 5.46 to Fig. 5.62 compare ATHLET 3.4 results with the corresponding experimentally measured parameters for a variety of physical quantities, proving the quality of the ATHLET simulation. Additionally, result achieved with ATHLET 3.3.1 are shown to evaluate also the progress of model development. The experimental result includes the designation of the measurement. Tab. 5.3 lists the sequence of events of both the experiment and the ATHLET calculation.

Tab. 5.3 Sequence of events for ROSA-III test Run 916

Event	Measured time (s)	ATHLET
Break opening, MRP tripped	0	0
Closure of FW supply	1.6 - 3.2	1.6 - 3.2
L2 level trip signal (level < 4.76 m)	5.6	5.7
L1 level trip signal (level < 4.25 m)	10.3	10.8

Main steam line closure	7.5 - 12.2	7 - 12
Jet pump suction nozzle uncovery	13.4	13.6
Recirculation line nozzle uncovery	18	16
Dryout at top of the core	22	20
Lower plenum flashing	38	36
ADS actuation	131	130
FW line flashing	142	143
LPCS initiation	143	142
LPCI initiation	183	185

Fig. 5.46 compares the pressure in the upper plenum, which is representative for all other pressure measurements. After the break has been initiated, the pressure decreases until the main steam valve is closed (at ca. 10 s). The following pressure increase is terminated by the uncover of the broken loop main circulation line due to the low mixture level in the downcomer, leading to an increasing vapor flow through the break (see density at break, Fig. 5.47). In the following time period till about 35 s, ATHLET overestimates the pressure drop, which can be explained by a too early transition to vapor flow at the MRP side of the break and a slightly too low density at the RV side of the break. In addition, the dry out of the top core region is overestimated (e.g. Fig. 5.48), which reduces the steam production there. In the time period until about 100 s, the calculated pressure approaches the measurement. Around 140 s, the feedwater injection line starts to flash and the LPCS injection is initiated which reduces the depressurization.

Fig. 5.49 to Fig. 5.51 show the total break mass flow and the contributions from the RV and the MRP side of the break. Although the density at the MRP side of the break as well as the differential pressure across the BL MRP are overestimated by ATHLET, the break mass flow from the MRP side seems to be underestimated. A good agreement between calculation and measurement can be stated for the main steam mass flow in Fig. 5.52.

The fluid densities at the jet pump exits and upstream of the break are presented e.g. in Fig. 5.47. At the jet pump exits, the calculation corresponds well with the experiment until 200 s, after that the density increase due to the ECC injection (LPCS and LPCI) is clearly overpredicted. As already mentioned, ATHLET calculates the first appearance of steam at the pump side of the break about 10 s too early. Between 40 and 160 s and once again after 250 s, the calculated density is clearly higher than the measured value.

During operational conditions, i.e. before the opening of the break, the pressure differences depend on the mass inventory as well as the flow losses. Since the mass inventory is well known at that time, a good consistency between calculation and experiment proves that the flow loss coefficients are correctly supplied. After the main recirculation pumps have been switched off, the pressure differences across vertical sections indicate mainly the liquid inventory (except near the leak).

The pressure difference between the lower and the upper plenum (including the core) is well predicted (Fig. 5.53), proving that the total liquid inventory in the RV is correctly calculated. This is pointed out here because the calculated fuel rod cladding temperatures indicate a wrong liquid inventory in that section or at least a wrong liquid distribution within the core. Major differences between calculation and experiment can be observed for the pressure differences from the jet pump drives to suctions. Under steady state conditions, the comparison is difficult since there are strong pressure gradients in the vicinity of the jet pump nozzles which, of course, are not resolved by the ATHLET discretization. During the transient, the deviation for the IL jet pump, which is nearly constant in time, seems to be caused by a measurement bias, whereas for the BL jet pump, the deviation may be caused by a too low mass flow towards the break (Fig. 5.49).

Altogether, the comparison of the pressure differences demonstrates that the steady state flow losses as well as the liquid distribution during the transient are calculated well by ATHLET.

The comparison of the calculated liquid and vapor temperatures with the measured fluid temperatures shows that as long as there is no vapor (liquid) in an ATHLET control volume, the vapor (liquid) temperature equals the saturation temperature. In general, both the calculated and measured fluid temperatures are close to the saturation values. Subcooled liquid can be observed only during the initial phase of the transient in the lower downcomer and lower plenum due to the injection of subcooled feedwater, and after the start of the ECC injection into the upper plenum and the core bypass. The latter is clearly overpredicted by ATHLET (Fig. 5.54), what indicates that the calculated condensation rates during ECC injection are too low. Even in the lower plenum (Fig. 5.55), ATHLET calculates subcooled ECC water whereas in the experiment all liquid temperatures remain close to saturation. Superheated vapor appears in pure vapor areas due to heat-up by the fuel bundles (Fig. 5.56) or by hot structures (Fig. 5.57).

Comparing the calculated and the measured fluid temperatures, one has to consider that the measurement shows the temperature history in a small spatial area (e.g. a sub-channel in the core) whereas ATHLET supplies values averaged over the entire control volume which represents - for example - not only the complete core channel flow area but even a finite axial range. Strong spatial temperature gradients in the core region or in the vicinity of the ECC injection points complicate the comparison between the calculation and the experiment.

The comparison of the cladding temperature of each an average and a hot rod in the hot channel box A (HV-ROD2x) and the channel boxes B, C, D (HV-ROD1x) at the axial positions 2 (close to top of core) to 6 (close to bottom of core) point out that the liquid inventory and distribution in the core is not exactly calculated by ATHLET 3.3.1/3.3 (e.g. Fig. 5.48), although the pressure difference between the upper and lower plenum agrees excellently with the experiment (Fig. 5.53). The current version ATHLET 3.3.1 (and 3.3) show a better agreement to the measured data than ATHLET 3.2.1. Within the first 50 s after the break, an early dry-out and rewetting is calculated in the top core region, in contrast to the experiment. At ca. 65 s, dry-out starts in the experiment at top of the core and propagates down through the core. Only for the hot rods in pos. 2 the ATHLET results agree well with the experiment. For lower positions the dry-out is calculated late and the cladding temperatures are clearly underestimated.

Finally, the Fig. 5.58 to Fig. 5.62 document the performance of the ATHLET simulation concerning numerical effort and conservation of the coolant mass balance. In general, ATHLET 3.3.1/3.3 needs more time steps compared to ATHLET 3.2.1. No numerical problems appeared and the maximum mass error for both code version of ca. 0.15 kg, which becomes smaller at the end for ATHLET 3.3, while the mass error for ATHLET 3.3.1 is predicted between ATHLET 3.3 and 3.2.1. For all versions the mass error is negligible compared to the initial mass inventory of about 775 kg.

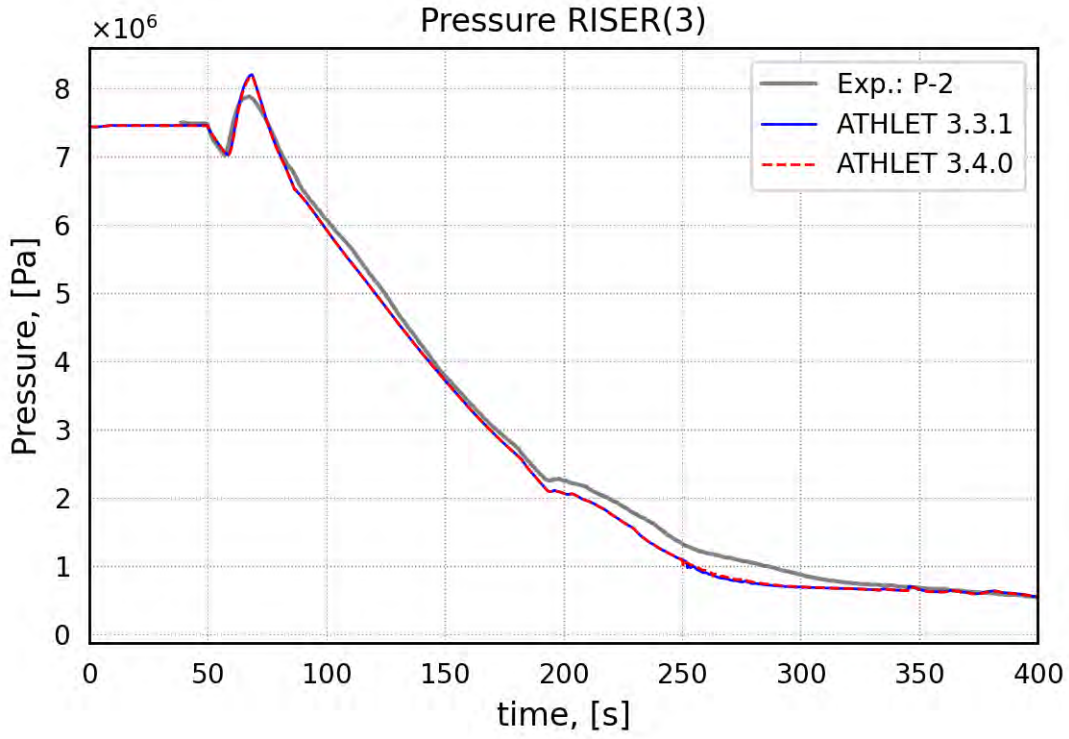

Fig. 5.46 Pressure in upper plenum

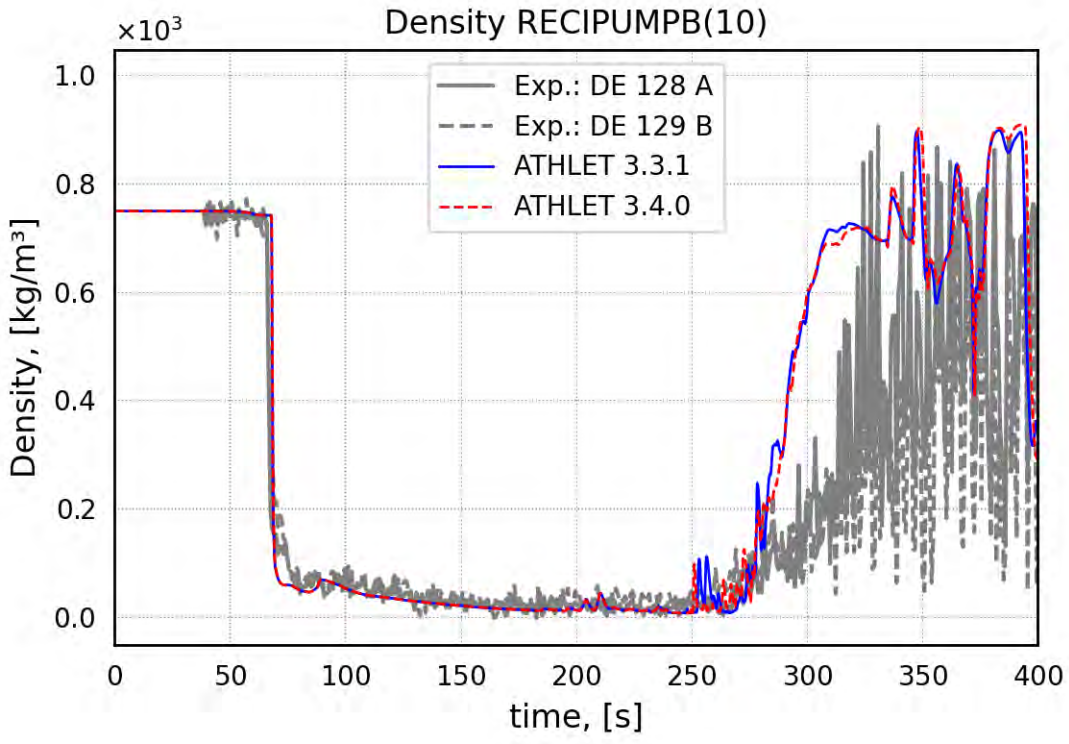

Fig. 5.47 Fluid density at break (RV side)

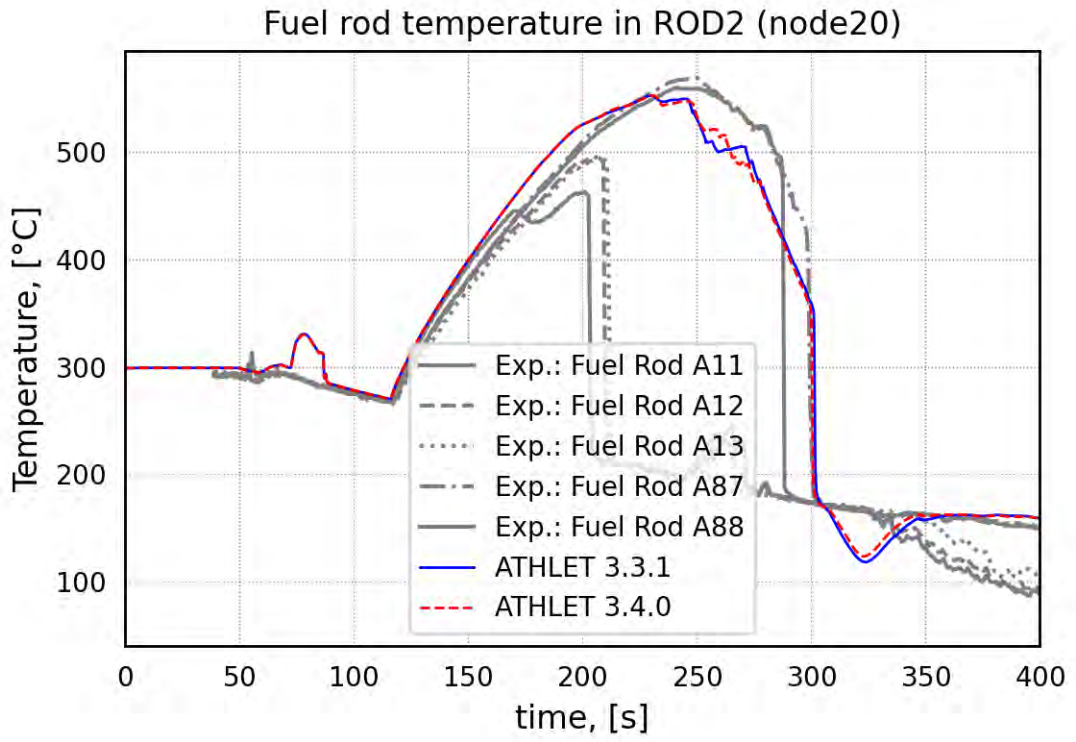

Fig. 5.48 Cladding temperature of fuel hot rods A at pos. 2

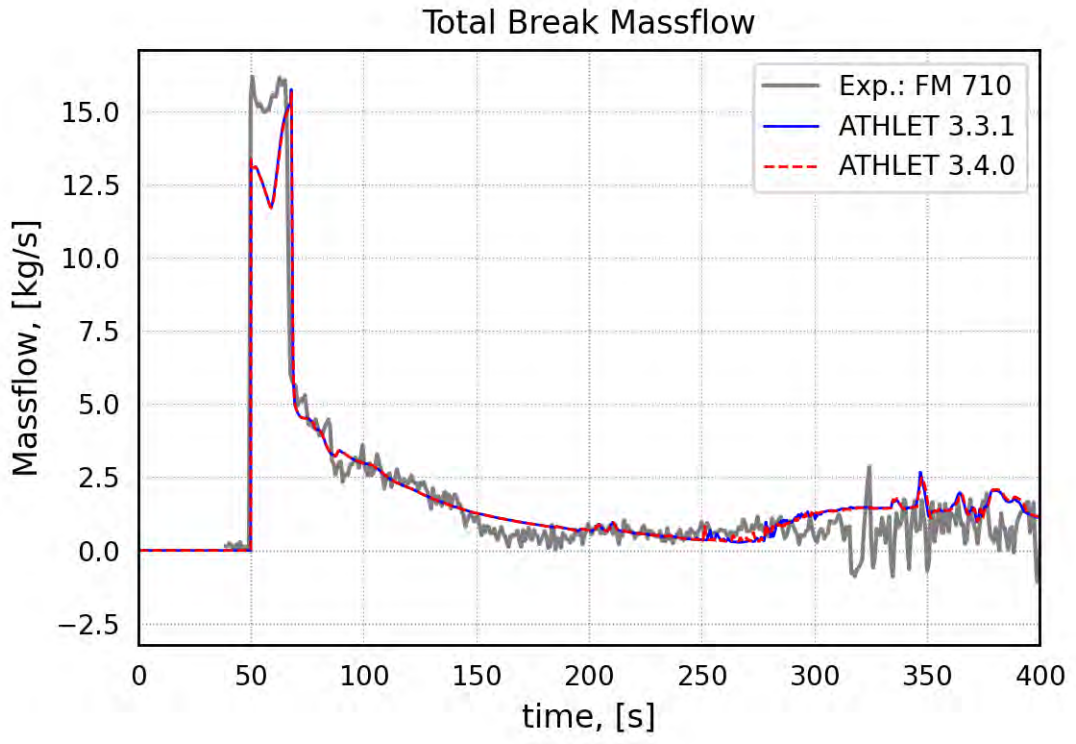

Fig. 5.49 Total break mass flow

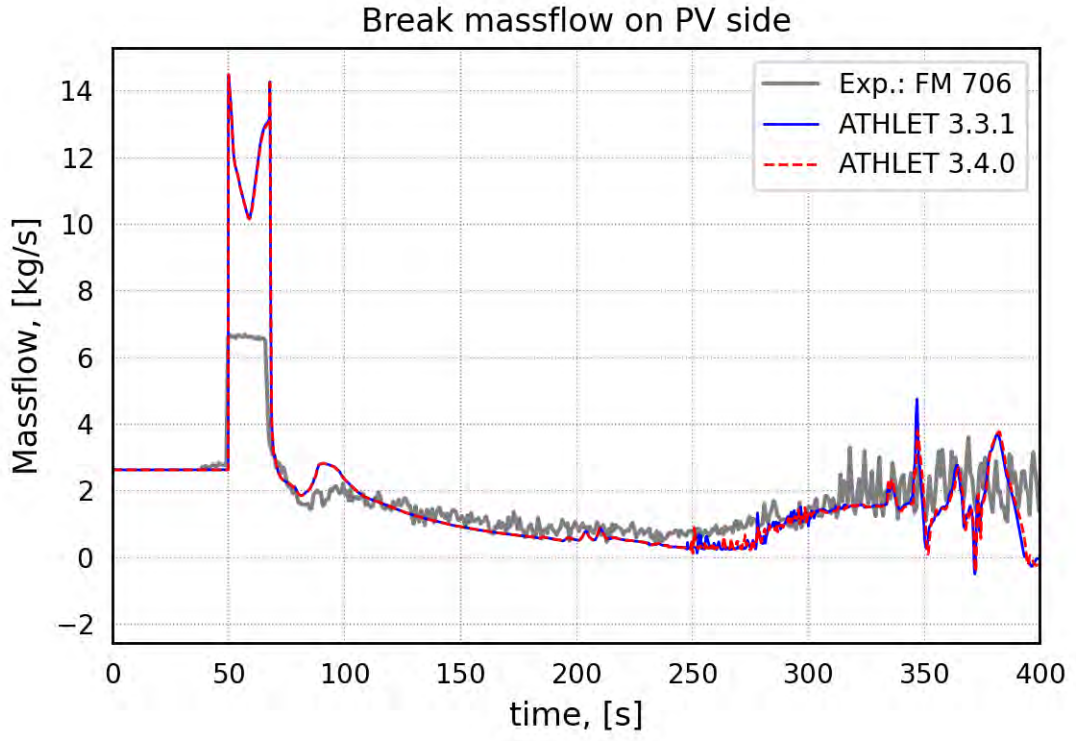

Fig. 5.50 Mass flow at PV side of break (low range measurement)

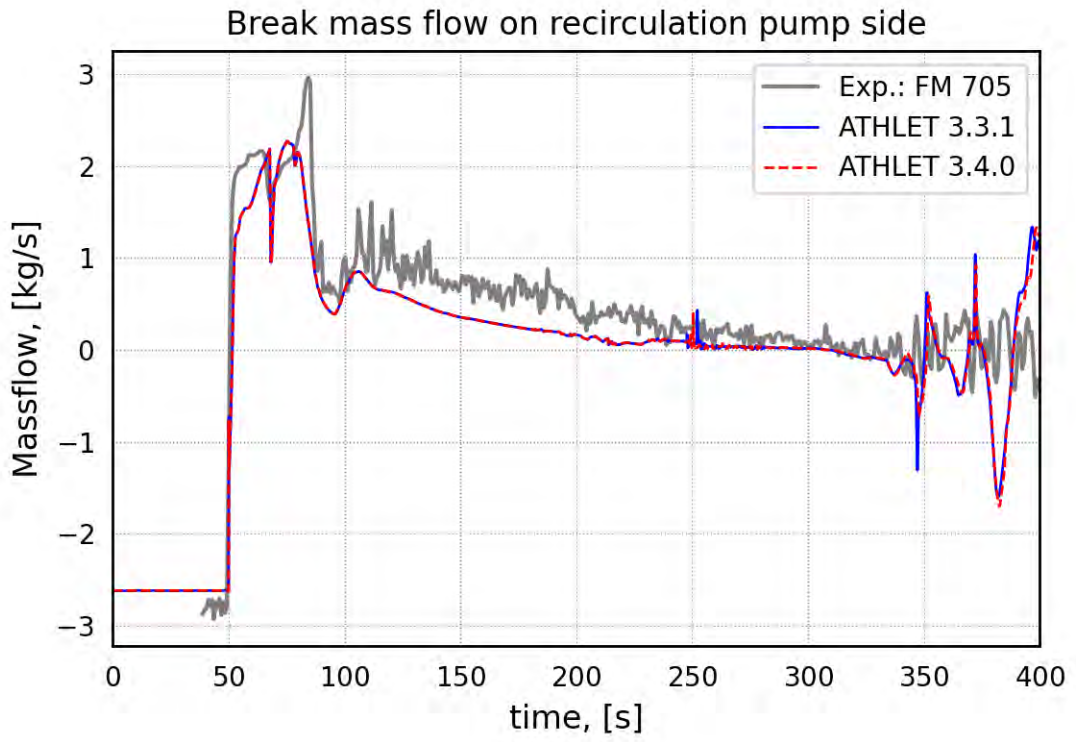

Fig. 5.51 Mass flow at MRP side of break (low range measurement)

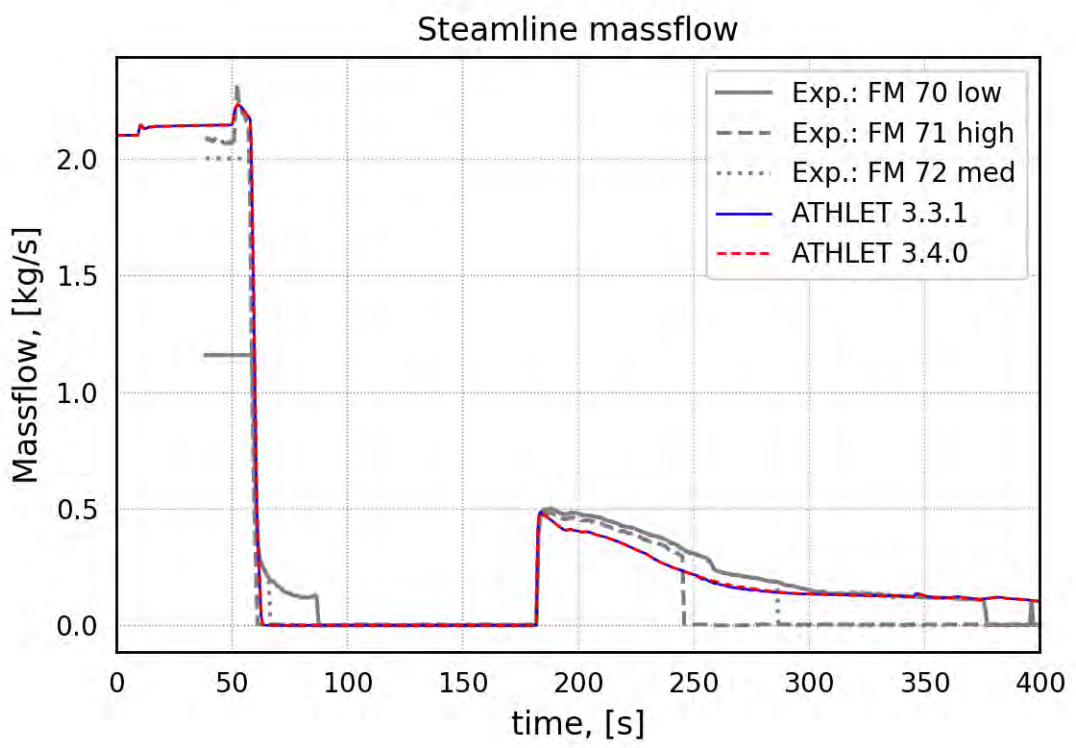

Fig. 5.52 Mass flow in main steam line

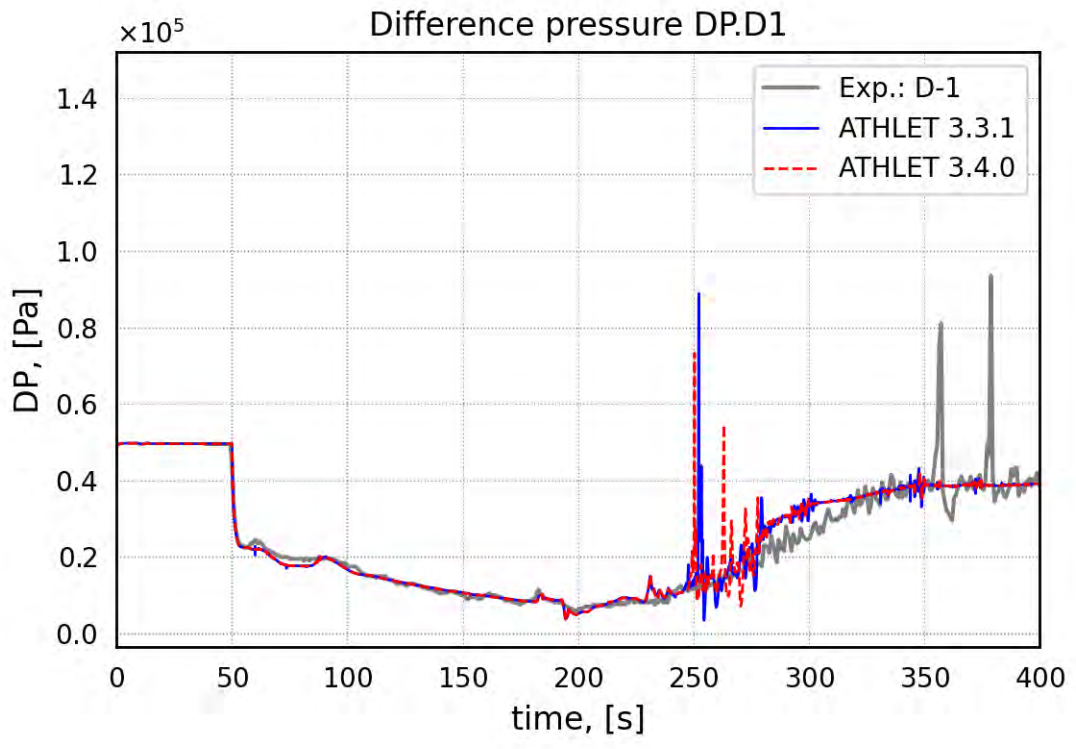

Fig. 5.53 Differential pressure between lower and upper plenum

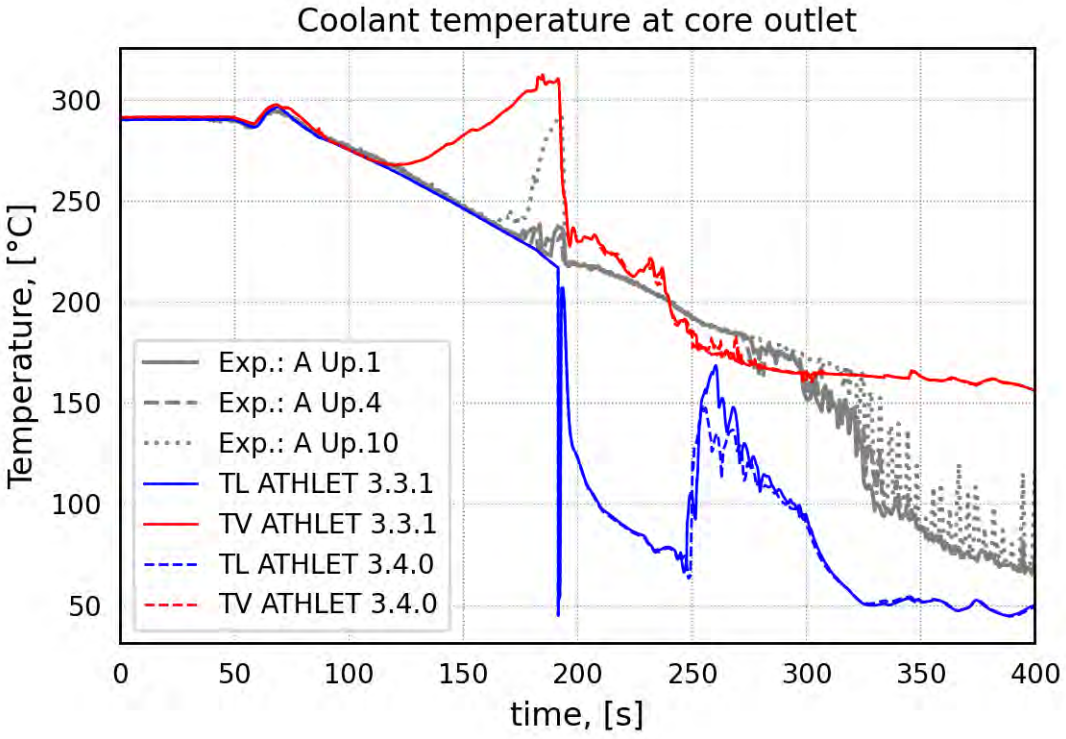

Fig. 5.54 Liquid and vapor temperature above tie plate

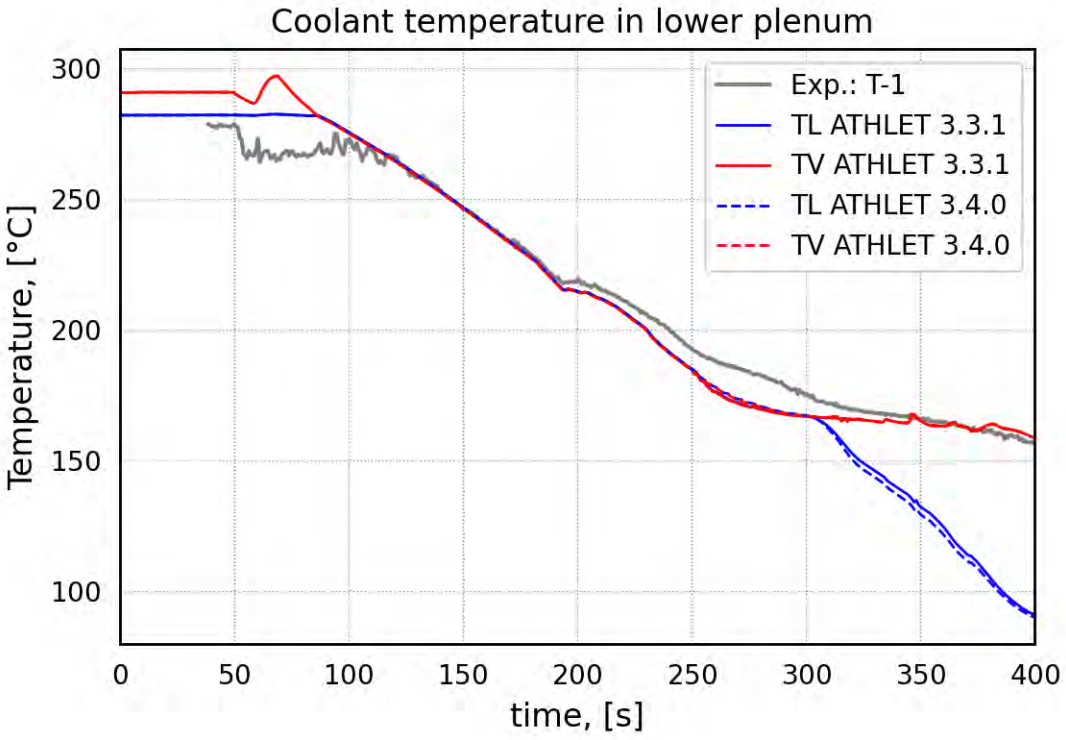

Fig. 5.55 Liquid and vapor temperature in lower plenum

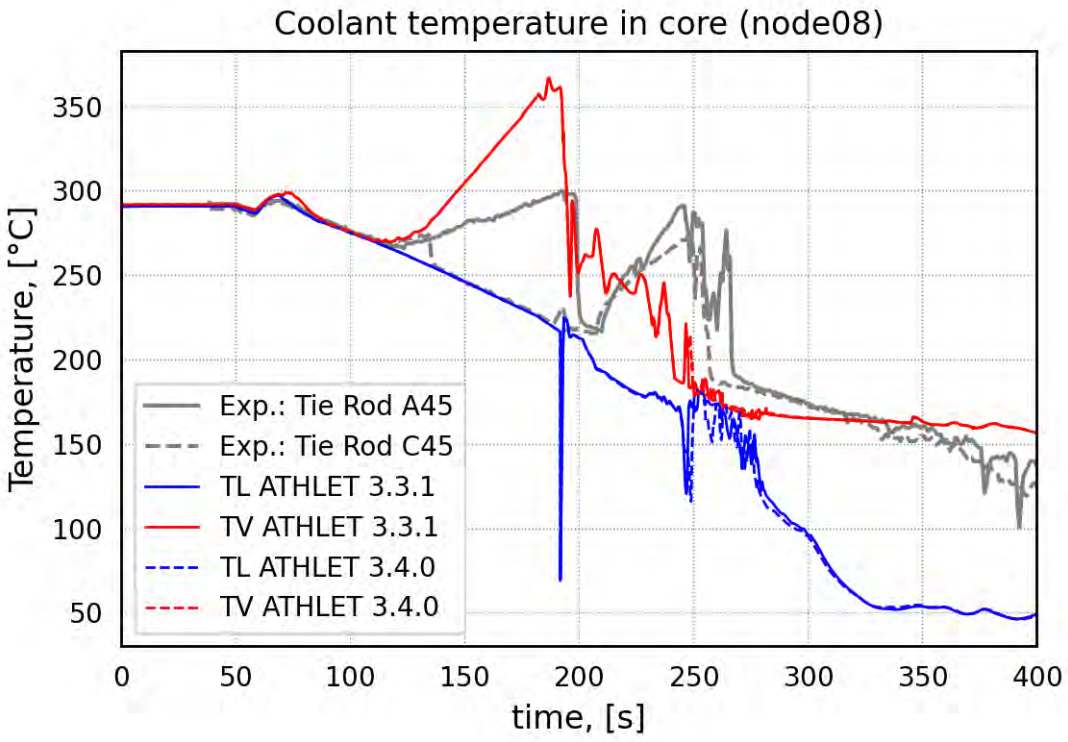

Fig. 5.56 Liquid and vapor temperature in the core (level 1)

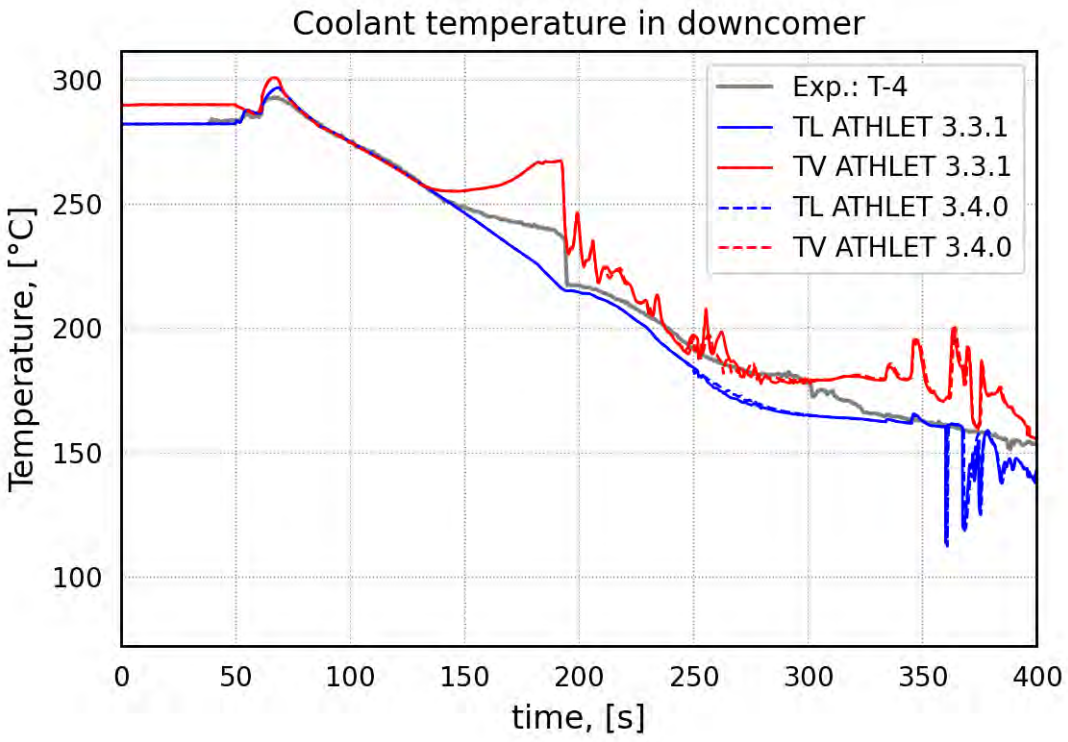

Fig. 5.57 Liquid and vapor temperature temperature in upper DC

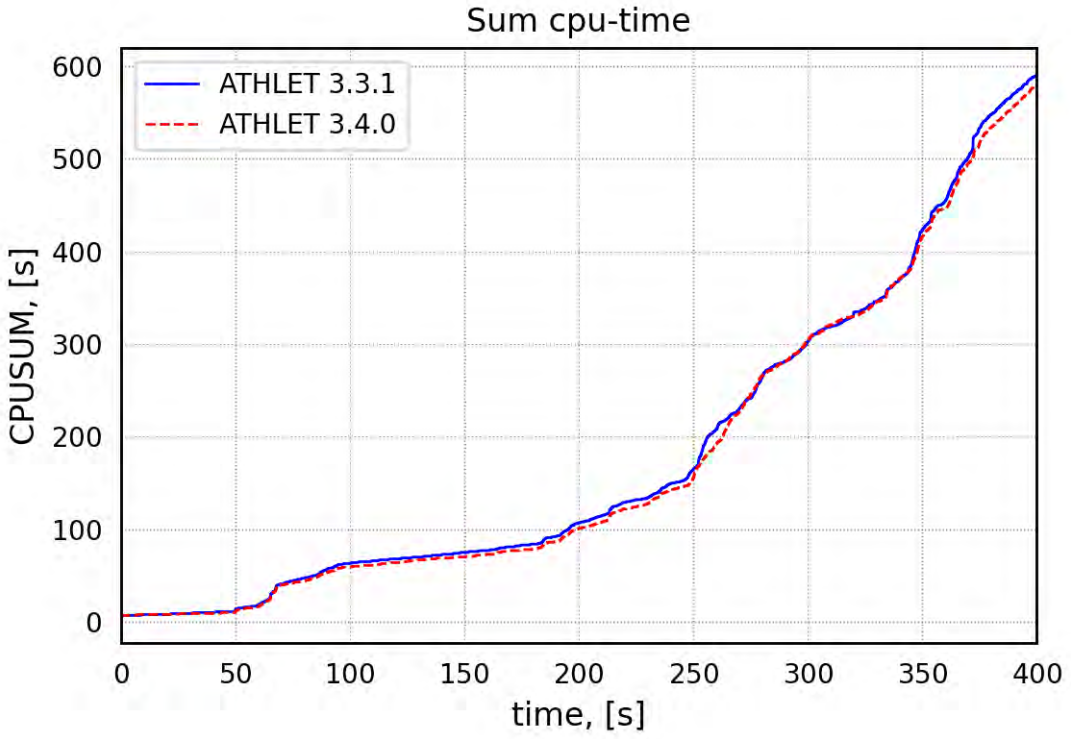

Fig. 5.58 CPU time consumption

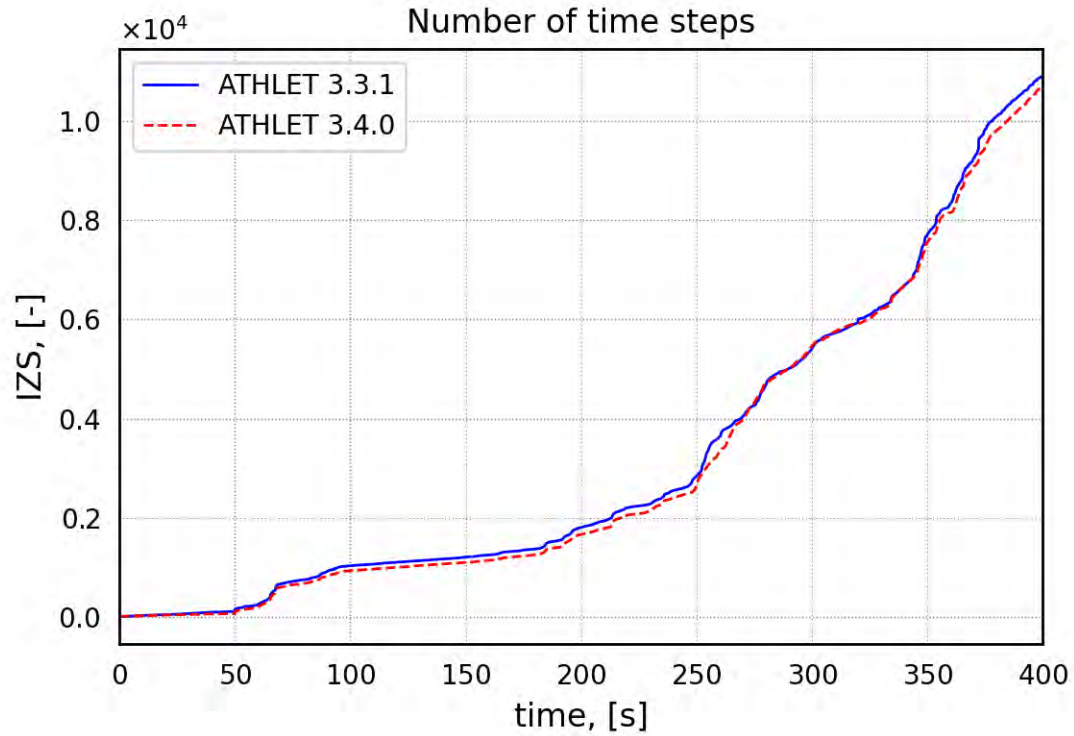

Fig. 5.59 Number of time steps (IZS)

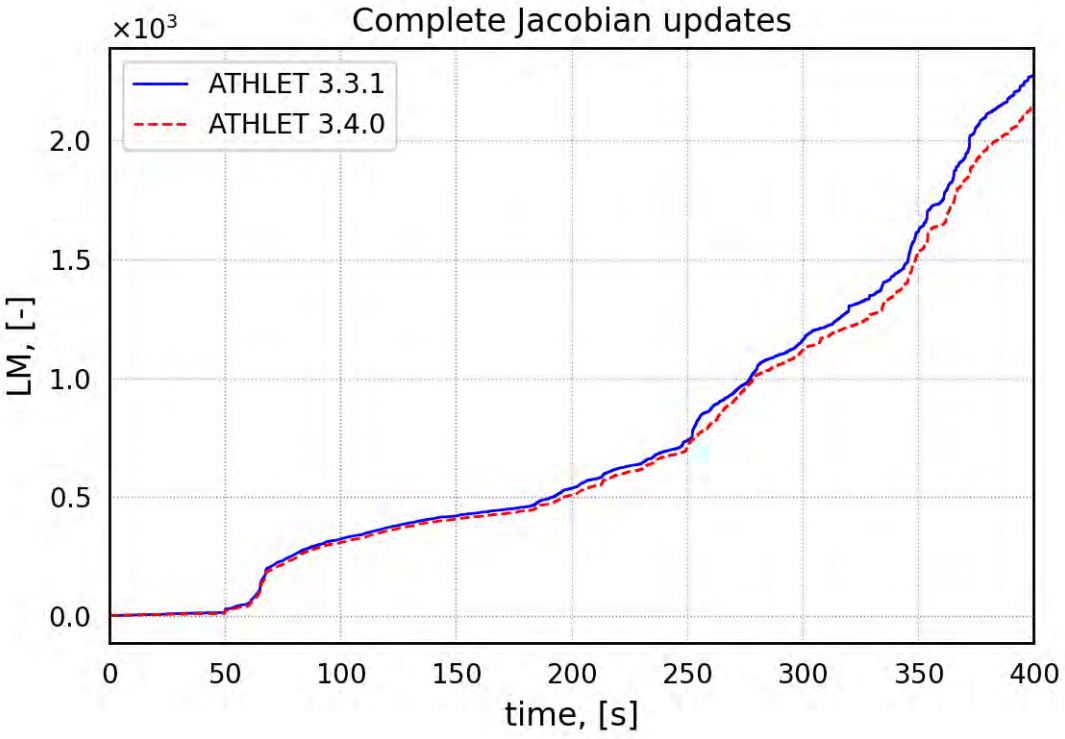

Fig. 5.60 Number of complete Jacobian updates

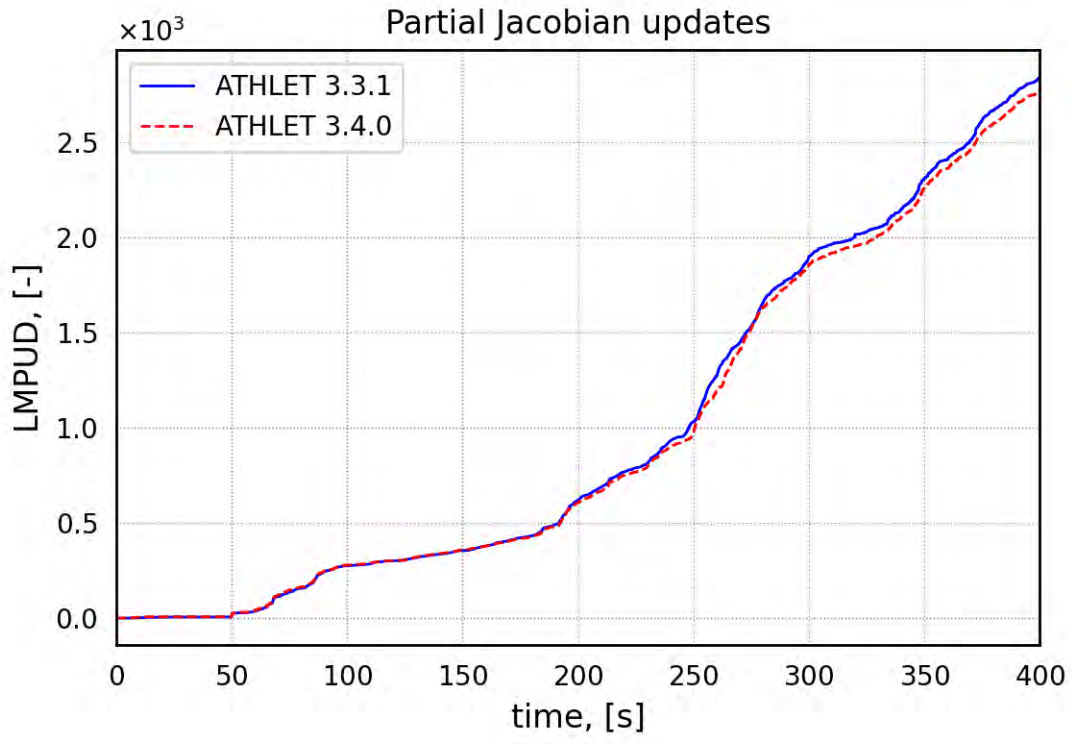

Fig. 5.61 Number of partial Jacobian updates

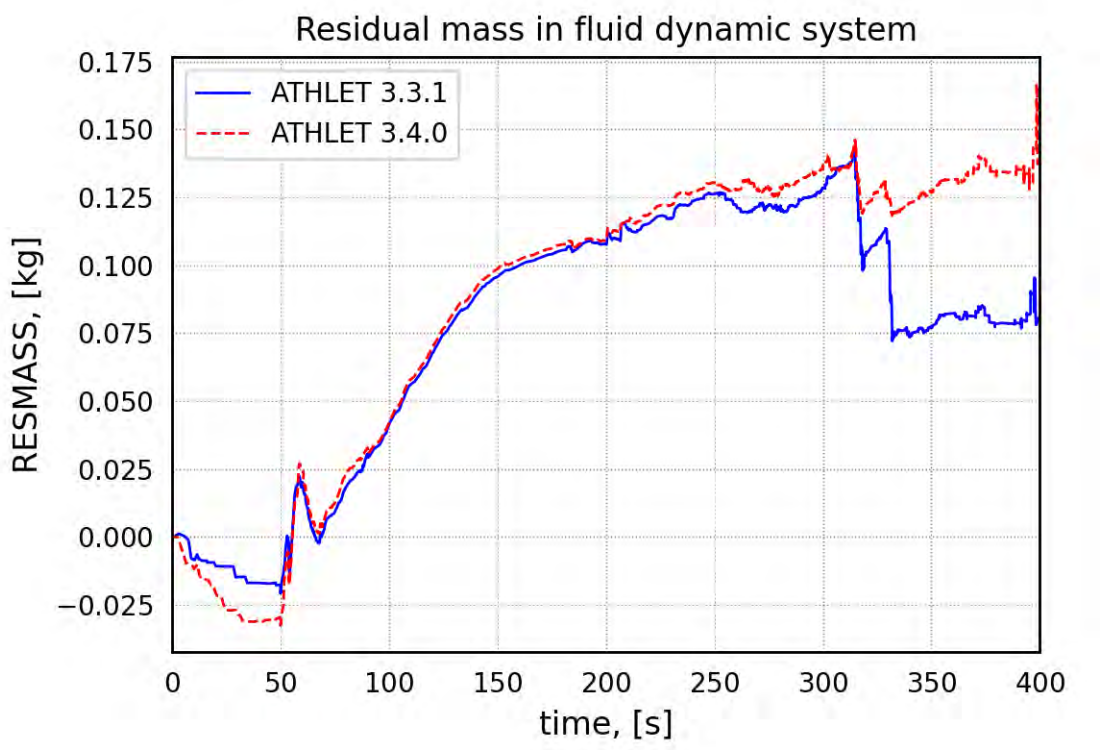

Fig. 5.62 Mass error

5.2.5 Main Findings

Summarizing the comparison of the ATHLET calculation with the experimental results, it can be stated that, in general, the calculated hydraulic parameters show a good, some of them even excellent agreement with the measurements. The main deviations concern the fuel cladding temperatures, in particular in the lower core region, which are underpredicted due to a too large liquid inventory in the core.

Generally, all code versions ATHLET 3.4, and ATHLET 3.3.1 predict a quite similar behaviour of the sequence. If deviations occur, all versions are better or weaker for some properties, which cancel each other in general.

5.3 LOFT LP-LB-1 Test

5.3.1 Test Facility

The LOFT test facility was a 50 MWt 1.5 loop PWR reactor designed to simulate the major components and system responses of a commercial PWR during LOCAs or

operational transient sequences /REE 78/.The reactor is 1:47 volumetrically scaled to an American type 1000 MWe PWR with some peculiarities in detail. It consists of five major subsystems: the reactor vessel including a small nuclear core, the intact loop with steam generator for operational heat removal, the broken loop, the blowdown suppression system and the emergency core cooling system. The systems were instrumented so that quantities important for phenomenological evaluation and system code could be measured with adequate precision.

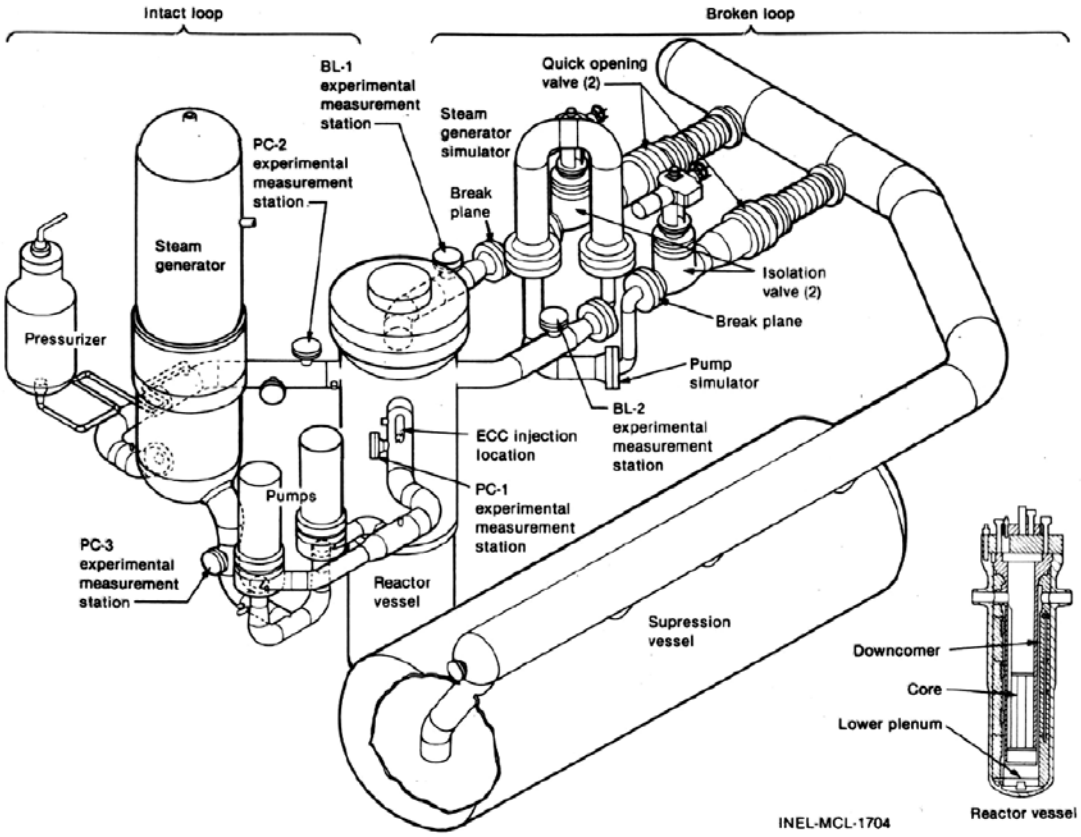

Fig. 5.63 LOFT components showing thermo-fluid instrumentation locations /ADA 84/, p. 5

The configuration of the major LOFT components is shown in Fig. 5.63. The intact loop simulates three loops of a commercial four-loop PWR and contains the one operating steam generator for this reactor, two reactor coolant pumps (RCP) operating in parallel, a venturi flowmeter, and is connected to the pressurizer and connection systems. The broken loop consists of a hot leg and a cold leg with separate connections to the blowdown suppression tank via a quick-opening blowdown valve. In those, an orifice represents the break plane. The broken hot leg also includes passive steam generator and main coolant simulators representing only the volume and pressure losses of those

components. A recirculation line establishes a small flow through the broken loop to maintain the fluid temperature equal to the intact loop cold leg temperature. They were isolated prior to the initiation of the experiment. In addition, the reflood assistance bypass (RABS) connects the broken cold and hot legs, and there is relevant leakage via the closed RABS valves even during operation.

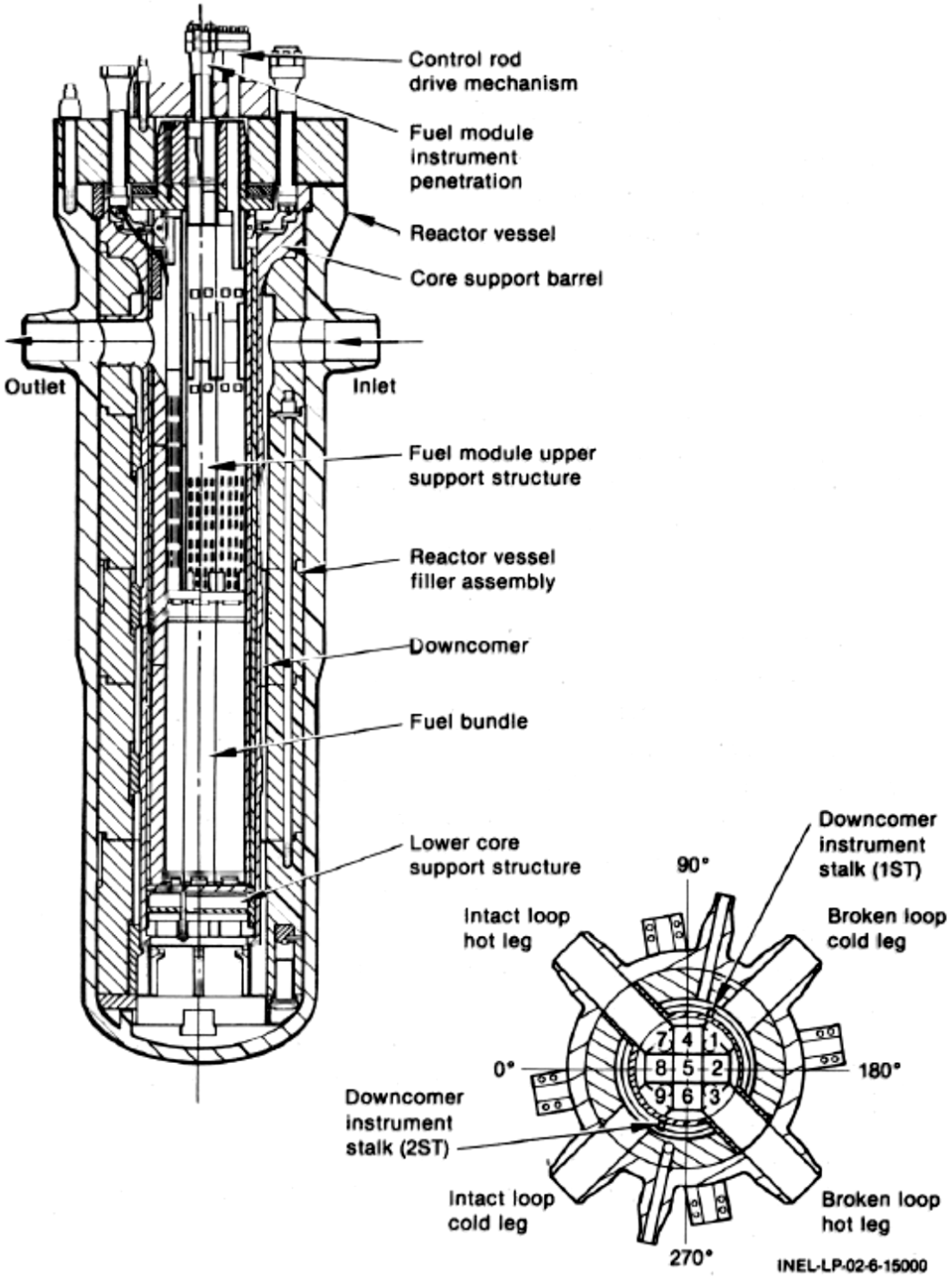

Fig. 5.64 LOFT reactor vessel assembly /ADA 84/, p. 8

The LOFT reactor vessel shown in Fig. 5.64 has an annular downcomer, a lower plenum, lower core support plates, a nuclear core, and an upper plenum. The downcomer is connected to the cold legs of the intact and broken loops, and the upper plenum is connected to the hot legs. Notably, the downcomer consists of a larger ~ 5 cm inner annulus and a

smaller ~ 0.6 cm outer gap, between which metal filler pieces ensure volumetric scaling. The core consists of 1300 enriched-uranium fuel rods arranged in five square and four triangular fuel assemblies. The fuel rods are designed to commercial PWR specifications, except that they are only 1.68 m (66 in.) long, and several fuel rods have special instrumentation. The fuel assemblies are extended with a box-like support structure into the upper plenum, which imposes complex flow paths and increases the overall structural area in that region.

Each one of the two LOFT ECC system consists of an accumulator, a high-pressure injection system (HPIS) and a low-pressure injection system (LPIS).

LOFT started operation in 1976. From 1976 till the end of the fiscal year 1982, a total of 30 nuclear and 7 non-nuclear experiments were run in the US Nuclear Regulatory Commission's (NRC) program. A summary of NRC LOFT program experiments and research findings can be found in /NAL 85/.

5.3.2 Test Conduct

The experiment LP-LB-1 (LOFT Project Large Break test No. 1 /ADA 84/), performed in February 1984, simulated a double-ended offset shear of a cold leg primary coolant pipe in a PWR, and was initiated from conditions representative of a normal operation /WAH 86/. Specific objectives included maximizing the core fraction not rewet at the end of the blowdown phase and investigating the reflood behaviour at hight-temperature conditions with ECC injection flow via the downcomer. Relevant boundary conditions included:

- Near equilibrium decay heat through initial steady state power operation of reactor.
- Assumed loss of off-site power coincident to LOCA, therefore MCP coast down after break initiation and delay of ECC injection for time needed to start-up EDGs. Additionally, trip of RCP and disconnect from flywheels to maximize core uncover after blowdown.

Minimum ECC injection assumptions as in a UK PWR safety case, i.e., no HPIS available, 2 out of 4 accumulators inject to intact loop only at 70 % of nominal injection volume (water level), both LPIS are operation, but at 50 % of nominal safety case injection rate for LOFT (based on Appendix K of 10CFR50.46 in 1983).

- All fuel rods in the core were unpressurized in the gas gap for this test.
- The steady state bypass flow via RABS valves is assumed to be 2.9% /WAH 86/ (or about 8.8 kg/s), total core bypass is 12.5 % using the values given in /WAH 86/ and /JOU 81/ and working notes from the 1980s, but neglecting 1.4 % guide tube bypass in /WAH 86/.

Tab. 5.4 summarizes several important initial and boundary conditions for LP-LB-1 and the corresponding conditions of the reference ATHLET calculation at 0 s.

Tab. 5.4 Initial and boundary conditions for LOFT LP-LB-1

Parameter	**Measured Value**	**ATHLET 3.4.0 (0 s)**
Primary Coolant System		
Core ΔT [K]	29.8 ± 1.4	29.6
Hot leg pressure [MPa]	14.90 ± 0.08	15.01
Cold leg temperature [°C]	282.9 ± 1	283.2
Mass flow rate intact loop [kg/s]	305.8 ± 2.6	304.2
Reactor vessel		
Reactor power [MW]	49.3 ± 1.2	49.12
Max. linear heat generation rate [kW/m]	51.7 ± 3.6	52.8
Pressurizer		
Water temperature [°C]	341.8 ± 5.8	341.6
Pressure [MPa]	14.92 ± 0.11	14.99
Liquid level [m]	1.04 ± 0.04	1.047
Broken loop		
Cold leg temperature [°C]	279 ± 6	279
Hot leg temperature [°C]	288 ± 1	288
Emergency Core Cooling System		
Accumulator pressure [MPa]	4.21 ± 0.06	4.19
Accumulator liquid temperature [°C]	32 ± 6	32

An overview of the main events during the experiment is given in Tab. 5.5. /ADA 84/, /WAH 86/. The cooling of the core was observed to be strongly asymmetric during blowdown in the outer fuel assemblies, with fuel assembly 4 near the intact hot leg quenched halfway through the blowdown and fuel assembly 6 near the intact cold leg/broken hot leg not experiencing cooling until reflooding. Both upper and lower quench fronts were observed during reflooding, with the area around 24 in (~ 40 % active core height) in the central assembly quenched last. Additionally, it was observed post-test that the cladding in hot areas of the core had largely collapsed onto the fuel pellets during the transient, although no substantial cladding failures were observed.

Tab. 5.5 Initial and boundary conditions for LOFT LP-LB-1

Event	**Time (s)**
Blowdown valves opened	0.
Reactor scrammed	0.13 ± 0.01
RCP tripped	0.24 ± 0.01
RCP disconnected from flywheels	0.63 ± 0.01
Control rods on bottom	1.83 ± 0.01
Maximum cladding temperature reached (blowdown)	12.9 ± 0.5
Pressurizer emptied	15 ± 1
Accumulator injection initiated	17.5 ± 0.05
LPIS pumps turned on	24.8 ± 0.5
Maximum cladding temperature reached (reflood)	26.8 ± 0.5
LPIS initiated	32 ± 1
Accumulator emptied	40 ± 1
Accumulator injection complete	46 ± 2
Core reflood complete	50 ± 2
Core quench complete	72 ± 2
Experiment terminated	132

5.3.3 Input Dataset

The LOFT input deck is based on a legacy input deck for LOFT developed in GRS over the last 30 years, however since ATHLET 3.2 /LER 19/ the input for the RPV was

significantly altered. Further changes in the UP have been introduced for version 3.3 /HOL 21/ and version 3.3.1. For version 3.4, four azimuthal channels in the RPV abbreviated by 1, A, 2, B have been implemented.

5.3.3.1 Nodalisation

The facility input deck includes all relevant parts of the LOFT facility except for the blowdown suppression system downstream of the broken legs (see Fig. 5.65) and is nodalized as follows:

- Core

  The core is represented by nine thermal hydraulic channels (Fig. 5.66) radially and azimuthally linked via cross-connections. The hot channel (PV-COR-H) simulates the central fuel assembly (No. 5). Three representative fuel rods are defined:

  - HPV-COR-HA for 104 rods with a peaking factor of 1.3083
  - HPV-COR-H1 for 68 rods with a peaking factor of 1.4268 and
  - HPV-COR-H2 for 32 hot rods with a radial peaking factor of 1.4798.

  The peripheral assemblies are represented by an inner and an outer ring to capture the strong radial power gradient, which each are further subdivided in four azimuthal channels assigned to the intact and broken legs. To each inner channel (PV-COR1/A/2/B-N), two representative rods are assigned:

  - HPV-COR1/A/2/BN1 for 476 average rods with peaking factor of 0.9606 and
  - HPV-COR1/A/2/BN3 for 284 high power rods with peaking factor of 1.2005.

- Each outer channel (PV-COR1/A/2/B-O) contains one representative rod:

  - HPV-COR1/A/2/BN2 for 398 lower rods with a peaking factor of 0.6598.

  Axially, all rods are divided into 18 HCVs, the axial power shape is shifted to the lower parts of the core with a peak factor of 1.58 at 0.556 m. The core power has been re-evaluated based on core maps in /REE 78/, the assignment of core positions to representative rods – and the resulting fraction of total core free flow area – are subtly different to the previous ATHLET model. Flow areas and volumes are adapted to the values in Annex A to /REE 78/.

- Lower plenum

  The lower plenum TFOs (PV-LP1/A/2/B-0, PV-LP1/A/2/B-M, PV-LP-MH) continue the nine core channels into the bottom of the reactor, where they are connected to a common branch object (PV-LP-B). Cross-connections allow for horizontal flow radially and azimuthally, and for the outer channel also to the downcomer TFOs in the LP. Pressure losses and flow constrictions by structures in the core inlet region are considered. Flow areas and volumes are adapted to the values in Annex A to /REE 78/.

  The lower core support structure and fuel end boxes are presented by several HCOs represented by plates with an estimated effective area for heat transfer. Similarly, the lower plenum wall is represented by an HCO with heat losses to the environment neglected.

- Upper plenum

  The upper plenum consists of the central assembly channel (PV-UPC-H, PV-UPB-H) and two outer rings split in four channels (PV-UPC1/A/2/B-N/0, PV-UPB1/A/2/B-N/0) for the peripheral fuel assemblies with respective cross connections – as in the LP and in the core. Radial flow is strongly inhibited where the support structure boxes have not flow holes in their walls. For each channel, there is a separate branch (PV-UPM-M, PV-UPM1/A/2/B-N/0) at the height of the loop nozzles. These branches are connected by single junction pipes. Flow areas and volumes are adapted to the values in Annex A to /REE 78/.

  The upper core support structure is represented by several HCOs that are modelled as plates with a reasonable area for heat transfer and constant thickness of 0.64 cm.

- Downcomer

  The downcomer below the loop connection consists of two annular rings, each split into four channels (PV-DC1/A/2/B-B and PV-DC1/A/2/B-0) assigned to the intact and broken loop respectively. The downcomer channels extend into the lower plenum and connect to the bottom branch PV-LP-B. At the loop connection, the branches PV-DC1/A/2/B-M combine the two rings but are separated from each other by the hot leg piping. Cross connections allow azimuthal flows in the downcomer and additionally radial flow in the lower plenum. Flow areas and volumes are adapted to the values in Annex A to /REE 78/.

  Between both downcomer channels, the solid metal filler is represented by a plate of 26 cm thickness. The inner ring is connected to the core bypass via HCOs representing the core barrel, the outer ring is connected to RPV wall HCOs.

- Bypasses

  There are numerous bypasses in the LOFT facility, which are represented as follows:

  - The RABS bypass is represented by a pipe with a small, but constantly open diameter in the control valve region. Limiting hydraulic diameter and pressure losses have been optimized to achieve 2.9 % bypass flow.

  - The core bypass is represented by an annular ring split into four channels (PV-COR1/A/2/B-BYP), combining the flow-skirt and the filler cooling channel bypasses. Flow areas and volumes are adapted to the values in Annex A to /REE 78/. The bypass at mid-core level between the filler cooling channel and the outer fuel assemblies is neglected. Pressure losses and limiting hydraulic diameter are optimized to achieve 4.6 % bypass flow. The core bypass starts below the active core and reconnects to the upper plenum somewhat below the branch object.

    The flow skirt and the core filler are represented by separate HCOs with an estimated heat transfer area and reasonable thicknesses.

  - The borehole bypass between the flow skirt and the downcomer is modelled by four small SJPs (PV-DB1/A/2/B-S1/2/34) between each downcomer and core bypass channel. The stations are at the heights indicated in /REE 78/ and /JOU 81/. Limiting diameters and flow losses are adapted to achieve 1.04 % bypass flow.

  - The hot leg to downcomer (to cold leg) bypasses are presented by two SJPs (PV-DU-1/2) between the hot leg and respective downcomer branch. This bypass includes any contribution from the hot leg via the upper downcomer annulus into the upper head. Diameters and flow losses are adapted to achieve 3.96 % of nominal flow.

- Loops

  The IL steam generator secondary side is nodalized in detail to simulate both the heat removal during the steady and heat addition during the transient phase of the experiment. The IL U-tubes are represented by one pipe object. The two parallel main coolant pumps and related piping's are combined to one pump. The pump head is calculated by means of homologous head curves; the pump speed is supplied as measured. The operation of the LOCE system post scram is modelled. The accumulator and its connecting line use the dedicated ACCU junction model. The pressurizer is modelled without heating, spray or level control.

The loops TFOs are modelled with adiabatic HCOs to represent pipe walls and other structures, neglecting heat losses to the environment.

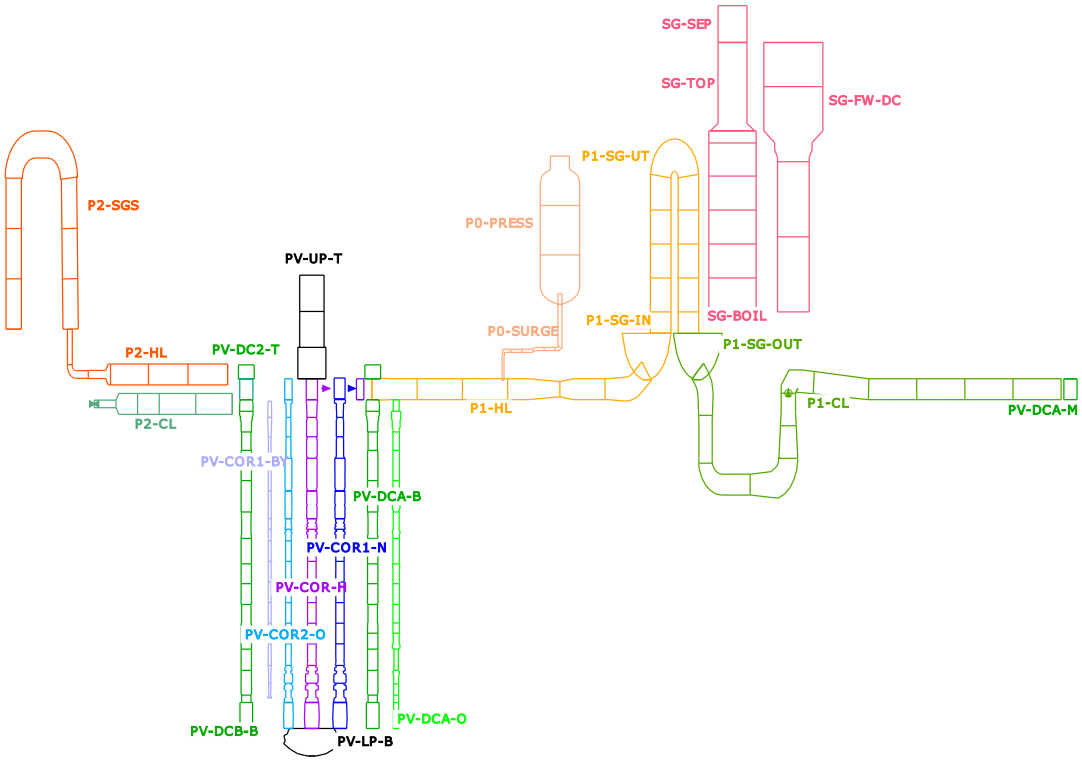

Fig. 5.65 LOFT nodalisation overview

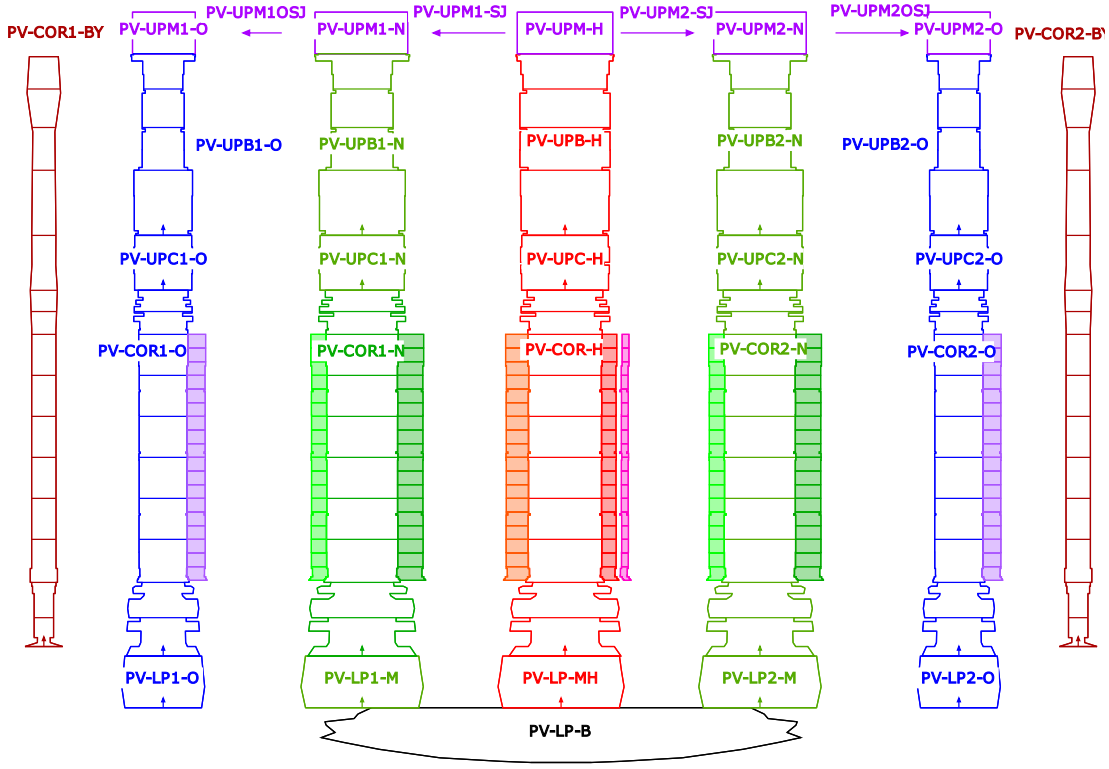

Fig. 5.66 LOFT reactor core, lower plenum and upper plenum nodalisation

The intact loop hot leg is connected to core channel 1, the cold leg to downcomer channel A. Broken loop hot leg is connected to core channel 2, cold leg to downcomer channel B.

5.3.3.2 Model Options

The following modelling settings are applied:

- The 6-equation model is applied in the primary circuit except for the pressurizer and the accumulator and their connection lines, where the 5-equation model is chosen. The secondary side is modelled with the 5-equation model.
- The T-junction model is applied at both ends of the pressurizer surge line to simulate the vapour pull-through when the mixture level reaches the surge line nozzle, as well as the vapour flow and liquid entrainment in case of a pressurizer in-surge.
- The critical discharge mass flow is calculated with the CDR1D model.
- Under CW `MULTICOMP`, hydrogen and nitrogen are activated in the whole primary circuit and solute nitrogen at 600 ppm is specified in the accumulator water phase.

- The point-kinetics neutronics model is active. The ZEROTRANS phase is 10 s.
- Via PW RADPOW, the power shape in each representative fuel rod follows the volumetric power curve given in /REE 78/.
- The gap conductance model is active with default settings, gap width is set to 0.095 mm.
- The quench front model is active with for all representative fuel rods with default settings at primary pressures below 4.7 MPa.
- The boron tracking model is applied. The initial boron concentration equals 513 ppm for the primary circuit and 3000 ppm for the accumulator and LPIS.
- The zirconium oxidation model MODOXI = 2 under PW ZROXIDAT is activated for all rods with a pre-oxidation layer thickness of 5 µm.

The following non-default model options were used:

- Under CW EVAPORATE: IGAM=1
- Under CW INTEGRAT: HMAX=1.0, and under KW DRUFAN: FCLIMA=0.1, FCLWML=0.1, FCLMWV=0.1 (for reducing RESMASS)

The following sensitivity cases were investigated:

- Simulation with ATHLET 3.4 omp version and with NuT with 1 process and default settings (_omp, _nut)
- Using the 5-equation model in the primary circuit (_1M)
- Activating the SBTL95 plugin (_sbtl)

5.3.4 Main Results

After the initial 100 s of steady-state simulation, initial conditions are well aligned to the experimental values (Tab. 5.5). After both blowdown valves open, primary pressure rapidly drops to the saturation pressure, inducing flashing in the primary system, which slows down depressurization. As shown for the intact leg hot leg pressure measurement PE-PC-02 (Fig. 5.67), this is well predicted by ATHLET. However, there is a slight underprediction around 15 s, probably related to an underestimation of structural heat

transfer in the model, and between 35 s and 55 s, which is possibly caused by a combination of overestimated steam condensation during ECC injection and underprediction of steam production at heat structures, and an underprediction of residual flashing into the broken loops. Differences between versions 3.4.0 and 3.3.1 are insignificant.

Break mass flows are also captured reasonably well if the measurement uncertainties are taken into account. Nevertheless, the rapid decrease of the density and - consequentially - of the mass flow in the cold leg around 5 s is not captured (Fig. 5.68), the reason is unknown. One possibility is that the current model only considers one pipe for both pumps and does not model two separate pipes explicitly. Between 30 s to 45 s, the short bursts of mass flow are not captured as well with the 2M model, which is reproduced also in the intact loop cold leg mass flow (Fig. 5.70). The hot leg break mass flow is well predicted in the initial phase (Fig. 5.69) and both peaks towards the end of the blowdown phase are captured qualitatively correct. However, the hot leg flow rate is systematically slightly underestimated with the 2M model between 5 s to 50 s. Only some of that deviation is likely due to limited measurement precision. The initial behaviour of the intact loop cold leg flow rate is captured well (Fig. 5.70), the later deviations are probably due to a somewhat different behaviour during quenching both in the core and in the downcomers, where ATHLET fails to predict some transient condensation-induced water hammers and/or flashing. The volumetric flow measured in the accumulator injection line (Fig. 5.71) is reproduced well as calculated by ATHLET up to 40 s, where the flow is subcooled water. Afterwards, the flow becomes dominated by nitrogen, and ATHLET results and measurements diverge noticeably. Overall, the ATHLET result appears more reasonable, and the peak of the gas flow, which appears to be captured by the measurement, is actually reproduced rather well. Again, differences in break flow prediction between ATHLET 3.3.1 and 3.4.0 are minor.

The comparison of temperatures in the core is a sensitive (and the only available) means of judging the quality of core heat-up and quenching behaviour. However, when interpreting the following signals, it has to be considered that some of the cladding – particularly in the middle of the core – did collapse onto the pellets during the transient. This effect is not captured by ATHLET. In the short term, this will lead to an underprediction of cladding temperature and heat removal from the fuel, whereas in the reflooding phase the fuel in the simulation will remain hotter, leading to a delayed prediction of quenching particularly during reflooding. Moreover, the specific power in the instrumented fuel rod will not exactly match the representative fuel rod in ATHLET. However, for the following

comparison, fuel rods have been chosen that are reasonably close to the representative rods in their respective TFO.

In Fig. 5.72, the wall temperature in a “normal” rod near the centre at 11 inch is compared to the respective ATHLET result at the same height. This shows a clear underprediction, the effectiveness of quenching after blowdown is overestimated, the subsequent heat-up during reflooding underestimated. This is an artefact of the nodalisation, as the HCV in question is assigned to the lower CV in the central channel. In the subsequent upper HCV, which is assigned to the CV above, the prediction of heat-up and quenching during blowdown and re-flood is a better fit to the data (dashed lines), although peak cladding temperature here is still underestimated by about 50 K. Importantly, the time of final clad quenching at 50 s is predicted merely 5 s early. In the middle of core height, the heat-up in a hot rod at 31 inch is slightly underpredicted during blowdown and the initial reflooding phase (Fig. 5.73). However, the final quench is predicted with some delay at about 85 s instead of 72 s and starting at about 100 K lower wall temperatures. In the upper core region, the temperature of a central normal rod at 49 inch shows considerable deviations (Fig. 5.74). While the time of initial heat-up is captured and the time of quench are qualitatively captured, the peak temperature is significantly underestimated. In the reflooding phase, the timing and degree of the heat-up is underestimated, while the final quench happens too late. In sensitivity calculation without the ATHLET quench model, the timing for final quench after reflooding could be improved, cladding temperatures during the reflooding phase we reduced, thus more investigations will be needed here.

Looking at the wall temperatures of homologous rods 2H14 and 6H14 at 32 inch in the peripheral fuel assemblies allows to gauge the degree of asymmetry simulated by ATHLET. In the current model, assembly 2 is assigned to core channel 2 and assembly 6 to the channel A. In Fig. 5.75 the data for both rods are compared with ATHLET results for both parts. The ATHLET results for channel A show a 200 K overprediction of peak temperature for fuel assembly 2 and only 50 K overprediction for assembly 6. Consequently, quenching is delayed by around 30 s. Notably, the ATHLET results for channel A do not fit to measurement values associate to that channel and are more similar to the results for average rods in the central channel. Overall, the thermal-hydraulic asymmetry in not well captured in the ATHLET model, despite a nodalisation with at least azimuthal peripheral channels as in /ADA 84/. In addition, the deviations in initial cladding temperature and temperature peak during blowdown throughout the core show indicate that firstly the power shape and distribution in the core might not be fully representative of

the experiment, and secondly that there might still be issues with the entrainment and de-entrainment modelling in ATHLET and the modelling of the complex flow paths in the upper plenum. In addition, there is some dependency on the core nodalisation, although other parts of the model, e.g., the upper and lower plena, might be more influential. In addition, the nodalisation changes compared to /HOL 22a/ did worsen the results in the reflooding phase for both code versions. Further optimisation of the input deck will be necessary to better reflect phenomena in the test.

In Fig. 5.76, data for fluid temperature at several positions in the upper end box of the central fuel assembly are compared with ATHLET results. The initial temperature peak in the central region of the fuel assembly during blowdown is missed by ATHLET, remaining at saturation temperatures. The subsequent peak during core uncovery ending with reflooding is predicted by ATHLET, but overpredicted by about 100 K and about 10 s late. This indicates that top quenching is underpredicted by ATHLET. The results for the blowdown phase motivate that outer rods in the central channel might be more similar to hot peripheral fuel rods. Moreover, as ATHLET does not explicitly compute radiative heat transfer to the fluid, adding this mechanism could be explored for further improvements.

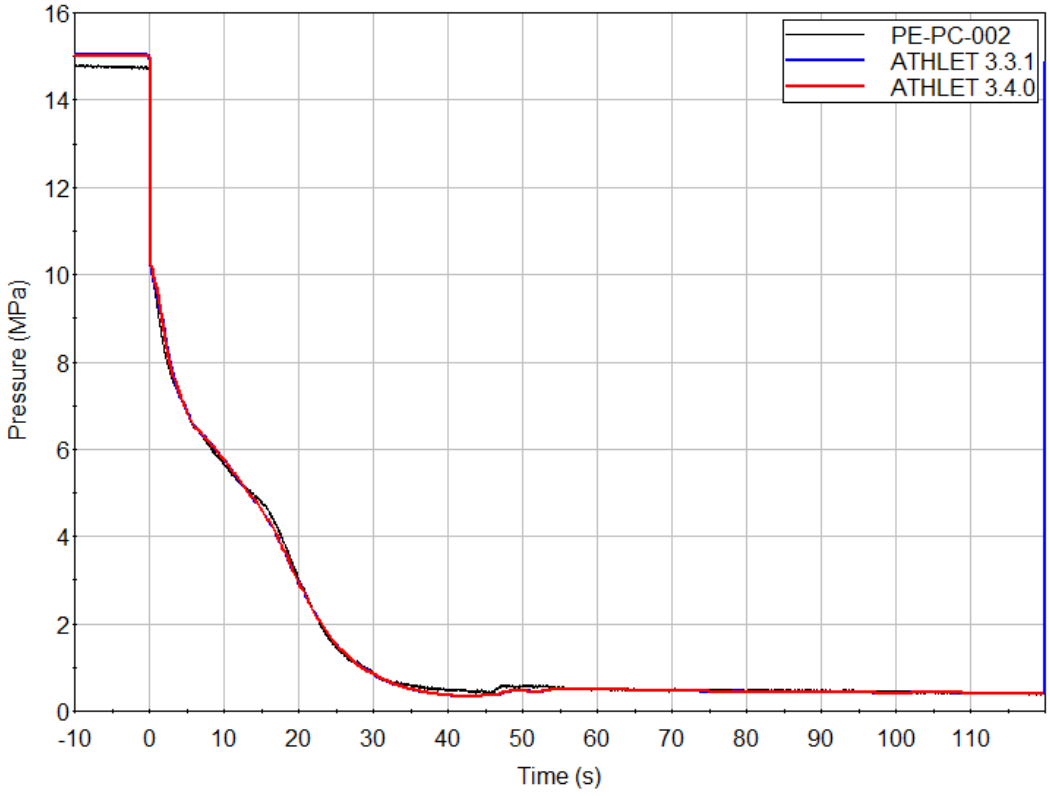

Fig. 5.67 LP-LB-1 primary side pressure PE-PC-02 with ATHLET 3.4.0 and 3.3.1 results

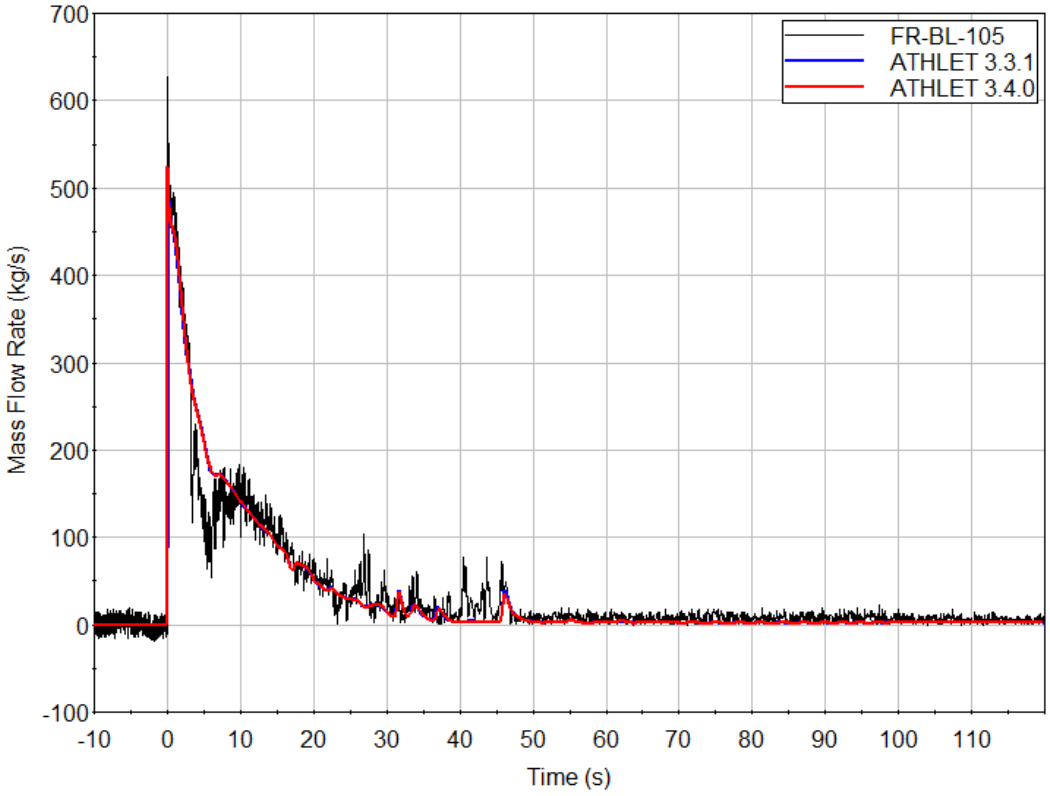

Fig. 5.68 LP-LB-1 broken cold leg mass flow rate FR-BL-105 with ATHLET 3.4.0 and 3.3.0 results

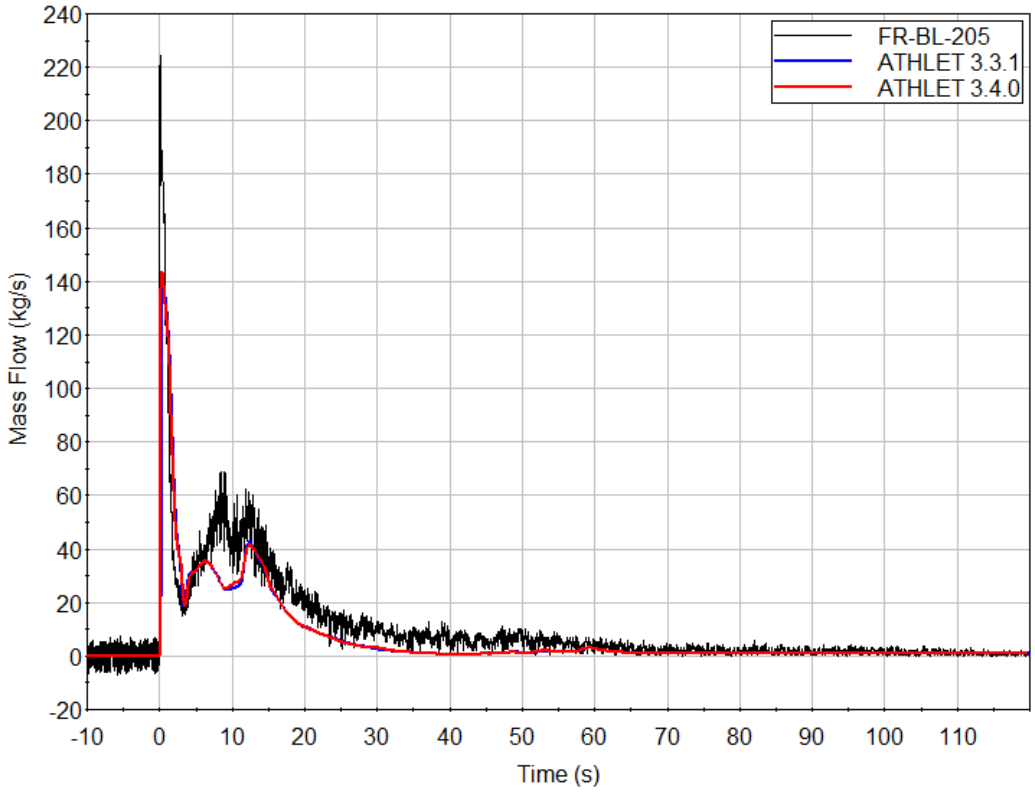

Fig. 5.69 LP-LB-1 broken hot leg mass flow rate FR-BL-205 with ATHLET 3.4.0 and 3.3.0 results

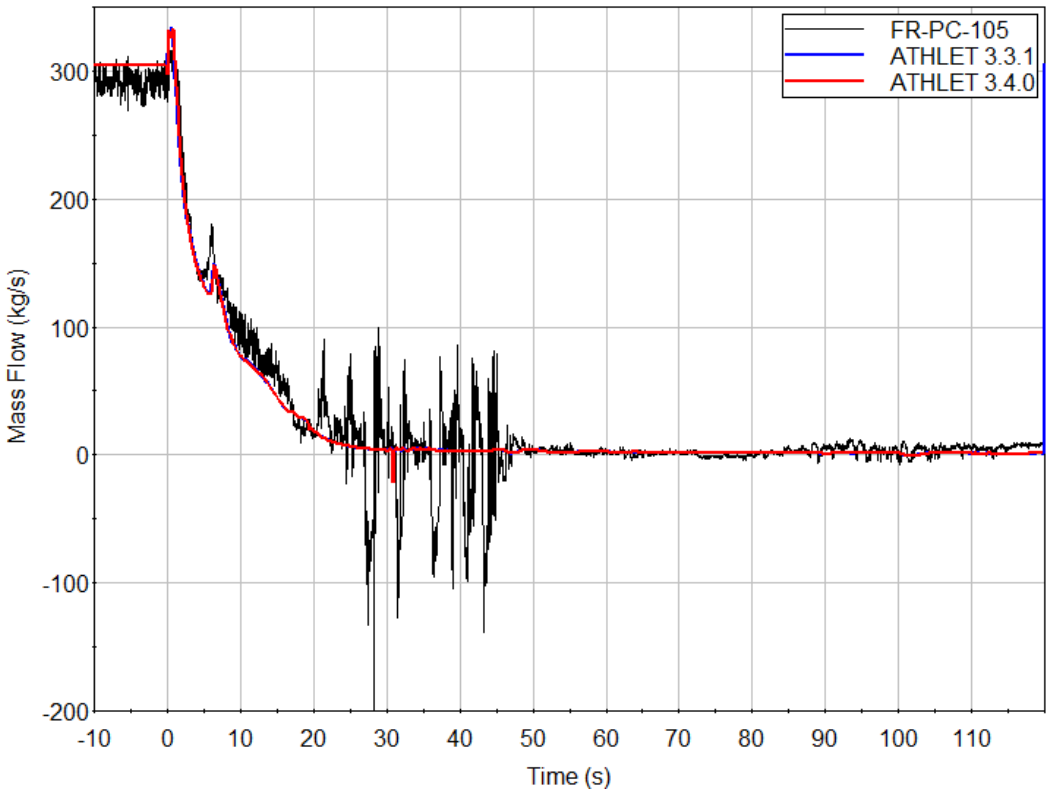

Fig. 5.70 LP-LB-1 intact loop cold leg mass flow rate FR-PC-105 with ATHLET 3.4.0 and 3.3.0 results

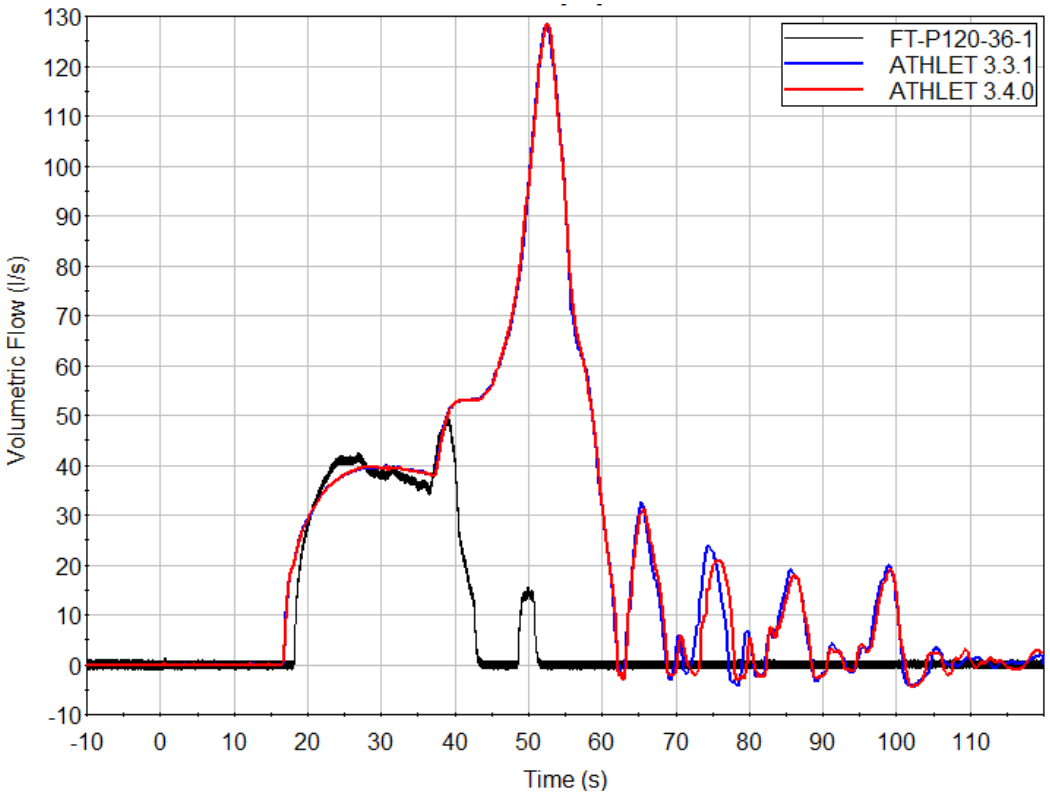

Fig. 5.71 LP-LB-1 accumulator volumetric flow rate FT-P120-36-1 with ATHLET 3.4.0 and 3.3.0 results

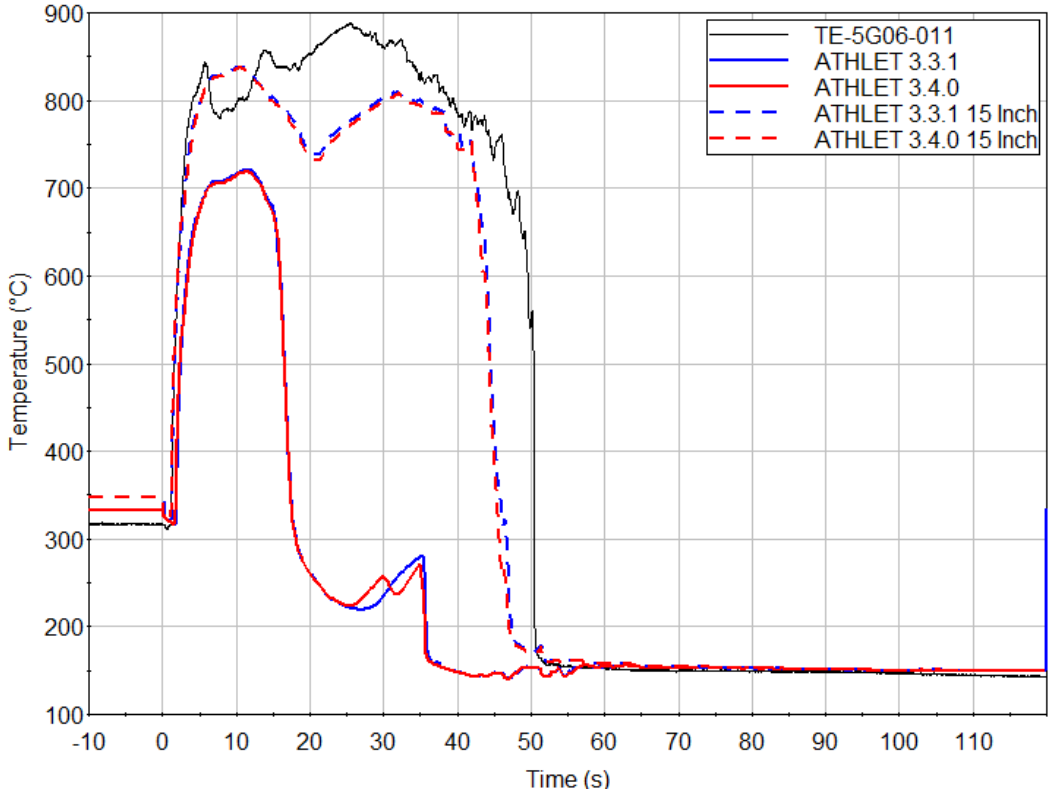

Fig. 5.72 LP-LB-1 central fuel assembly average rod wall temperature TE-5G06-011 at 11 inches with ATHLET 3.4.0 and 3.3.0 results

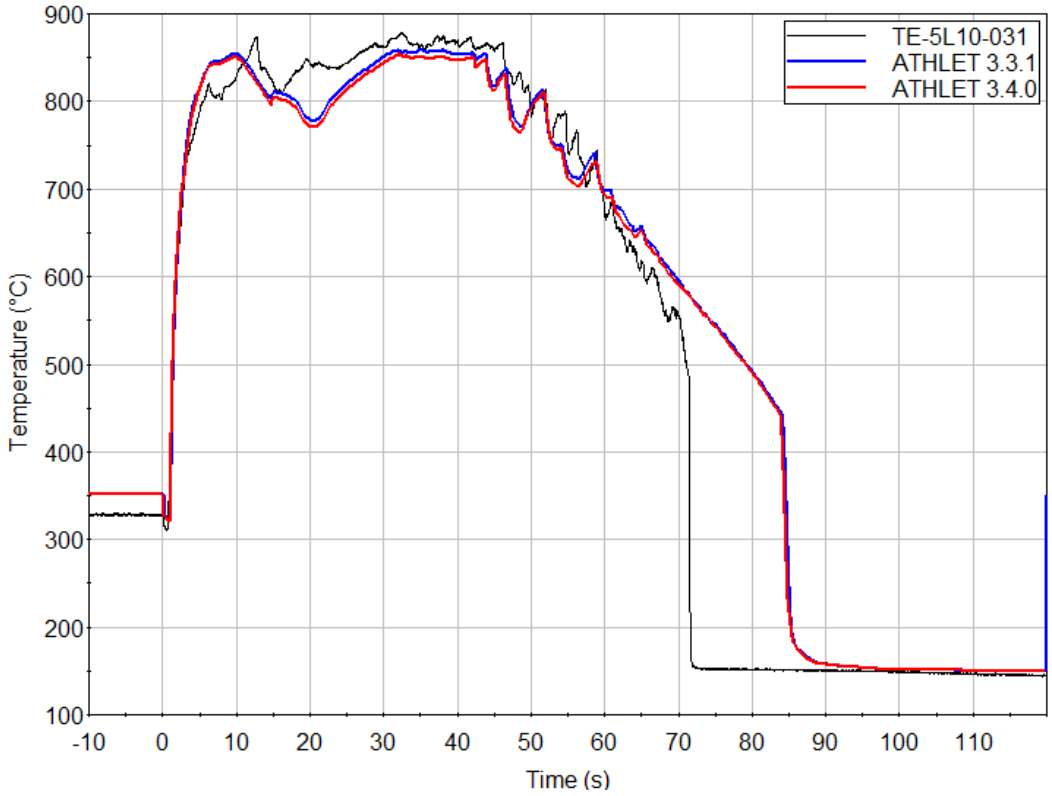

Fig. 5.73 LP-LB-1 central fuel assembly hot rod wall temperature TE-5L10-031 at 31 inches with ATHLET 3.4.0 and 3.3.0 results

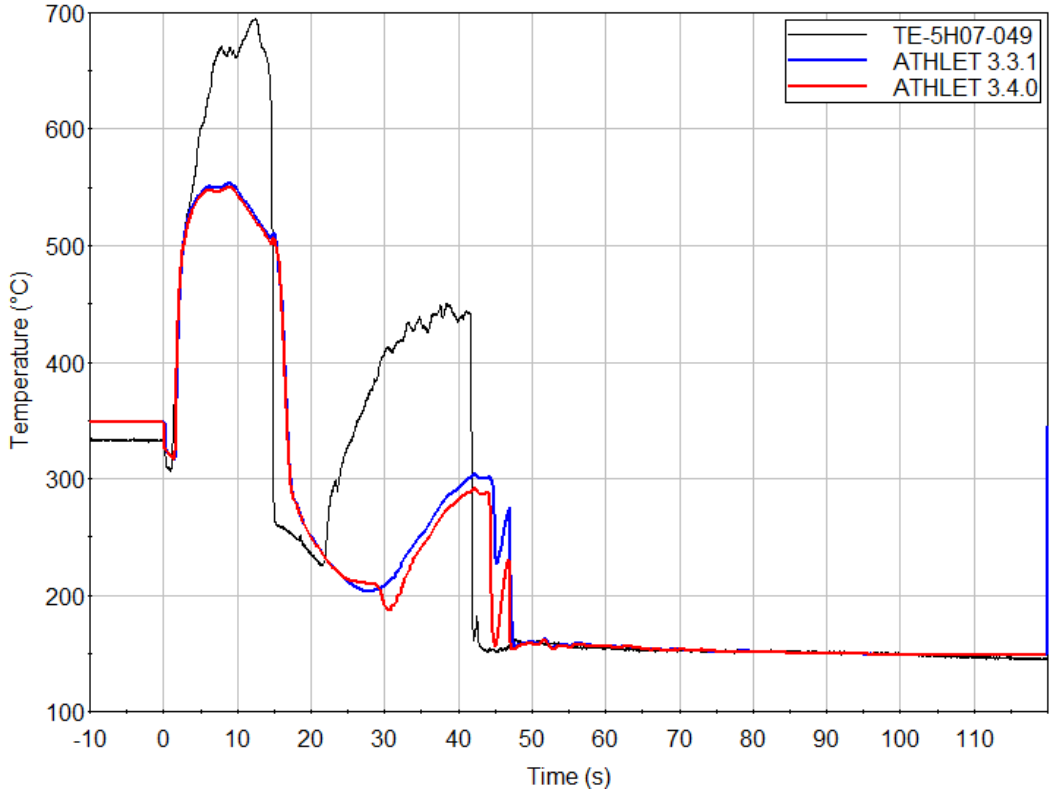

Fig. 5.74 LP-LB-1 central fuel assembly average rod wall temperature TE-5H07-049 at 49 inches with ATHLET 3.4.0 and 3.3.0 results

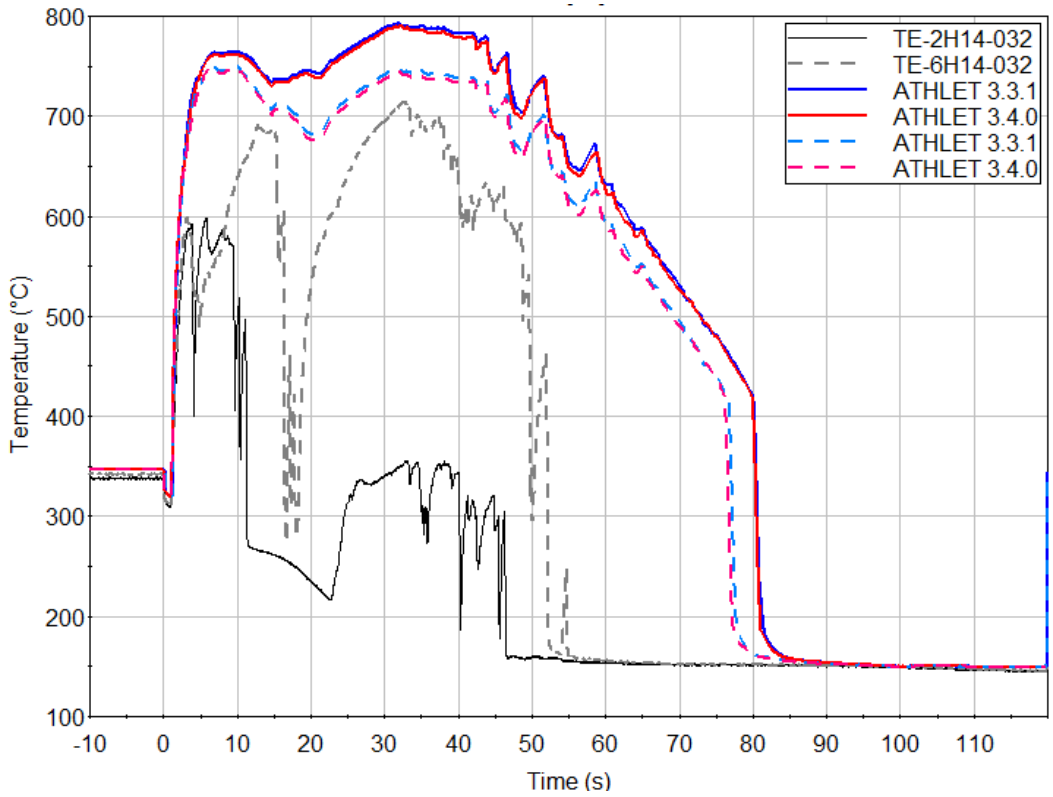

Fig. 5.75 LP-LB-1 peripheral fuel assembly 2 and 6 wall temperatures TE-2H14-032 and TE-6H14-32 at 32 inches with ATHLET 3.4.0 and 3.3.1 results

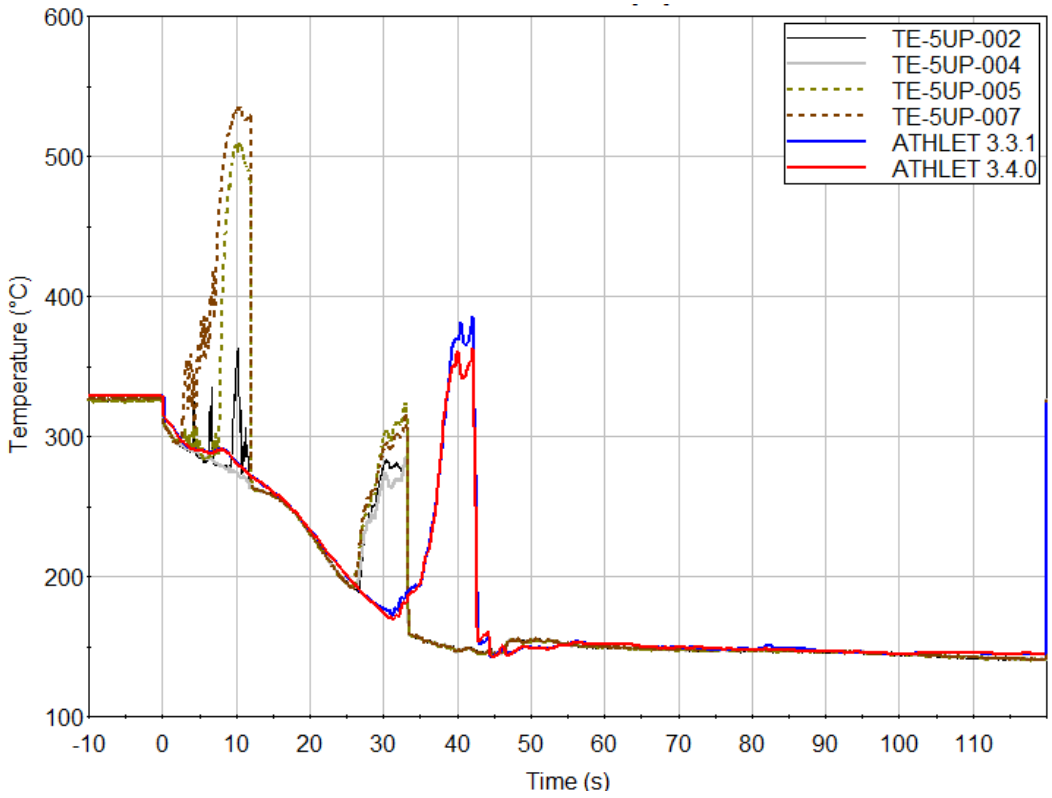

Fig. 5.76 LP-LB-1 central fuel assembly upper end box fluid temperatures with ATHLET 3.4.0 and 3.3.0 results

Regarding sensitivity cases, Fig. 5.77 and Fig. 5.78 illustrate that results with the SBTL95 data are almost identical to the standard version 3.4.0 results. This underscores the successful validation of that library for ATHLET. However, there are significant deviations between ATHLET 3.4.0 results with the 5-equation (1M) and the 6-equation model (2M). The break mass flows shown in Fig. 5.77 are generally consistent due to the nodalisation changes compared to /HOL 22b/. However, the 5-equation model with the current nodalisation overpredicts the intact cold leg mass flow rate systematically (FR-PC-105), for unknown reasons. For the broken hot leg, the 1M model produces a quite good fit for the initial 10 s and also overall. In the core, however, the 5-equation model predicts a very pronounced blowoff with more effective cooling, so that peak temperatures are underestimated by ~200 K. In addition and somewhat puzzling, the reflooding quenches the whole core at about 20 s. Due to the changed nodalisation compared to /HOL 22a/, no second heat-up also late in the transient can be observed. Overall, the 5-equation model simulation does not well reproduce the behaviour in the core, so that this validation calculation cannot be deemed successful. Further investigations are needed if this is an issue of the model itself or related to scaling effects from the multi-channel modelling employed here.

As shown in Fig. 5.79, the mass error for the primary circuit is consistently very small considering an initial inventory of about 9280 kg, although the systematic mass loss during steady state merits some follow-up. At the same time, number of time steps (about 22000 for the 2M model for ATHLET 3.4.0 and about 26000 for ATHLET 3.3.0) and calculational times (about 3800 s on a standard PC with ATHLET 3.4.0) are still reasonable. Using the OMP version allows some speed-up, while results remain identical. Consequently, the numerics settings have been appropriate. Similarly, use if NuT also allows some limited speed-up and results show only minor changes compared to version 3.4.0, which are expected. Thus, also the NuT version has been successfully validated.

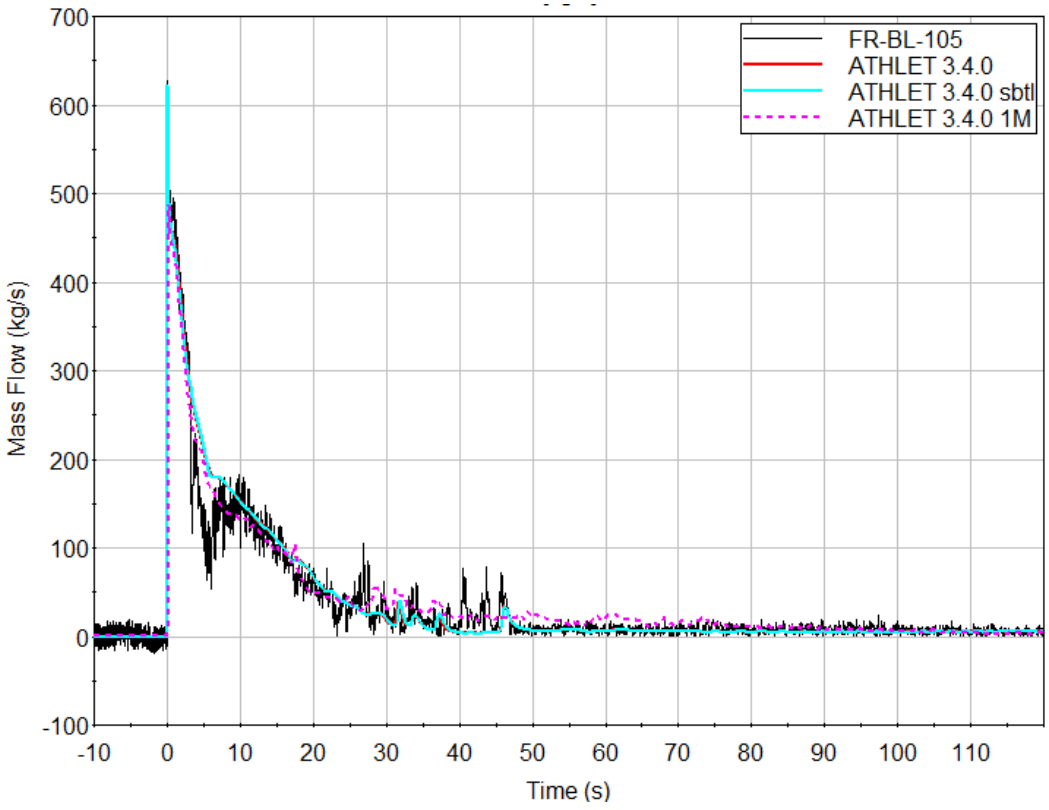

Fig. 5.77 LP-LB-1 broken cold leg mass flow rate FR-BL-105 with ATHLET 3.4.0 results and sensitivity cases 1M model and SBTL95

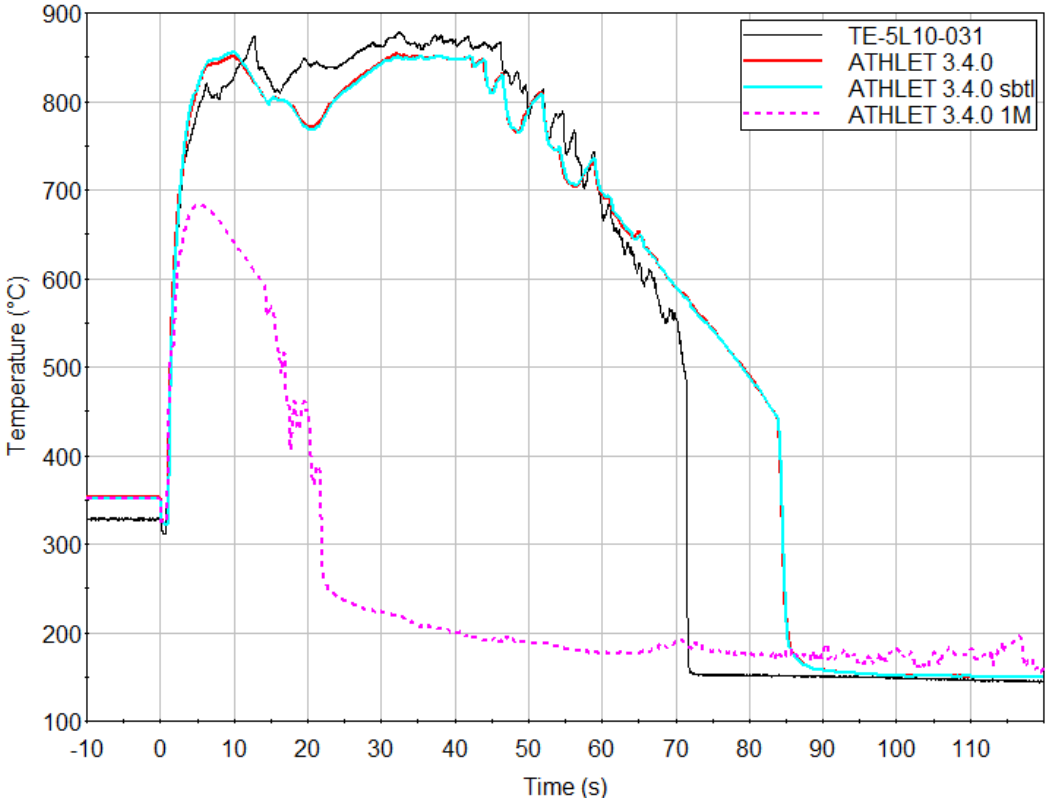

Fig. 5.78 LP-LB-1 central fuel assembly wall temperature TE-5L10-031 at 31 inches with ATHLET 3.4.0 results and sensitivity cases 1M model and SBTL95

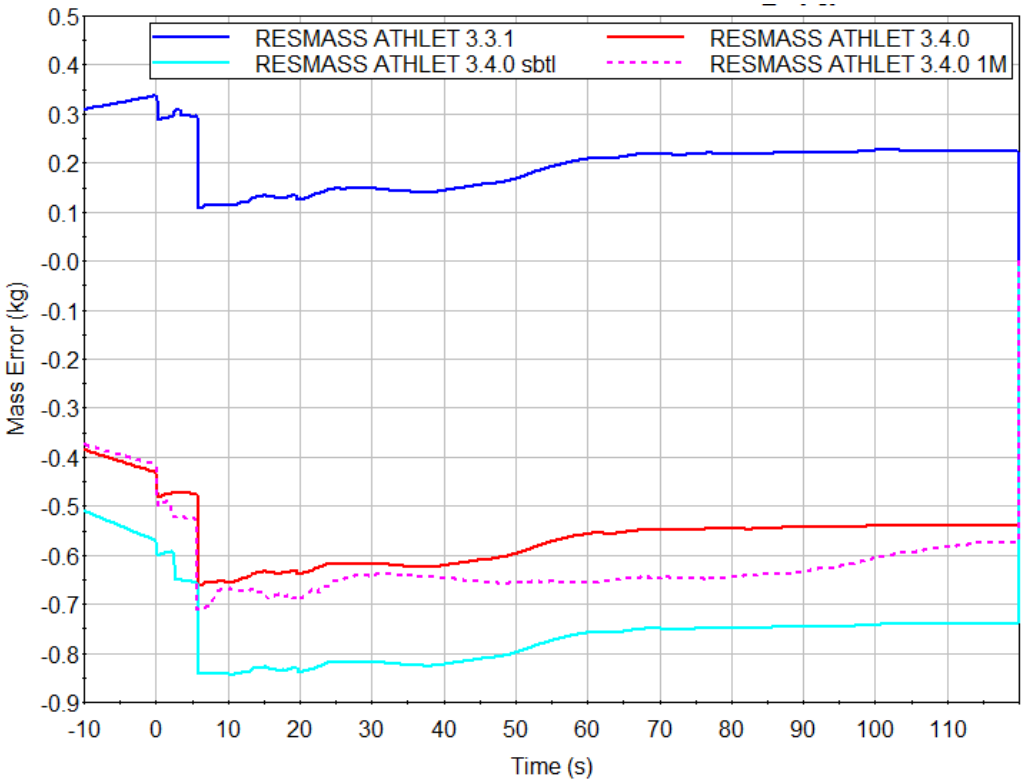

Fig. 5.79 LP-LB-1 primary side mass error for ATHLET 3.4.0, sensitivity cases 1M and SBTL, and ATHLET 3.3.1

5.3.5 Main Findings

Overall, the validation of ATHLET 3.4.0 with the 6-equation model against LOFT LP-LB-1 was successful, considering measurement uncertainties and peculiarities of the test and reactor as well as the input deck. Specifically:

- Explicit modelling of the outer downcomer channel and bypasses is important for best-estimate results. Similarly, structural masses in the RPV are important particularly for the reflooding phase.
- The entrainment and de-entrainment models appear not optimally suited for the complex phenomenology in the LOFT reactor. There are significant differences between 5- and 6-equation model, which require further analyses.
- More realistic predictions will require a resolution of asymmetric flow during blowdown. The current four channel version does not achieve this, yet.
- The quench front model appears reluctant to finally quench the core during re-flooding despite comparatively high liquid fractions in the core, which will require further analyses.
- For best-estimate prediction of quench front progression, a finer nodalisation of TFOs is more effective than more HCVs per CV. Unsurprisingly, there is a strong impact, if the quench front has to move across CV boundaries.

With regard to the 5-equation model, the validation was only partially successful. The predicted temperatures in the core deviate strongly, so that caution should be used if this option is applied to the core of a reactor with a multi-channel nodalisation for a fast blow-down scenario (LB-LOCA).

5.4 ISB-WWER Test SSP-2

5.4.1 Test Facility

The test facility ISB-WWER, designed and constructed by the Electrogorsk Research and Engineering Centre, is a full-pressure scaled-down model of the Russian reactor VVER-1000.The volume scaling is 1 : 3000 and the elevations are kept 1 : 1. The original four-loop primary circuit with horizontal steam generators is represented by a two-loop circuit with four vertical steam generators. The first loop represents a single loop (also

called broken loop) with one steam generator and the second loop represents a triple loop (also called intact loop) with three parallel connected steam generators. The volume ratio between both loops is 1 : 3. The main circulation pumps are installed as bypasses around the loop seals, and are isolated from the loops during the experiments.

The primary circuit further consists of an electrically heated pressurizer model, which can be connected to the single as well as to the triple loop, and models of the three independent emergency core cooling systems: high pressure injection system, hydro-accumulators and low-pressure injection system. The four hydro-accumulators of the VVER-1000 dispose of own connections to the reactor pressure vessel. This is a special feature of VVER. Two of the four accumulators are connected to the downcomer and the other two to the upper plenum of the reactor.

The reactor model is divided into the following parts:

- an external downcomer simulating the vertical downcomer annulus as well as the lower plenum of the reactor vessel,
- the core simulator based on a bundle of 19 directly heated fuel rod simulators with a length of 3.5 m,
- the upper plenum section simulating the upper plenum as well as the upper head of the reactor vessel, and
- the bypass section simulating the core coolant bypass channels; it allows to adjust the by- pass flow of the core in the range of 3 % to 20 % of the nominal mass flow rate.

The core simulator is connected to the downcomer and to the upper plenum via horizontal U-shaped tube junctions. The bypass is located between one lower and one upper connection line. The secondary circuit is not modelled in detail. The vertical steam generators are designed only to remove the power from the primary circuit. An isometric view of the main components of the ISB-WWER test facility is given in Fig. 5.80 and the principal scheme of ISB-WWER is shown in Fig. 5.81. An overview of the main design characteristics of the facility is given in Tab. 5.6.

The standard instrumentation of the ISB-WWER facility includes transducer for pressures, differential pressures, temperatures, mass flows, and for the electrical parameters of the fuel rod simulator and the other heating devices. The most important parameters

for the described experiment are the pressure in the primary circuit (P 13) and on the secondary side of the steam generators (P1 - P4). The transducers for the differential pressure are placed as a complete chain around the whole primary loops. The temperature is measured by thermocouples. Most important locations are the inlet and outlet temperatures of reactor vessel and steam generators as well as the surface temperatures of core heater claddings and the U-tubes in the steam generators. There are also thermocouples in additional locations for heat loss information. The flow rates in the loops are measured in both the single and the triple loop cold leg by differential pressure flowmeter (FL7 and FL9). In addition, the secondary side feed water mass flow rate is also measured. The electrical heat power for core, bypass and pressurizer heaters is defined by measured voltage and current. Special devices - the so-called needle shaped conductivity probes - are used as local void fraction sensors in 14 places. These probes provide especially useful local information about the time of structural changes of the flow. This includes the time of the transition from one-phase to two-phase flow and vice-versa, the time of significant changes of the void fraction and of the passing of a mixture level.

All measured signals are recorded and pre-processed by a data acquisition system. The channel information is scanned by the basic PC system with a maximum sampling rate of 18 Hz and stored on hard disk.

A more detailed description of the test facility is given in /GAX 95/.

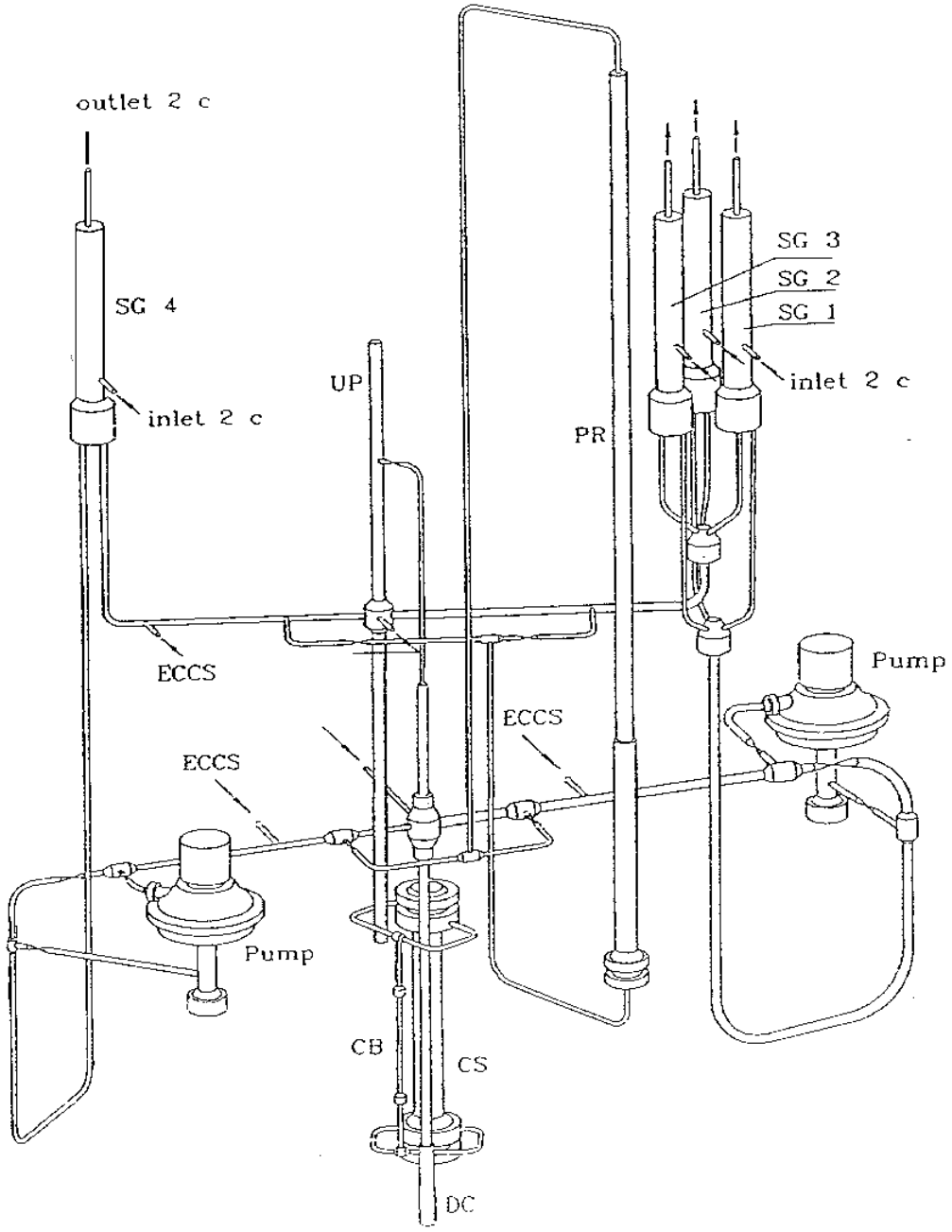

Fig. 5.80 Isometric view of ISB-WWER facility main components /GAX 95/

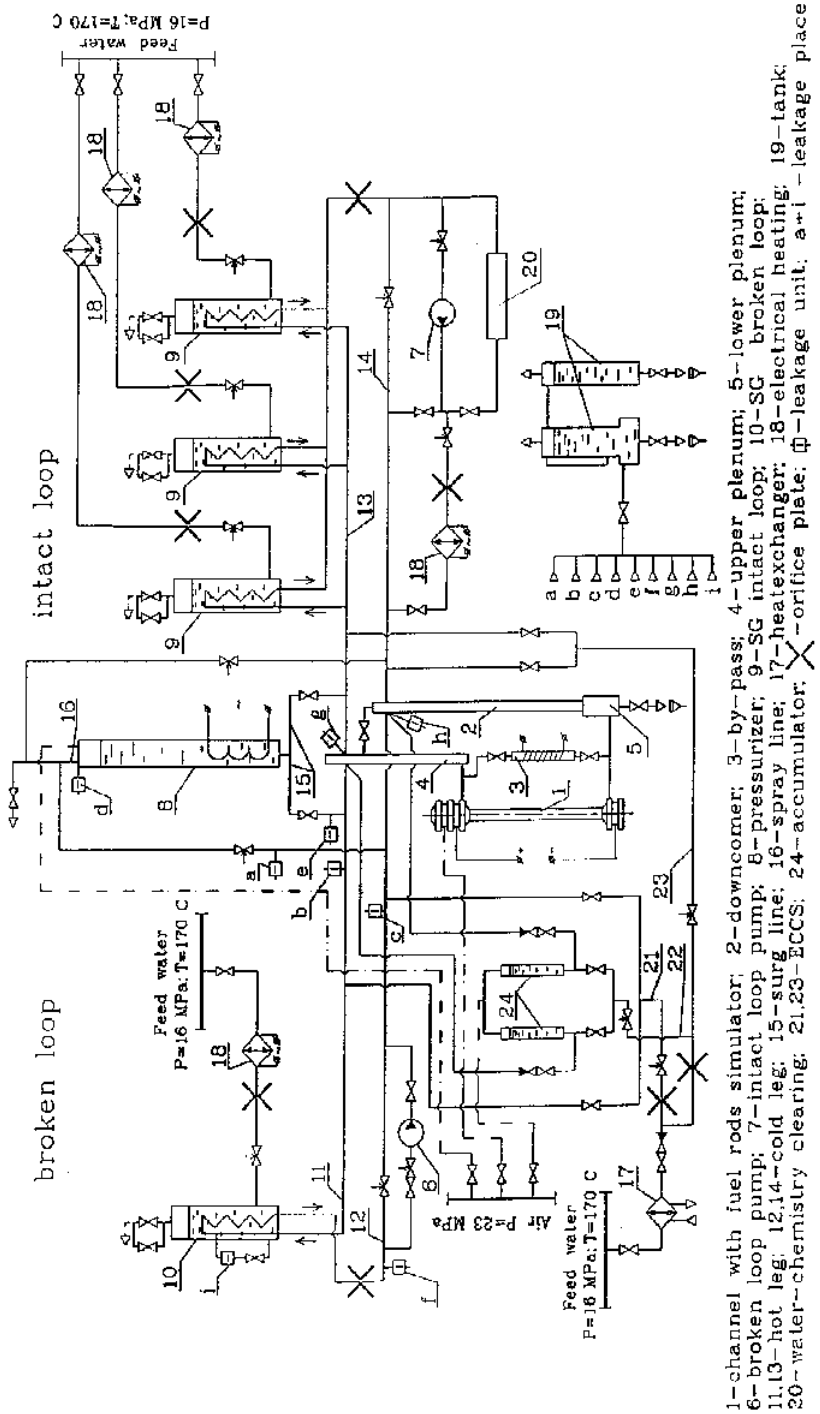

Fig. 5.81 Basic scheme of ISB-WWER test facility /GAX 95/

5.4.2 Test Conduct

The Second Russian Standard Safety Problem (SSP-2) was carried out in Electrogorsk Research and Engineering Centre of Nuclear Plants Safety in 1995/96. The scenario of the experiment simulates the rupture of an ECC injection line. As the initiating event, the rupture of one line connected to the upper plenum was assumed. The result is a 11 % break (in terms of main circulation line cross section) in the upper plenum of the reactor vessel, close to a medium size LOCA. In addition, the trip of all four main circulation pumps by blocking signal was assumed, and the emergency core cooling systems were assumed to be not available. The description of initial and boundary conditions is given in more detail in /GAX 97/, /STE 98a/.

The given scenario for the experiment is the following:

t = 0 s	Start of transient Break line opening (5.2 mm diameter, l/d = 10 at upper plenum)
t = 5 s	Start of electrical power reduction at the core and the bypass section; Steam generator secondary side feed water injection and steam release is switched off (closing valves W-3, W-5, W-7, W-9, S-7, S-9, S-11, S-13)
t = 9 s	Pump trip by blocking signal (UPP13 = 11.0 MPa) simulated by closing valves W-33,W-34 and by opening valves W-10a, W-64, W-16, W-52, and W-65
T_{clad}=273 K	When the maximum cladding temperature reaches 273 K for the first time, the core power is reduced from 100 kW to 52 kW. When the maximum cladding temperature reaches 273 K for a second time, the power is switched off completely.

Tab. 5.6 Main characteristics of the ISB-WWER test facility

Characteristics	**Value**
Coolant	Water
Number of loops	2
Volume ratio of coolant loops	1 : 3
Maximum pressure	25 MPa
Operational pressure (nominal)	16 MPa
Temperature at core outlet (max)	400°C
Core electrical heating power (max)	1.8 MW
Operational core heating power (nominal)	1.0 MW
Pressurizer heating power	20 kW
Core mass flow rate (max)	9.0 kg/s
Core mass flow rate (nominal)	6.0 kg/s
Cladding temperature (max)	1000°C
Number of fuel elements in core bundle	19
Scaling factor for heights	1 : 1
Scaling factor for volumes	1 : 3000

5.4.3 Input Dataset

5.4.3.1 Nodalisation

In the framework of participation in the Second Russian Standard Safety Problem, a new input data deck of the code version ATHLET Mod 1.1 Cycle C was developed for the ISB-WWER test facility. The basis for the geometrical information was mainly the data report /GAX 95/. This input deck was continuously adapted to new ATHLET versions.

The input model for the test facility consists of 72 thermo-fluid objects and 77 heat conduction objects, comprising 388 control volumes, 410 junctions and 390 heat conduction volumes. The overall nodalisation scheme is shown in Fig. 5.82.

For this small break calculation, the 6-eq. option of the code was chosen.

The modelling of the main components of the test facility is described in more detail below:

Reactor vessel model

The reactor vessel model is divided into three components: the downcomer/lower plenum, the core simulator and the upper plenum section (Fig. 5.83).

Due to their three-dimensional nature, it is difficult to model the downcomer/lower plenum with only one-dimensional thermo-fluid-objects. The downcomer/lower plenum section is represented by 10 TFOs.

In the downcomer, the inlets from the intact and the broken loops are connected to the annulus section represented by the branch PV-DC-2 and by the pipes PV-DC-1 and PV-DC-3. The branch PV-DC-5 connects then the annulus section with the rest of the downcomer: its upper head is represented with PV-DC-4, and its lower part – the pipe PV-DC-6. The upper head of the downcomer (PV-DC-4) is connected to the upper head of the upper plenum with the pipe PV-DC-UP, and to the top of the downcomer annulus (PV-DC-1) through a 4mm hole.

The bottom part of the downcomer (pipe PV-DC-6) starts at the branch PV-DC-5 and ends at the branch PV-LP-4, which models the entire bottom part of the lower plenum including the inner perforated pipe and the outer pipe. The outlets from the lower plenum in the core (PV-LP-21 and PV-LP-22) are connected to the branch PV-LP-2, which forms the lower plenum annulus together with the pipes PV-LP-1 and PV-LP-3. The top of the lower plenum annulus (PV-LP-1) is connected to the inner downcomer pipe (PV-DC-6) through a 4mm hole, and its bottom part (PV-LP-3) connects the annulus to the rest of the lower plenum represented by the branch PV-LP-4.

The core simulator is represented by 4 TFOs: PV-COR-IN, PV-COR, PV-COR-OUT and PV-COR-BYP. The pipes PV-LP-21 and PV-LP-22 connect the lower plenum with the inlet section of the core which is represented by the branch PV-COR-IN. The core simulator itself is modelled with the pipe PV-COR, which starts at the inlet section PV-COR-IN and ends at the core outlet represented by branch PV-COR-OUT. The outlet of the core simulator is connected to the upper plenum with two horizontal pipes PV-UP-11 and PV-UP-12. The external bypass section branches off from the pipe PV-LP-22 goes through PV-COR-BYP and ends at PV-UP-12.

The upper plenum, especially the outlet annulus section, is difficult to model too. The lower part of the upper plenum is represented by the branch PV-UP-1, which is connected to the core with PV-UP-11 and PV-UP-12, followed by the pipe PV-UP-2 and the branch PV-UP-3. The branch PV-UP-3 connects the lower part of the upper plenum to the annulus section, and to the upper part of the upper plenum. The upper part consists of the inner annulus section (PV-UP-36 and PV-UP-6) and the pipe PV-UP-7 representing the upper head of the reactor vessel, which contains a grid plate and the connection pipe to the downcomer PV-DC-UP. The upper plenum annulus is represented by two pipes (PV-UP-57 and PV-UP-4) and the branch PV-UP-5. While the top pipe PV-UP-57 connects the annulus to the upper head, the outlets in the hot legs and the leak P0-LEAK are connected to PV-UP-5.

Main circulation loops

The hot legs of the main circulation pipes are connected to the branch PV-UP-5. The hot leg of the single loop is represented by the pipe P1-HL. The triple loop hot leg has been modelled by the common part P2-HL, the branch P2-HL-BR and the pipe P2-HL-SGT representing the connections to the three steam generators (FPAR0=3). The cold legs have been modelled in a similar way. The single loop cold leg is given by the pipes P1-CL-1 to P1-CL-3 and the bypass line P1-PUMP including the main circulation pumps. The triple loop cold leg is represented in a similar way by the pipes P2-CL-1 to P2-CL-3 and the pump bypass P2-PUMP, but in addition there are the TFOs P2-CL-SGT and P2-CL-BR with FPAR0=3. The main circulation pumps (MCP) have been modelled with the ATHLET pump model. The nominal pump head has been taken as the corresponding value of the prototype VVER-1000 MCP (0.66 MPa), due to the lack of information about the pumps and local form losses. The pressure losses in the primary circuit have been adjusted to the measured pressure differences at steady state conditions. The pump coast down is simulated by a GCSM signal for pump head, on the basis of an input table.

Steam generator

The steam generators for both the single and the triple loop have been modelled similarly. An overview of their nodalisation is given in Fig. 5.82. According to the used nodalisation, the inlet into the steam generator of the broken loop is located within the P1-HL pipe, while the outlet is in the P1-CL-1 pipe. In the intact loop, the inlet and the outlet of the steam generator are modelled as a part of P2-HL-SGT and P2-CL-SGT respectively. The inlet and the outlet into the tube regions are represented by the branches

P1(2)-SG-IN and P1(2)-SG-OUT respectively. The 11 vertical U-tubes have been divided into three bundles with different lengths P1(2)-SG-UT1 to P1(2)-SG-UT3 in order to take into account the influence of the different elevations on natural circulation. The secondary side is represented by the pipe S1(2)-DRUM. The steam generator primary and secondary side are coupled by heat structures for every bundle.

Pressurizer

The pressurizer system is represented by 6 TFOs. The connection between the pressurizer itself P0-PRESS and the hot legs is modelled by the pipe P0-SURGE and P0-HL-SL, taking into account the possibility to connect the pressurizer to the single loop as well as to the triple loop. For the current calculation the pressurizer is connected to the single loop only because of the closed valve to the triple hot leg. The spray line is modelled by the TFOs P0-CL-SL and P0-PRES-SP, but it is not used for this experiment, due to the closed valves W30 and W31. The pressurizer safety valve is represented by the single junction pipe P0-PRES-RV.

Break modelling

The break line is modelled as a pipe that consists of 2 control volumes with a discharge valve assigned to it. The discharge rate is calculated by means of CDR tables. In order to take into account the stratification upstream of the leak, the option JFLO0 = 2 was chosen, as recommended in the ATHLET User's Manual.

Secondary circuit

The secondary circuit is modelled in a very simple way. Both the single loop as well as the triple loop secondary side except the steam generator drum have been modelled by the two pipes S1(2)-MSL and S1(2)-BPL only, representing the steam line and the bypass line toward the relief valve. The feed water injection system is simulated for both loops with a single junction pipe S1(2)-FWL at the bottom of the steam generator drum. The steam lines have been completed by the isolation valve S1(2)-MSV and the safety relief valve S1(2)-BPV.

Heat conduction structures

The heat losses to the environment have been modelled by taking into account all solid component structures of the test facility. Also, the heating structures as well as the heat exchange structures have been modelled by heat structure objects. For matching the

heat losses of the components given as boundary condition for the calculation, the outside heat transfer coefficients – considering the effect of the isolation material –- were estimated by the code on the basis of calibrated temperature-dependent tables. In the period of zero-transient calculation the heat losses in those parts of the components without mass flow have been switched off and are considered only after the start of the transient. The heater rods in the core simulator have been modelled in agreement with the single flow channel by only one heat structure HV-COR-R, taking into account the number of rods by using FPARH=19. Therefore, radial temperature differences inside the core simulator are not captured. The axial rod power distribution is kept constant for all elevations. The time evolution of the power for the core rods as well as for the pressurizer heaters is given by input tables.

GCSM

Besides the definition of a series of important process variables in the process signal block, there are 16 blocks for special tasks shortly described below:

`BLOCK-1'	Set of transient initialization signals like start of transient, scram, pump coast down, ECCS and valve actions.
`MCPUMP'	Main circulation pump coast down simulation.
`VALVES'	Isolation valve opening and closing position control, including accumulator and leak simulator valve.
`ECCS'	Emergency core cooling system control, especially mass flow and enthalpy behavior. This block is not used for this transient.
`SCRAM'	Scram power behavior in the core simulator.
`PRESHEAT'	Pressurizer heater controller for primary pressure control in the zero-transient period and heater behavior for transient according to the prescribed boundary conditions.
`BYPHEAT'	Core bypass heat behavior.
`RV-PRESS'	Pressurizer safety valve controller, including estimation of critical discharge through the valve.
`AIR'	Temperature boundary conditions for the environment.
`TDV'	Time dependent volume boundary conditions.
`FEEDW'	Feedwater mass flow and enthalpy.

`SG-STEAM'	Steam generator secondary side pressure controller for the zero-transient period and steam mass flow behavior for transient according to the prescribed boundary conditions.
`SG-SV'	Steam generator safety valve controller including estimation of critical discharge through the valve.
`HEATLOSS'	Estimation of outside heat transfer coefficient for the component heat losses according to the temperature dependent boundary conditions.
`MEASUREM'	Post processing of process signals for comparison with experimental data.
`POSTPROC'	Post processing information concerning heat losses and mass balance.

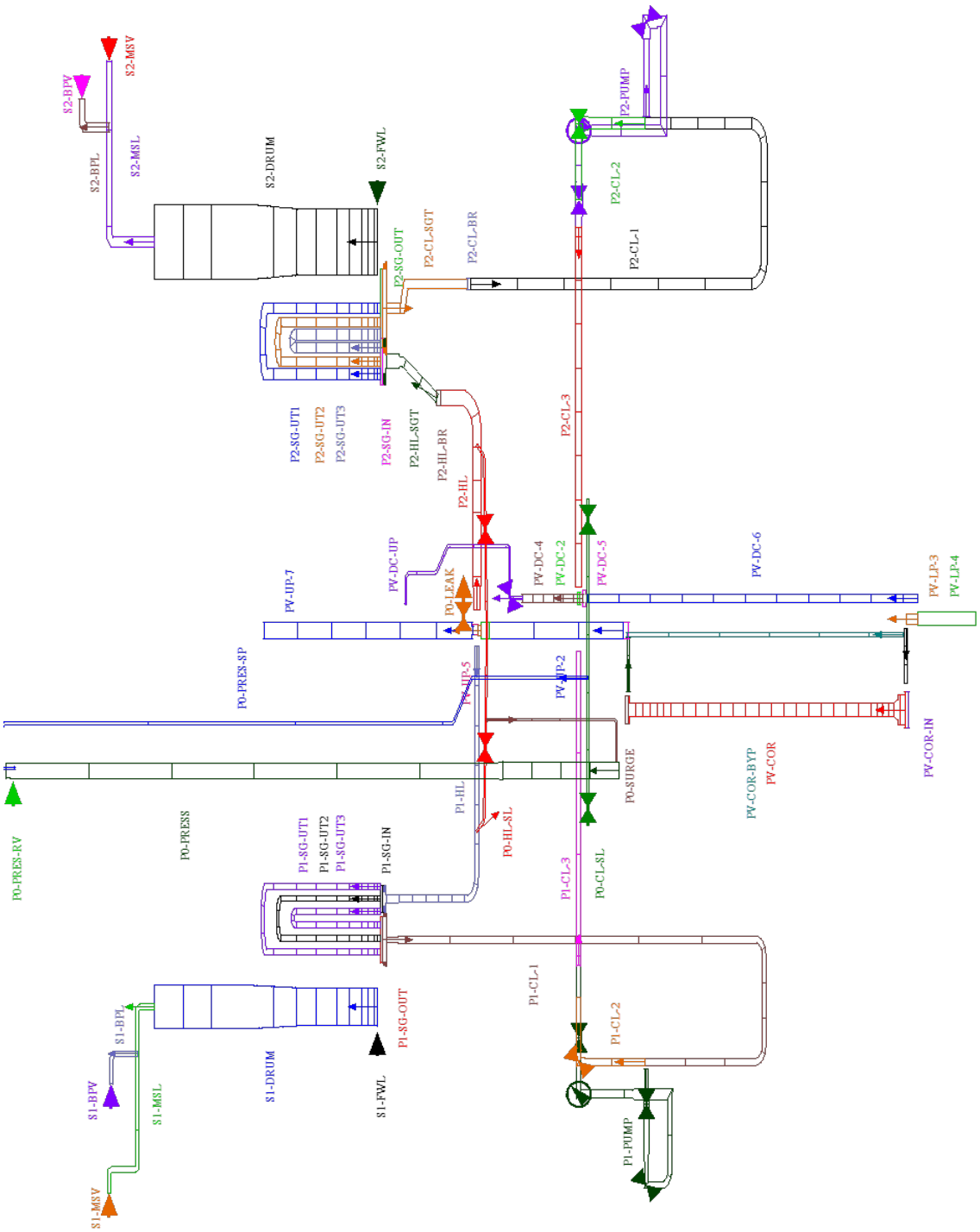

Fig. 5.82 ATHLET nodalisation scheme of ISB2-WWER facility (overview)

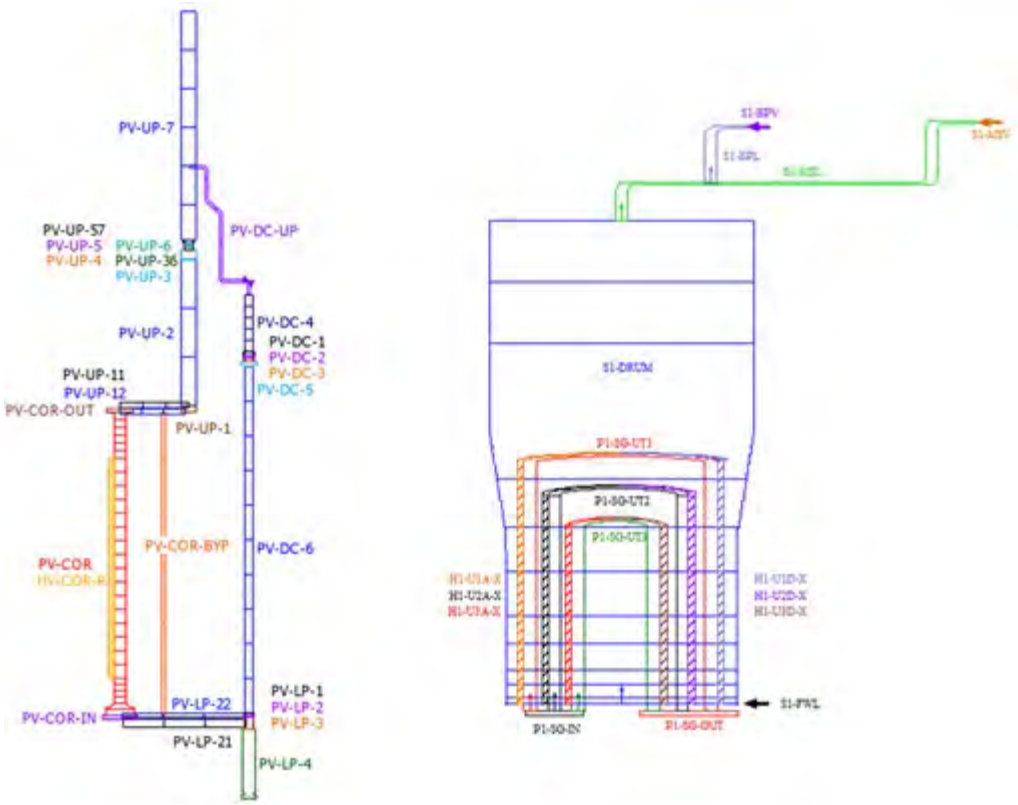

Fig. 5.83 ATHLET nodalisation scheme of reactor vessel and steam generator

5.4.4 Main Results

5.4.4.1 Comparison of different ATHLET versions

The figures Fig. 5.84 to Fig. 5.94 compare ATHLET 3.4.0 results with the corresponding experimentally measured parameters for a variety of physical quantities, proving the quality of the ATHLET simulation Additionally, results achieved with ATHLET 3.3.1 are shown to evaluate the progress of the model development. The transient was started by opening the leak valve in the upper plenum. The leak mass flow rate becomes critical very quickly and reaches its maximum value of 1.1 kg/s after about one second. The primary pressure decreases strongly from 15.8 MPa down to 12.6 MPa in 1.5 seconds (Fig. 5.84 and Fig. 5.85) and water from the pressurizer is discharged to the hot leg of the single loop. Therefore, the temperature at the SG inlet drops for a short time due to the relatively cold water of the surge line and then increases because of the saturated conditions in the pressurizer and the higher enthalpy of the injected water (Fig. 5.86). The temperature in the hot leg does not reach the same values as in the experiment because of the smaller flow rate in the surge line out of the pressurizer. For the same reason, the collapsed level in the pressurizer drops more slowly and the depletion will

occur later. After 3 s the electrical power supply to the core simulator starts to decrease, which slows down the pressure drop in the primary circuit.

Due to the fast pressure decrease, flashing at the steam generator inlet can be observed, first in the single loop and at about 6 s in the triple loop. The flashing in the single loop starts earlier because of the higher initial temperatures there. After 8 s the main circulation pumps were stopped without coast-down. The mass flow in the loops decreases in the next 4 s to small values (Fig. 5.87 and Fig. 5.88). That is the reason for the short temporary pressure increase in the primary circuit after about 10 s. At the same time flashing takes place in the upper plenum, and the leak mass flow, now saturated, starts to decrease (Fig. 5.89).

In the secondary circuits the feedwater valves and the steam outlet valves also start closing at 8 s. Therefore, the pressure on steam generator secondary side increases due to the remaining heat flow from the primary loops (Fig. 5.90). The collapsed level in the steam generator secondary side increases because of the mass balance between feedwater and steam release. Afterwards, the pressure decreases very slowly due to the heat losses to the environment. The parameters at the steam generators of the different loops are not comparable due to different initial conditions and different valve closing behavior. In addition, the pressurizer influences the behavior of the single loop.

Due to the fact that the emergency core cooling systems were assumed to be not available, the coolant inventory decreases continuously. The primary pressure still drops rapidly. After the appearance of the first vapor at the reactor outlet, the coolant flashed in the hot leg. After 19 s the pressurizer is completely empty. The state of the primary circuit after the depletion of the pressurizer is characterized by a counter-current flow. The vapor from the reactor outlet moves towards the steam generator and is condensed there. The condensate flows partially through the hot legs back to the reactor vessel. Only the remaining part of vapor condenses in the descending part of U-tubes and flows to the cold leg. Vapor appears in the cold leg of single loop after 35 s and of triple loop after 43 s respectively, and the liquid level in the cold leg decreases afterwards. This results in a reduction of the pressure difference (Fig. 5.91 and Fig. 5.94). The differences between the loops are mainly caused by the different secondary side parameters. Simultaneously, the primary temperature decreases and the heat sink in the steam generators loses effectiveness. Consequently, the primary pressure drop decelerates. When the primary pressure finally comes close to the secondary pressure at roughly 140 s, the condensation rate decreases and the level in the hot leg drops rapidly.

When the hot legs are depleted, the leak flow changed from two-phase mixture to vapor. Consequently, the pressure decrease was accelerated. This is caused by the increasing enthalpy losses via the leak. The intensification of the pressure drop initiated also an intensification of flashing in those parts of the circuit, which were still filled with two-phase mixture. As it is indicated by the measured differential pressures and voids, a cold leg loop-seal clearing does not occur. Therefore, the vapor generated in the loop seal has to flow towards the steam generator on the one side and towards the downcomer on the other side. The result is a reverse vapor flow through the steam generator, which is indicated by the temperatures at the inlet and outlet of the steam generator (Fig. 5.86 and Fig. 5.93). The temperature at the inlet is a little bit higher than at the outlet because the vapor is heated by the secondary side. The vapor flowing towards the downcomer leads to a level decrease in the downcomer. The level reached the holes connecting the downcomer to the lower plenum at app. 182 s. At this time, an entrainment of vapor from the downcomer to the core is presumed, as indicated by the differential pressure across the lower core region (Fig. 5.95). Finally, the inventory of the downcomer was pushed into the core simulator and out of the leak.

As expected, when no emergency core cooling system is operating, an overheating of the fuel rod simulators can be observed. The rise of the maximum cladding temperature starts at 170 s, approximately 20 s earlier than in the experiment, experiment and evolves similar to the experiment as shown in Fig. 5.96. At 203 s (220 s in the experiment), the maximum cladding temperature reached the value of 723 K, and the power supply to the core was reduced from 100 kW to 52 kW. This slowed down the overheating and the cladding temperatures start to decrease at a rate similar to the experiment. As the water continues to evaporate within the rod simulator, the residual power of 52 kW was sufficient for a second overheating to occur. The maximum cladding temperature went down to 681 K at 229 s and then started to rise, reaching 723 K again at 256 s, much earlier than in the experiment. After the second overheating, the power at the core was switched off completely, which explains why the cladding temperatures decreased afterwards.

Both code versions ATHLET 3.3.1 and ATHLET 3.4.0 predict similarly the evolution of all physical properties observed in the experiment.

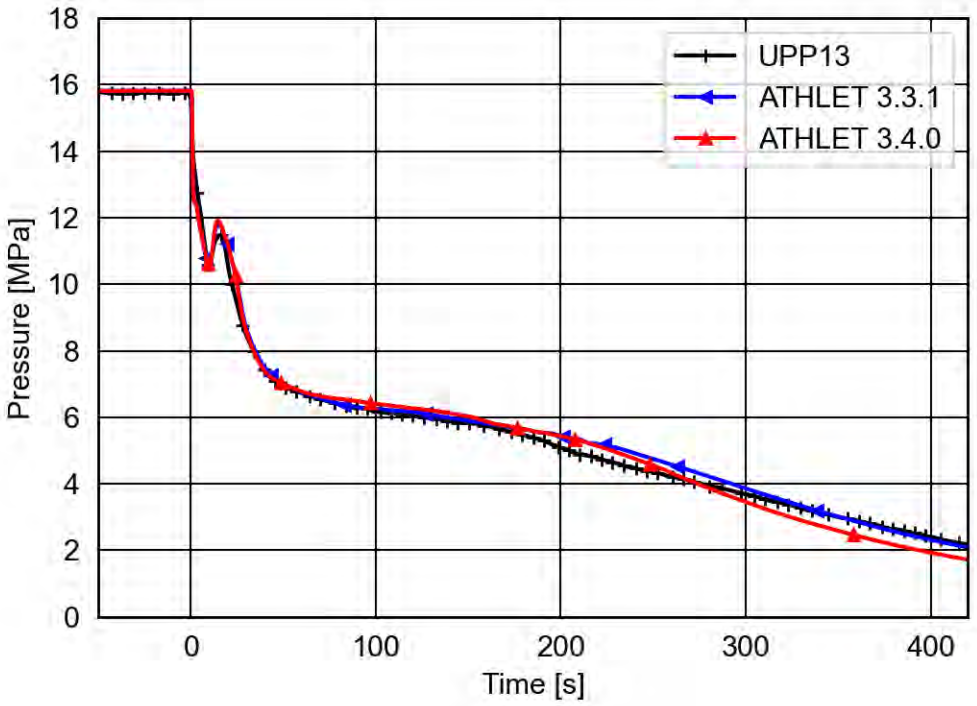

Fig. 5.84 Pressure in upper plenum

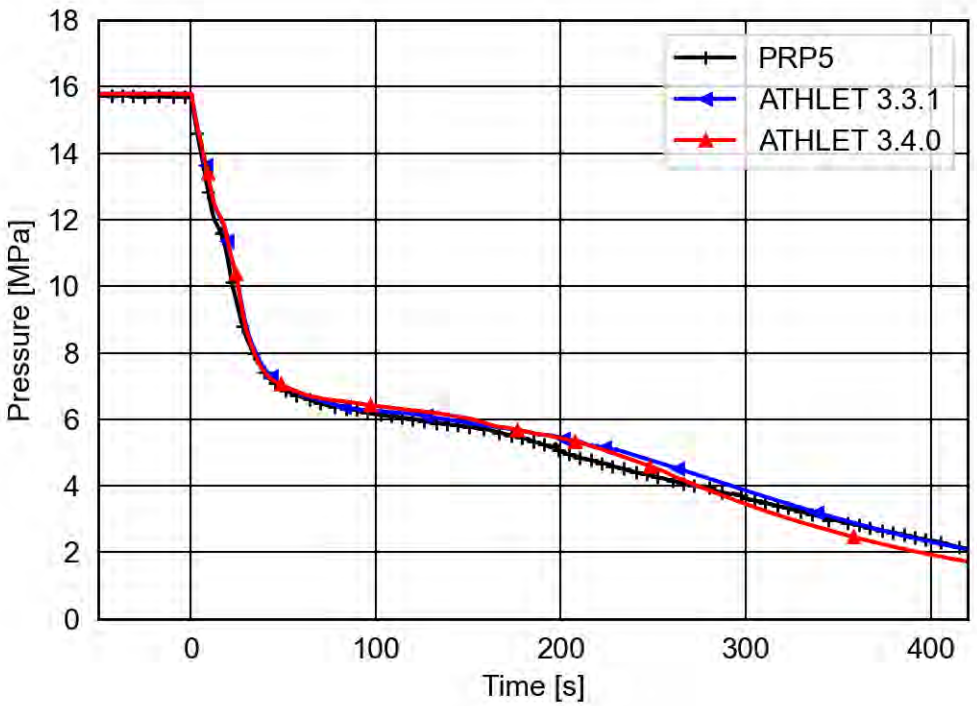

Fig. 5.85 Pressurizer pressure

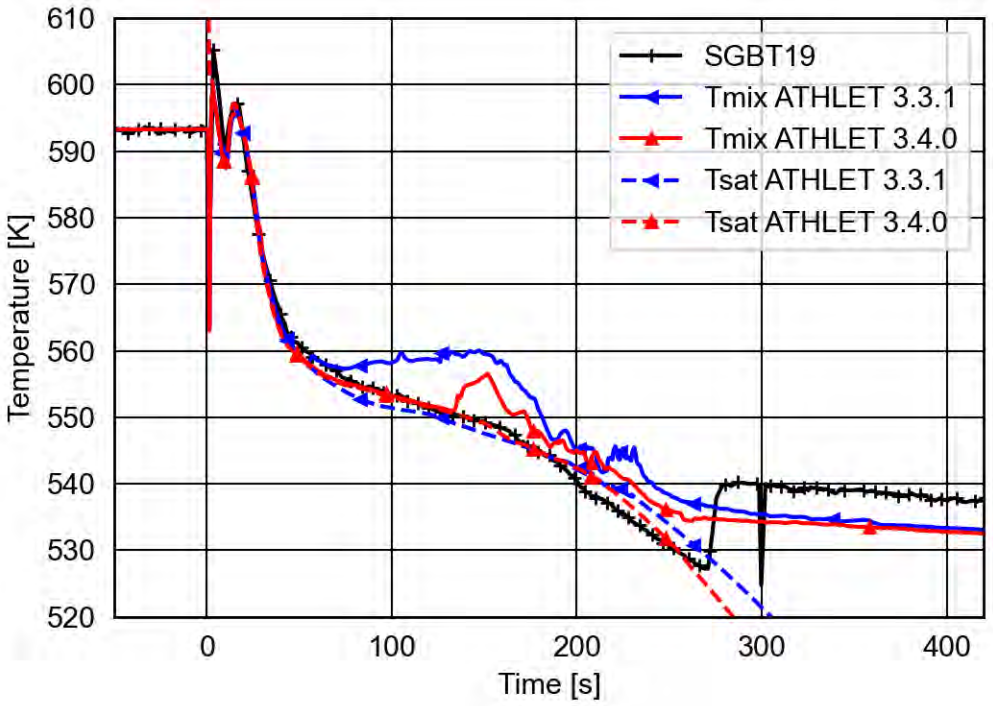

Fig. 5.86 SG inlet temperature (single loop): solid line – mixture temperature, dashed line – saturated temperature

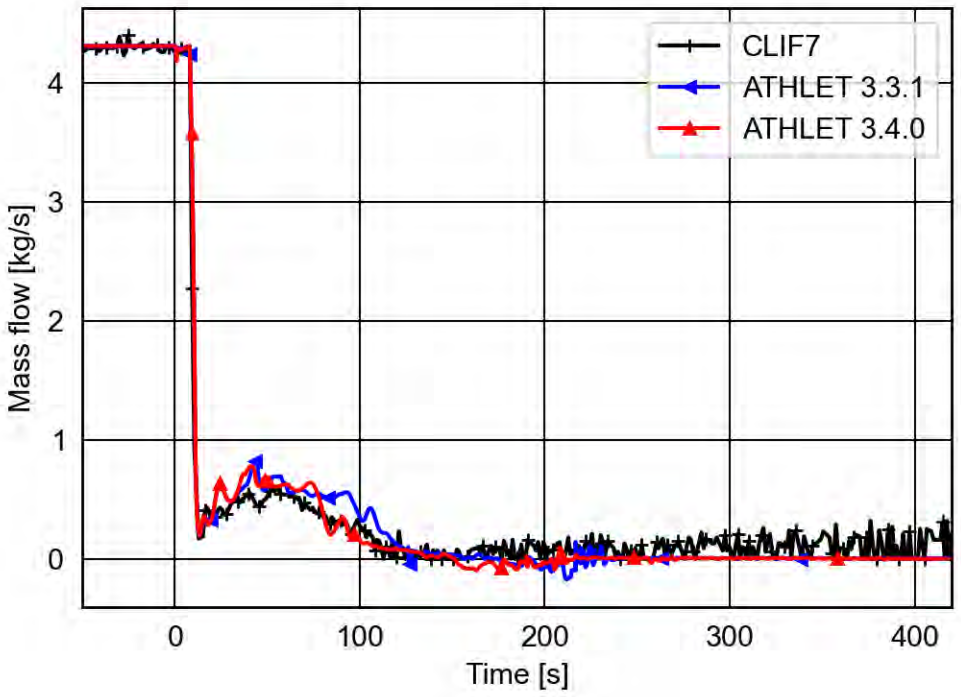

Fig. 5.87 Mass flow rate in cold leg (triple loop)

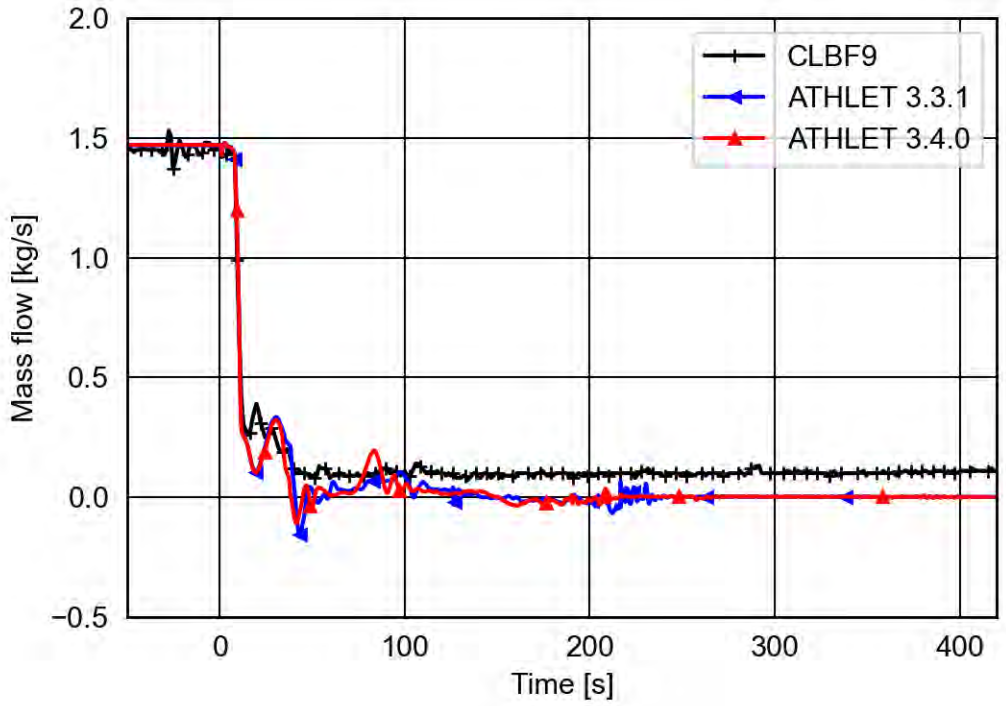

Fig. 5.88 Mass flow rate in cold leg (single loop)

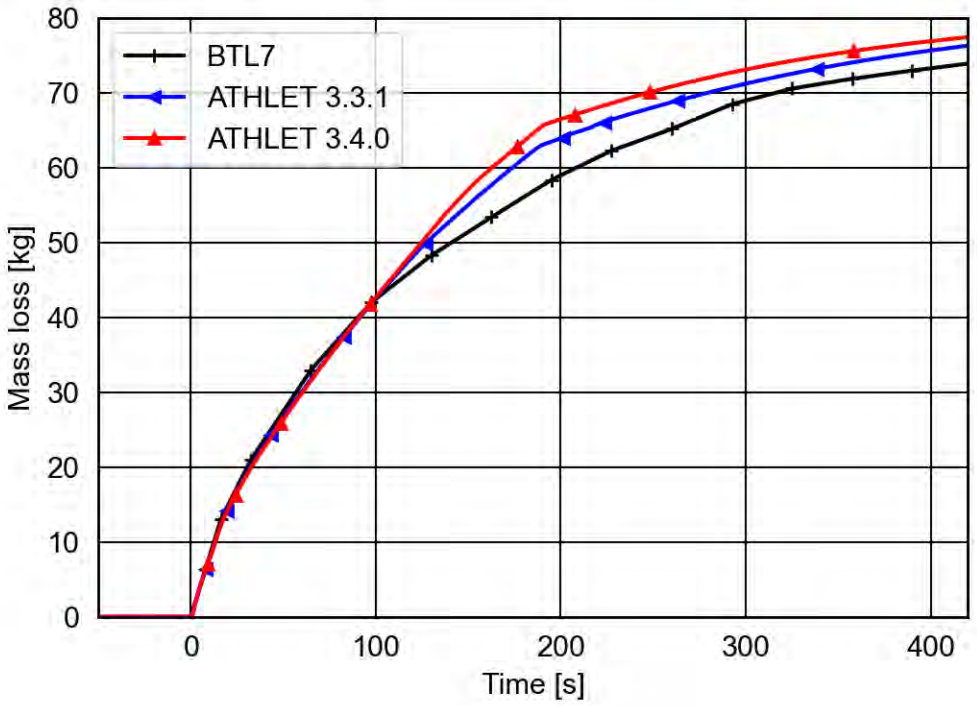

Fig. 5.89 Integrated break mass flow rate

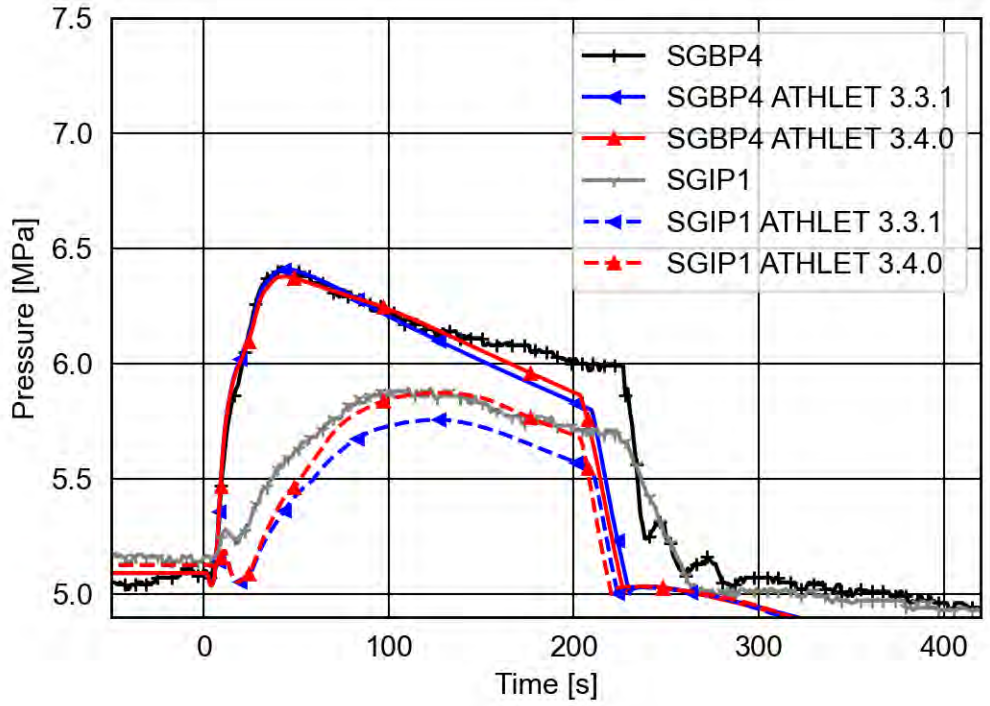

Fig. 5.90 Secondary pressure in broken (SGBP4) and tripple (SGIP1) loops

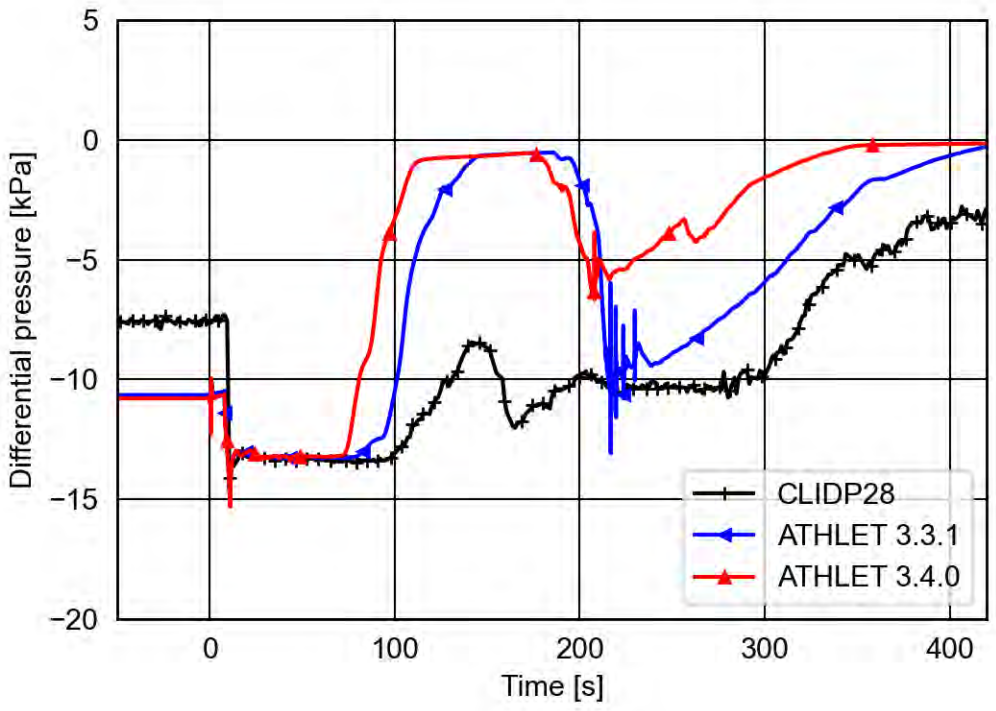

Fig. 5.91 Differential pressure in vertical part of triple loop cold leg (upflow)

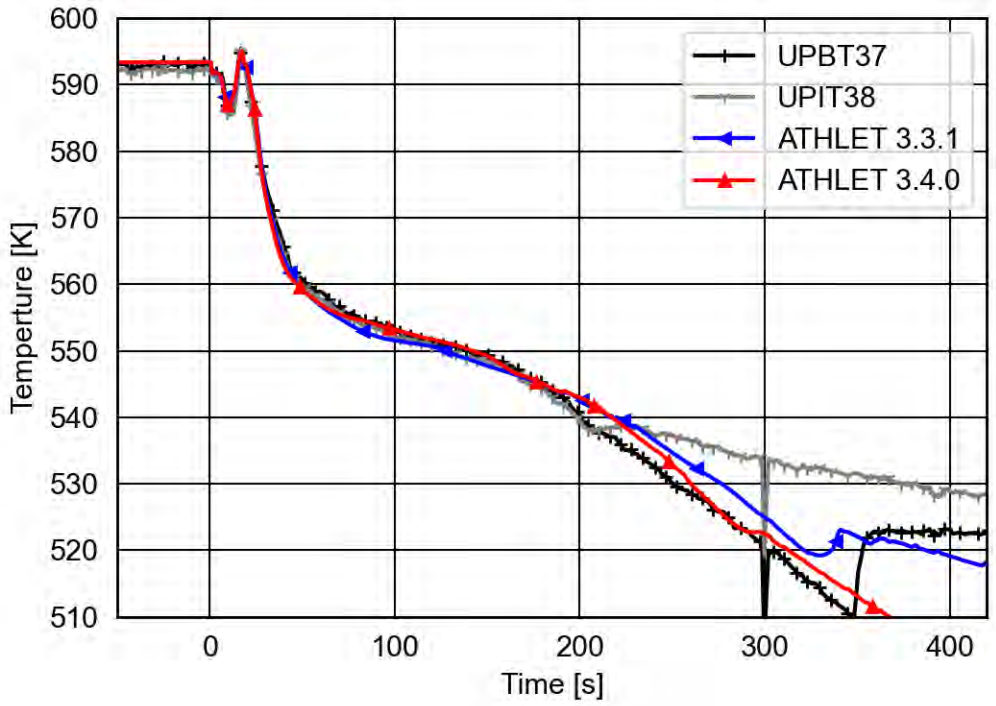

Fig. 5.92 Temperature at upper plenum outlets in hot leg of broken (UPBT37) and intact (UPIT38) loops.

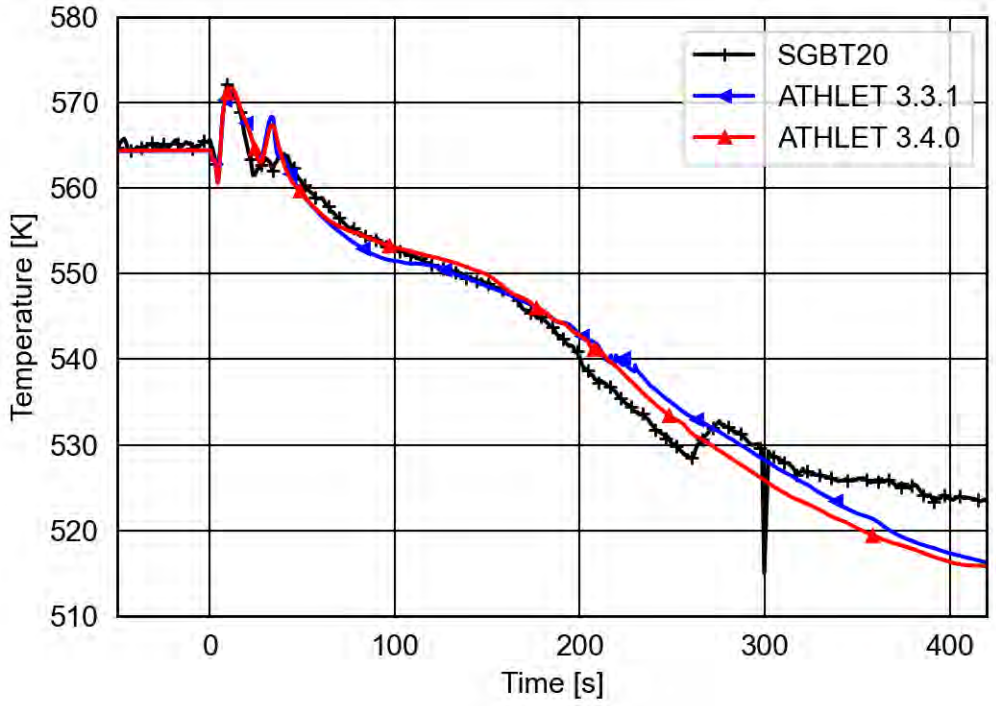

Fig. 5.93 SG outlet temperature (single loop)

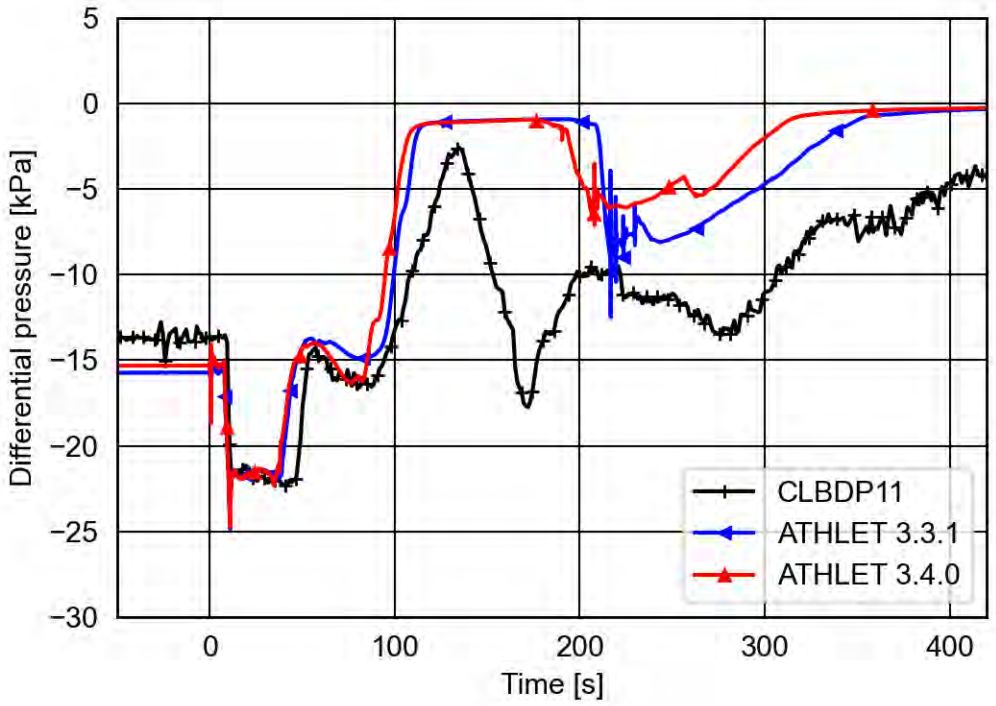

Fig. 5.94 Differential pressure in vertical part of single loop cold leg (downflow)

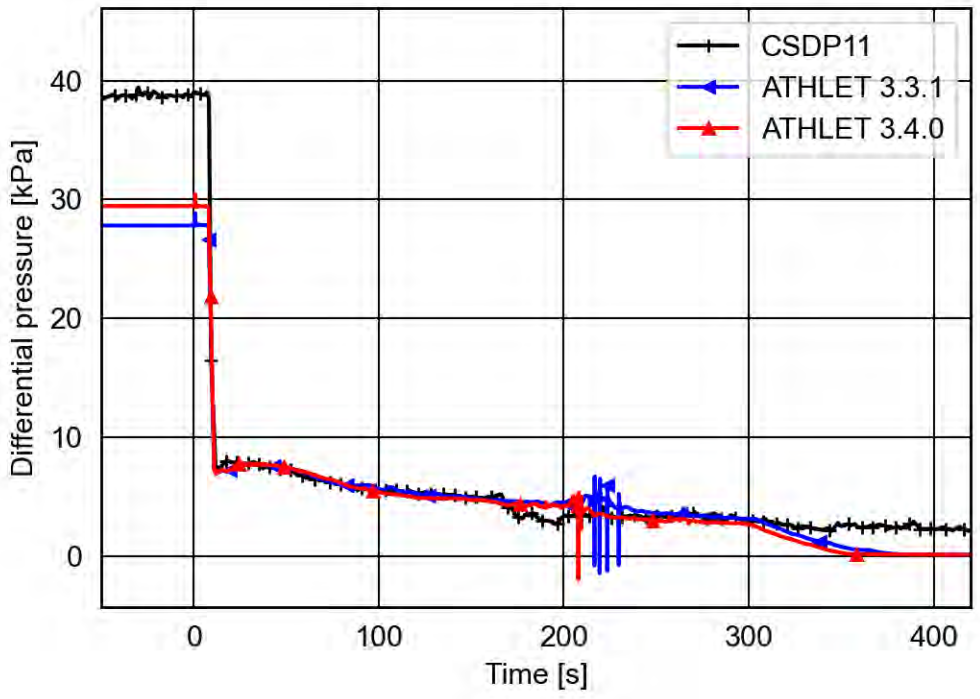

Fig. 5.95 Differential pressure across lower core region

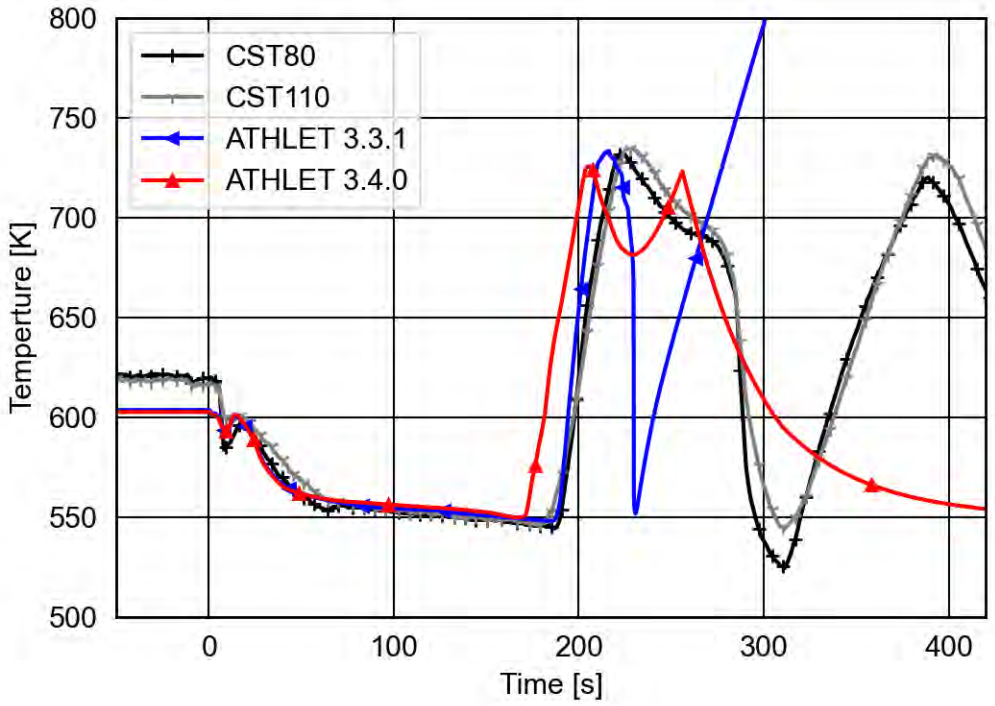

Fig. 5.96 Cladding temperatures top core simulator region (elevation between -1844 mm and -1623 mm)

5.4.4.2 Comparison of 5-eq. model and 6-eq. model

The difference between the 5-eq. model and the 6-eq. model is evaluated next using the ATHLET 3.4.0 version. Both modelling approaches provide the results which agree well with the experimental data.

The temperatures and pressures in the primary circuit are only minorly affected by the model change (Fig. 5.97). With the 6-eq model, the rise of cladding temperatures begins slightly earlier, but the first overheating occurs almost at the same time, since the temperatures rise faster with the 5-eq model (Fig. 5.98). During the first cooling phase, the cladding temperatures go below 550K using the 5-eq model, while they drop only to 700K with the 6-eq model. However, the tendencies in the upper plenum are captured better with the 6-eq model (Fig. 5.99 and Fig. 5.100).

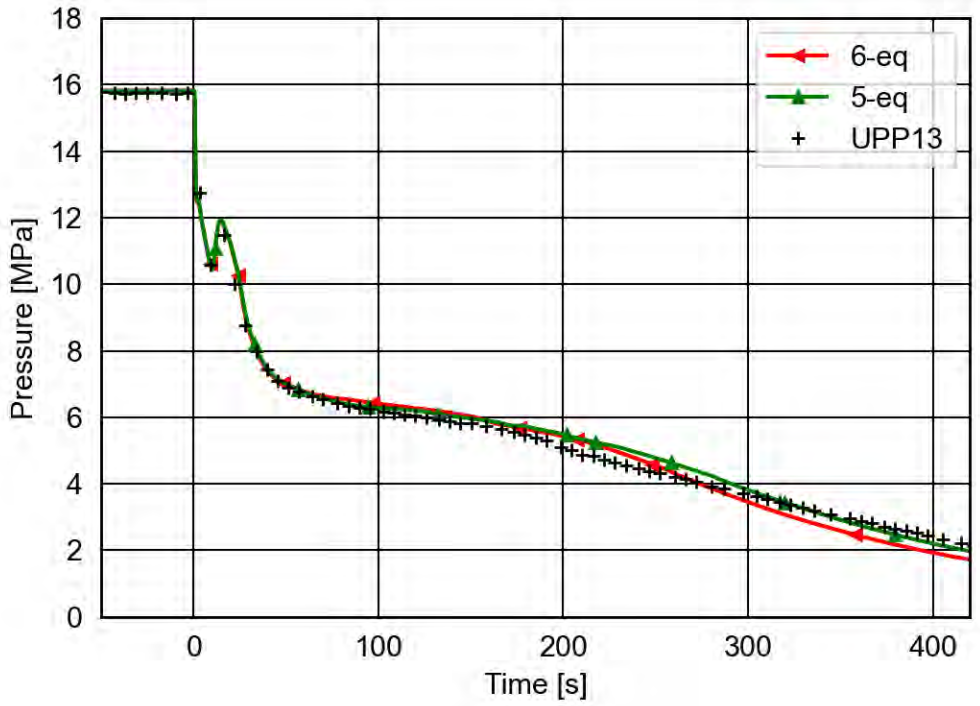

Fig. 5.97 Pressure in upper plenum

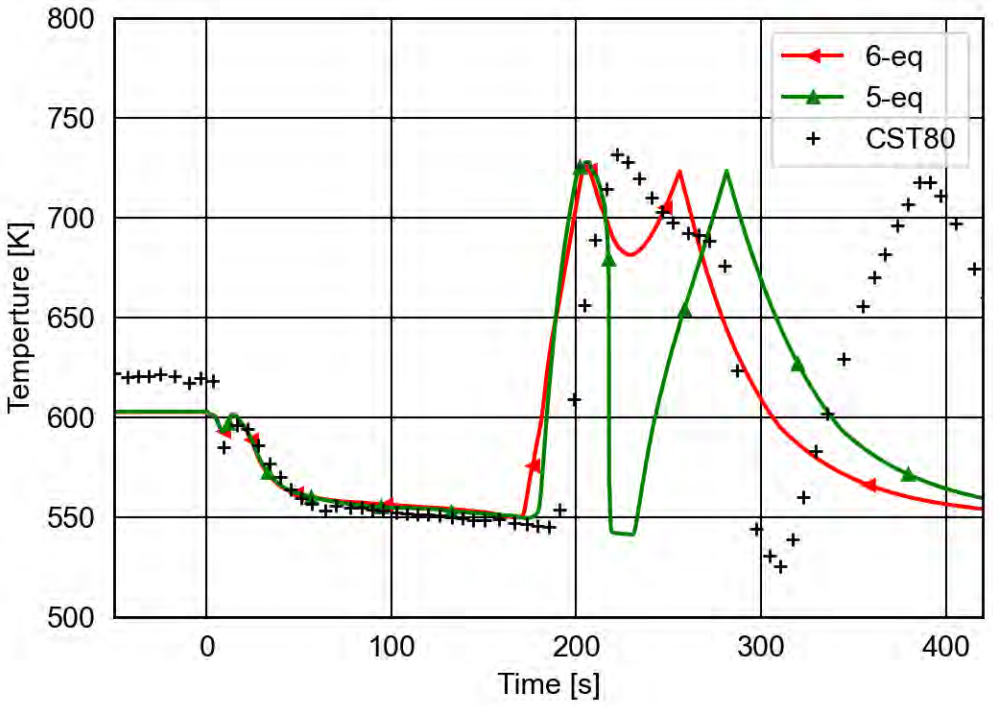

Fig. 5.98 Cladding temperatures at top core simulator region (elevation between -1844 mm and -1623 mm)

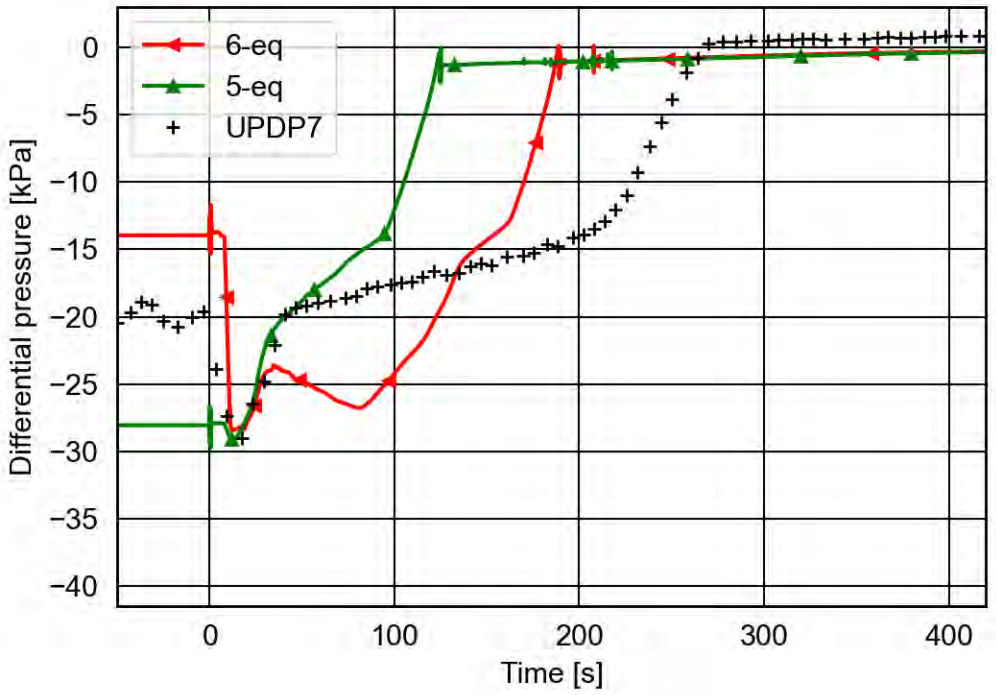

Fig. 5.99 Differential pressure across the upper head of upper plenum

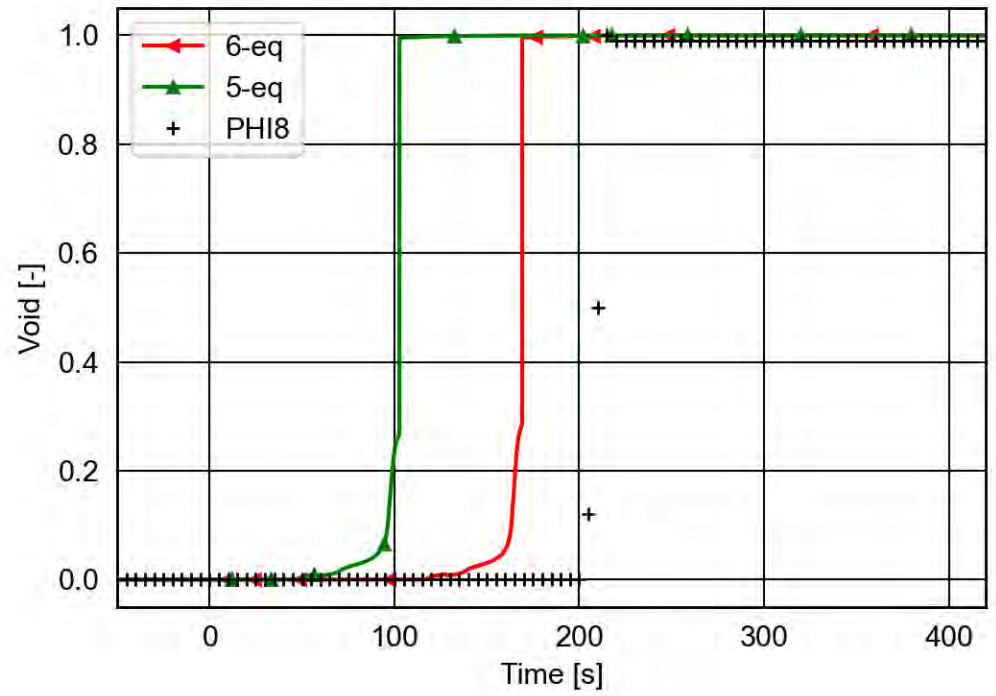

Fig. 5.100 Void fraction at the top of upper plenum

5.4.5 Main Findings

The comparison of the calculated results with the measured experimental data shows in general a good agreement. The main phenomena were reproduced by the code. Nevertheless, there are some disagreements between experimental and calculated results:

- Different from the experiment, the calculated natural circulation in the broken loop reached smaller values and stopped completely after 150 s.
- The steam generator secondary side U-tube surface temperatures deviate from the measured ones, especially in the triple loop.
- The calculated core bypass temperature increases considerably after pump trip, possibly due to an incorrect modelling of pressure losses.
- The simulation can reproduce the quenching after 201 s, which was not the case for older input decks. However, the quenching behavior is considerably different compared to the experiment.
- In the both, single and triple loop, the differential pressure in the vertical part of the cold leg (CLIDP11 and CLIDP28) deviates from the experiement especially from 100 to 210 s. This is caused by differences in the void fraction.
- The leak mass flow deviates from the experiment after 100 s.

The results illustrate the capability of ATHLET to analyze thermal-hydraulic problems for WWER plant configurations.

In general, both code versions ATHLET 3.3.1 and ATHLET 3.4.0 predicts the same evolution of most physical properties observed in the experiment.

5.5 PERSEO

A full documentation of the calculated PERSEO tests including results and comparison with the experimental data can be found in /BUC 19/, /BUC 20/ and /BUC 23b/.

5.5.1 PERSEO Test Facility

Passive residual heat removal is performed in some nuclear power plant designs by so called isolation condenser. Such heat exchangers are normally located above the reactor

pressure vessel and transfer heat to a water filled vessel. At its inner side, vapour is condensed, on its outer side, water is heated up and finally boiled. To activate the system, valves at the inlet and/or outlet pipe must be opened so that the initially fully water filled heat exchanger drains and gets filled again with vapour, which is subsequently condensed.

Within the PERSEO test facility (see Fig. 5.101) also such an isolation condenser is constructed. However, the starting behaviour is a little different to the above-mentioned sequence: In PERSEO, two water pools exist. The heat exchanger is located in the heat exchanger pool (HX pool) which is initially filled with air and vapour. Since also the heat exchanger itself is not filled with water but with vapour initially, heat losses are minimised when the condenser is not working. The other pool (overall pool) instead is filled with water, which can flow by a valve-blocked connection line at its bottom to the bottom of the HX pool. A second pipe connects the top parts the two pools in such a way, that the pipe is immersed into the overall pool inventory by a conically formed injector. The system is activated by opening the valve in the lower connection pipe, so that water gets into the HX pool and is heated up. Inside the heat exchanger vapour is condensed. On its primary side, the heat exchanger is connected via a steam and a return line to a large vessel below representing the reactor pressure vessel fed with steam. Due to the heat source at a low elevation and heat sink at a high elevation a natural circulation establishes during operation of the system. Steam created in the HX pool is directed by the injector into the overall pool water inventory.

Vapour can be injected into the pressure vessel equivalent to a power of 20 MW. To control the liquid level in the vessel, water can also be drained. The heat exchanger consists of two cylindrical collectors and 120 vertical heat exchanger pipes.

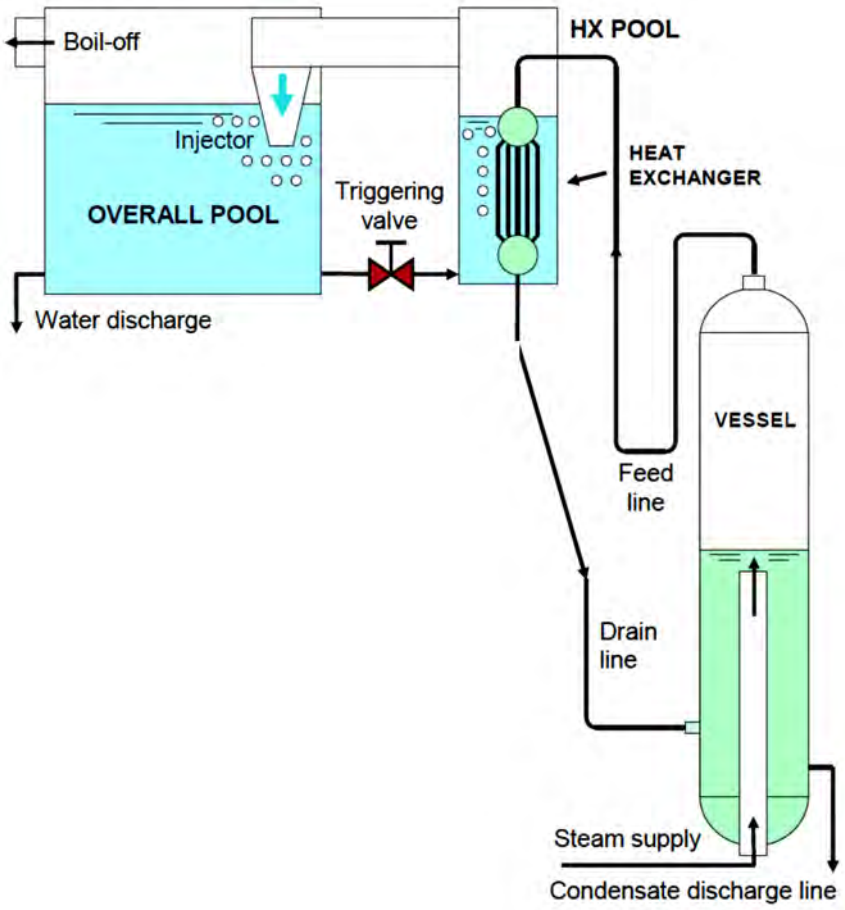

Fig. 5.101 PERSEO facility scheme Bandini /BAN 09/

5.5.2 Test Conduct

For PERSEO, the so-called Test 7 Part 1 and 2 as well Test 9 have been performed and compared with experimental data. Actually, both parts of Test 7 were conducted sequentially, but while in Part 1 the stability of the system for two different liquid levels in the HX Pool was investigated, in Part 2 the long-run behaviour was tested. Both phases were performed at a high pressure of approximately 70.5 bar. Test 9 also deals with the long-time behaviour of the system, but with a lower primary pressure of approximately 40 bar.

5.5.3 Input Dataset

Basically, two datasets have been developed to simulate the PERSEO test facility, differing in the approach to modelling the overall pool. In the first step, a two-channel model of the pool was created, just to take a mixing of the inventory into account. Secondly, a 3D model of the pool was built up to simulate its behaviour in more detail.

5.5.3.1 Nodalisation

The ATHLET nodalisation for the 1D overall pool is shown in Fig. 5.102. Steam injection into the pressure vessel is modelled by a pressure and enthalpy boundary object (TDV) connected to the pressure vessel, in which the desired pressure and enthalpy is specified according to the experimental data. The heat exchanger pipes are modelled only once, and a multiplication factor is used to account for the number of pipes of 120. The same has been done for the needed heat conduction objects representing the pipes walls.

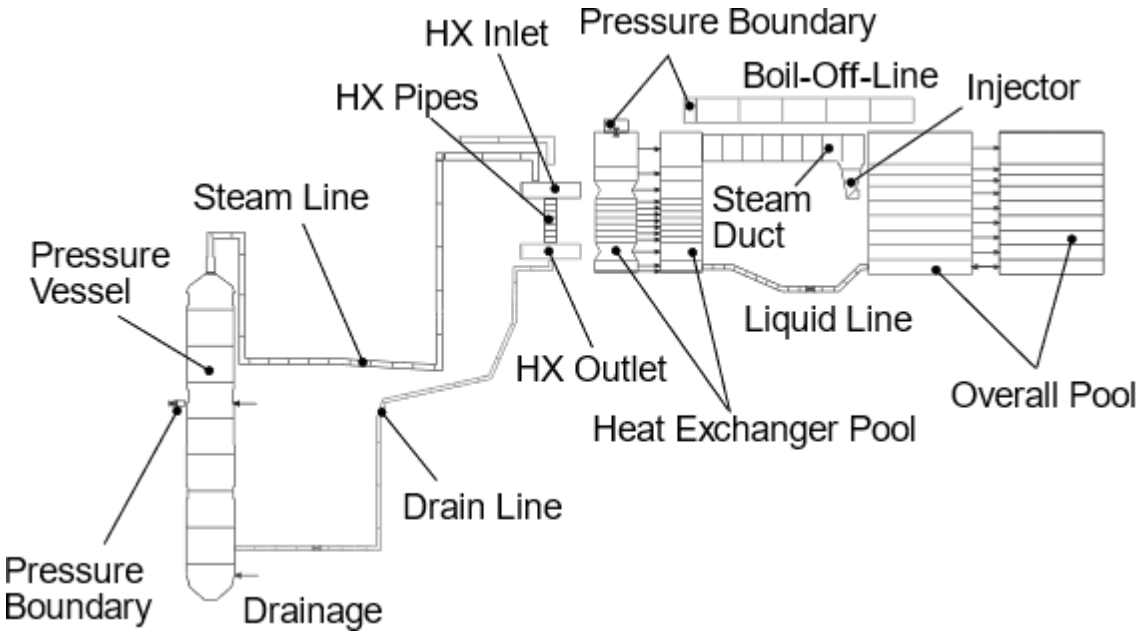

Fig. 5.102 ATHLET Nodalisation Scheme of PERSEO test facility for the 1D overall pool case

On the secondary side, TDVs at the HX pool and the so-called boil-offline were set. The first one was needed to get a stable steady state during the first seconds of the simulation, before opening the liquid line valve, because otherwise, due to condensation of vapour in the HX pool, pressure would have decreased rapidly leading ATHLET to stop the calculation. Using an additional valve, this TDV was isolated from the pool, when the transient started.

The second TDV was set to create the environmental boundary to which the generated vapour is discharged from the overall pool.

While in the 1D representation of the overall pool a two-channel model was chosen to simulate just the mixing of the water inventory, also a 3D model solution was created,

which is not shown in Fig. 5.102, but in which the pool is divided into nine parallel channels in a 3x3 matrix. The channels are equal in size.

5.5.3.2 Model Options

The new heat transfer correlation model was introduced in ATHLET to improve the simulation of condensation in vertical pipes, which is available since ATHLET 3.3 and was chosen as default for the simulation of such heat exchanger types. Therefore, all ATHLET 3.4 and 3.3.1 results, shown afterwards are using this feature.

5.5.4 Main Results

5.5.4.1 Test 7 Part 1

In Test 7 Part 1 starts with opening the connection pipe valve, which is subsequently closed again, opened again and finally closed. With opening the valve, water flows into the HX pool and the heat exchanger starts to transfer heat from the primary to secondary side. Power during first opening is about 1 MW, during the second opening approximately 20 MW (Fig. 5.103). A more exhaustive interpretation of the experiment and simulation can be found in /BUC 19/.

In the following pictures besides the experimental data also simulation results obtained with ATHLET 3.4 and ATHLET 3.3.1 are shown. Due to the enhanced calculation of condensation in vertical pipes taken from /PAP 10/, the agreement with the experimental data in the ATHLET 3.4 and 3.3.1 case is in a good agreement which is shown exemplarily in the figure of the power of the heat exchanger in Fig. 5.103. ATHLET 3.4 and 3.3.1 lead to similar results. Referring to the number of complete Jacobian updates it can be seen that for the simulations, the number of updates is identical for ATHLET 3.4 under Windows 10 and Linux of the code using serial or omp version indicating identical results (Fig. 5.104 with 1D and Fig. 5.105 with 3D representation of the overall pool).

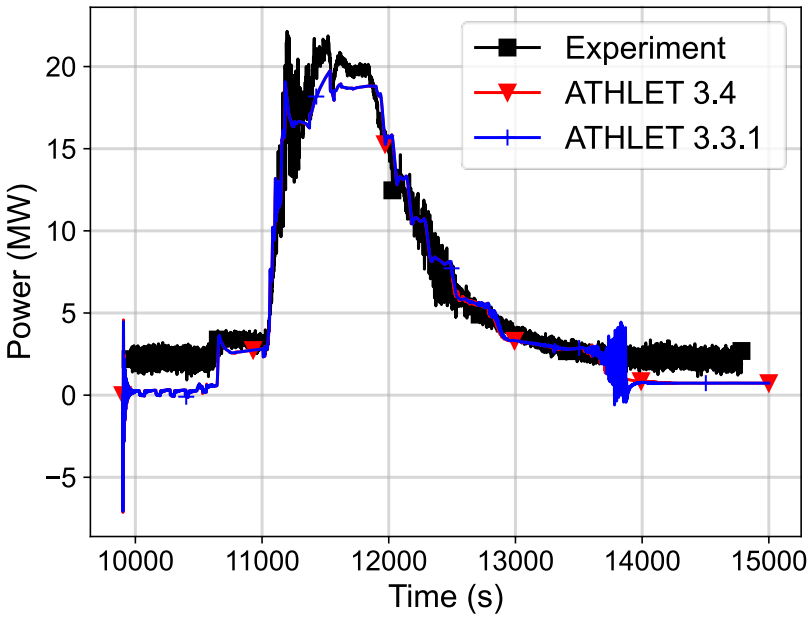

Fig. 5.103 Simulation results Test 7 Part 1 with 1D Overall Pool; Power condenser

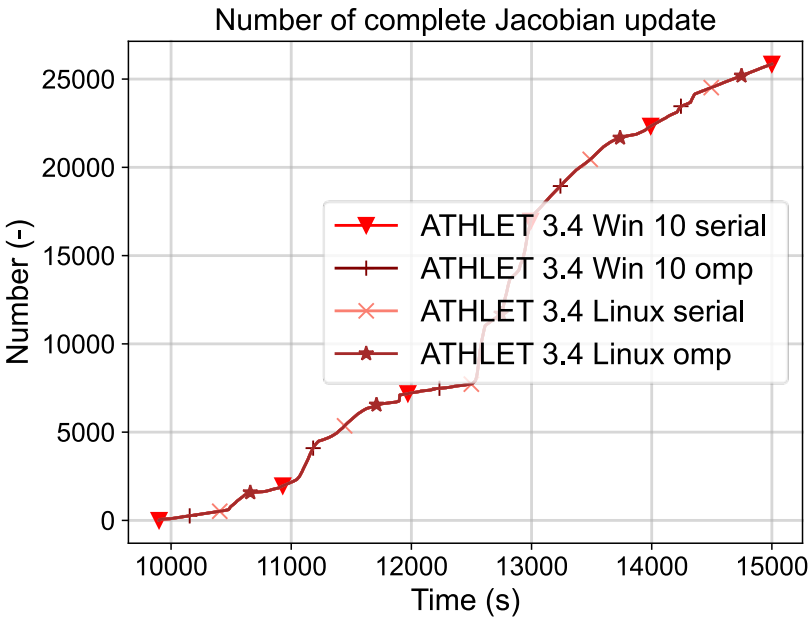

Fig. 5.104 Simulation results Test 7 Part 1 with 1D Overall Pool; Number of complete Jacobian updates

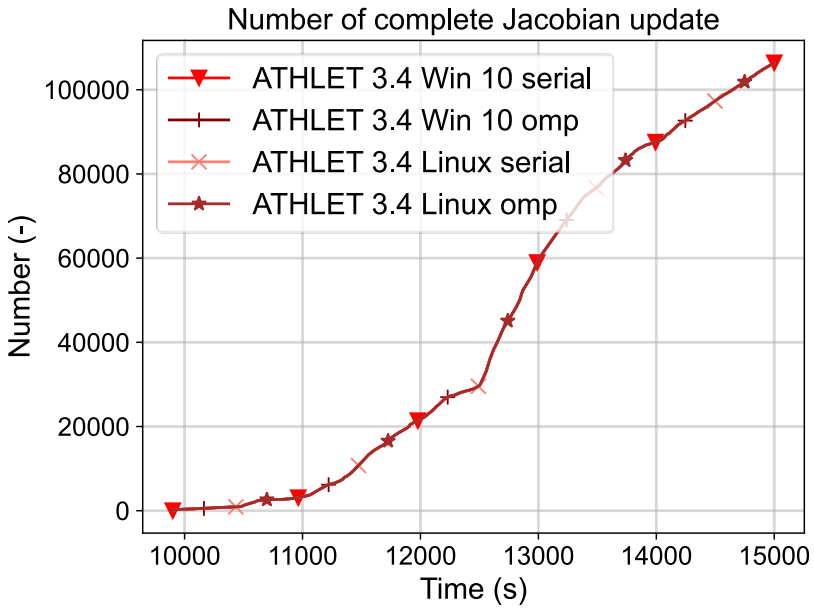

Fig. 5.105 Simulation results Test 7 Part 1 with 3D Overall Pool; Complete Jacobian Updates

5.5.4.2 Test 7 Part 2

In this test, the valve in the connection line between the pools is opened only once but longer than in part 1. With opening the valve at 300 s, the liquid level in the HX pool is rising and oscillating (Fig. 5.107). Power of the condenser follows the liquid level in the HX pool and reaches 20 MW (Fig. 5.106) but declines with decreasing pool level after closing the valve at 3,338 s. It can be seen, that with opening the valve, heat transfer starts due to water level increase in the HX Pool (Fig. 5.107). In ATHLET 3.3 and 3.3.1 the agreement of the heat exchanger power is good, although a slight underprediction of the power can be observed. With closing the valve, the water level inside the HX Pool decreases due to evaporation leading in the end to a decreasing power of the heat exchanger. A more detailed analysis of the experiment and simulation can be found in /BUC 19/. Also here, number of complete Jacobian updates are similar comparing Windows and Linux as well as serial and omp version (Fig. 5.108 and Fig. 5.109).

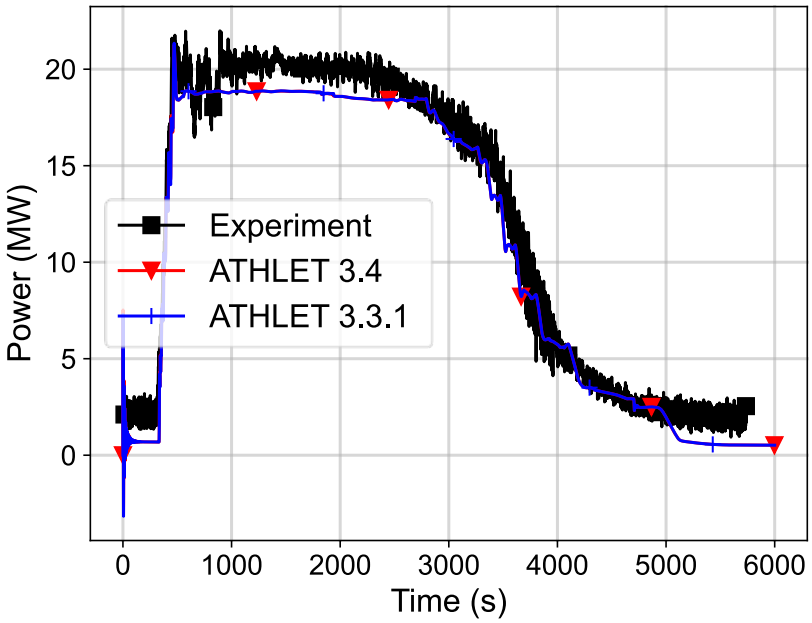

Fig. 5.106 Simulation results Test 7 Part 2 with 1D Overall Pool; Power condenser

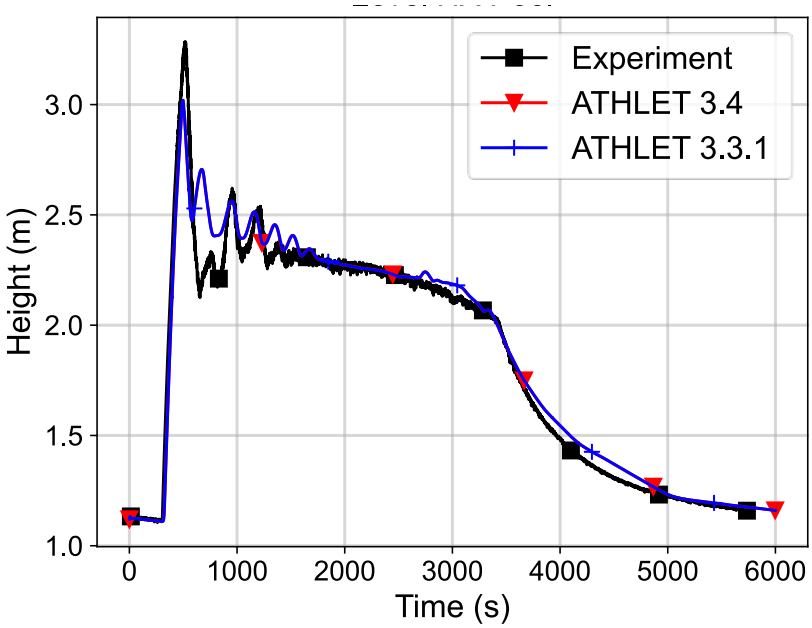

Fig. 5.107 Simulation results Test 7 Part 2 with 1D Overall Pool; Level HX Pool

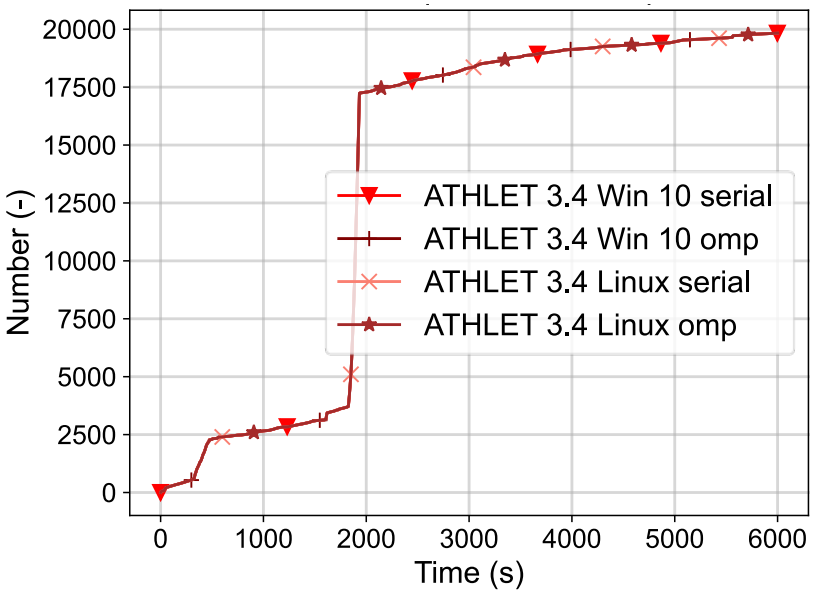

Fig. 5.108 Simulation results Test 7 Part 2 with 1D Overall Pool; Number of Jacobian updates

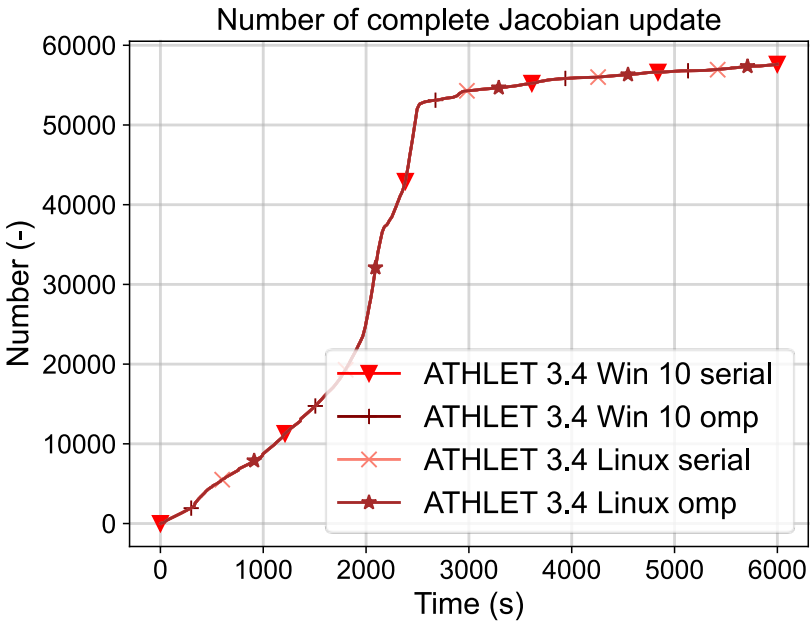

Fig. 5.109 Simulation results Test 7 Part 2 with 3D Overall Pool; Number of complete Jacobian updates

5.5.4.3 Test 9

Finally, Test 9 is quite similar to Test 7 Part 2 but in contrast to that, the primary pressure is reduced from 70.5 bar to 40.8 bar consequently leading to a lower condenser power during the experiment of approximately 14 MW (Fig. 5.110). The transferred heat is well

predicted by both ATHLET versions. The experiment and the related simulations are documented in /BUC 20/.

Simulations for Test 9 give reasonable results with all ATHLET versions. Testing results of serial and omp version of ATHLET 3.4 show same results under Windows and Linux in the 1D and 3D case indicated by the number of complete Jacobian updates in Fig. 5.111 and Fig. 5.112.

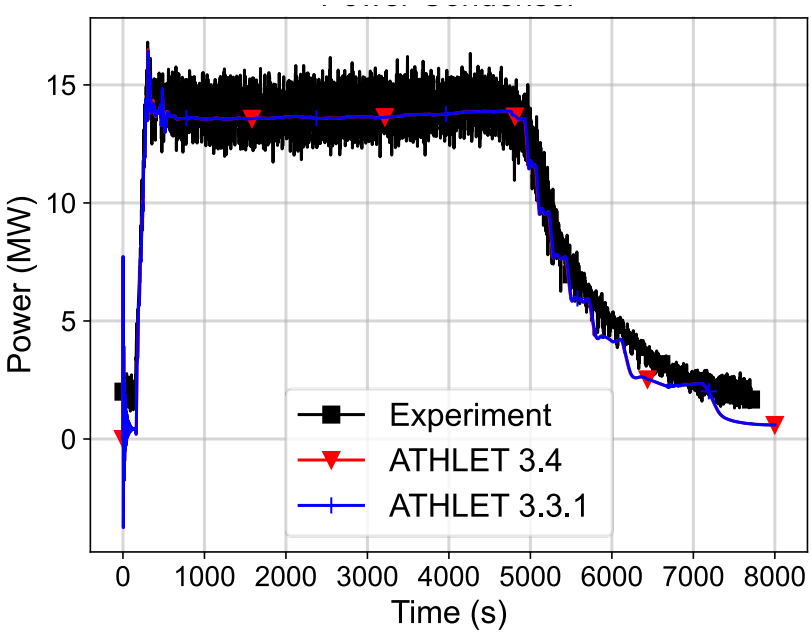

Fig. 5.110 Simulation results Test 9 with 1D Overall Pool; Power condenser

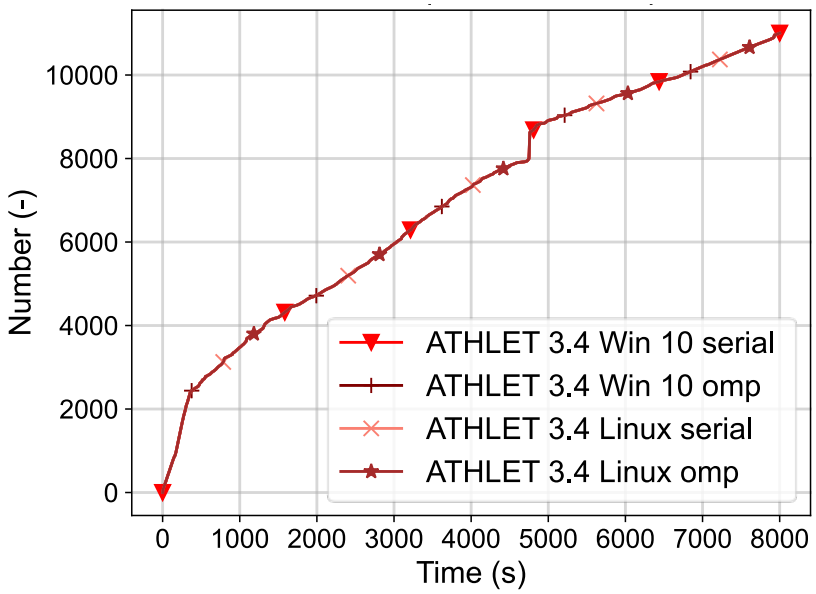

Fig. 5.111 Simulation results Test 9 with 1D Overall Pool; Number of complete Jacobian updates

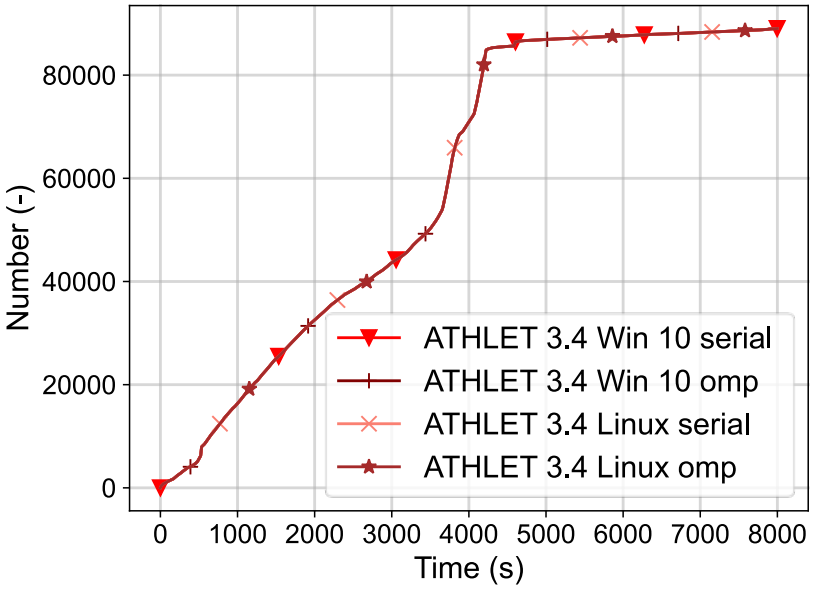

Fig. 5.112 Simulation results Test 9 with 3D Overall Pool; Number of complete Jacobian updates

5.5.4.4 Miscellaneous

In the following, restart possibility and usage of the numerical toolkit (NuT) is shown.

Using Test 9 for restart test capabilities results in consistent results as shown in Fig. 5.113 and Fig. 5.114. Simulation results seem to be identical, indicated by the same number of Jacobian updates.

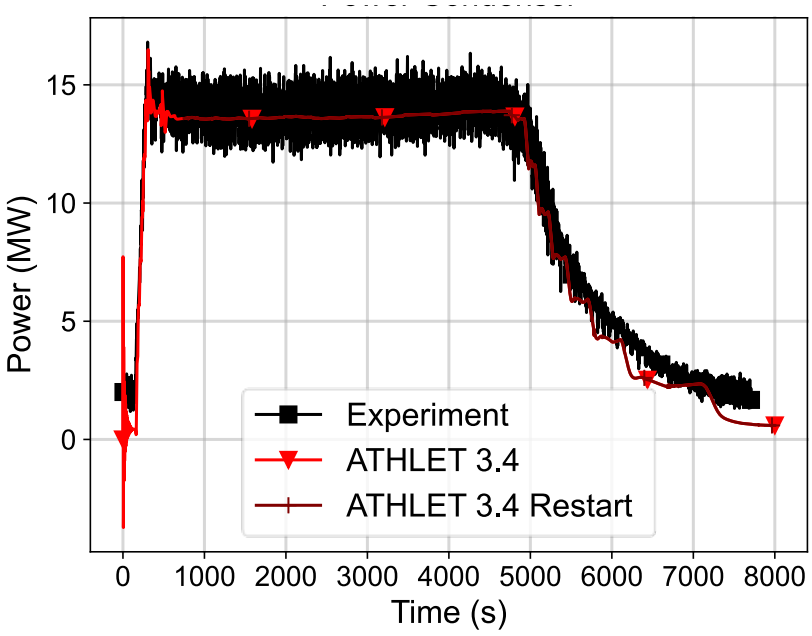

Fig. 5.113 Test of restart capability for Test 9 (Restart at 750 s); Power

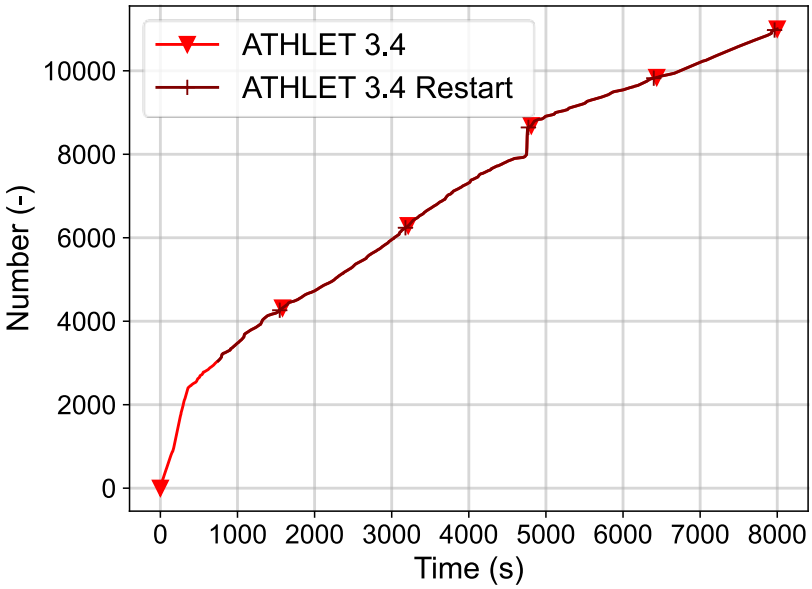

Fig. 5.114 Test of restart capability for Test 9 (Restart at 750 s); Complete Jacobian updates

Using the numerical toolkit leads to similar but slightly different results in the main figures of merit as shown in Fig. 5.115 and Fig. 5.116. While plotted power looks identical

between FEBE and NuT, the number of complete Jacobian updates indicates small differences. This is well within expectations.

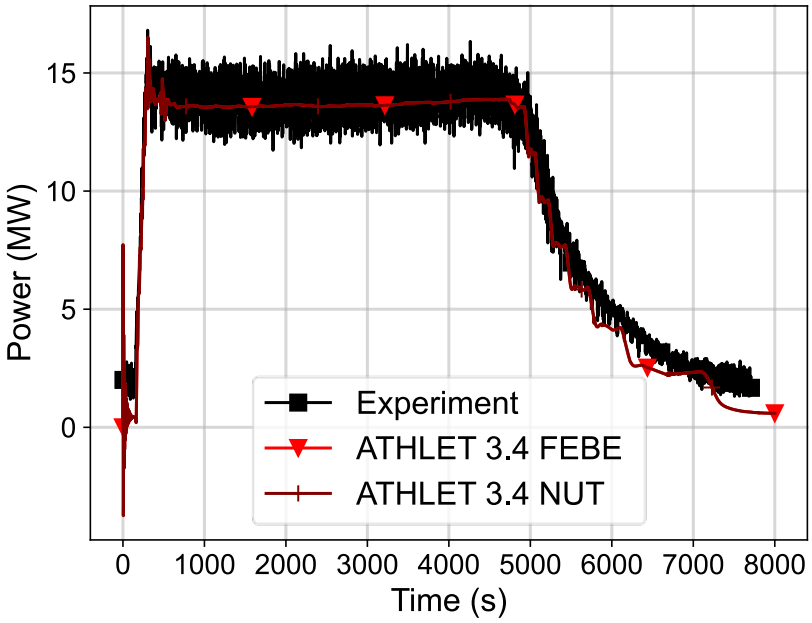

Fig. 5.115 Test of NuT for Test 9; Power condenser

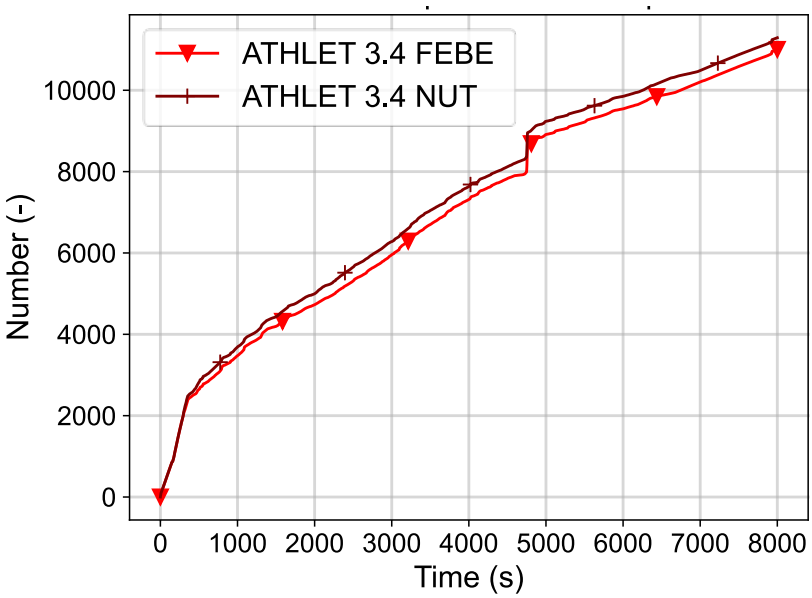

Fig. 5.116 Test of NuT for Test 9; Number of complete Jacobian updates

5.5.5 Main Findings

Simulation of all PERSEO tests with and without the 3D model show no fundamental differences in the figures of merit between ATHLET 3.4 and ATHLET 3.3.1. Serial and

omp version of ATHLET 3.4 lead to same results independent of the used operating system. Furthermore, restart capability works fine, and the restart run lead to same results as the original one, from which it was restarted. Calculations with NuT differ in results compared with FEBE calculations, but, as in the operating system case, no unexpected relevant differences can be observed.

5.6 EASY-4

The EASY-4 test was an experimental simulation of a station blackout in the BWR KERENA controlled by passive safety systems only. The test was conducted in the frame of the German joint research project EASY by Framatome. A detailed analysis of the experiment as well as the simulation results and a BEPU analysis can be found in /BUC 18/.

5.6.1 INKA Test Facility

The INKA test facility (Integral Teststand Karlstein) is a large experimental facility representing the BWR KERENA reactor. It is located in Karlstein (Main) and operated by Framatome. The main objective of the facility is to investigate the behaviour of the passive safety systems and safety approach of the KERENA concept during accident conditions.

The reactor circuit is represented by the large GAP vessel, a downcomer line, a return line and the emergency condenser (EC). GAP stands for Großarmaturenprüfstand. This vessel originates from the GAP facility Framatome uses to test large valves. The vessel is additionally equipped with a steam injection and a water drainage. Furthermore, during the EASY project between 2015 and 2018, a passive pressure pulse transmitter (PPPT) was added to the vessel, which is used to trigger the passive flooding valve.

Besides the cooling circuit, the flooding pool vessel, drywell vessel and wetwell vessel installed in INKA represent the different containment compartments of KERENA. While the whole facility is scaled 1 : 1 in height, the containment vessels are scaled 1 : 24 in volume and the GAP vessel scales the RPV of KERENA approximately 1 : 6. Finally, there is the shielding and storage pool located on the top of the facility. The different systems for pressure suppression, residual heat removal and coolant addition are scaled in number (1 : 4) but not in size. A simplified representation of INKA is shown in

Fig. 5.117. In this scheme the abbreviations are as follows: RPV for reactor pressure vessel; FPV for flooding pool vessel; DWV for drywell vessel; PSPV for pressure suppression pool vessel; SSPV for shielding and storage pool vessel; CCC for containment cooling condenser; EC for emergency condenser.

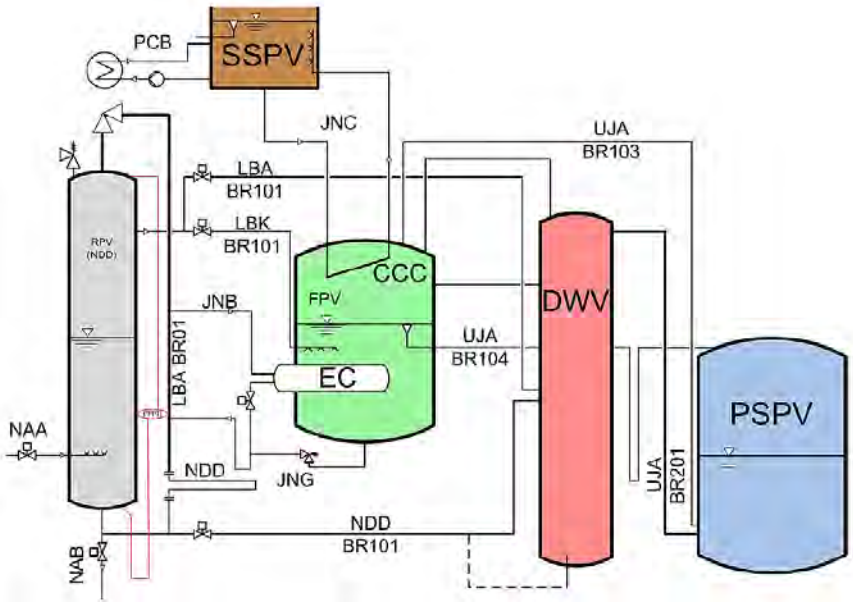

Fig. 5.117 INKA simplified process diagram /WAG 17/

5.6.2 Test Conduct

The test EASY-4 is a simulated station blackout in which the safety concept of KERENA to cope with the accident with passive safety features only was assessed. Since the experiment progress is mainly determined by the size of the passive heat exchanger. In the facility the heat exchangers are scaled (1 : 4), which is much smaller than the containment scaling (1 : 24). In order to decelerate the progress of the experiment, the heat exchanger scaling was adapted to 1 : 8 by plugging 50 % of the emergency condenser pipes and isolating one half of the containment cooling condenser.

5.6.3 Input Dataset

In the following the input data set for ATHLET and for the coupled ATHLET/COCOSYS calculation are described.

5.6.3.1 Nodalisation

The nodalisation for the stand alone ATHLET simulations is shown in Fig. 5.118. Here, the primary system including GAP vessel, downcomer line (DCL), emergency condenser (EC) and return line are modelled. Steam injection and water drainage are modelled as single junction pipes (SJP) with a fill. The PPPT was not included in the simulations since the GAP liquid level did not decrease so much as to activate it. For the EC, the pipes were arranged in groups according to their length. The plugged pipes were not simulated. In the containment, the flooding pool vessel (FPV), drywell vessel (DWV) and wet well vessel (WWV) have been modelled by a parallel channel approach including simulation of mixture level tracks. The vessels are interconnected by various connecting pipes. The containment cooling condenser (CCC) is connected to the top part of the FPV. One half of the CCC was deactivated by closed valves. Air is simulated in it. Finally, the CCC is connected to the shielding and storage pool (SSPV) by an inlet and outlet pipe. The outlet pipe is connected to the pool by a sparger. A pressure boundary for the ambient environment was set on the top of the pool. Heat losses are considered for pipes and vessels, which insulation is also included in the model.

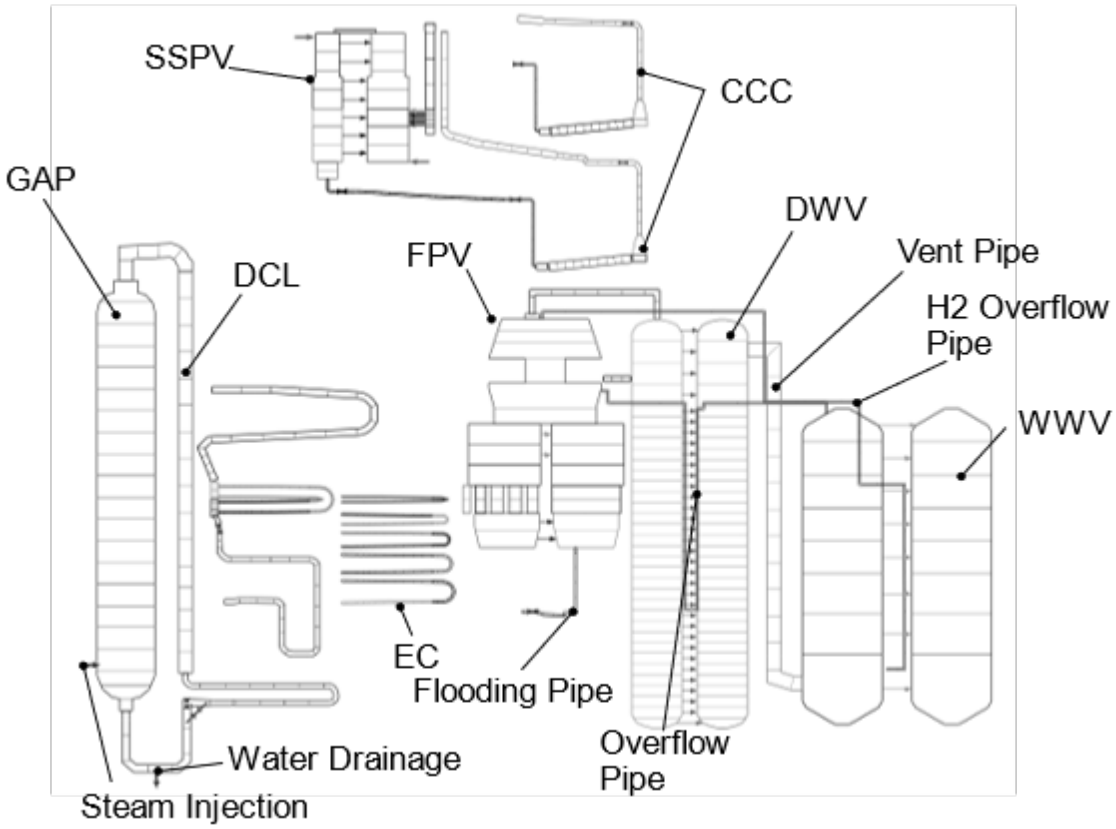

Fig. 5.118 ATHLET nodalisation of INKA for SBO experiment

The version of the dataset for AC² simulations (coupled ATHLET-COCOSYS) is shown in Fig. 5.119. In contrast to the ATHLET stand-alone dataset, the DWV and WWV were simulated by COCOSYS. The discharge coupling was used. Therefore, discharge valves have been implemented at the interfaces between ATHLET and COCOSYS, which are at the end of the connection lines between FPV and DWV, as well as at the end of the overflow pipe and the H_2 overflow pipe. Due to the coupling strategy, each of the connecting pipes ends in a ATHLET TDV, in which the pressure and enthalpy as well as gas mixture is taken from COCOSYS by GCSM. In the case of the H_2 overflow pipe, which is immersed in the water inventory of the WWV, the water column was needed to be added by GCSM controller to consider the hydrostatic pressure at the end of the pipe. The vent pipe is modelled fully in COCOSYS. The insertion model is used to simulate the ingress of steam/air into the wet well water inventory.

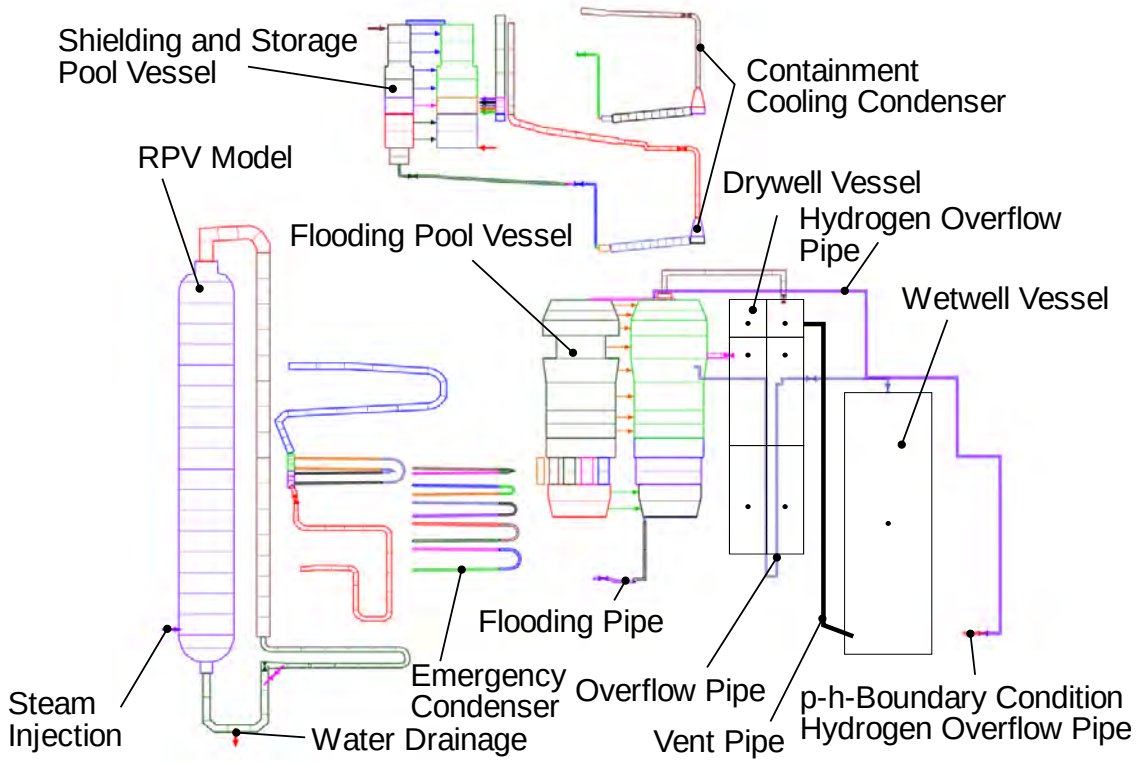

Fig. 5.119 ATHLET/COCOSYS nodalisation of INKA for SBO simulation

5.6.3.2 Model Options

It is needed to be noted, that the power of the emergency condenser as well as for the containment cooling condenser needed to be fitted to the experimental data, since ATHLET underestimated the heat transfer in both heat exchangers. The underlying reasons are still under investigation. For the EASY-4 simulation, the underestimation was

addressed by introduction of correction factors multiplied to the FPARH values of the respective heat exchanger HCOs. In the stand-alone case, for the EC a value of 1.3 and for the CCC a value of 1.8 were chosen. In the AC² simulation, EC parameter was still 1.3 but for the CCC only 1.1 was needed. Both parameters were used to reach the respective pressure in the GAP (EC parameter) and drywell (CCC parameter) although the actual EC and CCC power still differed from experimental data (as shown in Fig. 5.121 and Fig. 5.125). Depending on the used code version, an adjustment of both parameters could improve the results.

5.6.4 Main Results

A description of the progress of the experiment and a comparison with ATHLET simulations can be found in /BUC 18/. Fig. 5.120 and Fig. 5.122 show the pressures in the GAP and drywell vessel. It can be seen that primary pressure prediction is almost the same in both ATHLET versions. It agrees well with the experimental data, although the power of the emergency condenser is underpredicted by code versions (see Fig. 5.121). During air overflow from the drywell into the wet well by the vent pipe, pressure is rising in all cases until approximately 5,000 s when the air flow switches to steam flow. In the ATHLET 3.3.1 case, less air is moving into the wet well than in the ATHLET 3.4 case, leading to a lower drywell pressure (see Fig. 5.123). The lower the air ingress, the larger is the steam ingress into the wet well indicated also by a higher water temperature in the wet well in the ATHLET 3.3.1 case (Fig. 5.124). CCC power in the ATHLET 3.3.1 and ATHLET 3.4 are similar, since the conditions within the flooding pool and connected drywell are almost the same. However, the power is slightly higher in ATHLET 3.4 since the pressure and therefore temperature difference between inside and outside of the heat exchanger is slightly higher.

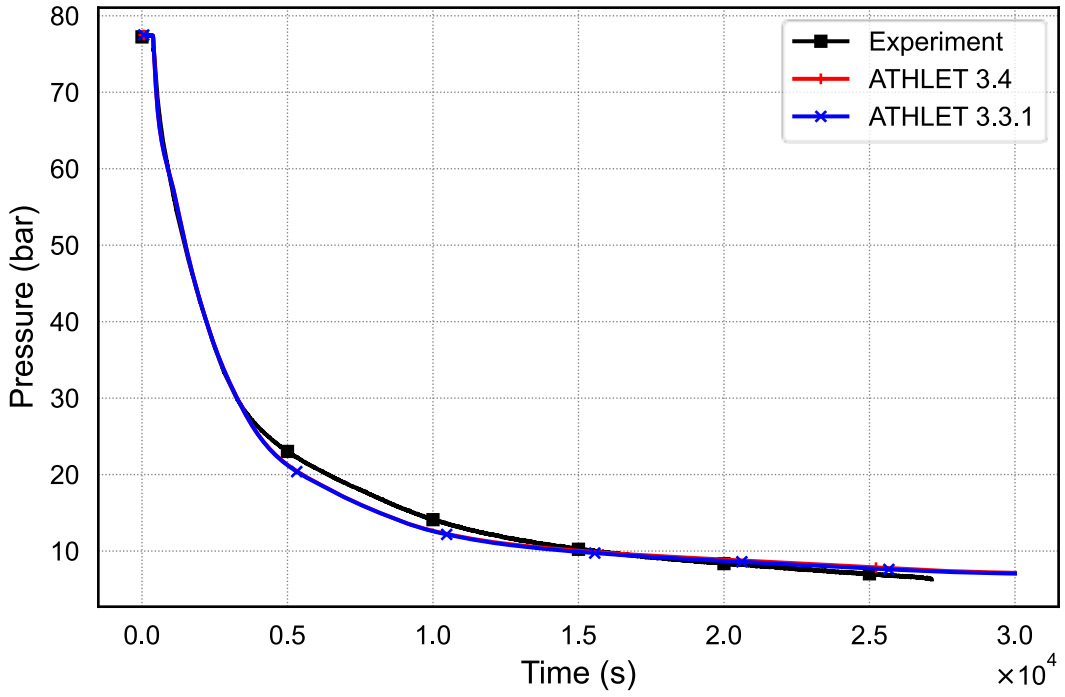

Fig. 5.120 Simulation results EASY-4 and comparison between different ATHLET versions and operating systems; Pressure GAP

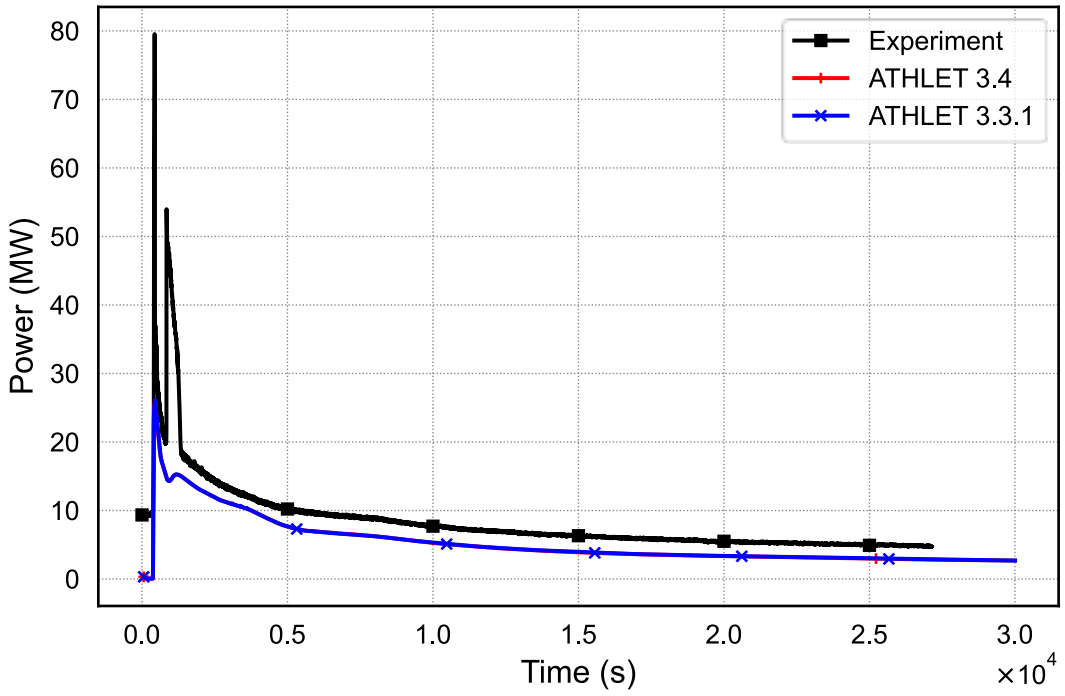

Fig. 5.121 Simulation results EASY-4 and comparison between different ATHLET versions and operating systems; Power EC

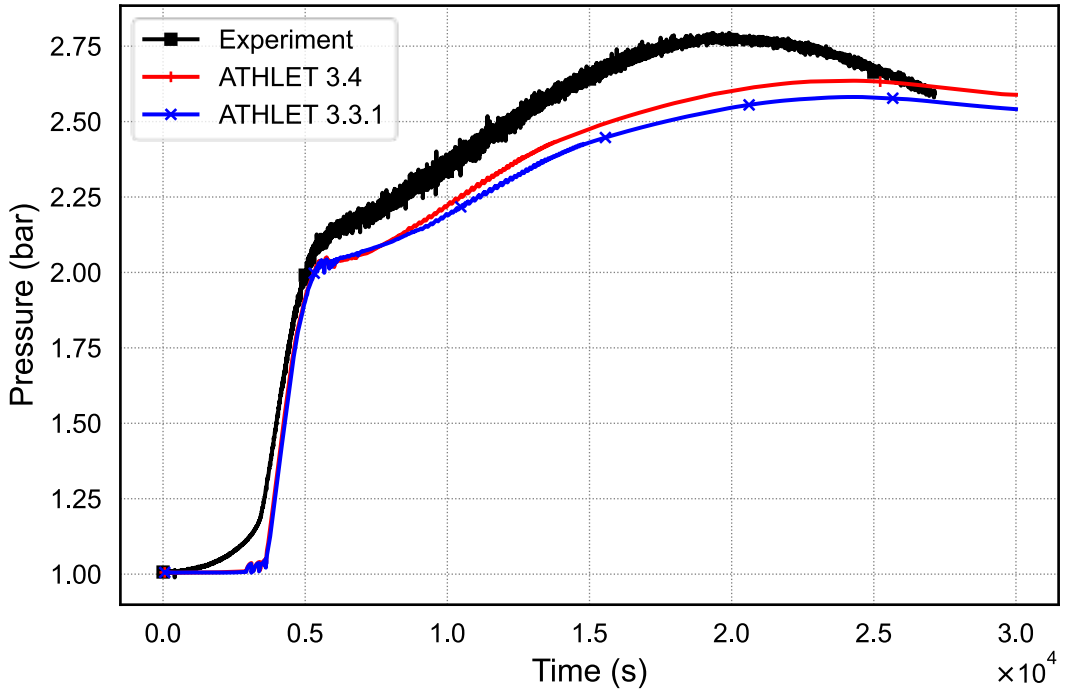

Fig. 5.122 Simulation results EASY-4 and comparison between different ATHLET versions and operating systems; Pressure drywell vessel

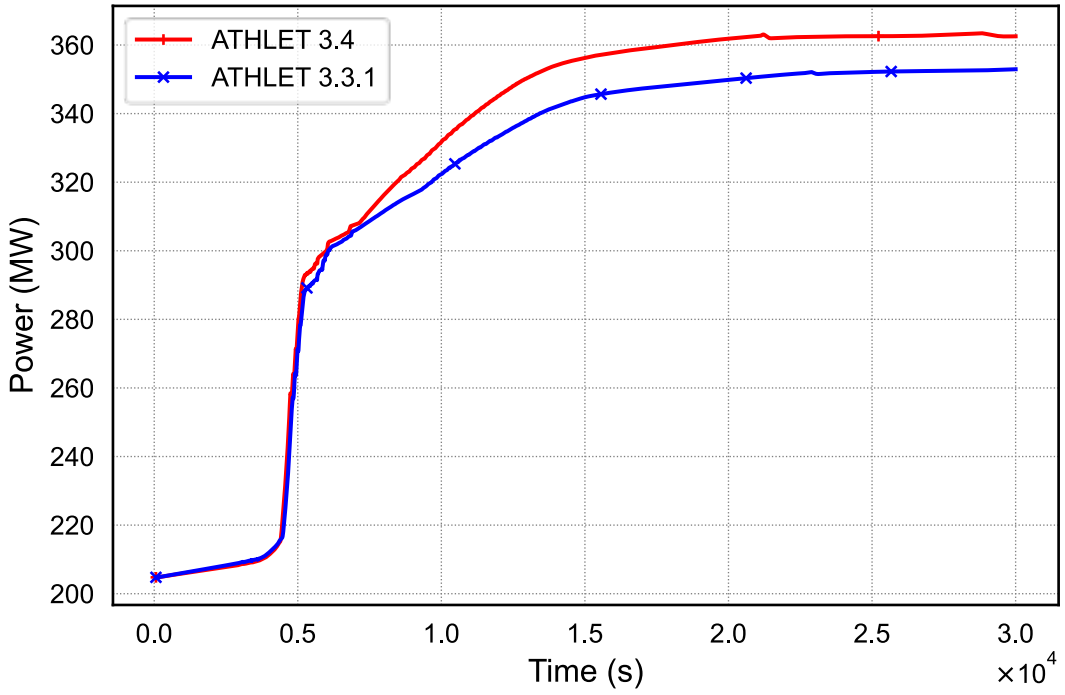

Fig. 5.123 Simulation results EASY-4 and comparison between different ATHLET versions and operating systems; Air mass in wet well

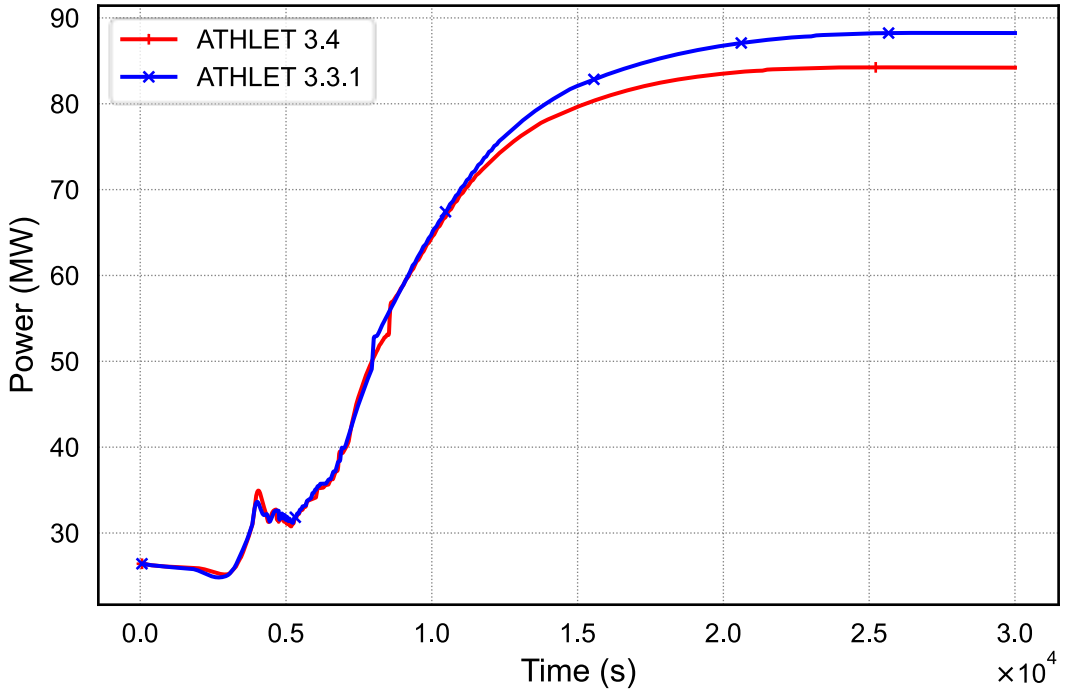

Fig. 5.124 Simulation results EASY-4 and comparison between different ATHLET versions and operating systems; Water temperature in wet well vessel

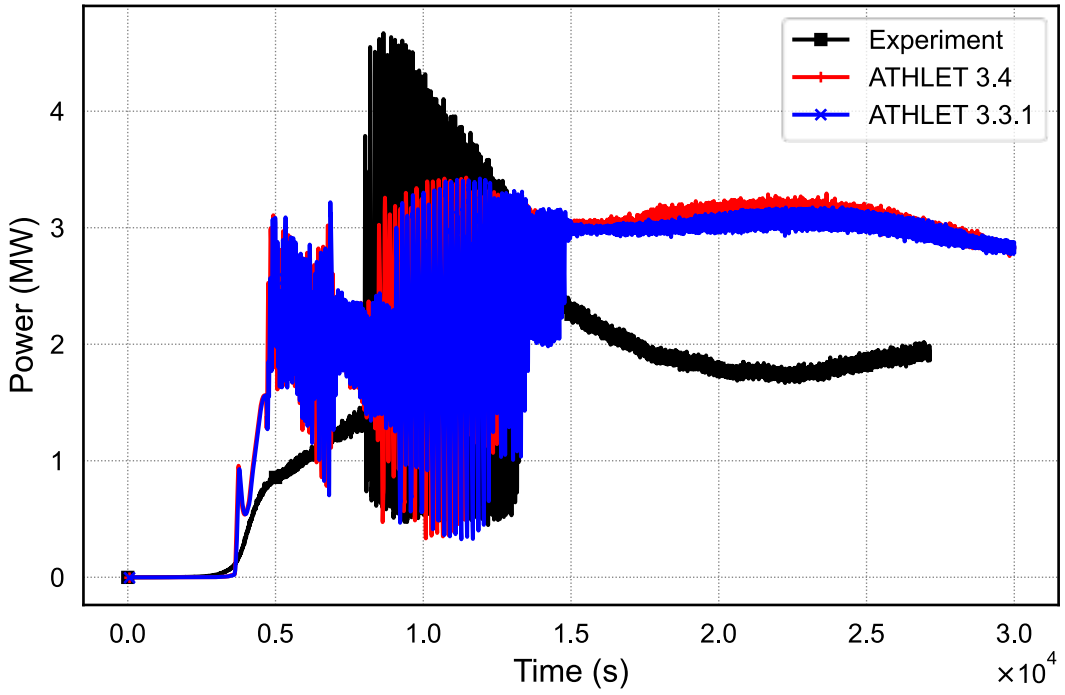

Fig. 5.125 Simulation results EASY-4 and comparison between different ATHLET versions and operating systems; Power CCC

Fig. 5.126 shows the number of timesteps for ATHLET 3.4 simulations with omp and serial executables and different operating systems indicating identical results.

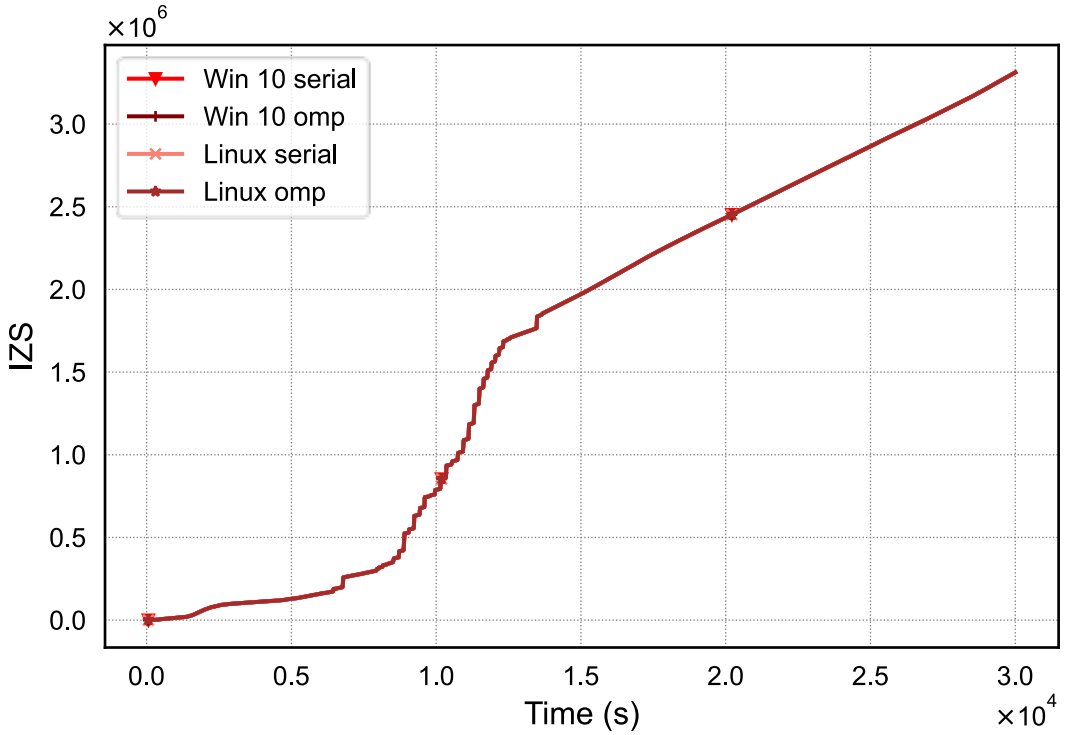

Fig. 5.126 Number of timesteps for the EASY4 simulation with ATHLET 3.4

Using the coupled version of ATHLET/COCOSYS similar results can be found for the different versions of AC² as shown exemplarily for the drywell vessel pressure in Fig. 5.127. Notably, there is good agreement between the experiment and AC² 2023, AC² 2021.1. The number of ATHLET timesteps in Fig. 5.128 indicate, that the simulation of the experiment lasts longer in the old version than with the new version of 2023 and that Linux and Windows 10 versions lead to the identical results. Data in both figures for AC² 2021.1 was obtained by using the so-called driver coupling method. Since the plugin method is not available anymore in AC² 2023, no additional comparison between both types was performed.

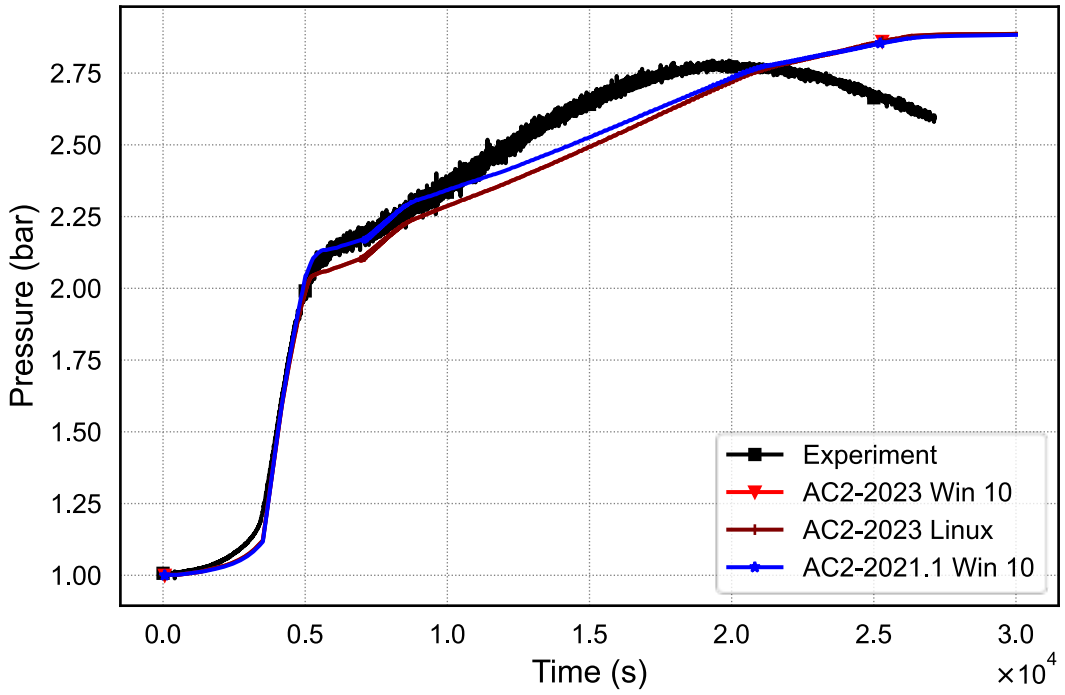

Fig. 5.127 Simulation results EASY-4 using coupled version of ATHLET/COCOSYS, pressure drywell vessel

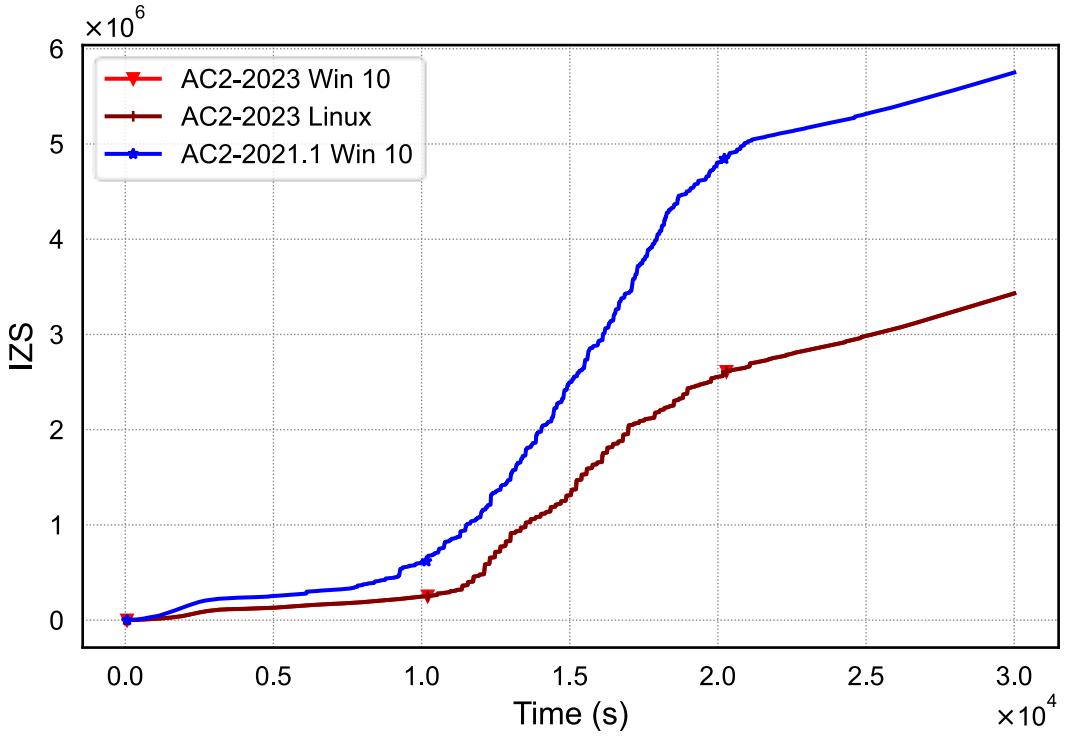

Fig. 5.128 Simulation results EASY-4 using coupled version of ATHLET/COCOSYS, number of timesteps

5.6.5 Main Findings

It was shown that using ATHLET 3.4 in comparison with ATHLET 3.3.1 the progress of the simulation of the EASY-4 experiment is similar. Only minor changes with respect to air ingress into the wet well was observed, which has a slight impact on other figures like pressure in the drywell or CCC power. The coupled version of ATHLET/COCOSYS of AC^2 2023 lead to similar results compared to the versions before with smaller calculation time.

Overall, the AC^2 2023 simulation demonstrates successful validation of AC^2 against the EASY-4 test, although further investigations into the code and the input deck is necessary.

5.7 Selected Reflooding Tests

In this section, the results of selected tests of the reflooding experiments FEBA, FLECHT and PERICLES will be presented. All tests mainly consist of a heated vertical rod bundle in a steam filled channel, which is then flooded with liquid water to simulate reflooding after a loss of coolant accident. The results for ATHLET 3.3 and 3.4 mostly overlap, except for minor differences in calculation time for some of the tests.

5.7.1 FEBA

The FEBA (Flooding Experiments with Blocked Arrays) facility was built by the Kernforschungszentrum Karlsruhe to obtain insights into heat transfer mechanisms during the reflooding process of a bundle from below or above. Eight test series were conducted during which the pressure, the blocked ratio of the channel, as well as the reflooding velocity and mechanism were varied.

5.7.1.1 Test Facility

The test section consists of a 5 x 5 rod bundle in a square stainless-steel housing. The housing has an inner length of 78.5 mm and its walls are 6.5 mm thick and insulated on the outside to reduce heat losses. The housing has the additional function to simulate heat from other rods surrounding the bundle. The rod bundle is electrically heated with a stepped cosine power profile as shown in Fig. 5.129 over the heated length of 3.9 m. The individual rods have an outer diameter of 10.75 mm and the bundle pitch is 14.3 mm.

Six spacer grids are axially distributed along the bundle length. A cross-section of the test section is also included in Fig. 5.129. Additional information on FEBA can for example be found in the evaluation report /IHL 84/.

5.7.1.2 Test Conduct

The simulated test is number 216 from the first series. In this test, an unobstructed bundle was flooded from below. Additional test parameters are listed in Tab. 5.7 below.

The desired initial cladding and housing temperatures are achieved by heating the fuel rod simulators in stagnant steam for about two hours before the test. To initiate the test, the bundle power is increased to the controlled decay heat transient, 120 % ANS-Standard /ANS 79/ 40 s after the shutdown of a reactor. Coolant is then pumped into the lower plenum and is quickly evaporated when it reaches the heated length. Steam and entrained liquid travel through the test section into a separator, where the liquid is drained into a collecting tank and the steam flows through a buffer tank and into the atmosphere. The flooding continues until the rod bundle is cooled down.

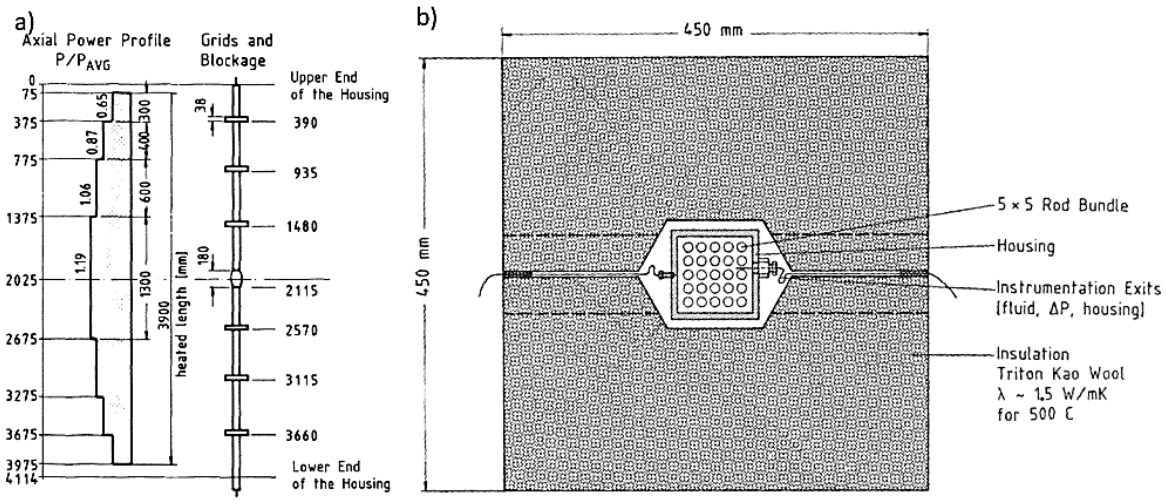

Fig. 5.129 a) Stepped cosine axial power profile and locations of the spacer grids.
b) Cross-section of the FEBA test section. Taken from /IHL 84/

Tab. 5.7 Test parameters of FEBA test 216 of series 1

Test No	Fluid Velocity [cm/s]	System Pressure [bar]	Feedwater Temp. [°C] 0-30s End		Cladding Temp. at 2025 mm [°C]	Housing Temp. at 2025 mm [°C]
216	3.8	4.1	48	37	787	640

5.7.1.3 Input Dataset

The FEBA test section is modelled as a one-dimensional pipe with 23 axial nodes. The spacer grids are considered as reductions to the pipe's cross-sectional area and as form losses. The initial temperature of the channel is chosen to be the temperature distribution of the wall and coolant is supplied by a fill at the lower end of the pipe. At the top end of the channel there is time dependent volume, which acts as a drain. Mass flow and enthalpy of the fill and the pressure and enthalpy of the time dependent volume are given by GCSM signals.

The heater rods are modelled with 23 axial nodes and 5 radial layers. The inner three layers are magnesium oxide, the outer two are made of nichrome. The initial temperature distribution of the rods is achieved by introducing a microchannel in the rod, for which a temperature distribution can be defined. The housing consists of four layers and the temperature on its outside is controlled by GCSM. The nodalisation is included below in Fig. 5.130.

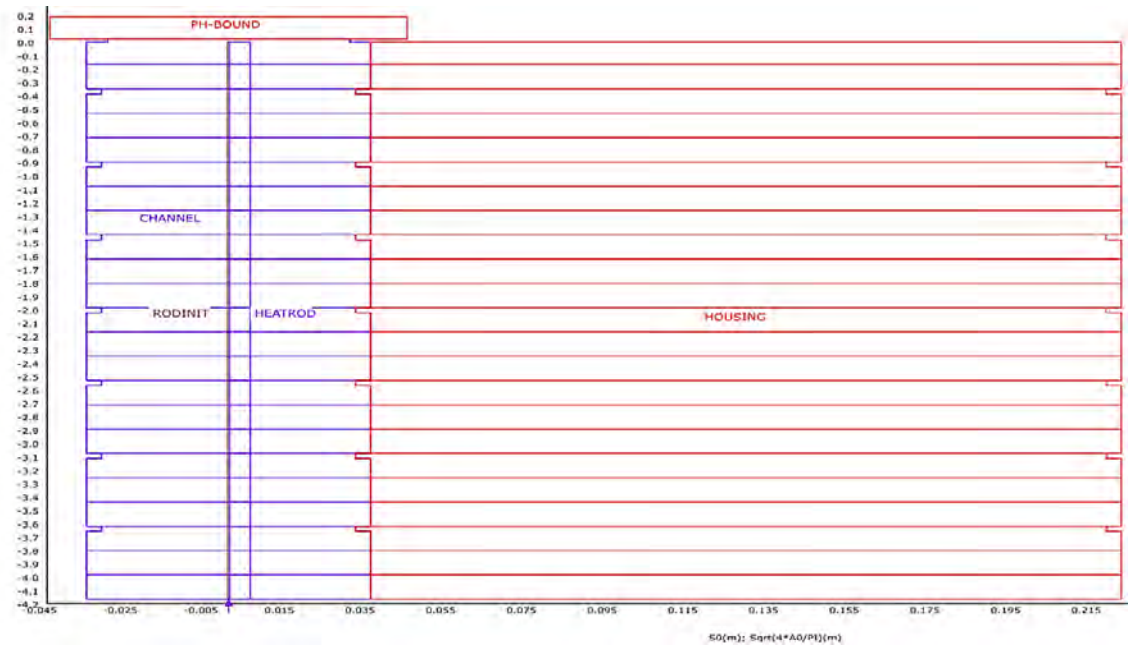

Fig. 5.130 Nodalisation of the FEBA test section in ATHLET

To delay the quench front progression, the parameter `CQHTWB` of the quench model is reduced by an order of magnitude from the default $3 \cdot 10^5$ to $3 \cdot 10^4$. The parameter controls the maximum possible heat transfer coefficient at the wetted side of the quench front.

5.7.1.4 Main Results

While the heating up phase of the rod cladding is barely affected by the version change, the cooling process is slowed down, which matches the experimental data better as can be seen for the cladding temperature trends at 1.942 m in Fig. 5.131. In the beginning of the test, the temperature rises as the coolant quickly evaporates when entering the test section and the steam cooling is not enough to compensate the heating power. The simulations reach their peak temperature of around 880°C 40 s before the experiment and start to cool down early. As the lower parts of the cladding are cooled down, the coolant temperature remains lower as liquid reaches the higher areas, so that more heat can be removed from the cladding. While the cooling process in the experiment continues until just after 210 s into the experiment, ATHLET 3.2.1 quenches about 40 s early. The prolonged cooling process in ATHLET 3.3 and 3.4 reduces the difference in quench time to 30 s.

The delay in the quench front resulting from the prolonged cooling down period can be seen in Fig. 5.132. The agreement between experiment and simulation is greatly increased in ATHLET 3.3 and 3.4, especially in the early phase of the experiment. The top of the heater rods is still quenched too early, but the difference is reduced from 140 s to 80 s.

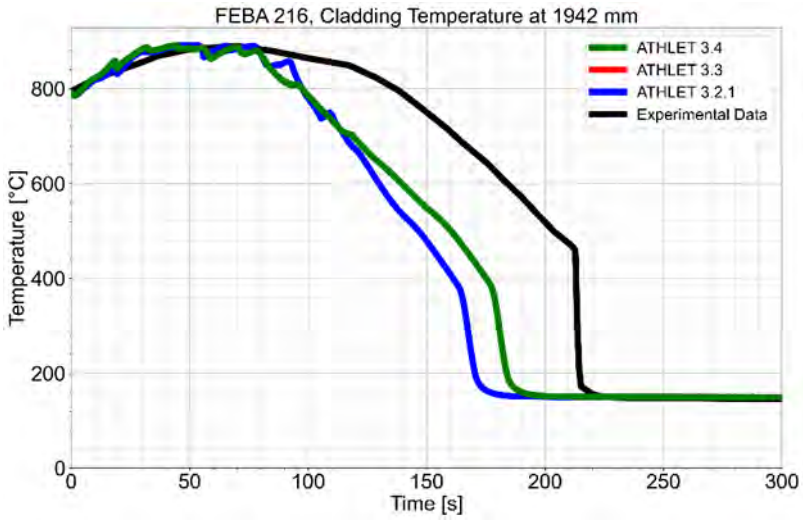

Fig. 5.131 Comparison of the simulated and experimental cladding temperature for FEBA 216 at 1.942m

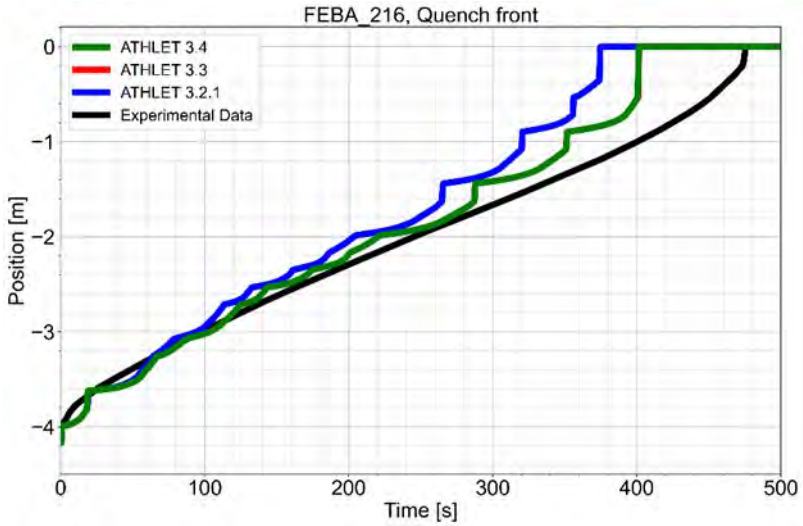

Fig. 5.132 Comparison of the simulated and experimental quench front progression for FEBA 216

5.7.2 FLECHT

5.7.2.1 Test Facility

The FLECHT SEASET (Full Length Emergency Core Heat Transfer – Systems Effects and Separate Effects Tests) program is a modified version of earlier tests by the Idaho National Engineering Laboratory, utilizing a new bundle geometry. Similar to the FEBA facility, mainly the test section consisting of a vertical rod bundle in an initially steam filled channel is of interest.

The new bundle contains 161 heater rods, arranged to similarly to the 17 x 17 Westinghouse fuel bundle design. The heater rods have an outer diameter of 9.5 mm, a bundle pitch of 12.6 mm. The bundle is housed in a cylindrical vessel with an inner diameter of 193.7 mm. A cross-section is included in Fig. 5.133. Also shown in Fig. 5.133 is the stepped cosine axial power profile over the heated length of 3.66 m. Additional information on the facility can be found in the data report /LOF 80/.

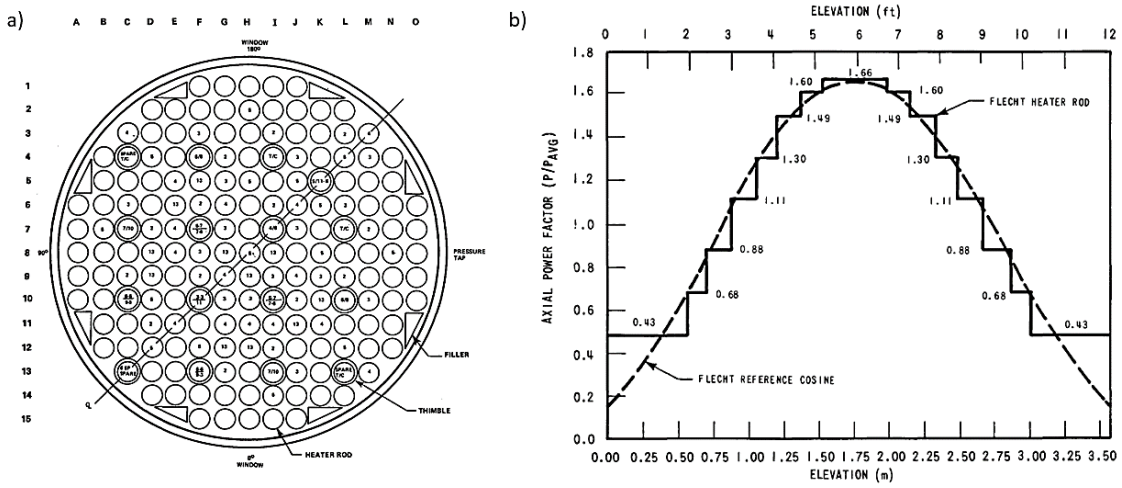

Fig. 5.133 a) Cross-section of the FLECHT test section.
b) Axial power profile of the heater rods. Taken from /LOF 80/

5.7.2.2 Test Conduct

Before the test, the test section and connected components are pressurized by opening the connection valve to a boiler and regulating the exhaust line with a control valve. The lower plenum is brought to coolant temperature and components above the test section are heated slightly above saturation temperature with clamp-on strip heaters.

Power is then supplied to the heater rods until the pre-set initial temperature value is reached in two of the designated thermocouples. This triggers the water injection into the lower plenum and the subsequent reflooding, as well as the power decay equalling 120% ANS standard /ANS 79/. Heating and water injection continue until all designated heater rods are quenched, at which point water and power supply are terminated and the system is depressurized.

Results are presented for the tests 31701 and 31805, which were conducted under similar conditions, except for the coolant velocity. Coolant injection in test 31701 was around

eight times faster than in test 31805. Additional test parameters can be found in Tab. 5.8. For these tests, the rods 4G and 5G were disconnected.

Tab. 5.8 Parameters of the FLECHT tests 31701 and 31805

Test No	Upper plenum Pressure [bar]	Init. clad temp. [°C]	Rod peak power [kW/m]	Flow rate [mm/s]	Coolant temp. [°C]
31701	2.8	872	2.3	155	53
31805	2.8	871	2.3	21	51

5.7.2.3 Input Dataset

The FLECHT test section is modelled as a pipe with 12 control volumes. The spacer grids are considered as form losses, but not as reductions of the cross-section. Below the main channel is an additional object acting as a lower plenum. The coolant is supplied into the lower plenum by a fill object and drained in a time dependent volume at the top of the channel. The initial temperature distribution of the heater rods is taken as the initial temperature of the channel.

The heater rod consists of 60 volumes axially, 5 per pipe section, and 8 layers radially. The two innermost layers are heated boron nitride, followed by four unheated layers of boron nitride and then two layers of stainless steel. There is no housing simulated. A schematic of the nodalisation is shown in Fig. 5.134.

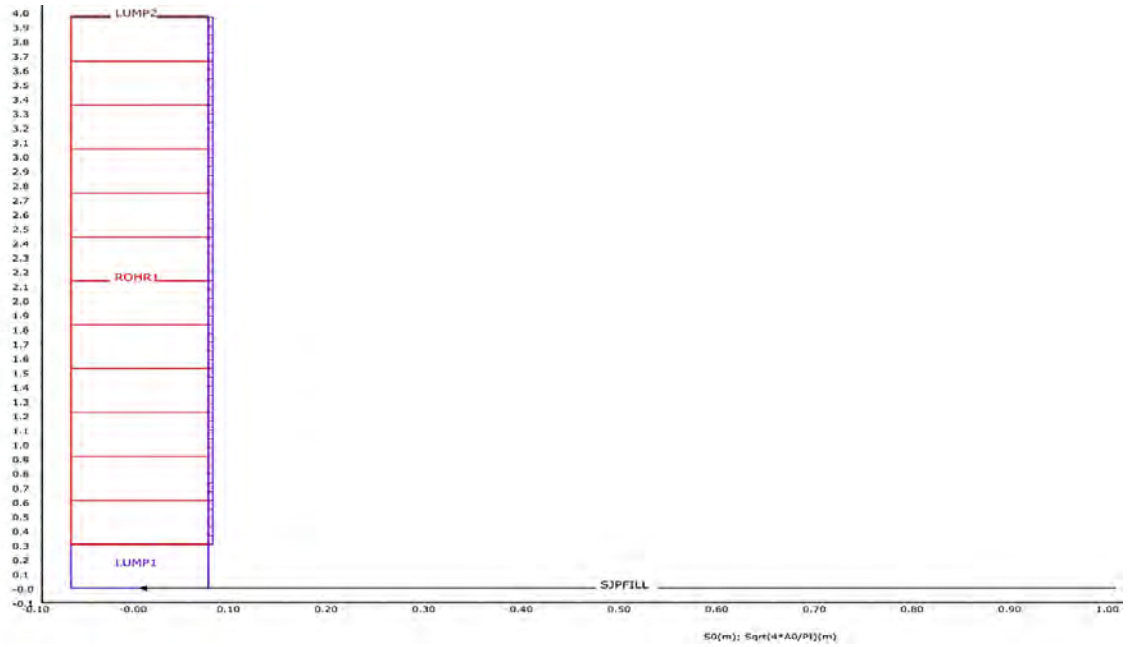

Fig. 5.134 Nodalisation of the FLECHT test section in ATHLET

5.7.2.4 Main Results

As with FEBA, the changes implemented in ATHLET version 3.3 and 3.4 mainly affect the cooling down process. Because of the high flooding rate in FLECHT 31701, the heating up phase is very short. The simulations' initial temperature is about 60°C lower than the experimental data but remains at a higher level for longer. In the first seconds, the temperature trend observed in the simulations is barely changed. Afterwards, the cladding cools down more slowly and the eventual quench is delayed. This delay improves the code's reproduction of the temperature trend, as can be seen in Fig. 5.135. Different to that, the prolonged cooling down of ATHLET 3.3 and 3.4 is barely visible in test 31805. As with FEBA, the simulated temperature begins to drop earlier, and the experimental data reaches its peak as the simulated data is already going down. The cladding is quenched prematurely at about 160 s as can be seen in the cladding temperature trend pictured below in Fig. 5.136.

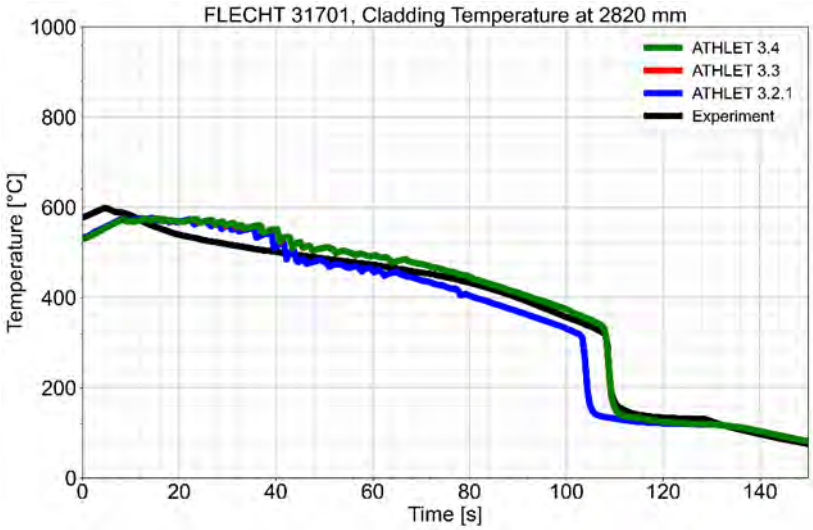

Fig. 5.135 Comparison of the simulated and experimental cladding temperature for FLECHT 31701 at 2.82 m

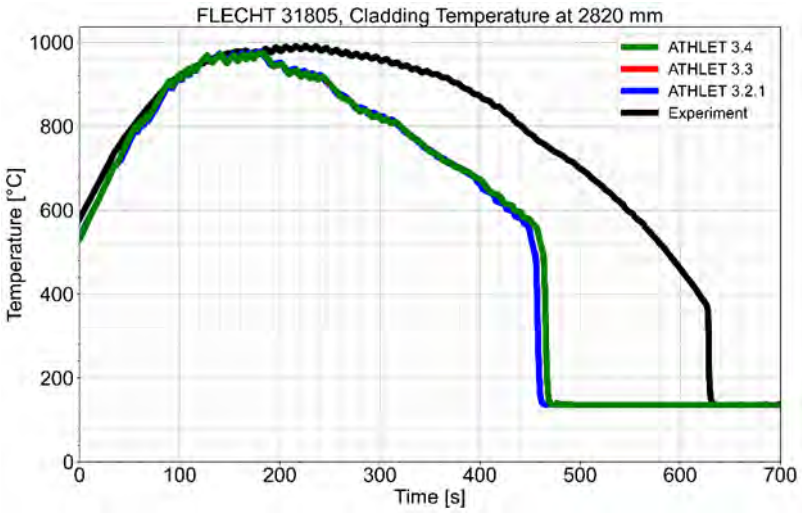

Fig. 5.136 Comparison of the simulated and experimental cladding temperature for FLECHT 31805 at 2.82 m

5.7.3 PERICLES

5.7.3.1 Test Facility

The PERICLES test program aimed to investigate 2-D effects in adjacent rod bundles with different heating power during reflooding.

The test section consists of three 7 x 17 bundles side by side, where the central one is supplied by a separate power source from the other two. The central bundle is considered the hot channel and has its heating power increased by a factor of 1.435 in some of the tests. The effectively 7 x 51 bundle is surrounded by steel housing with a rectangular cross-section (91.5 mm x 646.5 mm) and a wall thickness of 7 mm. The heater rods have an outer diameter of 9.45 mm and a bundle pitch of 12.6 mm. The cross-section is displayed in Fig. 5.137.

Like FEBA and FLECHT, the axial power profile of the heater rods is a stepped cosine shape, which is also included in Fig. 5.137. Unlike the other two test programs, the experiments were conducted with constant heating power rather than a decay curve.

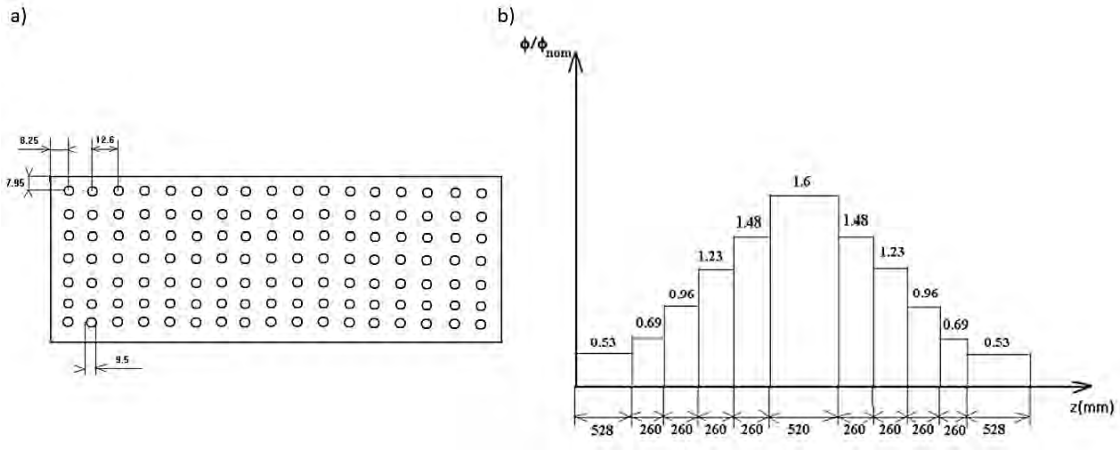

Fig. 5.137 a) Schematic cross-section of the PERICLES bundle.
b) Axial power profile of the heater rods. Taken from /SKO 11a/

5.7.3.2 Test Conduct

In preparation for the test, the outer wall is heated externally and kept a few degrees above saturation temperature. The initially steam filled bundles are then heated with the full operational power, until the desired initial temperature, generally 600°C, is reached at the section of maximum power in the heater rods. At this point, the reflooding process is started with a constant flow rate. The experiment continues until all three bundles are completely quenched.

In the selected experiment, the central bundle is heated with the same power as the outer ones.The other experimental parameters are included in Tab. 5.9 below.

Tab. 5.9 Parameters of PERICLES test RE0062

Test No	Nom. power [W/cm2]	Mass flow [g/cm2s]	Subcool-ing [°C]	Pressure [bar]	Initial temp. [°C]
RE0062	2.93	3.6	60	3	600

5.7.3.3 Input Dataset

The PERICLES test section is modelled as 3 parallel pipes containing 23 control volumes each. The central channel is connected to the other two with cross-connection objects, creating a quasi-two-dimensional representation. The spacer grids are considered as cross-section reductions and form losses. Below is a branch object connected to all three channels, into which the coolant is supplied. At the top is a time dependent volume, which

acts as a drain for the three channels. The nodalisation of the channels is included in Fig. 5.138. To create the initial conditions, the experimental preparatory procedure is simulated in the beginning of the simulation.

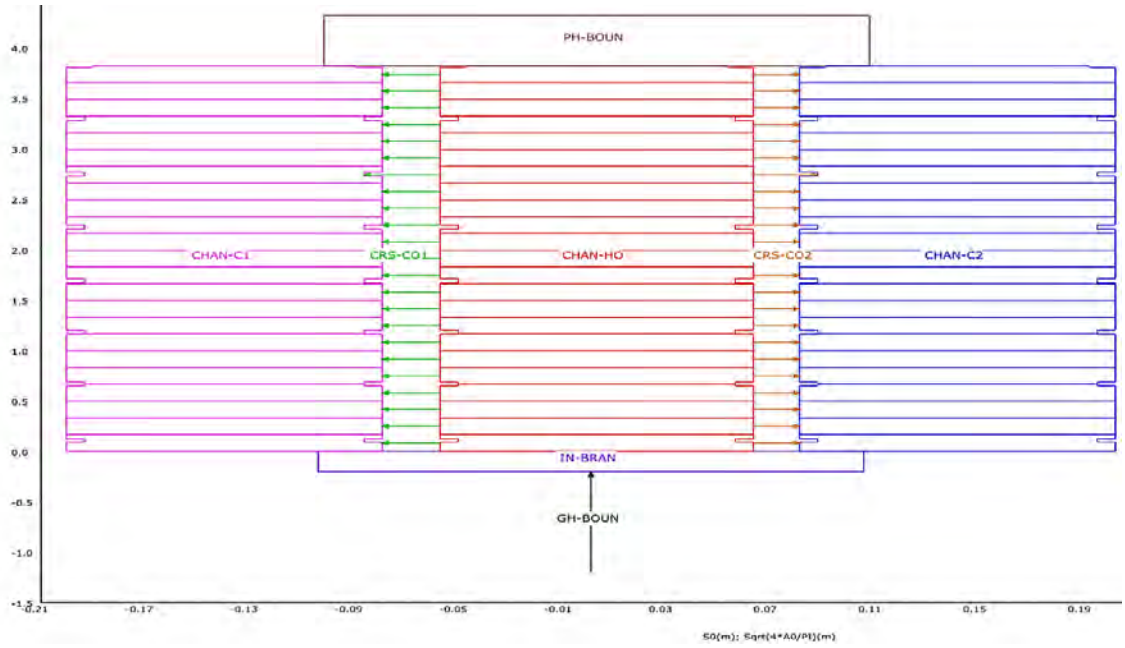

Fig. 5.138 Nodalisation of the PERICLES test section in ATHLET

Each channel is linked to a heater rod and a housing object, which consist of 23 axial volumes each. The heater rods consist of three radial layers, heated boron nitride, unheated boron nitride and stainless steel. The housings are simulated with two layers. For the quench model, a value of 10^5 was chosen for the parameter `CQHTWB` instead of the default $3 \cdot 10^5$ to achieve a slower quench front progression.

5.7.3.4 Main Results

Like in the tests shown earlier, the heating up phase in the simulations is barely affected by the version change but the temperature drops more slowly than before. This improves agreement between experimental and simulated data.

During the heating up phase, the experimental cladding temperature rises higher than the simulations. The simulated cladding temperature remains below the experimental data in all ATHLET versions, but the difference in quench times is reduced from 40 s to 10 s in version 3.3. and 3.4. The cladding temperature at 2.998 m for test 62 is displayed in Fig. 5.139 below.

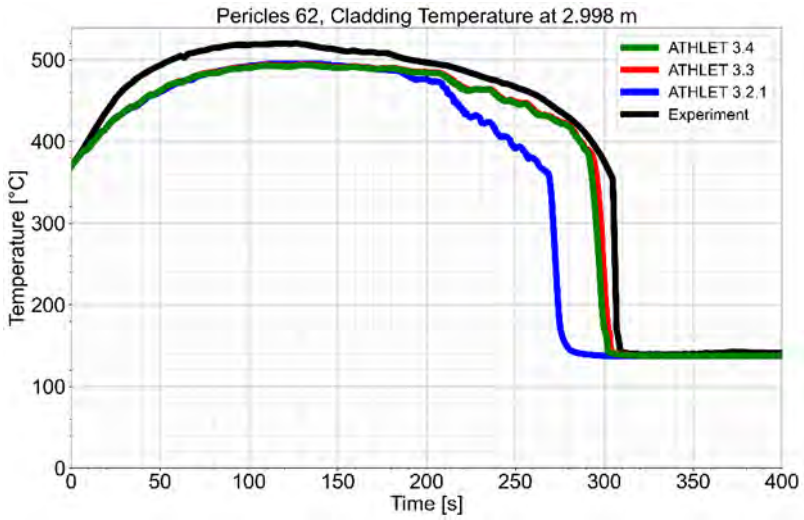

Fig. 5.139 Comparison of the simulated and experimental cladding temperature for PERICLES RE0062 at 2.998 m

5.7.4 Main Findings

The changes implemented in ATHLET version 3.3 generally reduce how much heat is removed from the rod cladding, which slows down the cooling process.

Since the implementation of the bundle factor to increase the heat transfer in rod bundles, many reflooding tests tended to cool down too fast and quench early. In many cases even adjustments of the parameters in the quench front model could not slow down the quench front progression enough. The new changes to heat transfer correlations counteract the accelerated heat loss in the cladding and delay the quench front in many cases, generally improving the simulation results for reflooding tests.

5.8 Mantilla

Mantilla /MAN 08/ performed the experiments to develop a mechanistic model of predicting the onset and maximum entrainment of gas-liquid flows in horizontal pipes.

5.8.1 Test Facility

Two horizontal test sections were constructed with a 2-inch diameter flow loop and a 6-inch diameter U-shaped loop. The schematic drawings of test facilities can be found in Fig. 5.140 and Fig. 5.141. In the experiment, various solutions such as air, tap water, water-Glycerin, and water-Butanol were injected to examine the effect of fluid properties.

However, for the code validation, only the experiments with the air-water mixture are considered. Entrainment fractions, pressure drops, and temperatures were measured where the flows were fully developed.

The 2-inch test section (avg. diameter = 48.6 mm) is 14.1 m long. The film extractor is installed at 12.3 m, and it measures the entrainment fraction of the flow. The pressure is recorded with three pressure transducers which involve two absolute and one differential. The locations of absolute pressure transducers are at 0.17 m and 11.6 m from the inlet. In the case of the differential one, it is located at 10.6 m and 11.6 m. The temperature is measured by a resistance temperature detector (RTD) at 14.01 m from the test section inlet.

The 6-inch test section (avg. diameter = 153 mm) has a U-shape with two 90-degree bent points. The first section of the loop is horizontally 15.61 m (L/D = 102) long. The second section has a length of 8.18 m (L/D = 53). The second pipe was inclinable from 0°to 25°degrees upward but in the experiment, the pipe was only placed at a 0°-angle. Two sections are connected through pipes as well and its length is assumed to be 3 m. The film extractor is installed at the end of the inclinable section. The pressure is measured with one absolute and one differential pressure transducers. The location of the absolute pressure transducer is 2.81 m downstream of the flexible connection. In the case of the differential one, the first tap is installed at the same point of the absolute pressure transducer and the second tap is positioned at 6.37 m downstream of the flexible connection. The temperature is measured at the inlet of the first section where the air and water are mixed.

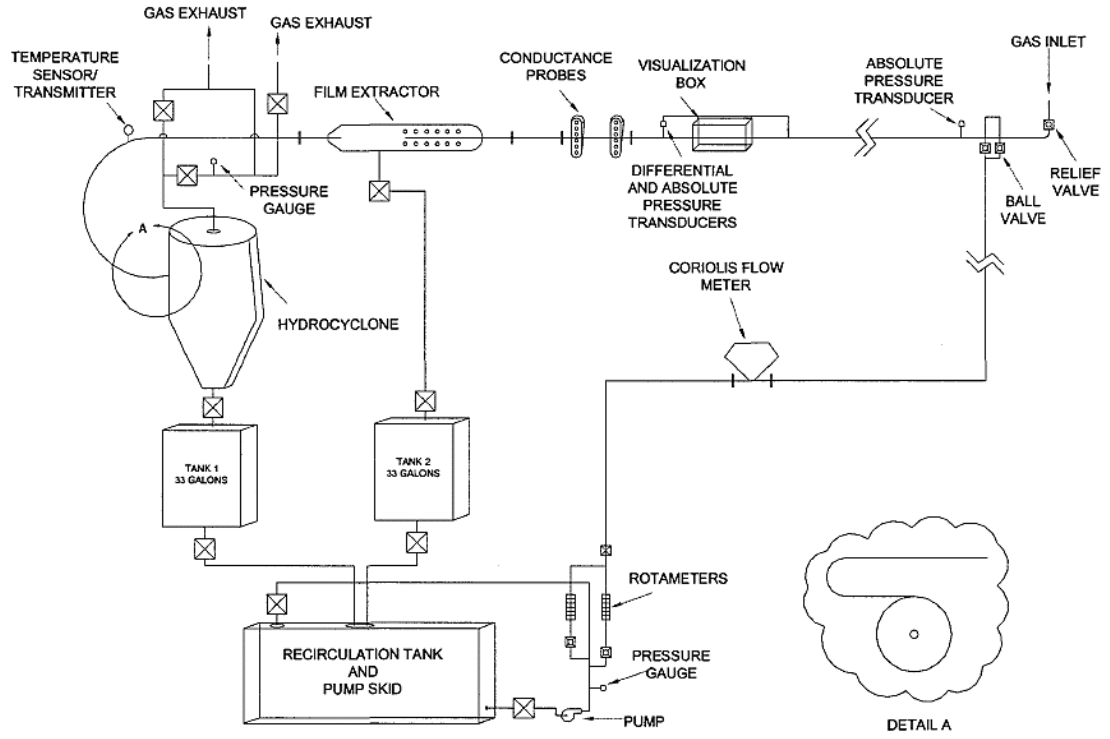

Fig. 5.140 Schematic drawing of 2-inch flow loop /MAN 08/

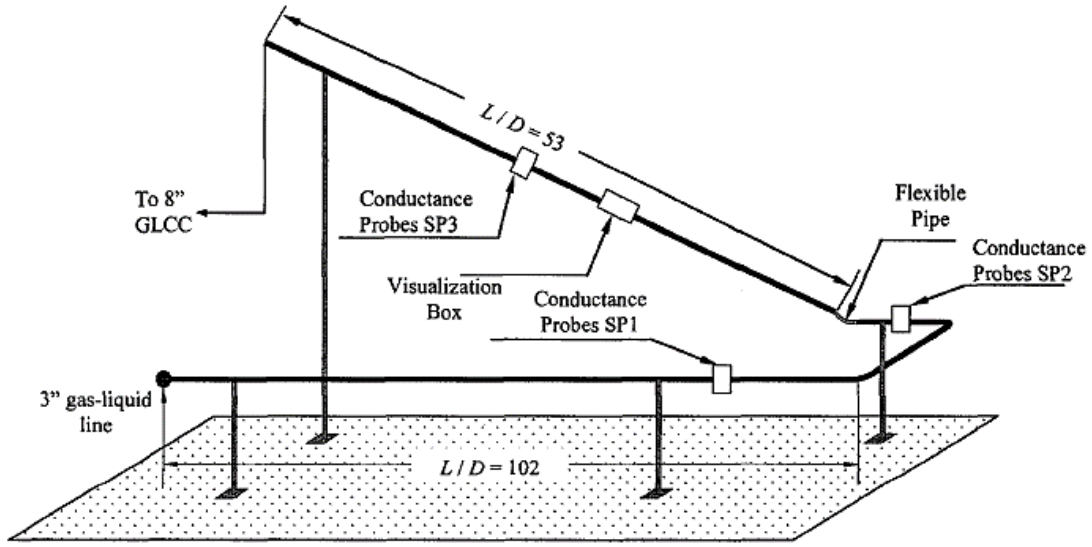

Fig. 5.141 Schematic drawing of 6-inch flow loop /MAN 08/

5.8.2 Test Conduct

The boundary conditions of the 2-inch and 6-inch test sections are given in Tab. 5.10 and Tab. 5.11. In addition, those are drawn over Mandhane's flow regime map for horizontal flow (see Fig. 5.142 and Fig. 5.143).

For the 2-inch test section, 49 experimental cases were performed, and the boundary and initial conditions (BIC) were j_V = 2.0 – 80 m/s, j_L = 0.004 – 0.1 m/s (Re_{SL} = 160 - 5300), 2 bar pressure, and 20°C temperature. The flow regimes of the experiments would belong to stratified, wavy, and annular-mist flows as shown in Fig. 5.142.

In the case of the 6-inch test section, 39 experimental cases were carried out with the BICs as j_V = 2.0 – 20 m/s, j_L = 0.004 – 0.1 m/s (Re_{SL} = 600 - 16000), 1 – 2 bar pressure, and 20°C temperature. The flow patterns of the experiments would belong to stratified and wavy flows as shown in Fig. 5.143.

Tab. 5.10 Boundary conditions of 2-inch test section of Mantilla

Run #	$\dot{m}_{v,\,in}$ (kg/s)	$\dot{m}_{l,in}$ (kg/s)	$j_{v,\,in}$ (m/s)	$j_{l,\,in}$ (m/s)	T_{out} (°C)	P (kPa)
1	9.61E-03	6.83E-03	2.1	0.0037	23.5	210.191
2	2.30E-02	6.68E-03	5.0	0.0036	23.0	209.958
3	3.13E-02	6.86E-03	6.9	0.0037	22.6	208.022
4	3.70E-02	6.51E-03	8.2	0.0035	21.8	206.495
5	4.85E-02	6.45E-03	10.5	0.0035	20.5	209.806
6	5.46E-02	6.32E-03	11.7	0.0034	19.8	212.580
7	6.00E-02	6.16E-03	13.3	0.0033	19.2	204.901
8	6.59E-02	6.09E-03	14.3	0.0033	18.9	208.841
9	7.07E-02	6.16E-03	15.2	0.0033	18.5	209.498
10	9.90E-02	6.64E-03	21.0	0.0036	18.5	211.371
11	1.41E-01	6.36E-03	29.9	0.0034	17.7	211.111
12	2.27E-01	6.35E-03	49.6	0.0034	17.5	204.652
13	3.12E-01	6.39E-03	69.1	0.0035	20.1	204.107
14	3.76E-01	6.65E-03	82.2	0.0036	19.7	206.001
15	9.64E-03	3.27E-02	2.1	0.018	23.3	211.787
16	2.41E-02	3.34E-02	5.4	0.018	22.2	205.960
17	3.26E-02	3.27E-02	7.1	0.018	21.5	210.858
18	3.66E-02	3.31E-02	7.9	0.018	21.0	210.162

Run #	$\dot{m}_{v,\,in}$ (kg/s)	$\dot{m}_{l,in}$ (kg/s)	$j_{v,\,in}$ (m/s)	$j_{l,\,in}$ (m/s)	T_{out} (°C)	P (kPa)
19	4.60E-02	3.36E-02	10.1	0.018	20.8	206.837
20	5.00E-02	3.37E-02	11.1	0.018	20.8	205.705
21	6.98E-02	3.23E-02	15.0	0.018	20.2	210.619
22	9.43E-02	3.30E-02	20.9	0.018	22.5	204.650
23	1.42E-01	3.38E-02	30.8	0.018	19.2	206.443
24	1.86E-01	3.32E-02	40.9	0.018	24.7	208.664
25	2.28E-01	3.31E-02	49.4	0.018	20.8	208.806
26	3.12E-01	3.33E-02	69.2	0.018	21.4	204.056
27	3.71E-01	3.31E-02	81.3	0.018	22.8	208.211
28	7.94E-03	6.37E-02	1.8	0.035	23.7	190.770
29	2.21E-02	6.35E-02	4.7	0.034	24.7	208.394
30	3.18E-02	6.29E-02	6.8	0.034	24.1	209.884
31	3.49E-02	6.35E-02	7.6	0.034	24.2	206.776
32	4.43E-02	6.29E-02	9.6	0.034	23.4	208.495
33	7.18E-02	6.33E-02	15.9	0.034	21.8	206.512
34	9.27E-02	6.31E-02	20.5	0.034	21.5	200.818
35	1.41E-01	6.26E-02	30.3	0.034	19.4	209.828
36	2.30E-01	6.40E-02	50.6	0.035	21.5	205.866
37	3.11E-01	6.35E-02	69.3	0.034	21.9	204.223
38	3.70E-01	6.31E-02	81.3	0.034	21.0	206.374
39	8.16E-03	1.82E-01	1.5	0.1	24.1	223.577
40	2.19E-02	1.86E-01	4.8	0.1	23.8	204.743
41	3.18E-02	1.85E-01	6.8	0.1	23.5	208.696
42	3.49E-02	1.86E-01	7.6	0.1	23.4	206.623
43	4.44E-02	1.85E-01	9.7	0.1	22.8	205.822
44	7.17E-02	1.85E-01	15.4	0.1	21.8	211.819
45	8.54E-02	1.83E-01	19.4	0.1	21.7	203.875
46	1.39E-01	1.85E-01	31.5	0.1	21.4	199.899

Run #	$\dot{m}_{v,\,in}$ (kg/s)	$\dot{m}_{l,in}$ (kg/s)	$j_{v,\,in}$ (m/s)	$j_{l,\,in}$ (m/s)	T_{out} (°C)	P (kPa)
47	2.29E-01	1.85E-01	51.4	0.1	20.8	201.928
48	3.13E-01	1.90E-01	70.1	0.1	21.6	202.533
49	3.69E-01	1.87E-01	81.7	0.1	21.3	204.711

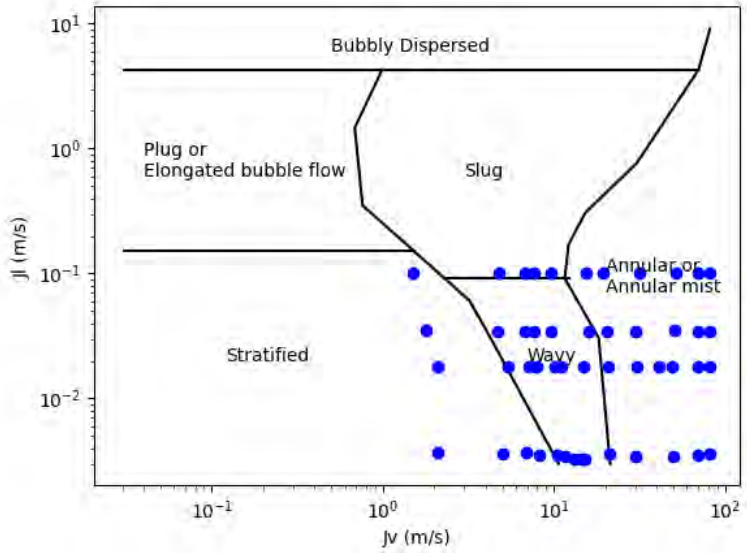

Fig. 5.142 Flow regimes of 2-inch experiments by Mandhane's flow pattern map

Tab. 5.11 Boundary conditions of 6-inch test section of Mantilla

Run #	$\dot{m}_{v,\,in}$ (kg/s)	$\dot{m}_{l,in}$ (kg/s)	$j_{v,\,in}$ (m/s)	$j_{l,\,in}$ (m/s)	T_{out} (°C)	P (kPa)
1	9.61E-03	6.83E-03	2.1	0.0037	23.5	210.191
2	2.30E-02	6.68E-03	5.0	0.0036	23.0	209.958
3	3.13E-02	6.86E-03	6.9	0.0037	22.6	208.022
4	3.70E-02	6.51E-03	8.2	0.0035	21.8	206.495
5	4.85E-02	6.45E-03	10.5	0.0035	20.5	209.806
6	5.46E-02	6.32E-03	11.7	0.0034	19.8	212.580
7	6.00E-02	6.16E-03	13.3	0.0033	19.2	204.901
8	6.59E-02	6.09E-03	14.3	0.0033	18.9	208.841
9	7.07E-02	6.16E-03	15.2	0.0033	18.5	209.498

Run #	$\dot{m}_{v,\,in}$ (kg/s)	$\dot{m}_{l,in}$ (kg/s)	$j_{v,\,in}$ (m/s)	$j_{l,\,in}$ (m/s)	T_{out} (°C)	P (kPa)
10	9.90E-02	6.64E-03	21.0	0.0036	18.5	211.371
11	1.41E-01	6.36E-03	29.9	0.0034	17.7	211.111
12	2.27E-01	6.35E-03	49.6	0.0034	17.5	204.652
13	3.12E-01	6.39E-03	69.1	0.0035	20.1	204.107
14	3.76E-01	6.65E-03	82.2	0.0036	19.7	206.001
15	9.64E-03	3.27E-02	2.1	0.018	23.3	211.787
16	2.41E-02	3.34E-02	5.4	0.018	22.2	205.960
17	3.26E-02	3.27E-02	7.1	0.018	21.5	210.858
18	3.66E-02	3.31E-02	7.9	0.018	21.0	210.162
19	4.60E-02	3.36E-02	10.1	0.018	20.8	206.837
20	5.00E-02	3.37E-02	11.1	0.018	20.8	205.705
21	6.98E-02	3.23E-02	15.0	0.018	20.2	210.619
22	9.43E-02	3.30E-02	20.9	0.018	22.5	204.650
23	1.42E-01	3.38E-02	30.8	0.018	19.2	206.443
24	1.86E-01	3.32E-02	40.9	0.018	24.7	208.664
25	2.28E-01	3.31E-02	49.4	0.018	20.8	208.806
26	3.12E-01	3.33E-02	69.2	0.018	21.4	204.056
27	3.71E-01	3.31E-02	81.3	0.018	22.8	208.211
28	7.94E-03	6.37E-02	1.8	0.035	23.7	190.770
29	2.21E-02	6.35E-02	4.7	0.034	24.7	208.394
30	3.18E-02	6.29E-02	6.8	0.034	24.1	209.884
31	3.49E-02	6.35E-02	7.6	0.034	24.2	206.776
32	4.43E-02	6.29E-02	9.6	0.034	23.4	208.495
33	7.18E-02	6.33E-02	15.9	0.034	21.8	206.512
34	9.27E-02	6.31E-02	20.5	0.034	21.5	200.818
35	1.41E-01	6.26E-02	30.3	0.034	19.4	209.828
36	2.30E-01	6.40E-02	50.6	0.035	21.5	205.866
37	3.11E-01	6.35E-02	69.3	0.034	21.9	204.223

Run #	$\dot{m}_{v,\,in}$ (kg/s)	$\dot{m}_{l,in}$ (kg/s)	$j_{v,\,in}$ (m/s)	$j_{l,\,in}$ (m/s)	T_{out} (°C)	P (kPa)
38	3.70E-01	6.31E-02	81.3	0.034	21.0	206.374
39	8.16E-03	1.82E-01	1.5	0.1	24.1	223.577
40	2.19E-02	1.86E-01	4.8	0.1	23.8	204.743
41	3.18E-02	1.85E-01	6.8	0.1	23.5	208.696
42	3.49E-02	1.86E-01	7.6	0.1	23.4	206.623
43	4.44E-02	1.85E-01	9.7	0.1	22.8	205.822
44	7.17E-02	1.85E-01	15.4	0.1	21.8	211.819
45	8.54E-02	1.83E-01	19.4	0.1	21.7	203.875
46	1.39E-01	1.85E-01	31.5	0.1	21.4	199.899
47	2.29E-01	1.85E-01	51.4	0.1	20.8	201.928
48	3.13E-01	1.90E-01	70.1	0.1	21.6	202.533
49	3.69E-01	1.87E-01	81.7	0.1	21.3	204.711

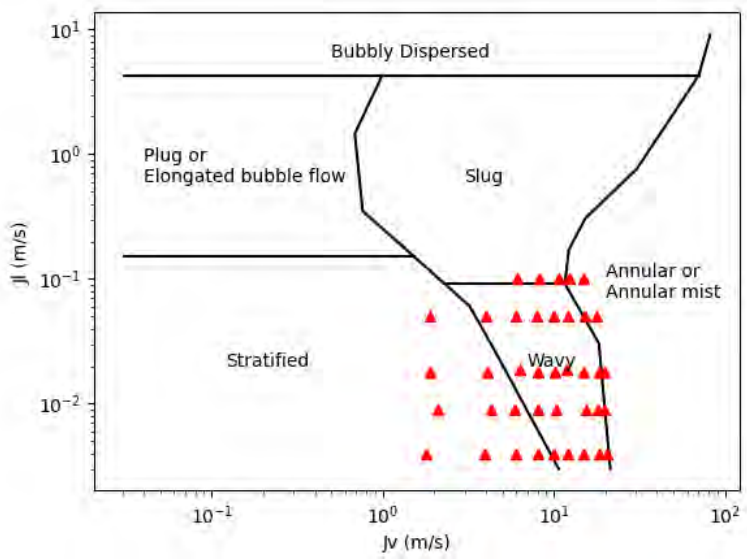

Fig. 5.143 Flow regimes of 6-inch experiments by Mandhane's flow pattern map

5.8.3 Input Dataset

In the following, the input data set for ATHLET and the models used in the calculation are described.

5.8.3.1 Nodalisation

The 2-inch test section of Mantilla is modeled for ATHLET simulations as shown in Fig. 5.144. The main part of the test section is modeled with a single Thermo-Fluid dynamic Object (TFO), `M_PIPE` which is 14.0 m long and uniformly divided into 70 nodes (L_{CV}/D = 4.1). A Time-Dependent Volume (TDV), `M_OUTLET`, is attached to describe the outlet of the system and the outlet pressure condition is assigned here. A short pipe, `M_INLET`, is linked to the upstream of `M_PIPE` with two additional single junctions, which simulate the injection of the air-water mixture. A very little amount of saturated steam is injected (`M_VAPIN`) together with pure air to prohibit the volatilization of water.

Fig. 5.145, on the other hand, shows the nodalized ATHLET model for the 6-inch test section. The U-shape loop is modeled with three TFOs `PIPE_INLET`, `PIPE_CONN`, and `PIPE_MAIN`. The discretization of `PIPE_MAIN` is a little bit finer than other TFOs by 0.2 m (L_{CV}/D = 1.3). A TDV, `PIPE_OUT`, is attached for the outlet of the system and three single junction pipes are connected to provide the injection of the air-water mixture. To consider the 90°-bends, the form loss factor 0.2 is assigned at the edges of `PIPE_CONN`.

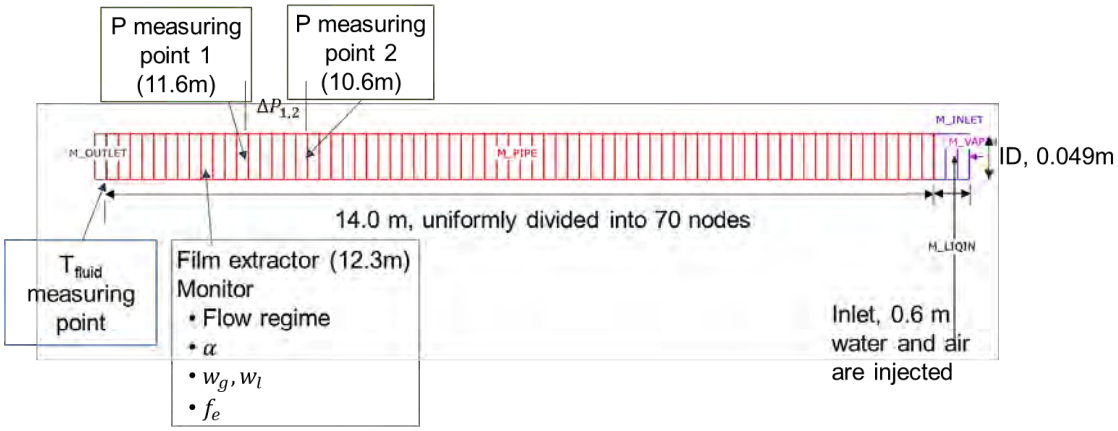

Fig. 5.144 Nodalisation of 2-inch test section of Mantilla for ATHLET simulation

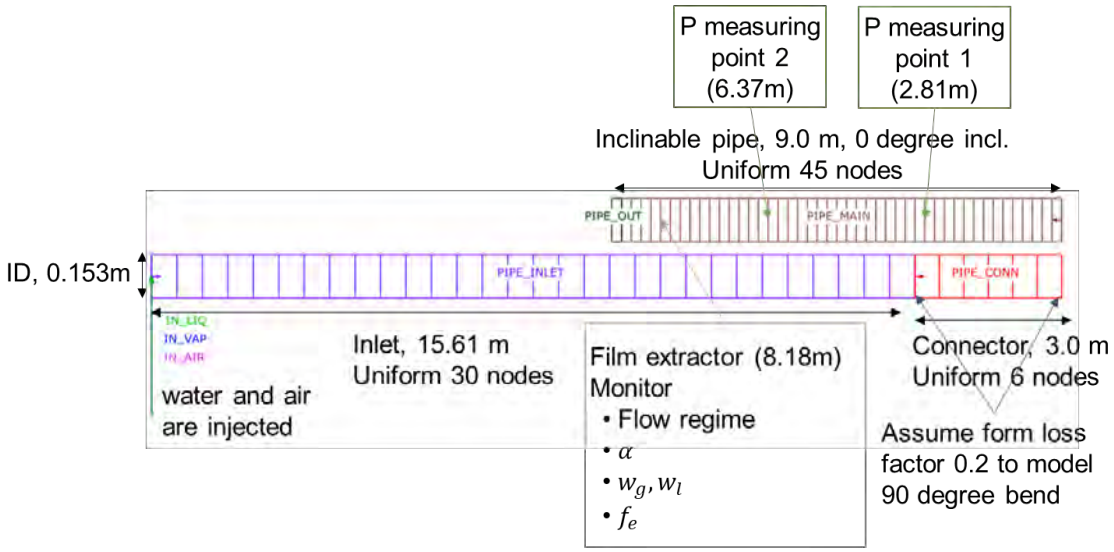

Fig. 5.145 Nodalisation of 6-inch test section of Mantilla for ATHLET simulation

5.8.3.2 Model Options

The following options are applied:

- The 6-eq. model is applied for all TFOs and all test cases.
- Different models for the onset of entrainment and the entrainment fraction in horizontal pipes are used between ATHLET 3.2.1 and ATHLET 3.3/3.4.
- The Martinelli-Nelson friction loss model (`ITPMO = 2`) is used with the wall roughness as 1.5 x 10^{-6} m for both 2-inch and 6-inch test section.

5.8.4 Main Results

The calculation results of entrainment fraction and pressure drop are compared with the experimental data. The results of the 2-inch test section are presented in Fig. 5.146 for the entrainment fraction and Fig. 5.147 for the pressure drop. For the entrainment fraction, ATHLET 3.2.1 shows high overestimations for the low j_L cases. This is because a term of the maximum entrainment fraction which may be a function of liquid flows was not included in the entrainment model of ATHLET 3.2.1. Meanwhile, ATHLET 3.3 shows good agreements especially for the cases with low j_L. Thus, the RMS error is significantly reduced from 33 % to 4.6 %. The predictions of the onset of entrainments are $j_V \approx 11$ m/s in most cases except the cases of $j_L = 0.0035$ m/s ($Re_{SL} = 160$). For that condition, the critical velocity by the Ishii & Grolmes criteria becomes $j_V \approx 23$ m/s, so ATHLET 3.3 based on those criteria shows delayed onset of entrainment while ATHLET 3.2.1 yields

early onset of entrainment, compared to the experimental observation. For the pressure drop results, the predictions between ATHLET 3.2.1 and ATHLET 3.3 are very similar. Both versions underpredict the pressure drops, and their errors increase as j_L (or Re_{SL}) increases. No difference is found between ATHLET 3.3 and 3.4.

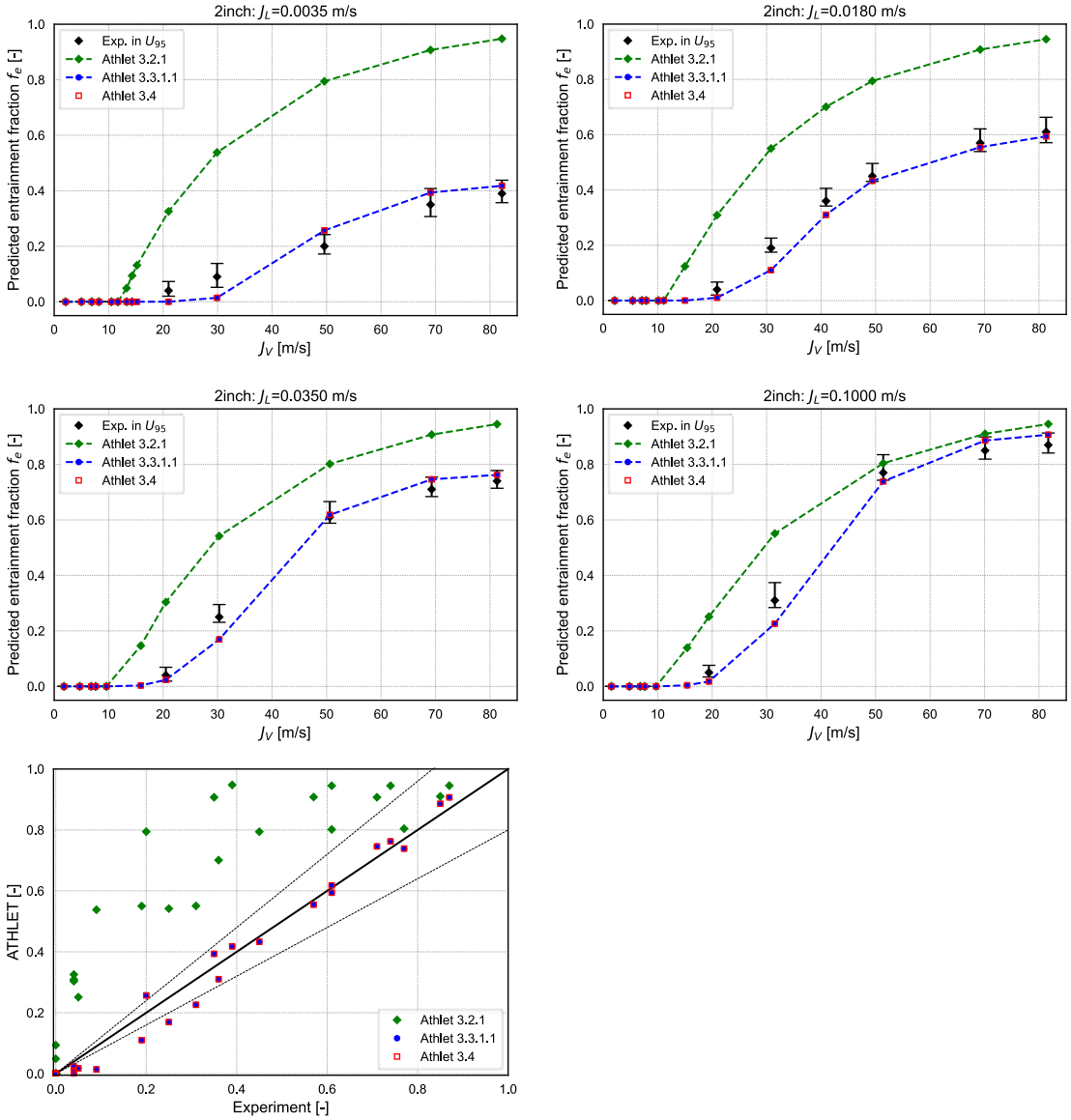

Fig. 5.146 Comparison between measured and calculated entrainment fraction in Mantilla 2-inch test section

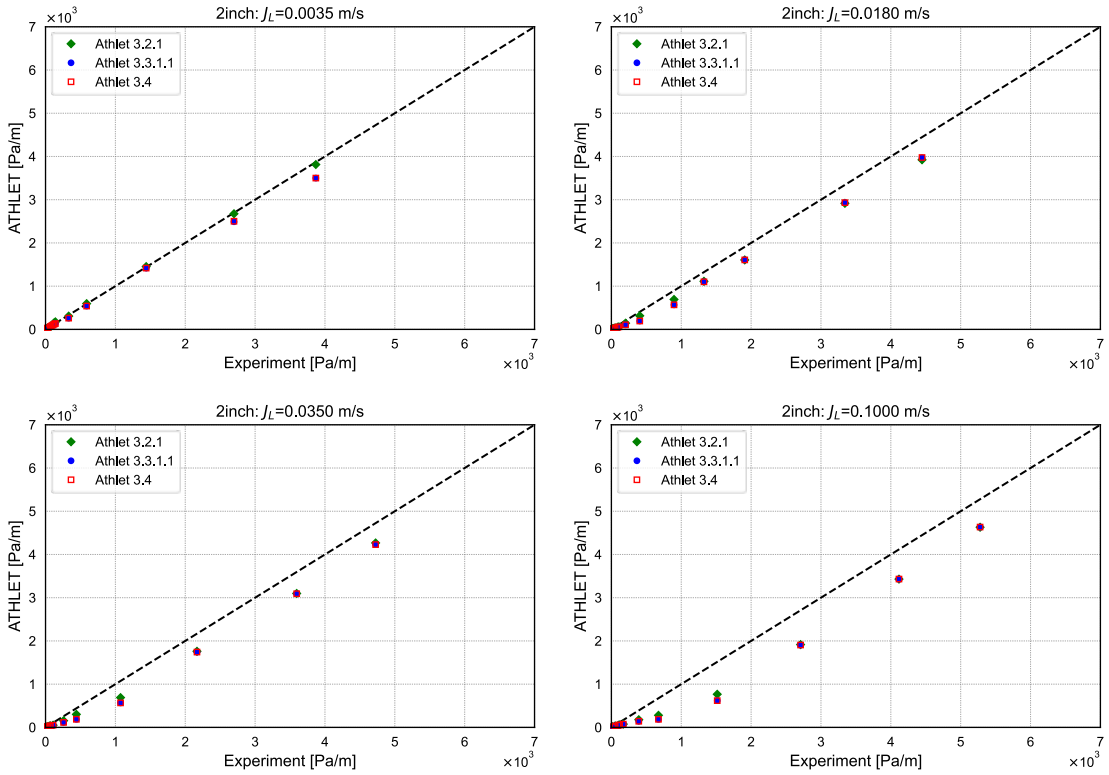

Fig. 5.147 Comparison between measured and calculated pressure drop in Mantilla 2-inch test section

The results of the entrainment fraction and the pressure drop in the 6-inch test section are demonstrated in Fig. 5.148 and Fig. 5.149, respectively. In the 6-inch test section, it turned out that ATHLET 3.2.1 estimates significantly too high entrainment fractions while ATHLET 3.3 shows low predictions. The model evaluation is unclear in this case, because all experiment measurements are very low entrainment factors (f_e < 0.05) with high uncertainties. The onset of entrainment was predicted at j_V ≈ 15 m/s in most cases, but it is delayed to j_V ≈ 20 m/s in the low Re_{SL} cases (j_L = 0.004 m/s, Re_{SL} = 600) with the Ishii & Grolmes criteria. For the pressure drops, because of higher predictions on the entrainment fraction, higher pressure drops are calculated by ATHLET 3.2.1 than ATHLET 3.3 for the cases where the onset of entrainment occurs. The underestimation issue observed in the 2-inch test section can be also found in the 6-inch test section. Thus, further investigation on the drag force model is necessary to improve the prediction of the pressure drop. Again, ATHLET 3.4 yields identical results as ATHLET 3.3.

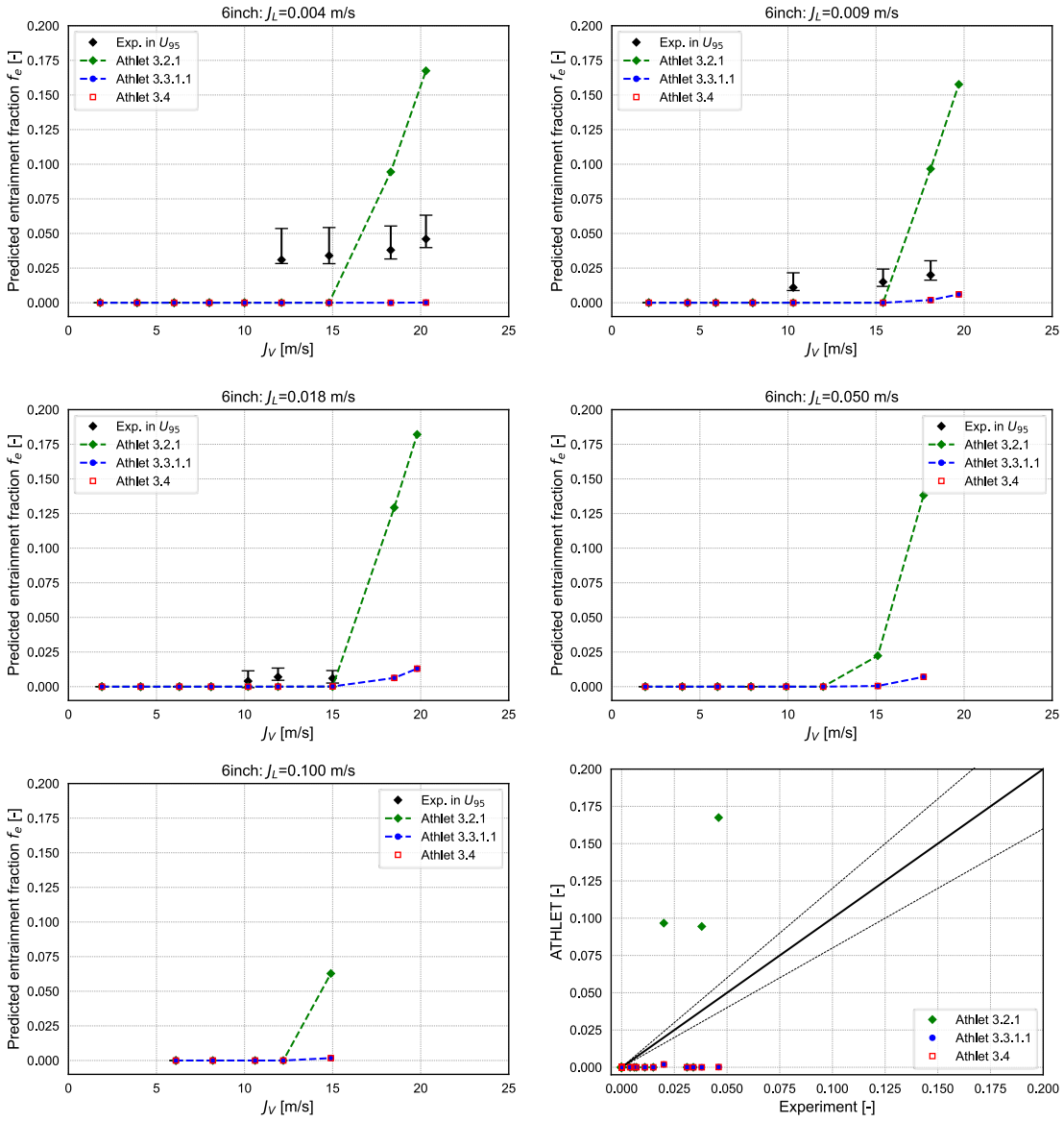

Fig. 5.148 Comparison between measured and calculated entrainment fraction in Mantilla 6-inch test section

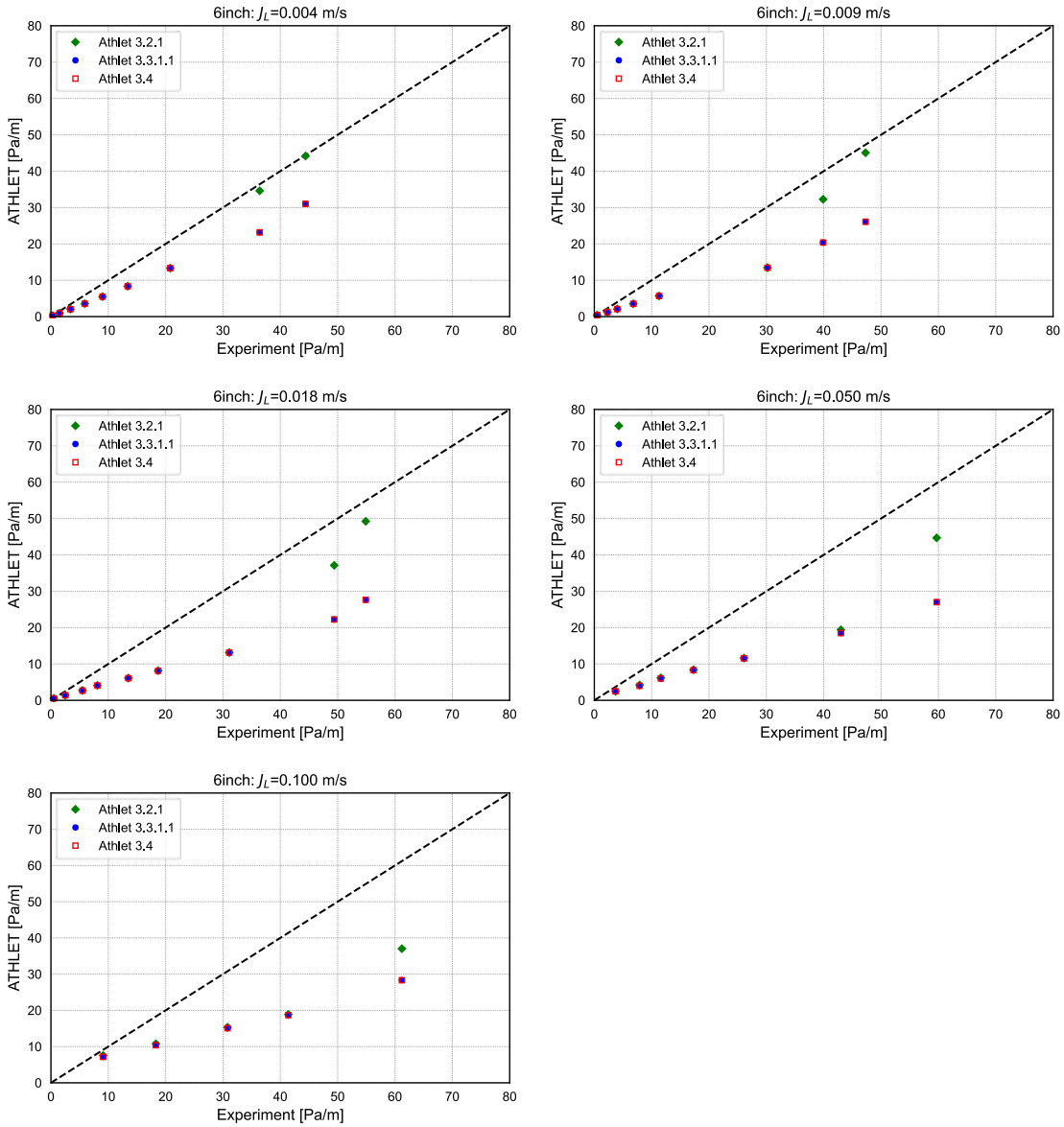

Fig. 5.149 Comparison between measured and calculated pressure drop for Mantilla 6-inch test section

The mean average (MA) error and the root mean square (RMS) error against the measured are given in Tab. 5.12. It demonstrates that the new entrainment fraction model in ATHLET 3.3 can significantly improve the result. To investigate numerical stability between the versions, the number of time steps for each simulation is presented in Tab. 5.13. In most cases, the number of time steps of ATHLET 3.3 is similar to or less than that of ATHLET 3.2.1. Especially, the cases with the numerical instability where the number of time steps is huge by ATHLET 3.2.1 (red colored in the table) are resolved in ATHLET 3.3. In ATHLET 3.2.1, there was `D2MDZC` subroutine which forcingly controlled the phase velocity for the phase-dissipating flow, but this induces instability for the cases

where the void fraction is very high. In ATHLET 3.3, this instability no longer occurs because D2MDZC subroutine has been deactivated.

Tab. 5.12 Relative and absolute errors of calculated results against measured data of Mantilla

Test section	Code version	Abs. err. f_e [%]		Rel. err. ΔP [%]	
		MA	RMS	MA	RMS
2-inch	ATHLET 3.2.1	29.5	33.1	24.9	30.6
	ATHLET 3.3.1/3.4	4.0	4.6	28.1	34.9
6-inch	ATHLET 3.2.1	3.6	5.1	39.1	42.2
	ATHLET 3.3.1/3.4	2.1	2.5	46.6	47.4

Tab. 5.13 The number of time steps during ATHLET simulation for Mantilla. Only minimal differences are observed between versions 3.3 and 3.4.

Exp. ID	2-inch		Exp. ID	6-inch	
	ATHLET 3.2.1	ATHLET 3.3.1		ATHLET 3.2.1	ATHLET 3.3.1
1	1313	1024	1	4235	4037
2	910	643	2	3328	3029
3	984	659	3	1350	1035
4	1034	672	4	1325	1042
5	1150	696	5	1310	1058
6	1156	709	6	1413	1070
7	1109	716	7	1527	1098
8	1157	716	8	1649	1121
9	1153	724	9	6787	733
10	28349	751	10	1187	746
11	48568	782	11	1179	735
12	1102	889	12	1312	724
13	1077	1005	13	3369	3077
14	1291	1241	14	2323	2037
15	1318	1061	15	973	654
16	1093	701	16	1072	669

Exp. ID	2-inch		Exp. ID	6-inch	
	ATHLET 3.2.1	**ATHLET 3.3.1**		**ATHLET 3.2.1**	**ATHLET 3.3.1**
17	1258	723	17	1146	696
18	1279	729	18	3093	2852
19	1085	533	19	2521	2179
20	878	334	20	1158	754
21	716	353	21	1194	734
22	588	355	22	1283	743
23	695	448	23	1288	738
24	48583	888	24	1334	769
25	64158	907	25	1296	779
26	137530	1017	26	1348	796
27	175504	991	27	2574	2330
28	1447	1139	28	2181	1874
29	1121	741	29	1204	825
30	1178	737	30	1216	807
31	1220	720	31	1238	796
32	1266	708	32	1304	804
33	1060	753	33	1361	792
34	1039	752	34	1306	818
35	1064	879	35	1309	938
36	1129	963	36	1341	939
37	150804	1332	37	1367	965
38	230035	1407	38	1394	949
39	1102	851	39	1434	906
40	1276	923			
41	1351	931			
42	1373	926			
43	1383	934			
44	1157	954			

Exp. ID	2-inch		Exp. ID	6-inch	
	ATHLET 3.2.1	**ATHLET 3.3.1**		**ATHLET 3.2.1**	**ATHLET 3.3.1**
45	1064	934			
46	1029	1060			
47	1271	1904			
48	1335	2258			
49	1468	2229			

5.8.5 Main Findings

- The prediction of the entrainment fraction in the 2-inch test section is remarkably improved from ATHLET 3.2.1 to ATHLET 3.3. For the 6-inch test section, ATHLET 3.2.1 strongly overestimates the entrainment fraction, while ATHLET 3.3 underestimates.
- The predictions for the pressure drops are barely changed between the versions. Thus, it is necessary to further investigate the drag force models for horizontal flows in ATHLET.
- The numerical instability in the high void fraction cases by ATHLET 3.2.1 is resolved in ATHLET 3.3 because of the deactivation of `D2MDZC` subroutine.
- The ATHLET versions 3.3 and 3.4 give identical results for all test cases.

5.9 TPTF: Water-vapor two-phase flow in horizontal pipe

5.9.1 Test Facility

The TPTF (two-phase flow test facility) experiments were started in 1982 by JAERI, Japan, to obtain fundamental data on the thermal-hydraulic responses in the primary components of LWR such as the core, the steam generator of a PWR and the horizontal and vertical pipes /NAK 83/. One of the test sections of TPTF was a horizontal pipe test section to study flow regime transition, interfacial friction, and interphase heat transfer in saturated steam-water two-phase flow conditions at pressure up to 12 MPa /KAW 87/, /NAK 96/ (see Fig. 5.150).

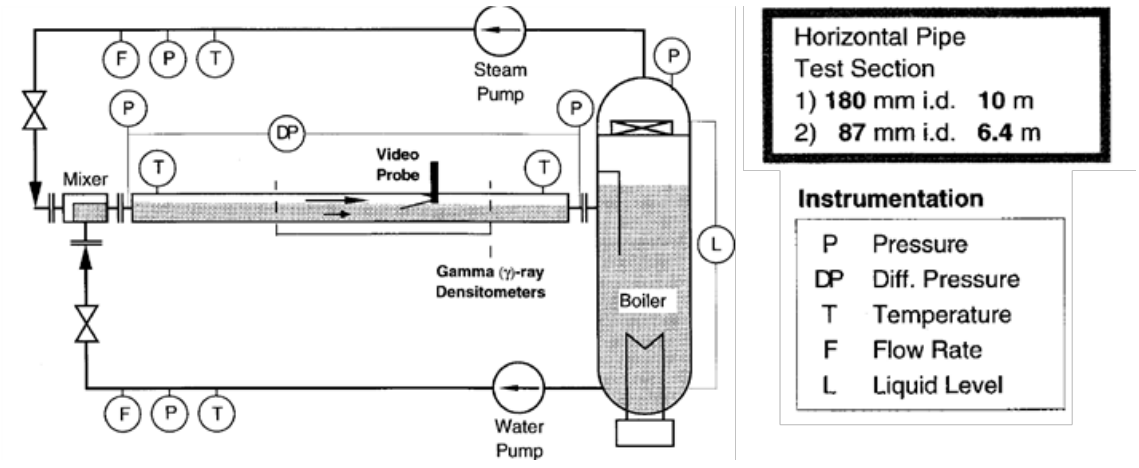

Fig. 5.150 Horizontal test section in the TPTF facility (from /LAN 22/)

Two test sections (4-inch TS or 8-inch) were used for the tests considered here: the 8-inch test section with 18 mm inner diameter and length 10 m, and the 4-inch test section with 87 mm inner diameter and length 6.4 m. Two different inlet flow mixers are available: a bubbly flow mixer for well-mixed flow conditions at the inlet, and a separated flow mixer, injecting fully separated fluid phases into the test section.

The test sections have measurement positions where quantitative values for velocities and void fractions are reported, and a video probe section; here, visually observed flow patterns are reported, including the occurrence of droplets in the gas phase. The locations of these measurement and the video probe are, in terms of L (length) and D (inner diameter) of the pipe:

- 8-inch test section: measurement at L/D = 17 and L/D = 48, video probe at l/D = 39
- 4-inch test section: measurement at L/D = 24, video probe at l/D = 56

5.9.2 Test Conduct

In total, 126 co-current tests are considered here:

- 56 tests with the 8-inch test section and the bubbly flow mixer, at a pressure of about 74 bar or 118 bar. The boiler liquid level was either below (28 cases) or above (28 cases) the outlet nozzle.
- 64 tests with the 8-inch test section and the separated flow mixer, pressure between 30 bar and 86 bar. In all these tests, the boiler liquid level was above the outlet nozzle.
- 19 tests with the 4-inch test section and the separated flow mixer, at a pressure of 30 bar, with the boiler liquid level above the outlet nozzle.

Measurement values (as reported in /LAN 20/) and test setup are given in Tab. 5.14 for the 8-inch test section, and in for the 4-inch test section in Tab. 5.15. The given velocity values (vL: liquid, vL: vapour) are used as inlet boundary condition (partial modelling approach for the 8-inch test section, and full modelling approach for the 4-inch test section; see section 5.9.3.1). The boiler liquid level is either above (H) or below (L) the outlet nozzle. Either a separated flow mixer (S) or a bubbly flow mixer (B) is used. Cases where entrainment is reported (through visual observation) are marked with a + in the last column.

Tab. 5.14 Test configuration and measured values for the tests in the TPTF 8-inch test section (sorted by pressure).

Run ID	Pres-sure [bar]	void [-] L/D=17	void [-] L/D=48	vL [m/s] L/D=17	vV [m/s] L/D=17	Boiler level	Mi-xer type	Droplet entrain-ment
475	30	0.402	0.402	1.6890	2.5124	H	S	
476	30	0.429	0.429	1.2680	2.3543	H	S	
479	30	0.538	0.538	2.1861	3.2342	H	s	
480	30	0.579	0.579	1.5962	2.9361	H	S	
483	30	0.547	0.547	2.2296	4.7166	H	S	
484	30	0.604	0.604	1.6313	4.2715	H	S	
493	30	0.606	0.606	1.5406	3.9439	H	S	
494	30	0.511	0.511	1.2904	3.0920	H	S	
486	30	0.730	0.730	1.5333	5.5890	H	S	
478	30	0.606	0.606	1.0508	2.8218	H	S	
482	30	0.683	0.683	1.3060	3.7628	H	S	
473	30	0.223	0.223	0.5328	1.8430	H	S	
474	30	0.429	0.429	0.7233	2.3543	H	S	
477	30	0.448	0.448	1.1159	2.2545	H	S	
481	30	0.565	0.565	1.2851	3.0088	H	S	
485	30	0.608	0.608	1.3750	4.2105	H	S	
495	30	0.452	0.452	1.0803	2.9867	H	S	
2473	30	0.398	0.398	0.9983	2.5377	H	S	
2474	30	0.519	0.519	1.2266	3.5067	H	S	
2475	30	0.628	0.628	1.5349	4.4268	H	S	
492	30	0.659	0.659	1.9912	5.2200	H	S	+
487	30	0.649	0.649	2.8775	6.3020	H	S	+
488	30	0.704	0.704	1.9696	5.8097	H	S	+
489	30	0.717	0.717	1.6714	5.7043	H	S	+
490	30	0.840	0.840	2.5938	9.2381	H	S	+
491	30	0.779	0.779	4.5701	9.9358	H	S	+
2476	30	0.709	0.709	1.8797	5.7687	H	S	+
2477	30	0.811	0.811	2.6243	8.3107	H	S	+
515	50	0.555	0.555	0.9258	3.0036	H	S	
519	50	0.669	0.669	1.2447	3.8087	H	S	
523	50	0.753	0.753	1.6721	5.3838	H	S	
513	50	0.386	0.386	1.0163	2.5907	H	S	
518	50	0.516	0.516	1.2438	3.2287	H	S	
2480	50	0.391	0.391	1.0230	2.5371	H	S	

Run ID	Pres-sure [bar]	void [-] L/D=17	void [-] L/D=48	vL [m/s] L/D=17	vV [m/s] L/D=17	Boiler level	Mi-xer type	Droplet entrain-ment
2481	50	0.507	0.507	1.2576	3.3412	H	S	
522	50	0.611	0.611	1.5424	4.1931	H	S	+
527	50	0.708	0.708	1.9795	5.7020	H	S	+
2482	50	0.609	0.609	1.4808	4.0345	H	S	+
2483	50	0.719	0.719	1.8754	5.5299	H	S	+
2484	50	0.814	0.814	2.4892	7.3145	H	S	+
524	50	0.644	0.644	2.8399	6.2873	H	S	+
525	50	0.794	0.794	4.9078	9.7003	H	S	+
526	50	0.864	0.864	3.0441	8.8819	H	S	+
779	73	0.06	0.09	1.4681	1.4167	H	B	
781	73	0.09	0.13	1.5055	1.4444	H	B	
775	73	0.13	0.15	1.5747	2.0000	H	B	
773	73	0.57	0.50	2.8837	4.5263	H	B	
730	73	0.66	0.64	1.2941	3.1212	H	B	
783	73	0.43	0.47	0.8947	2.5814	H	B	
785	73	0.26	0.27	0.7297	1.5769	H	B	
728	73	0.91	0.69	0.6111	1.7253	H	B	
708	73	0.65	0.53	0.2857	1.1692	H	B	
710	73	0.76	0.61	0.3858	1.3421	H	B	
720	73	0.63	0.48	0.0459	1.1429	H	B	
722	73	0.57	0.44	0.0512	1.0702	H	B	
712	73	0.48	0.38	0.0635	0.8542	H	B	
714	73	0.31	0.24	0.0638	0.6774	H	B	
542	73	0.690	0.690	1.3355	3.6667	H	S	
546	73	0.778	0.778	1.8559	5.1799	H	S	
2527	73	0.642	0.642	1.3631	3.5826	H	S	
2528	73	0.640	0.640	1.3694	3.5781	H	S	
541	73	0.549	0.549	2.2395	4.6630	H	S	+
543	73	0.468	0.468	3.4962	5.4487	H	S	+
544	73	0.581	0.581	4.4391	6.9535	H	S	+
545	73	0.656	0.656	2.9360	6.1585	H	S	+
547	73	0.895	0.895	3.9524	8.5698	H	S	+
751	74	0.19	0.15	1.6667	2.6842	H	B	
749	74	0.38	0.29	2.1129	3.3684	H	B	
747	74	0.48	0.41	2.4423	4.2083	H	B	
743	74	0.73	0.69	4.0741	6.9863	H	B	

Run ID	Pres-sure [bar]	void [-] L/D=17	void [-] L/D=48	vL [m/s] L/D=17	vV [m/s] L/D=17	Boiler level	Mi-xer type	Droplet entrain-ment
732	74	0.84	0.81	2.0625	4.8810	H	B	
755	74	0.13	0.13	0.6322	1.6154	H	B	
757	74	0.16	0.12	0.6190	0.6250	H	B	
759	74	0.08	0.06	0.5652	0.6250	H	B	
761	74	0.06	0.04	0.5532	0.5167	H	B	
726	74	0.97	0.83	0.9333	2.1237	H	B	
1545	74	0.32	0.31	0.1756	1.3750	H	B	
1547	74	0.2	0.20	0.1625	1.3000	H	B	
1549	74	0.12	0.11	0.1591	1.0833	H	B	
763	74	0.05	0.04	0.1474	0.5400	H	B	
857	74	0.67	0.64	3.3939	7.6866	L	B	
855	74	0.51	0.47	2.5714	5.2745	L	B	
853	74	0.35	0.33	2.0462	4.4286	L	B	
851	74	0.17	0.17	1.6506	3.0588	L	B	
849	74	0.08	0.10	1.5000	3.5000	L	B	
845	74	0.76	0.77	1.5833	5.4868	L	B	
843	74	0.42	0.42	0.9310	3.2619	L	B	
847	74	0.16	0.22	0.6786	1.4375	L	B	
838	74	0.83	0.87	0.3294	2.1566	L	B	
836	75	0.89	0.91	0.2727	2.6180	L	B	
834	75	0.82	0.88	0.1389	0.7561	L	B	
1561	76	0.67	0.68	0.4242	0.6716	L	B	
1563	76	0.65	0.66	0.4000	0.4154	L	B	
1565	76	0.64	0.65	0.4167	0.2344	L	B	
1567	77	0.64	0.67	0.4444	0.1719	L	B	
1559	77	0.79	0.82	0.2524	0.1646	L	B	
867	77	0.69	0.72	0.323	0.377	L	B	
1557	78	0.83	0.79	0.2882	0.2771	L	B	
868	78	0.76	0.78	0.292	0.355	L	B	
1555	80	0.87	0.83	0.3154	0.4828	L	B	
2487	86	0.370	0.370	1.0603	2.2351	H	S	
2489	86	0.466	0.466	1.1891	2.8112	H	S	
2490	86	0.606	0.606	1.4721	3.4653	H	S	
2458	86	0.268	0.268	2.5464	3.7313	H	S	+
2459	86	0.358	0.358	1.5717	2.8212	H	S	+
2462	86	0.441	0.441	1.8086	3.7868	H	S	+

Run ID	Pres-sure [bar]	void [-] L/D=17	void [-] L/D=48	vL [m/s] L/D=17	vV [m/s] L/D=17	Boiler level	Mi-xer type	Droplet entrain-ment
2463	86	0.349	0.349	2.8602	4.7851	H	S	+
2464	86	0.479	0.479	3.5701	5.3862	H	S	+
2465	86	0.557	0.557	2.2799	4.5961	H	S	+
2467	86	0.798	0.798	2.0396	5.0877	H	S	+
2468	86	0.676	0.676	3.1173	6.0355	H	S	+
2492	86	0.800	0.800	2.2000	5.1750	H	S	+
1581	116	0.68	0.74	0.287	0.838	L	B	
1596	117	0.85	0.87	0.173	0.412	L	B	
1597	117	0.80	0.85	0.195	0.300	L	B	
1601	118	0.61	0.66	0.333	0.492	L	B	
1603	118	0.58	0.64	0.333	0.276	L	B	
1600	118	0.56	0.62	0.364	0.000	L	B	
1598	118	0.77	0.82	0.217	0.182	L	B	
1599	118	0.73	0.79	0.248	0.000	L	B	

Tab. 5.15 Test configuration and measured values for the tests in the TPTF 4-inch test section (sorted by pressure).

Run ID	Pres-sure [bar]	void [-] inlet	void [-] L/D=24	vL [m/s] inlet	vG [m/s] inlet	Boiler level	Mixer type	Droplet entrain-ment
2172	30	0.510	0.530	0.0546	0.1571	H	B	
2173	30	0.476	0.425	0.0492	0.3013	H	B	
2174	30	0.458	0.370	0.0474	0.6196	H	B	
4304	30	0.517	0.552	0.0746	0.3874	H	B	
4305	30	0.503	0.508	0.0727	0.2852	H	B	
4306	30	0.477	0.430	0.0756	0.2195	H	B	
4307	30	0.457	0.368	0.0788	0.1656	H	B	
4308	30	0.536	0.611	0.0848	0.5228	H	B	
4309	30	0.448	0.342	0.0781	0.1359	H	B	
537	73	0.456	0.364	0.1955	0.2313	H	B	
541	73	0.516	0.549	0.2199	0.5229	H	B	+
542	73	0.563	0.690	0.0997	0.4739	H	B	
543	73	0.490	0.468	0.3840	0.5489	H	B	+

Run ID	Pres-sure [bar]	void [-] inlet	void [-] L/D=24	vL [m/s] inlet	vG [m/s] inlet	Boiler level	Mixer type	Droplet entrain-ment
544	73	0.526	0.581	0.4138	0.8089	H	B	+
545	73	0.551	0.656	0.2371	0.7725	H	B	+
546	73	0.593	0.778	0.1067	0.7159	H	B	
547	73	0.639	0.895	0.1210	1.2656	H	B	+
2527	73	0.547	0.642	0.1134	0.4436	H	B	
2528	73	0.546	0.640	0.1144	0.4422	H	B	

5.9.3 Input Dataset

5.9.3.1 Nodalisation

8-inch test section:

The nodalisation of the TPTF test section is shown in Fig. 5.151. Here, the so-called partial modelling approach is shown. In the partial modelling approach, the part of the test section up to L/D = 17 (first measurement position) is ignored, and values measured at this position are applied as boundary condition. This approach has turned out to be advantageous within the preparation of a benchmark test for different system codes performed within the frame of the FONESYS network /LAN 20/, /LAN 22/ and thus was the recommended one for all participants of the benchmark.

The boiler at the outlet is modelled as well, and the different boiler levels at the end of the test section in the experiments (above or below the outlet) are considered also in the ATHLET calculations. The level is set as an initial condition and then controlled in a simplified way via the single-junction pipe VSL-LEAK.

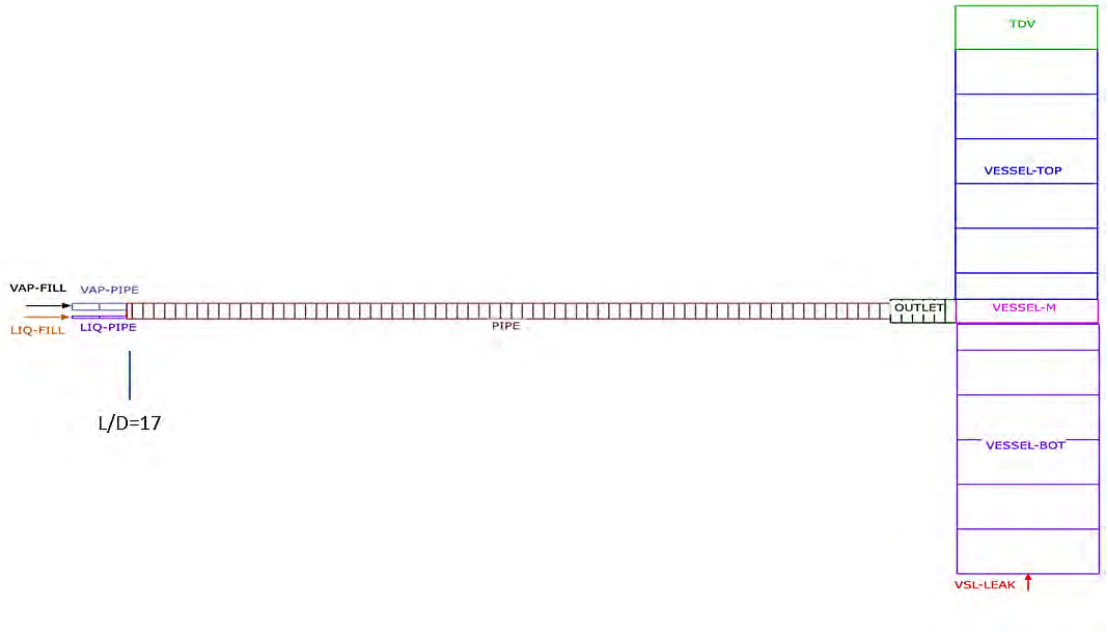

Fig. 5.151 ATHLET model for the 8-inch test section (partial modelling)

For a subset of cases, additional calculations were done with a full model. These calculations were done only for comparison with the partial model to make a final decision on the modelling approach. As the results were rather similar, it was decided to use the partial modelling approach in all cases for the 8-inch test section. Only the results from the partial model are provided for the 8-inch test section.

4-inch test section:

The ATHLET model for the TPTF 4-inch test section is shown in Fig. 5.152. In this case, the full modelling approach is applied, again following the recommendations for the FONESYS benchmark. Here, the boundary conditions are applied at the beginning of the converging inlet.

The values for the boundary conditions at L/D = 17 (partial approach, 8-inch), or the converging inlet (full modelling, 4-inch) respectively, are given in Tab. 5.14 and Tab. 5.15.

The void value cannot be directly applied as a boundary condition. Instead, the following approach was used. The mass flow of the phases is specified using fill objects (`VAP-FILL`, `LIQ-FILL`). The diameter of inlet pipes is adjusted to prescribe the given velocity values at the inlet of the test section.

The pressure is set at the time-dependent volume (TDV) at the top of the vessel.

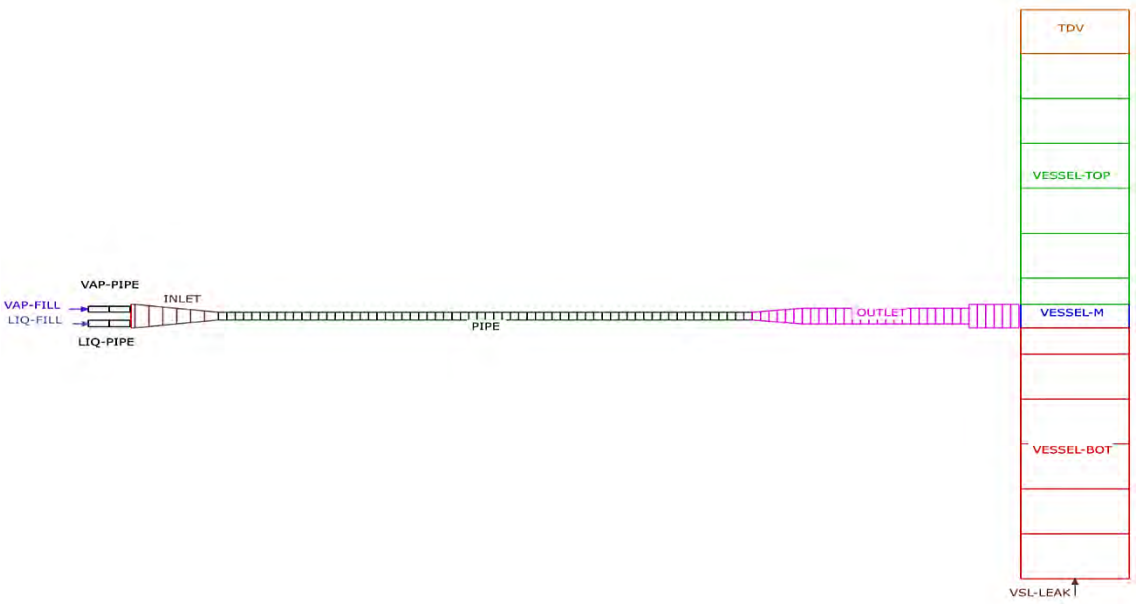

Fig. 5.152 ATHLET model for the 4-inch test section (full modelling)

In the test section (PIPE) itself, a very fine nodalisation (0.1 m) is used, both for the 8-inch test section and the 4-inch test section. Sensitivity tests have shown, however, that the results are mainly unchanged when using a coarser resolution (0.4 m).

5.9.3.2 Model Options

The 6-equation model in ATHLET was used for this test. As two-phase multiplier of the wall friction, the Martinelli-Nelson model, which is currently the default option in ATHLET, was used. The wall roughness was set to $5 \cdot 10^{-5}$ m. A form loss factor 1. was assigned at the end of the test section (opening to the vessel). Moreover, no heat loss through the wall is considered.

A new entrainment model was introduced with ATHLET version 3.3, influencing the results of those subset of test cases which show entrainment in the calculations when comparing with ATHLET version 3.2.1. For details of these changes in the entrainment model, see /LEE 22/ or the section on the Mantilla test in section 5.8; the new entrainment model was developed based on that benchmark.

5.9.4 Main Results

This validation focuses on a quantitative comparison of the void fraction at the downstream measurement position with experimental results, and on the occurrence of droplet

entrainment. In the experiments, the only information about droplet entrainment results from visual detection of the flow pattern at the video probe position; no quantitative measurement of the entrainment rate is available.

Regarding the predicted flow patterns there are, apart from discrepancies regarding occurrence of droplet entrainment, some differences in the predicted flow pattern. Slug flow, which was reported in several cases in the experiment, was not predicted in ATHLET calculations.

Fig. 5.153 shows the results for the void fraction in the 8-inch test section (at the measurement position L/D = 49) obtained with ATHLET 3.2.1, and the results for the 4-inch test section (measured at L/D = 24) are shown in Fig. 5.154. Most of the calculated values lie within a range of +/- 15 % deviation to the experimental values, with some larger relative deviation for very small void fractions, and two significant outliers in the 4-inch test section. Apparently, ATHLET tends to overestimate the void for cases with high (> 0.75) void fractions.

With ATHLET version 3.3, the picture does not change much at a first glance (Fig. 5.155 and Fig. 5.156). A closer look reveals that some points moved towards the diagonal line, i.e., are closer to the experimental values.

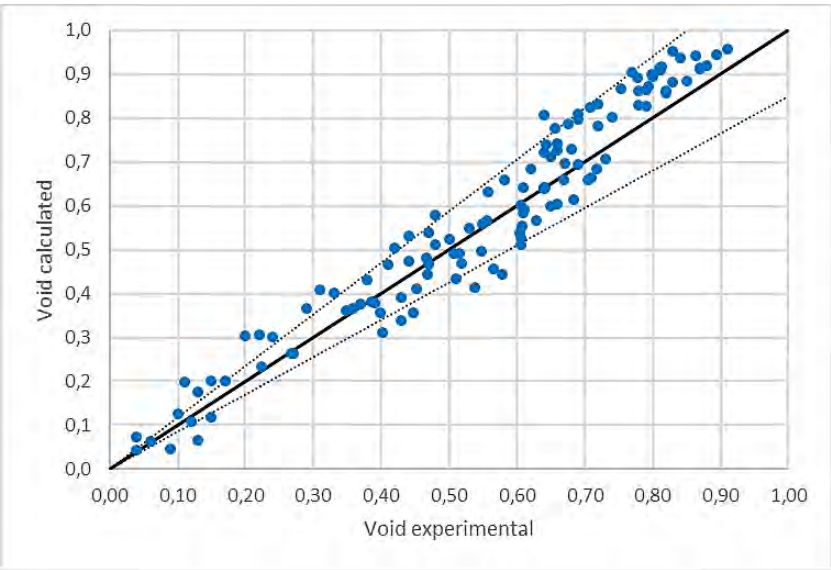

Fig. 5.153 Experimental vs. calculated values (obtained with ATHLET 3.2.1) of the void fraction at the downstream measurement position L/D = 49 in the 8-inch test section. The dotted lines indicate the 15 % error range

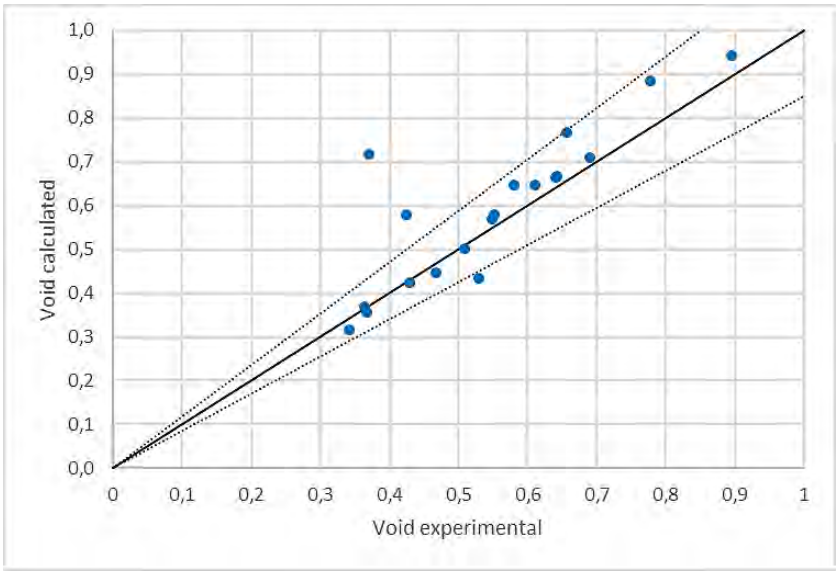

Fig. 5.154 Experimental vs. calculated values (obtained with ATHLET 3.2.1) of the void fraction at the downstream measurement position L/D = 24 in the 4-inch test section. The dotted lines indicate the 15 % error range

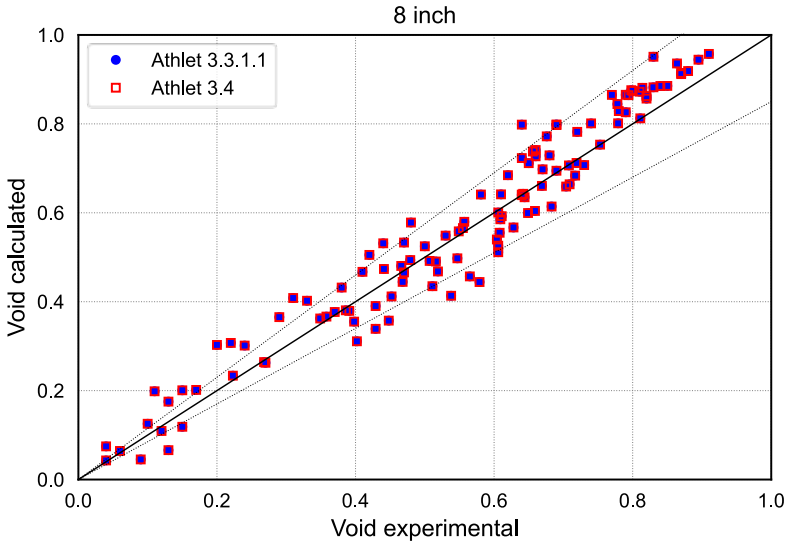

Fig. 5.155 Experimental vs. calculated values (obtained with ATHLET 3.3 and 3.4) of the void fraction at the downstream measurement position L/D=49 in the 8-inch test section. The dotted lines indicate the 15 % error range

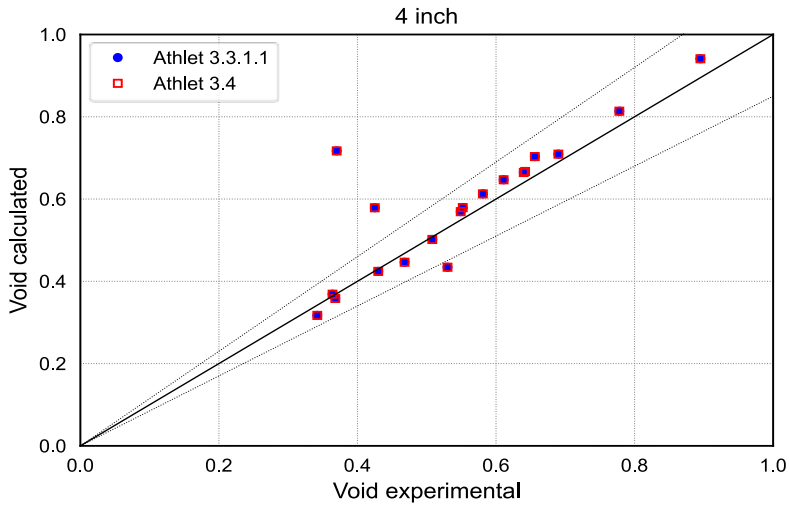

Fig. 5.156 Experimental vs. calculated values (obtained with ATHLET 3.3 and 3.4) of the void fraction at the downstream measurement position L/D = 24 in the 4-inch test section. The dotted lines indicate the 15 % error range

A quantitative comparison of the data shows that the relative difference of the considered quantities (void fraction, pressure, liquid and vapour velocity) between ATHLET 3.2.1 and ATHLET 3.3 is typically in the range of 10^{-5} or smaller for the cases without entrainment, while there are, as expected due to the change of the entrainment model (see chap. 5.9.3.2), notable differences for the cases with calculated entrainment. Between the code versions 3.3 and 3.4, with no relevant model change, the difference in these quantities is negligible for all cases.

Details for the cases with entrainment are given in Tab. 5.16. In almost all cases, with the new entrainment mode in ATHLET 3.3, the calculated void fraction shows a better agreement with the measured value than with ATHLET 3.2.1. The two exceptions show very small entrainment in ATHLET 3.3, but no entrainment with ATHLET 3.2.1 and in the experiment. In most cases, the relative difference between the calculated and measured void fraction is now less than 0.1. There are no cases where droplet entrainment is reported in the experiment with no calculated entrainment (though very small values are computed in a few cases). In most of the cases with no visually detected entrainment in the experiment, but with calculated entrainment, the entrainment rate is considerably reduced in ATHLET 3.3, indicating that the new entrainment model also improves the onset of entrainment. The relative deviation between the results of ATHLET 3.3 and ATHLET 3.4 is typically less than 10-5, thus no difference is made between these two versions in Tab. 5.16.

For the results presented so far, ATHLET was run on a Microsoft Windows platform using the serial version with the standard solver. Additional runs were, for comparison, also started using the OpenMP version, and using the Numerical Toolkit NuT (with the standard solver). With the OpenMP version, identical results were observed. When using NuT, small, but neglectable (order of magnitude 10^{-5} or smaller), differences to the standard version were observed.

Tab. 5.16 Detailed comparison of the void at the downstream measurement position of those cases (sorted by pressure) for which entrainment is observed either in the experiment or in the ATHLET calculation. Those cases where no entrainment is visually detected in the experiment are marked green. The respective better result of the two ATHLET versions is marked orange.

	Experiment		**ATHLET 3.2.1**			**ATHLET 3.3/3.4**	
8-inch test section							
Run ID	**void [-] L/D=48**		**void [-] L/D=48**	**entr. rate [-] L/D=48**		**void [-] L/D=48**	**entr. rate [-] L/D=48**
490	0.840		0.937	0.312		0.885	0.049
491	0.779		0.861	0.310		0.801	0.071
2477	0.811		0.910	0.228		0.812	0.025
523	0.753		0.868	0.104		0.753	0.040
524	0.644		0.739	0.103		0.635	0.012
525	0.794		0.872	0.482		0.865	0.271
526	0.864		0.943	0.480		0.936	0.208
527	0.708		0.825	0.102		0.707	0.008
2483	0.719		0.832	0.094		0.712	0.006
2484	0.814		0.916	0.327		0.881	0.069
541	0.549		0.558	0.000		0.558	0.002
543	0.468		0.444	0.000		0.445	0.005
544	0.581		0.660	0.235		0.641	0.121
545	0.656		0.778	0.235		0.738	0.071
546	0.778		0.893	0.234		0.844	0.041
547	0.895		0.945	0.617		0.944	0.498
773	0.500		0.524	0.000		0.525	0.003
845	0.770		0.905	0.259		0.865	0.049
855	0.470		0.539	0.016		0.533	0.007
857	0.640		0.808	0.386		0.798	0.211
732	0.810		0.915	0.249		0.872	0.042
743	0.690		0.809	0.380		0.799	0.201
2464	0.479		0.511	0.047		0.493	0.033

2465	0.557		0.632	0.043		0.580	0.016
2467	0.798		0.899	0.304		0.875	0.078
2468	0.676		0.787	0.307		0.772	0.143
2492	0.800		0.895	0.315		0.874	0.088
4-inch test section							
Run ID	**void [-] L/D=24**		**void [-] L/D=24**	**entr. rate [-] L/D=24**		**void [-] L/D=24**	**entr. rate [-] L/D=24**
541	0.549		0.569	0.0000		0.569	0.0011
542	0.690		0.709	0.0000		0.709	0.0003
543	0.468		0.446	0.0000		0.446	0.0028
544	0.581		0.647	0.2305		0.613	0.1033
545	0.656		0.766	0.2311		0.703	0.0614
546	0.778		0.886	0.2299		0.814	0.0341
547	0.895		0.943	0.6126		0.941	0.4280

5.9.5 Main Findings

In general, there is a satisfactory to good agreement of the void fraction calculated by ATHLET with the measured values. With the versions ATHLET 3.3/3.4, no changes are found for the cases without entrainment in the calculations, and a clear improvement in the entrainment cases. This results from the new entrainment model introduced in ATHLET 3.3. In the cases where ATHLET falsely (according to the reports from the experiment, purely based on visual observation) yields entrainment, the entrainment rates are reduced using the new model. In the few cases where entrainment is expected from the experiment, but was missed with ATHLET 3.2.1, the versions ATHLET 3.3/3.4 now calculate at least small entrainment rates. While the values of the entrainment rates cannot be compared with experimental values, the resulting void fraction in these cases is in almost all cases clearly improved with the new version.

Some deficiency is observed regarding the flow patterns. In general, the flow pattern map derived from the calculations matches roughly the experimental one; however, slug flow is never predicted by ATHLET, although some cases in the experiment are in the slug flow regime.

5.10 Boiling Test Facility of IKE of University of Stuttgart

5.10.1 Test Facility

The main part of the Boiling Test Facility is a 3 m prototype model for a large-scale straight two-phase closed thermosyphon related to passive spent fuel pool cooling in nuclear power plants. This test facility is built up at Institute of Nuclear Technology and Energy Systems at University of Stuttgart, Germany.

The thermosyphon is made from one tube, which consists of an evaporator, an adiabatic, and a condenser section, each one meter long, respectively. The inner surface of the tube is smooth. The pipe is made of 1.4301 stainless steel with an inner and outer diameter of 35 mm and 38 mm respectively. Double-tube heat exchangers are installed in the evaporator and condenser sections as heat source and heat sink, connected to process thermostats operated with water as sketched in Fig. 5.133. The adiabatic section is thermally insulated with 19 mm thick Armaflex XG pipe insulation. The thermosyphon is filled with deionised water near vacuum conditions /CÁC 23/.

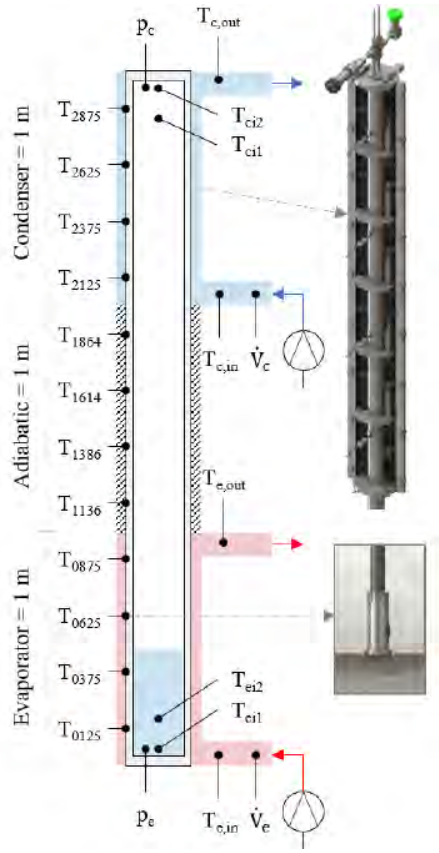

Fig. 5.157 a) Schematic representation of the experimental setup and the arrangement of the measuring instruments instrumentation.
b) Sketch of water double-pipe heat exchanger. Taken from /CÁC 23/

On the outer surface of the thermosyphon, 12 resistance thermometers PT100, with a Class A accuracy ± (0.15 + 0.002*T RD), are placed. The outer surface of the pipe is milled flat to ensure thermal contact between the pipe surface and the resistance thermometer. Four sheathed resistance thermometers PT100 are placed inside the thermosyphon, allowing the temperature measurement at different heights inside the evaporator and condenser section. The absolute pressure in the evaporator and condenser section is measured with absolute pressure transmitters PAA-33X with an accuracy of ±0.15 % FS. The inlet and outlet temperatures of both heat exchangers on the heating and cooling side are also measured with sheathed resistance thermometers PT100. The flow rate at the inlet of the evaporator and condenser section is determined with an ultrasonic flow meter with an accuracy of ± (0.7 % RD + 0.7 % FS). The Keysight data logger 34970A and the computer software Agilent VEE are used for the measurement data acquisition /CÁC 23/

5.10.2 Test Conduct

The test procedure starts with the evacuation of the thermosyphon with a vacuum pump to a final pressure of 0.2 Pa. Then, the thermosyphon is filled with degassed deionised water. After the filling procedure, the thermosyphon is heated up and the valve at the top is slowly opened to eliminate non-condensable gases in the system. Next, the inlet temperatures ($T_{e,in}, T_{c,in}$) and the volume flows ($\dot{V}_e, \dot{V}_c$) in the evaporator and condenser sections respectively are determined. The steady state is determined by checking that the fluctuations of inlet temperatures and volume flows are less than ± 0.1 °C and ± 0.2 l/min respectively /CÁC 23/.

As described above, two sheathed resistance thermometers are placed in both the evaporator (T_{ei1}, T_{ei2}) and condenser (T_{ci1}, T_{ci2}) sections. To determine the temperature distribution inside the evaporator and condenser section, measurements are repeated at the same filling ratio, heat source and sink temperature after displacing the movable resistance thermometers T_{ei2} and T_{ci1} to a new height. The resistance thermometers T_{ei1} and T_{ci2} are left in the same positions and serve as a reference /CÁC 23/.

The objective is to study the effect of the filling ratio (20 % - 100 %) of the working fluid deionised water on the thermosyphon's heat transfer performance and the temperature distribution along the thermosyphon under different heat source (45 °C – 80 °C) and heat sink (10 °C - 30 °C) temperatures. Due to the background of spent fuel pool heat removal the temperatures of the heat sink and source are chosen in accordance with German KTA 3303 /KTA 15/.

The Boiling test section is modelled as a pipe (named HP) of 3 m length with 9 control volumes, 3 CV for each section of the thermosyphon. A schematic of the nodalisation is shown in Fig. 5.134. The double-tube heat exchangers are modelled as pipes, too. Each pipe (named WT_COOL and WT_HEAT) is combined with a fill and a TDV (not sketched) to model the setting up of the starting and boundary conditions of the experiments during calculation. There is a further TFO modelling the environment named HP_EN which isn't sketched in Fig. 5.158.

The three TFOs of thermosyphon and heat exchangers are surrounded by 5 HECU objects modelling the wall material plus insulation, one for each section of the thermosiphon (H-HEAT_WT, H-COOL_WT, and H-ADI-EN) and one for the outsides of each heat exchanger (H-WTC-EN, and H-WTH-EN).

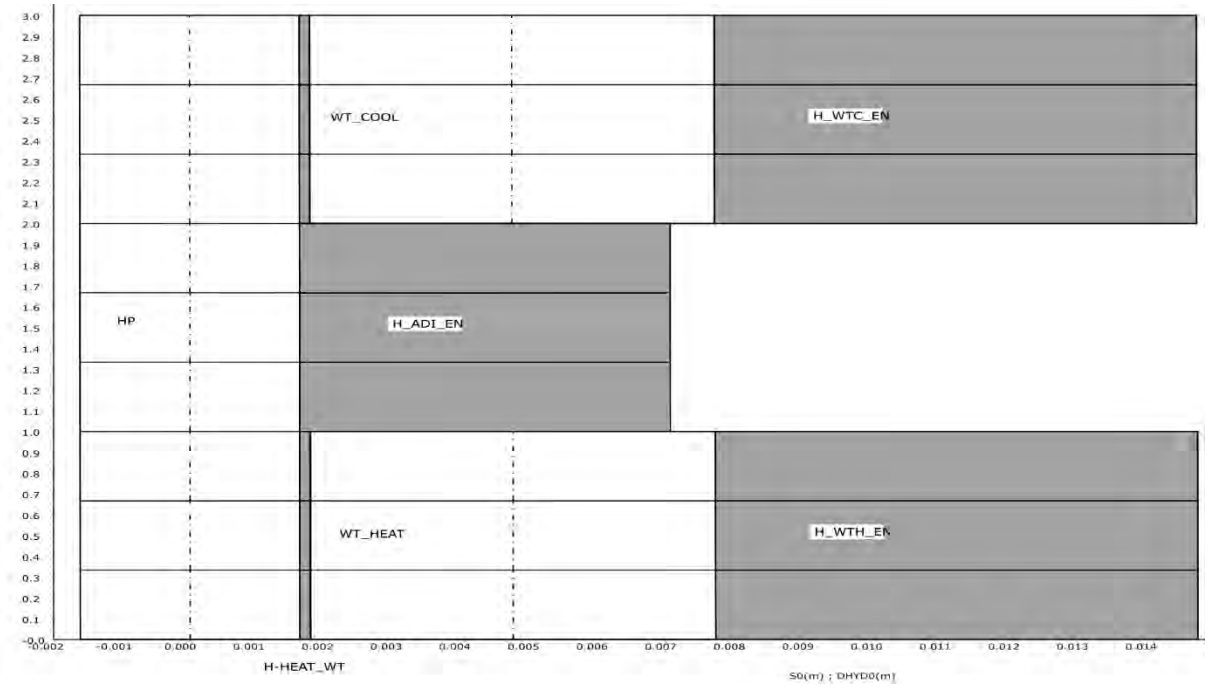

Fig. 5.158 Nodalisation of the test section in ATHLET

5.10.3 Main Results

The comparison of ATHLET calculations and experiments are done for the ATHLET versions 3.3.1 and 3.4 and for the experiments of 04 May 2022 starting at 10:00 for a temperature of 55 °C of the heat source, a temperature of 20 °C of the heat sink and a 100% filling ration of the heating zone. (The complete name of the experiment is S_Gl_Xx_55_20_100_x_V90_011_04May2022_10_00.) From all measured values the pressures and temperatures inside thermosyphon in the heating and in the cooling zone are chosen for comparison with ATHLET calculations. These values are a good indicator for the quality of the calculations, because this pressure and this temperature arises inside the thermosyphon as a result of the initial and boundary conditions.

As it can be seen in Fig. 5.159 the calculated pressure and temperature values in the heating and in the condenser zones meet the measured values. ATHLET overpredicts the mean value of the experimental pressure values slightly, by about 20 Pa in the heating and up to about 10 Pa in cooling zone. The differences between the two ATHLET versions are negligible.

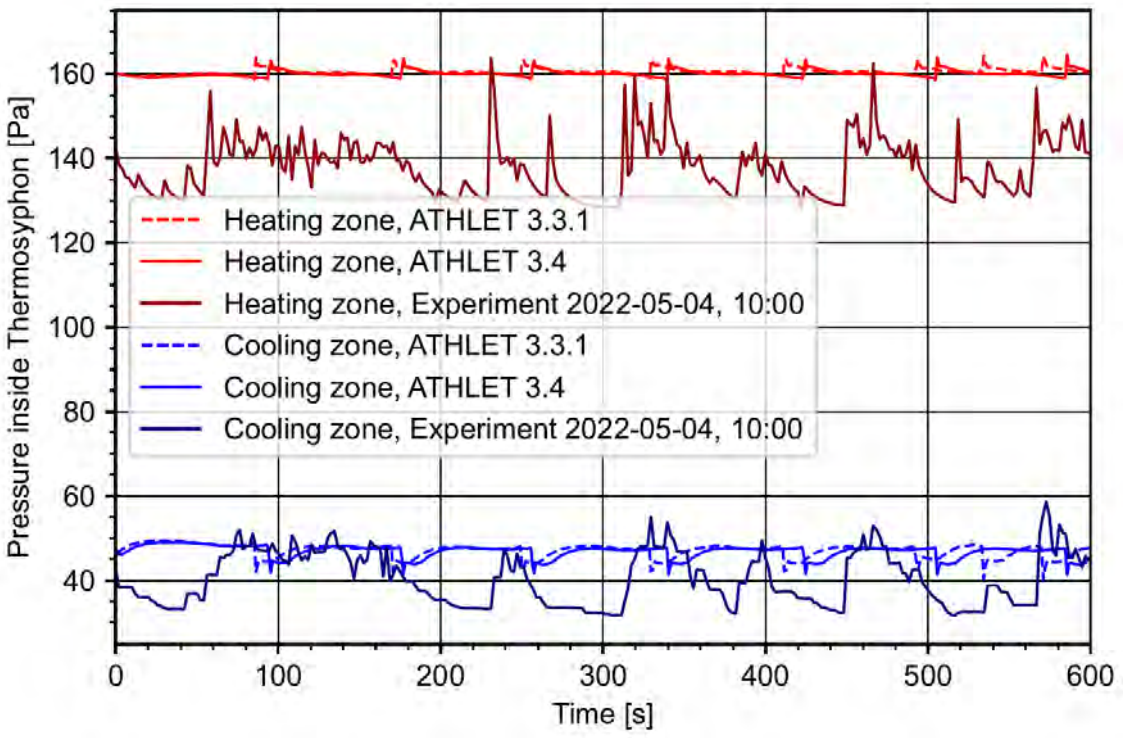

Fig. 5.159 Comparison of the simulated and experimental pressures inside heating and cooling zone of the thermosyphon for experiment of 04th May 2022, 10:00.

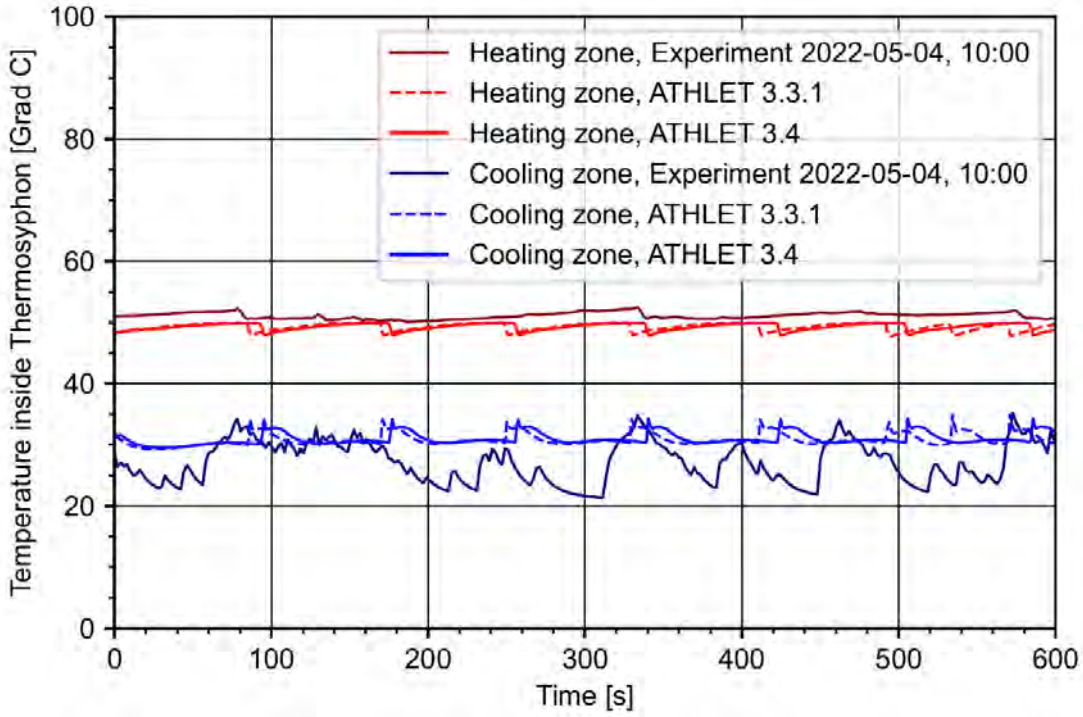

Fig. 5.160 Comparison of the simulated and experimental temperatures inside heating and cooling zone of the thermosyphon for experiment of 04th May 2022, 10:00.

5.10.4 Main Findings

Overall, ATHLET is calculation the thermosyphon qualitatively correct. There are however systematic deviations in predicted pressures and thus saturation temperatures in the range of about 10 % to 20 %. Comparing ATHLET 3.4 to ATHLET 3.3.1 there is no further progress in the simulation of the chosen Boiling Test.

6 Uncertainty Evaluation

In computational reactor safety analysis, conservative calculations are replaced by best estimate calculations. Best-estimate calculations are an attempt to predict the thermal-hydraulic behaviour of a nuclear power plant under normal and accidental conditions as realistic as the state of knowledge allows. Since a certain time, an increasing trend is observed to support the best-estimate calculations with uncertainty analysis. This approach called BEPU (Best Estimate Plus Uncertainty) is introduced to the safety analysis with the aim to increase the quality of the simulations and resulting safety statements.

6.1 Need for Uncertainty Analyses

ATHLET is a thermal-hydraulic system code with best-estimate models for the physical processes. Like in any best-estimate code, the models and methods in ATHLET approximate the physical behaviour with more or less accuracy. The comprehensive validation process described in the preceding chapters of this report establishes confidence in the general validity of the models and methods used and provides a qualitative statement on their accuracy.

Best-estimate codes are being applied for reactor safety analysis since several years throughout the OECD-countries. The field of application and the way to account for model uncertainties, however, vary from country to country /BES 96/. In Germany, ATHLET was applied with conservative initial and boundary conditions, thereby introducing a considerable amount of conservatism in the calculation. For future applications, full best-estimate analyses are foreseen, see also /IAEA 19/. It is mandatory, however, that best-estimate calculations with realistic boundary conditions are supplemented by a quantitative uncertainty analysis. In the US, NRC accepts licensing calculations with best-estimate codes if accompanied by uncertainty analysis /NRC 89/. Also, in European countries there is an increasing trend to apply BEPU approach for the licensing purposes.

There are several sources of uncertainties in code predictions, like the code models, chosen nodalisation, initial and boundary conditions, plant state, fuel parameters, scaling and numerical solution algorithm. Several code correlations are based on measurements, which show a scatter around a mean value. For example, data for two-phase pressure drop show a scatter range of about ± 20 to 30 %. Consequently, a range of

values should be taken into account for the respective model parameter instead of one discrete value only. The state of knowledge about all uncertain parameters is described by “subjective” probability distribution. The term “subjective” is used here to distinguish uncertainty due to imprecise knowledge from uncertainty due to stochastic or random variability. Such a distribution expresses how well the appropriate value of an uncertain parameter of the code application is known in the light of all available evidence according to the state of knowledge experts involved in determination of the probability distribution functions. A state of knowledge based on the minimum information at the parameter level is expressed by uniform distribution.

Stochastic variability due to possible component failures of the reactor plant is not considered in an uncertainty analysis as an input uncertainty. The possible failure of the reactor safety system components is taken into account in a deterministic way, assuming single failure criterion. The probability of system failures is rather a part of probabilistic safety analysis, not of demonstrating the effectiveness of emergency core cooling systems.

The aim of the uncertainty analysis is at first to identify and quantify all potentially relevant uncertain parameters. Their propagation through computer code calculations provides subjective probability distributions (and ranges) for the code results. The evaluation of the margin to a given acceptance criterion, e.g. the maximum fuel rod cladding temperature, should be based on the upper limit of this distribution for the calculated temperatures. Uncertainty analysis is thus needed, if conclusions are to be obtained from best-estimate thermal-hydraulic code calculations, otherwise only single values of unknown accuracy would be available for comparison with the acceptance limits.

An important field of uncertainty and sensitivity analyses is validation and development of the complex numerical codes. In the course of uncertainty and sensitivity analyses performed for experimental tests accuracy of the numerical simulation can be quantitatively estimated. On this basis conclusions can be drawn, if the simulations fulfil the acceptance criteria regarding experimental data and finally, if the expected accuracy of simulation is achieved. The sensitivity analysis enables to identify the input uncertainties which contribute significantly to the uncertainty of the calculated results. In the case of uncertainties related to the code physical models the weak points of the physical models can be identified. On this basis decisions concerning further code development can be performed.

6.2 Methods for Uncertainty Analyses

Methods for the quantification of uncertainties in thermal-hydraulic code calculation have been developed by various institutions. The most frequently applied statistical methods in uncertainty analyses are the input uncertainties propagation methods. The input uncertainties propagation methods consider the effect of uncertainties of input parameters like computer code models, initial and boundary conditions, other application specific input data and parameters of solution algorithms on the calculation results. As the first systematic methodology for performing the uncertainty analysis the CSAU methodology /BOY 89/ was introduced by NRC. Among the uncertainty evaluation methods based on input uncertainties propagation the most popular is the method based on Wilks' formula /WIL 41/, /WIL 42/, /WAL 43/. This method is also called GRS type method since it was proposed for use in simulations for nuclear facilities at first by GRS /HOF 85/, /GLA 08a/.

Comparisons of functioning and application of different methods for uncertainty analysis were perform in the frame of NEA/CSNI projects: UMS (Uncertainty Methods Study) /NEA 98/, BEMUSE (Best Estimate Methods - Uncertainty and Sensitivity Evaluation) /CRÉ 08/, /NEA 11/, PREMIUM (Post-BEMUSE Reflood Models Input Uncertainty Methods) /NEA 16/ and SAPIUM /BAC 20/. GRS participated in these international studies using ATHLET and the GRS uncertainty analysis method.

6.3 Description of the GRS Methodology

A methodology for uncertainty and sensitivity analyses has been developed by GRS where the computational effort is independent of the number of uncertain parameters /KRZ 94/. The implementation techniques are primarily based on tools from statistics. Statistics is used in order to evaluate the uncertainty and sensitivity with a reasonable number of calculations.

The state of knowledge about all uncertain parameters is described by ranges and probability distributions. In order to get information about the uncertainty of code results, a number of code runs have to be performed. For each of these calculation runs, all identified uncertain parameters are varied simultaneously. Uncertain parameters are uncertain input values, modelling options, initial and boundary conditions, numerical values like convergence criteria and maximum time step, among others. Modelling uncertainties are expressed by adding on or multiplying correlations by a corrective term, or by a set

of alternative model formulations. Finding the optimal nodalisation to describe the relevant thermal-hydraulic phenomena, is a task of code validation. However, alternative nodalisation schemes can be included in the uncertainty analysis.

Code validation results are a fundamental basis to quantify the uncertainty of physical models or their mathematical formulation. Experts specify the ranges and probability distributions of uncertainties that best express the state of knowledge. The state of knowledge dependence between parameters can be taken into account. Computerized support is provided for an inter- active construction of the probability distributions and for the state of knowledge dependence.

In the GRS methodology, all potentially important parameters are included in the analysis, based on judgement of the analyst. The number of calculations to be performed does not grow with the number of parameters. No ranking of input parameters to reduce their number is needed in order to cut computation costs. The reason is the simultaneous variations of all uncertain parameters for each code run, together with the statistical evaluation of these results. The uncertainty and sensitivity results have a well-founded probabilistic statistical interpretation.

The number of calculations depends only on the desired probability content and confidence level of the statistical tolerance limits used in the uncertainty statement of the results. The required minimum number n of these calculation runs is given by the Wilks' formula /WIL 41/, /WIL 42/, e.g. for one-sided tolerance limits:

$$1 - \alpha^n \geq \beta \tag{6.1}$$

where β x 100 is the confidence level (%) that the maximum code result will not be exceeded with a probability of a α x 100 (%) of the corresponding output distribution (percentile), which is to be compared to a given acceptance criterion. The confidence level is specified to account for the possible influence of the sampling error due to the fact that the statements are obtained from a random sample of limited size. For two-sided statistical tolerance, the corresponding formula is /SAC 69/:

$$1 - \alpha^n - n(1-\alpha)^{n+1} \geq \beta \tag{6.2}$$

The minimum number of calculations can be seen in Tab. 6.1. Evidently, increases in α to higher percentiles have a stronger impact on sample size than those for β.

Tab. 6.1 Minimum number of calculations n for one-sided and two-sided statistical tolerance limits at rank order 1

	One-sided statistical tolerance limits				**Two-sided statistical tolerance limits**		
β/α	**0.90**	**0.95**	**0.99**		**0.90**	**0.95**	**0.99**
0.90	22	45	230		38	77	388
0.95	29	59	299		46	93	473
0.99	44	90	459		64	130	662

These are limiting cases at rank order 1 of the generic formula given, e.g., by /TUK 47/, /WIL 48/ using the incomplete beta function. For (two-sided) limits of a sample with size N and coverage s (i.e. the number of samples retained after removing the extreme ranks for m figures of merit), the respective formula is:

$$1 - I_\alpha(s, N - s + 1) \geq \beta \tag{6.3}$$

Note that the formula does not depend on the specific number of ranks removed for an individual figure of merit or if ranks are removed from the low or high part or the specific ordering for that figure or in which sequence figures of merit are treated. Importantly, though, the actual limits for each figure of merit, i.e., the extreme ranks not removed, do depend on all these aspects in the general case.

If the rank order r for all m figures of merit is the same and rank order 1 means that no samples are actually removed, the resulting coverage (for two-sided limits) is $s = N - 2m(r-1)$ and the resulting formula becomes the following.

$$1 - I_\alpha(N - 2m(r-1), 2m(r-1) + 1) \geq \beta \tag{6.4}$$

Given that the proof of this formula assumes that actually at least one sample is removed per figure of merit, rank order 1 should be avoided. From this, the required minimum sample sizes can be determined. Tab. 6.2 gives some values.

Tab. 6.2 Minimum number of calculations N for statistical tolerance limits at different coverages s

	Tolerance limits (α / β)				
$N - s$	**0.90/0.90**	**0.90/0.95**	**0.95/0.95**	**0.95/0.99**	**0.99/0.99**
0	22	29	59	90	459
1	38	46	93	130	662
2	52	61	124	165	838
3	65	76	153	198	1001
4	78	89	181	229	1157
5	91	103	208	259	1307
6	104	116	234	288	1453
7	116	129	260	316	1596
8	128	142	286	344	1736
9	140	154	311	371	1874
10	152	167	336	398	2010
11	164	179	361	425	2144
12	175	191	386	451	2277
13	187	203	410	478	2409
14	199	215	434	504	2539
15	210	227	458	529	2669
16	222	239	482	555	2798
17	233	251	506	580	2925
18	245	263	530	606	3052
19	256	275	554	631	3179
20	267	286	577	656	3304
30	379	402	809	901	4533
40	490	515	1036	1139	5727
50	599	627	1260	1372	6898

If other numbers for the total samples N and coverage s than those provided in Tab. 6.1 and in Tab. 6.2 are used, it is a valid question where the percentile of the statistic corresponding to α is. For univariate distributions, this can be clearly answered using the same

formula as above and this can be answered for the same sample of code calculations. If we're looking at percentiles corresponding to $\alpha \geq 0.5$, a naïve estimator of the percentile is (obviously) a coverage $s = \lceil \alpha\, N \rceil$. For the correct answer at confidence level β we will have to modify the coverage by an offset k. This results in

$$1 - I_{\alpha}(\lceil \alpha\, N \rceil + k, \lfloor (1-\alpha) N \rfloor - k + 1) \geq \beta \tag{6.5}$$

If we are interested in percentiles $\alpha \leq 0.5$ and as we're faced with a cumulative distribution, the approach for a lower limit would be

$$\begin{aligned} & I_{1-\alpha}(\lceil (1-\alpha) N \rceil + 1 + l, \lfloor \alpha\, N \rfloor - l) \leq 1 - \beta \\ \Leftrightarrow \quad & I_{\alpha}(\lfloor \alpha\, N \rfloor - l, \lceil (1-\alpha) N \rceil + 1 + l) \leq \beta \\ \Leftrightarrow \quad & 1 - I_{\delta}(\lceil \delta\, N \rceil + (1+l), \lfloor (1-\delta)\, N \rfloor - (l+1) + 1) \leq \beta \end{aligned} \tag{6.6}$$

By transferring the lower percentiles to $\delta = 1 - \alpha$ and considering that the lower percentile offset is $l = k - 1$, which needs to be subtracted from the floor of $\lfloor \alpha\, N \rfloor$, the offsets for higher percentiles can be matched to the offsets of the lower percentiles. Obviously, eq. 6.5 can be used to estimate upper limits for the lower percentiles, and eq. 6.6 can be used to estimate lower limits for the higher percentiles. The apparent inconsistency in the offsets for the lower and higher percentiles is due to the following. The upper limit for the high percentile is the rank for which the coverage includes at least the required probability. For the lower limit, the resulting rank is that for which the complement of the percentile includes the required probability (i.e. $\delta = 1 - \alpha$). If you look for the rank outside of that coverage, the answer is $l + 1 = k$ offset from the naïve percentile rank. The remaining asymmetry is a result of rounding and properties of the incomplete beta function.

For multivariate distributions, even the definition of an order in the vector space spanned by the figures of merit includes choices by the analyst. More importantly, depending on the correlation of ranks between two (or more) figures of merit, ordering them by two or even more figures of merit might or might not be sensible. For example, if two figures of merit would be correlated with a rank correlation coefficient of 1, a separate rank ordering makes no sense. If ranks for two figures of merit are not correlated at all, it should not be relevant, which figure of merit is ranked first and which second.

As stated before, Wilks' formula gives the number of samples needed to cover a probability content of α at the confidence level of β. Consequently, the percentile coverages resulting from eq. 6.5 and eq. 6.6 can be used to investigate all combinations of s

samples that can be obtained by different ranking approaches via multiple figures of merit if at least one rank in the respective rank order from the bottom and (or) the top has been removed. The analyst could also decide to distribute the $N - s$ excluded samples more evenly to extreme ranks for the different figures of merit. There are other techniques to construct non-parametric and possibly non-convex multivariate percentile contours, but these are outside the scope of this discussion.

In the tables below, the offset values for k are given for relevant percentiles of 0.32, 0.5, 0.68, 0.8, 0.9, 0.95 and 0.999 for confidence levels of 0.9, 0.95 and 0.999 respectively, for selected N. It is not practicable to give a complete table for these off-sets because they switch between a higher and a lower value multiple times with increasing N because of the rounding procedure used to derive integer coefficients for the incomplete normalized beta function and the threshold of β, which can be narrowly missed or exceeded. As an example, the 0.9 percentile for sample size 22 at a confidence level 0.9 is $[0.9 \cdot 22] + k = 20 + 2 = 22$ (see Tab. 6.3), which is the expected result.

Tab. 6.3 Offset values for upper limits of naïve percentile estimator for different samples sizes and percentiles at confidence level 0.9

Size	**Offset for percentile α to upper limit at β = 0.9**						
N	**0.32**	**0.5**	**0.68**	**0.8**	**0.9**	**0.95**	**0.99**
22	3	4	4	3	2	N/A	N/A
38	4	5	4	3	2	N/A	N/A
52	5	6	5	4	3	2	N/A
65	6	6	5	5	3	3	N/A
78	6	7	5	5	3	2	N/A
91	6	7	6	5	4	3	N/A
100	7	7	7	6	5	4	N/A
120	7	8	7	7	5	4	N/A
140	8	9	7	7	5	4	N/A
160	8	9	8	7	6	4	N/A
180	9	10	8	8	6	5	N/A
200	9	10	9	8	6	5	N/A
250	10	11	10	9	7	5	2
300	11	12	11	10	8	6	3
400	13	14	13	11	9	6	3
500	14	15	14	12	10	7	4

And for the upper limit of the median (0.5 percentile) with sample size 181 at a confidence level of 0.95, $\lceil 0.5 \cdot 181 \rceil + k = 91 + 12 = 103$ (see Tab. 6.4), where the lower limit evaluates to $\lfloor 0.5 \cdot 181 \rfloor - k + 1 = 90 - 12 + 1 = 79$.

Tab. 6.4 Offset values for upper limits of naïve percentile estimator for different samples sizes and percentiles at confidence level 0.95

Size	**Offset for percentile α to upper limit at β = 0.95**						
N	**0.32**	**0.5**	**0.68**	**0.8**	**0.9**	**0.95**	**0.99**
59	7	7	6	5	4	2	N/A
93	8	8	7	7	5	3	N/A
124	9	10	9	7	6	4	N/A
153	11	11	9	8	7	4	N/A
181	11	12	10	9	7	5	N/A
208	12	13	11	10	7	5	N/A
220	12	13	12	11	8	6	N/A
240	13	14	12	11	8	6	N/A
260	13	14	13	11	9	6	N/A
300	14	15	14	12	9	7	3
350	15	16	15	13	10	7	3
400	16	17	16	14	11	8	4
450	17	18	17	15	11	8	4
500	18	19	18	16	12	9	4
550	19	20	19	16	12	9	4
600	20	21	20	17	13	10	5

Tab. 6.5 Offset values for upper limits of naïve percentile estimator for different samples sizes and percentiles at confidence level 0.99

Size	**Offset for percentile α to upper limit at β = 0.99**						
N	**0.32**	**0.5**	**0.68**	**0.8**	**0.9**	**0.95**	**0.99**
459	24	25	23	20	14	10	4
662	29	31	28	24	18	13	5
838	32	35	32	27	20	14	6
1001	35	37	35	30	22	16	7
1157	37	40	37	32	23	17	7
1307	40	43	40	34	25	18	8
1350	42	44	41	35	26	18	8
1400	42	45	41	35	27	19	9
1450	43	45	42	36	27	19	9
1500	43	46	43	37	27	20	9
1600	45	48	44	38	28	21	9

Size	**Offset for percentile α to upper limit at β = 0.99**						
N	**0.32**	**0.5**	**0.68**	**0.8**	**0.9**	**0.95**	**0.99**
1700	46	49	45	39	29	21	10
1800	47	50	47	40	30	22	10
1900	49	52	48	41	31	22	10
2000	50	53	49	42	32	23	11
3000	61	65	60	52	39	28	13

The probabilistic treatment of parameter uncertainties allows to quantify the state of knowledge about them (epistemic uncertainty). This means that, in addition to the uncertainty range, the knowledge is expressed by subjective probability density functions or probability distributions. The subjective interpretation of probability is used for a parameter with a fixed but unknown or inaccurately known value. The classical interpretation of probability as the limit of a relative frequency, expressing the uncertainty due to stochastic variability, is not applicable in that case.

The probabilistic distribution can express that some values in the uncertainty range are more likely the appropriate parameter value than others. In the case that no preferences can be justified, uniform distribution will be specified, i.e., each value between minimum and maximum is equally likely the appropriate parameter value. As a consequence of this specification of probability distributions of input parameters, the code results also show a subjective probability distribution, from which uncertainty limits or intervals are derived. Alternatively, Jeffries priors maximizing Shannon's information entropy can be chosen. But to apply these tools of Bayesian inference, assumptions about the distribution function and its support have to be made /JAY 68/.

Whether epistemic uncertainties can be combined with stochastic uncertainties in one common analysis or not, and what would be consistent approaches, is the subject of considerable debate. It can be pointed out, though, that parameter distributions for epistemic uncertainty can be interpreted as level 2 distributions in a two-level statistical model determining the parameters of level 1 distributions for stochastic uncertainty.

Finally, the application of Wilk's formula requires the sample to be random, which is a fundamental assumption in the order statistics approach used to derive the formulas given above (see, e.g., also /POR 19/). Consequently, Wilks formula cannot be applied to non-random samples, e.g., samples obtained by applying latin hypercube sampling. (Applying Wilks' formula to a non-random sample does not lead to grossly wrong results.

Worse, the results are meaningless, as there is no valid claim on any confidence interval.) There are methods to derive non-parametric confidence intervals for non-random samples, see, e.g., /LOH 96/, but these are outside the scope of this discussion.

As the sample has to be (sufficiently) random for Wilks' formula to be valid, ensuring sample randomness when using numerical pseudo-random number generators is important. Performing tests of randomness for the (unordered) samples from the uniform distribution that are commonly used to determine parameter value realizations via their inverse cumulative distribution functions is a good idea. Generally, larger samples sizes should be less susceptible to lack of randomness.

Further information on these topics can be found e.g. in the documentation of the GRS Software SUSA /KLO 20/, /KLO 17/.

6.3.1 Application to time series data

The original setting for which Wilks developed his approach was a sample from a discrete set of items (e.g., for quality control during production). Given that a simulation code produces time series for multiple output variables, looking into the application to time series data is important. Obviously, within each time point, output results have to be treated as completely dependent. However, also between the time points, the results should be assumed to be completely dependent – there is a reason for the "deterministic" in deterministic safety analysis with simulation codes. From this it follows that different time points do not increase the sample size and that removing extreme samples for a specific point in time will necessitate removing the whole time series data for the removed samples.

Moreover, this implies that care is needed when defining acceptance criteria. Criteria related to maximum or minimum results within a time window possibly aggregating over multiple output variables (like, e.g., peak cladding temperature) will be easier to handle than similar CV specific results possibly at a specific point in time. For the latter, a larger number of figures of merit have to be controlled simultaneously, increasing the number of required simulations runs. If, e.g., cladding temperatures of 5 fuel rods at 4 locations would be controlled separately, this would mean 20 figures of merit, requiring a coverage of $N - 20$ at a maximum for one-sided tolerance limits.

6.3.2 Reliability of passive safety systems

Passive safety systems are sometimes claimed to have exceptionally high reliability due to their reliance on physical phenomena and lack of active parts, excluding several common failure mechanisms (e.g., failure of electrical power supply). One question is then how to justify reliability claims for such systems. One approach would be to perform uncertainty analyses for such a system with a system code such as ATHLET. Neglecting that extreme percentiles of model parameter uncertainty distributions are hardly quantified reliably, although functional failures of a passive system might be associated with such extremes, we are faced with a practical challenge. If the reliability to be justified is 0.99999 (i.e., a failure probability of 10^{-5}) at a confidence level of 0.9, and if at least one sample should be outside of the coverage, then at least 388971 samples would be needed. This will hardly be feasible and motivates the search for more targeted approaches for determining failure modes of passive systems.

6.3.3 Treatment of Code Crashes

When performing uncertainty analyses following the GRS method, values for uncertain parameters are samples based on probability distributions. Given that the specific form of those distributions (e.g., normal, log-normal or uniform), their support (i.e., range) and the distribution parameters are often still the result of expert judgement or derived from the comparison of a correlation against experiments instead of applying inverse uncertainty quantification with the actual simulation code, the sampled values can be inconsistent with requirements of ATHLET. This can lead to the failure of a sample simulation (generally stops due to too small time step size or violations of ATHLET property package range of validity, but a more severe error can occur). Firstly, such failures should be analysed. It might be that the sampled uncertain parameter value is clearly unphysical and causes the crash. This should be reflected in an update of the underlying distribution at the next opportunity. Otherwise, a bug report should be raised, unless the stop is clearly spurious and due to well-known instabilities of two-phase thermal hydraulics with ATHLET.

From a practical point of view, the question is then what to do with the overall uncertainty analysis. As pointed out in /POR 19/, applying Wilks' formula with the minimum number of required simulations will not be possible with code crashes, since these cannot be subjected to ordering. However, as pointed out by Tukey /TUK 47/, /TUK 48/ and Wilks /WIL 48/, these results of order statistics are valid independent of the underlying distribution and only look at the sample. Consequently, they apply to any valid (i.e.,

uncensored and unbiased) subset of the N samples performed in the original analysis. That means, that different to /POR 19/, code crashes can be removed from the sample, if this clearly does not result in a censoring of valid extreme values or introducing a bias, which strongly distorts the sample from the results of the specified uncertainty distributions. While Porter is correct in pointing out that often code crashes are related to (input) parameter settings, this is not always the case. And even if, there might be simply unlucky parameter settings that triggered that crash and that do not invalidate the sample as random. (One example would be the water level of a mixture level track in ATHLET, which can take almost any value except *exactly* at a CV boundary.) This needs to be confirmed by the analysis mentioned above.

Importantly, if unjustified censoring of extreme values of the *sample* cannot be excluded, even replacing a crashed simulation by drawing a new sample is not admissible. This is also the case if significant bias in the extreme values of the *sample* is introduced. In this case, either ATHLET needs to be improved (a bug report) or the underlying uncertainty distributions need to be adjusted and the whole analysis repeated. Note that introducing a bias into the sample that only affects central ranks would not have an impact on results, but it might make the sample non-random. Notably, while Wilks' formula itself is distribution-free, any distorted sample can be used if and only if it is still a random sample.

A more formal approach to demonstrating randomness of the remaining samples would be the following. Usually, samples are drawn from a uniform distribution for each uncertain parameter in order to determine its specific value for the analysis. The unordered set of samples from the (multivariate) uniform distribution after removing those for code crashes can be considered and compared to the original unordered set. The hypothesis to be tested is that the pruned unordered set is still randomly uniformly distributed. If this hypothesis cannot be rejected (and if the test results are not worse than for the original sample from the uniform distribution), then the remaining sample can be seen as still random.

In order to make it possible to remove crashed simulations – and thus averting redoing the whole analysis or re-calculating a crashed case with a new sample – it is reasonable to initially specify more than the minimum needed simulations for the uncertainty analysis or even to choose a higher rank order than the minimum acceptable rank order for the analysis.

6.3.4 Sensitivity Analysis

Another important feature of the method is that one can determine sensitivity measures of the influence of uncertainties in input parameters on the uncertainties of results. This information can provide guidance as to where to improve the computer code or to perform additional experiments (i.e. improve the state of knowledge) in order to reduce the output uncertainties most effectively. Sensitivity measures like Standardized Rank Regression Coefficients and Correlation Ratios permit a ranking of input uncertainties with respect to their relative contribution to code output uncertainty. The difference to other uncertainty methods is that the ranking is a result of the analysis, not of prior estimates and judgements. Uncertainty statements and sensitivity measures are available simultaneously for all single-valued (e.g. peak cladding temperature) as well as continuous valued (time dependent) output quantities of interest. The GRS method relies only on actual code calculations without using approximations like fitted response surfaces.

The different steps of the uncertainty analysis are supported by the software system SUSA (Software System for Uncertainty and Sensitivity Analyses), also developed by GRS and continuously updated incorporating new features /KLO 20/.

6.3.5 Input uncertainties and the GRS method

The GRS method makes no assumptions on the underlying probability distributions. One question is then, how input uncertainties influence the results of the uncertainty analysis. That answer is straight forward in the general case: The values of any percentiles obtained by the GRS method do depend on the underlying uncertainty distributions, their specific range as well as percentiles, and on any correlations between those.

The next question is then, if extreme ranks in the sample of simulations correspond to extreme percentiles in the underlying input distributions. That answer in the general case, unfortunately, is no.

Simulation models for thermohydraulic analyses are non-linear, at times strongly so, and they can be non-monotonous for input values as well. They may exhibit cliff-edge effects, even without digitally operating model elements like switches. Moreover, the characteristics of a simulation can be different for different points in time. This has strong consequences. If we consider an analysis with n input uncertainty distributions and m figures of merit, the simulation model induces a function $A: \mathbb{R}^n \times \mathbb{R} \rightarrow \mathbb{R}^m \times \mathbb{R}$, $y_m(t) = A^{m \times n}(t) x_n(t)$. This function does not need to be continuous. The topological structure of

$\mathrm{Im}\big(A(t)\big)$ might be complicated, it might not be convex, it can consist of separate sub-manifolds and be non-contiguous. If two points in $\mathrm{Im}\big(A(t)\big)$ are close to each other, they might have any distance in the domain for the underlying distributions. Conversely, two points that are close in the input distribution domain might have any distance in the figure of merits codomain $\mathrm{Im}\big(A(t)\big)$. In short: $A(t)$ does not need to be a homeomorphism, neither globally nor even locally.

It is well known that thermohydraulic models can be non-hyperbolic, even without severe accident phenomena and I&C models. A consequence of this is that numerical integration might no longer converge weakly to a common solution, so that even without any model changes simple changes in details of integration could lead to cliff-edge effects. Explicit couplings and using numerical methods without effective error control for some models can exacerbate that situation. So small changes in input parameters can lead to uncontrolled variations in outputs. Unfortunately, the actual physical systems can and do sometimes show similar characteristics. Against this background, it is recommended to include numerical integration settings in uncertainty analyses.

So, in the general case, few if any conclusions can be drawn on the underlying input uncertainties from the results of an uncertainty analysis (with the GRS method). This will require expert judgement and a clear understanding of theoretical properties of a specific model. That has unfortunate consequences for ersatz-models used for uncertainty analysis. It has to be shown for each simulation model (i.e. input deck and analysis case) that the ersatz-model is representative of the full model. And, considering the remarks above, this might have to be demonstrated for each point in time. Stronger claims would need theoretical insights and expert judgement for specific models. This has not discouraged research in this field so far.

In actual analyses, it is often reasonable to assume that the non-central percentiles of input uncertainty distributions do strongly influence extreme ranks and/or percentiles of the figures of merit. For that reason, the estimation and/or determination of input uncertainty ranges as well as distribution forms merits attention by the analyst. As for any analysis, the common chestnut “rubbish in, rubbish out” does apply to uncertainty analyses as well. For this reason, determining adequate uncertainty distributions for a code and a simulation model is a continuous challenge for any simulation code that must be met during development, validation, and application.

6.4 Quantification of the Code Physical Model Uncertainties

Among input uncertainties evaluation the identification and quantification of physical model uncertainties in thermal-hydraulic codes appears to be particularly difficult. In the course of NEA/CSNI projects UMS /NUC 09/, BEMUSE /CRÉ 08/, /PER 11/, and PREMIUM /SKO 19/ a frequently observed problem was definition of unrealistic ranges of model uncertainties. Another problem was ignoring of some models by uncertainty analyses due to leak of information concerning the model. The reason is that the code users performing uncertainty analyses are frequently not really familiar with physical models of the code.

As the uncertainty analyses are always case related, input uncertainties identification and quantification are performed by code users within the actual analysis. In the past some systematic approaches for input uncertainties quantification have been proposed, e.g. /UNA 11/. However, the problem of physical model uncertainties quantification remains substantial. New code users performed uncertainty analyses, are faced with the same problems and frequently perform the same errors. The current trend is to develop more detailed approaches for input uncertainties evaluation to add users by the difficult task of input uncertainties quantification.

Whereas the input uncertainties like initial and boundary conditions, numerical integration settings, coupling schemes, facility geometry or transient related parameters are clearly related to the analysed case (facility and transient); the model uncertainties are rather code related. In the current approach the quantification of model uncertainties is an integral part of each uncertainty analysis. However, the users performing uncertainty analyses frequently expect information about model uncertainties from code developers. Following this need the quantification of the uncertainty of the models of the code ATHLET was undertaken.

It is advantageous to perform the quantification by a formalised approach. The evaluation of ATHLET model uncertainties was performed according to the steps of the methodology proposed in /SKO 04/.

1. Target (s) identification, e.g., uncertainty of best estimate calculation of a SB LOCA,
2. Elicitation process of potentially important uncertain input parameters
3. Parameter selection

4. Quantification of uncertain parameters

5. Transformation of input uncertainties into code input data

The basis of model uncertainties quantification is the evaluation of separate effect tests. Other information sources for quantification of model uncertainties are combined effect tests, experience from code validation by integral experiments, survey of the experts' state of knowledge, comparison with published related analyses, deriving uncertainties directly from literature, and if necessary, applying theoretical physical limitations. However, utilising published statements concerning model uncertainties, it should be made sure that the published results consider exactly the applied model, and that the correlations are implemented in the code correctly.

Modelling uncertainties are represented by additional uncertain input parameters. Generally, there are three possibilities of introducing output variations associated with its uncertainty into the code model:

Modelling uncertainties are represented by additional uncertain input parameters. Generally, there are three possibilities of introducing output variations associated with its uncertainty into the code model:

- adding on or multiplying correlations by a corrective term,
- variation of a key parameter of the model (frequently available in the code input)
- a set of alternative model formulations.

The results of the performed quantification are presented in Tab. 6.6

Tab. 6.6 Quantification of model uncertainties /AUS 09/, /AUS 13a/

No.	Parameter	Parameter explanation	Component/ Geometry	Ranges		Reference	Distribution	Quantification
				min	max			
Critical discharge								
1	TURB	Turbulence factor for evaporation in critical break flow model	Break	1.0	50.0	20.0	Log-normal μ=2.29, σ=0.65, shift=1.0, truncated over [0.0, 50.0]	Super Moby Dick and Sutherland – Sozzi separate effect experiments /SOZ 75/
2	FCONTR	Contraction factor for vapour discharge through an orifice – (CW DISCHARGE)	Break	0.6	1.0	0.9	Trapezium: 0.6 – 0.7 – 0.9 – 1.0	Literature /TRU 68/, /JOB 55/, /RIE 96/
Quench model								
3	CQHTWT	Heat transfer coefficient of rewetted side, upper quench front	Reactor core	$1x10^4$	$1x10^5$	$3x10^4$ W/m^2K	Log- uniform	FEBA, SCTF, FLECHT separate effect tests
4	CQHTWB	Heat transfer coefficient of rewetted side, lower quench front	Reactor core	$1x10^5$	$1x10^6$	$3x10^5$ W/m^2K	Log- uniform	FEBA, SCTF, FLECHT, PERICLES separate effect tests
Wall heat transfer								
5	OHWFC	Correction factor for single phase forced convection to water (Dittus-Boelter)	All heat slabs	0.85	1.15	1	Uniform	KWU tests with 25-rods bundle analyses /VOJ 82/ and expert judgement

No.	Parameter	Parameter explanation	Component/ Geometry	Ranges		Reference	Distribution	Quantification
				min	max			
6	OHWNC	Correction factor for single phase natural convection to water (Mc Adams)	All heat slabs	0.85	1.15	1	Uniform	KWU tests with 25-rods bundle analyses /VOJ 82/ and expert judgement
7	OHVFC	Correction factor for single phase forced convection to steam (Dittus-Boelter II)	All heat slabs	0.8	1.2	1.0	Uniform 50%	Literature /GOT 85/ and expert judgement
	OHVFC	Correction factor for single phase forced convection to steam (Mc Eligot)	All heat slabs	0.85	1.25	1.0	Uniform 50%	Literature /GOT 85/ and expert judgement
8	OHWFB	Correction factor for film boiling, modified Dougall-Rohsenow correlation	All heat slabs	0.65	1.3	1.0	Uniform 50%	Literature /GOT 85/, /NIJ 80/ and KWU tests with 25-rods bundle analyses /VOJ 82/
	OHWFB	Correction factor for film boiling, Condie-Bengston IV	Core	0.75	1.25	1.0	Polygonal 0.75-0.8-1.2-1.25 50%	Literature /GOT 85/, /NIJ 80/ and KWU tests with 25-rods bundle /VOJ 82/
10	OTRNB	Correction factor for critical heat flux, Biasi correlation – multiplication factor	All heat slabs	0.7	1.3	1.0	Uniform	Literature /GOT 85/, /WIC 91/, /NIJ 80/

No.	Parameter	Parameter explanation	Component/ Geometry	Ranges		Reference	Distribution	Quantification
				min	max			
10	OTRNB	Correction factor for critical heat flux, minimum value – multiplication factor	All heat slabs	0.7	1.3	1.0	Uniform	Literature /GOT 85/, /WIC 91/, /NIJ 80/
11	OHWNB	Correction factor for nucleate boiling (modified Chen correlation)	All heat slabs	0.8	1.2	1.0	Uniform	KWU tests with 25-rods bundle analyses /VOJ 82/ and expert judgement
12	OHWPB	Correction factor for pool film boiling at natural convection (Bromley correlation)	All heat slabs	0.75	1.25	1.0	Uniform	Literature /WAN 83/, tests with 25-rods bundle analyses /VOJ 82/ and expert judgement
13	OTMFB	Correction factor for minimum film boiling temperature (Groeneveld-Stewart correlation)	All heat slabs	0.9	1.30	1.0	Uniform	Literature /WIC 91/, KWU tests with 25-rods bundle analyses /VOJ 82/ and Ω experiment
Zr- oxidation								
14	OMOXR	Correction factor for oxidation rates	Fuel rods	0.9	1.1	1.0	Uniform	Literature /FIC 04/, /VOL 04/and expert judgement
Evaporation								

No.	Parameter	Parameter explanation	Component/ Geometry	Ranges		Reference	Distribution	Quantification
				min	max			
15	ZBO	Number of bubbles per unit volume (m^{-3})	Whole thermal-hydraulic system	10^8	10^{10}	$5x10^9$ $1/m^3$	Log-triangular	Moby Dick and Sozzi& Sutherland critical discharge experiments /SKO 97/, numerous integral experiments and user experience
16	ZTO	Number of droplets per volume (m^{-3})	Whole thermal-hydraulic system	10^8	10^{11}	$5x10^9$ $1/m^3$	Log-triangular	Moby Dick and Sozzi& Sutherland critical discharge experiments /SKO 97/, RBHT reflooding tests, numerous integral experiments and user experience
17	OADDI	Limiting of vapour specific volume for evaporation rate at low pressure	Whole thermal-hydraulic system	0.2	1.2	0.2	Uniform	Theoretical basis of evaporation model and expert judgement
Condensation								
18	OMCON	Correction factor for direct condensation	Whole thermal-hydraulic system	0.5	2.0	1.0	Histogram 0.5-1.0-2.0 / 50%-50%	HDR condensation tests /TES 93/, UPTF-TRAM experiment /PAP 96/ and expert judgement
Drift models								
19	ODBUN	Correction factor for relative velocity at vertical bundle (flooding based drift flux model)	Rod bundle	0.3	1.5	1.0	Normal $\mu = 0.84$, $\sigma = 0.28$, truncated over [0.3, 1.5]	Validation on the basis of bundle boil off experiments /LEF 98/ and expert judgement

No.	Parameter	Parameter explanation	Component/ Geometry	Ranges		Reference	Distribution	Quantification
				min	**max**			
20	ODVPI	Correction factor for relative velocity in vertical pipe flow	Vertical and inclined pipes	0.5	1.5	1.0	Trapezium 0.5 – 0.7 – 1.2 – 1.5	Validation on the basis of GE vessel blow-down tests, Wilson drift tests, Toshiba tests /SKO 88a/ and numerous other experiments
21	ODANU	Correction factor for relative velocity in vertical annular flow	Annular geometry – downcomer	0.4	2.0	1.0	Histogram 0.4-1.0-2.0 / 50%-50%	Expert judgement
22	ODHPI	Correction factor for interfacial shear in horizontal pipe flow	Horizontal flow paths	0.75	2.25	1.0	Polygonal	TPTF and IVO /SKO 88b/ experiments and expert judgement
23	ODHCC	Correction factor for relative velocity in horizontal cross-connections	Cross-connections in core and upper plenum	0.5	2.5	1.0	Uniform	LSTF experiment and expert judgement
Liquid entrainment (both one and two momentum equation models)								
24	OENBU	Correction factor for velocity of transition from non-dispersed to dispersed droplet flow in vertical bundle	Core	1.0	3.0	1.0	Uniform	FLECHT and FEBA experiments and expert judgement
Interfacial shear								

No.	Parameter	Parameter explanation	Component/ Geometry	Ranges		Reference	Distribution	Quantification
				min	max			
25	OIHST	Correction factor for interfacial shear in stratified and wavy horizontal pipe flow	Horizontal flow paths	0.2	2.0	1.0	Histogram 0.2-1.0-2.0 / 50%-50%	IME of Toulouse separate effect experiment /FAB 87/, /SKO 94/
26	OIHSB	Correction factor for interfacial shear in bubbly, slug and churn turbulent horizontal pipe flow	Horizontal flow paths	0.35	3.5	1.0	Histogram 0.35-1.0-3.5 / 50%-50%	ANL experiments analyses /ISH 79/ and expert judgement
27	OIHT1	Correction factor for critical velocity of transition from stratified to slug flow in horizontal pipes	Horizontal flow paths	0.5	1.5	1.0	Uniform	Validation on the basis of TPTF and Mantilla tests /LAN 22/ and UPTF experiments /SKO 01/
28	OIHT2	Correction factor for velocity of transition from non-dispersed to dispersed droplet flow in horizontal pipes	Horizontal flow paths	0.6	1.2	1.0	Uniform	Mantilla and TPTF experiments /LEE 22/, UPTF experiments and expert judgement
29	OIVPI	Correction factor for interfacial shear in non-dispersed vertical pipe flow	Vertical and inclined pipes	0.35	2.5	1.0	Histogram 0.35-1.0-2.5 / 50%-50%	GE vessel blow down tests, Wilson drift tests, Toshiba tests and numerous other experiments

No.	Parameter	Parameter explanation	Component/ Geometry	Ranges		Reference	Distribution	Quantification
				min	max			
30	OIBUN small scale	Correction factor for interfacial shear in non-dispersed vertical bundle flow	Core	0.15	2.5	1.0	Log-triangular 0.15 – 0.84 – 2.5	PERICLES and THETIS boil off tests
	OIBUN large scale	Correction factor for interfacial shear in non-dispersed vertical bundle flow	Core (rough nodalisation) (counter-current flow in reactor needs min. value 0.01)	0.01	2.5	1.0	Histogram 0.01-0.84-2.5 / 50%-50%	LOFT L2-5 experiment
31	OIANU small scale	Correction factor for interfacial shear in non-dispersed vertical downcomer flow	Annular geometry – downcomer	0.15	3.0	1.0	Histogram 0.15-1.0-3.0 / 50%-50%	Expert judgement and LOFT L2-5 experiment
	OIANU large scale (rough nodalisation)	Correction factor for interfacial shear in non-dispersed vertical downcomer flow	Annular geometry – downcomer (counter-current flow in reactor needs min. value 0.05)	0.05	3.0	1.0	Histogram 0.33-1.0-3.0 / 50%-50%	Expert judgement and LOFT L2-5 experiment

No.	Parameter	Parameter explanation	Component/ Geometry	Ranges		Reference	Distribution	Quantification
				min	**max**			
32	OIVTP	Correction factor for critical velocity of transition from non-dispersed to dispersed droplet flow in vertical pipe and downcomer	Vertical and inclined flow paths except core	1.0	2.0	1.0	Uniform	Validation on the basis of Harwell experiments by Whalley and Fells /SKO 99/ and expert judgement
33	OIVDI	Correction factor for interfacial shear in dispersed vertical droplet pipe flow	Vertical and inclined flow paths	0.3	1.5	1.0	Uniform	ANL experiments analyses /ISH 79/ and expert judgement
34	OIHDI	Correction factor for interfacial shear in dispersed horizontal droplet pipe flow	Horizontal flow paths	0.2	1.4	1.0	Uniform	ANL experiments analyses /ISH 79/ and expert judgement
Wall shear								
35	OFRIC	Void fraction dependent correction coefficient for fraction of water and steam in total wall friction (correction of standard distribution)	Whole thermal hydraulic system	-3.2	4.0	0.0	Uniform Max. correction of wall friction distribution at void=0.5 : vapour fraction of total wall friction is 80 % for k=-3.2; water fraction is 100% for k=4.0	Expert judgement

No.	Parameter	Parameter explanation	Component/ Geometry	Ranges		Reference	Distribution	Quantification
				min	max			
Two-phase pressure drop								
36	OFI2V	Correction factor for two-phase multiplier in vertical pipe, Martinelli-Nelson correlation	All flow paths in thermal-hydraulics system	~0.2	~2.0	1.0	Log-normal μ = -0.247, σ = 0.339	Literature /BEA 82/
37	OFI2H	Correction factor for two-phase multiplier in horizontal pipe, Martinelli-Nelson correlation	All flow paths in thermal-hydraulics system	~0.1	~2.0	1.0	Log-normal μ = -0.545, σ = 0.411	Literature /BEA 82/
Mixture level (M-L) model								
38		Heat transfer through the M-L surface	Vertical flow paths with M-L					Not yet quantified by GRS
39		Mass transfer through the M-L surface	Vertical flow paths with M-L					Not yet quantified by GRS
T-junction model								
40		Critical length for onset of water entrainment	T-Junction					Not yet quantified by GRS
41		Critical length for onset of vapour pull-through	T-Junction					Not yet quantified by GRS

6.5 Example of Application

In the course of ATHLET validation several uncertainty and sensitivity analyses have been performed. They are related directly to the code development. The sensitivity statements show which models contribute mostly to the uncertainty of the calculations. It indicates the potential code modifications and developments with the aim of improvement of code simulation accuracy.

The uncertainty and sensitivity analyses performed for the code ATHLET include different kinds of thermal-hydraulic experiments but also nuclear reactor applications.:

Analyses of combined effect tests:

- FEBA and PERICLES reflooding experiments /SCH 15/, /SKO 17/,
- French OMEGA rod bundle test 9, a blowdown experiment with a PWR type bundle /GLA 94a/, /GLA 94b/

Analysis of experiments performed at integral test facilities:

- PMK experiment “pressurizer surge line break” /HOR 01/
- LOFT test L2-5 200 % cold leg break /GLA 01a/, /CRÉ 08/
- ROSA/LSTF test SB-PV-09 small leak in the reactor upper head, /SKO 11b/
- ATLAS experiment 50 % break at the DVI line /AUS 13a/, /AUS 13c/

Analysis of experiment performed at NACIE test facility with molten metal as cooling medium - calculation of transient behaviour of two-phase flow in the closed loop /SCH 18/.

Analyses of reactor calculations, e.g.: 5 % cold leg break in a German 1300 MW PWR /GLA 01b/, 200 % cold leg break of Zion Westinghouse type PWR reactors /GLA 08b/, /SKO 09/.

To illustrate the application of the GRS methodology, the main results of the uncertainty analysis for the LSTF test SB-CL-18 will be presented in a summarized form. This

experiment belongs to the validation matrix of ATHLET, and the corresponding validation calculation with the current code version is described in chap. 5.1.

The main physical phenomena observed during this test were two dry outs of the heater rod bundle simulating the core. The first one was due to water level depression (120 - 155 s) before the loop seal cleared, and the second one (420 - 540 s) was due to the loss of water inventory at the break, which was finished by the accumulator injection.

All potentially important uncertain parameters have been included in the uncertainty analysis /GLA 01c/. Tab. 6.7 lists the selected input parameters, their specified ranges and distribution types. Included are 41 modelling parameters, 4 uncertainties related to the simulation of the bypass flow cross sections in the test vessel, 1 uncertain heater power and 2 uncertain convergence criteria of the numerical integration method of the code. The quantification of the model uncertainties is based on the experience gained from the ATHLET validation.

A total number of 100 ATHLET calculations was performed. According to Wilks' formula a minimum of 93 runs are required to establish two-sided tolerance limits with 95 % probability and 95 % confidence (see Tab. 6.1). Thus, at any time point, at least 95 % of the combined influence of all considered uncertainties on the calculated results is within the presented uncertainty range, at a confidence level of at least 95 %.

Tab. 6.7 List of uncertain input parameters for LSTF Test SB-CL-18 calculations

No.	Parameter	Ranges		Ref. value	Distribution	Explanation
		min	max			
Critical break flow						
1	DSCON	0.5	3	2.0	Polygonal	Contraction length
2	FD	0.02	0.22	0.02	Polygonal	Weisbach-Darcy wall friction coefficient
3	FF	0.7	1	0.775	Polygonal	Contraction coefficient for steam flow
4	PP	0.98	0.999	0.98	Polygonal	Void transition for contraction coefficient
Evaporation						
5	ZBO	10^8	10^{10}	$5x10^9$	Polygonal	Number of bubbles per unit volume
6	ZT	10^8	10^{10}	$5x10^9$	Polygonal	Number of droplets per unit volume
7	OMTCON	0.5	2	1	Uniform	Direct condensation multiplier
8	TURB	1	50	20	Log-normal	Turbulence factor for evaporation in CDR model
Drift models						
9	ODVRO	0.5	1.5	1	Polygonal	Correction factor for vertical pipes

No.	Parameter	Ranges		Ref. value	Distribution	Explanation
		min	max			
10	ODBUN	0.3	1.5	1	Normal	Correction factor for vertical bundles
11	ODVKU	0.7	1.3	1	Normal	Correction factor for vertical annulus
12	ODHPI	0.75	2.25	1	Polygonal	Correction factor for horizontal pipes
13	ODHBR	0.5	2	1	Uniform	Correction factor for horizontal cross flow connections
14	ODENT	1	3	1	Uniform	Correction factor for water entrainment in bundles
Two phase pressure drop						
15	ITMPO			1 or 4		Correlation selection (parameters 16 and 17)
16	OFI2H			1	Log-normal	Martinelli-Nelson correlation (ITMPO = 1) - horizontal Chisholm correlation (ITMPO = 4) - horizontal
17	OFI2			1	Log-normal	Martinelli-Nelson correlation (ITMPO = 1) - vertical Chisholm correlation (ITMPO = 4) - vertical
Pressure drop, wall friction						
18	ALAMO	0.01	0.03	0.02	Triangular	Pipe wall friction (ITMPO = 1)
19	ALAMO	0.01	0.03	0.02	Triangular	Rod bundle wall friction (ITMPO = 1)
20	ROUO	10^{-5}	10^{-4}		Polygonal	Pipe wall roughness (ITMPO = 4)
21	ROUO	1.510^{-6}	2.10^{-5}		Polygonal	Rod bundle wall roughness (ITMPO = 4)
Main coolant pump						
22	YHS	Table	Table	Table	Uniform	Two-phase multiplier for head and torque
Bypass flow paths						
23	CSA	0.01	0.6	0.47	Uniform	Bypass flow cross section between upper downcomer and upper plenum
24	CSA	0.2	1	0.62	Uniform	Bypass flow cross section between upper downcomer and upper head
25	ZFFJ/ZFBJ	0.4	2.5	1	Uniform	Correction factor for bypass form loss between rod bundle and upper head
26	ZFFJ/ZFBJ	0.33	3	1	Uniform	Correction factor for bypass form loss between upper plenum and upper head
Pressure drop, momentum term						
27	JDPA				0.25	Momentum flux term HL/UP from HL only (25%)
	JDPA				0.25	Momentum flux term HL/UP not computed (25%)
	JDPA				0.5	Momentum flux term HL/UP in both directions (50%)
28	JDPA				0.25	Momentum flux term CL/DC from CL only (25%)
	JDPA				0.25	Momentum flux term CL/DC not computed (25%)

No.	Parameter	Ranges		Ref. value	Distribution	Explanation
		min	max			
	JDPA				0.5	Momentum flux term CL/DC in both directions (50%)
29	JDPA				0.5	Momentum flux at rod bundle inlet not computed (50%)
	JDPA				0.5	Momentum flux at bundle inlet in both directions (50%)
27	JDPA				0.25	Momentum flux term HL/UP from HL only (25%)
Pressure drop, form losses						
30	ZFFJ/ZFBJ	0.667	1.5	1	Uniform	Correction factor for form loss at branches
31	ZFFJ/ZFBJ	0.5	2	1	Uniform	Correction factor for form loss at upper bundle plate
32	ZFFJ/ZFBJ	0.4	2.5	1	Uniform	Correction factor for form loss at DC cross connections
33	ZFFJ/ZFBJ	0.8	1.25	1	Uniform	Correction factor for form loss at surge line
Heat transfer						
34	IHTCI0			1 or 2		Selection of correlations (parameter 35)
35	OHWFB	0.65 0.75	1.3 1.25	1 1	Uniform Polygonal	Correction factor for FB, Dougall-Rohsenow (50%)Correction factor for FB, Condie-Bengston (50%)
36	ICHFI0			0 or 4		Selection of correlations (parameter 37)
37	OTRNB	0.7 0.7	1.3 1.3	1 1	Uniform Uniform	Correction factor for CHF, minimum value (50%) Correction factor for CHF, Biasi correlation (50%)
38	OHWFC	0.85	1.15	1	Uniform	Correction factor for single phase forced convection to water (Dittus-Boelter)
39	OHWNC	0.85	1.15	1	Uniform	Correction factor for single phase natural convection to water (Mc Adams)
40	IHTC30			1 or 2		Selection of correlations (parameter 41)
41	OHVFC	0.8 0.85	1.2 1.25	1 1	Uniform Uniform	Correction factor for single phase forced convection to steam (Dittus-Boelter II, 50%) Correction factor for single phase forced convection to steam (Mc Eligot, 50%)
42	OHWNB	0.8	1.2	1	Uniform	Correction factor for nucleate boiling (mod. Chen)
43	OHWPB	0.75	1.25	1	Uniform	Correction factor for pool film boiling (Bromley)
44	OTMFB	0.9	1.28	1	Uniform	Correction factor for minimum film boiling temperature
45	HTCL0	20	100	50	Uniform	Accumulator walls heat transfer coefficient (W/m^2K)

No.	Parameter	Ranges		Ref. value	Distribution	Explanation
		min	max			
Convergence criteria, heat power						
46	EPS	10^{-4}	10^{-2}	10^{-3}	Triangular	Convergence criterion (upper local relative error)
47	QROD0/00	0.99	1.01	1	Uniform	Correction factor for heater power (nominal: 10 MW)
48	CLIMX	0.1	1	0.2	Uniform	Correction factor for lower local absolute error for the void fraction (factor 1: $5x10^{-4}$)

Of special interest is the highest calculated cladding temperature. As it can be seen in Fig. 6.1, the experimental measurements at the elevation showing the highest temperatures, level 8, are generally inside the calculated uncertainty range. The calculated range of the second heat-up is slightly earlier than measured. The end of this heat-up phase is due to an early accumulator injection start due to a low range of calculated pressure in the primary coolant system.

The measured value for the first peak clad temperature at level 8 is 682 K, and the calculated upper uncertainty limit is 772 K. Sensitivity measures indicate the influence of the uncertainty in input parameters on the first peak clad temperature. For example, Fig. 6.2 shows the Spear- man Rank Correlation Coefficient used as sensitivity measure. The length of the bars indicates the sensitivity of the respective input parameter uncertainty on the result (here the peak clad temperature). The sensitivity measure gives the variation of the results in terms of standard deviations, when the input uncertainty varies by one standard deviation. Positive sign means that input uncertainty and results have the same direction., i.e. an increase of input uncertainty values tends to increase the clad temperature and vice-versa. For negative sign the input un- certainty and the result have opposite direction, i.e. increasing the parameter values tends to decrease the clad temperature and vice versa.

According to these quantities, the most important three parameters are the drift in horizontal pipes, the drift in vertical pipes, and drift in horizontal connections of the heater rod bundle. An increased drift in the horizontal bundle connection (decreased water droplet transport to the hot bundle regions) and increased drift in vertical pipes (impedes loop seal clearance) tend to increase clad temperature, whereas increased drift in the horizontal pipes impedes loop seal filling and results in lower clad temperatures.

A similar analysis can be made for the second peak clad temperature. The most important parameters in this case are the discharge contraction coefficient and drift in the heater rod bundle. An increased contraction coefficient leads to an earlier accumulator injection, and thus tends to decrease the peak clad temperature. A higher drift in the bundle results in increased clad temperatures in the upper bundle region.

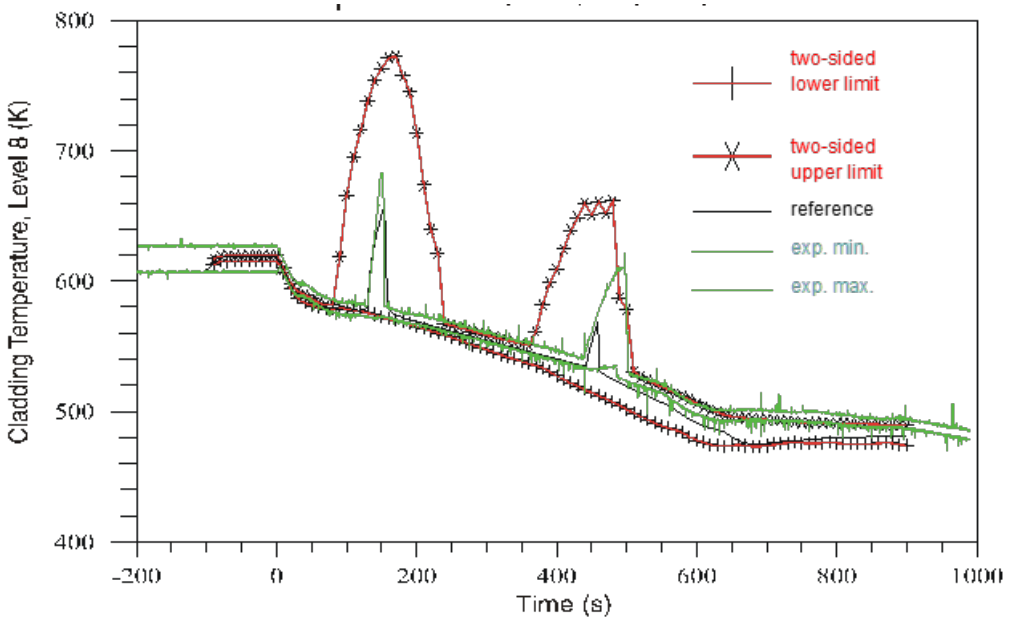

Fig. 6.1 Calculated uncertainty range and best-estimate reference calculation compared with measured minimum and maximum values of peak cladding temperatures at level 8 in LSTF Test SB-CL-18

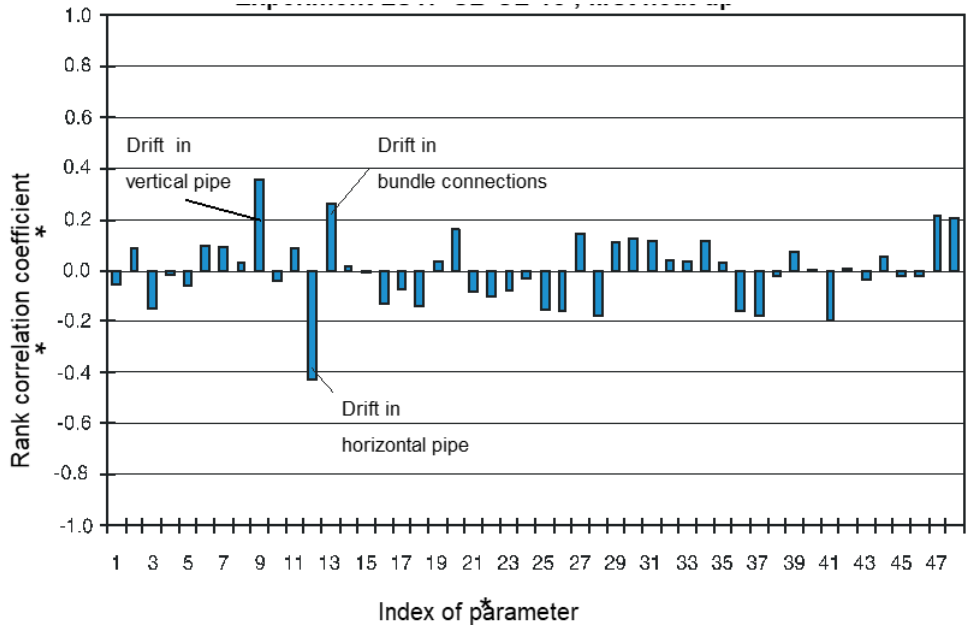

Fig. 6.2 Sensitivity measures of the first peak clad temperature for the 48 selected uncertain input parameters for the post-test calculation of LSTF SB-CL-18.

6.6 Conclusions

The validation concept for ATHLET is supported by a methodology to derive uncertainty statements quantifying the combined influence of all potentially important model, nodalisation, numerical, and experimental uncertainties of the calculated results.

A significant advantage of this methodology is that no a priori reduction in the number of uncertain input parameters by expert judgement or screening calculations is necessary to limit the calculation effort. All potentially important parameters may be included in the uncertainty analysis. The method accounts for the combined influence of all identified input uncertainties on code results.

The number of calculations needed is independent of the number of uncertain parameters accounted for in the analysis. It does, however, depend on the requested tolerance limits, i.e., the requested probability coverage (percentage) of the combined effect of the quantified uncertainties, and on the requested confidence level (percentage) of the code results. These tolerance limits can be used for quantitative statements about margins to acceptance criteria.

Another important feature of this method is that it provides sensitivity measures of the influence of the identified input parameter uncertainties on the results. The measures allow the derivation of an uncertainty importance ranking, which in turn provides guidance as to where to improve the state of knowledge in order to reduce output uncertainties most effectively, or where to improve code modelling. Different to other known methods, this ranking is a result of the analysis and its inputs, not of an a priori expert judgement. Uncertainty statements and sensitivity measures are available simultaneously for all single-valued parameters (e.g. peak cladding temperature) as well as for the time evolution of output quantities. This method relies only on actual code calculations without the use of approximations like fitted response surfaces.

The specification of ranges and probability distributions of input parameters may have a large influence on the uncertainty of code results, and thus on the quantification of the prediction capability. Current activities in the frame of prediction capabilities of best-

estimate codes are emphasizing these specifications. Investigations are underway to transform data measured in experiments and obtained in post-test calculations into thermal-hydraulic modelling parameters with uncertainties. It is more effective to concentrate on those uncertainties showing the highest sensitivity measures. The state of knowledge about uncertain parameters has to be further improved, and suitable experimental as well as analytical information has to be selected.

The GRS method has been used in different applications by various international institutions, e.g. in the frame of the OECD Uncertainty Methods Study /NEA 98/. Based on an increasing experience with generic applications to experiments and reactor transients, the method will allow the quantification of uncertainties in future ATHLET reactor calculations.

7 Summary and Validation Status of ATHLET 3.3.1

This report has briefly summarized the approach to the validation of ATHLET 3.4 for application to safety analyses of nuclear facilities and in particular LWR NPP. The overall validation approach for ATHLET 3.4 is firmly grounded in international good practice and used well-balanced validation matrices for all relevant phenomena and processes for LWR NPP, i.e. PWR, BWR and VVER reactor designs, and suitable integral test as well as separate test facilities. References to relevant validation calculations with ATHLET going back to the initial release version are given. These demonstrate the overall comprehensive validation status of the code for LWR NPP applications. In addition, further validation activities relating to passive safety systems, spent fuel pools as well as water-cooled pool-type research reactors are reported. This is complemented by validation of the coupling of ATHLET to 3D-neutron kinetics, coupling to CFD codes and validation to GEN-IV reactors.

Exemplary validation calculations demonstrate the quality of the current release version ATHLET 3.4 for twelve experimental facilities, covering both integral test as well as separate effect tests. Moreover, the range of tests presented in this report addresses are large subset of models in ATHLET, and most models needed for safety analyses of LWR NPP. The results show that ATHLET 3.4 has been successfully validated in all presented cases.

The validation report has also explained the quality assurance process for the on-going and systematic validation of ATHLET, which is part of the overall quality assurance processes of GRS for the verification and validation of ATHLET in line with IAEA SSG-2, Rev. 1. This includes important advice and guidance for organisations wanting to perform external validation of ATHLET.

The report closes with a brief explanation of the GRS method for uncertainty analyses and a brief example for its application for the in-depth validation of ATHLET.

Overall, the available information from validation calculations performed for the release of ATHLET 3.4 and the validation status previously reached for ATHLET 3.3.1 as well as earlier versions allows the following conclusions:

- ATHLET has been successfully validated for safety analyses of LWR reactor designs.

- ATHLET validation has been successfully extended to spent fuel pool applications as well as research reactors.
- ATHLET has been successfully validated for coupled thermal hydraulic-3D neutronics calculations with the combinations ATHLET/DYN3D (by HZDR), ATHLET/BIPR-VVER (by Kurchatov Institute) and ATHLET/FENNECS (by GRS).
- ATHLET has been successfully coupled to both ANSYS CFD as well as OpenFOAM. The extant coupling scheme work reliably for single-phase flow conditions. It can be considered validated, although care and targeted model qualification is needed when applying the coupling. Two-phase coupling is technically possible but should not be considered validated.
- ATHLET has been successfully applied to several Gen IV reactors, particularly liquid-metal cooled reactors. As validation matrices for these reactor types are still in development at GRS and there is a lack of systematic validation, no claims on validation of ATHLET for such reactor designs are made.

8 References

/ADA 84/ Adams, J. P., Birchley, J. C.: OECD LOFT Project, QUICK-LOOK REPORT ON OECD LOFT EXPERIMENT LP-LB-1. LOFT-T-3504: Idaho Falls, Idaho 83415, 1984.

/AKS 95/ Aksan, N., D'Auria, F., Städtke, H.: User Effects on the Transient System Code Calculations, Final Report. OECD Nuclear Energy Agency (NEA), NEA/CSNI/R(94)35, January 1995.

/ALT 98/ Alt, S., Lischke, W., Vandreier, B.: Verifikation des Thermohydraulikcodes ATHLET für die Bedingungen von WWER-Anlagen mit Experimenten der Versuchsanlagen PACTEL (Finnland) und HORUS-II (Hochschule Zittau/Görlitz), Schlussbericht. IPM-610205-05, 150 p., August 1998.

/ANO 80/ Anoda, Y., et al.: ROSA-III System Description, JAERI-M 9243. Japan Atomic Energy Research Institute (JAERI), December 1980.

/ANO 81/ Anoda, Y., et al.: ROSA-III System Description for Fuel Assembly No. 4, JAERI-M 9363. Japan Atomic Energy Research Institute (JAERI), February 1981.

/ANS 79/ American Nuclear Society (ANS): Decay Heat Power in Light Water Reactors, An American National Standard. American National Standards, ANSI/ANS-5.1-1979, 1979.

/ARI 95/ Arinine, V., Kirmse, R., Nikonov, S., Sakharova, O., Steinhoff, F.: Nachrechnung des Versuchs FIST6MSB1 mit ATHLET. GRS-A-, No. 2278, August 1995.

/ARN 97/ Arndt, S., Macek, J., Meca, R., Vojtek, I., Wolff, H.: Weiterentwicklung und Verifikation von Rechenprogrammen zur Analyse von Störfällen in WWER-Reaktoren, WTZ mit der Tschechischen Republik. GRS-A-, No. 2467, February 1997.

/ASN 17/ ASN: Qualification des outils de calcul scientifique utilisés dans la démonstration de sûreté nucleaire - 1re barrière, Réalisé conjointement avec IRSN. Guide No 28, 20 p., 25 June 2017.

/AUS 89/ Austregesilo, H., Barcus, M., Burwell, M. J., Kirmse, R., Loy, D., Müller, C. W., Pointner, W., Ringer, F. J., Sonnenburg, H.-G., Wolfert, K.: Auswertung von internationalen Integral- und Einzeleffekt-Experimenten. GRS-A-, No. 1625, November 1989.

/AUS 07/ Austregesilo, H.: Nachrechnung des ROSA/LSTF Versuchs SB-PV-09 mit ATHLET Mod 2.1 Cycle A. GRS-A-, No. 3369, March 2007.

/AUS 09/ Austregesilo, H., Krzykacz-Hausmann, B., Skorek, T.: Unsicherheits- und Sensitivitätsanalyse von Ergebnissen der Nachrechnung des ROSA/LSTF Versuchs SB-PV-09 mit ATHLET. Gesellschaft für Anlagen- und Reaktorsicherheit (GRS) mbH (GRS), GRS-A-, No. 3462, 132 p., March 2009.

/AUS 10/ Austregesilo, H., Bals, C., Erdmann, W., Horche, W., Krzykacz-Hausmann, B., Pointner, W., Schöffel, P. J., Skorek, T., Weber, S., Wielenberg, A.: Validierung des Rechenprogrammsystems ATHLET / ATHLET-CD, Abschlussbericht. Gesellschaft für Anlagen- und Reaktorsicherheit (GRS) gGmbH (GRS), GRS-A-3522, 557 p., April 2010.

/AUS 13a/ Austregesilo, H., Glaeser, H., Schöffel, P. J., Skorek, T.: Teilnahme am Internationalen Standardproblem ISP-50 mit ATHLET. Gesellschaft für Anlagen- und Reaktorsicherheit (GRS) mbH (GRS), GRS-A-, No. 3685, 137 p., March 2013.

/AUS 13b/ Austregesilo, H., Bals, C., Herb, J., Hollands, T., Papukchiev, A., Schöffel, P. J., Weber, S.: Validierung von Rechenprogrammen zur Simulation von Stör- und Unfällen im Reaktorkühlsystem. Gesellschaft für Anlagen- und Reaktorsicherheit (GRS) gGmbH (GRS), GRS-A-3706, 432 p., July 2013.

/AUS 13c/ Austregesilo, H., Skorek, T., Schöffel, P. J.: Simulation of the international standard problem ISP-50 with the system code ATHLET, Proc. Of the 15th International Topical Meeting on Nuclear Thermal-Hydraulics,. Pisa, Italy, May 2013.

/AUS 16/ Austregesilo, H.: Post-Test Calculation of ATLAS SBO Test A2.1 with ATHLET 3.1A. Presentation, 6th PRG Meeting of the OECD ATLAS Project, 17-18 October 2016, Korea Atomic Energy Research Institute (KAERI): Daejeon, 2016.

/BAC 20/ Baccou J., et al.: SAPIUM: Development of a Systematic Approach for Input Uncertainty Quantification of the Physical Models in Thermal-Hydraulic Codes, Good Practices Guidance Report. NEA/CSNI, NEA/CSNI/R, NEA/CSNI/R(2020)16, NEA/CSNI/R(2020)16, 2020.

/BAN 09/ Bandini, G., Meloni, P., Polidori, M.: Use of CATHARE at ENEA: Validation of CATHARE V2.5 against the PERSEO Tests, CATHARE Users' CLUB. Ed.: ENEA (ENEA): CEA / Grenoble, 3 June 2009.

/BEA 82/ Beattie, D. R. H., Whalley, P. B.: A simple two-phase frictional pressure drop calculation method. International Journal of Multiphase Flow, vol. 8, no. 1, pp. 83–87, 1982.

/BES 96/ Besette, D.: Status Report on the Use of Best-Estimate Methodology in Safety Analysis and Licensing, Report by the Task Group on Thermal-Hydraulic Applications (TG-THA o. OECD/NEA/CSNI, July 1996.

/BOR 93/ Bornemann, J.-T.: Nachrechnung des Versuches ROSA II Run 971 mit dem Rechenprogramm ATHLET/MOD1.0 - Cycle E. TÜV Bayern, May 1993.

/BOY 89/ Boyack, B., Duffey, R., Griffith, P., Lellouche, G., Levy, S., Rohatgi, U., Wilson, G., Wulff, W., Zuber, N.: Quantifying Reactor Safety Margins, Application of Code Scaling, Applicability, and Uncertainty Evaluation Methodology to a Large-Break, Loss-of-Coolant Accident. EG&G Idaho, Inc., NUREG/CR-, No. 5249, 31 December 1989.

/BRÄ 93/ Bräuer, B.: Dokumentation der Versuchsnachrechnung des Versuchs PKL III B2.1 mit ATHLET. Technische Notiz, TN-F3L-93-3, 46 p., 3 March 1993.

/BUC 15/ Buchholz, S., Cron, D. von der, Schaffrath, A.: System codes improvements for modelling passive safety systems and their validation. EUROSAFE Forum: Brussels, Belgium, 2015.

/BUC 18/ Buchholz, S., Mull, T., Wagner, T., Hristov, H., Gehr, R., Kaczmarkiewicz, N., Bonfigli, G., Sporn, M., Schuster, C., Schäfer, F., Schleicher, E.: EASY Integrale experimentelle und analytische Nachweise der Beherrschbarkeit von Auslegungsstörfällen allein mit passiven Systemen. Gesellschaft für Anlagen- und Reaktorsicherheit (GRS) gGmbH (GRS), GRS-, No. 527: Köln, August 2018.

/BUC 19/ Buchholz, S.: Nachrechnungen PERSEO Test 7 Part 1 und Part 2, TN-BUS-19/01. Technische Notiz, TN-BUS-19/01, February 2019.

/BUC 20/ Buchholz, S.: Nachrechnungen PERSEO Test 9, TN-BUS-20/01. Technische Notiz, TN-BUS-20/01, June 2020.

/BUC 23a/ Buchholz, S.: Recalculation of a PASI-Experiment. Technische Notiz, TN-BUS-23/01, March 2023.

/BUC 23b/ Buchholz, S.: AC2-ATHLET Simulations of PERSEO Test Facility. In: ANS (Ed.): NURETH 20. 20th International Topical Meeting on Nuclear Reactor Thermal Hydraulics, Washington, D.C., 20 - 25 August 2023, 2023.

/BUR 79/ Burtt, J. D.: International Standard Problem 13 (LOFT Experiment L2-5), Final Comparison Report, NUREG/CR-4115. December 1979.

/BUR 85/ Burwell, M. J., Romstedt, P.: Critical flow calculation and the evaluation of the critical plane location in a nozzle with a 1-D two phase flow model, Paper submitted to the “1985 European Two Phase Flow Group Meeting”,. Southampton, England, June 1985.

/BUR 89/ Burwell, M. J.: Post-Test Calculation of the LOBI Experiment A2-81 with ATHLET. GRS-A-, No. 1569, May 1989.

/BUR 92a/ Burwell, M. J.: Post-Test Calculation of the UPTF Test 10 Phase A (Run 80), Step 1 (0-200 s) with ATHLET. GRS-A-, No. 1893, March 1992.

/BUR 92b/ Burwell, M. J.: Post-Test Calculation of UPTF Test 30 with ATHLET. GRS-A-, No. 1890, March 1992.

/BUR 92c/ Burwell, M. J.: Post-Test Calculation of UPTF-Test Z3 Run 327 with Code System ATHLET-FLUT. GRS-A-, No. 1894, March 1992.

/BUR 94/ Burwell, M. J.: Nachrechnung des UPTF-TRAM A6 Run 01C Versuches mit ATHLET. GRS-A-, No. 2126, May 1994.

/BUR 01/ Burwell, M. J.: Nachrechnung des Einzeleffektversuchs UPTF C2 Run 7a und 9a mit ATHLET. GRS-A-, No. 2871, March 2001.

/BUR 03/ Burwell, M. J.: Nachrechnung des Einzeleffektversuchs UPTF TRAM C3 (Run 13a, Run14a) mit ATHLET. GRS-A-, No. 3123, June 2003.

/BUR 05/ Burwell, M. J., Pointner, W.: Auswertung der PKL-Versuche F1 und der ROCOM-Versuche zur Deborierung. GRS-A-, No. 3283, July 2005.

/CÁC 23/ Cáceres Castro, S. I., Kirsch, M., Kulenovic, R., Starflinger, J.: Heat transfer characteristics of a two-phase closed thermosyphon for passive spent fuel pool cooling. In: RMIT University: Joint 21st IHPC & 15th IHPS. Melbourne, 2023.

/CEU 15/ Ceuca, S., Pandazis, P.: Nachrechnung der ROCOM-Versuche 2.1 und 2.2 mit ATHLET unter Anwendung des 2D/3D-Modells im Ringraum und unteren Plenum, Technische Notiz TN-RCM-15/01. GRS, March 2015.

/CHO 12/ Choi, K. Y.: International Standard Problem No. 50, Final Integration Report. Ed.: NEA, NEA/CSNI/R, (2012)6, February 2012.

/CLE 92/ Clement, P., Chataing, T., Deruaz, R.: OECD/NEA/CSNI International Standard Problem No. 27, BETHSY Experiment 9.1B, 2”Cold Leg Break Without HPSI and With Delayed Ultimate Procedure, Comparison Report, Volumes 1 and 2. NEA/CSNI/R, (92) 20, November 1992.

/CON 98/ Consejo de Seguridad Nuclear (CSN): Garantía de calidad de las aplicaciones informáticas relacionadas con la seguridad de las instalaciones nucleares. Guía de Seguridad, No. 10.9, 14 p., 8 October 1998.

/CRÉ 08/ Crécy, A. de, Bazin, P., Glaeser, H., Skorek, T., Joucla, J., Probst, P., Fujioka, K., Chung, B. D., Oh, D.-Y., Kyncl, M., Pernica, R., Macek, J., Meca, R., Macian, R., et al.: Uncertainty and sensitivity analysis of the LOFT L2-5 test: Results of the BEMUSE programme. Nuclear Engineering and Design, vol. 238, no. 12, pp. 3561–3578, DOI 10.1016/j.nucengdes.2008.06.004, 2008.

/CRO 15/ Cron, D. von der, Hristov, H., Seubert, A.: Modeling of the Thermal Hydraulics of Very-High-Temperature Reactors with the System Code ATHLET. 2015.

/CSNI 89/ Committee on the Safety of Nuclear Installations (CSNI): Thermohydraulics of Emergency Core Cooling in Light Water Reactors, A State-of-the-Art Report by a Group of Experts of the NEA Committee on the Safety of Nuclear Installations. OECD Nuclear Energy Agency (NEA), CSNI Report No. 161, October 1989.

/DAV 22/ David, F., Al-Yahia, O. S., Prusek, T., Gomez, I., Buchholz, S.: PASI Pretests Analysis Results, PASTELS Deliverable D4.3. 31 January 2022.

/DEL 11/ Del Nevo, A.: Analytical Exercise on OECD / NEA / CSNI PKL-2 Project Test G.3.1: Main Steam Line Break Transient in PKL III Facility, TH / PKL-2 / 02 (10). Ed.: OECD /NEA / CSNI PKL-2 Project, March 2011.

/DFG 21/ Deutsche Forschungsgemeinschaft (DFG): Leitlinien zur Sicherung guter wissenschaftlicher Praxis, Kodex. korrigierte Version 1.1, September 2021.

/DIA 22/ Diaz-Pescador, E., Schäfer, F., Kliem, S.: On the validation of ATHLET 3-D features for the simulation of multidimensional flows in horizontal geometries under single-phase subcooled conditions. Nuclear Engineering and Technology, DOI 10.1016/j.net.2022.04.017, 2022.

/DRÄ 91/ Dräger, P.: Nachrechnung des Integralexperiments LOFT-LP-SB-3 mit ATHLET, GRS-A-1764. GRS, April 1991.

/DRÄ 98/ Dräger, P.: Nachrechnung des Versuchs UPTF/TRAM A7 (Run 1A) mit ATHLET. GRS-A-, No. 2557, April 1998.

/DRÄ 00/ Dräger, P., Horche, W., Jakubowski, Z., Pointner, W.: Störfallsimulator Unterweser, Qualifikation der Datenbasis. GRS-A-, No. 2802, March 2000.

/DRÄ 02/ Dräger, P., Horche, W., Jakubowski, Z., Pointner, W.: Störfallsimulator Philippsburg 2, Qualifikation der Datenbasis. GRS-A-, No. 3070, July 2002.

/EREC 95/ Electrogorsk Research & Engineering Centre on Nuclear Plants Safety (EREC): Russian Standard Safety Problem No. 1 (SSP-1) on ISB-WWER Test Facility 2.4% Small Leak From the Upper Plenum of the Reactor, Final Report 3.433 (in Russian language). Electrogorsk, Russia, 1995.

/EREC 97/ Electrogorsk Research & Engineering Centre on Nuclear Plants Safety (EREC): Russian Standard Safety Problem No. 2 (SSP-2) on ISB-WWER Test Facility 11% Leak From the Upper Plenum of the Reactor With Subsequent Trip of Circulation Pumps, Final Report 2.468 (in Russian language). Electrogorsk, Russia, 1997.

/FAB 87/ Fabre, J., Masbernat, L., Suzanne, C.: Experimental Data Set No. 8: Stratified Flow, Part II: Interfacial and Wall Shear Stress. Multiphase Science and Technology, vol. 3, No. 1-4, pp. 302–315, DOI 10.1615/MultSciEnTechn.v3.i1-4.130, 1987.

/FED 14/ Федеральная служба по экологическому, технологическому и атомному надзору (Ростехнадзор): АТТЕСТАЦИОННЫЙ ПАСПОРТ ПРОГРАММНОГО СРЕДСТВА Регистрационный номер 350 от 17 апреля 2014 года, «ATHLET (версия 2.1A_A)». 17 April 2014.

/FED 18/ Федеральная служба по экологическому, технологическому и атомному надзору (Ростехнадзор): АТТЕСТАЦИОННЫЙ ПАСПОРТ ПРОГРАММНОГО СРЕДСТВА Регистрационный номер 455 от 24 октября 2018 г, «ATHLET/BIPR-VVER (версия 1.0)». 24 October 2018.

/FEI 93/ Fei, L., Thiele, T.: Nachrechnung des Versuches UPTF-TRAM A2 mit dem Systemcode ATHLET, Report Nr. 9308. Dr. Pitscheider Ingenieur-Büro, 1993.

/FES 93/ Fessel, M., Kraus, B., Lischke, W., Vandreier, B.: Beiträge zur Verifikation des Rechencodes ATHLET: Analyse der Experimente am Einzelrohrversuchsstand HORUS I, Project BMFT-150 0856 0. HTWS Zittau, June 1993.

/FIC 04/ Fichot, F., Adroguer, B., Volchek A., Zvonarev, Y.: Advanced treatment of zircaloy cladding high-temperature oxidation in severe accident code calculations, Part III: Verification against representative transient tests. Nuclear Engineering and Design, no. 232, pp. 97–109, 2004.

/FJO 94/ Fjodorov, A., Kraus, B., Lischke, W., Schöße, T.: Analyse der Experimente am Einzelrohrversuchsstand HORUS II., Report THZ-61205-13. Hochschule für Technik, Wirtschaft und Sozialwesen TWS Zittau/Görlitz (FH), September 1994.

/FJO 96/ Fjodorov, A., Lischke, W.: Kondensation von Wasserdampf-Inertgas-Gemischen - Analyse der Experimente am Versuchsstand HORUS II mit den ATHLET-Code Versionen MOD 1.1 Cycle B und C, Report THZ-61205-15. Hochschule für Technik, Wirtschaft und Sozialwesen TWS Zittau/Görlitz (FH), May 1996.

/FJO 98/ Fjodorow, A.: Modellierung von Wärmeübergangsvorgängen bei der Kondensation in horizontalen Rohren mit Anwendung in der Störfallanalyse von Leichtwasserreaktoren. Dissertation, Technische Universität Dresden (TUD), 1998.

/FOR 90/ Forge, A., Mezza, M., Pochard, R., Porracchia, A., Hobbhahn, W., Skorek, T., Teschendorff, V., Weber, J. P., Schindler, M.: Comparative calculations on selected two-phase flow phenomena using major PWR system codes. Commission of the European Communities DG Science, Research and Development (EC), EUR 12901 EN, ISBN 92-826-1635-5, Commission of the European Communities: Luxembourg, 1990.

/GAR 73/ Garner, R. W.: Comparative analyses of standard problems - Standard problem 1, Straight Pipe Depressurization Experiments. Aerojet Nuclear Company: Idaho Falls, October 1973.

/GAS 91/ Gasteiger, H.: Post Test Calculation of UPTF Test 18 with the Code System ATHLET/FLUT. TÜV Bayern, June 1991.

/GAS 93/ Gasteiger, H.: Nachrechnung des Versuches PKL III B1.2 mit dem Rechenprogramm ATHLET/MOD1.1 - Cycle A. TÜV Bayern, May 1993.

/GAX 95/ Gashenko, M. P., Proshutinsky, A. P., Stolyarov, E., Elkin, I. V.: ISB-WWER: Description and Geometrical Characteristics, Measurement System Description, Heat Losses. Electrogorsk Research & Engineering Centre on Nuclear Plants Safety (EREC): Electrogorsk, Russia, 1995.

/GAX 97/ Gashenko, M. P., Proshutinsky, A. P., Stolyarov, E., Elkin, I. V.: The Russian Standard Problem No. 2 (SSP-2) at the Test Facility ISB-WWER, Final Report (in Russian language). Electrogorsk Research & Engineering Centre on Nuclear Plants Safety (EREC): Electrogorsk, Russia, 1997.

/GEP 90/ Geppert, J., Höppner, G., Miró, J. E.: Nachrechnung des LOBI-Versuches BT-01 (Frischdampfleitungsleck) mit dem Systemcode ATHLET. GRS-A-, No. 1679, June 1990.

/GEP 96/ Geppert, J., Steinhoff, F.: Nachrechnung des Integralexperiments PKL III B1.2 mit ATHLET. GRS-A-, No. 2337, February 1996.

/GLA 94a/ Glaeser, H., Hofer, E., Kloos, M., Skorek, T.: Unsicherheits- und Sensitivitätsuntersuchungen von Analysen mit Thermohydraulik-Rechenprogrammen. GRS-A-, No. 2177, July 1994.

/GLA 94b/ Glaeser, H., Hofer, E., Kloos, M., Skorek, T.: Uncertainty and Sensitivity Analysis of a Post-Experiment Calculation in Thermal Hydraulics. In: OECD Nuclear Energy Agency (NEA): Report on a CSNI Workshop on Uncertainty Analysis Methods. London, UK, 1 - 4 March 1994, NEA/CSNI/R(94)20, vol. 2, 1994.

/GLA 01a/ Glaeser, H., Hofer, E., Hora, A., Krzykacz-Hausmann, B., Leffer, J., Skorek, T.: Einfluss von Modellparametern auf die Aussagesicherheit des Thermohydraulik-Rechenprogramms ATHLET, GRS-A-2963. September 2001.

/GLA 01b/ Glaeser, H., Hofer, E., Krzykacz-Hausmann, B., Leffer, J., Skorek, T.: Einfluss von Modellparametern auf die Aussagesicherheit von ATHLET-Rechenergebnissen zum 5%-Leck im kalten Strang eines Druckwasser-Reaktors, GRS-A-2942. August 2001.

/GLA 01c/ Glaeser, H., Hofer, E., Krzykacz-Hausmann, B., Leffer, J., Skorek, T.: Einfluss von Modellparametern auf die Aussagesicherheit von ATHLET-Rechenergebnissen zum Integralexperiment LSTF-CL-18. GRS-A-, No. 2941, 2001.

/GLA 08a/ Glaeser, H.: GRS Method for Uncertainty and Sensitivity Evaluation of Code Results and Applications. Science and Technology of Nuclear Installations, vol. 2008, pp. 1–7, DOI 10.1155/2008/798901, 2008.

/GLA 08b/ Glaeser, H., Krzykacz-Hausmann, B., Luther, W., Schwarz, S., Skorek, T.: Methodenentwicklung und exemplarische Anwendungen zur Bestimmung der Aussagesicherheit von Rechenprogrammergebnissen. GRS-A-, No. 3443, November 2008.

/GOC 00/ Gocht, U., Lischke, W., Schaffrath, A.: Beiträge zur Validierung des Thermohydraulikcodes ATHLET anhand der Nachrechnungen der Experimente an der Versuchsanlage HORUS II. Hochschule Zittau/Görlitz (FH), IPM-610208-03, August 2000.

/GOT 85/ Gottula, R. C., et al.: Forced convective, non-equilibrium, post-CHF heat transfer experiment data and correlations comparison report. EG&G Idaho, Inc., NUREG, CR-3193, March 1985.

/GRS 21/ Gesellschaft für Anlagen- und Reaktorsicherheit (GRS) gGmbH (GRS): Softwareentwicklung (TKP 03-05). Managementhandbuch, Kapitel 2.2.3.5, Rev. 2, 2021.

/GRU 98/ Grundmann, U., Kliem, S., Krepper, E., Mittag, S., Rohde, U., Schäfer, F., Seidel, A.: Qualifizierung des Kernmodells DYN3D mit Komplex mit dem Störfallcode ATHLET als fortgeschrittenes Werkzeug für die Störfallanalyse von WWER-Reaktoren, Abschlussbericht (Teil 1). FZR-216, March 1998.

/GUO 22/ Guo, L., Hollands, T.: OECD/NEA International Standard Problem ISP-51, SBLOCA scenario in the ACME Facility, Phase 1: Open calculation. July 2022.

/GYÖ 95/ Györi, C., Horche, W., Trosztel, I.: ATHLET-Verifikation und Einsatz für Störfallanalysen des WWER-440. GRS-A-, No. 2293, October 1995.

/HAI 93/ A. Hainoun, Hicken, E. F., J. Wolters: ATHLET-Erweiterung zur Anwendung an Forschungsreaktoren. In: Kerntechnische Gesellschaft e.V. (KTG) (Ed.): Jahrestagung Kerntechnik 1993, Tagungsbericht. Köln, 25 - 27 May 1993, pp. 443, 1993.

/HER 16/ Herb, J., Chiriac, F.: One- and Two-Phase Coupling of OpenFOAM with the thermal hydraulic code ATHLET for nuclear safety analyses. Presentation, 11th OpenFOAM Workshop 2016: Guimaraes, 26 June 2016.

/HOB 89/ Hobbhahn, W., Weber, J. P., Forge, A., Mezza, M., Pochard, R., Porracchia, A.: Code Comparison based on a NEPTUNUS Pressurizer Experiment. In: Müller, U. (Ed.): Fourth International Topical Meeting on Nuclear Reactor Thermal Hydraulics (NURETH-4), October 10 to 13, 1989, Karlsruhe, Federal Republic of Germany. Kernforschungszentrum Karlsruhe (FZK), NURETH-4, Karlsruhe, 10 - 13 October 1989, vol. 1, ISBN 3765011169, Braun: Karlsruhe, 1989.

/HOF 85/ Hofer, E., Krzykacz-Hausmann, B., Ehrhardt, J., Fischer, F., Crick, M. J., Kelly, G. N.: Uncertainty and Sensitivity Analysis of Accident consequence Sub-models. In: Electric Power Research Institute (EPRI): Proc. ANS/ENS International Topical Meeting on Probabilistic Safety Methods and Applications. San Francisco, 14 February - 1 March 1985, vol. 2, pp. 130.1–130.17, 1985.

/HOL 16/ Hollands, T., Austregesilo, H., Bals, C., Buchholz, S., Ceuca, C. S., Hristov, H., Langenfeld, A., Pandazis, P., Palazzo, S., Preuß, J., Tiborcz, L., Weber, S.: Validierung von Rechenprogrammen zur Simulation des Reaktorkühlkreislaufs unter Stör- und Unfallbedingungen. Gesellschaft für Anlagen- und Reaktorsicherheit (GRS) gGmbH (GRS), GRS-404, 641 p., 2016.

/HOL 21/ Hollands, T., Austregesilo, H., Buchholz, S., Dünne, N., Junk, M., Lee, J., Lerchl, G., Schöffel, P. J., von der Cron, D., Wielenberg, A.: ATHLET 3.3 Validation. GRS-P-1/Vol. 3 Rev. 6, November 2021.

/HOL 22a/ Hollands, T., Austregesilo, H., Buchholz, S., Di Nora, V. A., Dünne, N., Eckert, D., Junk, M., Schöffel, P. J., Wack, J., Wielenberg, A.: ATHLET 3.3.1 Validation. GRS-P1/Vol.3 Rev. 7, November 2022.

/HOL 22b/ Hollands, T., Austregesilo, H., Lovasz, L., Pandazis, P., Tiborcz, L., Wielenberg, A.: ATHLET-CD 3.3.1 Validation. GRS-P-4 / Vol. 3, Rev. 2, November 2022.

/HÖP 93/ Höppner, G., Steinhoff, F.: ATHLET-Nachrechnung eines Ausfalls der Hauptwärmesenke in einem SWR. GRS-A-, No. 2100, December 1993.

/HOR 95/ Horche, W., Kauer, W., Lehnart, T., Roßner, L.: Qualifikation der Datenbasis für das KKWR Brokdorf mit dem Programmsystem ATLAS. GRS-A-, No. 2323, December 1995.

/HOR 98/ Horche, W., Jakubowski, Z., Pointner, W.: Qualifikation der Datenbasis für das KKW Neckar (GKN-2) mit dem Programmsystem ATLAS. GRS-A-, No. 2541, January 1998.

/HOR 99/ Horche, W., Hegyi, G., Keresztúri, A., Trosztel, I., Austregesilo, H., Langenbuch, S., Velkov, K.: Untersuchungen zur Weiterentwicklung und Verifikation von ATHLET zur Analyse von WWER-Anlagen (Band 1), WTZ mit der Republik Ungarn, Abschlussbericht. GRS-A-, No. 2798, December 1999.

/HOR 01/ Horche, W., Guba, A., Trosztel, I., Glaeser, H., Hofer, E., Krzykacz-Hausmann, B.: Untersuchungen zur Weiterentwicklung und Verifikation von

ATHLET zur Analyse von WWER-Anlagen (Band 2), WTZ mit der Republik Ungarn. GRS-A-, No. 2886, February 2001.

/HOR 09/ Horche, W.: Modellierung des ROCOM-Versuchsstandes und Nachrechnung von Experimenten aus der Serie T6655 mit ATHLET. GRS-A-, No. 3453, January 2009.

/HRI 15/ Hristov, H. V. et al.: Numerical Analyses on the Safety Aspects of KASOLA test facility. Proc. of the NURETH-16 conference: Chicago, USA, 2015.

/HRU 92/ Hrubisko, M.: Nachrechnung des ROSA III Versuchs Run 984 mit dem Rechenprogramm ATHLET. GRS-A-, No. 1981, December 1992.

/HRU 93/ Hrubisko, M., Pointner, W.: Nachrechnung des ROSA III Versuchs Run 952 mit ATHLET. GRS-A-, No. 2084, November 1993.

/HRU 95/ Hrubisko, M.: Nachrechnung des FIST-Versuchs 6SB2C mit ATHLET. GRS-A-, No. 2276, August 1995.

/IAEA 95/ International Atomic Energy Agency (IAEA): Simulation of a Loss of Coolant Accident Without High Pressure Injection But With Secondary Feed and Bleed, Results of the Fourth Standard Problem Exercise on the Simulation of Loss of Coolant Accidents, IAEA Technical Co-operation Project RER/9/004, AEA-TECDOC-848. IAEA-TECDOC-, No. 848, November 1995.

/IAEA 16/ International Atomic Energy Agency (IAEA): Safety Assessment for Facilities and Activities, General Safety Requirements. IAEA Safety Standards Series, GSR Part 4 (Rev. 1), 163 p., ISBN 978-92-0-109115-4, IAEA: Vienna, 2016.

/IAEA 19/ International Atomic Energy Agency (IAEA): Deterministic Safety Analysis for Nuclear Power Plants, Specific Safety Guide. IAEA Safety Standards Series, SSG-2 (Rev. 1), ISBN 978-92-0-102119-9, IAEA, 2019.

/IHL 84/ Ihle, P., Rust, K.: FEBA - Flooding Experiments with Blocked Arrays, Evaluation Report, KfK 3657. Kernforschungszentrum Karlsruhe (FZK), March 1984.

/ISH 79/ Ishii, M., Chawla, T. C.: Local drag laws in dispersed two-phase flow. Argonne National Laboratory (ANL), NUREG/CR-1230, December 1979.

/JAC 23/ Jacht, V., Scheuer, J., Schöffel, P. J., Wielenberg, A.: ATHLET 3.4 Programmer's Manual. GRS-P-1/Vol. 2 Rev. 11, November 2023.

/JAE 85/ Japan Atomic Energy Research Institute (JAERI): ROSA-IV Large Scale Test Facility (LSTF) System Description, The ROSA-IV Group, JAERI-M 84-237. 320 p., January 1985.

/JAE 89a/ Japan Atomic Energy Research Institute (JAERI): ROSA-IV / LSTF 5% Cold Leg Break LOCA Experiment Run SB-CL-18 Data Report, The ROSA-IV Group, JAERI-M 89-027. 112 p., March 1989.

/JAE 89b/ Japan Atomic Energy Research Institute (JAERI): LSTF Instrumentation Plan for Run SB-CL-18 Amendment to System Description (JAERI-M 84-237) and Data Report (JAERI-M 89-027), JAERI Handout at 1st ISP-26 Workshop. March 1989.

/JAY 68/ Jaynes, E. T.: Prior Probabilities. IEEE Transactions on Systems Science and Cybernetics, vol. 4, no. 3, pp. 227–241, DOI 10.1109/TSSC.1968.300117, 1968.

/JOB 55/ Jobson, D.: On the flow of compressible fluids through orifices. Proc. Instn. Mech. Engrs., vol. 37, no. 169, pp. 767–776, 1955.

/JOU 81/ Jouse, W. C.: Internal LOFT Reactor Vessel Core Bypass Flows. EG&G Idaho, Inc., LO-17-81-044, 20 November 1981.

/JUN 22/ Junk, M., Dünne, N., Wielenberg, A.: Simulation of the UPTF tests 5a and 8a using ATHLET 3.3, NUTHOS-13, Hsinchu, Taiwan, September 5-10, 2022. 2022.

/KAW 87/ Kawaji, M., Anoda, Y., Nakamura, H., Tasaka, T.: Phase and velocity distributions and holdup in high-pressure steam/water stratified flow in a large diameter horizontal pipe. International Journal of Multiphase Flow, vol. 13, no. 2, pp. 145–159, DOI 10.1016/0301-9322(87)90026-7, 1987.

/KHR 15/ Khrennikov, N. e. A.: Application of 3-D coupled code QUABOX/CUBBOX-ATHLET for RBMK-1000 vapor reactivity coefficient measurements, Annals of Nuclear Energy 84 (2015). 2015.

/KIR 87/ Kirmse, R., Malhotra, P. K.: Post-Test-Analyses of GE-Vessel Blowdown Tests #5803-2 (Bottom Leak) and #5702-16 (Top Leak) with ATHLET. GRS-A-, No. 1354, July 1987.

/KIR 89/ Kirmse, R.: Auswertung von LOBI Experimenten im Rahmen des "Shared Cost Action Research Programme" der Europäischen Gemeinschaften. GRS-A-, No. 1585, June 1989.

/KIR 96/ Kirmse, R., Pechterev, V., Steinhoff, F., Suslov, A. I.: Nachrechnung des Experiments UPTF-TRAM B1, Versuchsläufe B1a-2a, B1b-3c und B1b-2a, mit ATHLET. GRS-A-, No. 2377, July 1996.

/KLO 17/ Kloos, M., Berner, N.: SUSA Version 4.1 Manual of Methods. Gesellschaft für Anlagen- und Reaktorsicherheit (GRS) gGmbH (GRS), GRS-P-5 Vol. 2, 1. ed., 128 p., December 2017.

/KLO 20/ Kloos, M.: SUSA Version 4.2, User's Guide and Tutorial. GRS-P-5, Vol. 1, Rev. 6, October 2020.

/KOL 11/ Kolev, N. e. A.: VVER-1000 Coolant Transient Benchmark, Phase 2 (V1000CT-2), Summary Results of Exercise 2 and Exercise 3;, NEA/NSC/DOC(2011)3. 2011.

/KOP 20/ Koppers, V., Cuesta Morales, A.: Abschlussbericht zum Vorhaben 4717R01360 AP8 „Forschungskonzept für die Entwicklung eines generischen Analysesimulators für einen Forschungsreaktor“. Gesellschaft für Anlagen- und Reaktorsicherheit (GRS) gGmbH (GRS), GRS – 561, ISBN 978-3-947685-46-2, 2020.

/KOT 20/ Kotsarev, A. V., Lizorkin, M. P., Shumskiy, B. E.: Results of the ATHLET/BIPR-VVER Software System (Version 1.0) Certification. Kerntechnik, vol. 85, no. 5, pp. 387, 2020.

/KOZ 15/ Kozmenkov, Y., Kliem, S., Rohde, U.: Validation and verification of the coupled neutron kinetic/thermal hydraulic system code DYN3D/ATHLET. Annals of Nuclear Energy, vol. 84, pp. 153–165, DOI 10.1016/j.anucene.2014.12.012, 2015.

/KRE 96/ Krepper, E.: Post Test Calculations for a Small Break LOCA Experiment at the Integral Test Facility ISB-VVER using the Thermalhydraulic Code ATHLET. Ed.: Jahrestagung Kerntechnik (1996), 1996.

/KRE 98a/ Krepper, E., Schäfer, F.: Verifikation des ATHLET-Rechenprogramms im Rahmen der externen Verifikationsgruppe ATHLET BETHSY Test 5.2c - Totalverlust des Speisewassers. FZR-231, August 1998.

/KRE 98b/ Krepper, E., Schäfer, F.: Verifikation des ATHLET-Rechenprogramms im Rahmen der externen Verifikationsgruppe ATHLET BETHSY Test 9.3 - Heizrohrbruch mit Versagen der Hochdruck-Notseinspeisung. FZR-232, August 1998.

/KRE 99/ Krepper, E., Prasser, H.-M.: Natural Circulation Experiments at the ISB-VVER Integral Test Facility and Calculations Using the Thermal-Hydraulic Code ATHLET. Nuclear Technology, vol. 128, no. 1, pp. 75–86, DOI 10.13182/NT99-A3015, 1999.

/KRE 01/ Krepper, E., Schäfer, F.: Verifikation des ATHLET-Rechenprogramms anhand der Nachanalyse zweier Experimente an der CCTF-Versuchsanlage. Forschungszentrum Rossendorf (FZR), FZR-315, March 2001.

/KRI 22/ Krieger, J., Bratfisch, C., Koch, M. K.: Simulation of Heat Transfer in Helically Coiled Heat Exchangers with the System Code AC²-ATHLET. In: American Nuclear Society (ANS), SCK-CEN (Eds.): 19th International Topical Meeting on Nuclear Reactor Thermal Hydraulics. NURETH 19, virtual, 6 - 11 March 2022, pp. 35351, 2022.

/KRÜ 19/ Krüssenberg, A., Sarkadi, P., Weyermann, F. C.: Passive Lagerbeckenkühlung durch Wärmerohre - Verbesserung und Validierung numerischer Modelle. Gesellschaft für Anlagen- und Reaktorsicherheit, GRS-, vol. 564, 103 p., ISBN 978-3-947685-49-3, Gesellschaft für Anlagen- und Reaktorsicherheit gGmbH: Köln, Garching b. München, Berlin, Braunschweig, September 2019.

/KRY 91/ Krey, L.: Post Test Calculation of CCTF-Test C2-20, Run80 with the Code System ATHLET/FLUT N80a. Ed.: TÜV Bayern, June 1991.

/KRZ 94/ Krzykacz-Hausmann, B., Hofer, E., Kloos, M.: A Software System for Probabilistic Uncertainty and Sensitivity Analysis of Results from Computer Models. International Conference on Probabilistic Safety Assessment and Management (PSAM-II), San Diego, 1994.

/KTA 15/ KTA: Wärmeabfuhrsysteme für Brennelementlagerbecken von Kernkraftwerken mit Leichtwasserreaktoren. Sicherheitstechnische Regel des KTA KTA 3303:2015-11, 2015.

/KUK 92/ Kukita, Y., Nakamura, H., Watanabe, T.: OECD/NEA/CSNI International Standard Problem No. 26, ROSA-4 LSTF Cold Leg Small-Break LOCA Experiment, Comparison Report, NEA(CSNI. NEA/CSNI/R, No. 91, February 1992.

/KYN 89/ Kyncl, M., Kirmse, R.: Post-Test Calculation Report LOBI-MOD2 Test BL-01. GRS-A-, No. 1567, May 1989.

/LAN 03/ Langenbuch, S., Schmidt, K.-D., Velkov, K.: Analysis of the pressurized water reactor main steam line break benchmark by the coupled code system ATHLET QUABBOX/CUBBOX, Nuclear Technology 142 (2). 2003.

/LAN 04/ Langenbuch, S., Schmidt, K.-D., Velkov, K.: Analysis of the OECD / NRC BWR Turbine Trip Benchmark by the Coupled Code System ATHLET-QUABBOX/CUBBOX, Nuclear Science and Engineering 148 (2). 2004.

/LAN 20/ Lanfredini, M.: TPTF and Mantilla benchmark specification report. FONESYS, Rec-03(19) Rev. 4, 2020.

/LAN 22/ Lanfredini, M., Bestion, D., D'Auria, F., Aydemir, N., Carnevali, S., Fillion, P., Gaillard, P., Jeong, J. J., Junk, M., Karppinen, I., Kim, K. D., Kurki, J., Lee, J. H., Schöffel, P. J., et al.: TPTF horizontal flow prediction by SYS-TH codes - recent analyses made within the FONESYS network. In: American Nuclear Society (ANS), SCK-CEN (Eds.): 19th International Topical Meeting on Nuclear Reactor Thermal Hydraulics. NURETH 19, virtual, 6 - 11 March 2022, 2022.

/LAV 95/ Lavialle, G., Kimber, G., Leveque, C.: BETHSY International Standard Problem 38, Loss of Residual Heat Removal System During Mid Loop Operation, 1st Workshop Report. CEA Grenoble, France, October 1995.

/LEE 22/ Lee, J., Junk, M., Skorek, T., Schöffel, P. J.: Improvement of entrainment model for horizontal flow in ATHLET and application to Mantilla experiment and TPTF. In: American Nuclear Society (ANS), SCK-CEN (Eds.): 19th International Topical Meeting on Nuclear Reactor Thermal Hydraulics. NURETH 19, virtual, 6 - 11 March 2022, 2022.

/LEF 98/ Leffer, J., Skorek, T.: Untersuchung der Unsicherheit des Drift-Flux Modells an Hand von Experimenten THETIS und PERICLES. GRS, GRS Internal Report, TN-GRS-98-1: Garching, 1998.

/LER 02/ Lerchl, G.: Ein Modell zur Simulation des thermischen Mischens im Kaltstrang. Technische Notiz, TN-LER-01/02, 2002.

/LER 07/ Lerchl, G.: Simulation des unterkühlten und gesättigten Siedens mit ATHLET, (Nachrechnung von THTL-Versuchen zum Thema "Strömungsinstabilität in Forschungsreaktoren"). Technische Notiz, TN-LER-03/07, April 2007.

/LER 09/ Lerchl, G., Papukchiev, A.: Kopplung von ATHLET mit dem CFD-Programm ANSYS CFX, Ertüchtigung von ATHLET für eine semi-implizite Kopplung. Technische Notiz, TN-LER-09/01, 2009.

/LER 12/ Lerchl, G., Austregesilo, H., Schöffel, P. J., Cron, D. von der, Weyermann, F.: ATHLET Mod 3.0 Cycle A User's Manual. Gesellschaft für Anlagen- und

Reaktorsicherheit (GRS) gGmbH (GRS), GRS-P, GRS-P-1/Vol. 1 Rev. 6, November 2012.

/LER 19/ Lerchl, G., Austregesilo, H., Hollands, T., Schöffel, P. J., von der Cron, D.: ATHLET 3.2 Validation. Gesellschaft für Anlagen- und Reaktorsicherheit (GRS) gGmbH (GRS), GRS-P-1/Vol. 3 Rev. 5: Köln, February 2019.

/LIS 93/ Lischke, W., Vandreier, B.: Rechnungen zum ISP 33 an der finnischen Versuchsanlage PACTEL, Report THZ-61205-11. Hochschule für Technik, Wirtschaft und Sozialwesen TWS Zittau/Görlitz (FH), July 1993.

/LIS 94/ Lischke, W., Vandreier, B.: Nachrechnung der Experimente LOF-01 und LOF-04 (Loss of secondary side feed water) an der finnischen Versuchsanlage PACTEL, Report THZ-61205-14. Hochschule für Technik, Wirtschaft und Sozialwesen TWS Zittau/Görlitz (FH), December 1994.

/LIS 96/ Lischke, W., Vandreier, B.: Nachrechnung des Experimentes LSR-10 (Loop Seal Refilling Test) an der finnischen Versuchsanlage PACTEL mit dem Thermohydraulikcode ATHLET, Report THZ-61205-16. Hochschule für Technik, Wirtschaft und Sozialwesen TWS Zittau/Görlitz (FH), March 1996.

/LIS 97/ Lischke, W., Vandreier, B.: Nachrechnung des Experimentes SBL-22 (Small break loss-of-coolant test) an der finnischen Versuchsanlage PACTEL mit dem Thermohydraulikcode ATHLET, Report IPM-610205-022. Hochschule für Technik, Wirtschaft und Sozialwesen TWS Zittau/Görlitz (FH), February 1997.

/LOF 80/ Loftus, M. J., Hochreiter, L., Conway, C. E., Dodge, C. E., Tong, A., Rosal, E. R., Valkovic, M. M., Wong, S.: PWR FLECHT SEASET Unblocked Bundle, Forced and Gravity Reflood Task, Data Report, Volume I. Westinghouse Electric Company LLC (WEC): Washington, DC, June 1980.

/LOH 96/ Loh, W.-L.: On Latin hypercube sampling. The Annals of Statistics, vol. 24, no. 5, DOI 10.1214/aos/1069362310, 1996.

/MAN 08/ Mantilla, I.: Mechanistic Modeling of Liquid Entrainment in Gas in Horizontal Pipes. Dissertation, The University of Tulsa, 2008.

/MAN 21/ Manthey, R.: Two-phase flow instabilities in an open natural circulation system. Dissertation, 179 p., Technische Universität Dresden (TUD), 2021.

/MAR 22/ Martinez-Quiroga, V., Szogradi, M., Schollenberger, S., Sanchez-Perea, M., Sandberg, N., Zhongyun, J., Freydier, P., Suslov, M., Austregesilo, H., Glantz, T., Lee, J. H., Li, Z., Shvetsov, I., Mukin, R., et al.: OECD/NEA PKL-4 benchmark activity. Code assessment of the relevant phenomena associated to a blind IBLOCA experiment. Nuclear Engineering and Design, vol. 389, pp. 111632, DOI 10.1016/j.nucengdes.2021.111632, 2022.

/MEL 08/ Melikhov, O. I., Elkin, I. V., Lipatov, I. A., Gashenko, M. P., Kapustin, A. V.: Final AE Comparison Report, OECD PSB-VVER Project, Project Use Only. Ed.: Electrogorsk Research & Engineering Centre on Nuclear Plants Safety (EREC), PSB-29, 4 February 2008.

/MIS 23/ Mistry, H., Yang, Z., Herb, J., Papukchiev, A.: Weiterentwicklung und Validierung von OpenFOAM-Solvern und Kopplungsmethoden für die Thermohydraulik im Kühlkreislauf (WEVAFOAM). Gesellschaft für Anlagen- und Reaktorsicherheit (GRS) gGmbH, GRS-, GRS – 688, ISBN 978-3-949088-79-7: Garching b. München, 2023.

/MOS 97/ Moskalev, A., Roginskaja, V., Steinhoff, F.: Nachrechnung des Integralexperiments BETHSY 6.9c mit ATHLET. GRS-A-, No. 2466, March 1997.

/NAK 83/ Nakamura, H., Tanaka, M., Tasaka, K., Koizumi, Y., Murata, H.: System Description for ROSA-IV Two-Phase Flow Test Facility (TPTF). Japan Atomic Energy Research Institute (JAERI), JAERI-M, 83-042, March 1983.

/NAK 96/ Nakamura, H.: Slug Flow Transitions in Horizontal Gas/Liquid Two-Phase Flows (Dependence on Channel Height and System Pressure for Air/Water and Steam/Water Two-Phase Flows). Japan Atomic Energy Research Institute (JAERI), JAERI-96-022, 1996.

/NAL 85/ Nalezny, C. L.: Summary of the Nuclear Regulatory Commission's LOFT Program Research Findings. U.S. Nuclear Regulatory Commission (NRC), NUREG/CR-, No. 3305, April 1985.

/NEA 87/ OECD Nuclear Energy Agency (NEA): CSNI code validation matrix of thermo-hydraulic codes for LWR LOCA and transients. CSNI Report 132, 70 p., March 1987.

/NEA 89/ OECD Nuclear Energy Agency (NEA) (Ed.): CSNI Standard Problem Procedures. CSNI Report, No 17, 1989.

/NEA 93/ OECD Nuclear Energy Agency (NEA): Separate effects test matrix for thermal-hydraulic code validation, Vol.1: Phenomena Characterisation and Selection of Facilities and Tests and Vol 2: Facility and Experiment Characteristics. NEA/CSNI/R(93)14, 680 p., September 1993.

/NEA 96/ OECD Nuclear Energy Agency (NEA): CSNI Integral test facility validation matrix for the assessment of thermal-hydraulic codes for LWR LOCA and transients. NEA/CSNI/R(96)17, 388 p., July 1996.

/NEA 98/ Wicket, T., Sweet, D., Neill, A., D'Auria, F., Galassi, G., Belsito, S., Ingegneri, M., Gatta, P., Glaeser, H., Skorek, T., Hofer, E., Kloos, M., Chojnacki, E., Ousny, M., Lage Perez, C., Sánches Sanchis, J. I.: Report on the Uncertainty Methods Study, For Advanced Best Estimate Thermal Hydraulic Code Applications, Vol.1 & Vol. 2. OECD Nuclear Energy Agency (NEA), NEA/CSNI/R(97)35, 622 p., June 1998.

/NEA 00/ OECD Nuclear Energy Agency (NEA) (Ed.): CSNI International Standard Problems (ISP), Brief Descriptions. NEA/CSNI/, R(2000)5, 2000.

/NEA 01/ OECD Nuclear Energy Agency (NEA): Validation Matrix for the Assessment of Thermal-Hydraulic Codes for VVER LOCA and Transients, A Report by the OECD Support Group on the VVER Thermal-Hydraulic Code Validation Matrix. NEA/CSNI/R(2001)4, 249 p., June 2001.

/NEA 11/ OECD Nuclear Energy Agency (NEA): BEMUSE Phase VI Report: Status report on the area, classification of the methods, conclusions and recommendations. NEA/CSNI/R(2011)4, 28 March 2011.

/NEA 16/ OECD Nuclear Energy Agency (NEA): PREMIUM, a benchmark on the quantification of the uncertainty of the physical models in the system

thermal-hydraulic codes: methodologies and data review. NEA/CSNI/R(2016)9, 28 April 2016.

/NIJ 80/ Nijhawan, S., Chen, J. C., Sundaram, R. K., London, E. J.: Measurement of Vapor Superheat in Post-Critical-Heat-Flux Boiling. Journal of Heat Transfer, vol. 102, no. 3, pp. 465–470, DOI 10.1115/1.3244324, 1980.

/NIK 08/ Nikonov, S., Lizorkin, M., Langenbuch, S., Velkov, K.: Validation of the Coupled System Code ATHLET/BIPR-VVER on Local Core Measured Data. In: American Society of Mechanical Engineers (ASME): Proceedings of 16th International Conference on Nuclear Engineering, Volume 2: Fuel Cycle and High Level Waste Management; Computational Fluid Dynamics, Neutronics Methods and Coupled Codes; Student Paper Competition. ICONE 16, Orlando, Florida, USA, 11 - 15 May 2008, pp. 457–462, ISBN 0-7918-4815-9, DOI 10.1115/ICONE16-48604, ASMEDC, 2008.

/NIK 11/ Nikonov, S. P., Velkov, K., Pautz, A.: Detailed Modeling of KALININ-3 NPP VVER 1000 Reactor Pressure Vessel with the Coupled System code ATHLET/BIPR-VVER. Proc. of the M&C 2011: Rio de Janeiro, Brazil, 2011.

/NRC 89/ U.S. Nuclear Regulatory Commission (NRC): Best-Estimate Calculations of Emergency Core Cooling System Performance, Regulatory Guide 1.157 (Task RS 701-4). May 1989.

/NRC 05/ U.S. Nuclear Regulatory Commission (NRC): Transient and Accident Analysis Methods. Regulatory Guide, No. 1.203, 52 p., 2005.

/NUC 09/ Nuclear Science Committee (Ed.): Advanced reactors with innovative fuels, Proceedings of the 3rd workshop. Nuclear Energy Agency, Workshop Advanced Reactors with Innovative Fuels, ARWIF Workshop, Oak Ridge, Tennessee, 16 - 18 February 2005, 509 p., ISBN 9789264198470, OECD: Paris, 2009.

/ODA 00/ Odar, F.: Software Quality Assurance Procedures for NRC Thermal Hydraulic Codes. Ed.: U.S. Nuclear Regulatory Commission (NRC), NUREG, NUREG-1737, 1 December 2000.

/OEC 04/ OECD Nuclear Energy Agency (NEA): CSNI International Standard Problem Procedures, CSNI Report No. 17 - Revision 4. NEA/CSNI/R(2004)5, March 2004.

/ONR 19/ Office for Nuclear Regulation (ONR): Validation of Computer Codes and Calculation Methods. Nuclear Safety Technical Assessment Guide, NS-TAST-GD-042 Revision 4: Bootle, March 2019.

/PAL 13/ Palazzo, S., Velkov, K., Lerchl, G., van Tichelen, K.: Analyses of the MYRRHA spallation loop using the system code ATHLET. Annals of Nuclear Energy, vol. 60, pp. 274–286, DOI 10.1016/j.anucene.2013.05.010, 2013.

/PAL 18/ Palazzo, S., Koppers, V., Liao, X.: Verifizierung von Analysesimulatoren, Bericht zum Arbeitspaket 1 Vertiefte und generische Auswertung von Betriebserfahrungen - neue Bewertungsmethoden und Störfallanalyseverfahren. GRS-, No. 488, 41 p., ISBN 978-3-946607-73-1, Gesellschaft für Anlagen- und Reaktorsicherheit (GRS) gGmbH: Köln, Garching b. München, Berlin, Braunschweig, March 2018.

/PAL 20/ Palazzo, S., Pointner, W., Wenzel, S., Cuesta Morales, A., Périn, Y.: Fortschreibung des Standes von Wissenschaft und Technik bei der Durch- führung und Bewertung von Störfallanalysen und der Verwendung von Analysesimulatoren. Gesellschaft für Anlagen- und Reaktorsicherheit (GRS) gGmbH (GRS), GRS-Bericht, No. 581, 2020.

/PAN 15/ Pandazis, P., Ceuca, S., Schöffel, P. J., Hristov, H.: Investigation of multidimensional Flow Mixing Phenomena in the Reactor Pressure Vessel with the System Code ATHLET. Proc. NURETH-16: Chicago, 2015.

/PAP 96/ Papadimitriou, P. (Ed.): Kondensation an der Einspeisestelle und Modellierung in ATHLET. UPTF-TRAM Fachtagung V on Nutzung von UPTF-TRAM Ergebnissen für Reaktoranalysen mit ATHLET, Mannheim, October , 1996.

/PAP 10/ Papini, D., Cammi, A.: Modelling of Heat Transfer Phenomena for Vertical and Horizontal Configurations of In-Pool Condensers and Comparison with

Experimental Findings. Science and Technology of Nuclear Installations, vol. 2010, DOI 10.1155/2010/815754, 2010.

/PAP 12/ Papukchiev, A., Lerchl, G., Weis, J., Scheuerer, M., Austregesilo, H.: Multiscale Analysis of a Transient Pressurized Thermal Shock Experiment with the Coupled Code ATHLET – ANSYS CFX. ATW, International Journal for Nuclear Power, vol. 57, no. 6, pp. 402–409, 2012.

/PAP 14/ Papukchiev, A., Theodoridis, G., Lerchl, G., Scholz, D.: Assessment of Coupled Multiscale and Stand-Alone System Code Simulations Based on a Double T-Junction Mixing Experiment. In: Kerntechnische Gesellschaft e.V. (KTG): 45th Annual Meeting on Nuclear Technology, Jahrestagung Kerntechnik 2014. AMNT 2014, Frankfurt am Main, 6 - 8 May 2014, 2014.

/PAP 15a/ Papukchiev, A., Jeltsov, M., Kööp, K., Kudinov, P., Lerchl, G.: Comparison of different coupling CFD–STH approaches for pre-test analysis of a TALL-3D experiment. Nuclear Engineering and Design, vol. 290, pp. 135–143, DOI 10.1016/j.nucengdes.2014.11.008, 2015.

/PAP 15b/ Papukchiev, A., Geffray, C., Jeltsov, M., Kööp, K., Kudinov, P., Grishchenko, D.: Multiscale Analysis of Forced and Natural Convection Including Heat Trasfer Phenomena in the TALL-3D Experimental Facility. In: American Nuclear Society (ANS) (Ed.): NURETH-16, 16th International Topical Meeting on Nuclear Reactor Thermal Hydraulics. Chicago, 2015, pp. 13133, 2015.

/PAP 19/ Papukchiev, A., Scheuerer, M., Herb, J.: Anwendung und Validierung von CFD-basierten Verfahren für mehrskalige und multiphysikalische Simulationen in der Reaktorsicherheit. GRS-518, 205 p., ISBN 978-3-947685-03-5, July 2019.

/PER 11/ Perez, M., Reventos, F., Batet, L., Guba, A., Tóth, I., Mieusset, T., Bazin, P., Crécy, A. de, Borisov, S., Skorek, T., Glaeser, H., Joucla, J., Probst, P., Ui, A., et al.: Uncertainty and sensitivity analysis of a LBLOCA in a PWR Nuclear Power Plant: Results of the Phase V of the BEMUSE programme. Nuclear Engineering and Design, vol. 241, no. 10, pp. 4206–4222, DOI 10.1016/j.nucengdes.2011.08.019, 2011.

/POI 84a/ Pointner, W.: Posttest Calculation of the LOFT experiment LP-SB-1 with DRUFAN-02. GRS-A-, No. 1047, December 1984.

/POI 84b/ Pointner, W.: Posttest Calculation of the LOFT Experiment LP-SB-2 with DRUFAN-02. GRS-A-, No. 1048, December 1984.

/POI 89/ Pointner, W.: Nachrechnung des ROSA III Versuchs Run 916 mit den Rechenprogrammen ATHLET und FLUT, GRS-A-1624. Gesellschaft für Anlagen- und Reaktorsicherheit (GRS) gGmbH (GRS), November 1989.

/POI 91/ Pointner, W.: Wissenschaftlich-technische Zusammenarbeit mit der DDR: ATHLET-Analysen für WWER 440 Reaktoranlagen, Abschlussbericht. GRS-A-, No. 1768, March 1991.

/POI 92a/ Pointner, W., Steinborn, J.: Vorausrechnung des Integralexperiments BETHSY 9.1.b mit ATHLET. GRS-A-, No. 1949, August 1992.

/POI 92b/ Pointner, W., Fessel, M.: Nachrechnung des HDR Versuchs V 21.1 mit dem Rechenprogramm ATHLET. GRS-A-, No. 1950, August 1992.

/POI 94/ Pointner, W.: Qualifikation der Datenbasis für das KKW Gundremmingen mit dem Programmsystem ATLAS. GRS-A-, No. 2184, September 1994.

/POI 96/ Pointner, W.: Störfallsimulator Krümmel: Qualifikation der Datenbasis. GRS-A-, No. 2359, May 1996.

/POI 99/ Pointner, W.: Störfallsimulator Philippsburg I, Qualifikation der Datenbasis. GRS-A-, No. 2691, March 1999.

/POI 08/ Pointner, W., Austregesilo, H.: Nachrechnung des PKL-III Versuchs F4.2 mit ATHLET Mod 2.1 Cycle B. GRS-A-, No. 3402, January 2008.

/POI 17/ Pointner, W., Cuesta Morales, A., Koppers, V., Kowalik, M., Bröcker, A., Li, T., Mayer, G., Palazzo, S., Périn, Y.: Ermittlung des Standes von Wissenschaft und Technik bei der Durchführung und Bewertung von Störfallanalysen und der Verwendung von Analysesimulatoren. GRS-, No. 462, 354 p.,

ISBN 978-3-946607-45-8, Gesellschaft für Anlagen- und Reaktorsicherheit (GRS) gGmbH: Köln, March 2017.

/POL 22/ Polidori, M., Prusek, T., Sobecki, N., Lombardo, C., Herer, C., Vyskocil, L., Kecek, A., Buck, M., Cevikalp Usta, S.: Description of HERO-2 Facility and Simulations, PASTELS Deliverable 2.2. 8 March 2022.

/POM 96/ Pomier Baez, L. E., Dräger, P.: TPTF Experiment Post Test Calculation with ATHLET/MOD 1.1C. GRS-A-, No. 2358, March 1996.

/POR 19/ Porter, N. W.: Wilks' formula applied to computational tools: A practical discussion and verification. Annals of Nuclear Energy, vol. 133, pp. 129–137, DOI 10.1016/j.anucene.2019.05.012, 2019.

/PUR 94/ Purhonen, H., Kouhia, J., Holmström, H.: OECD/NEA/CSNI International Standard Problem No. 33, PACTEL Natural Circulation Stepwise Coolant Inventory Reduction Experiment, Comparison Report, Volumes 1 and 2. NEA/CSNI/R, (R94) 24, December 1994.

/REE 78/ Reeder, D. A.: LOFT System and Test Description, (5.5-FT Nuclear Core 1 LOCES). Ed.: EG&G Idaho, Inc., NUREG/CR-, No. 0247, July 1978.

/RIE 96/ Riest, D.: Dynamik realer Gase. Springer: Heidelberg, 1996.

/RIN 83/ Ringer, F. J.: Nachrechnung des Battelle-Versuchs SL1 mit dem Rechenprogramm DRUFAN-02. GRS-A-, No. 901, November 1983.

/RIN 87/ Ringer, F. J.: Nachrechnung des Marviken-Versuchs Nr. 22 mit dem Rechenprogramm ATHLET. GRS-A-, No. 1361, August 1987.

/RIN 90/ Ringer, F. J.: OECD-CSNI Internationales Standardproblem Nummer 26, Nachrechnung des LSTF-Versuchs SB-CL-18 mit dem Programmsystem ATHLET/FLUT. GRS-A-, No. 1683, June 1990.

/RIN 91/ Ringer, F. J.: Nachrechnung des TPTF-Ausdampfversuchs Nr. 6 mit dem 4-Gleichungs-Fluiddynamikmodell des Rechenprogramms ATHLET. GRS-A-, No. 1811, July 1991.

/RIN 93a/ Ringer, F. J.: Nachrechnung des Integralexperiments BETHSY 5.1a mit ATHLET. GRS-A-, No. 2112, December 1993.

/RIN 93b/ Ringer, F. J.: Nachrechnung des Integralexperiments BETHSY 4.3b mit ATHLET. GRS-A-, No. 2043, June 1993.

/RIN 94/ Ringer, F. J.: Nachrechnung des Integralexperiments BETHSY 5.2d mit ATHLET. GRS-A-, No. 2210, October 1994.

/RIN 95/ Ringer, F. J.: Nachrechnung des Integralexperiments PKL III B4.1 mit ATHLET. GRS-A-, No. 2291, July 1995.

/RIN 96/ Ringer, F. J.: Nachrechnung des Integralexperiments PKL III C 1.2 mit ATHLET. GRS-A-, No. 2427, December 1996.

/RIN 01a/ Ringer, F. J.: Nachrechnung des LOBI MOD2 Experiments A1-82. GRS-A-, No. 3000, October 2001.

/RIN 01b/ Ringer, F. J.: Nachrechnung des Einzeleffektversuchs UPTF 8 A mit ATHLET. GRS-A-, No. 2870, March 2001.

/RIN 03/ Ringer, F. J.: Nachrechnung des Experiments PKL III D2.2 mit ATHLET (Wiederholungsrechnung). GRS-A-, No. 3122, June 2003.

/ROH 10/ Rohde, U., Kozmenkov, Y., Pivovarov, V., Matveev, Y.: WTZ mit Russland - Transientenanalysen für wassergekühlte Kernreaktoren, Abschlussbericht. FZD-543, December 2010.

/ROS 12/ Rostechnadzor: Requirements to Quality Assurance Programs of Nuclear Facilities. Federal Rules and Regulations in the Area of Atomic Energy Use, NP-090-11, 7 February 2012.

/RUA 96/ Ruan, Y. Q.: On Entropy Balance Analyses of Non-Equilibrium Two-Phase Flow Models for Thermal-Hydraulic Computer Simulation, Dissertation. Technische Universität München (TUM), 1996.

/SAC 69/ Sachs, L.: Statistische Auswertungsmethoden. 2. ed., 677 p., ISBN 978-3540046950, Springer: Berlin, Heidelberg, New York, 1969.

/SCH 89/ Schall, M.: Unabhängige Verifikation des ATHLET-Rechenprogramms am Beispiel von LOBI-Versuchen. Battelle Institut, BF-R-66.762-01, December 1989.

/SCH 93a/ Schall, M.: Verifikation des ATHLET-Rechenprogramms im Rahmen der externen ATHLET Verifikationsgruppe, Report BF-R-67.836-01. Battelle Institut e.V., May 1993.

/SCH 93b/ Schaffrath, A., Sprünken, H., Krüssenberg, A.-K., Brockmeier, U.: Verifikation von ATHLET mit Hilfe der Einzeleffekttests ECTHOR und PATRICIA-SG2, Report RUB E-33. Ruhr-Universität Bochum, May 1993.

/SCH 94/ Schall, M.: Verifikation des ATHLET-Rechenprogramms durch Nachanalysen von BETHSY Versuchen (BETHSY 4.1a TC und BETHSY 3.4a), Report BF-R-67.836-01. Ed.: Battelle Ingenieurtechnik GmbH, October 1994.

/SCH 98a/ Schall, M.: Verifikation des ATHLET-Rechenprogramms im Rahmen der externen Verifikationsgruppe ATHLET (Versuche: BETHSY 6.2 TC, BETHSY 7.2c, BETHSY 4.1a, Phase 2), Report BF-R-68.355-01. Ed.: Battelle Ingenieurtechnik GmbH, March 1998.

/SCH 98b/ Schickel, H., Steinhoff, F.: Wiederholungsrechnungen mit ATHLET zu BETHSY 5.2d, PKL III B1.2 und UPTF TRAM B1. GRS-A-, No. 2570, April 1998.

/SCH 98c/ Schaffrath, A., Prasser, H.-M.: Theoretical Support to the NOKO Experiments. FZR-224, 1998.

/SCH 00/ Schall, M.: Verifikation des ATHLET-Rechenprogramms im Rahmen der externen Verifikationsgruppe ATHLET (Versuche LOFT L2-5 und CCTF C2-12). BF-R68.449-01, July 2000.

/SCH 08/ Schöffel, P. J.: Nachrechnung des Versuchs UPTF 20 mit ATHLET Mod 2.1 Cycle B. GRS-A-, No. 3400, January 2008.

/SCH 12/ Schöffel, P. J.: Nachrechnung der Versuchsreihe UPTF-TRAM C1 unter Verwendung des neuen ATHLET 2D/3D-Moduls, Validierung der 2D-Erhaltungsgleichungen für den Ringraum. Technische Notiz, TN-SCO-01/12, June 2012.

/SCH 15/ Schöffel, P. J., Ceuca, C. S., Deitenbeck, H., Kloos, M., Langenfeld, A., Lerchl, G., Peschke, J., Scheuer, J., Skorek, T., Cron, D. von der, Weyermann, F.: Weiterentwicklung des Systemrechenprogramms ATHLET für Anwendungen in der Reaktorsicherheit. Gesellschaft für Anlagen- und Reaktorsicherheit (GRS) gGmbH (GRS), GRS-, No. 387, September 2015.

/SCH 18/ Schöffel, P. J., Herb, J., Langenfeld, A., Lerchl, G., Skorek, T., Cron, D. von der: Rechenmethodenentwicklung für Reaktorsicherheitsanalysen mit dem Systemcode ATHLET. GRS-, vol. 497, 252 p., ISBN 978-3-946607-82-3, Gesellschaft für Anlagen- und Reaktorsicherheit (GRS) gGmbH: Köln, November 2018.

/SEN 94/ Senst, A., Petry, A.: Nachrechnung des Versuchs PKL III B 3.1 mit ATHLET. GRS-A-, No. 2166, April 1994.

/SEU 19/ Seubert, A., Behler, M., Bousquet, J., Henry, R., Herb, J., Lerchl, G., Sarkadi, P.: Weiterentwicklung der Rechenmethoden zur Sicherheitsbewertung innovativer Reaktorkonzepte mit Perspektive P&T. Gesellschaft für Anlagen- und Reaktorsicherheit (GRS) gGmbH (GRS), GRS-, vol. 553, ISBN 978-3-947685-38-7, 2019.

/SEU 22/ Seubert, A., Bousquet, J., Henry, R., Lo Muzio, S.: Entwicklung eines modernen Neutronenkinetikcodes für unregelmäßige Geometrien für (v)SMRs und fortschrittliche sowie innovative Reaktorsysteme. GRS-683, 115 p., 2022.

/SIA 15/ Sicherheitsanforderungen an Kernkraftwerke vom 22. November 2012 (SiAnf) as amended 3. März 2015 - Neufassung (BAnz AT 30.03.2015 B2).

/SKO 88a/ Skorek, T., Sonnenburg, H.-G.: ATHLET Calculations of Large Vessel Blowdown Experiments Using a Full-Range Drift-Flux Model. In: European Nuclear Society (ENS), American Nuclear Society (ANS) (Eds.):

Proceedings of the International ENS/ANS Conference on Thermal Reactor Safety. NUCSAFE 88, Avignon, France, 2 - 7 October 1988, vol. 2, pp. 613–622, 1988.

/SKO 88b/ Skorek, T.: Calculation of IVO Loop Seal Experiment with ATHLET. Technische Notiz, TN-SKT-88-1, May 1988.

/SKO 94/ Skorek, T.: Modelling of two-phase flow in horizontal piping junction. In: Oriolo, F., Vigni, P. (Eds.): Proceedings of International Conference on New Trends in Nuclear Thermohydraulics. Università di Pisa (UNIPI), Pisa, 30 May - 2 June 1994, Vol. 1, pp. 57–66, 1994.

/SKO 95/ Celata, G. P., Shah, R. K. (Eds.): Two-Phase Flow Modelling and Experimentation, Proc. First Int. Symposium on Two-Phase Flow Modelling and Experimentation. Rome, 9 - 11 October 1995: Pisa, 1995.

/SKO 97/ Skorek, T., Papadimitriou, P. (Eds.): A Simple model for Critical Flashing Flows in Nozzles: Development and Experimental Verification. 4th World Conf. on Experimental Heat Transfer, Fluid Mechanics and Thermalhydraulics, Brussel, June , vol. 3, 1701-1708, 1997.

/SKO 99/ Celata, G. P., Di Marco, P., Shah, R. K. (Eds.): Two-Phase Flow Modelling and Experimentation. 2nd Intern. Conference on Two-Phase Flow Modelling and Experimentation, Rome, May , 1999.

/SKO 01/ Skorek, T. (Ed.): Flooding Phenomenon and Determination of Interfacial and Wall Shear in One Dimensional Two-Fluid Model,. 5th World Conf. on Experimental Heat Transfer, Fluid Mechanics, and Thermodynamics, Thessaloniki, September , vol. 2, 1441-1446, 2001.

/SKO 04/ Skorek, T. (Ed.): Determination of Input Uncertainties of Uncertainty and Sensitivity Analyses. Probabilistic Safety Assessment and Management, PSAM 7 – ESREL'04, Berlin, June , vol. 4, Springer: Berlin, 2004.

/SKO 09/ Skorek, T.: Uncertainty and Sensitivity Analyses of Experiments and NPP Accidents: LB LOCA at cold leg of Zion NPP and comparison with LOFT test L2-5. In: Atomic Energy Society of Japan (AESJ): Proceedings

NURETH-13, 13th Topical Meeting on Nuclear Reactor Thermal Hydraulics. NURETH-13, Kanazawa, 27 September - 2 October 2009, Kanazawa, Japan, 2009, 2009.

/SKO 11a/ Skorek, T., de Crécy, A.: PREMIUM – Benchmark on the quantification of the uncertainty of the physical models in the system thermal-hydraulic codes, Workshop Proceedings OECD/CSNI Workshop on Best Estimate Methods and Uncertainty Evaluations Part 3. GRS, CEA Grenoble: Barcelona, Spain, November 2011.

/SKO 11b/ Skorek, T., Krzykacz-Hausmann, B., Austregesilo, H.: Investigation of the Uncertainty of Governing Equation Systems in the Thermal-Hydraulic Calculation. In: Canadian Nuclear Society (Ed.): Proceedings of the 14th International Topical Meeting on Nuclear Reactor Thermalhydraulics (NURETH-14). NURETH-14, Toronto, Ontario, Canada, 25 - 30 September 2011, ISBN 978-1-926773-05-6: Canada, 2011.

/SKO 17/ Skorek, T.: Input uncertainties in uncertainty analyses of system codes: Quantification of physical model uncertainties on the basis of CET (combined effect tests). Nuclear Engineering and Design, vol. 321, pp. 301–317, DOI 10.1016/j.nucengdes.2016.10.028, 2017.

/SKO 19/ Skorek, T., Crécy, A. de, Kovtonyuk, A., Petruzzi, A., Mendizábal, R., Alfonso, E. de, Reventós, F., Freixa, J., Sarrette, C., Kyncl, M., Pernica, R., Baccou, J., Fouet, F., Probst, P., et al.: Quantification of the uncertainty of the physical models in the system thermal-hydraulic codes – PREMIUM benchmark. Nuclear Engineering and Design, no. 354, DOI 10.1016/j.nucengdes.2019.110199, 2019.

/SON 90a/ Sonnenburg, H.-G.: Analysis of UPTF 11 (Hot Leg CCF) with a Full-Range Drift-Flux Model. GRS-A-, No. 1681, June 1990.

/SON 90b/ Sonnenburg, H.-G., Prassad, P. N.: Analysis of UPTF-Test 26 Run 230 by ATHLET Code with Full-Range Drift Flux Model. GRS-A-, No. 1723, October 1990.

/SON 94/ Sonnenburg, H.-G.: Berechnung der Phasendifferenzgeschwindigkeit von Wasser und Dampf in geometrisch unterschiedlich berandeten Kanälen, Dissertation. GRS-, vol. 109, No. 109, 162 p., Gesellschaft für Anlagen- und Reaktorsicherheit (GRS) gGmbH: Köln, 1994.

/SOZ 75/ Sozzi, G. L., Sutherland, W. A.: Critical Flow of Saturated and Subcooled Water at High Pressure. GE, GE Report NEDO, No. 13418, July / 1975.

/STÄ 84/ Städtke, H.: International Standard Problem No. 18 LOBI-MOD2 Small Break LOCA Experiment A2-81. CSNI-, No. 133, April 1984.

/STE 89/ Steinhoff, F.: Phasenseparation und Gemischspiegeldynamik bei instationären Zweiphasenströmungen, Zugl.: München, Techn. Univ., Diss., 1989. GRS-, vol. 73, No. 73, 147 p., ISBN 3-923875-23-1, Gesellschaft für Anlagen- und Reaktorsicherheit (GRS) gGmbH: Köln, 1989.

/STE 91/ Steinborn, J., Teske, H.: Nachrechnung des Integralexperiments BETHSY 4.1a mit ATHLET. GRS-A-, No. 1829, August 1991.

/STE 94/ Steinborn, J., Nikonov, S.: Voraus- und Nachrechnung des Integralexperiments PACTEL (ISP-33) mit ATHLET. GRS-A-, No. 2125, May 1994.

/STE 95/ Steinborn, J., Maltschewski, M.: Voraus- und Nachrechnung des IAEA Standardproblems SPE-4 mit ATHLET. GRS-A-, No. 2254, February 1995.

/STE 98a/ Steinborn, J.: Nachrechnung des 2. Russischen Standardproblems am integralen Versuchsstand ISB-WWER mit ATHLET. GRS-A-, No. 2562, April 1998.

/STE 98b/ Steinhoff, F.: Nachrechnung des Integralexperiments PKL III C 5.2 mit ATHLET. GRS-A-, No. 2606, September 1998.

/STE 99a/ Steinhoff, F.: Nachrechnung des Integralexperiments PKL III D 1.2 mit ATHLET. GRS-A-, No. 2766, December 1999.

/STE 99b/ Steinborn, J.: Voraus- und Nachrechnung des 3. Russischen Standardproblems am Integralversuchsstand ISB-WWER mit ATHLET. GRS-A-, No. 2768, November 1999.

/STE 01/ Steinhoff, F.: Nachrechnung des Integralexperiments PKL III B 4.5 mit ATHLET. GRS-A-, No. 2861, March 2001.

/STE 02/ Steinhoff, F.: Nachrechnung des Integralexperiments PKL III D2.1 mit ATHLET. GRS-A-, No. 3090, November 2002.

/STE 04/ Steinhoff, F.: Nachrechnung des Versuchs PKL III E2.2 mit ATHLET (Wiederholungsrechnung), Validierung des weiterentwickelten Rechenprogrammsystems ATHLET/ATHLET-CD, Technischer Bericht. GRS-A-, No. 3222, August 2004.

/STE 05/ Steinborn, J.: Results of Test 4: Primary to Secondary Leak Post-Test Calculation with ATHLET Computer Code (Participant's Report), OECD PSB-VVER Analytical Exercise (AE). December 2005.

/STE 06a/ Steinhoff, F.: Nachrechnung des Versuchs PKL III E2.3 mit ATHLET. GRS-A-, No. 3327, June 2006.

/STE 06b/ Steinhoff, F.: Nachrechnung des Versuchs PKL III E3.1 mit ATHLET. GRS-A-, No. 3298, April 2006.

/STF 91/ Steinhoff, F.: Nachrechnung des GERDA-Integral Tests 16 07 02 (20 cm2-Leck im Pumpenbogen) mit dem Rechenprogramm ATHLET, GRS-A-1828. Ed.: GRS, August 1991.

/STO 92/ Stolze, P.: Nachrechnung des TOSHIBA-Blowdown-Versuchs mit dem 5-Gleichungsmodell (ATHLET MOD 1.0-CycleE). Lehrstuhl für Reaktordynamik und Reaktorsicherheit, Technische Universität München: Garching, February 1992.

/TES 93/ Teschendorff, V., Skorek, T., Weber, J. P.: ATHLET Verifikation an HDR-Kondensationsversuchen und Druckhalterversuchen. GRS, GRS Report GRS-A, No. 2062: Garching, June / 1993.

/TES 01/ Teschendorff, V., Austregesilo, H., Bals, C., Deitenbeck, H., Hora, A., Lerchl, G., Luther, W., Romstedt, P.: Entwicklungsarbeiten für ATHLET. GRS-A-, No. 2938, November 2001.

/THI 90/ Thiele, T.: Post Test Calculation of UPTF TEST No. 20 Using Code System ATHLET/MOD1.0-Cycle C, Bericht Nr. 9058. Pitscheider Ingenieur-Büro: München, December 1990.

/THI 91/ Thiele, T.: Post Test Calculation of UPTF Test 29 A Using Code System ATHLET-FLUT Version N08. Pitscheider Report No. 9055, 1991.

/TIB 15/ Tiborcz, L.: Validation of the Reflooding Model in the Code ATHLET. Diploma Thesis, Budapest University of Technology and Economics, 2015.

/TRA 97/ Trambauer, K.: Computer and compiler effects on code results, Status report. OECD Nuclear Energy Agency (NEA), NEA/CSNI/R(96)15, 34 p., 1997.

/TRA 09/ Trambauer, K., Austregesilo, H., Bals, C., Cester, F., Deitenbeck, H., Klein-Heßling, W., Lerchl, G., Müller, C. W., Papukchiev, A., Schubert, J.-D.: Weiterentwicklung ATHLET/ATHLET-CD, Continued development of the computer code system ATHLET/ATHLET-CD. Gesellschaft für Anlagen- und Reaktorsicherheit (GRS) gGmbH (GRS), GRS-A-, No. 3461, March 2009.

/TRA 22/ Travleev, A., Bakalov, I., Iliev, D., Spengler, C., Sievers, J., Heckmann, K., Wielenberg, A., Henry, R., Périn, Y., Kilger, R.: Entwicklung und Validierung von Werkzeugen zur Durchführung von Störfallanalysen für WWER-Reaktoren. Gesellschaft für Anlagen- und Reaktorsicherheit (GRS) gGmbH, GRS-, vol. 685, ISBN 978-3-949088-76-6, 2022.

/TRU 68/ Truckenbrodt, E.: Strömungsmechanik. ISBN 978-3-662-41600-6, DOI 10.1007/978-3-662-41599-3, Springer Berlin Heidelberg: Berlin, Heidelberg, 1968.

/TUK 47/ Tukey, J. W.: Non-Parametric Estimation II. Statistically Equivalent Block and Tolerance Regions - The Continuous Case. The Annals of Mathematical Statistics, vol. 18, no. 4, pp. 529–539, 1947.

/TUK 48/ Tukey, J. W.: Nonparameteric Estimation, III. Stastically Equivalent Blocks and Multivariate Tolerance Regions - The Discontinuous Case. The Annals of Mathematical Statistics, vol. 19, no. 1, pp. 30–39, 1948.

/UNA 11/ Unal, C., Williams, B., Hemez, F., Atamturktur, S. H., McClure, P.: Improved best estimate plus uncertainty methodology, including advanced validation concepts, to license evolving nuclear reactors. Nuclear Engineering and Design, vol. 241, no. 5, pp. 1813–1833, DOI 10.1016/j.nucengdes.2011.01.048, 2011.

/VAN 98/ Vandreier, B., Lischke, W.: Nachrechnung der Experimente SIR-20 und SIR-21 (Stepped inventory reduction in low primary pressure) an der finnischen Versuchsanlage PACTEL mit dem Thermohydraulikcode ATHLET, Report IPM-610205-03. Hochschule für Technik, Wirtschaft und Sozialwesen TWS Zittau/Görlitz (FH), March 1998.

/VAN 99a/ Vandreier, B., Lischke, W.: Nachrechnung des PACTEL-Experimentes “Small break loss-of-coolant accident' SBL-31 mit dem Thermohydraulikcode ATHLET, Report IPM-610208-01. Hochschule für Technik, Wirtschaft und Sozialwesen TWS Zittau/Görlitz (FH), March 1999.

/VAN 99b/ Vandreier, B., Lischke, W.: Beiträge zur Validierung des Thermohydraulikcodes ATHLET anhand der Nachrechnung des PACTEL-Experimentes SBL-33., Report IPM-610208-02. Hochschule Zittau/Görlitz (FH), December 1999.

/VDI 10/ Verein Deutscher Ingenieure (VDI) (Ed.): VDI Heat Atlas. VDI-Buch, 2. ed., ISBN 978-3-540-77876-9, DOI 10.1007/978-3-540-77877-6, Springer-Verlag Berlin Heidelberg: Berlin, 2010.

/VEL 09/ Velkov, K., et al.: Boron Transient by the GRS Coupled System Codes QUABOX/CUBBOXATHLET and TORT-TD/ATHLET, Annual Meeting on Nuclear Technology. Dresden, Germany, 2009.

/VOJ 82/ Vojtek, I.: Untersuchung der Wärmeübertragungsverhältnisse in der Hochdruckphase eines Kühlmittelverluststörfalls mit mittlerem und grossem Bruchquerschnitt. GRS, GRS-A Report, No. 709: Garching, March 1982.

/VOJ 00a/ Vojtek, I., Macek, J., Arndt, S., Bencik, M., Denk, L., Lahovský, F., Meca, R., Parduba, L., Wolff, H., Zezula, L.: Validierung von Rechenprogrammen zur Analyse von Störfällen in WWER Reaktoren, WTZ mit der Tschechischen Republik, Abschlussbericht. GRS-A-, No. 2850, November 2000.

/VOJ 00b/ Vojtek, I., Panayotov, D., Ilieva, B., Avramova, M.: Anwendung und Validierung von Rechenprogrammen zur Analyse von Störfällen in WWER Reaktoren, STC with Bulgaria. GRS-A-, No. 2874, December 2000.

/VOJ 01/ Vojtek, I., Husarcek, J., Arndt, S., Kristof, M., Ruttkayova, M., Wolff, H.: Anwendung und Validierung von Rechenprogrammen zur Analyse von Störfällen in WWER-Reaktoren, WTZ mit der Slowakischen Republik. GRS-A-, No. 2916, June 2001.

/VOL 04/ Volchek, A., Zvonarev, Y., Schanz, G.: Advanced treatment of zircaloy cladding high-temperature oxidation in severe accident code calculations, Part II: Best fitted parabolic correlations. Nuclear Engineering and Design, no. 232, pp. 85–96, 2004.

/WAG 17/ Wagner, T., Mull, T.: The set-up of the INKA test facility at Karlstein within the frame of the German EASY Project. In: ANS (Ed.): NURETH-17, 17th International Topical Meeting on Nuclear Reactor Thermal Hydraulics. Xi'an, China, vol. 21599, 2017.

/WAH 86/ Wahba, A. B.: Post-Test Calculation of the OECD-LOFT-Experiment LP-LB-1 using DRUFAN-02, OECD LOFT-T-3506. GRS-A-, No. 1209, April 1986.

/WAL 43/ Wald, A.: An Extension of Wilks' Method for Setting Tolerance Limits. The Annals of Mathematical Statistics, vol. 14, no. 1, pp. 45–55, DOI 10.1214/aoms/1177731491, 1943.

/WAN 83/ Wang, S. W., Weisman, J.: Post-critical heat flux heat transfer: A survey of current correlations and their applicability. Progress in Nuclear Energy, vol. 12, no. 2, pp. 149–168, DOI 10.1016/0149-1970%2883%2990021-5, 1983.

/WEB 98/ Weber, J. P., Petry, A., Urbonas, R., Vaisnoras, M., Vileiniskis, V.: Analyses of Elektrogorsk 108 tests, Steam line ruptures at high power and 4000 MW Loss of AC Power ATWS event. Technische Notiz, TN-PEA-98-10, 82 p., October 1998.

/WEB 19/ Weber, S., Austregesilo, H., Bals, C., Herb, J., Hollands, T., Langenfeld, A., Lovasz, L., Pandazis, P., Sarkadi, P., Schubert, J.-D., Tiborcz, L.: Weiterentwicklung des Systemrechenprogramms ATHLET-CD zur Simulation von Unfällen im Primärkreislauf, Abschlussbericht. Gesellschaft für Anlagen- und Reaktorsicherheit (GRS) gGmbH (GRS), GRS-, vol. 535, 208 p., ISBN 978-3-947685-20-2, 2019.

/WEI 96/ Weisbrod, J., Brockmeier, U.: Verifikation von ATHLET anhand der Nachrechnung der Einzeleffekttests PATRICIA-SG2 und UPTF TRAM-A5, RUB E-145. Ruhr-Universität Bochum, March 1996.

/WEI 98/ Weisbrod, J., Unger, H.: ATHLET-Validierung anhand von Nachrechnungen der Einzeleffekttests CREARE und UPTF Test Nr. 10, Phase B und Phase C, RUB E-212. Ruhr-Universität Bochum, August 1998.

/WEI 00/ Weisbrod, J., Unger, H.: ATHLET Validierung anhand des Einzeleffektexperiments IVO-CCFL, Nachrechnung des Experiments, RUB E-257. Ruhr-Universität Bochum, June 2000.

/WEI 01/ Weisbrod, J., Bakay, G., Unger, H.: ATHLET Validierung anhand des Integralexperiments UPTF Test 27, Phase B, Nachrechnung des Experiments. RUB E-269, June 2001.

/WEI 02/ Weisbrod, J., Unger, H., Wagner, H.-J.: ATHLET Validierung anhand von Nachrechnungen der Experimente UPTF Test 6, Test7 und Test Z3, LEE-11. Ruhr-Universität Bochum, September 2002.

/WIC 91/ Wickett, A. J., Birchley, J. C., Holmes, B. J.: Quantification of large LOCA uncertainties. AEA Reactor Services, PWR/TUG/P(91)124: Winfrith, November 1991.

/WIE 98/ Wierum, H.-D.: Verifikation des ATHLET-Rechenprogramms im Rahmen der externen Verifikationsgruppe ATHLET durch Nachanalysen der PKL III-Versuche B4.3 und C6.1. TÜV Hannover/Sachsen-Anhalt e.V., 7/98, August 1998.

/WIE 00/ Wierum, H.-D.: Verifikation des ATHLET-Rechenprogramms im Rahmen der externen Verifikationsgruppe ATHLET durch Nachanalysen der PKL II-Versuche B-2 und B-5. Berichts-Nr. 8/2000, December 2000.

/WIE 06/ Wielenberg, A.: Nachrechnung des Einzeleffektversuchs UPTF Nr. 7 (Gegenströmung im Ringraum) mit ATHLET. GRS-A-, No. 3365, October 2006.

/WIE 08/ Wielenberg, A.: Nachrechnung des Versuchs PKL III F2.1 (Reflux-Condenser Mode bei Ausfall der Not- und Nachkühlsysteme im ¾-Loop-Betrieb) mit ATHLET. GRS-A-, No. 3401, March 2008.

/WIE 10/ Wielenberg, A.: Nachrechnung der Versuche PKL III G1.1 und G1.1a mit ATHLET. GRS-A-, No. 3513, February 2010.

/WIL 41/ Wilks, S. S.: Determination of Sample Sizes for Setting Tolerance Limits. The Annals of Mathematical Statistics, vol. 12, no. 1, pp. 91–96, DOI 10.1214/aoms/1177731788, 1941.

/WIL 42/ Wilks, S. S.: Statistical Prediction with Special Reference to the Problem of Tolerance Limits. The Annals of Mathematical Statistics, vol. 13, no. 4, pp. 400–409, DOI 10.1214/aoms/1177731537, 1942.

/WIL 48/ Wilks, S. S.: Order Statistics. Bulletin of the American Mathematical Society, vol. 54, no. 1, pp. 6–50, 1948.

/WIN 78/ Winkler, W.: Comparison Report on OECD-CSNI Standard Problem No. 6. CSNI Report No. 30, August 1978.

/WON 20/ Wong, K. W.: Recalculation of the THTL Flow Instability Experiment. Gesellschaft für Anlagen- und Reaktorsicherheit (GRS) gGmbH (GRS), Technische Notiz, TN-WON-20/10, 23 p., 2020.

/WON 21/ Wong, K. W.: Simulation of flow instability with modification in ATHLET evaporation and interfacial condensation model. Gesellschaft für Anlagen- und Reaktorsicherheit (GRS) gGmbH (GRS), Technische Notiz, TN-WON-21-02, 26 p., 2021.

/XU 21/ Xu, H., Badea, A. F., Cheng, X.: Development of a new full-range critical flow model based on non-homogeneous non-equilibrium model. Annals of Nuclear Energy, vol. 158, pp. 108286, DOI 10.1016/j.anucene.2021.108286, 2021.

/XU 22/ Xu, H., Badea, A. F., Cheng, X.: ATHLET Simulation of PKL I2.2 IB-LOCA Benchmark Test and Quantitative Assessment. Nuclear Technology, pp. 1–13, DOI 10.1080/00295450.2021.2014755, 2022.

/YON 85/ Yonomoto, T., Tasaka, K., Koizumi, Y., Anoda, Y., Kumamaru, H., Nakamura, H., Suzuki, M., Murata, H.: ROSA-III 50% Break Integral Test Run 916, (Break Area Parameter Test). Japan Atomic Energy Research Institute (JAERI), JAERI-M 85-109, August 1985.

9 Index

P

R

S

T

U

V

W